Investigating bifidobacteria-host interactions in the gut using organoid models and network biology approaches

Martina Poletti

A thesis submitted for the degree of Doctor of Philosophy

Supervisors:

Tamas Korcsmaros

Lindsay Hall

Conrad Nieduszynski

University of East Anglia

Earlham Institute

Quadram Institute Bioscience

United Kingdom

November 2022

Abstract

Despite numerous studies indicating that *Bifidobacterium* species exert beneficial effects a range of diseases, current knowledge about the specific modulating factors is limited. One mechanism is represented by autophagy, mediating key processes in intestinal epithelial cells, and which is often disrupted in gut disorders such as inflammatory bowel disease. In this regard, intestinal organoids represent a useful model to investigate these processes, allowing to study the effect of microbial-derived molecules on host epithelial cell function in a high-throughput and representative manner. The goal of this PhD thesis is to combine experimental and computational approaches, including intestinal organoids and network biology methods, to identify specific mechanisms by which *Bifidobacterium*-derived metabolites affect intestinal epithelial cell function, exerting a beneficial effect on the host.

To achieve these goals, mouse and human intestinal organoid models were developed, and in parallel with existing colon cancer cell lines, their culture conditions were further characterised to allow their co-culture with *Bifidobacterium*-derived metabolites. Subsequently, downstream applications were optimised to assess modulation of host intestinal barrier, cytokine release, autophagy, and gene expression changes. Host transcriptomics data from organoids was further integrated with *a priori* knowledge to build regulatory and molecular interaction networks, whose analysis can reveal specific mechanisms modulated by bifidobacteria.

This work resulted in the development and further characterisation of novel experimental models to investigate apical host-microbe interactions, including organoids with reversed polarity or organoid-derived monolayers. Furthermore, exposure of epithelial cultures to *Bifidobacterium* strains highlighted the ability of bifidobacterial metabolites to improve intestinal barrier function and modulate autophagy in epithelial cells. Transcriptomics analysis of human colonic organoids exposed to *Bifidobacterium* metabolites also revealed positive modulation of the immune response, epithelial differentiation and tight junctions through epigenetics mechanisms, and the downregulation of cholesterol biosynthesis.

Overall, this work has increased the understanding of the effects of bifidobacteria on the intestinal epithelium, while showing how a combination of experimental and network biology approaches can be used for these types of studies. Once further validated, results of this thesis will help unravel the beneficial effects of probiotics such as bifidobacteria in the gut, further aiding the development of management strategies for inflammatory diseases of the gut.

Acknowledgements

I would like to thank all the people who contributed to my thesis in the last five years, which have supported me both scientifically and personally.

First, I could not be more grateful to all the members of the Korcsmaros group, and my PhD supervisors Tamas, Lindsay, and Conrad. Without their scientific guidance, flexibility, and source of motivation in challenging moments, my PhD experience would have not been the same. A particular thanks goes to Isabelle, for her patience and support, and for the shared moments in the lab; and to my Norwich colleagues Márton, Matthew, Leila, and Dezso for the great scientific exchanges, their continuous help for the computational work, and the shared coffee breaks. I am also grateful to have worked together with other PhD students based in Budapest, Luca and Balazs, and with former members Amanda and Elena. It was a pleasure to work with all of you during these past 5 years.

This PhD would also not have been possible without the help of our collaborators. Lindsay and members of the Hall lab at QIB welcomed me in their group, shared their experimental and scientific expertise on microbiology, and provided the precious *Bifidobacterium* strains used in this thesis. Marc Ferrante at KU Leuven and Paul Wilmes at the University of Luxembourg hosted me in their respective labs, which have enriched this PhD thanks to their constructive collaboration and scientific exchange. A special thanks goes to Kaline, for being a great organoid collaborator in our joint publication, and to Audrey for the joint work on HuMiX. Finally, I am grateful to the Powell's group, for sharing their human organoid lines, and their insights about IBD.

The Norwich Research Park Doctoral (DTP) training program team, and the Biological Sciences Research Council (BBSRC) gave me the opportunity to start this journey, for which I am grateful. A special thanks goes to the Graduate Studies Office team, for their guidance through the administration process over the past years, and the Earlham and Quadram Institutes for welcoming me in their tremendous scientific community. This PhD program also gave me the chance to explore the world of microbiome research by working with the Gut Microbiology team at Nutricia Danone in Utrecht. This experience - and the visionary supervision of Sebastian - further steered my passion for this topic, which I will continue as an industrial postdoc following this journey.

I would have not completed my PhD without the support from friends, both close and far away. A special thanks goes to my closest Norwich friends Daniela, Ariadna, Anna, and Sonia for the beers and laughs after - sometimes demanding - days in the lab, and our Sunday gatherings over a stack of pancakes. Although geographically farther away, I want to thank Greta and Sofia, who were the driving force behind the initial undertaking of this doctorate, for always being there during my (too shorts) visits in Milan.

I am grateful to my parents and my sister Erika for their endless support. Without your help and continuous dedication, I would not have achieved my career goals in a field I love. Mamma and Papa', thanks for being so supportive, especially given the sometimes-abstract content of my lab adventures. Erika, thanks for being my continuous career coach, for pushing the best out of me, and for offering me a bed in London during my escapes from Norwich.

Finally, I could not be here without the support and love from my partner Nicolas. I am so proud how we have started and will finish this PhD path together, despite the geographical distance. I am also thankful for your numerous Brussels -> Norwich trips to visit me during the past 4 years, for standing me during my crisis moments, and always bringing me back to reality when signs of impostor syndrome arose.

The PhD path has been filled with ups and downs, but I would have not arrived at the finish line without the help from all of you.

Table of contents

List of abbreviations

2-ME	2-mercaptoethanol
3D	Three-dimensional
AMP	Antimicrobial peptide
ARN	Autophagy Regulatory Network
ASCL2	Achaete scute-like 2
ASC	Adult intestinal stem cell
ATG	Autophagy-related
ATOH1	Atonal BHLH transcription factor 1
B. animalis	*Bifidobacterium animalis*
B. bifidum	*Bifidobacterium bifidum*
B. breve	*Bifidobacterium breve*
B. dentium	*Bifidobacterium dentium*
B. infantis	*Bifidobacterium longum subsp. infantis*
B. longum	*Bifidobacterium longum* subsp. longum
B2M	Beta-2-microglobulin
BHI	Brain Heart Infusion
BMP	Bone morphogenetic protein
BMPR1A	BMP receptor type 1A
BSA	Bovine Serum Albumin
C. difficile	*Clostridioides difficile*
C. elegans	*Caenorhabditis elagans*
C. rodentium	*Citrobacter rodentium*
CALM	Calmodulin
CCR	C-C motif chemokine receptor
CD	Crohn's disease
CDX2	Caudal-type homeobox 2
CFU	Colony forming unit
ChIP	Chromatin immunoprecipitation
ChRE	Carbohydrate response element
ChREBP	ChRE binding protein
CLR	C-type lectin receptor
CM	Conditioned media
CRC	Colorectal cancer
CRS	Cytokine release syndrome

CSF1	Colony stimulating factor 1
CXCR	C-X-C motif chemokine receptor
DCLK1	Doublecortin-like kinase 1
DCs	Dendritic cells
DDI	Domain-domain interaction
DEG	Differentially expressed gene
DLL	Delta-like ligand
DMEM/F12	(Advanced) Dulbecco's Modified Eagle Medium/Nutrient Mixture F12
DMI	Domain-motif
DMSO	Dimethyl sulfoxide
DSS	Dextran sulphate sodium
E. coli	*Escherichia coli*
EACC	Enteroid Anaerobe Co-Culture
ECM	Extracellular matrix
EDTA	Ethylenediaminetetraacetic acid
EEC	Enteroendocrine cell
EFNA1	Ephrin A1
EGF	Epidermal growth factor
EGFR	Epidermal growth factor receptor
ELM	Eukaryotic Linear Motif (resource)
ENR	EGF, Noggin, R-spondin1
ENS	Enteric nervous system
EPS	Exopolysaccharide
ER	Endoplasmic reticulum
EVOM2	Epithelial Tissue Volt Ohmmeter 2
FACS	Flow cytometry activated sorting
FAS	Fas Cell Surface Death Receptor
FBS	Foetal Bovine Serum
Fcɣbp	Fc-gamma binding protein
FMT	Faecal Microbiota Transplantation
GABA	γ-aminobutyric acid
GALT	Gut-associated lymphoid tissue
GC	Goblet cell
GF	Germ free
GI	Gastrointestinal
GO	Gene Ontology
GPCR	G-protein coupled receptor

GSEA	Gene Set Enrichment Analysis
HD	Human α-defensin
HES1	Hes family BHLH transcription factor 1
HLA	Human leukocyte antigen
HMO	Human milk oligosaccharide
HNF	Hepatocyte Nuclear Factor
HNP	human neutrophil peptide
HSP	Heat-shock protein
HRA	Health Research Authority
HTA	Human Tissue Authority
HUB	Hubrecht Organoid Technology (organisation)
HuMiX	Human-microbial crosstalk module
IBD	Inflammatory Bowel Disease
IBS	Irritable Bowel Syndrome
ICAM1	Intercellular Adhesion Molecule 1
IECs	Intestinal epithelial cells
IFN	Interferon
iHACS	Intestinal Hemi-Anaerobic Co-culture System
IL	Interleukin
iPSC	Induced pluripotent stem cell
ITG	Integrin
JAK-STAT	Janus kinase-signal transducer and activator of transcription pathway
KCL	King's College London (organisation)
L. lactis	*Lactococcus lactis*
L. rhamnosus	*Lacticaseibacillus rhamnosus*
LC3	Microtubule-associated protein 1A/1B-light chain 3
LDH	Lactate dehydrogenase
LGR5	Leucine-rich repeat-containing G-protein coupled receptor 5
lncRNA	Long non-coding RNAs
LPS	Lipopolysaccharide
LRP1	LDL Receptor Related Protein 1
LTA	Lipoteichoic acid
LYZ	Lysozyme
M cell	Microfold cell
MAMP	Microbe-associated molecular pattern
MAP1LC3B/LC3	Microtubule-associated proteins 1A/1B light chain 3B
MAPK	Mitogen-activated protein kinase

miRNA	MicroRNA
MoDC	Monocyte-derived dendritic cell
mRNA	Messenger RNA
MRS	De Man, Rogosa and Sharpe
MTA	Material Transfer Agreement
mTOR	Mechanistic target of rapamycin
mTORC1	RPM complex 1
MUC2	Mucin 2
MyD88	Myeloid differentiation primary response 88
NAD	Nicotinamide adenine dinucleotide
NES	Normalised Enrichment Score
NEUROG3	Neurogenin3
NF-kB	Nuclear Factor kappa-light-chain-enhancer of activated B cells
NGPs	Next-generation probiotics
NK	Natural killer
NLR	Nucleotide oligomerization domain-like receptor
NNUH	Norfolk and Norwich University Hospital
NOD2	Nucleotide-binding oligomerization domain-containing protein 2
OD	Optical density
ODM	Organoid Differentiation Medium
OGM	Organoid Growth Medium
P/S	Penicillin/streptomycin
PBMC	Peripheral blood mononuclear cell
PBS	Phosphate buffered saline
PC	Paneth cell
PCA	Principal Component Analysis
PFA	Paraformaldehyde
PKC	Protein Kinase C
PLAU	Plasminogen Activator
PMA	Phorbol myristate acetate
POU2F3	POU Class 2 Homeobox 3
PP	Peyer’s patches
PPI	Protein-protein interaction
PRR	Pattern recognition receptor
QC	Quality control
RCM	Robertson's Cooked Meat
RegIII	Regenerating islet-derived protein 3

RELMβ	Resistin-like molecule beta
RIPK1	Receptor-interacting serine/threonine-protein kinase 1
RLR	Retinoic acid inducible gene I like receptor
RNAseq	RNA sequencing
RPMI	Roswell Park Memorial Institute
rRNA	Ribosomal RNA
S. enterica	*Salmonella enterica*
SARS-CoV-2	Severe acute respiratory syndrome coronavirus 2
SC	Stem cell
scRNAseq	Single-cell RNA sequencing
SD	Standard deviation
serpins	Serine protease inhibitors
SHIME®	Simulator of Human Intestinal Microbial Ecosystem
SMAD4	Decapentaplegic homolog 4
SPDEF	SAM pointed domain ETS factor
sPLA2	Secretory phospholipase A2
SQSTM1/p62	Sequestosome 1
STAR	Spliced Transcripts Alignment to a Reference
STAR (bis)	Stem Cell ASCL2 Reporter
Sup.	Supernatant
TA	Transit-amplifying
Tad	Tight adherence
TCF	T-cell factor
TEER	Transepithelial electrical resistance
TF	Transcription factor
TFF	Trefoil factor peptides
TG	Target gene
TGF-β	Transforming growth factor beta
Th	T helper
TieDIE	Tied Diffusion Through Interacting Events
TJ	Tight junctions
TLR	Toll-like receptor
Tn5	Transposon 5
TNF	Tumour necrosis factor
Treg	Regulatory T cell
Trm	Resident memory T cell
tRNA	Transfer RNA

UC	Ulcerative colitis
UEA	University of East Anglia
UMAP	Uniform manifold approximation and projection
VDR	Vitamin D receptor
vWF	Von Willebrand factor
WNT	Wingless-related integration site
WT	Wild-type

List of Figures

List of Tables

List of Peer Reviewed publications

Peer-reviewed journal articles published during my PhD (2018-2022). Those covered in Chapter 1 and 5 are reproduced in **Appendix 3**.

Chapter 1:

- **Poletti, M**., Arnauts, K., Ferrante, M., & Korcsmaros, T. (2021). Organoid-based Models to Study the Role of Host-microbiota Interactions in IBD. *Journal of Crohn's & Colitis,* 15(7), 1222–1235.
- Hautefort, I., **Poletti, M.**, Papp, D., & Korcsmaros, T. (2022). Everything You Always Wanted to Know About Organoid-Based Models (and Never Dared to Ask). *Cellular and Molecular Gastroenterology and Hepatology,* 14(2), 311–331.

Chapter 5:

- **Poletti, M**., Treveil, A., Csabai, L., Gul, L., Modos, D., Madgwick, M., Olbei, M., Bohar, B., Valdeolivas, A., Turei, D., Verstockt, B., Triana, S., Alexandrov, T., Saez-Rodriguez, J., Stanifer, M. L., Boulant, S., & Korcsmaros, T. (2022). Mapping the epithelial-immune cell interactome upon infection in the gut and the upper airways. *NPJ Systems Biology and Applications,* 8(1), 15.
- Treveil, A., Bohar, B., Sudhakar, P., Gul, L., Csabai, L., Olbei, M., **Poletti, M.,** Madgwick, M., Andrighetti, T., Hautefort, I., Modos, D., & Korcsmaros, T. (2021). ViralLink: An integrated workflow to investigate the effect of SARS-CoV-2 on intracellular signalling and regulatory pathways. *PLoS Computational Biology,* 17(2), e1008685.

Others (not presented in the thesis)

- Olbei, M., Hautefort, I., Modos, D., Treveil, A., **Poletti, M.**, Gul, L., Shannon-Lowe, C. D., & Korcsmaros, T. (2021). SARS-CoV-2 Causes a Different Cytokine Response Compared to Other Cytokine Storm-Causing Respiratory Viruses in Severely Ill Patients. *Frontiers in Immunology,* 12, 629193.

- Vickers, A., Tewary, M., Laddach, A., **Poletti, M.**, Salameti, V., Fraternali, F., Danovi, D., & Watt, F. M. (2021). Plating human iPSC lines on micropatterned substrates reveals role for ITGB1 nsSNV in endoderm formation. *Stem Cell Reports*, 16(11), 2628–2641.

- **Poletti, M.,** Hautefort I., Treveil A., Demeter A., Rodriguez E., Brion A., Goldson A., & Korcsmaros T. (2020). P071 Studying the effects of the probiotic bifidobacteria on gut health and intestinal epithelial cells function, *Journal of Crohn's & Colitis,* 14(Supplement_1), S171.

Chapter 1: General Introduction

1. Introduction

The human gut is colonised by trillions of endogenous microorganisms, including bacteria, viruses, archaea and fungi, which constitute one of the most complex microbial communities on earth (Bäckhed et al., 2005; Gill et al., 2006; Turnbaugh et al., 2007). This community, known as the gut 'microbiota', plays a pivotal role in human health (de Vos and de Vos, 2012). The intestinal microbiota interacts with the epithelium of the gut through metabolites or other released factors (Earle et al., 2015; Geva-Zatorsky et al., 2015; Peterson and Artis, 2014). By doing so, it takes part in various processes including the maintenance of intestinal barrier functions and integrity (Earle et al., 2015; Geva-Zatorsky et al., 2015), modulation of the host immune system (Zelante et al., 2013), and prevention of colonisation from pathogens (Zelante et al., 2013). Microbial metabolites such as short chain fatty acids (SCFAs), produced by microbial fermentation of dietary fibre in the gut, also serve as energy source (Sanderson, 2004) and immunomodulators (Russo et al., 2019). Conversely, the intestinal epithelium also plays a crucial role in maintaining gut homeostasis, by acting as a physical barrier as well as coordinating the immune defence and crosstalk between bacterial and immune cells (Allaire et al., 2018).

Maintaining balance of the complex molecular interplay between the gut microbiota, the intestinal epithelium and immune cells in the gut is essential for the host (Kim et al., 2017). Compositional perturbations of the microbiota, caused by antibiotics, changes in diet, and host genetics, are associated with various diseases, including obesity (Shen et al., 2013), diabetes (Naseer et al., 2014), colorectal cancer (CRC) (Azcárate-Peril et al., 2011), and Inflammatory Bowel Disease (IBD) (Ott et al., 2004). Importantly, these diseases are characterised by a significant decrease in beneficial bacterial populations such as Bifidobacteriaceae, while exhibiting an increased in potential pathogenic ones such as Enterobacteriaceae, Pasteurellaceae, Fusobacteriaceae, and Neisseriaceae (Gevers et al., 2014). Furthermore, dysfunction of epithelial cells associated with genetic genetic defects in key epithelial functions (i.e. bacterial sensing, autophagy and epithelial barrier) is associated with inflammatory conditions such as IBD (Koch and Nusrat, 2012; McCole, 2014).

One member of the microbiota, *Bifidobacterium*, shows promising results towards the protection against a range of diseases, including IBD. Evidence suggests that bifidobacteria can affect cellular processes in intestinal epithelial cells including autophagy, a cellular degradation mechanism important for intestinal homeostasis and maintenance of barrier function (Alessandri et al., 2019; Engevik et al., 2019; Inaba et al., 2016; Lin et al., 2014). However, the specific bacterial modulating factors, as well as the mechanisms and host targets involved in these effects, are largely unknown. Investigating the interactions between bifidobacteria and intestinal epithelial cells is key to understanding the mechanisms behind the beneficial effects of bifidobacteria on gut health.

Studying host-microbe interactions *in vitro* can be challenging. Recently, organoids have been proposed as an extremely useful model allowing the analysis of interactions between microbes and epithelial cells (Bozzetti and Senger, 2022; Puschhof et al., 2021a). As I described in my published review (see **Appendix 3**), organoids can be exposed to selected bacterial strains and/or their metabolites, following which several readouts, including 'omics (transcriptomics, proteomics) and other measures such as barrier function, immunostaining of autophagy proteins, and cytokine production, can be generated to study the effect of bacteria on the host (Poletti et al., 2021). Furthermore, network biology approaches can be employed to integrate 'omics readouts with available data to create molecular interaction networks. The analysis of these networks enables us to make predictions about the most important factors involved in these interactions at the transcriptional, post-transcriptional and post-translational levels, as well as the role played by host genetics (Sudhakar et al., 2021). Because organoid research is still in its infancy, several optimisations are required for their exposure to anaerobic microbes such as bifidobacteria, and to allow several molecular applications to decipher mechanisms involved in bifidobacteria-host interactions.

The goal of this thesis is to explore mechanisms involved in bifidobacteria-host interactions in the gut, in particular the effect on epithelial cell function (including autophagy), using intestinal organoid-based models and network biology approaches. In **Chapter 1**, I will introduce general concepts about the intestinal epithelium and the microbiome, bifidobacteria, autophagy, organoid models and network biology approaches. The section of this introduction related to organoids has also been published as review article (see **Appendix 3**). In **Chapter 2**, I will introduce experimental work to optimise different methodologies to develop organoid-based and other *in vitro* models to investigate bifidobacteria-host interactions studies, as well as to generate and analyse 'omics data from these studies. In **Chapter 3**, I will present a study where I used these models to investigate the effects of bifidobacteria on epithelial barrier, inflammation and autophagy in the gut. In **Chapter 4**, I will present a study where I investigated

the molecular mechanisms behind bifidobacteria-host interactions in the gut using organoid models and network biology. Additionally, in **Chapter 5**, I have included an additional project carried out during the COVID-19 pandemic, which was not part of my PhD, but resulted in a first author publication due to its relevance for the research community (see **Appendix 3**). In this chapter, I will explore the effect of SARS-CoV-2 on epithelial cell functions and epithelial-immune interactions in the gut in infected human organoids. Finally, in **Chapter 6**, I will discuss all results together, present advantages and limitations of the used methodologies and elucidate future work and potential applications.

Thanks to this work, I successfully developed optimised experimental protocols for the exposure of mouse and human organoid cultures with *Bifidobacterium*-derived metabolites. These improved organoid cultures, together with the standard Caco-2 cell culture model, were used to study the effect of bifidobacterial metabolites on host autophagy processes and to generate 'omics readout to decipher the main mechanisms involved in these interactions. The results of these studies elucidated the role of bifidobacteria on increasing barrier function, and proposed several pathways by which bifidobacteria can affect host intestinal epithelial cells. Furthermore, the integrated experimental and computational methodology used in this thesis can be applied to other studies to unravel mechanisms of action and the role of probiotic bacteria in the gut. Overall, I hope the outcomes of my PhD will help achieve a greater mechanistic understanding of how bifidobacteria influence host cellular response in health or chronic inflammatory diseases, and consequently pave the way for translational developments in prevention and treatment of the disease using live biotherapeutics.

2. The intestinal epithelium

2.1. Intestinal epithelial composition and structure

The intestinal epithelium, composed of a single layer of cells, plays a crucial role in maintaining gut homeostasis, by acting as a physical barrier as well as coordinating the immune defence and crosstalk between bacterial and immune cells (Allaire et al., 2018). The intestinal epithelium is formed by a single layer of cells, generally organised into crypts and villi (Peterson and Artis, 2014). The architecture and cellular composition of the intestinal epithelium greatly differs between the small and large intestines. While the small intestine is characterised by the presence of villi that increase the mucosal surface and nutrient absorption, villi are absent in the colon, as this limits the potential damage caused by the semi-solid stool transitioning through the large intestine. Intestinal crypts contain fast-cycling stem

cells (SCs) residing at the crypt base (Barker et al., 2007). SCs give rise to proliferative transit-amplifying (TA) daughter cells, which will differentiate and migrate upwards, eventually moving onto the flanks of the villi to die at the villus tips (Crosnier et al., 2006). Intestinal crypts undergo constant cycles of replenishment and renewal, with a turnover of about 4-5 days in homeostatic conditions (van der Flier and Clevers, 2009) (**Figure 1.1A**).

Various differentiated cell types are found in the gut epithelium, each of them carrying unique and specialised functions. These cell types include absorptive enterocytes/colonocytes, responsible for nutrient and water absorption and secretory cell types, such as Paneth cells (PCs) releasing antimicrobial factors, goblet cells (GCs) secreting mucins, and enteroendocrine cells (EECs) secreting hormones (Crosnier et al., 2006; Gribble and Reimann, 2016; Johansson and Hansson, 2016; Rodríguez-Colman et al., 2017). Finally, we can find tuft cells playing a role in defence against helminths and microfold (M) cells that are responsible for uptake and presentation of luminal antigens to the immune system (Gerbe et al., 2016; Howitt et al., 2016; Ohno, 2016; von Moltke et al., 2016). Most IECs are present in both the small and large intestine (enterocytes/colonocytes, EECs, GCs and tuft cells, M cells), however some cell types are unique to the small intestine (PCs) (**Figure 1.1B**).

In addition to IECs, resident immune cells, including phagocytes and lymphocytes, are also present in the gut and play a role in host-microbe crosstalk. Phagocytes, which include macrophages, neutrophils and dendritic cells (DCs), are innate immune cells that perform phagocytosis by engulfing bacteria and other foreign particles, subsequently killing them and presenting their antigens to other immune cells. Lymphocytes, which include T cells and B cells, are adaptive immune cells that get activated in response to the detection of foreign antigens. Finally, Natural Killer (NK), which are innate immune cells (but increasingly being recognised in the adaptive immune response), play a role in the removal or tumours and virus-infected cells, as well as coordinating the response of DC and macrophages.

Gut immune cells are mainly located in the gut-associated lymphoid tissue (GALT), containing 70% of all body's immune cells (Heel et al., 1997). GALT includes effector sites and organised tissues (Heel et al., 1997). Effector sites include intraepithelial lymphocytes within the epithelium and other immune cells (DCs, macrophages, T cells) within the lamina propria (Macdonald and Monteleone, 2005; Mowat et al., 2003). Conversely, organised tissues include Peyer's patches (PP) and mesenteric lymph nodes. PPs are present only in the small intestine, and consist of lymphoid aggregates of B cells and T cells separated from the gut lumen by the follicle-associated epithelium, a particular type of epithelium containing M cells,

and other immune cells (B cells, T cells, macrophages, DCs). Smaller individual lymphoid follicles also line the small intestine and colon (Brandtzaeg, 2017).

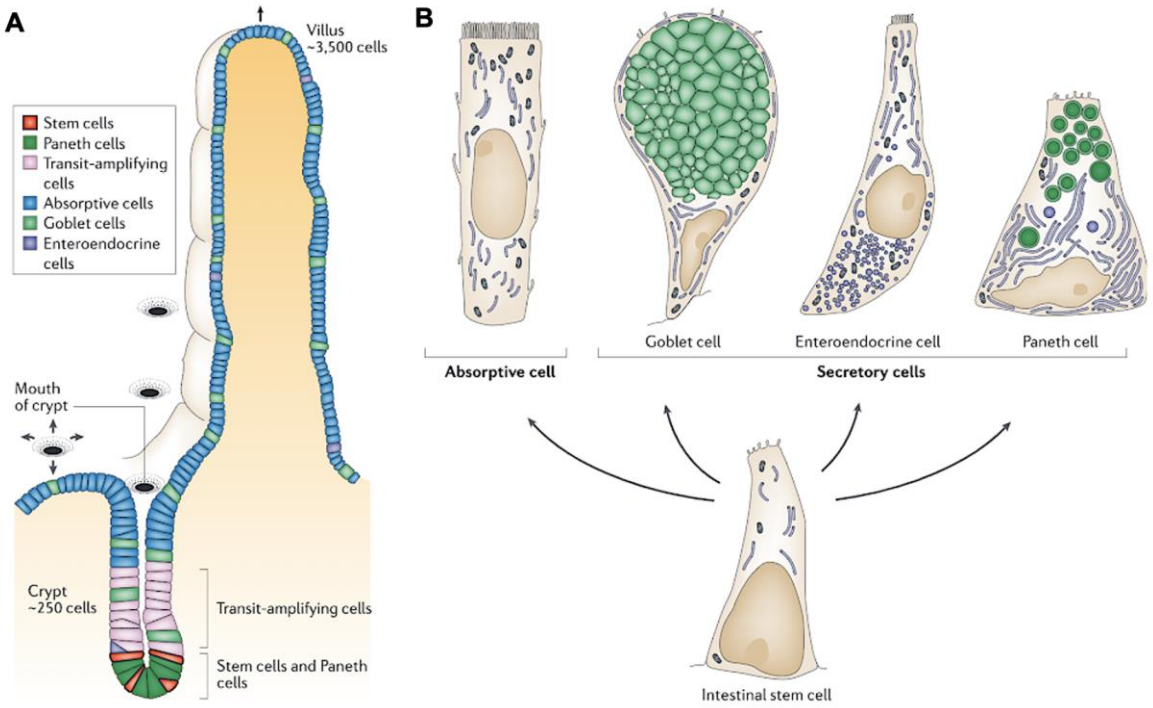

Figure 1.1. Overview of the main epithelial cell types present in the small intestine. A) Representation of a villus with one of the crypts contributing to the renewal of its epithelium. Stem cells reside at the crypt base, interspersed between Paneth cells. Transit-amplifying cells, dividing progenitors, some of which are partially differentiated, move upwards. At the villus tip, differentiated cells (absorptive cells, goblet cells and enteroendocrine cells) can be found. **B)** There are four classes of terminally differentiated cells, which include absorptive enterocytes, Goblet cells, enteroendocrine cells and Paneth cells. Their functions are explained in the text. Figure from (Crosnier et al., 2006).

2.2. Intestinal epithelial cells (IECs)

In this paragraph, the main IECs will be described in more detail. A short summary of these cell types, their subsets and main function can be found as **Table 1.1.**

2.2.1. Absorptive enterocytes and colonocytes

Absorptive enterocytes and colonocytes, represents the majority of cells bordering the intestinal lumen (10% in the small intestine and 20% in the colon) and have a lifespan of 5-7 days (Barker, 2014; Cheng and Leblond, 1974). Enterocytes are specialised in metabolic and digestive functions. Thanks to their characteristic microvilli brush border increasing their

surface area, they absorb nutrients apically and transport them, and contribute to maintain water/electrolyte homeostasis (Zachos et al., 2016).

2.2.2. Enteroendocrine cells

Enteroendocrine cells, making up 1% of the intestinal epithelium, comprise different subsets of cells secreting various types of hormones, mainly regulating the digestive function (Haber et al., 2017). In particular, they can release peptide hormones (e.g. secretin, gastrin) in response to luminal nutrients, but also cytokines in response to microbial metabolites (Worthington et al., 2018). Interestingly, location specific differences in EECs were found between villi and crypts based on bone morphogenetic protein (BMP) signalling gradient (Beumer et al., 2018).

2.2.3. Stem cells

Stem cells reside in intestinal crypts, are present in low numbers (4-6 cells) and are mainly involved in the regeneration of the intestinal epithelium. The identity and position of stem cells in the gut is still a question under debate (Barker et al., 2008). According to the “+4 position” model, quiescent SCs are present in the +4 position of the crypt, with PCs occupying the first three positions (Potten et al., 1974). Conversely, according to the “stem cell zone” crypt base columnar cells - fast cycling SCs characterised by a high expression of Leucine-rich repeat-containing G-protein coupled receptor 5 (LGR5) - are present at the base of the crypt interspersed between PCs (Barker et al., 2007; Barker et al., 2010; Cheng and Leblond, 1974; Jaks et al., 2008; Muñoz et al., 2012). Despite initial reports of molecular markers for the +4 SC population (Montgomery et al., 2011; Powell et al., 2012; Sangiorgi and Capecchi, 2008; Takeda et al., 2011), subsequent studies confirmed that their expression was not cell-type specific (van der Flier et al., 2009; Wong et al., 2012). The general consensus is that these cells exist, and evidence shows that this population is key during intestinal injury to potentially replenish LGR5+ cells by increasing their stem cell activity (Montgomery et al., 2011; Tian et al., 2011). Throughout this thesis, any reference to SCs will refer to LGR5+ cells, as further research is needed to clarify the role of the +4 SCs.

2.2.4. Goblet cells

Goblet cells are secretory cells present in 5-15% of the small intestinal and up to 50% of the colonic epithelium (Kim and Ho, 2010; Noah et al., 2011). GCs play a key role in barrier function thanks to their secretion of mucin glycoproteins (e.g. mucin 2, MUC2) and other bioactive molecules such as membrane-bound mucins (e.g. MUC1, MUC3, MUC17), trefoil factor peptides (TFF), resistin-like molecule beta (RELM**β**), and Fc-gamma binding protein

(Fcɣbp) (Kim and Ho, 2010). Importantly, the formation of trimers by disulfide bonding between cysteine-rich C-terminal von Willebrand factor (vWF) domains of MUC2, coupled with crosslinking between MUC2 vWF domains and TFF and Fcɣbp proteins results in the formation of a highly viscous extracellular mucus layer (Godl et al., 2002; Kim and Ho, 2010).

2.2.5. Paneth cells

Paneth cells are secretory cells present in the small intestinal epithelium, interspersed amongst stem cells at the base of crypts, as previously mentioned. PCs possess a long life (>30 days) compared to the other intestinal cell types and play a key role in host defence against pathogens, modulation of host commensal community, immune regulation and intercellular communication thanks to the release of a series of molecules (Bjerknes and Cheng, 2006; Zachos et al., 2016).

The main secreted products include antimicrobial peptides (AMPs) such as defensins and lysozyme, as well as pro-inflammatory mediators and signal transduction proteins, which collectively help regulate microbial composition in the gut (Ouellette, 2011; Vaishnava et al., 2008). Additionally, PCs play a key role in maintaining the crypt associated stem cell population and regulate constant rejuvenation of the small intestinal epithelium by secreting Wingless-related integration site 3 (WNT3), the Notch ligand Delta-like ligand 4 (DLL4), and epidermal growth factor (EGF) (Bevins and Salzman, 2011; Clevers and Bevins, 2013; van Es and Clevers, 2014; Wittkopf et al., 2014).

2.2.6. Tuft cells

Tuft cells represent about 0.5% of the intestinal epithelial cells (Banerjee et al., 2018) and they are characterised by the presence of apical microvilli and high expression of doublecortin-like kinase 1 (DCLK1) (Gerbe et al., 2009). Their role differs based on the location in the gut: in the small intestine, they play a key role in type II immunity against eukaryotic infections; in the colon, their role is poorly understood but seems to be different in specification and function (Banerjee et al., 2018).

2.2.7. Microfold cells

Microfold cells are mainly present in the follicle associated epithelium, where they make up 5-10% of cells (Nicoletti, 2000; Ohno, 2016). M cells play a key role in delivering microbial antigens to gut associated lymphoid tissue, thus contributing to mucosal and systemic immune responses (Ohno, 2016).

Table 1.1. Subtypes of intestinal epithelial cells and their subsets. Taken from (Allaire et al., 2018).

IEC subtype	Localization	Role	Subsets
Enterocyte	Small intestine (enterocyte) Colon (colonocyte)	Physical barrier Nutrient/water absorption Epithelial shedding Secrete antimicrobials	Differentiate as they migrate up the crypt axis Cells at apical tips metabolise microbial short chain fatty acids → consume oxygen in colon Cells at the base of crypts ferment glucose to lactate and do not consume oxygen
Goblet cell	Small intestine Colon	Mucin secretion Goblet cell-associated passage Secret antimicrobials	Sentinel goblet cells Detect and endocytosis bacterial products Are directly responsible for pathogen-induced compound mucus exocytosis
Paneth cell	Small intestine	Secrete antimicrobials Support the stem cell niche	
Tuft cell	Small intestine Colon	Helminth detection ILC2 expansion through production/secretion of IL-25	Tuft 1: TSLP; Tuft2: CD45 Tuft cells develop differently depending on if they are located in the small intestine or colon
Enteroendocrine cell	Small intestine Colon	Secrete hormones	Enterochromaffin cells, G cells, K cells, I cells, S cells, and other
M cell	Small intestine (follicle-associated epithelium)	Antigen uptake	Inflammation-induced M cells Cholera toxin treatment causes M cells to form at villus tips

2.3. Signals driving differentiation of the intestinal epithelium

In the intestinal epithelium, differentiated IECs originate from intestinal SCs residing at the base of intestinal crypts. Local signals in the intestinal crypts are key to maintaining SCs in an undifferentiated state and to minimise cellular and DNA damage caused by environmental stress (Gehart and Clevers, 2019). As previously mentioned, PCs are key to controlling SCs proliferation (Sato et al., 2011b; Zhang and Liu, 2016). In this regard, WNT signalling, with β-catenin and T-cell factor (TCF) transcription factors (TFs) as the main primary mediators (Korinek et al., 1998), and Achaete scute-like 2 (ASCL2) acting downstream of WNT, are the main pathways involved in this regulation (Schuijers et al., 2015; van der Flier et al., 2009).

Intestinal SCs drive the rapid renewal of the intestinal epithelium, and generate progenitor cells that in turn differentiate into all the different IECs (Snippert et al., 2010). Currently, it is believed that every IEC belonging to a specific intestinal villus-crypt originates from a single SC (Snippert et al., 2010). When SCs divide, one daughter cell stays in the crypt, while the other migrates upwards through the transit amplifying region where cell division occurs. Here, different pathways and TFs will control differentiation of these cells into the main epithelial lineages (Gehart and Clevers, 2019). Mature IECs will end their journey at the extrusion zone of the villus tip, where they will undergo apoptosis and shed from the epithelial layer through a process called anoikis (Gilmore, 2005)**.**

Three pathways are believed to control differentiation of SCs into the different IECs: Notch, WNT and BMP signalling pathways (Noah et al., 2011; Worthington et al., 2018). Notch signalling, mainly mediated by the Hes family BHLH transcription factor 1 (HES1), drives differentiation of absorptive cell types. Additionally, HES1 inhibits the activity of atonal BHLH transcription factor 1 (ATOH1), which in turn promotes differentiation into secretory cell types (Shroyer et al., 2007; Yang et al., 2001). Because high Notch absorptive progenitor cells can proliferate more than low Notch secretory cells, this results in the epithelial layer being dominated by absorptive enterocytes (Stamataki et al., 2011).

WNT signalling can also interact with Notch signalling, influencing the secretory/absorptive lineage decision. Furthermore, other key TFs important for specific secret-ory cell types include SAM pointed domain ETS factor (SPDEF) for goblet and Paneth cells (Gregorieff et al., 2009), neurogenin3 (NEUROG3) for enteroendocrine cells (López-Díaz et al., 2007) and POU Class 2 Homeobox 3 (POU2F3) for tuft cells (Gerbe et al., 2016).

BMP signalling has been shown to play a key role in epithelial differentiation by limiting epithelial expansion through inhibiting self-renewal of stem cells (Qi et al., 2017). Additionally, through BMP receptor type 1A (BMPR1A), it negatively regulates proliferation and differentiation of secretory lineage cells in the transit amplifying region (Auclair et al., 2007). Finally, through the downstream transcription factor small mother against decapentaplegic homolog 4 (SMAD4), it participates in a feedforward loop with the transcription factor hepatocyte nuclear factor 4α (HNF4A) to promote enterocyte fate (Chen et al., 2019).

A detailed explanation of the signalling gradient and additional pathways and transcription factors involved in epithelial differentiation can be found in **Figure 1.2**.

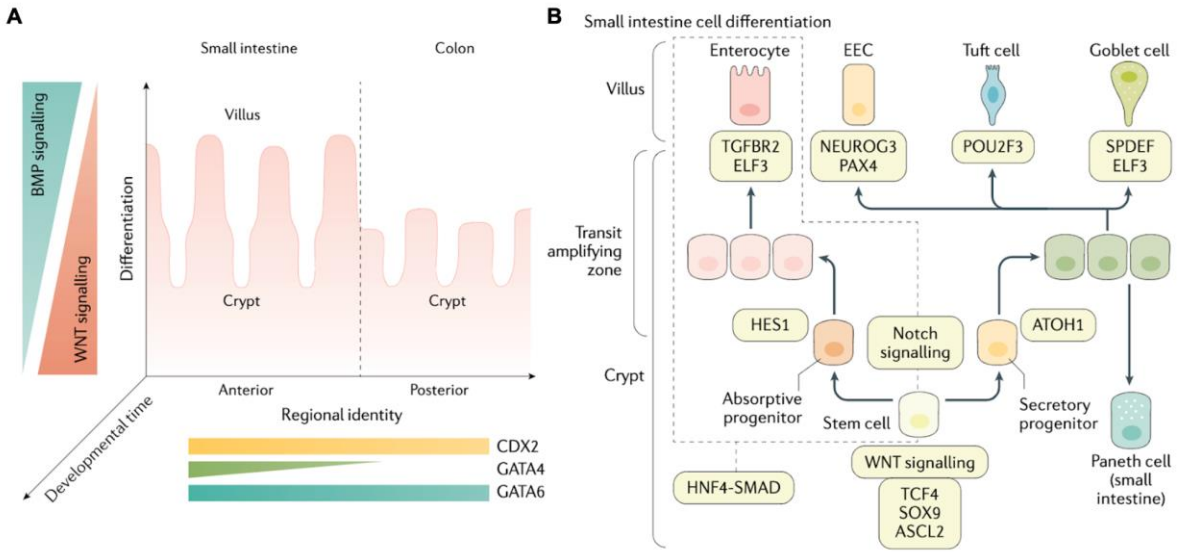

Figure 1.2. **Intestinal epithelial cell differentiation into multiple cell types. A)** The intestinal epithelium is characterised by three separate gradients: anterior–posterior, crypt–villus and developmental time. **B)** Cell differentiation from stem cells into differentiated cell types in the intestinal epithelium is regulated by different transcription factors and signalling pathways. ATOH1, atonal BHLH transcription factor 1; BMP, bone morphogenetic protein; CDX2, caudal type homeobox 2; EEC, enteroendocrine cell; HNF4, hepatocyte nuclear factor 4. Reproduced from (Heppert et al., 2021).

2.4. Mechanisms controlling gut homeostasis and barrier function

One of the main functions of IECs is to maintain a physical and biochemical barrier between the gut lumen and the lamina propria (Peterson and Artis, 2014), protecting against harmful bacteria, antigens and toxins while permitting passage of nutrients and immune sensing functions (Vancamelbeke and Vermeire, 2017). Loss of epithelial barrier function can be observed in a number of diseases including Inflammatory Bowel Disease (IBD) (Mehandru and Colombel, 2021), coeliac disease and type I diabetes (Groschwitz and Hogan, 2009).

Intestinal homeostasis and gut barrier function is controlled by several different players and mechanisms. The intestinal epithelium plays a key role thanks to the formation of the mucus layer, the correct proliferation and differentiation of IECs with expression of junctional complexes, and AMPs production. Additionally, the gut microbiota also contributes to the regulation of intestinal structure, barrier function and integrity (Earle et al., 2015; Geva-Zatorsky et al., 2015; Yu et al., 2012a), through interactions with both epithelial and immune cells (Zelante et al., 2013). This is exemplified by the observation that the intestinal mucosa of germ free (GF) mice, that has no microbiota, is very thin, and characterised by a reduced IECs proliferation and impaired production of mucins and other IEC-derived mediators (Hooper, 2004). Finally, resident immune cells (macrophages, neutrophils, lymphocytes) also contribute to the barrier function through endocytosis, antigen presentation, and secretion of

cytokines in response to microbes or inflammation (Bui et al., 2018; Ho et al., 2020; Luissint et al., 2019).

2.4.1. Intestinal epithelium

2.4.1.1. Mucus layer

The mucus layer lines the gut epithelium, thus contributing to increasing barrier function. As previously mentioned, the mucus layer is formed of gel-forming glycoproteins called mucins which are secreted by GCs, where MUC2 represents the main component in both the small and large intestines (Schroeder, 2019). Regional differences exist between the small and large intestine, with the former characterised by a single thin mucus layer, and the latter by bi-layered and thick mucus structure, with an impermeable inner layer and a permeable outer layer (Schroeder, 2019). The mucus layer plays a key role in facilitating uptake of dietary molecules, representing a physical barrier for opportunistic pathogens, a site of long-term bacterial colonisation and a carbon and energy source for intestinal microbiota (Sicard et al., 2017; Vancamelbeke and Vermeire, 2017). Reduction in the mucus layer either by decreased mucin production or reduced GC number can be observed in various conditions such as IBD (Johansson et al., 2014; Swidsinski et al., 2007). Mucus production can be modulated by the gut microbiota (commensals, pathogens) and their metabolites (Caballero-Franco et al., 2007; Sperandio et al., 2013; Wrzosek et al., 2013). Autophagy plays an important role in regulating GC functions, as even a partial loss of autophagy was shown to result in GC hyperplasia, perturbations in the secretory pathway and defects of the mucus layer (Lassen et al., 2014; Patel et al., 2013; Wlodarska et al., 2014)

2.4.1.2. Junctional complexes

Epithelial barrier function depends on the correct formation of the epithelial layer, formed by a coherent monolayer of cells connected by junctional complexes, including (apical) tight junctions (TJs), (central) adherens junctions and (basal) desmosomes. Furthermore, the correct modulation of cellular shedding – a process of apoptotic extrusion of intestinal epithelial cells at the tip of the villi, is also very important to maintain an intact epithelial layer (Groschwitz and Hogan, 2009; Williams et al., 2015). In this way, the gut epithelium can protect the host against pathogenic bacteria, antigens and toxins, whilst allowing nutrients translocation and immune sensing (Vancamelbeke and Vermeire, 2017). Dysregulated cellular shedding or expression/synthesis of junctional complexes, is linked to an altered barrier function, which can be observed in pathological gut conditions including IBD (Groschwitz and Hogan, 2009; Williams et al., 2015). Gut bacteria play a key role in the modulation of barrier function, by

regulating the intestinal epithelial cell turnover, and promoting epithelial regeneration and expression and reorganisation of tight junctions (Yu et al., 2012a).

2.4.1.3. Antimicrobial peptides

Antimicrobial peptides play a major role in maintaining gut barrier function by protecting against pathogens and modulating the gut microbiome composition (Muniz et al., 2012). Although primarily acting as antimicrobials, they can also neutralise bacterial exotoxins by acting as chemoattractants for immune cells and modulating their differentiation and maturation (Muniz et al., 2012). AMPs are mainly secreted by PCs in the small intestine, but they can also be released by enterocytes and immune cells such as neutrophils (Bevins and Salzman, 2011; Muniz et al., 2012).

AMPs can be subdivided in three classes, which include defensins, cathelicidins and C-type lectins. Defensins are small cationic peptides that can disrupt bacteria cell walls or membranes. Six α-defensins can be found in the human gut, which are expressed by neutrophils (human neutrophil peptides, HNPs 1–4) and PCs (human α-defensins, HD-5 and HD-6). In the mouse gut, 19 α-defensins can be found, known as cryptdins, mainly expressed by Paneth cells, as well as numerous β-defensins expressed by different types of IECs (Muniz et al., 2012). Cathelicidins (human LL-37 and mouse CRAMP) are also small cationic peptides with broad antibacterial activity (Muniz et al., 2012). Finally, C-type lectins, consisting of a carbohydrate recognition domain and an N-terminal peptide, exert their antimicrobial activity by binding to peptidoglycan in Gram positive bacteria. Regenerating islet-derived protein 3 alpha (RegIIIα) and islet-derived protein 3 gamma (RegIIIγ) are the main C-type lectins found in humans and mice, respectively (Muniz et al., 2012). Other AMPs also exist, including lysozyme C (lysozyme, LYZ1) - a glycoside hydrolase that cleaves peptidoglycan in Gram-positive bacteria, mainly secreted by Paneth cells and macrophages (mouse only); secretory phospholipase A2 (sPLA2), which degrades bacterial phospholipids on the cell wall, and is expressed by Paneth cells (Muniz et al., 2012). Dysregulation of AMPs production has been associated with increased susceptibility to infection and pathologies such as IBD (Adolph et al., 2013; Zhao et al., 2010).

2.4.2. The gut microbiome

The gut microbiome plays a key role in the modulation of intestinal homeostasis and gut barrier function, interacting with IECs through a series of mechanisms.

One mechanism is through the recognition of specific microbe-associated molecular patterns (MAMPs) such as lipopolysaccharide (LPS), nucleic acids, and flagellin by pattern recognition

receptors (PRRs), initiating a number of responses including phagocytosis, inflammation and maturation of antigen-presenting cells (Hato and Dagher, 2015). Four families of PRRs exist, which include membrane-bound toll-like receptors (TLRs) and C-type lectin receptors (CLRs) as well as cytoplasmic nucleotide oligomerization domain-like receptors (NLRs) and retinoic acid inducible gene I like receptors (RLR) (Gourbeyre et al., 2015). The continuous recognition of commensal and pathogenic bacteria by PRRs, and the subsequent fine-tuning and balance of these responses contributes to the maintenance of intestinal homeostasis and barrier function (Sánchez et al., 2017). For instance, the recognition of bacterial muramyl dipeptide by nucleotide-binding oligomerization domain-containing protein 2 (NOD2), a type of NLR, controls Paneth cells activation and **β**-defensin 2 production (Voss et al., 2006). Furthermore, recognition of bacterial components, such as LPS, lipoteichoic acid (LTA) or flagellin by TLRs results in increased MUC2 expression, the main component of the intestinal mucus layer (Dharmani et al., 2009; Hayashi et al., 2001).

In addition to PRR, bacteria can also interact with host IECs via protein-protein interactions (PPIs) facilitated by molecular mimicry strategies, whereby bacterial proteins have developed to contain eukaryotic-like domains to mimic host proteins (Doxey and McConkey, 2013). Although this mechanism is mainly used by pathogens to hijack host processes to enhance invasion and reduce intracellular clearance (Sudhakar et al., 2019), commensal bacteria also exhibit similar mechanisms, although these are less studied (Cohen et al., 2017). For instance, specific G-protein coupled receptors (GPCRs), in addition to sensing SCFAs (Husted et al., 2017; Tan et al., 2017), can bind to other microbiota-derived ligands such as N-acyl amides (Cohen et al., 2017). GPCRs are the largest family of membrane proteins encoded in the human genome, and regulate various aspects of host physiology including immunity (Wacker et al., 2017). Their regulation by microbial ligands shows the key role played by the microbiome in modulating intestinal homeostasis. Indeed, GPCRs have also been implicated in various diseases exhibiting shifts in microbial communities such as IBD (Zeng et al., 2020).

Finally, microbial derived metabolites such as SCFAs can also mediate the host-microbe crosstalk, contributing to intestinal homeostasis and barrier function through the modulation of mucus production, cell proliferation and tight junction expression (den Besten et al., 2013; Ríos-Covián et al., 2016). More details about these mechanisms are highlighted below in the section ‘Bifidobacteria-epithelial cell crosstalk’.

2.4.3. Resident immune cells

Resident immune cells also contribute to the barrier function by communicating with IECs in response to signals derived from microbes or inflammation through mechanisms such as

endocytosis, antigen presentation, and cytokines secretion (Bui et al., 2018; Ho et al., 2020; Luissint et al., 2019). Cytokines - small, secreted proteins acting in a paracrine manner to induce various effects on their targets - can affect IECs in various ways by binding to receptors present on their membrane. Some of these effects include the promotion of IECs proliferation by interleukin (IL)-2 (Mishra et al., 2012), PC-related RegIIIγ expression (Kinnebrew et al., 2012; Pickert et al., 2009), mucin production and TJ expression (Soderholm and Pedicord, 2019) by IL-22, and epithelial repair by IL-10 (Soderholm and Pedicord, 2019). Hence, a tight regulation of cytokines production is key to maintaining intestinal homeostasis and barrier function, and their dysregulation is typical of inflammatory conditions of the gut including IBD (Friedrich et al., 2019).

3. Inflammatory Bowel Disease

Inflammatory Bowel Disease encompasses Crohn's disease (CD) and ulcerative colitis (UC), both of which are characterised by chronic intestinal inflammation. While in UC inflammation is continuous from the rectum to the proximal colon, CD inflammation is patchy and discontinuous, and frequently occurs in the distal ileum or colon. Both forms of IBD are thought to be driven by environmental factors in genetically susceptible individuals, resulting in an exacerbated immune response towards components of the gut microbiota (Geremia et al., 2014). However, the underlying mechanisms are not yet completely understood. In particular, whether the loss of tolerance towards the microbiota is a cause or consequence of the disease and what is the exact effect of the interactions between intestinal epithelial cells and the dysbiotic microbiota remain unclear. The aetiology of IBD is multifactorial, but growing evidence suggests that the crosstalk between the luminal microbiota and the intestinal epithelium play a key role in the onset of IBD (Neurath, 2020).

3.1. Role of the epithelium in IBD

The intestinal epithelium plays an important role in IBD (Coskun, 2014; Strugala et al., 2008; Zeissig et al., 2007). Indeed, several IBD-associated genetic defects are involved in key IECs function, including bacterial sensing (*NOD2*), inflammation (*IL-23R*), autophagy (*ATG16L1*), endoplasmic reticulum stress, and epithelial barrier function (*HNF4α, CDH1, MEP1A, CARD15, ATG16L1*) (Koch and Nusrat, 2012; McCole, 2014). For instance, chronic inflammation in UC results in long-term changes in GC function as associated mucus production (Singh et al., 2022; Swidsinski et al., 2007), resulting in increased barrier permeability (Kaser et al., 2008; Mankertz and Schulzke, 2007; Rioux et al., 2007), and increased bacterial and metabolite translocation (Johansson et al., 2014; Sun et al., 2016). Overall, this results in overactivation of immune cells activation and inflammation (Neurath,

2019). Pro-inflammatory factors released in the intestinal mucosa during active disease also progressively damage the epithelial layer (Johansson et al., 2014; Sun et al., 2016).

3.2. The role of the gut microbiome in IBD

The gut microbiome plays a key role in IBD, and alterations in microbiota composition and homeostasis (known as “dysbiosis”) have been observed in both forms of IBD (Halfvarson et al., 2017; Joossens et al., 2011; Kostic et al., 2014). Patients with IBD show decreased microbial diversity (Macfarlane et al., 2004) and a shift in the balance between commensal and pathobionts (Ni et al., 2017). For example, a reduction in the Firmicutes *phylum* and an increase in Proteobacteria (Mirsepasi-Lauridsen et al., 2018) as well as a decrease in *Bifidobacterium* spp. during active disease (Macfarlane et al., 2004) has been observed. This change in microbiota is also associated with a shift in fermentation products, such as SCFAs (Zeng et al., 2017). For instance, a decrease in butyrate-producing species has been observed in UC (Machiels et al., 2014).

The causal role for the gut microbiota in IBD development has been demonstrated (Gkouskou et al., 2014). Using mouse colonic inflammation models, it was shown that only conventionally-raised mice developed inflammation, while GF mice did not (Pils et al., 2011). Furthermore, transferring the gut microbiota from a colitis mouse model to a wild-type (WT) mouse resulted in the induction of inflammation (Zhou et al., 2019). In addition, recurrence of CD in patients who had undergone an (ileocolonic) resection could be prevented in the absence of faecal stream (and thus microbiota), and triggered in the presence of intestinal fluids (D’Haens et al., 1998; Rutgeerts et al., 1991).

3.3. Microbial-based treatments for IBD

Because of the strong relationship between dysbiosis and IBD, probiotics formulations (O’Toole et al., 2017; Sheil et al., 2007; Venturi et al., 1999), microbial metabolites (Russo et al., 2019; van der Beek et al., 2017) and Faecal Microbiota Transplantation (FMT) (Imdad et al., 2018) have been explored for their ability to restore the microbiota composition and inflammatory status associated with IBD (Hart et al., 2002).

Current probiotics formulations mainly rely on the use of cultivable and aerotolerant species that can be produced at an industrial scale, including *Bifidobacterium* spp., *Lactobacillus* spp., and yeasts (O’Toole et al., 2017). Supplementation with *Bifidobacterium* for IBD treatment will be described in more detail under the section “Bifidobacterial supplementation”. New therapies such as next-generation probiotics (NGPs), encompassing key commensals of the human gut and their metabolites as the main product of interest, are also increasingly being proposed as

promising therapy, although regulatory barriers hinder their use compared to regular probiotics (O'Toole et al., 2017). So far, the most promising candidate is represented by the anti-inflammatory bacterium *F. prausnitzii,* which is currently undergoing preclinical evaluation (Martín et al., 2014; Martín et al., 2017). Furthermore, microbial-derived metabolites such as SCFAs and tryptophan have also been investigated for IBD treatment. For tryptophan metabolites, a placebo-controlled, crossover trial is currently undergoing to assess the effect of oral 5-hydroxytryptophan administration on fatigue in IBD patients (NCT03574948) (US National Library of Medicine, 2019). For SCFAs, although beneficial effects against inflammation have been observed *in vitro*, no consensus has been achieved for their effects in the clinic (Galvez et al., 2005). Finally, FMT has shown promising results towards the induction of remission in UC patients (Costello et al., 2019; Moayyedi et al., 2015; Paramsothy et al., 2017). Furthermore, in paediatric UC patients, responders were characterised by a change in microbial and metabolic profile towards the donor, as well as a reduction in acetate and increase in butyrate levels post-FMT (Nusbaum et al., 2018).

Despite some promising findings, the overall understanding of the effectiveness and mechanisms behind probiotics as treatment strategies for IBD is still lacking (Fang et al., 2018; Sanders et al., 2019). It remains unclear which specific bacterial strains (single or complex mixtures) are required to induce and maintain remission in IBD patients. Moreover, given the heterogeneous nature of IBD, it is likely that a microbial intervention will need to be tailored to each individual, to reduce dysbiosis and promote immune tolerance and homeostasis in IBD. Throughout this thesis, I tried to elucidate some potential bifidobacterial strains that have beneficial effects on the epithelium, and study the mechanisms involved in these effects.

4. Bifidobacteria

Bifidobacteria are Gram-positive, heterofermentative, anaerobic bacteria with a distinctive bifid (i.e. Y) shape, after which they are named. Isolated for the first time in 1899 from the faeces of the breast-fed infants by Tissier, they are found in the gastrointestinal (GI) tract of various mammals (Ventura et al., 2007). Around 80 sub-species of bifidobacteria have been characterised in different ecological niches (Turroni et al., 2011). In humans, bifidobacteria represent the first colonisers of the human gut, and are the dominant bacterial genus in the breast-fed infant microbiota, accounting for 40% to 80% of the total gut microbiota (Makino et al., 2015; Nuriel-Ohayon et al., 2016).

In particular, *Bifidobacterium longum* subsp. *infantis, Bifidobacterium longum* subsp. *longum, Bifidobacterium breve* and *Bifidobacterium bifidum* are the primary species present within the

infant gut, with increasing diversification of the genus seen with age (Di Gioia et al., 2014). While newly born infants have the highest proportions of bifidobacteria (45-95% for breastfed babies) (Arboleya et al., 2016; Bezirtzoglou et al., 2011; Fallani et al., 2010), their abundance decreases rapidly following weaning (30-40%) (Arboleya et al., 2016; Turroni et al., 2012), and continues gradually to do so during childhood and adolescence where it stabilises (0-18%), and furtherly decline only in the elderly phase (Arboleya et al., 2016; Vaughan et al., 2005) (**Figure 1.3**).

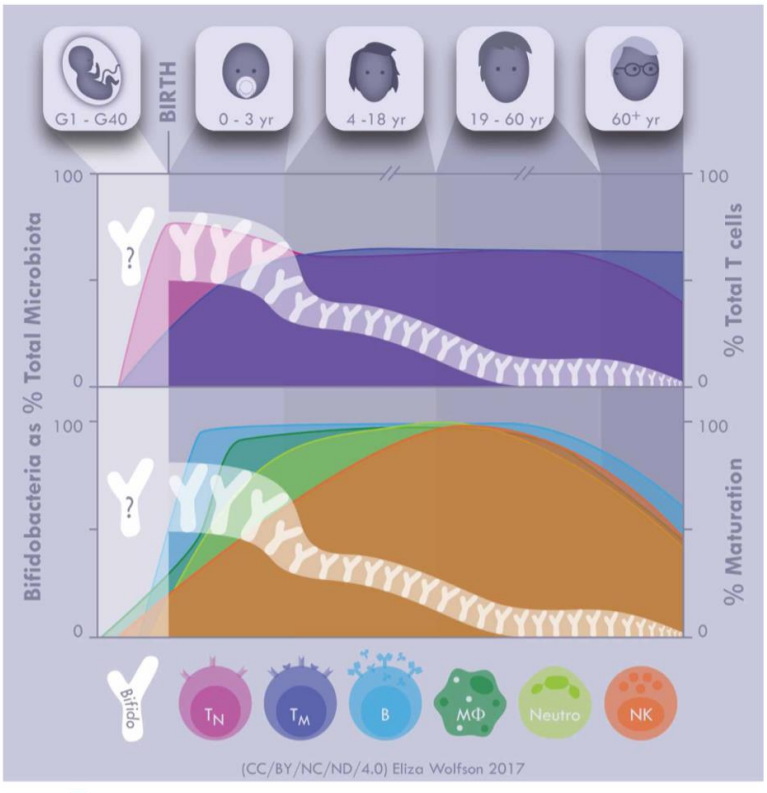

Figure 1.3. Relative abundance of gut bifidobacteria and immune cell maturation during the human life cycle. Figure reproduced from (O'Neill et al., 2017).

4.1. Bifidobacterium levels in health and disease

Bifidobacterium levels across life course along with key stages of immune maturation and are associated with improved host well-being. Several studies have identified an association between decreased bifidobacterial levels accompanied by a reduced microbial diversity with increased disease symptoms (O'Callaghan and van Sinderen, 2016; O'Neill et al., 2017; Tojo et al., 2014). In early life, lower *Bifidobacterium* levels are observed in low-birth-weight premature babies, which can often suffer from pathologies such as necrotising enterocolitis

(NEC) leading to death. In children, lower levels of the genus *Bifidobacterium* were found in those with active coeliac disease compared to those with non-active disease or healthy controls (Collado et al., 2008). Additionally, a lower proportion of *B. longum* was found in children with allergy compared to healthy controls (Akay et al., 2014; Ouwehand et al., 2001). Despite the low levels of Bifidobacterium in adulthood, minor changes in their relative abundance have been associated with major changes in health state. For instance, in adults, decreased *Bifidobacterium* levels were linked to diseases such as Irritable Bowel Syndrome (IBS) and UC (Khalif et al., 2005; Kim et al., 2015; Macfarlane et al., 2004; Parkes et al., 2012). Additionally, levels of mucosal *Bifidobacterium* have been inversely associated with the number of days patients with IBS experienced pain or discomfort (Parkes et al., 2012).

4.2. Bifidobacterial supplementation

Because of their decreased numbers in disease conditions, several members of the *Bifidobacterium* genus have been studied for their health-promoting effects. In extreme preterm infants, supplementation with a probiotic mix containing four *Bifidobacterium* strains (*B. breve* HA-129, *B. bifidum* HA-132, *B. infantis* HA-116 and *B. longum* HA-135) and *Lacticaseibacillus rhamnosus* HA-111 accelerated gut microbiome maturation and reduced intestinal inflammation (Samara et al., 2022). Similarly, supplementation of NEC babies with bifidobacteria has shown to significantly reduce disease symptoms and premature death, supporting the role of Bifidobacterium levels in this disease (Patole et al., 2016). In healthy women, supplementation with *Bifidobacterium animalis* DN-173 010 decreased transit time (Marteau et al., 2002). Mechanistic studies have further identified the ability of different bifidobacterial species in limiting pathogen colonisation and invasion, modulating gut homeostasis, regulating the innate and adaptive immune responses, and possessing anti-tumor immunity activities (Alessandri et al., 2019; Hart et al., 2004; Silva et al., 2004; Sivan et al., 2015).

Bifidobacteria has been employed as a promising therapy for patients with disorders of the GI tract, including IBD (Jakubczyk et al., 2020; O'Neill et al., 2017). One trial for CD and six for UC have been published so far (Jakubczyk et al., 2020). However, some studies used *Bifidobacterium* in combination with other probiotic strains or prebiotic mixes, making it difficult to attribute specific outcomes solely to bifidobacteria (Furrie, 2005; He et al., 2008; O'Mahony et al., 2005). When a single species was used, only a limited number (*B. longum subsp. longum, B. breve, and B. longum subsp. infantis*) has been tested. Additionally, the treatment duration, number of patients, and disease markers for each trial vary greatly, making the comparison between studies challenging. Nevertheless, these studies suggest bifidobacteria could represent a promising therapy for IBD. In two consecutive studies, a 28-day treatment

with *B. longum* subsp. *longum* combined with a prebiotic mix resulted in a reduction of tumour necrosis factor (TNF)-α and clinical symptoms in UC patients, and reduction of CD activity index and histology score in active CD patients compared with the controls (Fujimori et al., 2009; Steed et al., 2010)**.** In another study, 6 weeks treatment *B. longum* subsp. infantis 35 624 resulted in a reduction in pro-inflammatory C-reactive protein and IL-6 (non statistically significant) in UC patients compared with the baseline (Groeger et al., 2013)**.** Finally, a 8-week supplementation of *B. longum* subsp. *longum* 536 resulted in a significant decrease in disease activity in mild-to-moderate UC, which was not observed in the control group (Tamaki et al., 2016).

Although it is established that bifidobacteria could confer positive health benefits to the human host, there is a lack of knowledge concerning the specific modulating factors that explain these beneficial effects (Cronin et al., 2011). Progress in this field is generally hindered by the complexity (microbial genomics, impact of diet, host responses, etc.) and inaccessibility of the GI tract (O'Neill et al., 2017; Russell et al., 2011). Nevertheless, unravelling these complex interactions is key to understanding the role played by bifidobacteria in promoting health.

4.3. Bifidobacteria-epithelial cell crosstalk

Bifidobacteria was shown to directly interact with intestinal epithelial cells through their apical side, and a number of studies have shown their ability to directly modulate IECs functions through a variety of effector molecules including metabolites, proteins/peptides, exopolysaccharides (EPS), and indirectly through cross-feeding mechanisms (Castro-Bravo et al., 2019; Fanning et al., 2012b; Lee et al., 2018; O'Connell Motherway et al., 2019).

4.3.1. Bifidobacterial effector molecules

4.3.1.1. Pili

Pili are long proteinaceous appendages protruding from the extracellular cell surface of bacteria which are involved in promoting adhesion to the intestinal epithelium or facilitating aggregation with other bacterial cells (Foroni et al., 2011; Kline et al., 2010; Scott and Zähner, 2006). In bifidobacteria, two different types of pili have been described: (i) the sortase dependent pili and (ii) the type IVb pili, also known as tight adherence (Tad) pili (Milani et al., 2017; O'Connell Motherway et al., 2011).

In a recent study, *B. breve* UCC2003 Tad pili, in particular the TadE protein, was shown to promote *in vivo* colonic epithelial proliferation 5 days post-administration in a mouse model, showing how Tad pili may contribute the maturation of epithelial cells of newborns, stimulating growth of their thin intestinal mucosa and contributing to host mucosal homeostasis (O'Connell

Motherway et al., 2019). Moreover, addition of a genetically modified *Lactococcus lactis* strain producing *B. bifidum* pili, lowered level of anti-inflammatory IL-10 and increase that of pro-inflammatory cytokine TNF-α mouse cecal mucosa (Turroni et al., 2013).

4.3.1.2. Extracellular polysaccharides

Exopolysaccharides are carbohydrate polymers that are synthesised and presented in the outer surface of bifidobacteria (Hidalgo-Cantabrana et al., 2014). *In silico* analysis showed a lack of consensus on functional-structural organisation in the *eps*-encoding clusters of bifidobacteria, highlighting inter/intra species variability in terms of length and number of genes (Ferrario et al., 2016; Hidalgo-Cantabrana et al., 2014). This hidden diversity in EPS biosynthesis, together with variation in EPS production levels, may represent a great potential for strain-specific immune responses (Ruiz et al., 2017).

Bifidobacterial EPS was shown to act as an anti-inflammatory molecule. In mouse models, the EPS-producing strain *B. breve* UCC2003 was associated with increased protection against *Citrobacter rodentium* infection (Fanning et al., 2012a), and intestinal epithelial cell shedding *via* Myeloid differentiation primary response 88 (MyD88) dependent signalling (Hughes et al., 2017). Additionally, the presence of *B. longum* BCRC 14634 derived EPS increased IL-10 production and decreased TNF-α production following *in vitro* exposure of murine macrophages to LPS (Wu et al., 2010). Furthermore, *B. longum* subsp. *longum* 35624 surface-associated EPS prevented expansion of the proinflammatory T helper (Th) 17 response compared to the corresponding EPS-negative mutant (Schiavi et al., 2016)

4.3.1.3. Serpins

Serine protease inhibitors, or serpins, constitute a family of proteins able to bind and irreversibly inactivate proteases. The serpin-coding gene is not ubiquitously present in all *Bifidobacterium* species, but restricted to *B. breve, B. longum* subsp. *longum, B. longum* subsp. *infantis, B. longum* subsp. *suis, Bifidobacterium cuniculi, Bifidobacterium scardovii,* and *Bifidobacterium dentium* (Turroni et al., 2011).

An *in vitro* study suggested that bifidobacterial serpin-encoding genes are activated by specific serine proteases (Turroni et al., 2010a). For example, *B. longum* NCC2705 serpin was shown to target two pro-inflammatory proteases, including human neutrophil and pancreatic elastases (Ivanov et al., 2006). Serine proteases are generally released during inflammation caused by bacterial infection or intestinal tissue damage as observed in IBD. Hence, production of serpins by bifidobacteria may play a role in anti-inflammatory activities and maintenance of gut homeostasis by allowing bifidobacteria to survive in a competitive environment (Alvarez-Martin et al., 2012; Turroni et al., 2010a).

4.3.1.4. Short chain fatty acids (SCFAs)

The intestinal microbiota, including bifidobacteria, generates a series of compounds from the metabolism of undigested carbohydrates or their own metabolic activity, with a direct effect on IECs. The most important include those derived from the degradation of host-derived mucins (Glover et al., 2022), and SCFAs such as acetate, butyrate and propionate (den Besten et al., 2013; Ratajczak et al., 2019).

Bifidobacterium spp. can produce acetate and lactate by degrading mucin or diet-derived, non-digestible carbohydrates, which can be further fermented by other microbes to produce butyrate and propionate (Flint et al., 2015). For instance, *B. bifidum,* one of the main bifidobacterial species capable of digesting mucin (Turroni et al., 2010b), produces several mucin-associated mono- and oligo-saccharides, as well as acetate and lactate, which in turns favours the growth of butyrate producer *Eubacterium hallii* (Bunesova et al., 2018). SCFAs production by bifidobacteria has very important health-related implications. Acetate was shown to promote GCs differentiation, secretion of mucin and terminal decoration of mucin glycans with sialic acid in a gnotobiotic rodent model (Wrzosek et al., 2013). Additionally, being the preferred energy source of IECs, butyrate promotes epithelial integrity by stimulating cell proliferation, tight junctions, and mucin production by GCs (den Besten et al., 2013; Ríos-Covián et al., 2016). Moreover, butyrate has been shown to promote an anti-inflammatory response, by inducing the production of transforming growth factor beta (TGF-β), IL-18, and IL-10 by both antigen presenting cells and IECs, and romoting the differentiation of naïve T cells to Regulatory T cells (Tregs) (Furusawa et al., 2013; Zhang et al., 2016). Finally, propionate was shown to act as a precursor for gluconeogenesis in the liver and to affect intestinal homeostasis through anti-inflammatory and anticarcinogenic actions (Bunesova et al., 2018; Reichardt et al., 2014)**.**

4.3.1.5. Other molecules

In addition to pili, EPS and serpins, other *Bifidobacterium*-derived molecules have been associated with specific effects on the host. For instance, the peptidoglycan hydrolase TgaA, a surface-associated protein in *B. bifidum*, was shown to induce IL-2 production in monocyte-derived dendritic cell (MoDC), which is a key cytokine regulating the expansion of Tregs (Guglielmetti et al., 2014a; Guglielmetti et al., 2014b; Zelante et al., 2012). Additionally, another peptide contained within the sequence of the protein translocase subunit SecA of *B. longum* DJ010A was shown to induce a marked Th17 response when incubated with human peripheral blood mononuclear cells (PBMCs) (Hidalgo-Cantabrana et al., 2017).

4.3.2. Effects of bifidobacteria on epithelial cells

4.3.2.1. Cell growth, differentiation, apoptosis

Bifidobacteria has been shown to affect fundamental cellular processes, such as cell growth, differentiation and apoptosis (**Figure 1.4A**). *B. breve* UCC2003 was found to reduce intestinal epithelial cell shedding in a mouse model, in an EPS-dependent manner, which likely involved MyD88, a downstream effector molecule of TLR signalling (Hughes et al., 2017). *B. breve* UCC2003 also modulated several genes involved in IEC cell differentiation in the neonatal murine gut, in particular SC proliferation marker genes (Kiu et al., 2020). Additionally, it increased colonic epithelial cell proliferation in monoassociated mice compared to GF mice through the pilin subunit TadE (O'Connell Motherway et al., 2019). *Bifidobacterium*-derived lactate was also found to promote stem cell proliferation and protect against gut injury *via* G-protein-coupled receptor Gpr81 and WNT/β-catenin signals of Paneth cells and intestinal stromal cells in newborn mouse intestine (Lee et al., 2018). Finally, soluble factors from *B. breve* prevented oxidant-induced IEC death through induction of autophagy-related (ATG) proteins (*Atg5* and *7)* and proteasomal blockade (Inaba et al., 2016).

4.3.2.2. Barrier function

Several studies have highlighted the role of bifidobacteria in promoting or dampening the loss of epithelial barrier function (**Figure 1.4B**), caused by pro-inflammatory treatments such as dextran sulphate sodium (DSS) or TNF-α. In a transcriptomics study in neonatal murine IECs, *B. breve* UCC2003 modulated key genes linked with epithelial barrier function, including cadherins, gap junctions, tight junctions and integrin-related genes (Kiu et al., 2020). One mechanism could be through the modulation of tight junctions: *B. longum* CCM 7952, *B. longum* subsp. longum YS108R and *B. bifidum* ATCC 29521 were shown to be prevent against the downregulation TJs (occludin, zonulin-1) (Srutkova et al., 2015) or maintain the expression of TJs (claudin-1, claudin-3 and zonula occludens-1) following DSS-treatment in mice (Din et al., 2020; Yan et al., 2019). Bifidobacterial-derived SCFAs could be mediating these effects, as one study showed that *B. bifidum* spp. prevented TNF-α induced loss of transepithelial electrical resistance (TEER) *via* acetate production (Hsieh et al., 2015).

4.3.2.3. Mucus layer

Several studies have revealed the ability of bifidobacteria to enhance the mucus layer *via the* modulation of GC function (**Figure 1.4C**). However, these results seemed to suggest that only viable bifidobacteria can exert these beneficial effects. In one study, heat inactivated *B. breve* increased mucin *Muc1* expression, but not *Muc2* expression in cell line LS174T (Becker et al., 2013). Furthermore, *B. dentium* metabolites acetate and γ-aminobutyric acid (GABA) were able to increase MUC2 levels in T84 cells (a colonic adenocarcinoma cell line), and mucin

secretion *via* autophagy mechanisms, respectively (Engevik et al., 2019). In the same study, *B. dentium* monoassociated mice showed increased expression of GC Krüppel-like factor 4 (*Klf4*), Trefoil factor 3 (*Tff3*), Relm-β, and *Muc2* in the colon compared to GF mice, but only with alive *B. dentium* and not with the heat-killed equivalent (Engevik et al., 2019). Similarly, only viable *Bifidobacterium pseudolongum Patronus* increased colonic mucus thickness using a rat model (Mangin et al., 2018), while *B. longum* NCC 2705 ameliorated damages in mucus growth following a Western diet, but not repair penetrability (Schroeder et al., 2018).

4.3.2.4. Antimicrobial peptides production

The role of bifidobacteria in modulating AMPs production was also evaluated (**Figure 1.4D**). Yet, results of these studies are still controversial. For instance, on the one hand, supplementation of *B. bifidum* in premature rad decreased the expression of PC-derived phospholipase A2 (*sPla2*) and lysozyme (*Lyz1*) compared to those fed with milk formula only (Underwood et al., 2012). Similarly, oral administration of *B. infantis* Natren Life Start super strain (NLS-SS) to celiac patients resulted in decreased PC-derived duodenal α-defensin-5 (HD-5) (Pinto-Sánchez et al., 2017). On the other hand, opposite effects were observed. For instance, mono-colonisation with *B. breve* NCC2950, upregulated *RegIIIγ* expression in GF mice (Natividad et al., 2013), and *Bifidobacterium*-derived lactate increased PCs growth and upregulated PC-derived *Lyz1* and *RegIIIβ* and *RegIIIγ* expression (Lee et al., 2018). Interestingly, bifidobacteria is not susceptible to lysozyme, suggesting that AMP production is not unlikely to be a specific immune response against bifidobacteria (Dan et al., 2018; Sakurai et al., 2017).

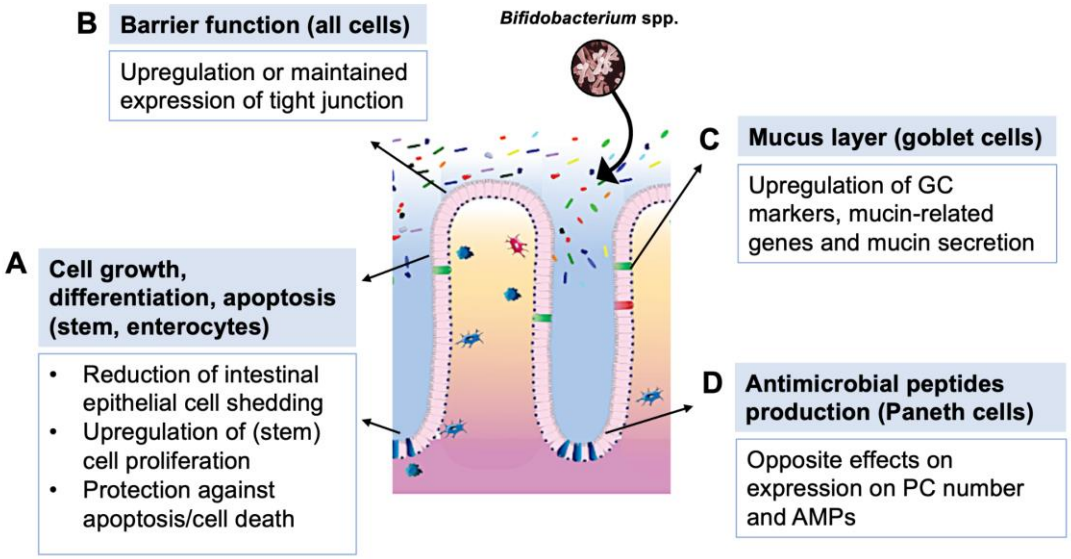

Figure 1.4. Mechanisms in which bifidobacteria have been shown to modulate the intestinal epithelium. Original figure adapted from (Poletti et al., 2021).

5. Autophagy

5.1. Role of autophagy in host-microbiome crosstalk

Autophagy - a key molecular mechanism in which intracellular components are sent to the autolysosomal compartment for degradation and recycling - plays a role in maintaining intestinal homeostasis. Indeed, it is involved in the modulation of the inflammatory response, prevention of intracellular waste accumulation (damaged organelles, misfolded proteins), protection against intracellular pathogens, membrane dynamics (transport or secretion), and regulation of cell differentiation and survival (Foerster et al., 2022; Khandia et al., 2019; Levine and Kroemer, 2019). Three main types of autophagy have been described so far (Galluzzi et al., 2017). During macroautophagy (generally referred as 'autophagy'), cellular components are sequestered within a double-membrane vesicle, called "autophagosome". Based on the inducing factor, this process can be non-selective ("bulk autophagy") or involve a highly regulated elimination of specific cellular components ("selective autophagy") (Dikic and Elazar, 2018; Gohel et al., 2020; He and Klionsky, 2009; Sica et al., 2015). During chaperone-mediated autophagy, proteins bearing a KFERQ-like motif are selectively recognized by the heat-shock protein (HSP)-A8/heat shock cognate (HSC)-70 and enter the lysosome for degradation (Kaushik and Cuervo, 2018). Finally, microautophagy eliminates cellular material directly *via* membrane invaginations formed at the surface of late endosomes or lysosomes (Mejlvang et al., 2018; Sahu et al., 2011; Uytterhoeven et al., 2015).

The central role of autophagy in maintaining homeostasis is evidenced by the association of numerous diseases and disorders with autophagy defects (Kuma et al., 2017; Levine and Kroemer, 2019). Additionally, several studies have also highlighted the modulation of other autophagy-independent pathways, including phagocytosis, exocytosis, cytokinesis, DNA repair, or innate and adaptive immune signalling (Galluzzi and Green, 2019). To achieve so, autophagy proteins interact with molecular sensors which respond to microbial stimuli (TLRs and NLRs), stress (HMGB1, Sestrins, ER-stress sensor proteins, P2XR, and cGAS-STING pathway), or changes in energy status (AMPK and mTOR pathways) (Kang et al., 2011; Kroemer et al., 2010; Oh and Lee, 2014; Rashid et al., 2015; Ro et al., 2020; Young et al., 2015; Zierhut and Funabiki, 2020). In the gut, autophagy plays a central role in regulating the function of secretory (PCs, GCs) and Lgr5+ SCs growth and differentiation (Foerster et al., 2022).

5.1.1. Mucus layer

Successful mucus secretion by GCs relies on the packaging of the mucin protein into secretory granules localised on the apical side, and constitutively secretion of these granules by fusion

with the plasma membrane. This process depends on the activity of core autophagy machinery proteins, such as ATG5, ATG7 and microtubule-associated proteins 1A/1B light chain 3B (MAP1LC3B/LC3) (Patel et al., 2013). This is supported by observations that Atg7-deficient mice are characterised by a decreased GC-dependent mucus secretion, resulting in increased bacterial burden in the colon and exacerbated sensitivity to DSS-induced colitis (Tsuboi et al., 2015). Additionally, the NLR64 inflammasome has been identified as a key regulator of GCs secretory functions (Elinav et al., 2011; Wlodarska et al., 2014)**.** In fact, Nlrp6-deficient mice exhibit defective autophagy in intestinal cells including GCs, which is accompanied by impaired mucous layer formation. The impaired mucus layer formation also results in an abnormal representation of Bacteroidetes and Saccharibacteria phyla (Elinav et al., 2011)**,** and increased penetration and invasion by *Citrobacter rodentium* (Wlodarska et al., 2014)**.**

5.1.2. Antimicrobial peptides

As mentioned above, AMPs are packaged and released in the gut lumen by PCs, enterocytes and immune cells (Bevins and Salzman, 2011; Muniz et al., 2012), and play an important role in gut homeostasis and shaping the microbiome composition (Muniz et al., 2012). Autophagy is required for AMP release in the gut lumen, as shown by defective packaging and secretion observed in mice harbouring Atg5/Atg7/Atg16l1-deficient Paneth cells, as well as in CD patients with *NOD2* and *ATG16L1* variants (Cadwell et al., 2008; Cadwell et al., 2009; VanDussen et al., 2014). Interestingly, these defects required the presence of an infectious (viral, bacterial) trigger to appear (Bel et al., 2017; Cadwell et al., 2010).

Furthermore, autophagy also contributes to other functions in PCs that could play a role in gut homeostasis. In a study carried out in our lab, a multi-omics analysis of small-intestinal organoids enriched in *Atg16l1*-mutant Paneth cells found that autophagy impairment affected key proteins involved in processes such as exocytosis, apoptosis and DNA damage repair, with most changes happening at the protein level, rather than gene expression (Jones et al., 2019). Additionally, it was found that PCs use the autophagy machinery to secrete lysozyme in the gut lumen during *Salmonella enterica* Serovar Typhimurium infection *via* an unconventional autophagy pathway called “secretory autophagy” (Bel et al., 2017). Interestingly, vitamin D binding to the vitamin D receptor (VDR) expressed by PCs could sustain autophagy activity over time (Lu et al., 2021)**.** Furthermore, other studies have suggested the role of autophagy in the expression and secretion of other AMPs, such as defensins and cathelicidins, yet the exact mechanisms have not yet been determined (Muniz et al., 2012; Tsuboi et al., 2015)**.**

5.1.3. Inflammation

Autophagy is a key contributor to the regulation of inflammatory processes, by acting both as inflammatory or an anti-inflammatory agent (Chen et al., 2018; Deretic and Levine, 2018; Tsuboi et al., 2015). Indeed, autophagy is able to alleviate the activation of inflammasomes - multimeric protein complexes involved in the maturation of pro-inflammatory cytokines (Tsuboi et al., 2015) - either by removing stimuli inducing them (e.g. intracellular infectious agents) or by degrading inflammasome components (e.g. NLRP1, NLRP3, AIM2, or pro-CASP1) (Deretic and Levine, 2018). Conversely, an overactivated autophagy level, indicated by higher levels of autophagosomes and LC3-II protein expression, has been observed in patients with rheumatoid arthritis in correlation to inflammation (Chen et al., 2018).

The importance of autophagy genes in maintaining gut homeostasis was shown in a study where DSS-treated mice harbouring the CD risk allele *ATG16L1* T300A showed alterations of the gut microbiota (e.g. increase *Bacteroidetes* abundance) and enhanced local Th1 and Th17 responses compared to DSS-treated WT mice (Tsuboi et al., 2015). Similar effects were also found in gnotobiotic mice expressing the CD risk allele *ATG16L1* T300A and inoculated with human stools from active CD patients (Tsuboi et al., 2015)**.** In another study, using IEC-specific deletion of *ATG16L1* in a chronic colitis mouse model, autophagy was required to protect against TNF-induced apoptosis, showing how epithelial autophagy controls inflammation-induced apoptosis and barrier integrity to limit chronic intestinal inflammation (Pott et al., 2018).

5.2. Autophagy impairment in IBD

Significant evidence exists to link defective autophagy and onset and development of IBD (Matsuzawa-Ishimoto et al., 2018). The presence of the *ATG16L1* T300A variant that makes this protein susceptible to CASP3-dependent cleavage, increases the risk for CD (Lassen et al., 2014; Murthy et al., 2014). Paneth cells from CD patients harbouring this variant or knock-in T300A mouse models are characterised by defective AMP secretion and production of secretory granules (Bel et al., 2017; Cabrera et al., 2015; Cadwell et al., 2008; Cadwell et al., 2009), which results in increased sensitivity to viral infection, and enhanced inflammatory response during DSS-induced colitis (Cadwell et al., 2010; Kernbauer et al., 2014; Matsuzawa-Ishimoto et al., 2017). Similarly, Atg7-deficient mice are characterised by a decreased GC-dependent mucus secretion, resulting in increased bacterial burden in the colon and exacerbated sensitivity to DSS-induced colitis (Tsuboi et al., 2015).

Because ATG proteins are involved in damaged organelle recycling, they also play a key role in promoting resilience of the intestinal barrier to metabolic and immune-mediated damages and preventing epithelial cell death (Aden et al., 2018; Matsuzawa-Ishimoto et al., 2017;

Matsuzawa-Ishimoto et al., 2020; Xie et al., 2020). Indeed, studies have shown that PC-specific deletion of Atg genes endoplasmic reticulum (ER) stress gene *Xbp1* results in intestinal inflammation (Adolph et al., 2013). Further, CD susceptibility genes such as *NOD2* were found to stimulate autophagy downstream of bacterial invasion to diminish inflammasome overactivation (Matsuzawa-Ishimoto et al., 2018; Travassos et al., 2010), supporting the notion that autophagy can repress the inflammatory cascade in IBD.

Because IBD-sensitising mutations occur at the germline level, it is assumed that a generalised impairment of autophagy contributes to the clinical outcomes of IBD, which for instance has been shown for epithelial cells (Pott et al., 2018). Non-canonical roles of ATG proteins could also contribute to IBD. For instance, the CD risk gene immunity-related GTPase family M member 1 *(IRGM1)* (Parkes et al., 2007) was shown to promote autophagy-mediated degradation of NLRP3 and PYCARD/ASC, thereby reducing inflammation in a CD mouse model (Mehto et al., 2019).

5.3. Modulation of autophagy by probiotics

Because of the key role played by autophagy mechanisms in barrier function, gut homeostasis and inflammation, probiotic supplementation strategies have been explored to enhance autophagy in the gut. Previous studies have shown *Bifidobacterium* species were able to initiated autophagy in the rat ileal IEC18 cell line by the upregulation of *Atg5*, *Atg12* and *Atg16* (Lin et al., 2014), and to prevent oxidant-induced intestinal epithelial cell death through induction of autophagy (Hughes et al., 2017; Inaba et al., 2016). Additionally, *B. dentium* was shown to enhance goblet cell function, including mucin production and secretion, *via* the upregulation of autophagy in *in vitro* and *in vivo* studies (Engevik et al., 2019). Treatment with *L. rhamnosus* GG and *B. longum* in *Salmonella*-infected Caco-2 cell model also enhanced autophagy and suppressed inflammatory IL-1β expression *via* autophagy related ATG16L1 protein (Lai and Huang, 2019). In another study, live *Lactobacillus acidophilus* alleviated colitis and improved intestinal barrier in UC rats by increasing SCFAs and inhibiting NLRP3 inflammasome, compared to the supernatant and heat-killed bacteria only, which was likely to be mediated by G-protein coupled receptors (Li et al., 2022a).

5.4. Measuring autophagy flux in mammalian cells

Because of the role played by autophagy in mediating host-microbiome crosstalk, including the potential effects of bifidobacteria, it is useful to employ methods to detect this process within intestinal epithelial cells. Several different screening platforms have been proposed to identify and measure the different steps of autophagy processes in mammalian cells, which

are summarised in **Figure 1.5** (Seranova et al., 2019). In particular, the LC3 protein (LC3-II form associated with autophagosomes throughout their life span) is used as a marker of autophagy, while Sequestosome 1 (SQSTM1/p62) can be used as an autophagy substrate (Seranova et al., 2019). Quantification of the number of LC3-II positive puncta inside host cells is considered as a gold-standard assay for assessing the numbers of autophagosomes in cells (Runwal et al., 2019). Additionally, p62 dot intensity can also be used to monitor the autophagy flux as an indication of autolysosomes formation to eliminate damaged proteins (Elbialy, 2021; Peng et al., 2017).

In the work highlighted in this thesis, I developed a method for the quantification of p62 and LC3 puncta to assess autophagy flux within mouse and human intestinal organoids (**Chapter 2**), as well as to assess the modulation of autophagy by *Bifidobacterium* metabolites in a Caco-2 monolayer system (**Chapter 3**).

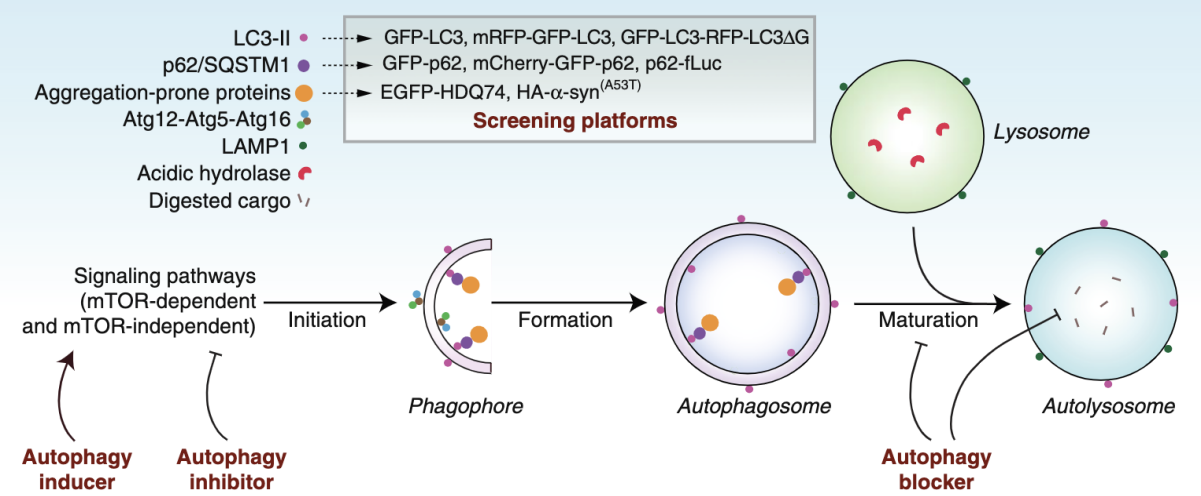

Figure 1.5. Schematic overview of autophagy process and different screening platforms available to monitor autophagy in mammalian cells. Autophagy starts with the target recognition, formation of the initiation complex, lipidation of LC3 protein, and nucleation of the membrane which expands engulfing materials from the cytoplasm to form an autophagosome. These structures subsequently fuse with lysosomes to generate autolysosomes, whereby the cargo is degraded. Commonly used screening platforms for autophagy detection are based on LC3, p62/SQSTM1, and aggregation-prone proteins. Figure and caption adapted from (Seranova et al., 2019).

6. *B. breve* UCC2003 as a model strain to study the beneficial effects of bifidobacteria on the intestinal epithelium

Most *in vivo* studies that investigated the effect of *Bifidobacterium* spp. on intestinal epithelial cells, have focused on the protective effects of pre-colonisation of *Bifidobacteirum* strains in the gut against acute or chronic inflammation (Din et al., 2020; Hsieh et al., 2015; Pinto-Sánchez et al., 2017; Schroeder et al., 2018; Srutkova et al., 2015; Yan et al., 2019). However, results were mainly applicable to adult life rather than during early development, where the effects of *Bifidobacterium* spp. are expected to be more pronounced and long-term. Subsequent studies have shown that bigger effects are found in new-born mice compared to adult mice (Lee et al., 2018).

Three *Bifidobacterium* species are among the most abundant in the infant gut and for which a good amount of evidence for their effects in the gut was found: *B. longum, B. breve, and B. bifidum* (Arboleya et al., 2016; Makino, 2018). Among these, *B. breve* UCC2003, which was originally isolated from a nursing stool (O'Connell Motherway et al., 2011), has gained interest for their potential beneficial effects in the gut. Indeed, previous studies have shown its ability to reduce epithelial cell shedding and increase epithelial proliferation (Hughes et al., 2017; O'Connell Motherway et al., 2019). Additionally, it has been shown to be able to evade adaptive B cell responses, to protect mice against colonisation by gut pathogen *C. rodentium*, to protect *Caenorhabditis elegans* against *Salmonella* infection and to modulate the gut microbiota composition through EPS cross-feeding (Christiaen et al., 2014; Fanning et al., 2012a; Fanning et al., 2012b; Püngel et al., 2020). Finally, a transcriptomics study found that *B. breve* UCC2003 modulated over 4,000 genes in neonatal murine IECs, mainly involved in cell differentiation (including SCs proliferation) and barrier function, suggesting its ability to modulate epithelial homeostasis and regeneration under stress conditions (Kiu et al., 2020).

In addition to their health benefits, *B. breve* is a useful model to study the effects of bifidobacteria on IEC function, as it has been shown to be highly efficient at colonising the murine gastrointestinal tract (small intestine, caecum and colon), and to stably persist at high levels for at least seven weeks (Cronin et al., 2008; O'Connell Motherway et al., 2011). Moreover, a transposon 5 (Tn5) insertion library of nearly 20,000 transposon insertion mutants of *B. breve* UCC2003 has been developed using random mutagenesis, making it the first genome-wide random mutagenesis approach for bifidobacteria to our knowledge (Ruiz et al., 2013). Together with the fully sequenced genome, these factors make *B. breve* UCC2003 a particularly useful strain with which to study *Bifidobacterium*-host interactions in the gut. For this reason, *B. breve* UCC2003 will be the main strain employed to study the effects of bifidobacteria on the mouse and human intestinal epithelium.

7. Experimental models to study the effect of bifidobacteria on the intestinal epithelium

7.1. Animal models and cell lines

Studying bifidobacteria-host interactions in the gut *in vivo* is hindered by the limited accessibility of epithelial cells such as intestinal aspirates and biopsies (Dave et al., 2012). Additionally, the manipulation and precise control over experimental variables in human studies, including host and microbial genetics, also remains a difficult task. While the effects of the bifidobacteria are location (e.g. sites of inflammation) and time dependent, *in situ* spatio-temporal measurements of bifidobacterial and host responses at sufficient resolution are not currently possible in humans (Halfvarson et al., 2017).

Microbe-host interaction studies have been generally carried out in mice (Faith et al., 2014), due to their similar gastrointestinal architecture, and because they allow an easier sample collection and better control over both diet and genetics (Kostic et al., 2013). Indeed, animal models have proven crucial to study the effect of microbes on gut epithelial barrier, cell function and inflammation. However, mouse models are not able to fully represent the physiological conditions of the human gut (Nguyen et al., 2015), nor do they perfectly recapitulate human disease (Seok et al., 2013). Additionally, they show limited applicability for high-throughput studies due to costs and ethical concerns (Kostic et al., 2013). Alternatively, human colorectal adenocarcinoma cell lines such as Caco-2, T84 and HT-29 have also been employed(Krishnan et al., 2016; Martz et al., 2017; Munoz et al., 2016). Yet, cell lines do not reflect tissue heterogeneity and location specific characteristics (duodenum, colon, etc) (May et al., 2017). To overcome these limitations, co-culture systems with immune and intestinal cells have been proposed (Duell et al., 2011; Pozo-Rubio et al., 2011). However, these models have not been able to generate data of clinical relevance so far (Noel et al., 2017).

Thus, to gain a better understanding into the mechanisms behind host-microbiota interactions, including the effect of specific members in modulating host function, specific *in vitro* systems mimicking the intestinal epithelium in a representative model are needed. To this regard, the development of intestinal organoids - three-dimensional (3D) *in vitro* models of the human intestinal epithelium - has represented a major advancement in the field (Bartfeld, 2016). Indeed, intestinal organoids represent a unique tool to study host-microbiota crosstalk, overcoming some of the disadvantages associated with human studies, mouse models and cell lines. Furthermore, organoids allow repeated experiments and maintain organ, disease and patient characteristics (Dotti and Salas, 2018; Sato et al., 2011b).

7.2. Intestinal organoids

Intestinal organoids are 3D *in vitro* epithelial structures derived from primary tissue, capable of self-renewal and self-organisation, and recapitulating the architecture and function of the human gastrointestinal tract (Fatehullah et al., 2016) (**Figure 1.6**). Intestinal organoids can be derived either from adult intestinal stem cells (ASCs), ASCs containing crypts (Sato et al., 2009) or induced pluripotent stem cells (iPSCs) (Spence et al., 2011). When stem cells are embedded in a cell culture matrix mimicking the extracellular matrix (ECM), and given the appropriate niche factors, they will self-assemble in a crypt-villi structure where the luminal surface of epithelium is projected towards the centre of the organoid and the basolateral side is in contact with the ECM and surrounding medium (Sato et al., 2009; Spence et al., 2011). While ASC-derived organoids can be differentiated into the different intestinal epithelial cell types (Sato et al., 2009), iPSC-derived organoids also contain the intestinal mesenchyme (Spence et al., 2011). However, iPSC-derived organoids are characterised by a low grade of maturation and therefore resemble more foetal tissue compared to ASC-derived organoids, making them less favourable to model adult tissue biology (Kin et al., 2013) (**Figure 1.7**).

Organoids derived from human biopsies represent a great experimental tool to study host-microbe interactions as they maintain the crypt-villi structure of the intestine, contain the majority of intestinal cell types and retain the genetic, transcriptional and epigenetic characteristics of the donor and intestinal segment (duodenum, jejunum, ileum) they were derived from (Cramer et al., 2015; Dekkers et al., 2016; Kraiczy et al., 2019; Middendorp et al., 2014). Contrary to intestinal cell lines, differentiated intestinal organoids contain all the epithelial cell lineages populating the intestinal crypt (Sato et al., 2009), including cells that could not be previously cultured *in vitro* (e.g. Paneth cells) (Sato et al., 2011a). Additionally, organoids can contain rare intestinal cells (enteroendocrine, tuft, or M cells) if specific culturing protocols are used (Basak et al., 2017; de Lau et al., 2012; Rouch et al., 2016)

The culture media used to grow human intestinal organoids include EGF, R-spondin (Wnt agonist binding to LGR5 (Kim et al., 2005; Smith et al., 2017)), and Noggin (a BMP inhibitor), which combined promote SC hyperplasia and maintenance of the stem cell niche by promoting WNT and inhibiting BMP signalling (Clevers, 2013; Haramis et al., 2004). However, by manipulating the standard organoid culture conditions, organoids can also be maintained in a non-differentiated status, containing mainly SCs and progenitor cells (Sato et al., 2011b), or differentiated towards different IECs such as absorptive or secretory cell types (Jones et al., 2019; Kaiko et al., 2016; Sato et al., 2011b). In this way, organoids represent a unique tool to investigate the cell-type specificity of bifidobacterial-host interactions in the human gut.

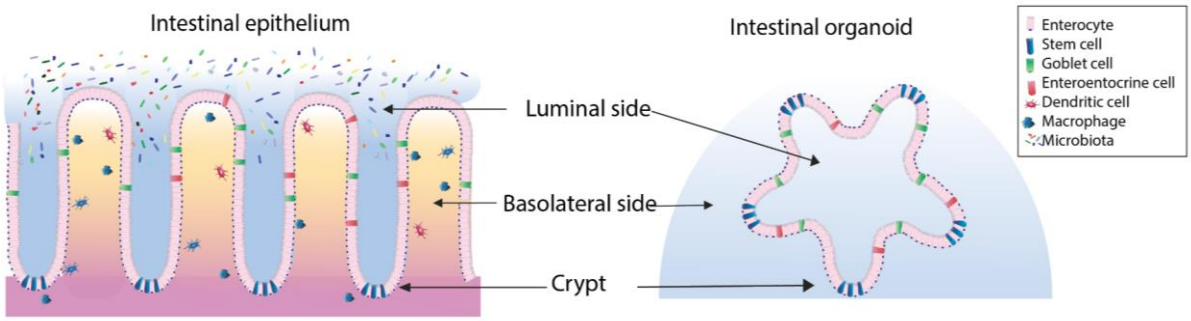

Figure 1.6. The intestinal epithelium and the organoid model. Original figure, published in (Poletti et al., 2021).

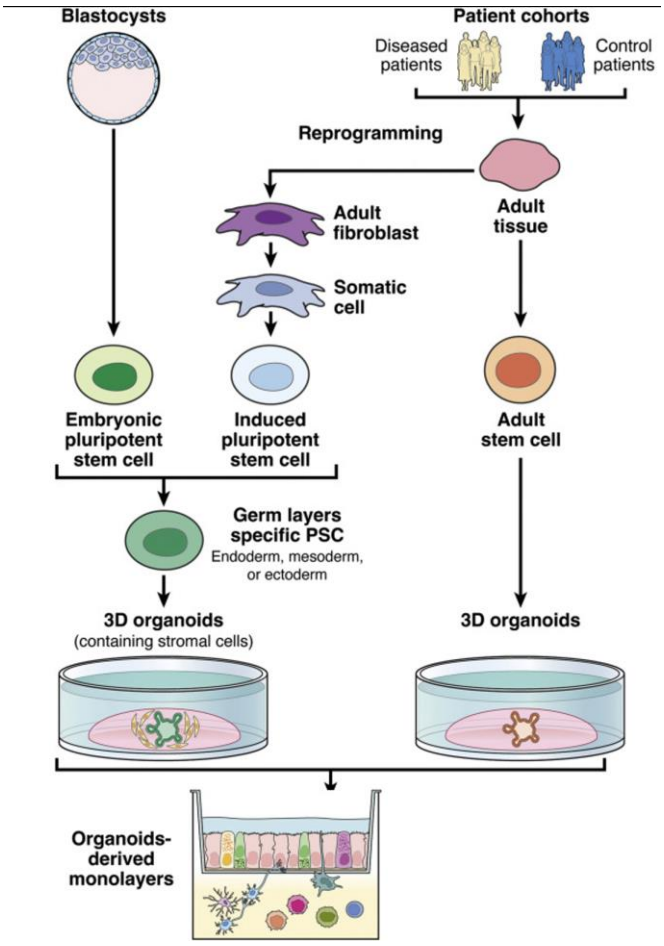

Figure 1.7. Intestinal organoid cultures. Stem cells can be obtained from embryonic blastocysts or generated from adult tissue. Adult stem cells (aSCs) can be used immediately to grow tissue-specific organoids. Embryonic pluripotent stem cells or reprogrammed induced pluripotent stem cells first need to develop into somatic cells and then the relevant germ layer (endoderm, mesoderm, or ectoderm) before being grown in tissue-specific organoids. Adapted from (Hautefort et al., 2022).

7.2.1. Organoid models for host-microbe interactions studies

So far, different techniques have been developed to expose organoids to microbes and/or their metabolites (Puschhof et al., 2021b). These include the microinjection of 3D organoids, or establishment of organoids with reversed polarity ("apical-out") and organoid monolayers on Transwells (**Figure 1.8A, B, C**). Additionally, more advanced models have been developed where either Caco-2 cells or organoids have been introduced within microfluidics devices to achieve a more physiologically relevant model (**Figure 1.8D, E**). These models, including their advantages and disadvantages, and the bacteria tested with them will be presented below.

7.2.1.1. Microinjection of 3D organoids

Microinjection of microorganisms directly into the lumen of the differentiated 3D organoids has been employed in several labs, representing a useful technique to access the apical side of the epithelium (**Figure 1.8A**) (Bartfeld et al., 2015; Leslie et al., 2015; McCracken et al., 2014). The lumen of organoids is characterised by hypoxic conditions (Bartfeld, 2016), which facilitates the study of facultative or obligate anaerobic bacteria. Microinjection of organoids has been employed to look at the effects of *Bifidobacterium adolescentis* and faecal containing complex microbiota (Williamson et al., 2018), as well as *Clostridioides difficile* (Leslie et al., 2015), *Escherichia coli* (Karve et al., 2017), *E. coli* ECOR2 (Hill et al., 2017). Microinjection represents a useful approach when looking at facultative anaerobes or for high-throughput studies (Williamson et al., 2018). However, it requires a highly specialised automated set-up which is not easily available and proper training is needed to correctly use it (Williamson et al., 2018).

7.2.1.2. 3D organoids with reversed polarity

Another model that has been recently developed is represented by organoids with reversed polarity ("apical-out") (**Figure 1.8B**). In this system, the apical side of the epithelium is easily accessible, making it possible to study epithelial-microbe interactions by adding the microbes directly in the culturing medium (Co et al., 2019), which is technically more convenient than microinjection. These organoids can be generated by disrupting the ECM matrix in which organoids are grown, and subsequently continue the organoid culture in suspension using low-attachment plates. After 3 days in culture, an inversion of the organoid polarity with the apical side on the "outside" can be observed, and further differentiation of the organoid in differentiated cell types is obtained over time (Co et al., 2019). Previously, it has been shown that the ECM removal interferes with the β1-integrin signalling required to maintain basolateral-out polarity, which results in morphogenetic eversion of the organoid epithelium (Co et al., 2019).

This method has been applied to human (Co et al., 2019; Co et al., 2021; Stroulios et al., 2021; Stroulios et al., 2022), porcine (Joo et al., 2022; Li et al., 2020) and chicken (Nash et al., 2021) primary cell-derived intestinal organoids, as well to human iPSC-derived organoids (Kakni et al., 2022). In humans, apical out organoids have been generated for all the different segments of the GI tract (gastric antrum, small intestine, colon) (Co et al., 2019) and have been shown to be a useful model to study gut infection by invasive enteropathogens (*S. enterica* serovar Typhimurium and *Listeria monocytogenes*) (Co et al., 2019) and viruses (Stroulios et al., 2022). However, apical out organoids could be used to evaluate aerobe bacteria or bacterial metabolites as well (Co et al., 2019; Co et al., 2021; Stroulios et al., 2021).

Apical out organoids present multiple advantages. These include (i) the absence of the ECM, which promotes molecule diffusion; (ii) the release of mucins in the culture medium instead of the lumen, making their manipulation easier based on the experiment (left as part of an intact mucosal barrier or removed for more rapid access to the epithelial surface); (iii) the suspended culture in which organoids are grown allows simple division into multiple wells for high-throughput experiments (Co et al., 2021).

However, some limitations associated with this model also exist: (i) several media changes are required for this protocol, making it more time consuming (Co et al., 2021); (ii) apical-out organoids exhibit slower proliferation and accelerated differentiation, hindering their maintenance in culture over time (Co et al., 2019); (iii) a complete polarity reversion is not guaranteed, making it difficult to distinguish between apical and basolateral interactions (Co et al., 2019). In the future, a thorough characterisation of how polarity reversion affects apical-out organoids phenotype, metabolism and response to microbial challenge will be needed to understand critical similarities and differences between this model and self-organised and polarised organoids.

7.2.1.3. Organoid-derived epithelial monolayers on Transwells

Another type of organoid where the apical side is made accessible is represented by organoid-derived monolayers (**Figure 1.8C**). To create monolayers, human small intestinal (Ettayebi et al., 2016; Foulke-Abel et al., 2014) or colonic (Wang et al., 2017b) organoids generated from patient biopsies are cultured using the standard protocols (Sato et al., 2011b), fragmented into small clumps of cells/single cells and subsequently plated onto a ECM-coated dish well or Transwell insert (Ettayebi et al., 2016; In et al., 2016; VanDussen et al., 2015). Differentiation towards the different epithelial cell lineages and polarisation occurs during a period of 7-10 days, resulting in confluent monolayer. Upon differentiation, the production of mucus by goblet cells is also observed (VanDussen et al., 2015).

In this model, introduction of microorganisms is executed *via* addition to the culture media (Bartfeld and Clevers, 2015; Schlaermann et al., 2016; VanDussen et al., 2015). This model enables co-culture of organoids with aerobic bacteria and microbial-derived metabolites for several hours (<24 hours for bacteria, <48 hours for metabolites) (In et al., 2016; Noel et al., 2017; Vancamelbeke et al., 2019; VanDussen et al., 2015) in an easily applicable set-up, and enables comparison of several conditions in one experiment. However, co-culture with strictly anaerobic bacteria is not feasible, as the system is kept in aerobic conditions to guarantee the organoid's survival.

7.2.1.4. Anaerobic Transwell models

Recently, new systems have been developed to maintain the apical chamber of organoid-derived monolayers on Transwells in an anaerobic environment, while keeping the basolateral chamber in aerobic conditions (Fofanova et al., 2019; Kim et al., 2019; Sasaki et al., 2020). In one model, the Enteroid Anaerobe Co-Culture (EACC) system, human jejunal organoid-derived monolayers grown on Transwells inserts were placed onto modified gaskets sealed in place using double-sided adhesive tape on a gas-permeable plate. When keeping the entire system in an anaerobic chamber, the EACC system allowed co-culture with the obligate anaerobic bacteria *Bacteroides thetaiotaomicron* and *Blautia* spp. for 24 hours (Fofanova et al., 2019). One disadvantage of this model is that it is not commercially available, and reproducing it could be time-consuming and would require optimization.

In another model, the Intestinal Hemi-Anaerobic Co-culture System (iHACS), human colonic-derived epithelial monolayers were grown on Transwell inserts whose upper compartment is sealed off by a plug, enabling the co-culture with obligate anaerobe bacteria *B. adolescentis* and *Akkermansia muciniphila* for 24 hours. Upon availability of the plug, the model can be implemented in every laboratory although co-culture is also limited to 24 hours (Sasaki et al., 2020).

Finally, an alternative model has been developed where human colonic-derived epithelial monolayers are seeded within a micro-fabricated insert with tailored oxygen permeability properties, which allows the creation of an oxygen gradient between the apical and basolateral compartments (0.8±0.1% O_2; 11.1±0.5% O_2). With this device, co-culture with facultative and obligate anaerobes *L. rhamnosus*, *B. adolescentis,* and *C. difficile* was achieved for 24 hours(Kim et al., 2019). One disadvantage of this model is that the culture area is relatively large (equivalent to a 12-well Transwell® insert), thus requiring a substantial amount of starting material for the epithelial compartment.

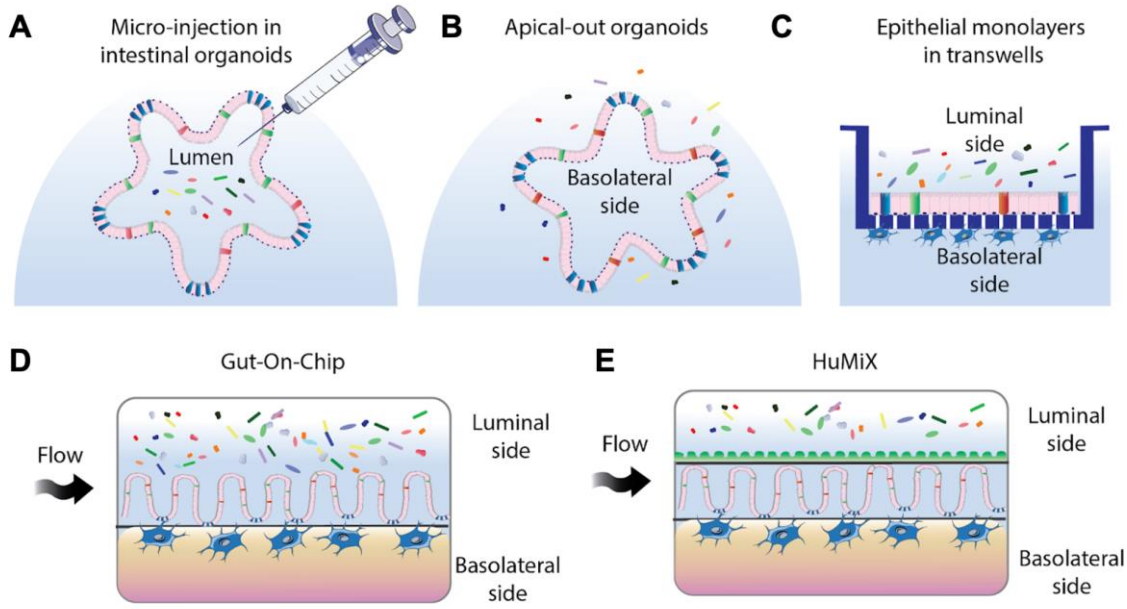

Figure 1.8. 3D organoids, organoid-derived models, and microfluidics models for the study of host-microbe interactions in the gut. Original figure, published in (Poletti et al., 2021).

7.2.2. Challenges to co-culture bifidobacteria with organoids

Introducing microbes within the organoid system can be challenging for several reasons (Dotti and Salas, 2018; Poletti et al., 2021; Puschhof et al., 2021b). First, 3D organoids have closed structures, with the apical side of the epithelium where microbial-epithelial interactions take place projected inwards and therefore not very easily accessible. Second, epithelial cells require an aerobic environment while commensals such as bifidobacteria are (facultative) anaerobes, requiring a (virtually) oxygen-free environment. Third, bacterial and epithelial cells require different mediums to support their metabolism and growth, which are often not compatible with each other. Fourth, the static nature of culture conditions of organoids can result in microbial overgrowth and potential damage to epithelial cells due to nutrients and oxygen depletion, and accumulation of organic waste (e.g. acetate or lactate). So far, this issue has been tackled by keeping the microbial and epithelial culture compartments separate (Zachos et al., 2016), or by using a short co-culture time (from a half-hour to several hours), followed by bacterial elimination using bacteriostatic antibiotics (Payne et al., 2012). However, to properly mimic host-microbiome interactions *in vitro*, viable and functional intestinal tissue and microbial cells must be kept within the same confined space for a longer period of time (Kim et al., 2012; Park et al., 2017).

Additionally, organoid models also lack certain features that are characteristics of the epithelium *in vivo.* First, all organoid models also lack the typical peristalsis-like motion of the gut, which is important to stimulate proper intestinal differentiation in *in vitro* models such as mucus production (Gjorevski et al., 2016; Kim et al., 2016). Furthermore, organoid-derived monolayers lack the crypt-villus structure observed *in vivo* (Wang et al., 2017a). Additionally, mucus layer of organoids is either challenging to access as it is enclosed in the central lumen (in 3D organoids) (Lock et al., 2018) or present only as a thin mucus layer (< 36 µm thick) (in organoid-derived monolayers) (In et al., 2016; VanDussen et al., 2015), making it an unsuitable model to replicate microbial-host interaction happening at the mucosal surface (Lock et al., 2018).

Finally, organoids are composed of epithelial cells only, making them a key model to look at the direct microbial-epithelial crosstalk (Stelzner et al., 2012). However, other cell types can play a major role in mediating these interactions and should be included in the organoid system to make it more physiologically relevant (Fatehullah et al., 2016; Hollins and Parry, 2016). Indeed, co-culture of organoids with immune cells (macrophages (Noel et al., 2017), neutrophils (Karve et al., 2017), T-lymphocytes (Rogoz et al., 2015) and intraepithelial lymphocytes (Nozaki et al., 2016)), as well as fibroblasts (Pastuła et al., 2016), adipocytes (Takahashi et al., 2017), and enteric nervous system (ENS) cells (Workman et al., 2017), has been key to gain knowledge on the role of these cell types in host-microbial interactions (Kuhn, 2016). However, introducing an additional cell type brings additional challenges in terms of requirement for their metabolism and growth, which could be different to that of epithelial and microbial cells, adding an additional layer of complexity.

Introducing organoids within microfluidic systems has worked towards solving part of these issues, thanks to the presence of fluid flows facilitating nutrient and oxygen uptake, and fluid shear stresses providing physiologically relevant mechanical signals to organoid cells (Qian et al., 2016).

7.2.3. Microfluidic-based and organoid-on-chip models

Within microfluidic systems, organoid cells are cultured with the organ-relevant spatiotemporal chemical gradients and dynamic mechanical cues, to achieve the same structural tissue arrangement and functional complexity of the living organism *in vitro* (Huh et al., 2012). These models provide a more representative and physiologically relevant model to investigate bifidobacteria-host interactions than simple organoid systems (von Martels et al., 2017).

7.2.3.1. Gut on-chip and organoid-on-chip

One of these models is the “gut-on-chip” system consisting of two channels simulating the gut lumen and the blood vessel, separated by an ECM-coated membrane and epithelial cells (**Figure 1.8D**) (Kasendra et al., 2018; Kim et al., 2012; Villenave et al., 2017; Walsh et al., 2018). Within this device, the application of fluid flow and peristalsis-like deformations to the epithelial layer induces epithelial multi-lineage differentiation and crypt-villi formation (Kasendra et al., 2018; Kim and Ingber, 2013). While in initial set-up Caco-2 cells were used, in a further model (the microfluidic primary human Intestine Chip model (“organoid-on-chip”)) they were replaced by human duodenal organoids (Kasendra et al., 2018). In both systems, other cell types (endothelial or PBMCs) can also be introduced in the lower channel to obtain a more advanced model (Kasendra et al., 2018; Kim et al., 2016). Additionally, while the gut-on-chip and organoid-on-chip models were initially characterised by the epithelial chamber being kept in aerobic conditions (Kim et al., 2012; Kim et al., 2016), a recent development (the “anaerobic human Gut-Chip”) has introduced a transluminal hypoxia gradient that allowed to co-culture human ileal organoids with a complex microbiota community for up to 5 days (Jalili-Firoozinezhad et al., 2019).

Advantages of organoid-on-chip systems include the better mimicking of epithelial functions thanks to the peristalsis and fluid flow applied to the epithelial layer. For instance, a spontaneous differentiation of goblet cells is observed, giving rise to a bilayer mucus structure while still maintaining a subpopulation of proliferative epithelial cells (Sontheimer-Phelps et al., 2020). This is not observed in organoid-derived monolayers, where the epithelial layer is less developed and goblet cells produce less mucus than what is observed *in vivo* (Kim et al., 2016). Furthermore, investigating direct interactions between microbes and epithelial cells is possible, as there is no separation between the epithelial and microbial compartments (Kasendra et al., 2018; Kim and Ingber, 2013). However, some limitations exist including the need for specific training and reduced application for high-throughput experiments. Finally, the anaerobic human gut-on-chips are not commercially available yet in the used set-up.

7.2.3.2. The human-microbial crosstalk module

In addition to the gut-on-chip and organoid-on-chip models, a third model has been developed to look at host-microbe interactions, called the human-microbial crosstalk module (HuMiX) (**Figure 1.8E**) (Shah et al., 2016). This device is composed of three parallel microfluidic chambers (microbial, epithelial, and perfusion chamber) separated by semipermeable membranes, including specific controllable inlets for each chamber (Eain et al., 2017; Shah et al., 2016; von Martels et al., 2017). Within this system, Caco-2 cells are grown for one week under continuous basal perfusion, followed by bacterial inoculation into the microbial chamber

for 24 hours in anaerobic sheer-free conditions. Using this system, Caco-2 cells have been successfully co-cultured with the anaerobic bacteria *B. caccae* and *L. rhamnosus* (Shah et al., 2016), as well as immune cells (CD4+ T cells) (Shah et al., 2016).

HuMiX has some advantages, including its modular design that allows easy disassembly and cell collection, as well as the ability to generate multiple readouts (RNA sequencing/qPCR, immunostaining, Western Blot) within one device, which makes it perfect for detailed mechanistic studies(Shah et al., 2016). Additionally, the mucus-coated membrane separating the microbial and epithelial compartments enables the study of host-metabolites interactions, although limiting the direct host-microbe contact.

Among the disadvantages, gut peristalsis and differentiation of the epithelium into various cell types is not present (Kasendra et al., 2018; Marzorati et al., 2014), and the “microbial microchamber” is not completely devoid of oxygen, making this model less physiologically relevant (Shah et al., 2016). Finally, Caco-2 cells are employed in the current model although the introduction of organoids is feasible.

In this chapter, I have presented the different models available to introduce microbes within intestinal organoid systems. Among these, in my PhD I have only focused on four main models: (i) 3D organoids, (ii) apical out organoids, (iii) organoid-derived monolayers on Transwells and (iv) HuMiX. With regard to HuMiX, I worked together with collaborators (KU Leuven, Belgium) to assess the feasibility of introducing human intestinal organoids within the epithelial chamber of this microfluidics system.

7.2.4. Organoid applications

Organoids and organoid-derived models are amenable to various applications, which can be combined to understand the role of host-microbe interactions in gut health and disease.

7.2.4.1. Organoid reporter systems and high-content imaging platforms

Organoids co-cultured with microbes or their metabolites can be fixed and subsequently stained for bioimaging approaches (Dekkers et al., 2019; Pleguezuelos-Manzano et al., 2020). Several studies have provided lists of markers to check to evaluate the differentiation status on intestinal epithelial organoids: some of these include tight junctions (F-actin (phalloidin), E-cadherin, ZO-1), stem cell proliferation (Ki67), specialised cell markers (MUC2 for goblet cells, LYZ for Paneth cells, NEUROG3 for EECs) (Dekkers et al., 2019). However, the 3D structure and high variability between organoids makes it quite difficult to establish high-quality and reproducible protocols for imaging based organoid analyses. In this regard, integrated high-

throughput methods have been developed to culture, image and quantify large numbers of organoids (All-in-one approach to culture, image and quantify large numbers of organoids at all scales., 2022; Brandenberg et al., 2020). For instance, a platform has been developed to grow patient-derived organoids within a pre-formed U-shaped microcavity, resulting in a highly homogeneous organoid culture positioned in the same Z-place, facilitating the bio-imaging screening of various bacterial-derived molecules (Brandenberg et al., 2020). Methods to collect several Z-stacks of organoids in a standardised way have also been developed (Li et al., 2022b). Furthermore, microscopy image analysis softwares such as Imaris (Oxford Instruments) have also been implemented for 3D and 3D stereo visualisation and segmentation of confocal organoid images (Dekkers et al., 2019).

Live bioimaging and analysis of complex structures such as organoids have also been explored thanks to the development of high throughput systems and related protocols (Alsehli et al., 2020; Kerz et al., 2016). These systems, combined with the integration of fluorescent reporter systems within organoids, could allow the study of specific cellular processes upon microbial exposure, as has been done for the Stem Cell ASCL2 Reporter (STAR) integrated in intestinal organoids (Heinz et al., 2020).

In the work highlighted in this thesis, I have developed a method to image 3D human and mouse intestinal organoids without prior removal from the Matrigel matrix, which was the previously described technique (**Chapter 2**) (Pleguezuelos-Manzano et al., 2020). Additionally, I used this method to set-up a protocol for the assessment of autophagy flux in 3D organoids by immunostaining, confocal imaging, and quantification of autophagy-related p62 and LC3 puncta using the Imaris cell imaging software (Oxford Instruments) (**Chapter 2**). Finally, I contributed to the work of a senior post-doc in our group (Dr. Isabelle Hautefort, EI), with the aim to develop a method for high-content imaging of human colonic organoids containing an autophagy-reporter system developed in the Hall group (QIB) (not presented).

7.2.4.2. Omics data

Organoid models are amenable to ‘omics data readout generation, which consists of the comprehensive sequencing and measure of different biological molecules (DNA, RNA, proteins, metabolites) within a cell. 3D organoid models and organoid monolayers on Transwells are more suited for generating a single type of ‘omics readout in many different samples, while systems such as HuMIX, given their lower throughput, are better for generating multiple ‘omics from the same sample in a limited number of conditions.

Among omics readout, transcriptomics is the study of all RNA molecules, including messenger RNA (mRNA), ribosomal RNA (rRNA), transfer RNA (tRNA), and other non-coding RNAs (microRNAs (miRNAs), long non-coding RNAs (lncRNA)). To measure the transcriptome, the two main methods include (i) microarrays, which are based on oligonucleotide probes that hybridise to specific RNA transcripts, and (ii) RNA sequencing (RNAseq), which allows for direct sequencing of RNAs without the need for probes (Micheel et al., 2012). While initially these measurements were only possible on a mixed population of cells ("bulk sequencing"), later technologies have been developed to obtain 'omics measurements on single cells ("single-cell sequencing") (Tang et al., 2011; Teague et al., 2010).

Both bulk and single cell approaches have been applied to organoid models to decipher host-microbe interactions in the gut. Bulk RNAseq has been used to look at the effect of specific microbes or microbial-derived metabolites on epithelial cell gene expression (Forbester et al., 2015; Kaiko et al., 2016; Lukovac et al., 2014). In combination with the applications of protocols to skew organoid differentiation towards a specific lineage (e.g. Paneth cells or goblet cells), cell-specific responses upon microbial exposure can be evaluated (Jones et al., 2019; Kaiko et al., 2016). In a ground-breaking study, the effect of 92 microbial metabolites on epithelial cell proliferation was tested using stem- and progenitor cell–enriched colonic organoids from mice with a Cdc25A-luciferase construct. Interestingly, butyrate was found to dramatically reduce proliferation of stem and progenitor cells at physiologic concentrations (Kaiko et al., 2016). Additionally, flow cytometry activated sorting (FACS) (Fujimichi et al., 2019) or mass cytometry (Qin et al., 2020) could be used to isolate cells from organoids after microbial exposure, similarly to what has been achieved with mouse intestinal tissue (Wang et al., 2013).

Single cell RNAseq (scRNAseq) has also been applied to organoids. By combining this readout with high-throughput platforms, achieving high-resolution snapshots of organoid heterogeneity in different conditions over time is becoming increasingly possible (Brazovskaja et al., 2019; Bues et al., 2022). For instance, these approaches have been used to screen for modulators of intestinal SC differentiation (Mead et al., 2022), to find disease activity-dependent modification of SC properties in CD small intestinal organoids (Suzuki et al., 2018), or investigate the cell-specific response to bacterial infection (Haber et al., 2017) and severe acute respiratory syndrome coronavirus 2 (SARS-CoV-2) viral infection (Triana et al., 2021).

In the work highlighted in this thesis, I used bulk RNAseq on healthy human colonic organoids to gain new insights into the mechanisms by which bifidobacteria influence intestinal epithelial cells in the gut (**Chapter 4**). Furthermore, I used scRNAseq datasets from infected human

colonic and ileal organoids and resident immune cell populations to understand the role of epithelial-immune interactions in the gut during SARS-CoV-2 infection (**Chapter 5**).

7.2.4.3. Disease models

Co-culturing organoids where specific genes linked to genetic susceptibility (e.g. *NOD2, ATG16L1* in IBD) have been genetically modified using clustered regularly interspaced short palindromic repeats (CRISPR) / associated protein 9 (Cas9) technology (Drost et al., 2015; Drost et al., 2016; Fujii et al., 2015; Schwank et al., 2013) can help gain better understanding on the role of these genes in mediating microbial effects on the epithelium (Limanskiy et al., 2019; Matano et al., 2015). Additionally, the use of healthy patient-derived organoids in parallel with organoids derived from patients with diseased conditions such as IBD (Zilbauer and Kraiczy, 2017) could help elucidate the role of the genetic susceptibility in response to bacterial challenges. In combination with high-throughput approaches (Brandenberg et al., 2020; Gracz et al., 2015), different microbial species or their metabolites could be tested for their beneficial effects on the epithelium during disease (Francies et al., 2019; Fujii et al., 2016; VanDussen et al., 2015; van de Wetering et al., 2015). Additionally, the introduction of patient-derived or engineered organoids within microfluidics devices also helps re-create a better *in vivo*–like disease phenotype(Dutta et al., 2017), facilitating the development of even more robust disease models for microbial screening (Astolfi et al., 2016; Mack et al., 2014). Overall, organoids are useful for target identification and validation in the early stages of drug discovery, thanks to their similarity with actual organs. Conversely, organ-on-a-chip models are more suited for subsequent efficacy and safety screening, as they provide a more reproducible and controllable environment (Esch et al., 2015).

8. Networks

In biology, networks can be employed to describe complex relationships between molecules, organisms, microbes, metabolic reactions, genetic interactions, etc. The analysis of networks can help visualising and studying system dynamics, tracing signal flow, and understanding functional relationships between different entities in the network (Han, 2008). In particular, molecular networks are a type of network used to visualise direct or indirect interactions and/or functional associations between molecules (genes, transcripts, proteins), representing key functions such as metabolism or transcriptional regulation within a cell, organ, or organism. Molecular networks are composed of “nodes”, which represent the molecular entities, and “edges”, which represent the physical or functional interaction between them (**Figure 1.9A**). Molecular networks possess a number of features: (i) they can be directed or undirected, based on whether the molecular interaction/edge has a direction, and can be signed, indicating

activation (+) or inhibition (-) (**Figure 1.9B**); (ii) they can be multi-layered, with each layer being made of a different type of molecule (gene, transcript, protein) or include one single layer with the different molecules in the same network (**Figure 1.9C**); (iii) they can be constructed either using experimental or computational methods (Papin et al., 2005; Siahpirani and Roy, 2017).

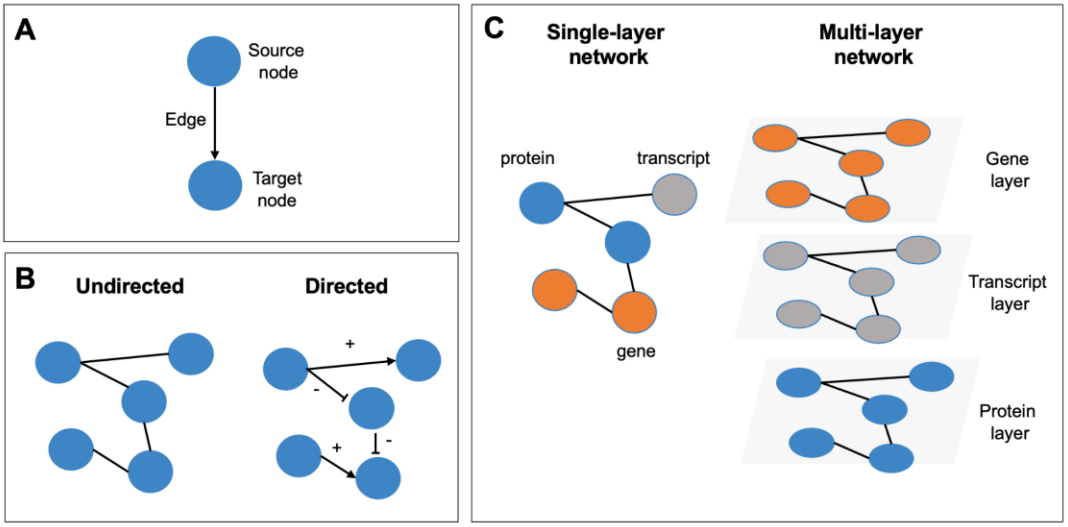

Figure 1.9. Overview of molecular networks and their properties. **A)** Directed interaction (edge) between two molecular entities (nodes). **B)** Undirected and directed networks. **C)** Single and multi-layered networks. Original figure.

Experimental methods used to construct molecular networks include yeast-two-hybrid methods and tandem affinity purification (Brückner et al., 2009) for protein-protein interactions (PPIs), chromatin immunoprecipitation (ChIP) methods (coupled with microarray analysis (ChIP-on-chip) or sequencing (ChIP-seq)) for DNA-protein interactions (Furey, 2012), and High-throughput sequencing of RNA isolated by crosslinking immunoprecipitation (HITS-CLIP) for miRNA/lncRNA-mRNA interactions (Chi et al., 2009). Once experimentally identified, molecular interactions are stored in specific databases, which can focus on a specific interaction (e.g. HTRIdb for human transcription factor (TF) - target gene (TG) interactions (Bovolenta et al., 2012), pathway or set of pathways (e.g. SignaLink3 (Csabai et al., 2022; Fazekas et al., 2013)) or cellular process (Autophagy Regulatory Network (ARN) (Türei et al., 2015)). Most databases collect multiple experimental results together ("second-party") (e.g. HTRIdb (Bovolenta et al., 2012), while others combine multiple databases ("third-party") (e.g. OmniPath for molecular interactions and DoRothEA for TF-TGs interactions (Garcia-Alonso et al., 2019; Türei et al., 2016; Türei et al., 2021). One disadvantage of datasets based on experimentally verified interactions is that they can be biassed or miss important interactions depending on the data availability.

To overcome some of these issues associated with experimentally-derived interactions, network inference methods can be used to predict molecular interactions using expression information, structural profiles and sequence homology (Chai et al., 2014; Chan et al., 2017; Huang et al., 2016; Siahpirani and Roy, 2017). However, disadvantages of using this approach include under-sampling, lack of generalisation potential, and high variability depending on the method and input dataset used. Due to these limitations, approaches have been developed to integrate both experimental and computationally derived molecular interactions (Castro et al., 2019).

In the work outlined in this thesis (**Chapter 4** and **5**), I have mainly used experimentally determined interactions, which were further contextualised based on experimental expression data to restrict the knowledge to those interactions relevant for the research question under study.

8.1. Signalling networks

Cells can sense different stimuli from the surrounding environment as well as internally from different regions of the cell. In both cases, signals are captured when a receptor binds with the internal or external signalling molecule, also known as “ligand”, which will cause the receptor to undergo a conformational change that starts a signal transduction ultimately leading to the cell molecular response. In the case of external interactions, the signalling cascade will involve altered function of different effector enzymes, which can in turn regulate protein function through post-translational events. In the case of internal signals such as for steroid hormones, this interaction will lead to direct modulation of transcription resulting in altered gene levels (Buchanan et al., 2010). Because signalling pathways are complex systems involving many interacting molecules, they are often visualised and analysed using network approaches. One example of a resource collecting intra- and intercellular signalling pathways is OmniPath (Türei et al., 2016; Türei et al., 2021). Given the nature of signalling pathways, these networks mainly include PPIs, with directed interactions according to the flow of molecular signals (Winterbach et al., 2013).

8.2. Regulatory networks

Regulatory networks are molecular networks describing regulatory interactions between molecules, such as transcriptional and post-transcriptional regulatory interactions between TF-TG, TF-lncRNAs, TF-miRNAs, miRNA-mRNAs and lncRNA-miRNA (Winterbach et al., 2013). For instance, a curated collection of signed TF-TG gene interactions in humans is represented by DoRothEA (Garcia-Alonso et al., 2019). miRNAs and lncRNAs are key

regulators of gut function and homeostasis and can mediate the effect of bacteria on the gut (Chapman and Pekow, 2015; Mirza et al., 2015). In one study, *B. animalis* subsp. lactis Bb12 modulated miRNAs in swine monocytes that in turn were interacting with at least 26 proteins of the TLR2 pathway, leading to immunomodulation effects (Arenas-Padilla et al., 2022). Interestingly, a multiplex single-cell analysis pipeline has been developed to establish post-translational modification signalling networks that can be altered in diseases using organoids co-cultured with fibroblast and leukocytes (Sufi et al., 2021). Similar platforms could be used to unravel the regulatory mechanisms through which bacteria act on epithelial cells, exerting their beneficial effects.

8.2.1. Transcription factors

In a human cell, only 10-50% of all genes are expressed at a single time (Campbell et al.; Marinov et al., 2014) and cells continuously change their gene expression profiles to adapt their function in response to external and internal stimuli. The main gene regulatory mechanism in humans is represented by regulation of gene transcription by TFs. To regulate gene expression, TFs bind *cis*-regulatory elements on the DNA, and in cohort with coactivators and/or corepressors recruited to the TF-DNA complex, they act to promote or block the binding of RNA polymerase to these regions. Additionally, histone modifying enzymes can control histone acetylation/deacetylation, making these sites more or less accessible for RNA polymerase binding. *Cis*-regulatory elements, including enhancers, promoters or silencers, can be present upstream the regulated gene initiation side, or downstream, within gene introns or at a distance to the gene itself. Ultimately, the level of transcription is determined by the combined action of TFs, coactivators and corepressors at the different *cis*-regulatory regions of a gene (Campbell et al.).

In the work highlighted in this thesis, knowledge from signalling and regulatory networks collected in OmniPath and DoRothEA has been used to study the effect of exposure to *Bifidobacterium* metabolites on intestinal epithelial cells function using colonic human organoids (**Chapter 4**). Furthermore, it has been used to reconstruct the inter- and intracellular signalling altered by SARS-CoV-2 infection in ileal and colonic human organoids (**Chapter 5**).

8.2.2. Non-coding RNAs

In addition to the regulation of gene transcription, post-transcriptional mechanisms can also be used to modulate gene expression levels. One example is represented by miRNAs, which are made of 22 nucleotides sequences of non-coding RNAs, and can post-transcriptionally regulate gene expression by binding to a (nearly) complementary mRNA sequence (Bartel, 2018). Following binding of miRNAs to their sequence, mRNAs are either degraded or

translationally repressed (Chapman and Pekow, 2015). Currently, almost 2,000 mature human miRNAs sequences are recorded in the miRbase (version 22.1) – the primary archive of miRNA sequences and annotations (Kozomara et al., 2019).

In addition to miRNAs, lncRNAs - defined as being more than > 200 nucleotides long non-coding RNAs - also exist, although their regulatory role is not fully clear (Goff and Rinn, 2015; Long et al., 2017). For some of them, it seems that their regulatory action is fulfilled by either recruiting protein complexes to DNA or by preventing TFs from binding to DNA. Additionally, they are able to block the binding of miRNAs (Jalali et al., 2013; Paraskevopoulou and Hatzigeorgiou, 2016) or modulate the post-transcriptional processing of mRNA, interfering with splitting factors and alternative splicing (Bhat et al., 2016).

In the work highlighted in this thesis, I will look at the effect of SARS-CoV-2 derived miRNAs on the function of intestinal epithelial cells by reconstructing intracellular signalling networks of SARS-CoV-2 infected human colonic organoids (**Chapter 5**).

8.3. Network contextualisation using ‘omics data

Network contextualisation methods can be used to construct biological networks by integrating context specific ‘omics data with experimentally determined molecular interactions (known as *a priori* interactions) (Dugourd and Saez-Rodriguez, 2019). For this purpose, transcriptomics is the most commonly used method, due to the limited availability and associated cost of the other types of ‘omics data (phosphoproteomics, metabolomics) (Dugourd and Saez-Rodriguez, 2019).

Because the activity of signalling pathways is only weakly correlated with gene expression levels (Vogel and Marcotte, 2012), molecular networks contextualised with transcriptomics data are generally used to investigate regulatory interactions, such as TFs regulating differentially expressed genes (DEGs). Once identified, these regulators can be further filtered using various strategies, such as (i) ranking regulators by the number of genes they target; (ii) hypergeometric significance tests to identify regulators targeting genes with the largest differential expression profiles, as implemented in the CHAT tool (Muetze et al., 2016); (iii) analytic rank-based enrichment analysis to compute transcription factor activity, as developed in VIPER (Alvarez et al., 2016).

Some methods have also been developed to predict the activity of signalling pathways contextualised with transcriptomics data, without directly inferring protein activity from gene

expression. One example is PROGENy, which uses a footprint based approach to predict pathway activity based on gene expression of pathway responsive genes, which were previously obtained during perturbation experiments (Schubert et al., 2018). However, this approach is limited to specific tested pathways and could be biased by the perturbation dataset used.

Finally, by combining contextualised signalling pathways and regulatory networks, causal networks can be constructed (**Figure 1.10**). These networks follow the signal from an internal/external perturbation affecting a membrane receptor, through intracellular signalling pathways to TFs which in turn regulate the expression of specific genes. Causal networks can be constructed by identifying the most likely PPI interactions connecting the upstream perturbation or affected receptor to the regulated TF downstream using 'omics data. One method, named Tied Diffusion Through Interacting Events (TieDIE) relies on diffusion algorithms that computes a subnetwork of gene and protein interactions connecting the upstream and downstream input perturbations. Conversely, another recently developed tool called CARNIVAL, can reconstruct causal networks with or without an upstream perturbation by combining VIPER and PROGENy using an integer linear programming optimization problem. Here, the most optimal PPI paths are identified using interaction direction and sign alongside perturbation, pathway and TF constraints (Liu et al., 2019).

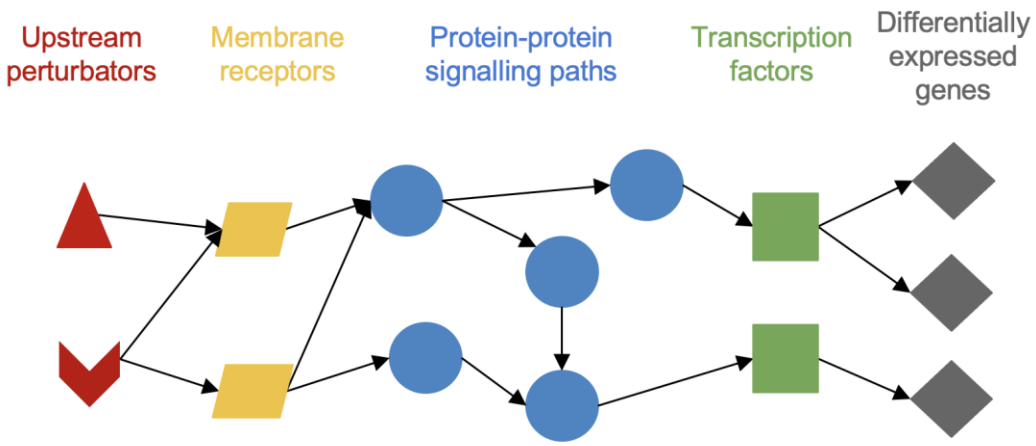

Figure 1.10. **Overview of causal molecular networks**. Molecular network representing the signalling cascade going from an upstream perturbation (e.g. a ligand binding to a membrane receptor) to the downstream perturbation (e.g. a TF regulating differentially expressed genes), through an intermediary protein-protein signalling network.

8.4. Network analysis and applications

Once constructed, the analysis of molecular interaction networks can help understand specific cellular processes, find perturbed functions, predict key regulators and novel drug targets (Miryala et al., 2018). Different methods exist to analyse molecular networks, including topology, modularity and functional enrichment.

Topology is the study of the arrangement and structure of a network (Winterbach et al., 2013). Topology measures such as “degree centrality” (the number of connections that a specific node has) or “betweenness centrality” (the number of shortest paths passing through a node when every pair of nodes is connected) can be used to define important nodes in a specific network. Furthermore, clustering methods can also identify different modules/clusters in a network by groups of highly interconnected nodes, which will often represent biological pathways or functions (Tripathi et al., 2016). Finally, functional analysis methods such as ClusterProfiler (Wu et al., 2021; Yu et al., 2012b) and ReactomePA (Fabregat et al., 2018; Gillespie et al., 2022) can help identify the functional role of the reconstructed set of interactions. Using these tools, networks are assigned functional annotations such as Gene Ontology (GO) (Ashburner et al., 2000)) or Reactome (Fabregat et al., 2018; Yu et al., 2012b). Subsequently, over-representation (or enrichment) analyses can be performed on the network to determine whether genes from pre-defined sets (i.e. characterised by a specific GO or Reactome annotation) are present more than would be expected by chance (over-represented) in the network.

9. Primary research aims

The main hypothesis behind this PhD research is that *Bifidobacterium*-derived metabolites can modulate epithelial cell function in the gut, thereby exerting a beneficial effect on the host. In particular, one mechanism thought to mediate these effects is represented by autophagy. To assess these hypotheses, I set up a series of research goals, which were addressed across the different chapters of this thesis:

1) Develop and optimise experimental protocols to establish intestinal epithelial cell models (mouse and human intestinal organoids, Caco-2 cells) and to expose them to bifidobacterial metabolites.

2) Develop experimental methodologies to evaluate changes in epithelial functions (autophagy, epithelial barrier, inflammation, gene expression) in mouse and human intestinal organoids upon exposure to bifidobacteria.

3) Assess the effects of bifidobacteria on barrier function, inflammation, and autophagy.

4) Develop computational methodologies to investigate the effect of bifidobacterial metabolites on host intestinal epithelial cells, using organoid transcriptomics data and network biology approaches

5) Use the developed experimental and computational methodologies to identify molecular interactions involved in the effect of bifidobacteria on epithelial cell function in the healthy human colonic epithelium.

6) As an additional goal (for the COVID-related project), use the developed computational methodologies to identify molecular interactions involved in viral-epithelial cell and epithelial cell-immune cell interactions in the human ileum and colon upon SARS-CoV-2 infection.

10. Thesis structure

This thesis is organised in 6 chapters:

- In **Chapter 1,** general concepts about the intestinal epithelium and the microbiome, autophagy, bifidobacteria, organoid models and network biology approaches will be discussed.
- In **Chapter 2**, a series of experiments with the aim of developing or optimising organoid-based and other *in vitro* models to investigate bifidobacteria-host interactions in the gut will be presented. In particular, these include methods to establish different organoid models, co-culture organoids with bifidobacteria, quantify the autophagy flux in epithelial cells, and to generate and analyse omics' data from these models.
- In **Chapter 3**, a study investigating the protective effects of bifidobacterial metabolite exposure on cell viability, barrier function, pro-inflammatory cytokine release and autophagy during gut inflammation in a Caco-2 cell model will be presented.
- In **Chapter 4**, a study exploring the molecular mechanisms behind bifidobacteria-host interactions in the gut using organoid models and network biology will be introduced.
- In **Chapter 5**, a separate study will be presented, focusing on the effects of SARS-CoV-2 infection on epithelial cell function and epithelial-immune interactions in the gut using human ileal and colonic organoids. This project is outside my PhD scope, making the thesis length longer than expected, and for this reason it can also be referred to as published article only.
- In **Chapter 6,** the main results of the previous chapters will be discussed, including future work, potential applications and impact of my thesis.

Chapter 2: Optimisation of organoid models and their applications to investigate bifidobacteria-interactions in the gut

1. Introduction

Organoid models represent a unique tool to study bifidobacteria-host crosstalk in the gut, overcoming some of the disadvantages associated with human studies, mouse models, and cell lines, as explained in **Chapter 1**. Furthermore, organoids allow repeated experiments to be performed, while maintaining organ, disease, and host characteristics (Dotti and Salas, 2018; Sato et al., 2011). Different organoid-based models can be employed to study bifidobacteria-host interactions in the gut and the related mechanisms; however several issues need to be addressed.

Organoids are closed structures, with the apical side of the epithelium, where most microbiota-epithelial interactions take place, projected inwards and not very easily accessible. Therefore, to expose the apical side of the epithelium, organoids can be grown as monolayers (**Figure 2.1A**). These organoids can be established by plating cell fragments derived from human small intestinal (Ettayebi et al., 2016; Foulke-Abel et al., 2014) or colonic (Wang et al., 2017) organoids onto an ECM-coated Transwell insert (Ettayebi et al., 2016; In et al., 2016; VanDussen et al., 2015). Using these models, bacterial cells or metabolites can be added directly apically to the culture media (Bartfeld and Clevers, 2015; Schlaermann et al., 2016; VanDussen et al., 2015). Alternatively, organoids can be grown with a reversed polarity ("apical-out") such that the apical side of the epithelium is facing outwards (**Figure 2.1B**) (Co et al., 2019; Co et al., 2021; Stroulios et al., 2021).

These novel models will present some advantages compared to standard organoid models. Organoid-derived monolayers allow the easy application of imaging techniques and a medium level of throughput. Conversely, apical-out organoids are more high-throughput, allowing to test the effect of several strains on the epithelium, but imaging can be more challenging due to the 3D structure (Poletti et al., 2021). Challenges also exist for the use of these models to study the effect of bifidobacteria on the epithelium. For organoid derived-monolayer, a significant amount of starting organoid material is required to establish them, and obtaining a confluent monolayer is sometimes challenging due to the specific culturing conditions required

(Poletti et al., 2021). For apical-out organoids, protocols for their establishment and characterisation are still in their infancy. Hence, optimisations are still required to ensure a complete polarity reversion is achieved, and to establish defined protocols to allow collection of other readouts, such as immunostaining and RNA extraction (Poletti et al., 2021; Stroulios et al., 2021).

When using any of these models for bifidobacteria-organoid co-culture, it is important to find the suitable environmental conditions that allow both organoids and bifidobacteria to cope well during the co-culture period. One of such requirements is the oxygen level, as bifidobacteria cells require an anaerobic environment for their metabolism and survival, while IECs require an aerobic one. Unless specialised equipment is used, such as the use of specific microfluidics devices or other adaptations (see **Chapter 1**), this cannot be done in Transwells or simple culture plates (Fofanova et al., 2019; Kim et al., 2019; Sasaki et al., 2020). For instance, within the human-microbial crosstalk module (HuMiX), anaerobic bacteria can be maintained in an (almost) anoxic compartment (Shah et al., 2016) **(Figure 2.1C).** Currently, Caco-2 cells have been used in HuMiX to model the epithelial layer (Shah et al., 2016). However, introducing human organoid-derived monolayers within HuMiX would make this device much more suitable to replicate bifidobacteria-host interactions in the gut happening *in vivo*, especially when looking at multi-omics readouts (Poletti et al., 2021).

Besides the different oxygen requirements, finding the optimal co-culture media to keep the bacterial and epithelial culture stable over time and support their metabolism, while maintaining cell viability, remains a challenge. In fact, bacterial media, such as the conventionally used De Man, Rogosa and Sharpe (MRS) broth, often contain components that damage mammalian cells (Allen-Vercoe, 2013). This implies the need for compromises in terms of the most optimal medium to be used during the co-culture, and finding the optimal co-culture medium for bifidobacteria and epithelial cells is indeed crucial to study the effect of bifidobacteria on the epithelium.

The goal of the work presented in this chapter is focused on the optimisation of these three different models (organoid-derived monolayers, apical-out organoids, introduction of organoid-derived monolayer in HuMiX) for the co-culture of bifidobacteria and epithelial cells. Furthermore, I aimed to determine the ideal medium to co-culture bifidobacteria with intestinal organoids. Subsequently, the best performing model and associated conditions would be used to assess the ability of selected bifidobacterial strains to modulate epithelial cell function in the gut exerting beneficial effects, and decipher the mechanisms involved. While these optimisation experiments were initially carried out on (mouse) small intestinal organoids,

subsequent experiments were done using (human) colonic organoids. The transition from small intestinal to colonic organoid models was due to the highest success in culturing mouse small intestinal organoids during the initial implementation phase, when human organoids were not yet available. In a later phase, once human organoids models were obtained, the focus was shifted to the colon, as this is more relevant to evaluate the effect of bifidobacteria as a probiotic treatment during adulthood in humans.

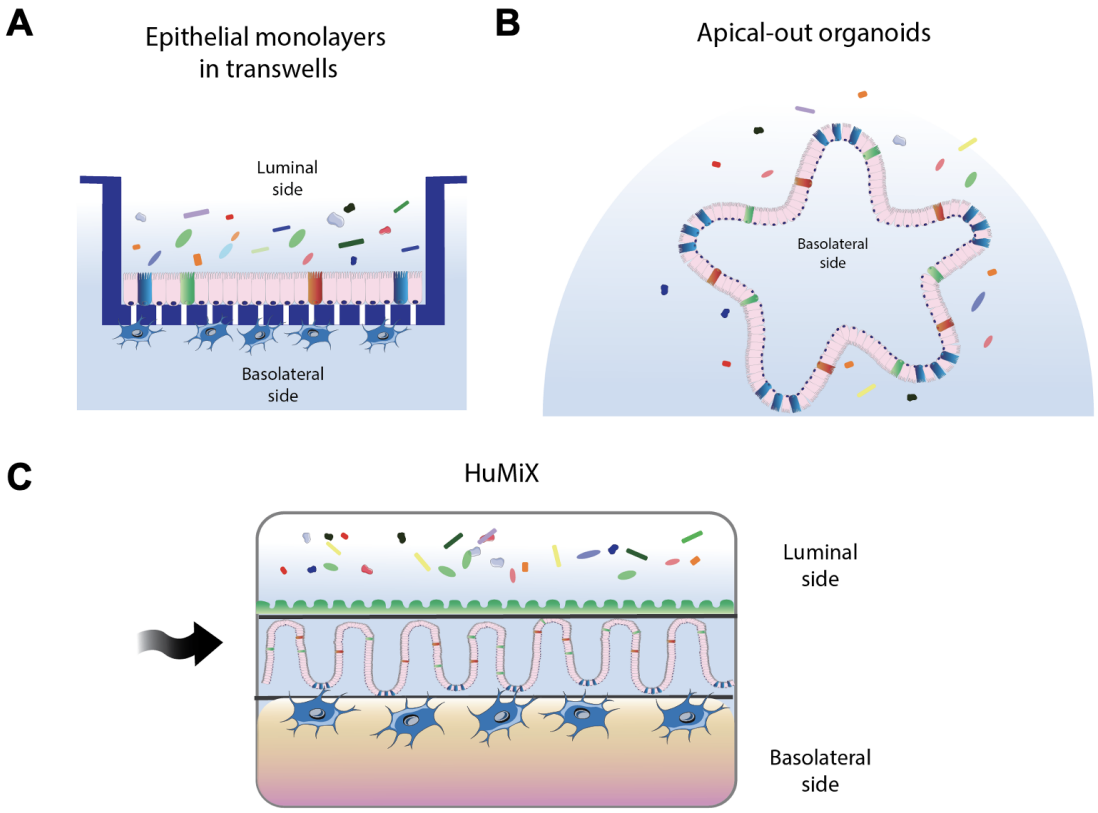

Figure 2.1. **Schematic overview of organoids and microfluidics models available to study host-microbe interactions in the gut**. **A)** Organoid-derived monolayers on Transwells. **B)** Organoids with reversed polarity ("apical out"). **C)** The human-microbial crosstalk module (HuMiX). Figure adapted from (Poletti et al., 2021).

To assess the effect of bifidobacteria on IECs, different parameters can be measured. One of the hypotheses of my PhD project is that some bifidobacterial strains can modulate autophagy, thereby improving intestinal cell function. Autophagy is an important mechanism for intestinal cell function (Lassen and Xavier, 2018) and it is often disrupted in diseases such as IBD (Shao et al., 2021). Autophagy can be assessed using different methods, one of which includes quantifying the number of LC3 and p62 puncta in the cell (see **Chapter 1**) (Seranova et al., 2019). This method has been successfully used to monitor autophagy in Caco-2 cell

monolayers. However, no method has been developed so far to identify and quantify the intracellular level of these proteins in (3D) human colonic organoids. P62 and LC3 immunostaining of organoid cultures presents multiple challenges including the 3D structure of organoids as well as the presence of different cell types with different levels of basal autophagy processes. Hence, in this chapter I aim to establish a protocol to assess autophagy by quantification of intracellular LC3 and p62 puncta in epithelial organoid cells by immunostaining.

Finally, to understand better the possible mechanisms of action underlying the effect of the function of IECs function, one way is to measure changes in gene expression profiles of IECs following exposure to bifidobacterial metabolites. For this purpose, it is important to optimise the RNA extraction protocol from organoids, determine the maximum amount of RNA that can be extracted, and establish how much initial organoid material is required for such experiments. Hence, in this chapter I illustrate a series of experiments I carried out to (i) optimise RNA extraction from mouse small intestinal and human colonic organoids using conventional kits, and (ii) determine the quality and quantity of RNA that can be extracted from different starting amounts of organoids.

2. Aims and objectives

In this chapter, I am going to describe different experiments with the goal of implementing the organoid model to study the effect of bifidobacteria and their metabolites on epithelial cell functions in the gut. To do so, I had a series of complementary goals:

1. Assess and further adapt protocols to establish and expand mouse intestinal and human intestinal organoids.

2. Evaluate different organoid-based models (organoid-derived monolayers, apical-out organoids, organoids within HuMIX) to find the most effective for the co-culture of bifidobacteria and host epithelial cells, including possible downstream applications (high-throughput experiments, confocal imaging, and transcriptomics).

3. Develop protocols to grow different bifidobacterial strains and to generate growth curves for the identification of the late exponential phase of bacterial growth for metabolites extraction.

4. Find the best media for epithelial-bacterial cell co-culture, by addressing three sub-goals:
    a. Assess whether conventional epithelial media could be used as a substitute for organoid media to reduce cost.
    b. Find media supporting bifidobacterial growth that also shows reduced cytotoxicity towards epithelial cells in organoids.
    c. Determine the amount of non-cytotoxic bifidobacterial media to use for exposure of organoids to bacterial supernatants.

5. Develop protocols to quantify autophagic proteins LC3 and p62 in intestinal organoids.

6. Develop protocols to extract high quality and high amounts of RNA from organoids for subsequent RNA sequencing experiments.

3. Methods

3.1. Mouse organoids establishment

Mouse ileal or duodenal organoids were established from C57BL/6J mice, following a previously described protocol (Jones et al., 2019; Sato and Clevers, 2013; Sato et al., 2009). Briefly, 5 cm pieces of ileal or duodenal tissue were collected, flushed to remove the intestinal content, and stored in ice-cold PBS. Fat/mesenteric tissue was removed, tissue portions were cut open and villi and excess mucus scraped off using a glass coverslip. Tissue portions were cut into segments of 5-8 mm long and collected in ice-cold phosphate buffered saline (PBS). Remaining villi fragments were washed off by vigorous shaking for 15 seconds in ice-cold PBS for 7-9 times or until the washing solution was clear. Intestinal crypts were dissociated from the tissue fragment following a 15 min incubation in Gentle Cell Dissociation Reagent (StemCell Technologies), at 37°C on a rocking platform (70-80 rpm). The crypt enriched fraction was collected by centrifugation at 300x g for 5 min at 4°C after removal of remaining tissue portions, and resuspended in ice-cold Advanced Dulbecco's Modified Eagle Medium/Nutrient Mixture F12, 15 mM HEPES (DMEM/F12, StemCell Technologies) or PBS for cell counting. Crypts were counted by eye under the brightfield microscope by placing a small drop (10 µl) on a Petri dish. The volume needed was collected in a pre-coated LoBind tube using a pre-coated pipette tip.

Collected crypts were subsequently spun down at 300x g for 5 min at 4°C, and resuspended in 50% Matrigel (Corning)/50% DMEM/F12 (StemCell Technologies) solution. Embedded crypts were plated into 40 µl bubbles onto a pre-warmed 24-well plate, and incubated for at least 20 minutes to let the Matrigel solution set. Organoids were fed with 500 µl Mouse Organoid Growth media (OGM) (Intesticult, StemCell Technologies) supplemented with 100 U/ml penicillin (P)/100 µg/ml streptomycin (S) and 10 µM Y-27632 (ROCK inhibitor; Tocris) per well and incubated et 37°C, 5% CO_2. Medium was replaced every 2 days. Y-27632 (Tocris) is added when plating intestinal crypts to improve cell attachment and reduce anoikis, but it was removed at the subsequent feeding.

3.2. Mouse organoid expansion and differentiation

After medium removal, organoids were collected in ice-cold Cell Recovery Solution (Corning). If the total volume exceeded 2 ml, organoid suspension was spun down for 5 min at 300x g at 4°C, and resuspended in 1.5 ml Cell Recovery Solution (Corning). Organoids were mechanically disrupted by pipetting several times using a pre-coated (2% Foetal Bovine Serum (FBS) in PBS solution) 1 ml pipette tip for 50 x, 200 µl tip for 50x and 20 µl tip for 50x and collected by spinning down for 5 min at 300x g at 4°C. Organoid fragments were

resuspended in 50% Matrigel (Corning)/50% DMEM/F12 (StemCell Technologies) solution and 40 µl organoid-containing domes were formed into each well of a pre-warmed 24-well plate, and incubated for at least 20 minutes to let Matrigel set. Organoids were fed with 500 µl mouse OGM (Intesticult, StemCell Technologies) supplemented with 100 U/mL/100 µg/mL P/S and 10 µM Y-27632 (Tocris) per well and incubated at 37°C, 5% CO_2. Medium was replaced every 2 days. Y-27632 (Tocris) is added after splitting to improve cell attachment and reduce anoikis, but it is removed at the subsequent feeding.

In this medium, mouse organoids differentiate spontaneously and the proportion of stem cells is low. Instead, to grow organoids in the stem cell-enriched form ("cystic"), 2 days after splitting, the media was changed to mouse Organoid Differentiation Medium (ODM) (Intesticult, StemCell Technologies) supplemented with 100 ng/ml Wnt3a (Bio-Techne), 10 mM Nicotinamide adenine dinucleotide (NAD) (Sigma) and 3 µM CHIR99021 (GSK-3 inhibitor, Tocris) for 3-4 days.

3.3. Human organoids establishment

Human colonic organoid cultures were established either from crypts isolated from patient biopsies, or from resuscitating cryovials containing organoids.
Patient biopsies were obtained through the Norwich Biorepository, an Human Tissue Authority (HTA) - licensed tissue bank, with ethics approval granted by the NHS Health Research Authority (HRA) (East of England-Cambridge East Research Ethics Committee) in March 2014 (reviewed in July 2018). Biopsies were collected at the NNUH endoscopy unit (Norwich, UK) after written informed consent from tissue donors, which was collected by a member of the biorepository team staff or appropriately-trained NHS staff. Use of human tissue samples for this project was approved by the Faculty of Medicine and Health Sciences Research Ethics Committee of the University of East Anglia (UEA) (Reference: 2017/18-113; project title: "*In vitro* culture and use of intestinal crypt-derived organoids from human intestinal biopsies as a patient-specific model to investigate host-microbe interactions and cell to cell communication").
Organoid lines were received in cryovials either from collaborators or purchased from Hubrecht Organoid Technology (HUB) biobank (Utrecht, The Netherlands). More details about the organoid lines used can be found in **Table 4.1**. Ethics statements relative to the human organoid lines are also reported in **Chapter 4**.

To establish organoid cultures from crypts isolated from patient biopsies, 4-6 biopsies were collected from healthy patients during routine endoscopy either at the University Hospitals

Leuven (Leuven, Belgium) or the Endoscopy Unit at the Norfolk and Norwich University Hospital (NNUH) (Norwich, UK). Biopsies were washed thoroughly in chelating solution (5.6 mM Na_2HPO_4, 8.0 mM KH_2PO_4, 96.2 mM NaCl, 1.6 mM KCl, 43.4 mM sucrose, 54.9 mM D-sorbitol, 0.5 mM DL-dithiothreitol) using a pre-coated (2% FBS in PBS solution) glass pipette. Next, biopsies were incubated for 45 minutes in a chelation solution supplemented with 2 mM ethylenediaminetetraacetic acid (EDTA) (Sigma-Aldrich) at 4°C on a rocking platform (70 rpm). Subsequently, biopsies were disrupted by rigorously pipetting with chelating solution using a pre-coated (2% FBS in PBS solution) glass pipette to loosen and collect the crypts. 10 µl of the crypt suspension was plated onto a Petri dish for crypt counting using a brightfield microscope.

To establish organoid cultures from frozen stocks, cryovials containing organoids were removed from liquid nitrogen storage and thawed quickly at 37 ºC in the incubator. Once thawed, they were diluted with ice-cold DMEM/F12 (StemCell Technologies). Organoid fragments were centrifuged at 300x g for 5 minutes and resuspended in ice-cold DMEM/F12 (StemCell Technologies). 10 µl of the organoid suspension was plated onto a Petri dish for crypt counting using a brightfield microscope.

3.4. Human organoid expansion and differentiation

Isolated crypts or organoid fragments were resuspended in 50% Matrigel (Corning) / 50% DMEM/F12 (StemCell Technologies) and 40 µl domes were formed into each well of a pre-warmed 24-well plate, and incubated for at least 20 minutes to let Matrigel set. To grow organoids in a stem-cell rich form (“cystic”), isolated crypts or organoid fragments were cultured in 500 µl human OGM (Intesticult, StemCell Technologies) supplemented with 100 U/mL/100 µg/mL P/S and 10 µM Y-27632 (Tocris) per well, and incubated et 37ºC, 5% CO_2. Medium was replaced every 2 days. Y-27632 was added after splitting to improve cell attachment and reduce anoikis, and removed at the subsequent feeding.

Organoids were passaged mechanically every 7-10 days, approximately. After medium removal, organoids were collected in ice-cold Cell Recovery Solution (Corning). If the total volume exceeded 2 ml, organoid suspension was spun down for 5 minutes at 300 g at 4ºC, and resuspended in 1.5 ml Cell Recovery Solution (Corning). Organoids were mechanically disrupted by pipetting several times using a pre-coated (2% FBS in PBS solution) 1 ml pipette tip for 50 x, 200 µl tip for 50x and 20 µl tip for 50x and collected by spinning down for 5 minutes at 300x g ar 4ºC. Organoid fragments were resuspended in 50% Matrigel (Corning) / 50% DMEM/F12 (StemCell Technologies), and 40 µl domes were formed into each well of a pre-warmed 24-well plate. Organoid fragments were cultured in 500 µl Human OGM (Intesticult,

StemCell Technologies) supplemented with 100 U/mL/100 µg/mL P/S +ad 10 µM Y-27632 (Tocris) per well and incubated at 37ºC, 5% CO_2.

In this medium, human organoids grow as cystic, where the proportion of stem and progenitor cells is relatively high. To grow organoids in a differentiated form, organoids were first expanded in 500 µl human OGM (Intesticult, StemCell Technologies) in each well of a 24-well plate. 3-4 days after splitting, the media was removed, organoids washed with PBS and 500 µl of human ODM (Intesticult, StemCell Technologies) was added to each well. Media was replaced every 2 days.

3.5. Human organoid cryofreezing

Human colonic organoids were grown in human OGM (Intesticult, StemCell Technologies). Mouse ileal organoids were grown in mouse OGM (Intesticult, StemCell Technologies) supplemented with 3 µM CHIR99021 (Tocris), which further preserved organoids in a stem-cell enriched form. Organoids were passaged as described above. The content of 3 wells of organoids (24-well plate) were collected into a 15 ml LoBindtube (Merck), centrifuged for 5 min at 300x g, and resuspended in 1 ml CryoStor® CS10 freezing medium (StemCell Technologies) by slowly pipetting up and down with a pre-coated (2% FBS in PBS solution) tip. Subsequently, organoid fragments were transferred into a cryovial, frozen slowly in isopropanol at -80 ^{0}C for one day, and subsequently transferred to liquid nitrogen for long term storage.

3.6. Organoid-derived monolayer establishment

3.6.1. On Transwells

To establish organoid monolayers, I used a method adapted from (VanDussen et al., 2015). This protocol was carried out at the facilities of collaborators (KU Leuven, Belgium). Briefly, human intestinal organoids were first expanded as 3D organoids in a 24-well plate, maintaining a dense culture of 150-200 organoids per well. Organoids were expanded in 500 µl human OGM (Intesticult, StemCell Technologies) per well or an equivalent made in-house (from KU Leuven collaborators) for 3-4 days. One day prior to monolayer establishment, Transwell inserts (6.5 mm, 0.4 µm) (Costar) were coated with 0.1 mg/ml collagen (Corning) in acetic acid solution and incubated at 37 ^{0}C overnight. On the seeding day, collagen-coated Transwell inserts (6.5 mm, 0.4 µm) (Costar) were washed with PBS to remove excess collagen solution for 2-3 times. If seeding was not performed immediately, 100-200 µl PBS was added on top to avoid drying and inserts incubated at 37 ^{0}C until seeding. Coated inserts were also

prefused with 50% human OGM (Intesticult, StemCell Technologies) / 50% DMEM/F12 (StemCell Technologies) (supplemented with 100 U/mL/100 µg/mL P/S and 10 µM Y-27632 (Tocris) and incubated at 37ºC for at least 30 minutes prior to seeding. Organoids were passaged as above mentioned, incubated with 1 ml TryPLE Express Enzyme (Fisher Scientific) for 5-7 minutes at 37ºC until cells were dissociated into fragments of 2-3 cells but not as single cells. 7-10 ml DMEM/F12 (StemCell Technologies) supplemented with 10% FBS was added to stop the dissociation. Cells were counted using a hemocytometer. Subsequently, cells were collected by centrifuging at 300 g for 5 minutes at 4ºC, and resuspended in human ODM (Intesticult, StemCell Technologies) supplemented with 100 U/mL/100 µg/mL P/S and 10 µM Y-27632 (Tocris). 100 µl of the organoid cell suspension was added to each of the coated Transwell inserts (6.5 mm, 0.4 µm) (Costar) and 600 µl of human ODM (Intesticult, StemCell Technologies), supplemented with 100 U/mL/100 µg/mL P/S and 10 µM Y-27632 (Tocris), was added to the basal compartment of the well. Medium was refreshed after 24 hours, by adding 200 µl fresh human ODM (Intesticult, StemCell Technologies) without Y-27632 (Tocris) to the apical compartment and 600 µl Human ODM (Intesticult, StemCell Technologies) to the basolateral compartment. Medium was changed every 2 days, and organoid monolayer differentiation was followed by measuring transepithelial electrical resistance (TEER) or under the brightfield microscope prior to medium change.

3.6.2. Onto HuMiX membrane

The HuMiX epithelial membrane was received from collaborators at the Wilmes group (University of Luxembourg), and pre-cut into a smaller disc (0.96 cm^2) using a precise cutter. Each membrane was coated with 0.1 mg/ml collagen (Corning) in acetic acid solution and incubated at 37ºC overnight. On the next day, collagen-coated membranes were washed with PBS to remove excess collagen solution for 2-3 times, and incubated with 100-200 µl PBS at 37ºC prior to seeding to avoid drying.

Organoids were passaged as previously explained, and subsequently incubated with 1 mL TryPLE Express Enzyme (Fisher Scientific) for 5-7 minutes at 37ºC until cells were dissociated into clumps of cells (2-3 cells). 7-10 ml DMEM/F12 (StemCell Technologies) supplemented with 10% FBS was added to stop the dissociation. Cells were counted using a hemocytometer. Cells were collected by centrifugation at 300x g for 5 minutes at 4ºC, and resuspended in human ODM (Intesticult, StemCell Technologies) supplemented with 100 U/mL/100 µg/mL P/S and 10 µM Y-27632 (Tocris). 500 µl of the organoid cell solution was added to each well. Medium was refreshed 24 hours post-seeding, by adding 200 µl fresh Human ODM (Intesticult, StemCell Technologies) without Y-27632 (Tocris). Subsequent medium changes were performed every 2 days, and organoid monolayer formation was monitored under a brightfield

microscope and polarity confirmed by staining for the presence of tight junctions (anti-ZO1), mucus (anti-MUC2) and cell nuclei (DAPI). A more detailed explanation of this immunostaining can be found in the 'Organoid-derived monolayers on Transwells' paragraph of this methods section.

3.7. Organoids with reversed polarity ("apical-out") establishment

To establish organoids with reversed polarity ("apical out"), I used an adapted protocol from (Co et al., 2019)**.** Briefly, mouse ileal organoids or human colonic organoids (healthy) were grown mouse or human OGM (Intesticult, StemCell Technologies) supplemented with 100 U/mL/100 µg/mL P/S, 10 µM Y-27632 (Tocris) and 3 µM CHIR99021 (Tocris). 3 days after passaging, organoids were removed from Matrigel (Corning) by incubation of the organoid bubbles with 0.5 mM ice-cold EDTA (Sigma-Aldrich) solution in PBS for 1 h at 4ºC on a rolling platform (100 rpm). Subsequently, organoids were pelleted by centrifugation 150-200x g for 3 minutes, resuspended in mouse or human OGM (Intesticult, StemCell Technologies) supplemented with 100 U/mL/100 µg/mL P/S, 10 µM Y-27632 (Tocris) and 3 µM CHIR99021 (Tocris). 400 µL of the organoid suspension was transferred in each well of a 24-well ultra-low attachment plate (Corning, Costar) and organoids were grown in suspension at 37ºC, 5% CO_2 for 3 days. One day after seeding, a partial medium change was performed by removing 300 µl and adding 300 µl of fresh mouse or human OGM medium (Intesticult, StemCell Technologies) supplemented with 100 U/mL/100 µg/mL P/S. On day 3, organoids were washed several times to get rid of the excess mucus and dead cells, and resuspended in fresh mouse or human OGM medium (Intesticult, StemCell Technologies) or DMEM/F12 (StemCell Technologies) for further applications (e.g immunostaining).

3.8. Immunostaining of organoids

3.8.1. Organoids embedded in Matrigel

For the immunostaining of organoids embedded in Matrigel, two different procedures were adopted. In the initial set-up, organoids were removed from Matrigel (Corning) and staining steps were performed on the organoid pellet only. Briefly, Matrigel (Corning) was dissolved by incubation with Cell Recovery Solution (Corning) for 1 h on ice on a rolling platform (70 rpm). Subsequently, organoids were transferred into a pre-coated (2% FBS in PBS solution) Low-bind 1 ml tube (Merck) and spun down at 200x g for 3 minutes at 4°C (or left to sediment at 37ºC). Subsequent steps were performed after removal of the supernatant on the organoid pellet. In a later set-up, organoids were stained without prior removal from Matrigel. Briefly, the day before or a few hours before organoid seeding, 1 µm thick round glass sterile coverslips were placed into each well of a 24-well plate and the entire plate warmed at 37ºC.

Following passaging, organoid fragments embedded in Matrigel were seeded directly onto the glass coverslip and grown in mouse or human OGM (Intesticult, StemCell Technologies) for 3-5 days. Human colonic organoids were further differentiated for 3-4 days prior to treatment and/or immunostaining. Subsequent steps were performed directly in each well of the 24-well plate. Primary and secondary antibody labelling was performed by inverting the coverslip onto a drop of antibody solution. Successful staining was achieved for the following components: brush border using phalloidin-iFluor488 (1:500, Abcam) or mouse anti-EpCAM (1:250-1:500, Abcam), tight junctions using mouse anti-ZO1 - iFluor488 (1:250-1:500, Invitrogen) and proliferating cells using the EdU assay-iFluor488 (Abcam) or rabbit anti-Ki67 (1:250-1:500, Abcam). Autophagy proteins were also successfully identified using goat anti-p62 (1:250-500, Abcam) or mouse anti-p62 (1:250-500, Invitrogen), and goat anti-LC3 (1:250-500, Abcam).
After staining was completed, organoids were mounted by adding a small amount of Aqua-Poly/Mount (Polysciences Europe GmbH) to the organoid pellet, and embedded organoids were dispensed on the cavity formed by a spacer onto a microscopy slide (to maintain the 3D structure of the organoids). Mounted organoids were covered with a glass coverslip and sealed with nail varnish. Representative images of organoids were collected using a LSM880 confocal microscope with AiryScan (Zeiss), using 63x oil immersion lens.

3.8.2. Organoid-derived monolayers on Transwells

The immunostaining of organoid-derived monolayers on Transwells was performed by our collaborator Dr. Kaline Arnauts (KU Leuven, Belgium). Briefly, the membrane of the Transwell insert (6.5 mm, 0.4 µm) (Costar) was cut-out of the plastic support using a surgical blade, and placed into a 24-well plate. Next, monolayers were washed with PBS, followed by fixation with 4% paraformaldehyde (PFA) solution (Merck) for 20 minutes at 37°C. Monolayers were subsequently washed three times with 70% ethanol and kept at 4°C until further processing.

Immunofluorescence staining was performed as described earlier using antigen retrieval in sodium citrate buffer (Vancamelbeke et al., 2019; Vanhove et al., 2018). Primary antibody staining was performed using mouse anti-ZO1 antibody (1:50, Thermo Scientific) and rabbit anti-MUC2 (1:150, Santa Cruz Biotechnology), while secondary antibody staining was performed using goat anti-mouse antibody (1:1000; Alexa Fluor 488, ThermoFisher Scientific) and donkey anti-rabbit antibody (1:1000; Alexa Fluor 594, ThermoFisher Scientific). Monolayers were also counterstained with DAPI (1:1000-2000, ThermoFisher Scientific) to identify nuclei. Stainings were visualised with a BX41 microscope (Olympus, Tokyo, Japan). Bright field images were made using a SC30 camera whereas the immunofluorescence images were made using a XM10 camera. To evaluate the polarity of the epithelial cell monolayers, Z-stack images were obtained from immunofluorescent-stained whole mount

monolayers on a Zeiss LSM 880 Airyscan (Carl Zeiss Inc, in collaboration with the Lab for Enteric NeuroScience, KU Leuven). Image processing was done using Fiji software (ImageJ).

3.8.3. Apical-out organoids

For the immunostaining of apical-out organoids, organoids grown in suspension were transferred into a pre-coated LoBind 1 ml tube (Merck), spun down at 200x g for 2-3 minutes at 4°C (or left to sediment at 37°C). The supernatant was removed and organoids were fixed with 4% PFA (Merck), permeabilized with 3% Bovine Serum Albumin (BSA) (Sigma Aldrich) + 1% Triton-X-100 (Sigma), stained with DAPI (1:1000, ThermoFisher Scientific) and phalloidin-iFluor488 (1:500, Abcam) in blocking buffer (3% BSA) to stain for nuclei and brush border, respectively.

3.9. Immunostaining of autophagy proteins p62 and LC3

For LC3 and p62 immunostaining, organoids were fixed with 4% PFA (Merck) for 30-60 minutes at 37^0C with gentle shaking (70 rpm). For LC3 staining, organoids were permeabilized with methanol for 10 minutes at 37^0C and subsequently blocked with 1% BSA (Sigma Aldrich) in PBS. For p62 staining, organoids were permeabilized and blocked with 1% BSA (Sigma) + 0.1% saponin (Sigma) in PBS solution. For LC3 staining only, organoids were subsequently quenched with 50 mM NH_4Cl in PBS for 30 minutes at 37^0C. Organoids were stained with goat anti-p62 (1:250-500, Abcam), goat anti-LC3 (1:250-500, Abcam) antibodies solution in 1% BSA in PBS (LC3) or 1% BSA + 0.1% saponin (p62) overnight at 4^0C. Here, a different set of samples was used to stain for p62 and LC3 if antibodies raised in the same species (goat) were used. Antibodies dilution was dependent on the amount and type (human, mouse) of organoids stained. The following day, organoids were washed and secondary antibody goat anti-rabbit Alexa Fluor 594 (1:250, ThermoFisher Scientific) prepared in 1% BSA in PBS (LC3) or 1% BSA + 0.1% saponin in PBS (p62) was also applied for 2 hours at 37^0C to each set of samples. Samples were also counterstained by adding phalloidin-iFluor488 (1:500, Abcam) and DAPI (1:500, ThermoFisher Scientific) to the secondary antibodies solution to visualise the cell shape and nuclei.

This protocol was further implemented by myself using anti-p62 antibodies raised in different species. Briefly, organoids were fixed with 4% PFA (Merck) for 30-60 minutes at 37^0C with gentle shaking (70 rpm). Organoids were permeabilized with methanol for 10 minutes at 37^0C, washed 3 times with PBS, quenched with 50 mM NH4Cl in PBS for 30 minutes at 37^0C, and washed again twice with PBS. Subsequently, organoids were blocked with 5% BSA in PBS for 1 h with gentle shaking (70 rpm) and washed twice with 0.1% BSA solution. Organoids were stained with mouse anti-p62 (1:250-500, Invitrogen) and goat anti-LC3 (1:250-500,

Abcam) antibodies solution in 0.1% BSA in PBS overnight at 4^0C. Antibodies dilution was dependent on the amount and type (human, mouse) of organoids stained. The following day, organoids were washed and secondary antibodies goat anti-rabbit Alexa Fluor 594 (1:250, ThermoFisher Scientific), goat anti-mouse Alexa Fluor 488 (1:250, Abcam) in 0.1% BSA in PBS were applied for 2 hours at 37 ^{0}C. Samples were also counterstained by adding Alexa Fluor 660 phalloidin (1:500, ThermoFisher Scientific) and DAPI (1:500, ThermoFisher Scientific) to the secondary antibodies solution to visualise the cell shape and nuclei.

In both set-ups, after staining was completed, organoids were washed once with 1% BSA (LC3 only), 1% BSA + 0.1% saponin (p62 only) or 0.1% BSA (LC3 and p62 together), once with PBS and once with dH_20 for 5 minutes with gentle shaking (70 rpm). Subsequently, organoids were mounted by adding a small amount of Aqua-Poly/Mount (Polysciences Europe GmbH) to the organoid pellet, and embedded organoids were dispensed on the cavity formed by a spacer onto a microscopy slide (to maintain the 3D structure of the organoids). Mounted organoids were covered with a glass coverslip and sealed with nail varnish. Representative images of organoids were collected using a LSM880 confocal microscope with AiryScan (Zeiss), using 63x oil immersion lens.

3.10. Quantification of autophagy by identification of p62 and LC3 puncta

Representative images of antibody-labelled organoids were collected for each condition using a LSM880 confocal microscope with AiryScan (Zeiss), 63x oil immersion lens. Cell segmentation and quantification of p62 and LC3 puncta was performed using the Imaris cell imaging software (Oxford Instruments). Briefly, a batch analysis was set-up to analyse multiple images. First, pre-processing of the images was applied to improve the phalloidin staining for the cell border, by applying a gaussian filter (0.05) and a gamma correction (1.5). Next, the “Cell module” was used to segment individual cells using the green channel (phalloidin-iFluor488) as cell border marker for cytoplasmic identification. In particular, a cell size of 5 µm and membrane detail of 0.9 µm and local contrast as filter type were used for the analysis. Subsequently, any object touching the border was removed. As part of the “Cell module”, p62 and LC3 puncta were identified as vesicles using the red channel (Alexa Fluor 594), a 0.6 µm as puncta diameter and using the background subtraction method. Statistics were exported for each batch analysis as a .csv file. For both p62 and LC3, data about the mean signal intensity and number of vesicles per segmented object/cell was used to quantify LC3 or p62 puncta (autophagosomal structures) signal for each condition.

3.11. RNA extraction from organoids

3.11.1. Preparation of cell lysates

Mouse ileal or human colonic organoids were grown in mouse or human OGM (Intesticult, StemCell Technologies), as previously described. For RNA extraction, 500 µl of Cell Recovery Solution (Corning) was added to each well and plates incubated on ice for 20 minutes on a shaking platform (70 rpm). Using a pre-coated P1000 pipette (2% FBS in PBS), organoids were transferred into a 15 ml LoBind tube (Merck), pooling 1, 2 or 3 wells for each technical replicate together. Organoid suspensions were collected by centrifugation for 3 minutes at 300x g, and washed once with 1 ml PBS. Cells were lysed with 350 µl of lysis buffer (provided by the RNA extraction kit) supplemented with 0.1 mM 2-mercaptoethanol (2-ME), vortexed and stored at -20^{0}C for at least 2 hours prior to RNA isolation.

3.11.2. RNA extraction

RNA was extracted using commercially available kits RNAesy (QIAGEN) and Isolate II RNA Mini (BIOLINE) following manufacturers' instructions. Briefly, cell lysates were filtered by running the samples through a spin column followed by centrifugation (for BIOLINE kit only) and purified by adding a 1:1 volume of 70% ethanol, and mixed by pipetting. Next, RNA was collected by running the sample through a spin column followed by centrifugation. RNA was bound to the silica membrane by adding a provided buffer followed by centrifugation. An additional DNAse I digestion step was performed by adding DNase I (RNase-Free DNase Set, QIAGEN) to the spin column membrane, and incubating for 15 minutes at 37^{0}C. RNA was washed repeatedly by addition of the provided washing buffer followed by centrifugation. Finally, RNA was eluted by adding 60–80 µl RNAse-free water (provided by the RNA isolation kit) (in two times) to the spin column membrane followed by centrifugation.

3.11.3. Ethanol precipitation

Following RNA extraction, an additional ethanol precipitation step was performed to further concentrate and de-salt the isolated RNA samples. Briefly, sample volumes were brought to a 300 µl minimum by adding RNAse free water. Subsequently, 1 µl glycogen, 1:10 volume of 3M sodium acetate and two volumes of 96 % ethanol were added to the samples. Samples were mixed by inversion and placed at -80ºC for at least 16 hours. The following day, samples were centrifuged at 13,000x g at 4ºC for 30 minutes, supernatants discarded, and pellets washed with 70% ethanol for 5 minutes. Subsequently, samples were centrifuged at 13,000x g at 4 ºC for 20 minutes, and pellets dried to remove the remaining ethanol. Once pellets were

dried, RNA was re-hydrated by adding 30 µl of RNAse-free water and incubating on ice for 5 minutes.

3.11.4. Nanodrop and Qubit measurements

The quality and quantity of RNA was measured on a Nanodrop using the RNA50 for Nucleic acids program. In parallel, RNA was also quantified using the Qubit kit and Qubit 3 instrument following the standard kit instructions. Briefly, two tubes of standards and one tube for each sample were prepared by mixing standard RNA samples or experimental samples to the Qubit™ working solution (Qubit reagent diluted 1:200 in Qubit buffer) to obtain a final volume of 200 µl. Tubes were vortexed for 2-3 seconds and incubated for 2 minutes at 37ºC before measurements. RNA was quantified by measurement with a Qubit Fluorometer. Standard curves were prepared using the RNA of the standards, and subsequently used to determine the RNA concentration in each sample.

3.12. Cytotoxicity assay

Cytotoxicity was evaluated by measuring the amount of lactate dehydrogenase (LDH) released by organoids in the medium using the CytoTox 96® Non-Radioactive Cytotoxicity Assay kit (Promega). Measurements were performed following the manufacturer's instructions. Briefly, after organoid treatment, culture supernatant was transferred to a V-bottom 96-well plate (Greiner CELLSTAR®, Sigma), spun down at 300x g for 5 minutes to remove remaining cells, and 50 µl was transferred to a flat-bottom 96-well plate. To perform cytotoxicity measurements, an equal volume of CytoTox 96® Reagent (Promaga) was added to each well and incubated for 30 minutes. During this enzymatic assay, the tetrazolium salt substrate (violet) is converted into a formazan product (red), where the amount of colour formed is proportional to the number of lysed cells. After 30 minutes, 100 µl of stop solution (Promega) was added to each well to stop the reaction, and the absorbance signal at 490 nm was measured immediately using a standard 96-well plate reader. Lysed cells were used to find the maximum LDH released (maximum cytotoxicity). Cytotoxicity was expressed as a percentage of the maximum toxicity.

3.13. Culturing Bifidobacterial strains

Bifidobacterium breve UCC2003 (**Table 2.1**) was streaked from frozen glycerol stocks into pre-reduced Robertson's Cooked Meat (RCM) (supplemented with 0.05% (wt/vol) L-cysteine HCl) and incubated in the anaerobic cabinet at 37ºC for 2-3 days. 3-4 isolated colonies were inoculated into RCM liquid broth (supplemented with 0.05% (wt/vol) L-cysteine HCl), and grown in the anaerobic cabinet at 37 ºC for one day. Subsequently, cultures were diluted 20-

fold into De Man, Rogosa and Sharpe (MRS) broth (supplemented with 0.05% (wt/vol) L-cysteine HCl) and incubated in the anaerobic cabinet at 37ºC for 15-16 hours.

Table 2.1. *B. breve* UCC2003 characteristics.

Isolate	Strain designation	Relevant feature	Genome size (bp)	Accession number	Reference
UCC2003	*B.breve*	Isolate from nursling stool (expressing UCC2003 EPS)	2,422,684	CP000303	(Mazé et al., 2007)

3.14. Bacterial growth curves

To assess bacterial growth in different media combinations, cultures pre-grown in MRS were diluted 100-fold into the following media conditions: 100% epithelial media (DMEM/F12, StemCell Technologies), 100% organoid medium mouse OGM (Intesticult, StemCell Technologies), 50% bacterial media MRS/50% DMEM/F12 (StemCell Technologies) or PBS alone. Bacterial cultures were incubated in the anaerobic cabinet at 37ºC, and bacterial growth was measured over time (0-21 hours) by optical density (ΔOD_{600}) measurements. 3 biological replicates were used for each condition.

4. Results

4.1. Optimisation of protocols to establish mouse and human organoid cultures

As described in the introduction of this chapter, organoid-based models represent a useful tool to study the effect of bifidobacterial metabolites in the gut. The initial goal of my PhD was to successfully establish cultures of mouse and human organoids that could be expanded enough to obtain the required starting material for subsequent experiments. Additionally, establishing an attainable alternative to the standard culturing protocol to achieve fully differentiated or stem-cell enriched organoids cultures was an important step to assess the effect of bifidobacteria during epithelial differentiation. Subsequently, protocols to cryopreserve organoids needed to be optimised too, as this would be important to establish organoid cultures without relying on the availability of intestinal tissue portion or patient biopsy. This is particularly relevant for patient biopsies, as the access to the initial material is more rare. Once organoid cultures were obtained, further characterisation of the presence of a brush border, tight junctions and major IEC populations was important to ensure they were properly modelling the intestinal layer observed *in vivo.*

Mouse ileal and duodenal organoid cultures were successfully established from intestinal crypts isolated from mouse (C57BL/6 mice) intestinal portions (**Figure 2.1A,** and Methods). Initial attempts to establish these cultures resulted in a very low organoid density in each well, and subsequent loss of organoids during each passaging step (**Figure 2.1B**). However, an improvement was achieved by increasing the amount of intestinal crypts seeded during organoid establishment (from 250 to 500) as well as the amount of organoid fragments seeded in each well after organoid passaging (from 150 to 200-250) **(Figure 2.1C)**.

When grown in standard medium (mouse OGM), mouse ileal/duodenal organoids grow in a fully differentiated form. A variation of the standard protocol was also implemented to obtain mouse ileal organoids grown in a stem-cell enriched form (**Figure 2.1D,** and Methods). This optimisation included growing organoids in standard medium (mouse OGM) until a big enough size was reached (2-3 days), but without the presence of visible budding (indicating differentiation of the epithelium). Subsequently, the standard media was supplemented with Wnt3a, NAD and CHIR99021 (GSK-3 inhibitor) for 3-4 days, which combined promote stem cell proliferation while blocking further epithelial differentiation.

Finally, cryofreezing of mouse organoids was also troubleshooted several times using mouse organoid cultures grown in standard medium (mouse OGM), but the yield of organoid resuscitation from frozen stocks was generally low. Nevertheless, a small improvement in yield was obtained when cryofreezing mouse organoid cultures previously grown in the stem-enriched form.

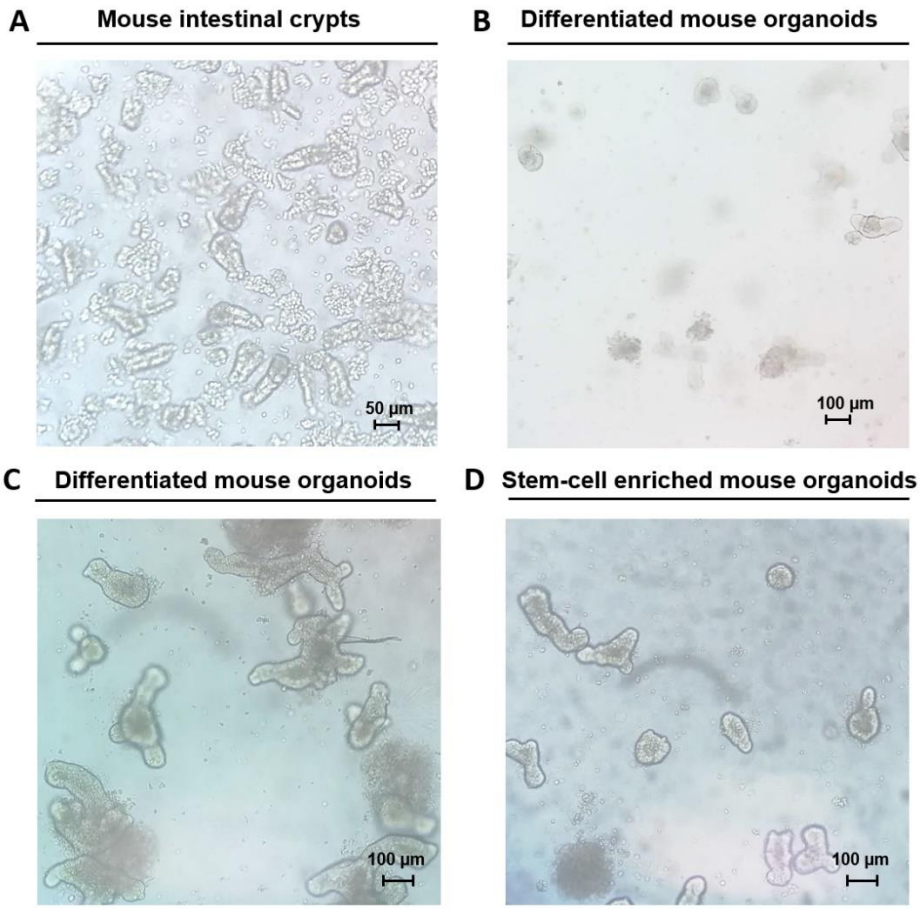

Figure 2.2. **Mouse ileal organoids culture. A)** Brightfield microscopy image of intestinal crypts isolated from mouse ileal tissue. **B, C)** Brightfield microscopy images of differentiated mouse intestinal organoid cultures grown in Matrigel and fed with mouse OGM for 5 days. Images refer to cultures with poor (B) or good (C) recovery, respectively. **D)** Brightfield microscopy image of stem-cell enriched organoid cultures grown in Matrigel and fed with mouse OGM medium for 2-3 days, followed by supplementation with 100 ng/ml Wnt3a, 10 mM NAD and 3 µM CHIR99021 for 3-4 days.

Human colonic organoid cultures were established from intestinal biopsies either from UC patients (KU Leuven hospital, Belgium) or from healthy patients obtained through the NNUH Endoscopy Unit (Norwich, UK). As described in the Methods, intestinal crypts were first isolated from 4-6 biopsies, and subsequently embedded in Matrigel and grown in human OGM for 7-10 days. During initial attempts, similar to what was achieved for mouse organoid

cultures, the density of human colonic organoids was relatively low, due to the low yield of crypt isolation from patient biopsies. Indeed, one critical step identified was the seeding density for intestinal crypts, which was optimised at 6-8 crypts per well. If too scarce, not enough organoids would be obtained for organoid passaging (where the organoid density needs to be high for a high yield) **(Figure 2.3A)**. On the contrary, if the density was too high, this would result in cell loss due to the lack of stem cell niche factors (from the media) reaching the cells **(Figure 2.3B)**. Because of the initial low yield of crypt isolation, it was difficult to maintain organoid cultures for longer than 3-4 weeks. Finally, contamination of the organoid culture was often encountered 2-3 weeks after organoid establishment. In the case of healthy colonic organoids, because of the scarce availability of intestinal biopsies from the NNUH (Norwich UK), the establishment protocol could be repeated only a few times, which made it difficult to achieve enough starting organoid material for further applications. During a collaboration with KU Leuven (Belgium), this protocol was tested again on UC biopsies leading to the successful development of UC colonic organoid cultures.

Because of the issues encountered in Norwich in sourcing intestinal biopsies, we decided to expand organoid cultures from previously-established frozen stocks, either purchased from the HUB biobank (Utrecht, The Netherlands) or provided as part of another collaboration effort (King's College London, UK). When established from frozen stocks, healthy or UC organoids were successfully grown over multiple passages, and expanded to allow cryofreezing and further applications (**Figure 2.3C**).

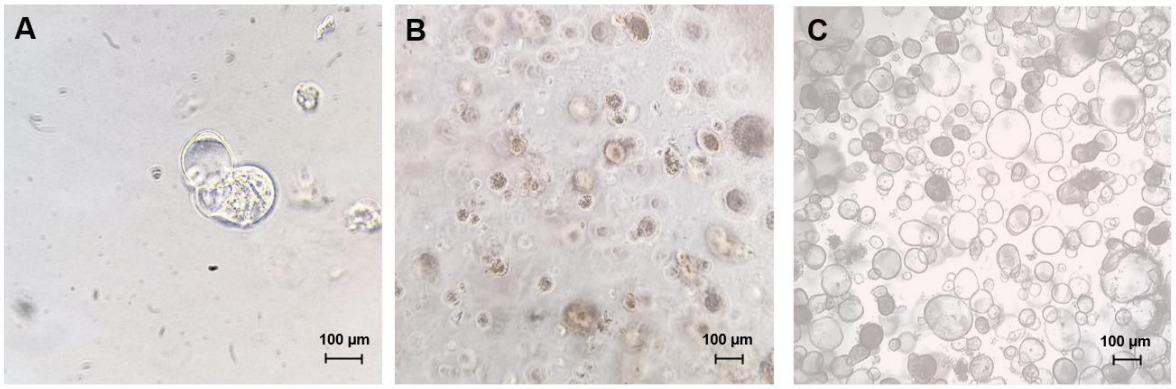

Figure 2.3. Human colonic organoids culture. A, B) Brightfield microscopy image (20X) of human colonic organoid cultures with poor recovery, either due to the too low (A) or too high (B) seeding density. Organoids were established from colonic crypts isolated from biopsies of healthy patients, and subsequently grown embedded in Matrigel and fed with human OGM for 5 days. **C)** Brightfield microscopy image (20X) of human colonic organoid cultures with good recovery. Organoids were established from frozen vials and subsequently grown embedded in Matrigel and fed with human OGM for 5 days.

4.2. Optimisation of protocols to establish organoid-derived monolayers

Once (3D) mouse and human organoid cultures were successfully established and characterised, the next objective was to develop protocols to generate organoid-derived monolayer. As mentioned in **Chapter 1**, organoid-derived monolayers are a better model to study the effect of bifidobacterial metabolites on epithelial function, as the apical side of the epithelium is more accessible. To establish organoid-derived monolayers, organoids were first grown embedded in Matrigel, and subsequently fragmented into small clumps of cells and plated on a collagen-coated Transwell (**Figure 2.4**).

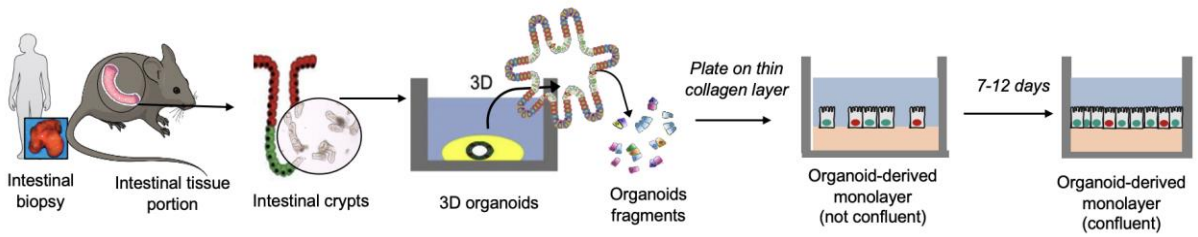

Figure 2.4. Steps for the generation of organoid-derived monolayers. Mouse intestinal tissue or biopsies obtained from a patient donor are used to obtain intestinal crypts through a series of washing steps. Intestinal crypts are embedded in Matrigel and grown in expansion media (mouse or human OGM) to generate organoid cultures. Organoids are expanded until enough material is obtained. Subsequently, organoids are broken down into small fragments and plated on a collagen coated Transwells or flat bottom plates. Organoid cells are subsequently grown in differentiation media (mouse or human ODM) for 7-10 days, after which they will give rise to a confluent and differentiated monolayer.

For mouse organoids, attempts to establish organoid-derived monolayers were not successful. Although enough starting material of organoid fragments was obtained from splitting organoid cultures and enough fragments (~200) were seeded on top of the coated Transwells insert, organoids would die off a few days after seeding.

For human organoids, organoid-derived monolayers were achieved thanks to a collaboration with the Vermeire group (KU Leuven, Belgium), with the work being carried out together with Dr. Kaline Arnaut, a current Postdoc in this group. As part of this collaboration, colonic or ileal organoid-derived monolayers on Transwells were established from organoid cultures derived from patient biopsies. Following successful crypt isolation (**Figure 2.5A**), organoid cultures were established and expanded by feeding them with an in-house organoid growth medium until the desired number was achieved (**Figure 2.5B**). Subsequently, a single cell suspension was obtained and plated onto collagen coated Transwell inserts on a 24-well plate (**Figure 2.5C**). Here, the critical step was to ensure enough cells (~600) were plated in each Transwell

so that most surface was covered prior to differentiation (**Figure 2.5C**). Subsequently, organoid-derived monolayers were differentiated for 7 days. Differentiation and increased barrier function were monitored over time by trans-epithelial electrical resistance (TEER) and microscopic observation. A fully confluent and differentiated monolayer could be obtained after 7 days in culture, as shown by a plateauing of the TEER and observation of under a brightfield microscope (**Figure 2.5D**).

Thanks to these optimisations, I was able to show that confluent colonic organoid-derived monolayers could be established on Transwells for further applications, including the study of the effect of bacterial metabolites on the epithelium. As an important note, this model was not used further, aside from the collaboration with KU Leuven, as the availability of human organoid cultures in Norwich came at very late stages of my PhD project, which made it difficult to establish and characterise these cultures for further experiments (described in **Chapter 3** and **4**).

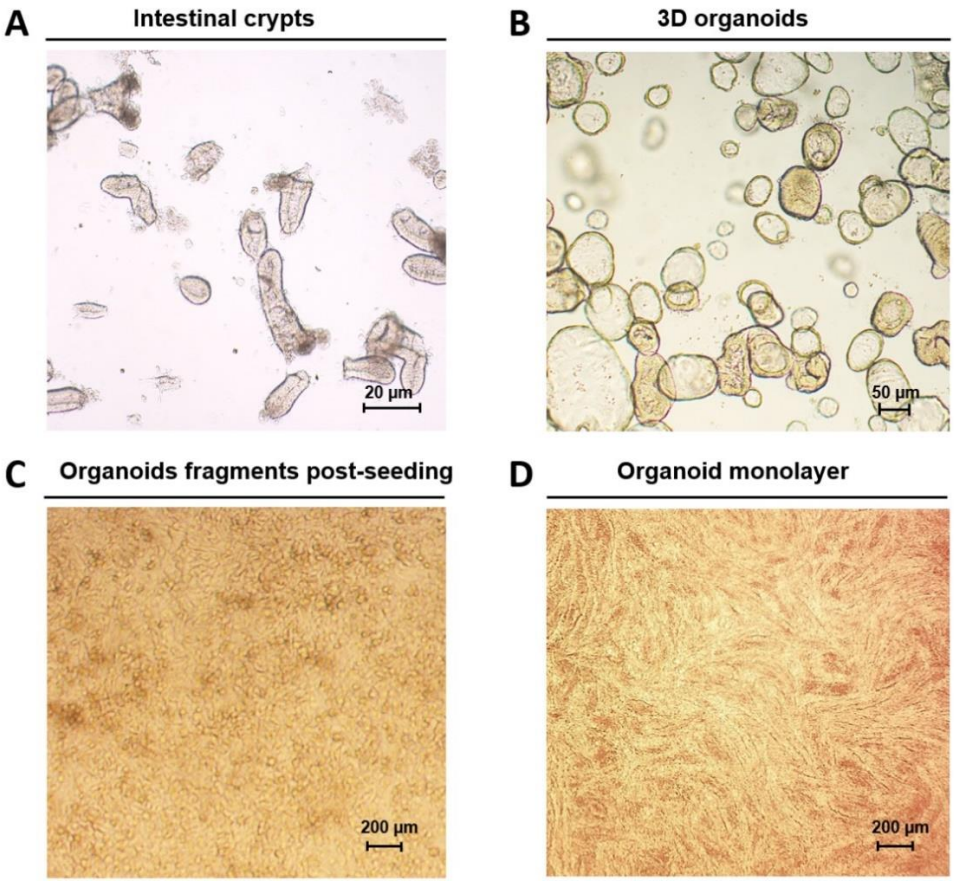

Figure 2.5. Human colonic organoid-derived monolayer culture. Brightfield images of the different steps of organoid-derived monolayer generation on Transwells from human colonic organoids. **A)** Intestinal crypts isolated from colonic biopsies from human patients. **B)** Colonic organoid cultures which were grown in expansion medium. **C)** Organoid fragments post-seeding on collagen coated Transwells. **D)** Confluent human organoid-derived monolayer 7 days post-seeding.

4.3. Introduction of patient-derived organoid monolayers into HuMiX

One disadvantage of organoid-derived monolayers on Transwells is that bacterial cells cannot be kept in an anaerobic environment while keeping epithelial cells in aerobiosis. The HuMiX module, developed by collaborators in Luxembourg, overcomes this problem by keeping the bacterial and epithelial separate in two different oxygen environments. However, the initial HuMiX system was using Caco-2 cells to model the epithelial layer. Hence, during a joint collaboration with KU Leuven and University of Luxembourg, we aimed to show that human colonic organoid-derived monolayers can be introduced within the epithelial chamber of the HuMiX module to overcome the limitations associated with Caco-2 cells. Experiments were carried out by myself, Dr. Kaline Arnauts (KU Leuven) for the organoid part and Audrey Frachet (University of Luxembourg) for the HuMiX part.

For this proof-of-concept study, the epithelial membrane of HuMiX received from the collaborators was first pre-cut into smaller disks to fit the size of a Transwell insert of a 24-well plate (0.96 cm^2, 0.4 µm). Subsequently, membranes were pre-coated with a thin layer of collagen before organoid fragments were seeded on top (**Figure 2.6**, and Methods).

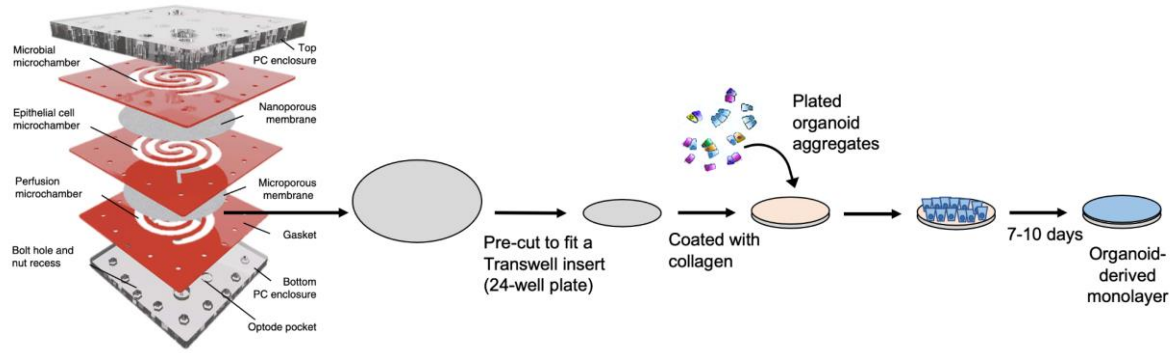

Figure 2.6. Introduction of organoid-derived monolayers into HuMiX. Schematic overview of the different steps required to test the feasibility of introducing human colonic organoid-derived monolayers into the epithelial chamber of HuMiX. Figure adapted with permission from (Shah et al., 2016).

Following the protocol, we successfully demonstrated that human colonic organoids can form a confluent and differentiated monolayer when seeded onto the epithelial membrane used in the HuMiX module. After 7-10 days from seeding, organoid fragments gave rise to a differentiated epithelial layer. The correct differentiation and polarity of the organoid-derived monolayer was also confirmed by immunostaining, which showed the presence of tight junctions (ZO-1, green) and mucus production (MUC2, red) (**Figure 2.7**). This finding supports

the potential to introduce patient-derived human colonic organoids into the HuMiX module, therefore allowing host-microbe interaction studies where both bacteria and the epithelium can be kept at their corresponding physiological oxygen conditions, whilst allowing exchange of metabolites and other signalling molecules.

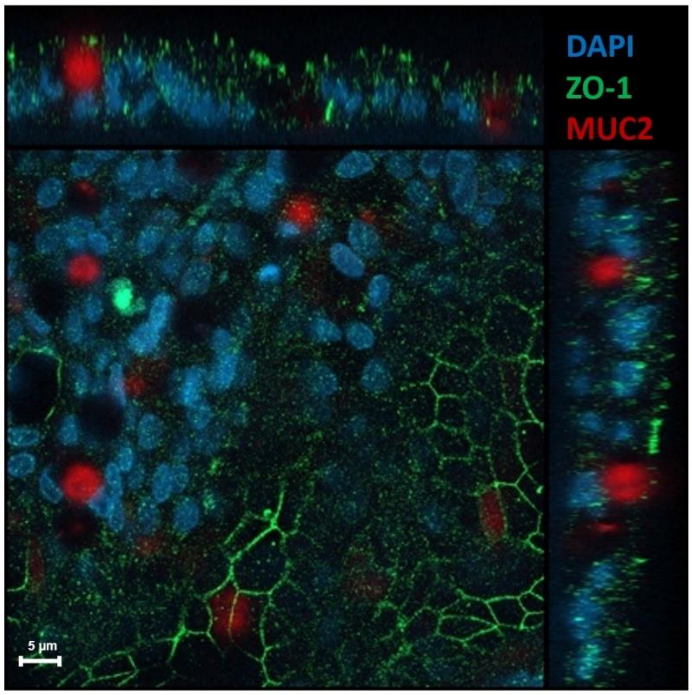

Figure 2.7. Confirmation of polarity of human colonic organoid-derived monolayers seeded within HuMiX by immunostaining. Z-stack fluorescence image of human colonic organoid-derived monolayer on Transwells. Stainings: nuclei (DAPI, blue), tight junctions (ZO-1, green) and mucus (MUC2, red). Z-stack images were obtained from immunofluorescent-stained whole mount monolayers on a Zeiss LSM 880 Airyscan (Carl Zeiss Inc, in collaboration with the Lab for Enteric NeuroScience, KU Leuven).

4.4. Organoids with reversed polarity (“apical-out”)

An alternative experimental system for modelling host-microbe interactions, which requires less starting material than organoid-derived monolayers, is represented by apical-out organoids. These organoids can be established from the direct reversion of polarity of 3D organoid cultures. This can be done by removing organoids from Matrigel and growing them in suspension, after which polarity reversion is observed within 3 days (**Figure 2.8**). Because the initial published protocol from Co and collaborators (Co et al., 2019) was based on duodenal mouse organoids, the goal of this experiment was to test and optimise this protocol further to establish mouse ileal and human colonic organoids with reversed polarity (**Figure 2.8**).

Initially, I tested this protocol on mouse ileal organoids or human colonic organoids grown in expansion media (mouse or human OGM). When testing it on mouse ileal organoids, all organoids would die 24 hours after being seeded in suspension using ultra-low attachment plates (**Figure 2.9A**). Subsequently, I tested whether the addition of Y-27632 (which improves cell attachment and blocks anoikis) and CHIR99021 (which promotes stem cell growth *via* WNT signalling) would enhance the stem-cell compartments of mouse ileal organoids and prevent cell death. This implementation resulted in some cell death, but intact mouse apical-out organoids could be observed at this stage.

Despite achieving polarity reversion for both mouse ileal and human colonic organoids (**Figure 2.10A, B**), organoid aggregation could be observed after the reversion process, in addition to the presence of high quantities of debris, as a consequence of the polarity reversion **(Figure 2.9B**). This was observed more frequently for mouse organoids compared to human ones, probably due to the higher proportion of stem-cells in the initial culture of human organoids compared to mouse ones associated with the culture media used (**Figure 2.10A, B**). In order to improve the protocol further, and reduce the amount of debris, a partial media change was performed one day after seeding. Subsequently, on day 3, organoids were collected, and multiple washes were performed, which successfully detached organoids and got rid of the debris (**Figure 2.9C, D**).

The correct reversion of the organoid polarity could be confirmed both under the brightfield microscope (**Figure 2.10A,B**), as well as by confocal microscopy imaging of brush border (phalloidin, green) and nuclei (DAPI, blue) (**Figure 2.10B,C**).

Despite the successful establishment of both mouse and human apical-out organoids, the tested protocol led to several organoids being lost and the reversion of polarity was not always complete (100%). Using apical out-organoids for co-culture experiments with bifidobacteria would require additional optimization to increase the yield of reversion and further characterization by marker staining to confirm whether these organoid models possess all the different epithelial cell types and proper mucus production like their normal polarity counterparts. Hence, similarly to what happened with organoid-derived monolayers, it was difficult to obtain a sufficient quantity of properly characterised apical out organoids for further experiments. Therefore, to perform further co-culture experiments with bifidobacteria, 3D organoids or Caco-2 cell models were used instead (described in **Chapter 3** and **4**).

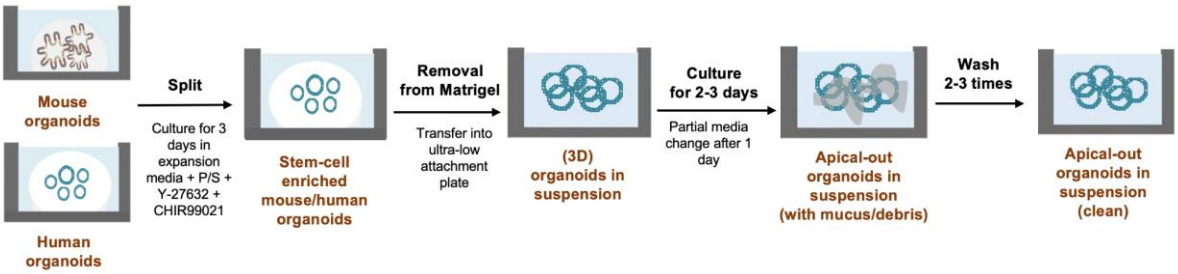

Figure 2.8. Schematic representation of apical-out organoid generation from mouse ileal and human colonic organoids from a healthy donor. Mouse ileal organoids and human colonic organoids were first grown expanded in mouse OGM, and subsequently split and grown for 3 days in a stem-cell enriched form with mouse OGM supplemented with 3 µM CHIR99021, 100 U/mL/100 µg/mL P/S and 10 µM Y-27632. Organoids were then removed from Matrigel and seeded in suspension using a ultra-low attachment plate. A partial medium change was performed the next day. 3 days after seeding, organoids were washed several times to remove excess mucus, after which clean apical-out organoids were obtained.

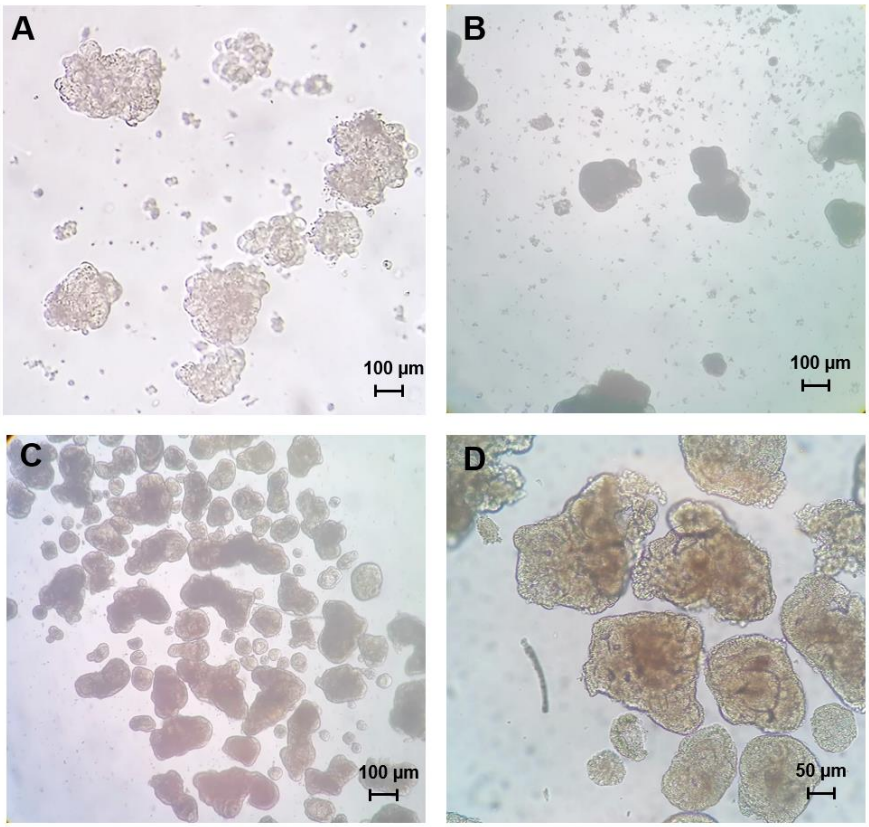

Figure 2.9. Optimisation of protocols to establish apical-out organoids. Brightfield images of different steps of mouse and human apical-out organoid establishment. **A)** Mouse ileal organoids die 24 hours after being seeded in suspension using ultra-low attachment plates. **B, C, D)** Human apical-out organoids grown for 3 days in suspension using ultra-low attachment plates before any washing step was performed (B), after one wash (C) and after two washes (D).

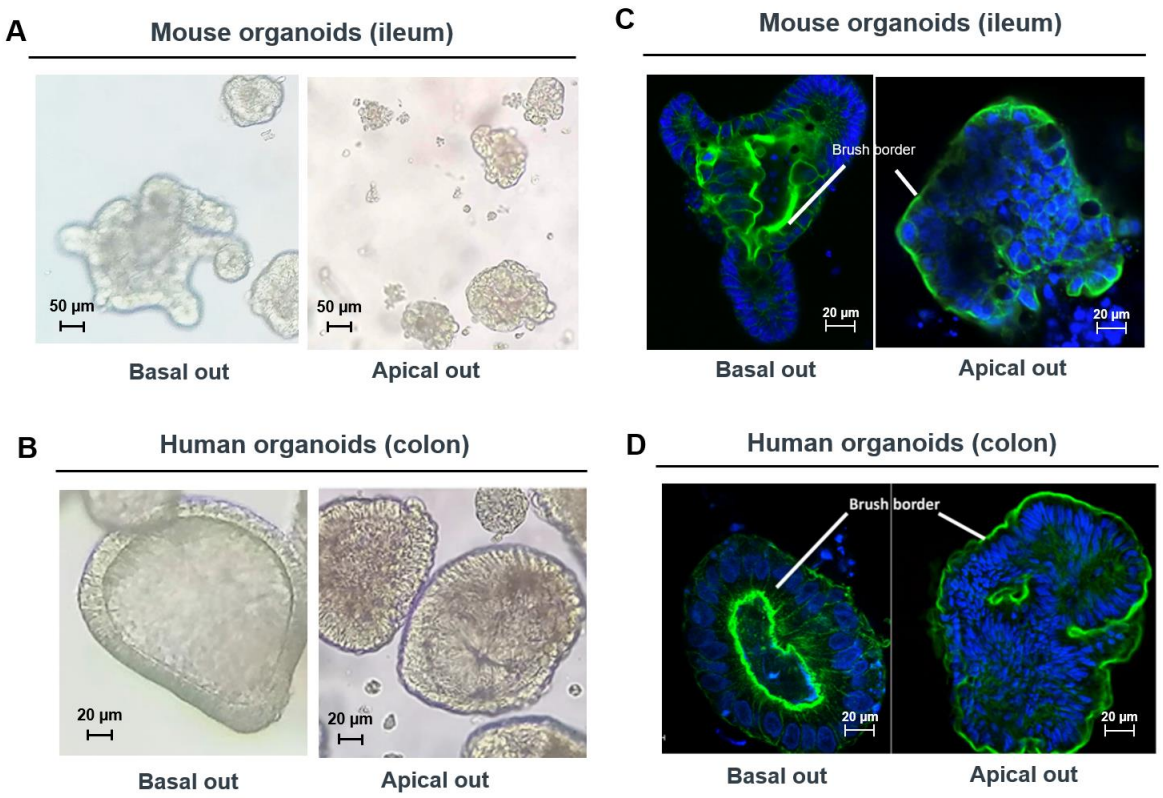

Figure 2.10. Human and mouse apical out organoids. A, B) Brightfield images of mouse ileal organoids (A) and human colonic organoids (B) with normal polarity (basal out, left), and with reversed polarity (apical out, right). **C, D)** Confocal images of mouse ileal organoids (C) or human colonic organoids (D) with normal polarity ("basal out", left) and reversed polarity ("apical out", right). Organoids were stained for nuclei (blue, DAPI) and the actin brush border (green, phalloidin-iFluor488). Images were collected using a LSM880 confocal microscope with AiryScan (Zeiss), using a 63x oil immersion lens.

4.5. Improvement of protocols for immunostaining of organoid cultures without removal from the ECM matrix

After optimising different methods to establish organoids, the next goal was to develop a protocol for the successful immunostaining of mouse and human (3D) organoids. One of the main issues for the success of organoids staining is the accessibility of antibodies for the intestinal cells, given they are embedded into a thick Matrigel matrix. Most protocols available in the literature advised removing organoids from Matrigel before proceeding with the staining. Hence, I initially tested the protocol when the organoids were first taken out of Matrigel by incubation with Cell Recovery Solution, while subsequent fixation, permeabilization and

primary and secondary antibody staining steps were performed using LoBind 1 ml tubes. However, this method led to a significant amount of organoid loss, not only during the organoid removal stage, but also during all the staining and washing steps. Here, organoids would be collected either by centrifugation or by waiting for them to sediment to the bottom of the LoBind 1 ml tube, after which the supernatant could be removed. However, both methods would lead to significant organoid loss, either due to the organoid damage as a consequence of repeated centrifugation, or sequential organoid loss after the sedimentation step, as some organoids would remain in the floating solution. Therefore, in collaboration with the senior post-doc in our group (Dr. Isabelle Hautefort), we set-up a series of optimisation experiments to improve the organoid immunostaining protocol.

An improvement of this protocol was brought about when we noticed that organoids could be grown directly on glass coverslips and that subsequent fixation with 4% PFA would make the Matrigel matrix dissolve over time. In this way, stainings could be performed directly on the organoid domes without the need for prior extraction from Matrigel. Following this, we found that the optimal fixation time was around 30 minutes, resulting in at least 75% of Matrigel to be dissolved, whilst avoiding too much crosslinking. Subsequently, permeabilization and antibody staining steps could be performed directly on the organoids grown on coverslips. With this protocol, not only the amount of organoid loss was minimal, but we were able to preserve the structure of organoids which was instead damaged by repeated centrifugation. Additionally, the drop method for primary and antibody staining could be implemented, while still performing the washing steps onto the plate well, as round coverslips where organoids were seeded could be easily removed from the 24-well plate. In this way, we were able to not only achieve a homogeneous antibody staining, but also decrease the amount of antibody solution used.

We successfully implemented this protocol in mouse ileal organoids to identify cell nuclei (DAPI), cell edges (actin/phalloidin) and proliferating cells (Ki67) **(Figure 2.11A**), as well as autophagy processes (p62, LC3) (**Figure 2.12A, B**). Furthermore, we successfully applied it to healthy human colonic organoids to identify nuclei (DAPI), cell edges (actin/phalloidin, EpCAM), tight junctions (ZO-1) and proliferating cells (EdU) (**Figure 2.11B-D**), as well as autophagy processes (p62, LC3) (**Figure 2.12C, D**). Immunostaining of lysozyme (LYZ) for Paneth cells and mucin (MUC2) for goblet cells was also tested on both mouse and human organoids, but it did not lead to satisfactory results.

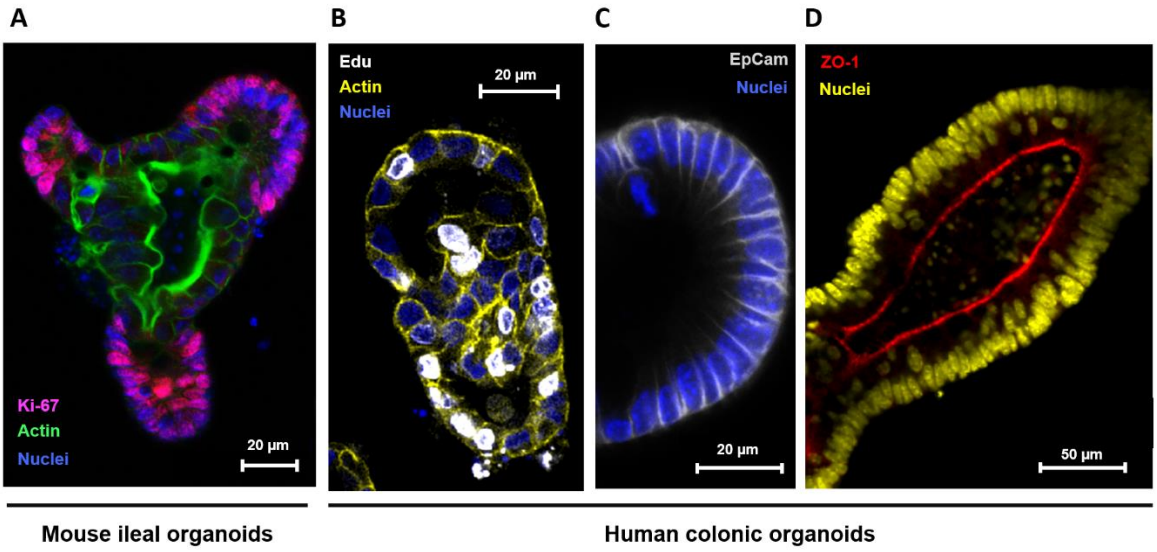

Figure 2.11. **Immunostaining of mouse and human intestinal organoids embedded in Matrigel.** Confocal images of representative mouse ileal (A) and human healthy colonic (B, C, D) organoids. Images were collected using a LSM880 confocal microscope with AiryScan (Zeiss), using a 63x oil immersion lens. **A)** Organoids were stained for nuclei (blue, DAPI), actin brush border (green, phalloidin-iFluor488) and proliferating cells (violet, anti-KI67 - Alexa Fluor 594). **B)** Organoids were stained for nuclei (blue, DAPI), actin brush border (yellow, phalloidin - iFluor488) and proliferating cells (EdU assay - iFluor488). **C)** Organoids were stained for nuclei (blue, DAPI) and actin brush border (white, anti-EpCAM - Alexa Fluor 647). **D)** Organoids were stained for nuclei (blue, DAPI) and tight junctions (red, anti-ZO1 - iFluor488).

4.6. Immunostaining and quantification of p62 and LC3 puncta applied to mouse ileal organoids identified differences in autophagy flux

A central process regulating epithelial cell function, which could mediate the effect of bifidobacterial metabolites on the gut, is represented by autophagy. One method to quantify autophagy processes in epithelial cells is by quantification of intracellular p62 and LC3 puncta (see **Chapter 1**). Hence, the goal of this experiment was to set-up a protocol to quantify autophagy processes in mouse and human intestinal organoids by means of immunofluorescence staining of intracellular autophagy proteins LC3 and p62. To do that, together with Dr. Isabelle Hautefort (QIB), I adapted a protocol previously used to identify these proteins on Caco-2 cell monolayers, by implementing it following the improved methodology developed for immunostaining of organoids (see methods of this chapter). With this implementation, I was able to identify both LC3 and p62 puncta within mouse (**Figure 2.12A, B)** and human **(Figure 2.12C, D)** organoids.

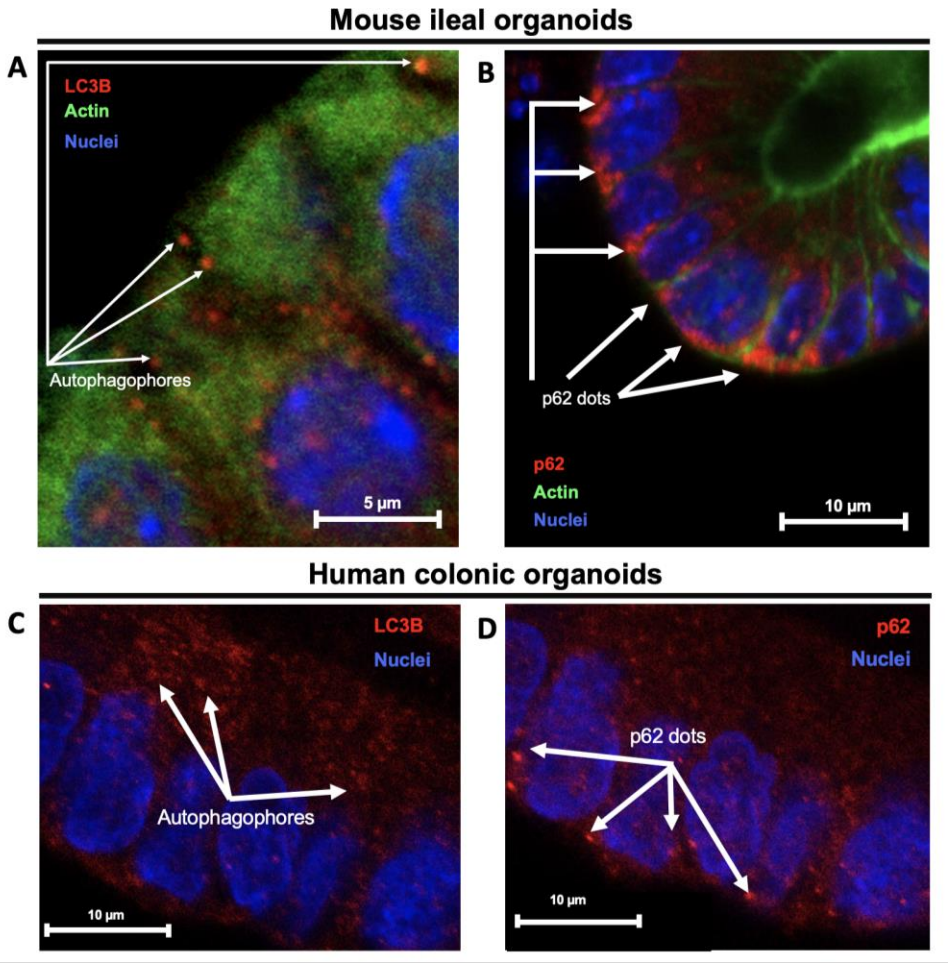

Figure 2.12. **Immunostaining of autophagy proteins p62 and LC3 in different sets of samples of organoids embedded in Matrigel.** Confocal images of representative mouse ileal **(A, B)** and human healthy colonic **(C, D)** organoids. Images were collected using a LSM880 confocal microscope with AiryScan (Zeiss), using 63x oil immersion lenses. Cells were stained for nuclei (blue, DAPI), actin brush border (green, phalloidin-iFluor488) (A,B), LC3 (red, Alexa Fluor 594) and p62 (red, Alexa Fluor 594) (A-D). A different set of samples were used for LC3B and p62 staining due to the anti-LC3 and anti-p62 primary antibodies used being raised in the same species.

One downside of this protocol was that two separate sets of samples were needed for each condition to identify p62 and LC3, respectively. The reason was that antibodies used in this protocol were raised in the same species**.** However, it is often important to identify changes in LC3 and p62 puncta relative to each other, since the concomitant change of these proteins' expression is indicative of autophagy flux. Hence, it was important to be able to identify these two proteins in the same cell simultaneously for each condition tested. An improvement of this protocol was achieved by optimising the use of anti-p62 and anti-LC3 antibodies raised in different species, therefore allowing the staining of p62 and LC3 in the same sample (**Figure 2.13A, B**).

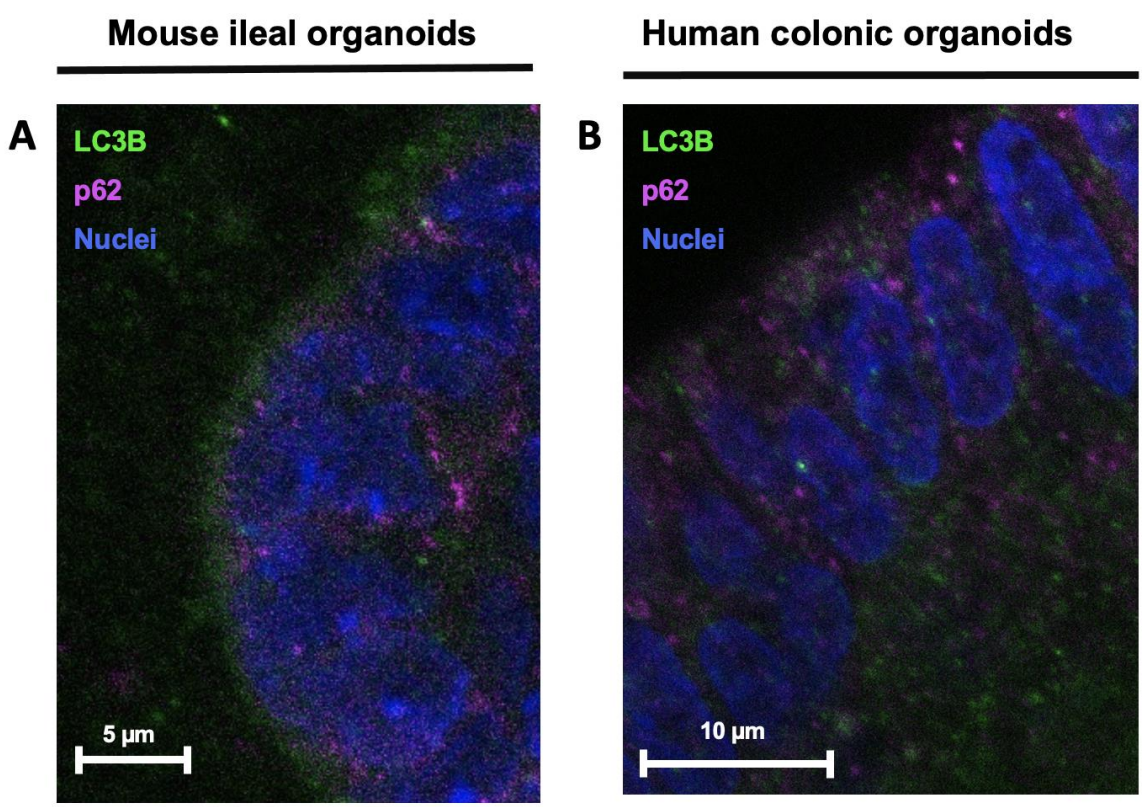

Figure 2.13. **Immunostaining of autophagy proteins p62 and LC3 within the same sample of organoids embedded in Matrigel.** Confocal images of representative mouse ileal **(A)** and human healthy colonic **(B)** organoids. Images were collected using a LSM880 confocal microscope with AiryScan (Zeiss), using 63x oil immersion lenses. A, B) Cells stained for nuclei (blue, DAPI), LC3B (green, AlexaFluor 594) and p62 (violet, AlexaFluor 488).

Once immunostaining protocols were successfully implemented, it was important to develop an analytical pipeline to correctly identify and quantify the expression of LC3 and p62 proteins within the cell as a measure of autophagy flux. To do so, representative images of LC3 and p62 immunostaining collected by confocal microscopy were further analyzed using the image analysis software Imaris. Using this software, a pipeline was built to first identify/segment epithelial cells within organoids based on membrane immunostaining (**Figure 2.14A**). Subsequently, LC3 or p62 puncta were identified based on LC3 or p62 immunostaining (**Figure 2.14B**). Finally, the number of puncta and average intensity per cell for each set of images was computed to quantify autophagy processes (**Figure 2.14C**).

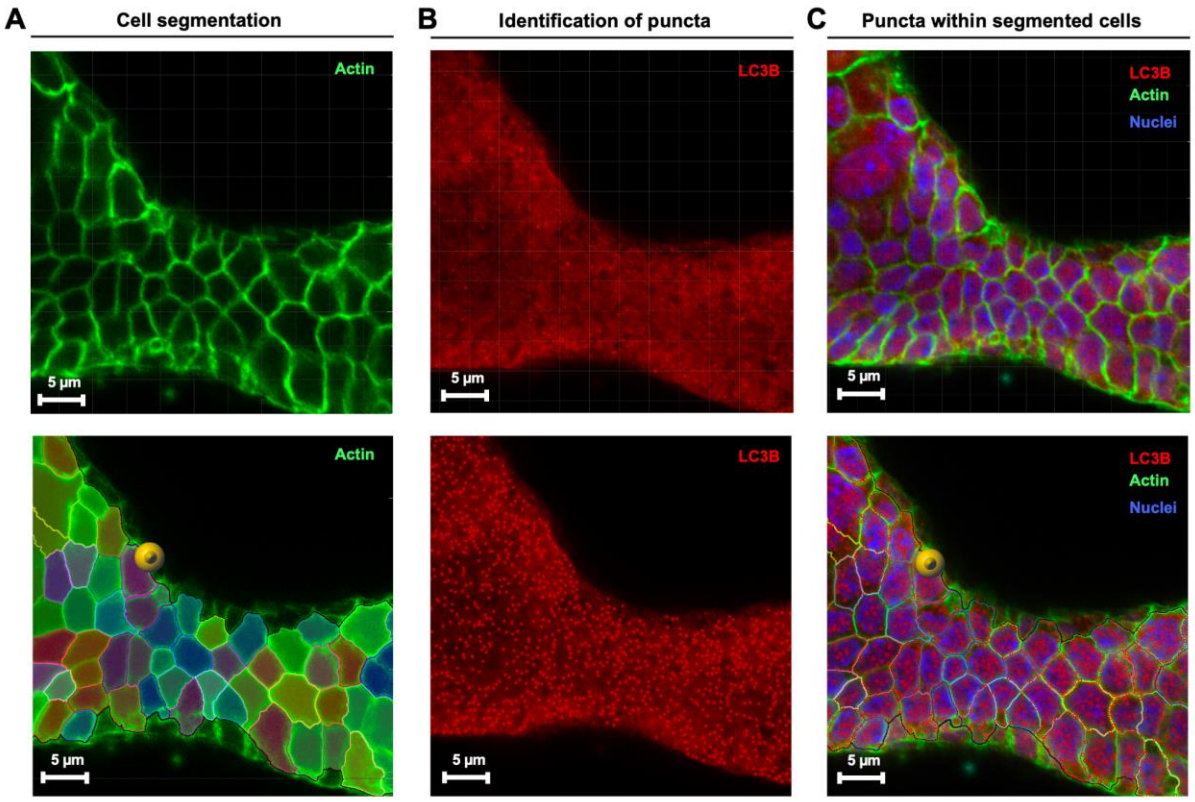

Figure 2.14. Analysis and quantification of LC3 and p62 puncta in organoids. A) Cell segmentation; single cells within organoids were identified using the cell membrane identification function within the Cell Module function. Segmentation was based on actin immunostaining (phalloidin-iFluor488). The following parameters were used: cell size 5 µm, membrane thickness 0.9 µm, local contrast method applied. **B)** Identification of puncta; the number of puncta in each cell was identified based on the p62/LC3 proteins staining (Alexa Fluor 594) using the spot identification function within the Cell Module function. The following parameters were used: 0.6 µm as puncta diameter, and background subtraction method was applied. **C)** Puncta within segmented cells; the number of p62/LC3 puncta and average intensity of puncta per cell were identified by combining the identification of spots and cell segmentation layers. **A, B, C)** Organoids were fixed, permeabilized and stained for nuclei (blue, DAPI), actin brush border (green, phalloidin-iFluor488) and p62/LC3 proteins (red, Alexa 594). A different set of samples were used for LC3B and p62 staining due to the anti-LC3 and anti-p62 primary antibodies used being raised in the same species. Images were collected with a LSM880 confocal microscope with AiryScan (Zeiss), using 63x oil immersion lenses. Image analysis was performed using the Imaris cell imaging software (Oxford Instruments).

Next, to show the ability of this staining protocol to identify differences in intracellular autophagy, mouse ileal organoids (5-days post splitting) were treated with 33 µM rapamycin, which is a potent activator of autophagy by suppressing the mechanistic target of rapamycin complex 1 (mTORC1) (**Figure 2.15A**). Alternatively, organoids were left untreated, which was

used as media control. Next, the protocol for organoid staining described above was used to identify LC3 and p62 proteins, and phalloidin and DAPI staining to identify cell edges and nuclei, respectively (**Figure 2.15A**). When observing organoids treated with rapamycin compared to the media control, the LC3 signal was more homogeneous within the cell, but different signal intensities could be observed in specific cells localised along the intestinal crypt-villi structure (**Figure 2.15B, D**). Because the presence of LC3 puncta is indicative of autophagy activation, this indicated that these cell types were characterised by a higher autophagy flux, and are likely to indicate the presence of Paneth cells in the small intestinal epithelium of mice. Conversely, p62 signal was less homogeneous, and characterised by the widespread presence of very bright puncta localised in specific positions within the cell (**Figure 2.15C, E**). Additionally, p62 proteins seem to localise more at the cell edge (**Figure 2.15C, E**).

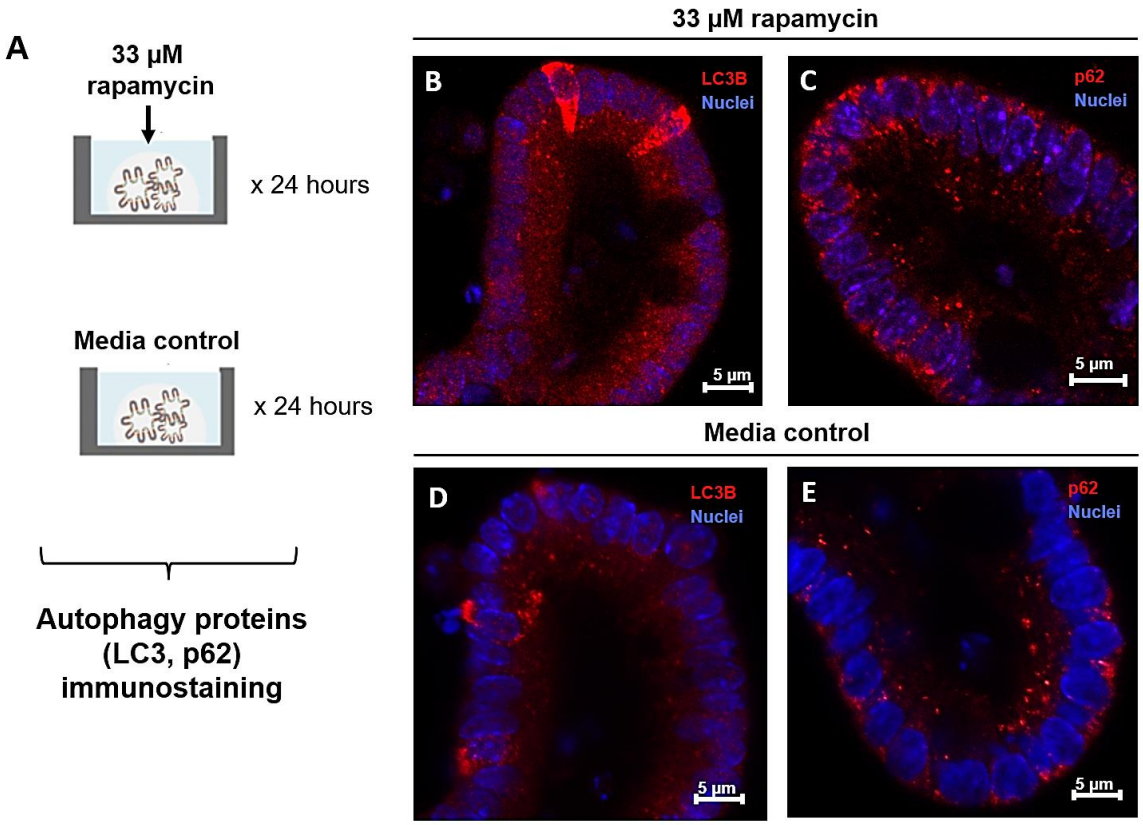

Figure 2.15. Evaluating autophagy flux within organoids by p62 and LC3 immunostaining. A) 5-days ileal organoids grown in mouse organoid growth medium (Intesticult) were treated with 33 µM rapamycin (autophagy activator) or left untreated for 24 hours. Organoids were fixed, permeabilized and stained for p62/LC3 proteins. A different set of samples were used for LC3B and p62 staining due to the anti-LC3 and anti-p62 primary antibodies used being raised in the same species. **B-E)** Representative confocal images of LC3 (B,D) or p62 (C,E) puncta within mouse ileal organoids treated with 33 µM rapamycin (B, C) or left untreated (D, E) for 24 hours. Images were collected using a LSM880 confocal microscope with AiryScan (Zeiss), using 63x oil immersion lens. Organoids were stained for nuclei (blue, DAPI) and p62/LC3 proteins (red, Alexa Fluor 594) are shown.

When looking at the autophagy flux in organoids treated with rapamycin compared to those untreated, both the number and average signal for LC3 puncta was higher in rapamycin-treated compared to the organoid control, although this difference was not statistically significant (**Figure 2.16A**). Conversely, the number and mean intensity of p62 puncta was slightly lower in organoids treated with rapamycin compared to controls, although again the difference was not statistically significant (**Figure 2.16B**). Nevertheless, differences between conditions could be confirmed by observing the number of spots and signal intensity by immunostaining, which was higher for LC3 and lower for p62 in rapamycin-treated organoids compared to controls, respectively (**Figure 2.16C,D**). Because the increase in LC3 and decrease in p62 puncta is an indication of autophagy activation, these results seem to indicate a trend towards the activation of autophagy by rapamycin treatment, as well as correct identification and quantification of this activation by immunostaining of organoids. The fact that the observed difference between conditions was not statistically significant could be attributed to several reasons, including the length or concentration of rapamycin treatment, the quality of immunostaining, image collection, or imaging analysis pipeline used.

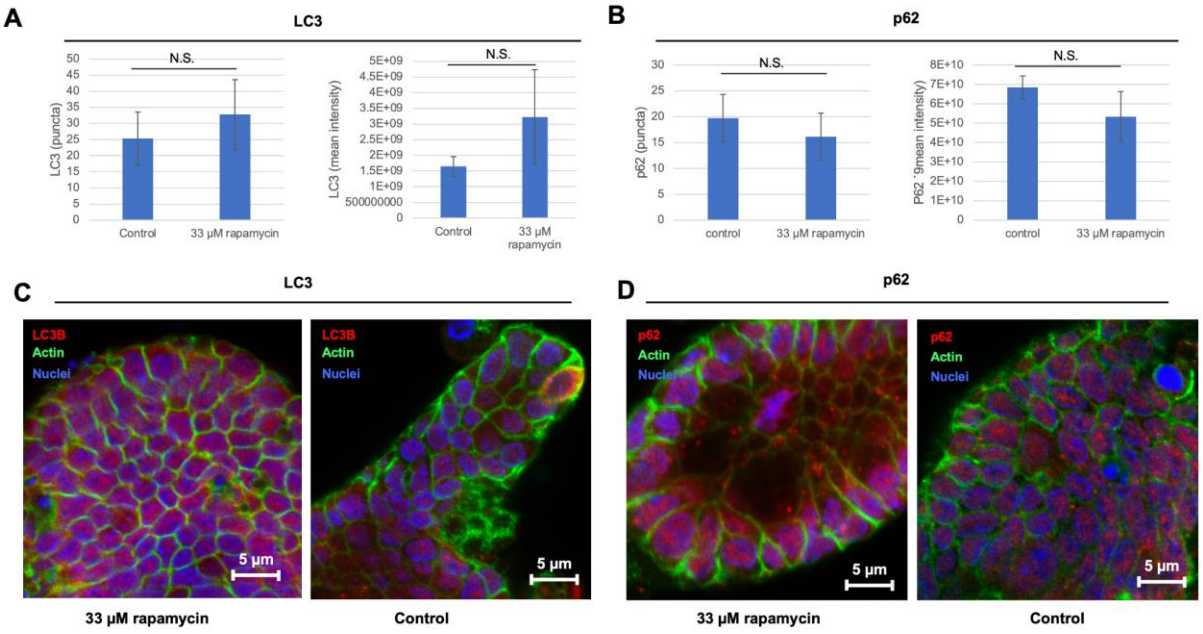

Figure 2.16. Quantification of p62 and LC3 puncta in mouse ileal organoids upon rapamycin treatment or no treatment. A, B) Bar chart indicating the average number and signal intensity of LC3 (A) and p62 (B) puncta in rapamycin-treated or untreated mouse ileal organoids. Error bars indicate the standard deviation (SD) (n=5). Statistical significance was calculated relative to the media control by performing a Student t-test. N.S., non significant (p-value > 0.05); * p-value < 0.05; **p-value < 0.01; *** p-value < 0.001. **C, D)** Immunostaining of LC3 (C) and p62 (D) proteins within rapamycin treated and untreated organoids. Organoids were stained for nuclei (blue, DAPI), actin brush border (green,

phalloidin-iFluor488) and p62/LC3 proteins (red, Alexa Fluor 594). A different set of samples were used for LC3B and p62 staining due to the anti-LC3 and anti-p62 primary antibodies used being raised in the same species. Images were collected using a LSM880 confocal microscope with AiryScan (Zeiss), using 63x oil immersion lens. Image analysis was performed using the Imaris cell imaging software (Oxford Instruments).

4.6. RNA extraction from human colonic organoids

The goal of this set of experiments was to compare the yield of two commonly used kits for RNA extraction (Isolate II RNA Mini BIOLINE and RNAesy Mini QIAGEN) and the number of wells (24-well plate) required to obtain the highest amount of RNA from mouse ileal and human colonic organoids. First, I compared the amount of RNA extracted with the BIOLINE kit starting with 1 well, 2 wells or 3 wells of both mouse and human organoids. The quality of RNA was measured by Nanodrop, and RNA was quantified both using Nanodrop and Qubit. Qubit was employed in addition to Nanodrop as it is a more accurate method to quantify RNA concentration.

In general, the amount of RNA was lower in mouse ileal organoids compared to human colonic organoids **(Figure 2.17A)**. Additionally, I found a small increase in the yield of RNA extracted from 2 wells compared to 1 well of both mouse and human organoids **(Figure 2.17A)**. For mouse organoids, there was an increase in RNA with 3 wells, while for human organoids no further increase could be achieved. On the contrary, the amount of extracted RNA from 3 wells was lower compared to that obtained from 2 wells **(Figure 2.17A)**. Hence, I decided to further test the RNA extraction from 1 or 2 wells of organoids.

Because the yield using the BIOLINE kit was quite low (close to 1 µg which is the minimum needed for cDNA synthesis), I compared the amount of RNA that could be extracted from 1 or 2 wells of human colonic organoids using the BIOLINE kit compared to another commonly used kit for RNA extraction from QIAGEN. Generally, in all conditions the use of the QIAGEN kit resulted in a higher amount of extracted RNA compared to the BIOLINE kit, as measured by Nanodrop (1.2-1.6-fold) (**Figure 2.17B**) and Qubit (1.1-1.7 fold) (**Figure 2.17C**).

Furthermore, the total amount of RNA extracted from 2 wells of human colonic organoids was always higher than that obtained from a single well for both kits tested (**Figure 2.17B, C**). In particular, with the BIOLINE kit, the obtained total RNA was 1.5-fold higher, as measured by Nanodrop **(Figure 2.17B)** and 1.6-fold higher when measured by Qubit **(Figure 2.17C)**. With

the QIAGEN kit, the obtained total RNA was 2.1-fold higher (Nanodrop) (**Figure 2.17B**) and 1-fold higher (Qubit) (**Figure 2.17C**). Results were slightly different when measuring RNA concentration using the Nanodrop and Qubit, but Qubit measurements were considered as more accurate compared to Nanodrop, due the intrinsic higher sensitivity of the measurement used in the assay.

Although in both cases the amount of RNA would be sufficient for cDNA synthesis, the total RNA extracted from 2 wells combined was higher than for 1 well alone. To account for further RNA losses during the further steps of RNA sequencing, I therefore decided to carry out all further experiments using 2 pooled wells of human colonic organoids, as well as to perform RNA extraction using the QIAGEN kit, which had the best performance among the ones tested.

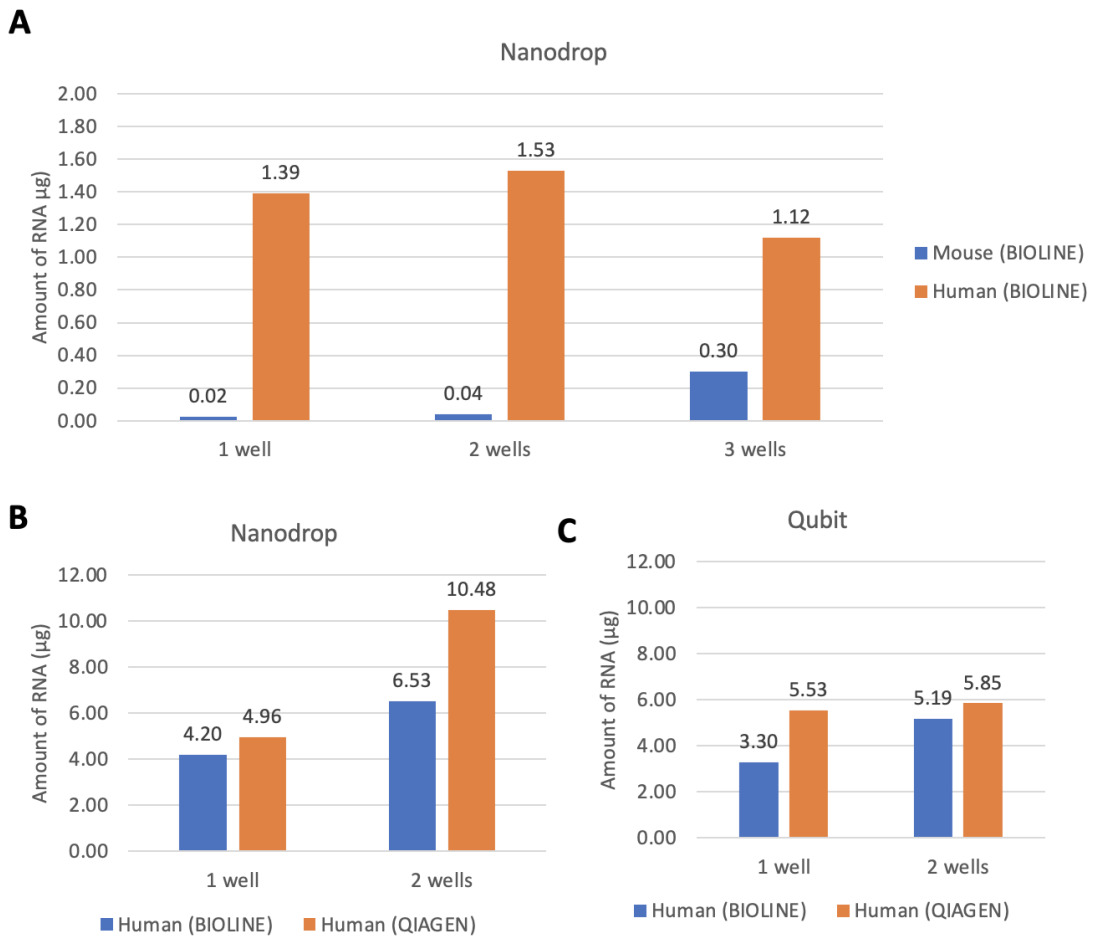

Figure 2.17. Yield of RNA extraction from organoids comparing two commercially available kits. A) Nanodrop measurements of the extracted RNA (µg) from mouse ileal and human colonic 3D organoids using the BIOLINE kit. Results are shown for 1 well, 2 wells or 3 wells (24-well plate) of pooled organoids. **B, C)** Nanodrop and Qubit measurements of extracted RNA (µg) from human colonic organoids using the BIOLINE or QIAGEN kits. Results are shown for 1 well or 2 wells (24-well plate) of pooled organoids.

Additionally, I tested whether an ethanol precipitation step could be used to further concentrate and de-salt the extracted RNA samples, leading to a better RNA quality and higher concentration. For this purpose, absorbance ratios A260/A280 and A260/A230 (obtained through the measurements of absorbance spectra of RNA by Nanodrop) can be used as an indication of RNA purity and quality. In particular, a A260/A280 ratio lower than 1.8 indicates the presence of impurities (DNA, proteins), while a A260/A230 ratio lower than 2.0 can be indicative of contamination with wash solutions, chaotropic salts, phenols or proteins. After performing an ethanol precipitation step, the concentration of RNA slightly decreased, as measured by either Nanodrop or Qubit (**Figure 2.18B**). However, the purity of RNA was increased, as shown by the higher A260/230 ratio, especially for those samples with poor initial RNA quality (S1, S4) (**Figure 2.18A, B)**.

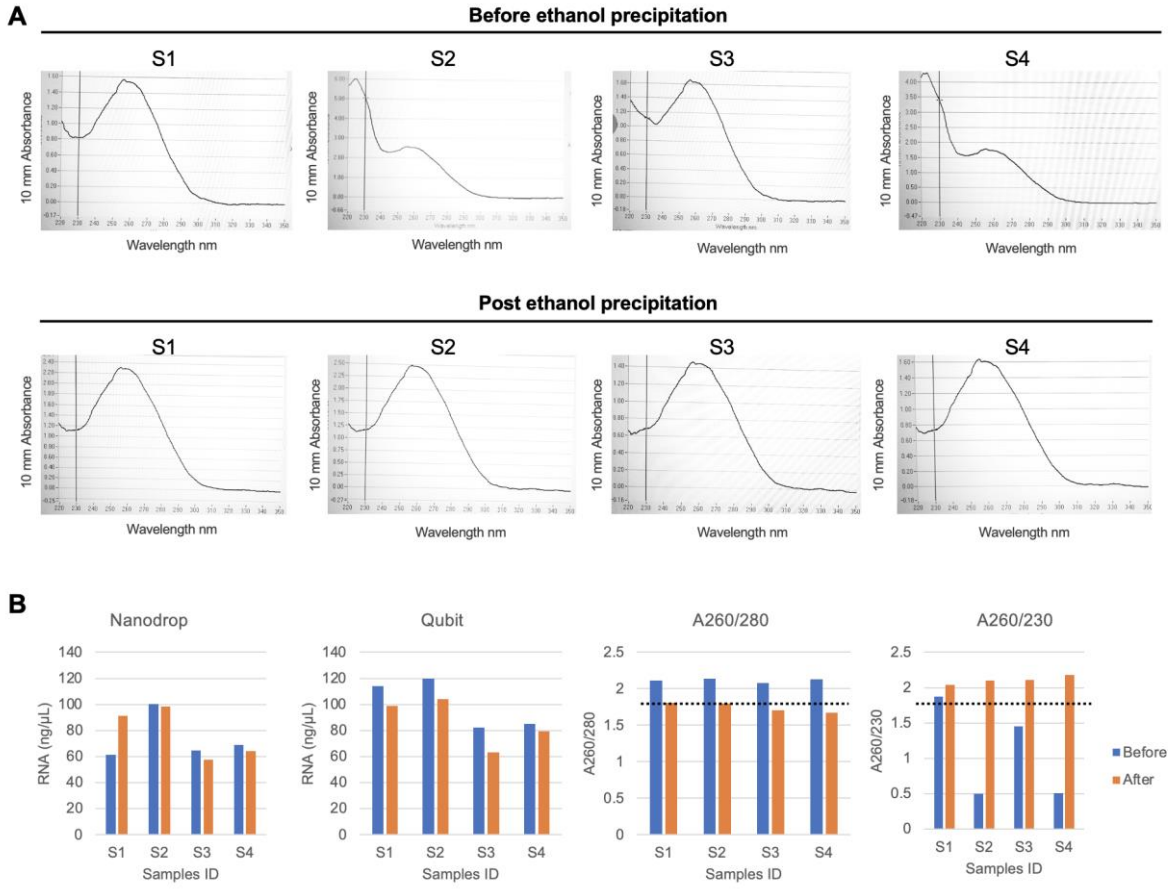

Figure 2.18. Effect of ethanol precipitation of RNA quantity and quality extracted from organoids. **A)** Absorbance (10 mm) spectra across different wavelengths (nm) of extracted RNA samples, measured by Nanodrop before and after ethanol precipitation. **B)** Bar plots indicating the concentration of extracted RNA samples, measured by Nanodrop and Qubit, and the 260/280 and 260/230 absorbance values obtained by Nanodrop measurements. Results are shown for values collected before and after ethanol precipitation. The dotted line indicates the threshold of 260/280 and 260/230 absorbance for a high-quality RNA.

4.7. Optimisation of media to expose organoids to bifidobacterial metabolites

As explained in the introduction of this chapter, finding the optimal media to co-culture bacterial and epithelial cells within organoids over time still remains a challenge. Hence, the goal of this experiment was to understand the best media to use to expose organoids to *Bifidobacterium* metabolites while maintaining both epithelial and bacterial cell viability. One of the media conventionally used to grow bifidobacteria is MRS. To assess bifidobacteria growth in the presence of epithelial media, *B. breve* UCC2003 was exposed to different media combination including 100% epithelial media (DMEM/F12), 100% organoid medium (mouse OGM (Intesticult), 50% bacterial media (MRS)/50% DMEM/F12 or PBS alone. Bacterial growth was monitored over time (0-21 hours) in anaerobic conditions by measuring the delta optical density (ΔOD_{600}). Results showed that the highest growth (21 hrs) could be observed in the presence of MRS, followed by 50% MRS/50% DMEM/F12 (**Figure 2.19**). Additionally, *B. breve* UCC2003 could grow in the presence of 100% epithelial or organoid media only, with the highest growth observed in mouse OGM (Intesticult). Despite this, growth was higher in the presence of at least 50% bacterial media (MRS) (**Figure 2.19**). In PBS, no growth was observed over time (**Figure 2.19**). Overall, these results show that *B. breve* UCC2003 can survive in epithelial or organoid media, but its growth is facilitated when at least half of the media is represented by bacterial media.

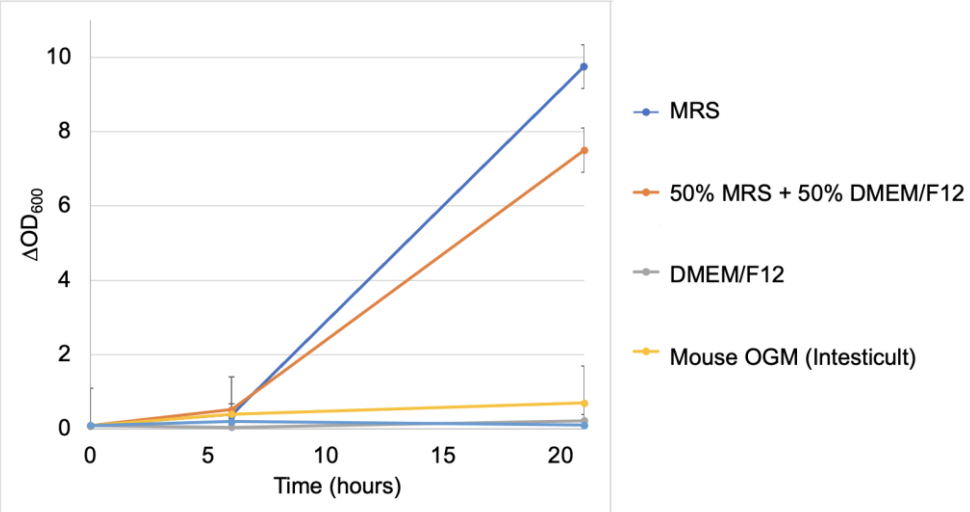

Figure 2.19. Bifidobacterial growth over time in different co-culture media combinations. Optical density measurements at 600 nm (ΔOD_{600}) are shown (y axis) over time (0-20 hours) (x axis). B. breve UCC2003 was pre-grown in MRS media and subsequently grown in different co-culture media combinations over time (0-21 hours) in anaerobic conditions. Mean and standard deviation (SD) measurements for 3 biological replicates for each time points are shown.

Next, to find a possible co-culture media when exposing epithelial cells to bifidobacteria, we tested the cytotoxicity of different media combinations with and without the presence of bacterial media MRS. To test this, mouse ileal organoids (5-days post splitting) were grown in epithelial medium (DMEM/F12) alone or supplemented with 30% or 70% MRS, or organoid medium supplemented with 70% MRS for 24 hours. Furthermore, organoids grown in organoid medium alone (mouse OGM, Intesticult) were used as (media) control. To assess cytotoxicity, visible signs of cell death were monitored under a brightfield microscope at the end of the exposure period. Results showed that the organoid survival was similar, at least visibly, between cultures grown in epithelial medium DMEM/F12 compared to organoid medium alone (**Figure 2.20A, B**). However, introduction of even small quantities of MRS (30%, 70%) can compromise organoids survival, leading to visible organoids death (**Figure 2.20**). Overall, these results suggest that epithelial medium could be used during the bacterial exposure period for at least 24h without compromising organoids survival. Conversely, bacterial media MRS should be used either at lower percentages (<30%) or substituted with an alternative bacterial medium that is less cytotoxic.

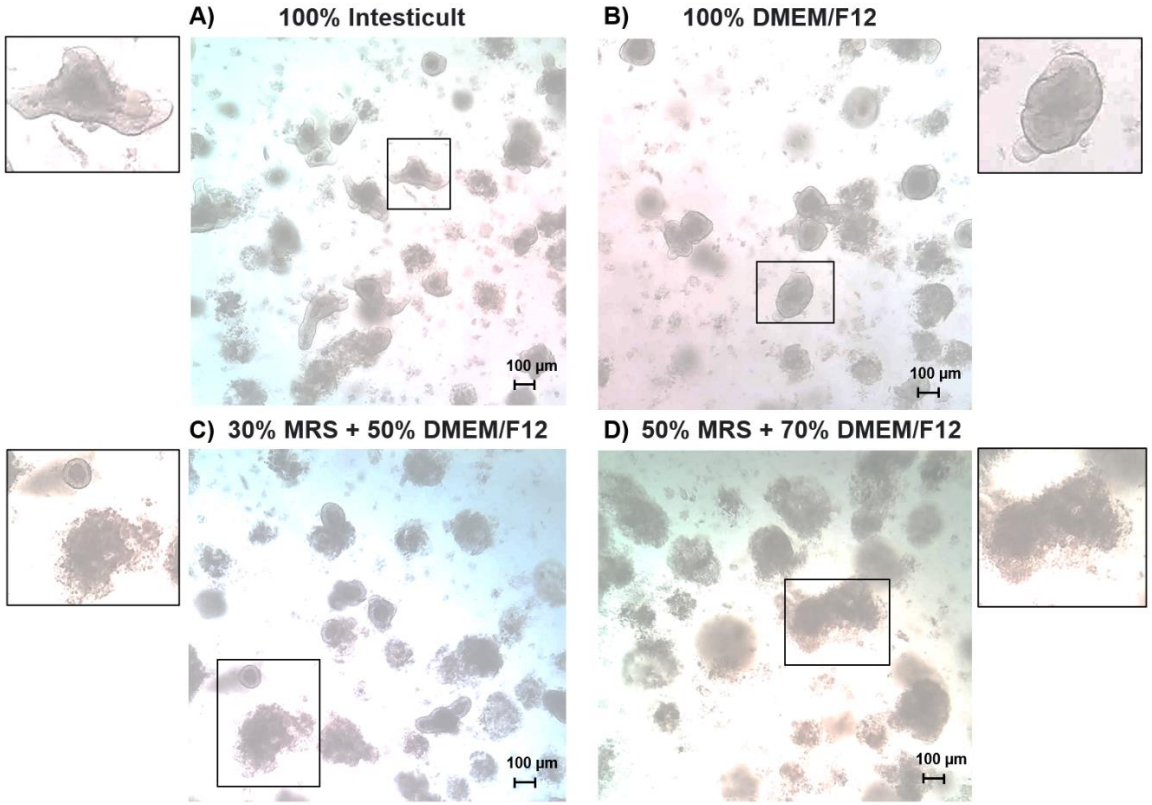

Figure 2.20. Mouse ileal organoids' survival in different co-culture media combinations. Mouse ileal organoids were grown for 5 days in standard mouse OGM (Intesticult) in 24-well plates and subsequently exposed to different co-culture media combinations for 24 hours. Media combinations included standard organoid medium mouse OGM (Intesticult) (A), which was used as negative control,

or standard epithelial media (DMEM/F12), either alone (B) or supplemented with 30% (C) or 50% (D) bacterial medium MRS. Visible cell death could be observed for epithelial media supplemented with 30% and 50% MRS, while no visible change was observed for standard organoid and epithelial media.

An alternative medium to MRS is Brain Heart Infusion (BHI), which had been previously used by other groups in co-culture experiments between bacteria and macrophages. Hence, in a follow-up experiment, I aimed to assess the cytotoxicity of increasing concentration of BHI medium for epithelial cells in mouse ileal organoids. To determine the maximum concentration of BHI that could be added to organoid cell cultures without causing cytotoxicity, mouse ileal organoids (5-days post splitting) were exposed to increasing concentrations (5, 10, 15, 20%) of BHI broth for 24 hours. Additionally, mouse OGM (Intesticult) alone was used as (media) control, while supplementation with 20% dimethyl sulfoxide (DMSO), a potent cytotoxic reagent, was used as positive control. Additionally, one sample containing lysed cells was used to calculate the maximum cytotoxicity. Cytotoxicity of epithelial cells within organoids was evaluated after the 24 hours period by measuring the amount of released LDH in the media using a commercial kit, which is a better measure compared to the simple observation under a brightfield microscope used in the previous experiment.

Upon exposure to BHI, a small level of cytotoxicity was observed across all conditions, as expressed by the amount of LDH release, with a slight increase of cytotoxicity for 15%-20% BHI compared to the media control (mouse OGM, Intesticult), although this increase was not statistically significant (**Figure 2.21**). However, these levels were much lower than that observed for the positive control 20% DMSO, where the cytotoxicity was significantly (p-value < 0.001) increased compared to the media control (mouse OGM, Intesticult) (**Figure 2.21**).

Based on these results, 10% BHI was chosen for mouse ileal organoids exposure to bifidobacterial metabolites collected in BHI media.

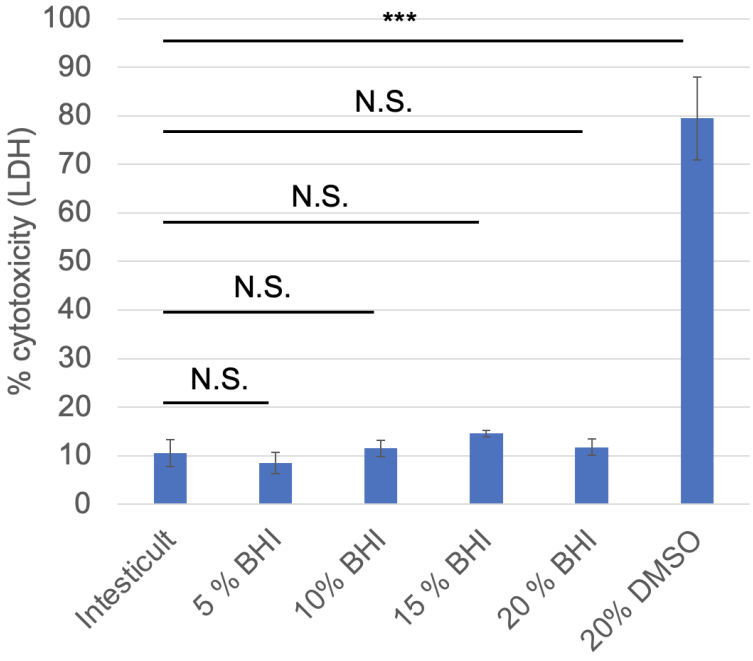

Figure 2.21. Bar chart showing the amount of LDH released in the media, as a measure of cytotoxicity, for mouse ileal organoids. Mouse ileal organoids were grown in Matrigel for 5-6 days before being exposed to increasing concentrations (5, 10, 15, 20%) of BHI broth for 24 hours. Mouse OGM (Intesticult) and 20% DMSO in mouse OGM were used as negative and positive controls respectively. Lysed epithelial cells were also used as an indication of the maximum cytotoxicity. Cytotoxicity was evaluated in the medium after 24 hours using the CytoTox 96® Non-Radioactive Cytotoxicity Assay kit (Promega). Cytotoxicity was evaluated as delta optical density (ΔOD_{490}), which is proportional to the amount of LDH released in the media. The height of the bar chart indicates the percent (%) cytotoxicity ± standard deviation (SD). % cytotoxicity was calculated as follows: (cytotoxicity of each condition / maximum cytotoxicity of lysed cells) x 100. Statistical significance was calculated relative to the media control mouse OGM (Intesticult) by performing a Student t-test. N.S., non-significant (p-value > 0.05); * p-value < 0.05; **p-value < 0.01; *** p-value < 0.001,

5. Discussion

In this chapter, I presented the results of different optimisations with the goal to establish mouse and human intestinal organoid cultures for subsequent applications, including confocal microscopy and host transcriptomics experiments. In terms of mouse organoids, ileal organoid cultures were successfully established and maintained during several passages from fresh intestinal tissue portions (**Figure 2.2**). In terms of human organoids, healthy colonic organoid cultures were successfully established from frozen stocks and maintained for several weeks for further applications (**Figure 2.3**). Despite this, setting up organoid cultures directly from patient biopsies was more challenging. Although several laboratories are establishing organoids from biopsies routinely, I faced several difficulties: (i) the process of obtaining biopsies from the clinical facilities was very slow and dependant on the patient giving consent; (ii) the yield of crypt isolation was low and multiple attempts were required to obtain enough organoids for later passaging and expansion; (iii) organoid cultures would often get contaminated. Culturing of organoids directly from biopsies requires specialised workflows to routinely obtain them from the clinicians without having to depend on the consent of the patient. Additionally, specific laboratories and equipment space should be dedicated for this work to avoid cross-contamination. Finally, defined protocols that have been perfectioned over time should be used to maximise the results. For smaller scale studies like ours, starting from an already established 3D organoid culture purchased from a biobank or obtained from collaborators was a more cost-efficient option to obtain organoids for co-culture studies.

In this chapter, I also illustrated different ways to establish mouse and human organoid-derived monolayers from 3D organoid cultures (**Figure 2.4**). Human colonic organoid-derived monolayers were successfully established on Transwells from 3D colonic organoid cultures thanks to a collaboration with collaborators at KU Leuven (Belgium) (**Figure 2.5**). In terms of mouse ones, despite several attempts, I was not able to generate monolayers from ileal organoids for subsequent co-culture experiments. Previous studies have reported the establishment of mouse organoid monolayers (Moon et al., 2014; Thorne et al., 2018). However, these studies were modelling a different tissue location - either jejunum (Thorne et al., 2018) or the colon (Moon et al., 2014). Additionally, while in one case monolayers were established from 3D organoids (Thorne et al., 2018), in the other cases they were established by seeding crypts directly on top of a Matrigel-coated surface (Moon et al., 2014). Finally, in both studies a specific modified in-house medium such as the L-WRN conditioned media (CM) or EGF, Noggin, R-spondin1 (ENR) media, supplemented with additional factors (Y-27632, CHIR99021) was used. When trying to establish monolayers from 3D cultures, using a

specialised medium, which preserves organoids in a more undifferentiated, stem-cell like richer state would potentially help decreasing the amount of cell death when seeding organoids cells on the collagen-coated Transwell, and increase the chance of cell survival and success of establishing a confluent monolayer.

Results presented in this chapter support the potential to introduce human colonic organoid-derived monolayers into the HuMiX module, therefore allowing host-microbe interaction studies in which both bacteria and the epithelium are kept in physiological oxygen conditions (**Figures 2.6** and **2.7**). Future experiments will require repeating this protocol using the full set-up of the microfluidics device. To achieve this, multiple considerations need to be done. First, the amount of starting organoid cells required to cover the entire surface of the device is relatively big, making it a long and expensive experimental protocol. Second, in a real set-up, single organoid cells would be injected inside the device through a system of sterile tubes. Follow-up experiments done by our collaborators showed that this step would result in some cells getting stuck, clogging the injection tubes, and resulting in cell loss and more difficult to obtain a confluent monolayer. Third, running an experiment requires the continuous flow of relatively higher quantities of organoid media than the one required for a static Transwell set-up, making it again an expensive type of experiment. Once further implementations addressing these aspects will be successful, the introduction of organoids within devices such as HuMiX would allow the investigation of host-microbiota interactions in real-time.

As discussed in the introduction, 2D organoid models would have some advantages over their 3D counterparts (Braverman and Yilmaz, 2018): (i) they allow easy access to the apical side of the epithelium for host-microbe interaction studies; (ii) they simplify staining techniques allowing antibodies' direct contact with epithelial cells; they can be used easily to look at the effect of microbial metabolites on barrier function; (iii) the role of immune cells can be studied more easily by growing immune cell on the basolateral side of the Transwell (Poletti et al., 2021). However, organoid-derived monolayers also present some disadvantages: (i) high quantity of starting organoid material is required, increasing cost and time, which hinders their application for high-throughput experiments; (ii) they are not fully differentiated and are characterised by diminished mucus production compared to their 3D counterparts, which could impede their use to look at these processes (Poletti et al., 2021)**.** To overcome some of the issues related to organoid monolayers, 3D organoids with reversed polarity (apical out) could represent an alternative solution (Co et al., 2019). In this chapter, I presented the work related to the establishment of mouse and human colonic apical-out organoids (**Figures 2.8 and 2.9**), and demonstrated the successful polarity reversion by immunofluorescence staining of the nuclei and actin brush border (**Figure 2.10**). However, using these models for further

applications, including co-culture experiments, would require additional experiments to increase the yield of reversion and further characterise the different epithelial cell types present, and for their functionality to match the normal polarity counterparts. Since the initial paper, further improvements have been made to improve the yield of mouse and human gut epithelial organoids (Stroulios et al., 2021). Additionally, human airway and porcine gut apical out organoids have been used to study the effect of viral infections on the epithelium (Li et al., 2020; Stroulios et al., 2022).

In this chapter, I illustrated several optimisations performed to obtain a protocol that could be used for the immunostaining of mouse and human intestinal organoids. In particular, an optimised protocol was obtained to stain organoids directly within the culture well. This variation eliminated the need for organoid removal from Matrigel, resulting in less organoid material loss. This protocol was successfully used in mouse ileal organoids and human colonic organoids to identify cell nuclei and cell edges, as well as proliferating cells and tight junctions (in human organoids only) (**Figure 2.11**). One limitation was that I could not obtain satisfactory results for lysozyme (LYZ) and mucin (MUC2) staining in both mouse and human organoids, which are markers for Paneth cells and goblet cells, respectively. Despite some researchers have successfully performed this staining in intestinal organoids, most are still struggling. For 3D organoid cultures, the antibody used for MUC2 staining was since then discontinued, making it difficult to replicate these protocols (Parmar et al., 2021). Furthermore, other studies have performed this staining either on apical-out organoids (Co et al., 2019) or organoid-derived monolayers (Liu et al., 2020), where the accessibility of antibodies is higher due to the absence of the Matrigel matrix.

In this chapter, I presented a methodology to monitor the autophagy flux in epithelial cells in the gut by immunofluorescence staining and quantification of LC3 and p62 puncta within mouse and human organoids (**Figures 2.12-14**). To show the ability of the protocol to distinguish differences in autophagy flux, mouse ileal organoids were treated with rapamycin (an autophagy activator) or left untreated and the number and signal intensity of LC3 and p62 puncta was assessed (**Figure 2.15A**). Results of the immunostaining showed that LC3 and p62 proteins could be successfully identified within organoids. Interestingly, LC3 puncta and signal intensity were much higher in specific cell types at the edge of the organoid bud, suggesting the presence of cells with a higher autophagy flux (**Figure 2.15B**). However, because I was not able to find markers for specific intestinal cell types, the identity of these cells, where the increased autophagy flux was taking place, could not be confirmed. Furthermore, results showed that different autophagy fluxes could be distinguished in organoid cells using the current methodology, yet differences measured were often non-statistically

significant (**Figure 2.16A, B**). These results could be due to the timing chosen to capture autophagy (24 hours), or the efficiency of the staining. Indeed, changes in autophagy levels are time-dependent and capturing the right moment when these changes take place is crucial (Brattås et al., 2021). Additionally, the immunostaining may have not been homogeneous across the area of the well, or images analysed were not being fully representative of the entire surface of the well. In the future, implementations to the staining protocol should be made to ensure the homogeneity of the staining. High-throughput imaging systems could be used to collect multiple z-stacks of the well to ensure a more refined image of the autophagic puncta and better coverage of the surface area.

One goal of my PhD was to optimise protocols to extract high quality RNA from mouse and intestinal organoids and determine the amount of initial material required to obtain enough RNA for subsequent applications (e.g. cDNA synthesis and sequencing). Results showed that the amount of RNA obtained from mouse organoids was always lower than the one obtained from human organoids, when comparing similar densities per well (**Figure 2.17A**). This could be due to the differentiation status of mouse organoids, where a high proportion of differentiated cells shedding from the nucleus was already present when RNA was isolated. Instead, human organoids are grown in a medium that maximises the number of fast-cycling stem cells, which may result in a higher yield of RNA extraction. Additionally, despite 1 well of human organoids yielding enough RNA, 2 wells of organoids were the safest option to ensure enough RNA for further applications, where additional RNA could be lost (**Figure 2.17A**). This amount of starting material may bear a relatively high associated cost, when multiple conditions need to be tested and a minimum number of biological replicates are included in organoid RNA sequencing experiments. Additionally, this may lead to high variability of different technical replicates due to different amounts/density of organoids present in each well, and hence accessibility to stem-cell niche factors, which may amplify the inherent in between-wells and in between-organoids variability of organoid cultures (Gehling et al., 2021). Finally, choosing the right kit for RNA extraction from any sample is key to achieve the right amount and quality of RNA for subsequent applications. In my work, the RNAesy Mini QIAGEN kit performed better in all conditions tested compared to the isolate II RNA Mini BIOLINE kit (**Figure 2.17B, C**). One reason could be due to the initial step included in the BIOLINE kit, where cell lysates are filtered prior to the ethanol purification step (see methods of this chapter). While this step may not be necessary to achieve high quality RNA, it may be contributing to initial loss of material, overall resulting in a lower yield.

When co-culturing microbes with intestinal organoids, it is important to find a medium recipe that can ensure the needs of both organoids and microbial cultures are addressed (Puschhof

et al., 2021). This is a vital prerequisite to ensure that the output measured is the most accurate possible. Through the experiments presented in this chapter, I attempted to find a possible combination of media that could be used to expose mouse and human organoid cultures to bifidobacteria metabolites. Results show that bifidobacteria can survive in epithelial or organoid media, although its growth is facilitated when at least half of the media is represented by bacterial media MRS (**Figure 2.19**). However, because the conventionally used MRS resulted to be toxic towards epithelial cells within organoids (**Figure 2.20**), I tested the use of an alternative media, BHI, which resulted to support microbial growth while having minimum cytotoxicity for intestinal epithelial cells within organoids. Additionally, I was able to demonstrate that 10% bacterial supernatant in BHI added to standard organoid medium (mouse/human OGM) could be used for the co-culture assay (**Figure 2.21**). This is similar to what other co-culture studies were using to expose epithelial cells to different bacteria (Puschhof et al., 2021; von Martels et al., 2017). One limitation of this approach is that the media used for the co-culture does not properly reflect the environment we find *in vivo* in the gut, and metabolites produced in this medium may differ from the ones that would be the ones produced by bifidobacteria in an *in vivo* model.

6. Future research directions

Overall, the results of this presented chapter show how I successfully developed protocols to establish mouse and human organoid cultures. These include alternative models that could be used for the study of the apical interactions between bifidobacteria and epithelial cells, such as apical out organoids and organoid-derived monolayers on Transwells or within microfluidics platforms like HuMiX. Furthermore, I found a possible co-culturing media that could be used for these assays, as well as developed protocols for downstream applications such as immunostaining and RNA sequencing, which could be used to decipher molecular mechanisms behind the beneficial effects of bifidobacteria or its metabolites. Among these, I developed a protocol to quantify autophagy flux within organoids by immunostaining and quantification of LC3 and p62 puncta, which would be extremely useful to look at the effect of bifidobacteria on this key cellular process, which is often altered in inflammatory conditions such as IBD.

During this PhD, I was not able to characterise organoid models such as apical out or organoid-derived monolayers within HuMiX for subsequent studies. In the future, if characterised and improved further, these models could be helpful for future host-microbe studies. For instance, once the successful introduction of patient-derived organoids within

HuMiX is achieved, the subsequent addition of microbes such as bifidobacteria within the microbial chamber would enable us to evaluate the direct effect of bacterial metabolites on different epithelial host cell populations under highly controlled conditions. Furthermore, once apical out organoids are fully characterised and the reversion process optimised to obtain a higher yield, these organoid cultures could be used to screen several strains of bifidobacteria and or their metabolites for their effect on the host.

As above-mentioned, the media combinations selected for co-culture studies between bifidobacteria and epithelial cells is still a compromise between bacterial culture media and epithelial/organoid media, none of which properly reflect the environment we find *in vivo* in the gut. Future studies could consider the use of novel media, such as the gut-microbiota specific medium (GMM), which has been shown to promote the growth of *Bifidobacterium* spp. within a complex microbiota community, and better reflect the conditions of the gut environment (Yousi et al., 2019). Alternatively, bifidobacteria could also be grown within a system such as the Simulator of Human Intestinal Microbial Ecosystem (SHIME®) model, which simulates the environment found in both the upper and the lower digestive tract to obtain a better physiological representation of bifidobacterial-derived metabolites produced in the human gut (Van de Wiele et al., 2015). Because *Bifidobacterium* spp. grow best at pH levels around 6.5–7.0, controlling pH conditions during the co-culture is also key to ensure proper bacterial growth and metabolism during such experiments (Ruiz et al., 2011). Finally, addition of specific dietary components such as human milk oligosaccharides (HMOs), which promote *Bifidobacterium* growth, could also contribute to improving the profile of secreted metabolites to mimic what is observed *in vivo* (Thomson et al., 2018).

As mentioned above, autophagy is not a static process, and the use of live reporters coupled with live imaging platforms could represent an advantageous solution when monitoring autophagy over time in future studies. Recently, our group in collaboration with a former senior post-doc within the Hall group (Diana Papp, QIB) has developed a human healthy colonic organoid autophagy reporter line which contains a LC3 dual mCHERRY-GFP reporter, characterised by a different emission spectrum of LC3 signal based on the step of autophagy process being activated. The use of this organoid reporter line for the live detection of autophagy fluxes using high-throughput platforms such the INCell Analyzer 6000 is currently being tested. Once further optimised, these methods could be applied to assess the effect of different bifidobacterial strains and/or their metabolites on the restoration of epithelial autophagy in specific cell types playing a role in IBD, and whose autophagy is impaired such as Paneth and Goblet cells.

In conclusion, I successfully developed protocols to establish organoid models and co-culturing conditions that, upon further optimisation, can be employed to assess the beneficial effect of bifidobacterial or other bacterial strains and their metabolites on the intestinal epithelium in a more physiologically relevant manner. Additionally, improvements of immunostaining and RNA extraction protocols, including successful identification of specific intestinal cell populations within organoids, could be used to investigate specific mechanisms involved in these beneficial effects in a cell-type specific manner. Finally, protocols to quantify the autophagy flux within organoids by immunostaining represent a starting point to study this key cellular process in the gut, which could be further implemented with the use of live reporters and high-throughput imaging systems, to unravel the role played by this process in mediating the beneficial effects of bifidobacteria on the intestinal epithelium.

Chapter 3: Effect of bifidobacterial metabolites on inflammation, barrier function, and autophagy in the gut using Caco-2 monolayers

1. Introduction

Alteration of the intestinal barrier is generally associated with several inflammatory diseases of the gut, such as IBD (Nalle and Turner, 2015; Vancamelbeke and Vermeire, 2017). Barrier integrity is maintained by various mechanisms, including mucus production by goblet cells, expression of tight junctions, and regulation of immune responses (Foerster et al., 2022). Autophagy is a very important host process involved in the maintenance of the epithelial barrier, and it is often disrupted in IBD (Foerster et al., 2022; Pott et al., 2018; Shao et al., 2021).

Several *in vitro* studies have shown the ability of bifidobacteria to modulate host function, including the maintenance of barrier integrity, regulation of immune responses (Alessandri et al., 2019; Lin et al., 2014) and autophagy processes (Zaylaa et al., 2019). Modulation of autophagy by bifidobacteria has been demonstrated both *via* direct interactions and by production of key metabolites (e.g. SCFAs). *B. infantis, B. longum, B. bifidum and B. adolescentis* spp. were shown to activate autophagy in the rat small intestinal cell line IEC-18 (Lin et al., 2014), and *B. breve* spp. in a human colonic cell line C2BBe1, which was mediated by a small secreted molecule (Inaba et al., 2016). In another study, *B. dentium* enhanced mucin production by goblet cells *via* upregulation of autophagy, resulting in increased mucus layer and barrier function (Engevik et al., 2019). Furthermore, preliminary data generated by Dr. Diana Papp (former postdoc in the Hall group, QIB) has pointed towards the ability of two strains of bifidobacteria (*B. breve* UCC2003 and *B. longum* LH206) to activate autophagy in Caco-2 cells (unpublished). The anti-inflammatory properties of bifidobacterial molecules (proteins and peptides, EPS, metabolites, and DNA) have also been studied, and autophagy seems to be a key mediator of these effects (Zaylaa et al., 2019). In the past, probiotics supplementation has been successfully used to dampen inflammation and maintain remission in UC patients (Iheozor-Ejiofor et al., 2020), although they still remain inefficient in CD (Limketkai et al., 2020). It is therefore important to better understand the molecular mechanisms of action behind the immunomodulatory properties of probiotics. Furthermore, the link between regulation of autophagy processes, barrier function and anti-inflammatory properties of bifidobacteria has not yet been investigated. In this chapter, I aim to investigate

protective effects of bifidobacteria in the context of inflammation, and study their ability to modulate barrier integrity, pro-inflammatory cytokine release and autophagy processes in epithelial cells.

To evaluate the effect of bacteria on host epithelial cells, several challenges need to be addressed. Bifidobacteria and epithelial cells require different oxygen environments and growth media to support their metabolism, while the static nature of culture conditions can result in microbial overgrowth and potential damage to epithelial host cells (Dotti and Salas, 2018). To overcome these problems, different methods can be used, including keeping bacterial and host cells in separate chambers, limiting the experiment to a short exposure time, or studying the impact of metabolites only. Each of these options will have their own advantages and disadvantages, some of which have been explained in more detail in **Chapter 1**. Here, to assess the preventive effect of bifidobacteria during intestinal inflammation, I decided to evaluate the effect of *Bifidobacterium*-derived metabolites. In particular, two bifidobacterial strains (*B. breve* UCC2003 and *B. longum* LH206), which had been previously shown to modulate autophagy in Caco-2 cells, were selected. To model the epithelium, Caco-2 monolayers were established on Transwell inserts. In this model, inflammation was induced using phorbol myristate acetate (PMA), which is a specific activator of Protein Kinase C (PKC), and activates Nuclear Factor kappa-light-chain-enhancer of activated B cells (NF-kB) signalling in a dose-dependent way, thereby acting as a pro-inflammatory agent (Chang et al., 2005; Hellweg et al., 2006). Additionally, to assess the contribution of autophagy processes in mediating these beneficial effects, Caco-2 monolayers were exposed to rapamycin for 24 hours, which is a potent inducer of autophagy through the inhibition of mTORC1 (Sekiguchi et al., 2012)

First, a set of experiments was carried out to find the ideal concentration of bacterial media BHI, which could be used to expose Caco-2 cells while maximising epithelial cell viability (see **Chapter 2**). To do so, I performed cytotoxicity measurements on Caco-2 cells exposed to increasing concentration of BHI, and found that 20% BHI could be used as an acceptable quantity for exposure of Caco-2 monolayers to bacterial metabolites. Next, I tested the ability of bifidobacteria to grow in this medium, and found the time-point at which they would reach the late exponential (i.e. lag) phase of bacterial growth. This time point was chosen for metabolites extraction, as it indicates the late points of bacterial growth before reaching the stationary phase, which is likely the time when most metabolites will have accumulated. Next, I set up an experiment to assess the beneficial effects of the two *Bifidobacterium* strains (*B. breve* UCC2003, *B. longum* LH206) during short-term and long-term inflammation. To do so, Caco-2 monolayers grown on Transwells were exposed to 20% *Bifidobacterium*-derived

metabolites collected in BHI for 24 hours, during which inflammation was induced for either a short (4 hours) or long (20 hours) time before the end of the experiment (**Figure 3.1**). To assess the beneficial effects of bifidobacterial metabolites against inflammation-induced loss of barrier integrity, cytotoxicity and pro-inflammatory cytokine production, epithelial barrier by TEER measurements, cell viability and the release of proinflammatory cytokine interleukin-8 (IL-8) in the media were evaluated at baseline, before induction of inflammation and at the end of the experiment. Finally, autophagy processes were evaluated for *Bifidobacterium*-treated Caco-2 monolayers by immunostaining and quantification of autophagic LC3 and p62 puncta, following an adaptation of the protocol developed in **Chapter 2.**

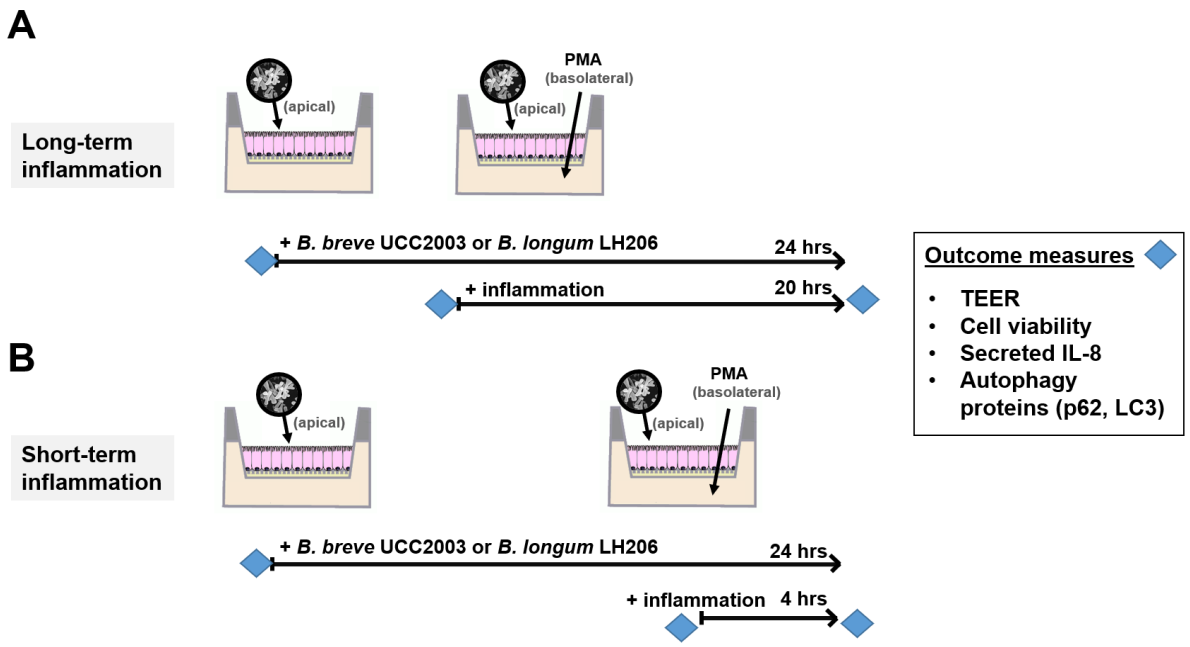

Figure 3.1. Experimental set-up to evaluate the effects of pre-exposure to bifidobacterial metabolites during long-term and short-term inflammation. Schematic representation of the two separate set-ups used to expose Caco-2 cells to bifidobacterial metabolites (*B. breve* UCC2003, *B. longum* LH206). **A)** Pre-exposure to bifidobacterial supernatants for 4 hours, followed by long PMA stimulation for 20 hours. **B)** Set-up 2, long pre-exposure to bifidobacterial supernatants for 20 hours, followed by a short PMA stimulation for 4 hours. For both set-ups, TEER, cell viability, IL-8 release and autophagic p62 and LC3 puncta were measured at each time point. Abbreviations: PMA, phorbol myristate acetate; TEER, transepithelial electrical resistance; IL-8, interleukin-8.

2. Aims and objectives

The main objectives of this study were:

1) Find the maximum concentration of bacterial medium BHI to use to expose Caco-2 cells to *Bifidobacterium* metabolites without compromising Caco-2 cells viability.

2) Determine the concentration of PMA to use for inducing epithelial inflammation without compromising Caco-2 cell viability.

3) Determine the beneficial effects of *Bifidobacterium*-derived metabolites against inflammation-induced loss of barrier function, epithelial cell cytotoxicity, and pro-inflammatory IL-8 release.

4) Evaluate differences in the effects of *Bifidobacterium* metabolites between short-term and long-term inflammation induction.

5) Determine the effect of *Bifidobacterium*-derived metabolites in the modulation of autophagy processes, with a focus on LC3 and p62 proteins.

6) Assess any differences in effects between metabolites from the two strains tested: *B. breve* UCC2003 and *B. longum* LH206.

3. Methods

3.1. Establishment of Caco-2 monolayers

Caco-2 cells were expanded in Roswell Park Memorial Institute (RPMI) 1640 medium (Gibco), supplemented with 10% FBS and 100 U/mL penicillin (P)/100 µg/mL streptomycin (S), in flasks until the right cell density was reached. To test the cytotoxicity of increasing concentrations of BHI medium and PMA solutions, single Caco-2 cells were seeded on 96-well plates and fed in RPMI 1640 medium (Gibco), supplemented with 10% FBS and 100 U/mL/100 µg/mL P/S, for 7 days or until the monolayer was formed. Caco-2 monolayer formation was observed under a brightfield microscope. For the exposure to bifidobacterial metabolites, single Caco-2 cells were seeded on Transwells (0.96 cm^2, 0.4 µm) using 24-well plates and feeded in RPMI 1640 media (Gibco) supplemented with 10% FBS and 100 U/mL/100 µg/mL P/S. An empty Transwell was added to the experiment to serve as baseline TEER measurement. Caco-2 monolayers were differentiated on Transwells for 18-24 days or until confluence was reached, as measured by monitoring TEER once a week using Epithelial Tissue Volt Ohmmeter 2 (EVOM2^{TM}) and STX-100 electrodes.

3.2. Culturing Bifidobacterial strains

Bacterial strains used in this study are indicated in **Table 3.1**. Bifidobacterial strains were streaked from frozen glycerol stocks into pre-reduced Robertson's Cooked Meat (RCM) (supplemented with 0.05% (wt/vol) L-cysteine HCl) and incubated in the anaerobic cabinet at 37ºC for 2-3 days. 3-4 isolated colonies were inoculated into RCM liquid broth (supplemented with 0.05% (wt/vol) L-cysteine HCl) respectively, and grown in the anaerobic cabinet at 37 ºC for one day. Subsequently, cultures were diluted 20-fold into De Man, Rogosa and Sharpe (MRS) broth (supplemented with 0.05% (wt/vol) L-cysteine HCl), followed by incubation in the anaerobic cabinet at 37ºC for 15-16 hours.

Table 3.1. Bacterial strains characteristics.

Isolate	Strain designation	Relevant feature	Genome size (bp)	Accession number	Reference
UCC2003	*B.breve*	Isolate from nursling stool (expressing UCC2003 EPS)	2,422,684	CP000303	(Mazé et al., 2007)
LH206	*B.longum* subsp. *longum*	Isolate from infant stool	2,350,538	ERS2658036	(Lawson et al., 2020)

3.3. Bacterial growth curves

To assess bacterial growth in BHI, *B. breve* UCC2003 and *B. longum* LH206 bacterial cultures pre-grown in MRS (supplemented with 0.05% (wt/vol) L-cysteine HCl) were diluted 50-fold into BHI media and incubated in the anaerobic cabinet at 37ºC. Growth was measured over time (0-28 hours) by optical density (ΔOD_{600}) measurements. 2 biological replicates were used for each bacterial strain tested.

3.4. Extraction of bifidobacterial metabolites

B. breve UCC2003 and *B. longum* LH206 cultures pre-grown in BHI for 2 days (supplemented with 0.05% (wt/vol) L-cysteine HCl) were diluted 100-fold into pre-warmed BHI broth (supplemented with 0.05% (wt/vol) L-cysteine HCl). Growth curves were monitored until late exponential phase, determined by constructing bacterial growth curves in BHI. Liquid cultures were spun down at 8000 rpm for 10 minutes at 37ºC, and supernatants filter-sterilised using a 0.22 µm filter. Collected supernatants were either used immediately or kept frozen at -20^{0}C for 1-2 days. On the day of exposure, supernatant fractions were quickly thawed using a water bath.

3.5. Treatment of Caco-2 cells

One day before the experiment, Caco-2 cell media was changed into a phenol-free RPMI 1640 media (Gibco) (supplemented with 20% FBS, 100 U/mL/100 µg/mL P/S, 25 mM HEPES and 2 mM L-glutamine) to allow for cytotoxicity experiments, as phenol red interferes with the colorimetric reaction of the kit used. The following solutions were prepared in phenol-free RPMI 1640 media (supplemented with 20% FBS, 100 U/mL/100 µg/mL P/S, 25 mM HEPES and 2 mM L-glutamine) for exposure of Caco-2 cells to different conditions. For treatment with increasing concentrations of BHI medium, BHI solutions at different concentrations (5, 10, 15, 20%) were prepared. For PMA treatment at increasing concentrations, PMA solutions (0.1 nM, 1 nM, 10 nM, 100 nM, 1 µM) were prepared from stock (10 mM in DMSO). For exposure to bacterial metabolites, a 20% bifidobacterial supernatant solution (collected in BHI) was prepared. For short-term and long-term induction of inflammation, 1 µM PMA solution was prepared from stock (10 mM in DMSO). For rapamycin treatment, 5 µM rapamycin solution was prepared from stock (1100 µM in DMSO), and used as positive control for the autophagy staining. 20% DMSO solution was prepared from stock, and used a positive control for the cytotoxicity assay.

In both short-term and long-term inflammatory set-ups, the apical medium (250 µl) was fully replaced with 20% bacterial supernatants in phenol-free RPMI 1640 (Gibco) (supplemented with 20% FBS, 100 U/mL/100 µg/mL P/S, 25 mM HEPES and 2 mM L-glutamine), while the

basolateral media (750 µl) was fully replaced with 1 µM PMA solution in phenol-free RPMI 1640 (Gibco) (supplemented with 20% FBS, 100 U/mL/100 µg/mL P/S, 25 mM HEPES and 2 mM L-glutamine). For the long-term inflammation set-up, media was collected from the apical chamber at baseline and at the end, and from the basolateral chamber at baseline, before PMA treatment and at the end. For the short-term inflammation set-up, both apical and basolateral media were collected at baseline, before PMA treatment, and at the end. At each of these time points, apical and basal media were collected separately in a V-bottom 96-well plate (Greiner CELLSTAR®, Sigma), spun down for 5 minutes at 300x g at 4ºC to remove excess cells, and subsequently transferred to a flat-bottom 96-well plate using a multi-channel pipette. 50 µl of the collected media was used to perform cytotoxicity measurements, while the remaining medium was frozen at -80ºC for subsequent cytokine measurements.

3.6. TEER measurements

TEER measurements of Caco-2 cell monolayers on Transwells were collected using EVOM2^{TM} and STX-100 electrodes. Final TEER measurements were calculated by multiplying the surface area of the Transwell (0.96 cm^2) by the net TEER (Ω), computed by subtracting the measured resistance minus the resistance of the blank Transwell (containing cell culture media only). Measurements were collected at different intervals throughout the expansion and polarisation of the Caco-2 cell monolayers (4-24 days). Additionally, TEER measurements were collected at baseline, after PMA-treatment and at the end of the short-term and long-term inflammation set-ups of bifidobacterial metabolites exposure.

3.7. Cytotoxicity Assay

Cytotoxicity measurements of the Caco-2 cell monolayer were performed on both the apical and basolateral media. Measurements were taken at baseline, before PMA treatment and at the end. For apical media during short-term inflammation only, measurements were taken only at the beginning and at the end of the experiment. Cytotoxicity was measured using the CytoTox 96® Non-Radioactive Cytotoxicity Assay kit (Promega), which measures the amount of Lactate dehydrogenase (LDH) released in the media. Measurements were performed following the manufacturer's instructions. Briefly, 50 µl culture supernatant was transferred to a V-bottom 96-well plate, spun down at 300x g to remove any remaining cell, and transferred to a new flat bottom 96-well plate using a multi-channel pipette. Then, an equal volume of CytoTox 96® Reagent (Promaga) was added to each well and incubated for 30 minutes. During this enzymatic assay, the tetrazolium salt substrate (violet) is converted into a formazan product (red), where the amount of colour formed is proportional to the number of lysed cells. After 30 minutes, 100 µl of stop solution (Promega) was added to each well to stop the

reaction, and the absorbance signal at 490 nm was measured immediately using a standard 96-well plate reader. Lysed cells were used to find the maximum LDH released (maximum cytotoxicity). Cytotoxicity was first expressed as LDH/ml, accounting for the volume of the apical chamber (250 µl) and basolateral chamber (750 µl). Next, cytotoxicity in the different conditions was expressed as a percentage of the maximum cytotoxicity observed for the lysed cell condition after 24 hours.

3.8. IL-8 measurements

Secreted IL-8 was quantified in the media at the beginning, before PMA treatment and at the end, with some exceptions. For the long-term inflammation set-up, IL-8 was quantified at all time points for the basolateral compartment, and at the beginning and end of the experiment for the apical compartment. For the short-term set-up, only the basolateral compartment was assessed at all time points. For the long-term set-up, IL-8 measurements were performed using a U-PLEX assay plate (MSD), based on the sandwich immunoassay method, according to the manufacturer's instructions. Quantification of the IL-8 signal was assessed using the MESO QuickPlex SQ 120 instrument (MSD) and the associated Discovery Workbench Desktop Analysis Software (MSD). Measurements were performed by a former postdoc Dr. Diana Papp (previously at QIB).

For the short-term set-up, IL-8 concentrations were quantified using the Human IL-8 Uncoated ELISA assay (Invitrogen) and measurements of IL-8 signal were collected using a standard plate reader. Measurements were performed by our collaborator Audrey Frachet Bour (Wilmes group, University of Luxembourg).

3.9. Autophagy proteins p62 and LC3 antibody labelling

Immunostaining of autophagy proteins LC3 and p62 was performed only on Caco-2 monolayers exposed to *Bifidobacterium*-derived metabolites or 5 µM rapamycin for 24 hours, without the presence of inflammation. At the end of the experiment, Caco-2 cell monolayers were fixed, permeabilized and stained for intracellular quantification of autophagy proteins p62 and LC3. For LC3, Caco-2 monolayers were permeabilized using 100% methanol (5 minutes), quenched in NH_4Cl (10 minutes) and blocked in 1% Bovine serum albumin (BSA) (30 minutes). For p62, Caco-2 cell monolayers were permeabilized and blocked using 1% BSA + 0.1% saponin solution (30 min). Primary antibody staining was performed using rabbit anti-p62 (1:1000, Invitrogen), rabbit anti-LC3 antibodies (1:1000, Abcam) and mouse anti-EpCAM antibodies (1:1000, Abcam) prepared in 1% BSA + 0.1% saponin (for p62) and 1% BSA (for LC3) overnight at 4 ^{0}C. Secondary antibody was performed using goat anti-rabbit Alexa Fluor 594 (for p62 and LC3 staining) (1:1000, ThermoFisher Scientific). Two separate sets of

samples were prepared to stain for p62 and LC3, as these antibodies were raised in the same species. Monolayers were also counterstained with DAPI (1:2000, ThermoFisher Scientific) and phalloidin-iFluor488 (1:1000, Abcam) to visualise nuclei and actin cytoskeleton, respectively.

3.10. Image acquisition and analysis

Four to five representative images of stained Caco-2 cell monolayers were collected for each condition using LSM880 confocal microscope with AiryScan (Zeiss), and a 63x oil immersion lens. Cell segmentation and quantification of p62 and LC3 puncta was performed using the Imaris cell imaging software (Oxford Instruments). Briefly, a batch analysis was set-up to analyse multiple images. First, pre-processing of the images was applied to improve the phalloidin staining for the cell border, by applying a gaussian filter (0.05) and a gamma correction (1.5). Next, the Cell module was used to segment individual cells using green channel (phalloidin) as cell border marker for cytoplasmic identification. In particular, a cell size of 7 µm and membrane detail of 0.1 µm and local contrast as filter type were used for the analysis. Subsequently, any object touching the border was removed. As part of the Cell module, p62 and LC3 puncta were identified as vesicles using the red channel (Alexa Fluor 594), a 0.9 µm as cell diameter and using the background subtraction method. Statistics were exported for each batch analysis as a .csv file. For both p62 and LC3, data about the mean signal intensity and number of vesicles per segmented object/cell was used to quantify LC3 or p62 puncta (autophagosomal structures) signal for each condition.

4. Results

4.1. BHI represents a less cytotoxic alternative to bacterial medium MRS

In **Chapter 2**, I showed that bacterial MRS media is toxic for epithelial cells in organoids and that BHI represents a less cytotoxic alternative to use for exposure of epithelial cells to bifidobacterial metabolites. Even if not tested directly, a similar level of cytotoxicity for MRS would be expected for Caco-2 cells as well. Hence, I aimed to assess the maximum concentration of BHI that could be added to Caco-2 cells without causing cytotoxicity. Similarly to what was done for mouse ileal organoids, differentiated Caco-2 cell monolayers (7 days post splitting) were exposed to increasing concentrations (5, 10, 15, 20%) of BHI broth for 24 hours, and cytotoxicity was evaluated by measuring the amount of released LDH in the media after exposure. Epithelial medium RPMI with or without 20% DMSO was used as negative and positive control, respectively. Additionally, one sample containing lysed cells was also used as an indication of the maximum cytotoxicity. For Caco-2 cells, all conditions tested resulted in no significant differences in the levels of cytotoxicity compared to the media control RPMI (**Figure 3.2**). Conversely, treatment with 20% DMSO resulted in a significant (p-value < 0.001) increase in cytotoxicity levels, up to 100% relative to the lysed cell condition **(Figure 3.2**). Based on these results, 20% BHI was selected as the maximum acceptable concentration of bacterial media to expose for Caco-2 monolayers.

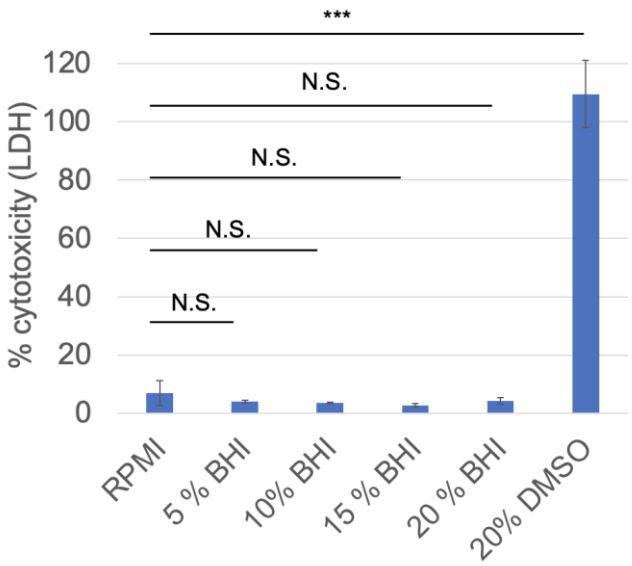

Figure 3.2. Cytotoxicity of increasing concentrations of BHI media in Caco–2 monolayers. Bar chart showing the percent (%) cytotoxicity measured for Caco-2 monolayers exposed to increasing BHI concentrations for 24 hours. Caco-2 monolayers were differentiated on 96-well plates for one week before being exposed to increasing concentrations (5, 10, 15, 20%) of BHI broth for 24 hours. Epithelial

media (RPMI 1640) and 20% DMSO were used as negative and positive controls, respectively. Lysed epithelial cells were also used to calculate the maximum cytotoxicity. Cytotoxicity was evaluated in the medium after 24 hours using the CytoTox 96® Non-Radioactive Cytotoxicity Assay kit. Cytotoxicity was evaluated as delta optical density (ΔOD_{490}), which is proportional to the amount of LDH released in the media. The height of the bar chart indicates the percent (%) cytotoxicity ± standard deviation (SD) (n=3). % cytotoxicity was calculated as follows: (cytotoxicity of each condition / maximum cytotoxicity of lysed cells) x 100. Statistical significance was calculated relative to the media control (RPMI 1640) by performing a Student t-test. N.S., non-significant (p-value > 0.05); * p-value < 0.05; **p-value < 0.01; *** p-value < 0.001.

4.2. Bifidobacterial strains reach the lag phase of growth in BHI media after 9 hours

Because BHI proved to be a good alternative media to expose epithelial cells to bacterial metabolites, I next aimed to test whether bifidobacteria was able to grow in BHI medium. Furthermore, I aimed to determine the time at which bifidobacterial strains reach the late exponential (or beginning of lag) phase of growth in this medium, where metabolites would be extracted. This phase was chosen as it represents the time when most produced metabolites would have accumulated, leading to the highest concentration. To achieve these goals, the growth of bifidobacterial strains (*B. breve* UCC2003 and *B. longum* LH206) in BHI was followed over time.

For both strains, growth began after 5 hours from inoculation (start of exponential phase), and started to plateau around 10 hours (**Figure 3.3A, B**). Compared to *B. longum* LH206, where the stationary phase of growth remained between 10-28 hours (ΔOD_{600} ~ 1), *B. breve* UCC2003 seemed to continue to grow, based on OD_{600} reaching values of 1.4. This could be due to an actual second phase of growth or accumulation of dead cells in the media, which would contribute to an increase in OD_{600} values. Nevertheless, based on the constructed growth curves, I was able to determine the late exponential phase needed for metabolites extraction, which was established at 9 hours for both *B. breve* UCC2003 and *B. longum* LH206 (**Figure 3.3A, B**).

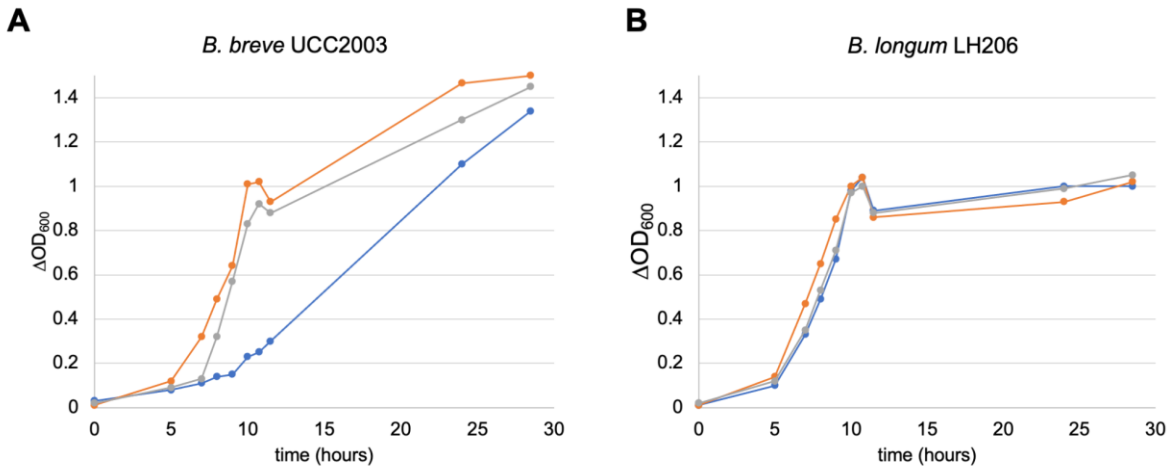

Figure 3.3. Bifidobacterial growth curves in BHI broth. Delta optical density measurements at 600 nm (OD_{600}) are shown (y axis) over time (0-28 hours) (x axis) for *B. breve* UCC2003 (A) and *B. longum* LH206. Single colonies were picked, and grown into BHI broth for 2 days. Subsequently, cultures were diluted 1:50, the point at which the growth curve was started. Measurements for 2 biological replicates of *B. breve* UCC2003 (A) and *B. longum* LH206 (B) are shown. No statistical analysis was carried out due to the insufficient number of replicates (n=2).

4.3. Caco-2 cell monolayers polarise within 18-23 days from seeding on Transwells

To assess the effect of bifidobacterial exposure during long-term and short-term inflammation of the epithelium, two full 24-well plates of Caco-2 cell monolayers were established on Transwells. The correct differentiation of the monolayer was assessed by monitoring TEER, which is an indication of barrier integrity.

Generally, measured TEER of Caco-2 cells seeded on Transwells grew over time, indicating the increased confluency and polarisation of the epithelial layer (**Figure 3.4A, B**). Conversely, the TEER stayed virtually zero for the Transwell inserts where no cells had been seeded (**Figure 3.4A, B**), and the absence of cells could be confirmed by observing the empty Transwell under a brightfield microscope, indicating absence of contamination (**Figure 3.5A**).

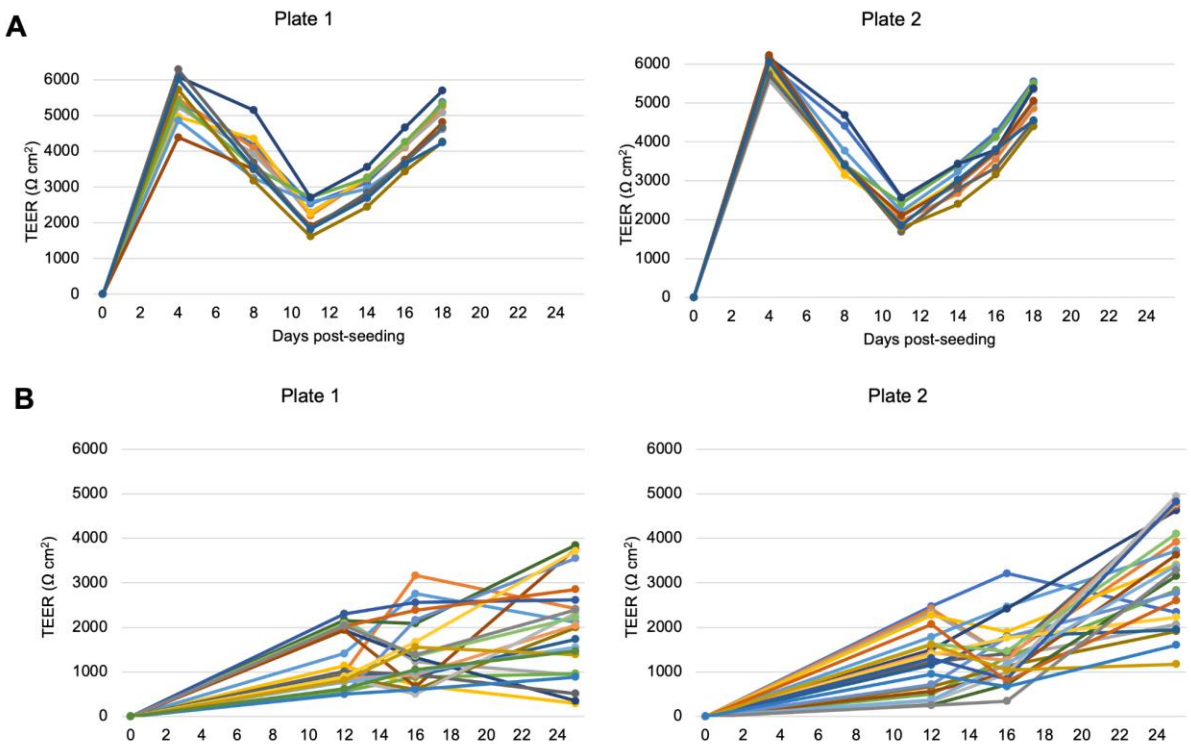

Figure 3.4. TEER measurements during differentiation of Caco-2 monolayers on Transwells. TEER measurements were collected using an EVOM2 and STX-100 electrodes to monitor epithelial barrier during Caco-2 monolayer expansion and differentiation on Transwells established for the long-term inflammation (A) and short-term inflammation (B) experimental set-ups. TEER measurements are expressed as Ω cm^2 by adjusting the measured TEER for the surface area of the Transwell used (0.96 cm^2).

In the two plates established for the long-term inflammation set-up, TEER measured was very high (6000 Ω cm^2) at day 4, followed by a sharp decrease between day 4-11 and a further increase between day 11-18 (**Figure 3.4A**). The initial peak in TEER values could be explained by the presence of a double layer of cells, which may have confounded the TEER measurements. This could be indeed noticed by microscopical observation of the Caco-2 cell monolayer under a brightfield microscope (**Figure 3.5B**). This is not commonly observed, and it could be due to the overseeding of the Transwell insert. At day 18, cells had reached an overall TEER of 6000 Ω cm^2, and the monolayer was considered as confluent (**Figure 3.4A**). This was also confirmed based on the observation under the brightfield microscope showing a differentiated Caco-2 monolayer (**Figure 3.5B**). This time-point was a little bit earlier compared to the normal timing of Caco-2 differentiation, but it may be due to the highest seeding density used at the beginning.

In the two plates established for the short-term set-up, TEER measurements recorded were quite variable, with the variability not attributable to a specific measurement or time point **(Figure 3.4B**). Interestingly, variability in TEER was much higher compared to the growth of Caco-2 monolayers established for the long-term set-up and could be attributed to an issue related to the measuring instrument. Nethertheless, the general trend indicated increasing TEER of the monolayer over time (**Figure 3.4B**). After 24 days, TEER measurements had reached between 4000-5000 Ω cm^2, which was lower than the ones obtained during the first set-up (**Figure 3.4A**). Based on microscopic observation at day 12 and day 24, it seemed that the monolayers had reached confluency but a quite large surface was covered by a double layer of cells (**Figure 3.5C**), which may have had an impact on the TEER measurements. To avoid possible cell loss after 24 days, I decided to use these monolayers for the experiment, despite the lower measured TEER.

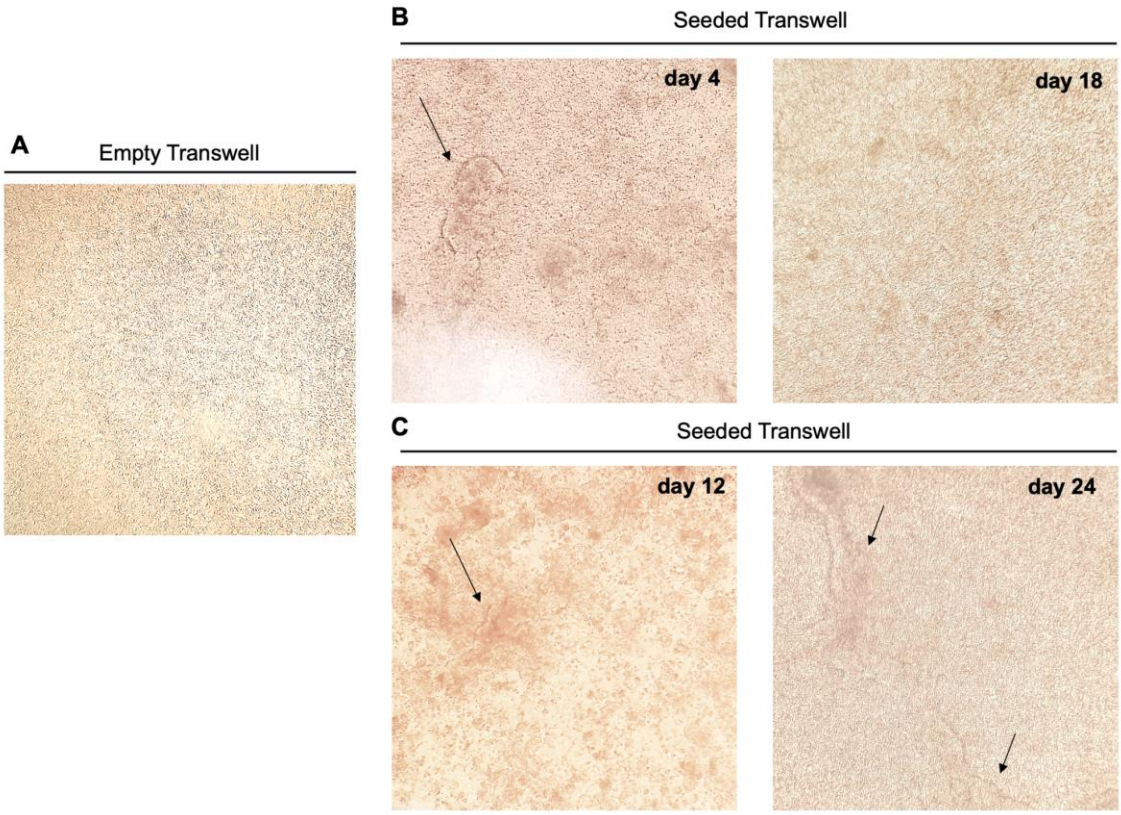

Figure 3.5. Representative brightfield microscopy pictures of seeded Transwell inserts. **A)** Blank Transwell with no cells; **B)** Long-term inflammation set-up; Transwell insert seeded with Caco-2 cells 4 and 18 days post-seeding. **C)** Short-term inflammation set-up; Transwell insert seeded with Caco-2 cells 12 and 24 days post-seeding.

4.4. PMA-induced inflammation does not affect Caco-2 cell viability

When inducing inflammation in Caco-2 monolayers, it was important to establish the maximum concentration of inflammatory agent PMA to use without causing extended cell death and reduced cell viability. To determine the ideal concentration, 7-days Caco-2 monolayers were treated with increasing concentrations of PMA (0.1 nM, 1 nM, 10 nM, 100 nM, 1 µM) for 24 hours, and cell cytotoxicity was measured at the end of the experiment. Additionally, Caco-2 grown in RPMI 1640 media and 20% DMSO were used as media control and positive control, respectively.

Cytotoxicity levels measured after 24 hours in Caco-2 cells exposed to increasing PMA concentrations resulted in a similar level of cytotoxicity (40%), which was not significantly increased compared to the media control RPMI (40%) (**Figure 3.6**). These values were also about half of those measured for Caco-2 cells exposed to 20% DMSO (positive control), where cytotoxicity levels significantly (p-value < 0.001) increased compared to the media control RPMI (**Figure 3.6**). The relatively high levels of cytotoxicity observed across all conditions could be due to some pre-existent levels of cell death present at baseline, due to an overseeding of the 96-well plate, and not dependent on PMA-treatment. Hence, the highest concentration of PMA tested (1 µM) was selected as a safe concentration for the establishment of inflammation in Caco-2 monolayers, without causing excess loss in cell viability.

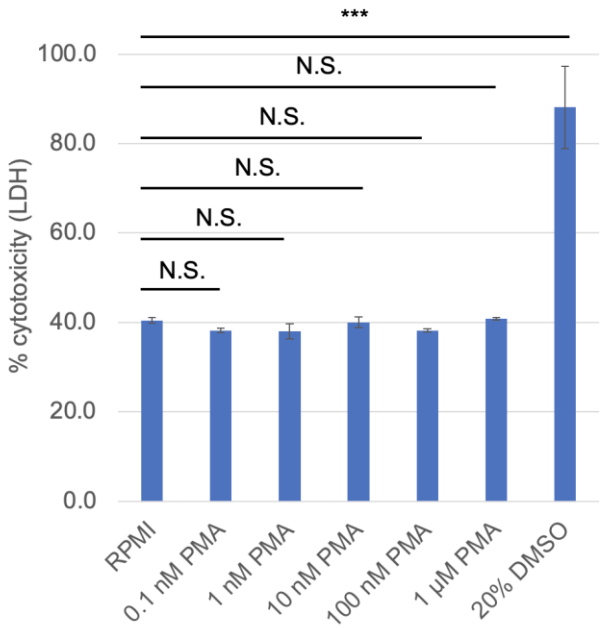

Figure 3.6. Cytotoxicity of increasing concentration of PMA in Caco–2 monolayers. Bar chart showing the amount of % cytotoxicity measured for Caco-2 monolayers exposed to increasing PMA

concentration for 24 hours. Caco-2 monolayers were differentiated on 96-well plates for one week before being exposed to increasing concentrations (0.1 nM, 1 nM, 10 nM, 100 nM, 1 µM) of PMA for 24 hours. Epithelial media (RPMI) and 20% DMSO were used as media and positive controls respectively. Lysed epithelial cells were also used to calculate the maximum cytotoxicity. Cytotoxicity was evaluated in the medium after 24 hours using the CytoTox 96® Non-Radioactive Cytotoxicity Assay kit (Promega). Cytotoxicity was evaluated as delta optical density (ΔOD_{490}), which is proportional to the amount of LDH released in the media. The height of the bar chart indicates the percent (%) cytotoxicity ± standard deviation (SD). % cytotoxicity was calculated as follows: (cytotoxicity of each condition / maximum cytotoxicity of lysed cells) x 100. Statistical significance was calculated relative to the media control (RPMI) by performing a Student t-test. N.S., non significant (p-value > 0.05); * p-value < 0.05; **p-value < 0.01; *** p-value < 0.001.

4.5. Effect of bifidobacterial metabolites exposure against short-term and long-term induced inflammation

To determine the beneficial effect of bifidobacterial metabolites on the epithelium during long-term and short-term inflammation, differentiated Caco-2 cell monolayers on Transwells were exposed to 20% bifidobacterial metabolites (extracted from *B. breve* UCC2003 and *B. longum* LH206), followed by induction of inflammation by PMA treatment for either 20 hours (long-term) (**Figure 3.7A**) or 4 hours (short-term) **(Figure 3.7B**), for a total experimental time of 24 hours. Furthermore, to study how bifidobacterial metabolites modulate autophagy, Caco-2 cell monolayers were alternatively exposed at baseline to rapamycin, which is a potent activator of autophagy (see introduction of this chapter), without inducing inflammation.

In both short-term and long-term inflammation set-ups, the effect on barrier integrity, cell viability and pro-inflammatory IL-8 release was evaluated at the beginning, before induction of inflammation and at the end. Autophagy processes (LC3 and p62 puncta) were also evaluated at the end in Caco-2 monolayers exposed to *Bifidobacterium* metabolites and rapamycin.

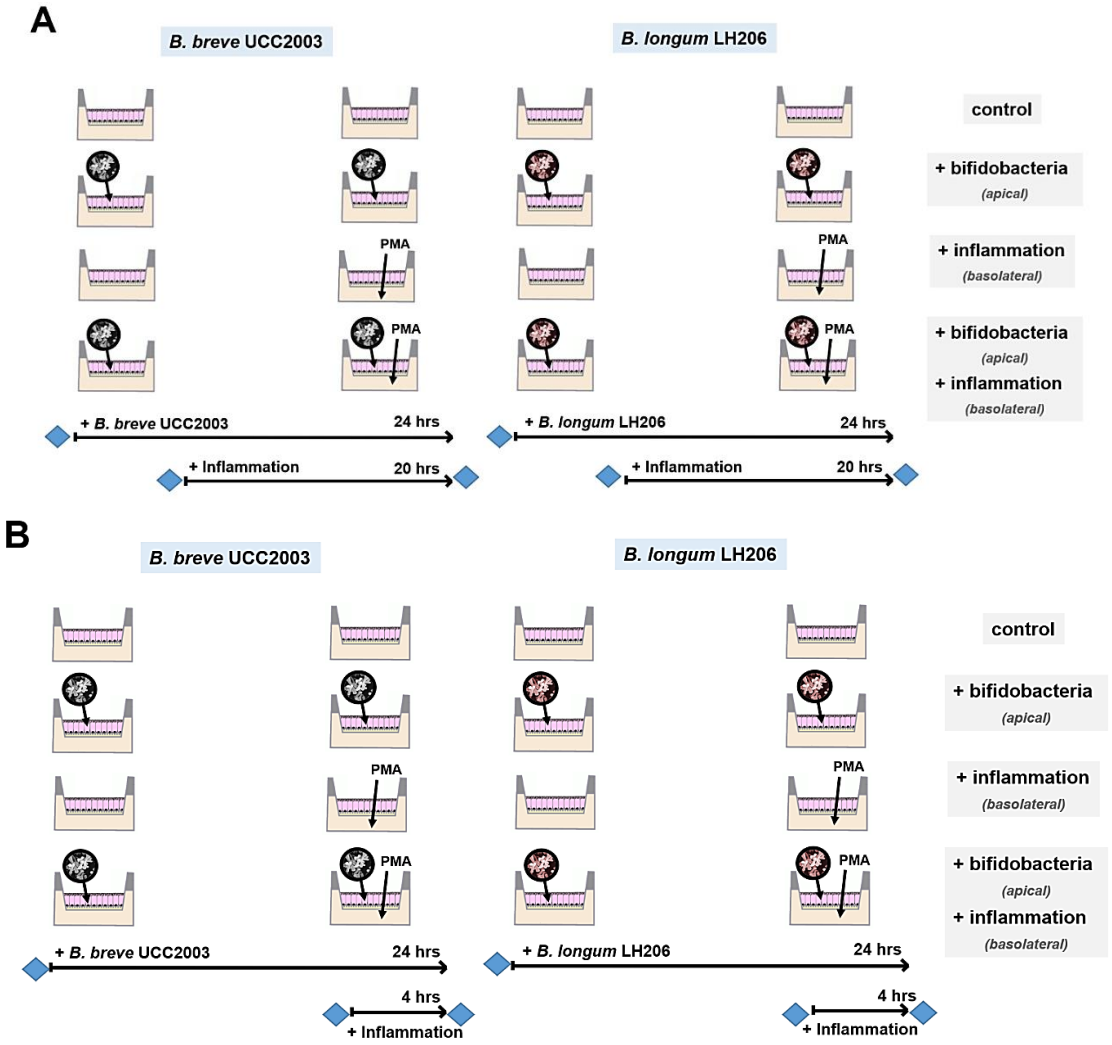

Figure 3.7. Experimental set-up to evaluate the protective effects of bifidobacterial metabolites during long-term and short-term inflammation. A) Set-up where long-term inflammation was induced (20 hours). B). Set-up where short-term inflammation was induced (4 hours).

4.6. Beneficial effects of bifidobacterial metabolites during long-term inflammation

4.6.1. Bifidobacterial metabolites increase barrier function, but does not protect against inflammation-induced loss of epithelial barrier

To evaluate the protective effects of bifidobacterial metabolites on barrier function during long-term inflammation, TEER was measured at baseline, before PMA-treatment (4 hours) and at the end (24 hours). In the first 4 hours after addition of bifidobacterial metabolites or rapamycin, a small increase in TEER was observed, which was similar between strains tested (*B. breve* UCC2003, *B. longum* LH206). Conversely, a decrease in TEER was recorded for untreated

(RPMI) or DMSO-treated Caco-2 cell monolayers, with the highest decrease observed in DMSO-treated samples, as it would be expected when giving a cytotoxic agent **(Figure 3.8)**. This suggests that exposure to bifidobacterial metabolites or activation of autophagy results in increased barrier function in Caco-2 cells.

Between 4 and 24 hours, in the absence of inflammation or DMSO treatment, TEER values slightly increased, both in absence (RPMI) or presence of bifidobacterial metabolites, and with rapamycin treatment (**Figure 3.8**). Conversely, PMA-treatment samples showed a decrease in TEER, both in the presence or absence of bifidobacterial metabolites, which was comparable to the DMSO-treated samples (**Figure 3.8**). This would suggest that in the presence of inflammation exposure to bifidobacterial metabolites did not protect Caco-2 cells against the loss of epithelial barrier.

At the end of the experiment, the highest TEER values could be observed samples exposed to bifidobacterial supernatants for the whole duration of the experiment; intermediate values for those pre-exposed to bifidobacterial supernatants followed by inflammation or those left untreated (RPMI); the lowest values for PMA-treated samples where no pre-exposure with bifidobacterial supernatants was performed, or for DMSO-treated samples **(Figure 3.8).**

Overall, these results indicate that exposure of Caco-2 cells to bifidobacterial metabolites or rapamycin, an autophagy activator, results in increased epithelial barrier, but this positive effect cannot be maintained when the barrier function is disrupted by a long-term inflammation induction by PMA treatment.

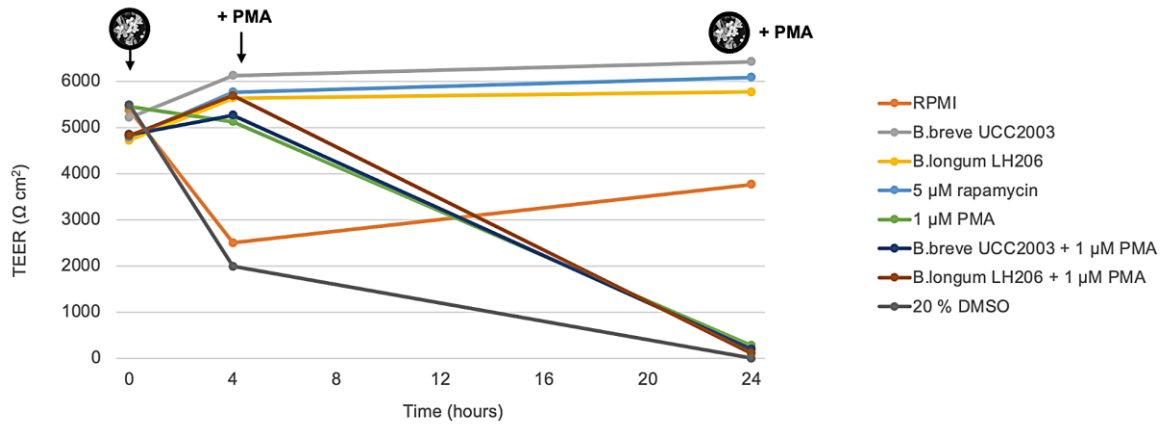

Figure 3.8. Changes in TEER measurements of Caco-2 monolayers on Transwells upon bifidobacterial metabolite exposure and long-term induced inflammation. Line graphs showing changes in TEER over time. Measurements were taken at the beginning, before PMA-treatment (4 hours) and at the end (24 hours) for all conditions. Measurements were collected prior to medium

removal using an EVOM2 and STX-100 electrodes. TEER measurements are expressed as Ω cm^2 by adjusting the measured TEER for the surface area of the Transwell used (0.96 cm^2). Average values are shown (n=2).

4.6.2. Bifidobacterial metabolites protects against inflammation-induced decrease in epithelial cell viability

Next, to assess the protective effect of bifidobacterial metabolites exposure against increased cytotoxicity induced by long-term inflammation, cell viability of the Caco-2 monolayer was measured in the absence or presence of bifidobacterial metabolites and inflammation. Cytotoxicity levels were evaluated in the culturing media by measuring the release of LDH, which is an indication of membrane integrity. Measurements were taken at the beginning, before PMA-treatment (20 hours) and at the end (24 hours) for the basolateral compartment, and at the beginning and end for the apical compartment.

In the absence of inflammation, cytotoxicity levels measured in the apical compartment showed a decrease over time (0-24 hours) in samples exposed to bifidobacterial metabolites, rapamycin, or left untreated, with the highest decrease observed for those exposed to bifidobacterial metabolites (**Figure 3.9**). When measured in the basolateral compartment, cytotoxicity slightly decreased in the first 4 hours upon bifidobacterial metabolite exposure or in the untreated samples, while it increased slightly between 4-24 hours in the bifidobacteria-treated samples, and remained stable or slightly decreased in the untreated or rapamycin treated samples (**Figure 3.9**).

In the presence of inflammation, when measured in the basolateral compartment, all PMA-treated samples showed an increased cytotoxicity compared to the non-treated samples, which was independent of whether Caco-2 cells had been exposed to bifidobacterial metabolites or not (**Figure 3.9**). However, when measured in the apical compartment, cytotoxicity increased in all PMA-treated samples, but did not increase or increased less for samples exposed to *B. longum* LH206 and *B. breve* UCC2003-derived metabolites, respectively (**Figure 3.9**).

Overall, these observations support an inflammation-induced decrease in cell viability, which can be partially restored by pre-exposure with bifidobacterial metabolites, with a bigger effect for those derived from *B. longum* LH206.

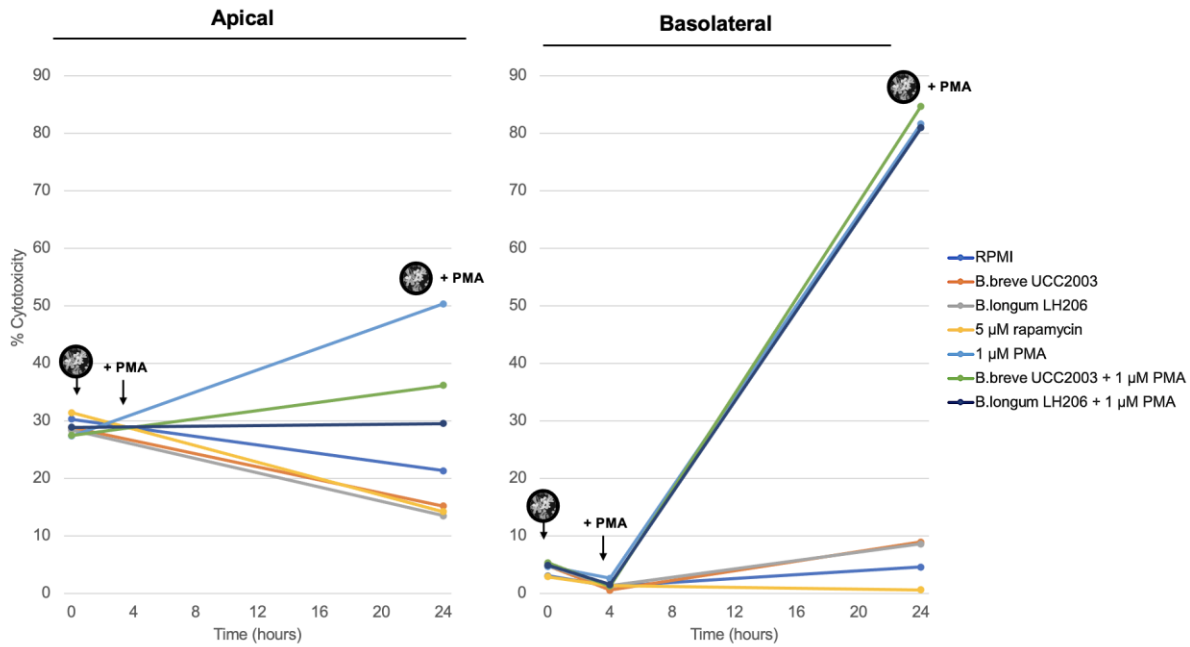

Figure 3.9. Epithelial cell cytotoxicity of Caco-2 cell monolayers on Transwells upon bifidobacterial metabolite exposure and long-term induced inflammation. Line graphs indicating average cytotoxicity measurements relative to the long-term inflammation set-up for all conditions. Measurements for the apical (left) and basolateral (right) compartments are shown separately. Cytotoxicity measurements were taken at the beginning (0 hours), after bifidobacterial exposure (4 hours) and at the end (24 hours) for the basolateral compartment; at the beginning (0 hours) and at the end (24 hours) for the apical compartment. Line graphs show average measurements (n=2) of percent (%) cytotoxicity, which was calculated relative to the maximum cytotoxicity obtained for Caco-2 cells treated with 20% DMSO for 24 hours. No statistical analysis was carried out due to the insufficient number of replicates (n=2).

4.6.3. Bifidobacteria does not protect against inflammation-induced increase in IL-8 production

Next, to assess the protective effects of bifidobacterial metabolites against long-term inflammation, we measured the amount of pro-inflammatory cytokine IL-8 released in the absence or presence of bifidobacterial metabolites and inflammation.

In the apical compartment, exposure to bifidobacterial metabolites resulted in an accumulation of IL-8. The accumulation of IL-8 was higher for *B. breve* UCC2003 than *B. longum* LH206, and it was not recorded in the basolateral compartment (**Figure 3.10**). Furthermore, in PMA-treated samples, IL-8 levels increased in both apical and basolateral compartment, with a higher increase in the basolateral compartment. Surprisingly, this increase was independent of whether samples had been exposed to bifidobacterial metabolites prior to induction of

inflammation (**Figure 3.10**). At the end of the experiment, IL-8 levels measured in both compartments were the highest for samples pre-exposed to bifidobacterial metabolites and where inflammation was induced, with a higher increase for those exposed to *B. breve* UCC2003 than *B. longum* LH206 supernatant (**Figure 3.10**).

Overall, these results suggest that exposure of Caco-2 cells to bifidobacterial metabolites triggers an apical accumulation of IL-8, especially for *B. breve* UCC2003-derived metabolites. Additionally, pre-exposure to *Bifidobacterium* metabolites did not result in any protective effects against IL-8-induced release upon long-term inflammation. In this context, it could be that other cytokines than IL-8 were released by epithelial cells following induction of inflammation, which could be mediating the anti-inflammatory effects of bifidobacterial-derived metabolites.

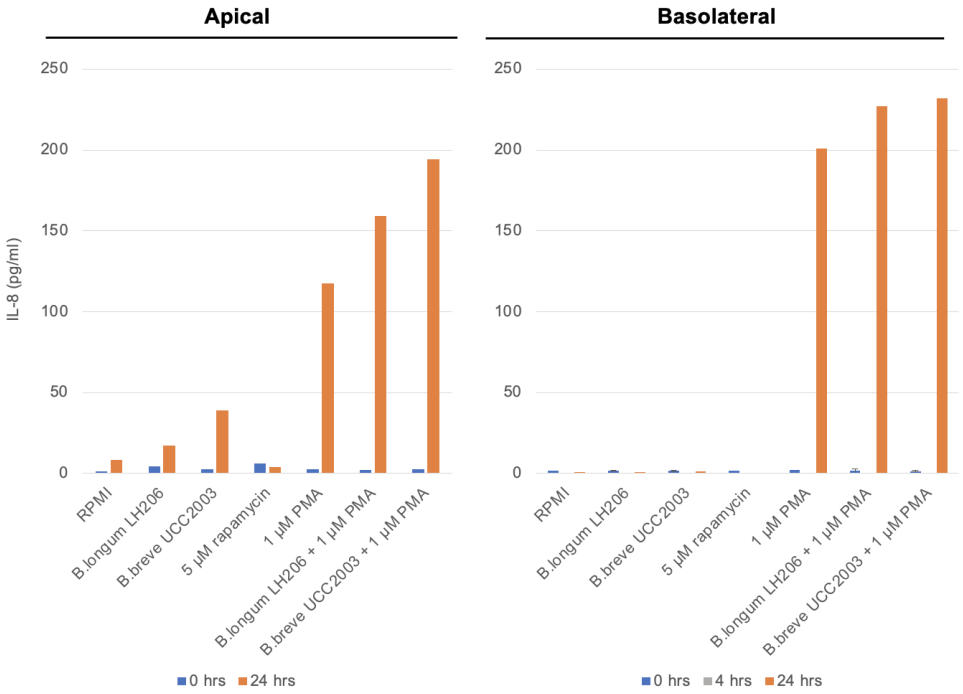

Figure 3.10. **IL-8 accumulation in the apical and basolateral compartments of Caco-2 cell monolayers on Transwells upon bifidobacterial metabolite exposure and long-term induced inflammation**. Bar showing the amount of IL-8 released in the media by Caco-2 cells. Measurements for the apical (left) and basolateral (right) compartments are shown separately. IL-8 was quantified at the beginning, after bifidobacterial exposure (4 hours), and at the end (24 hours) in the basolateral compartment media; at the beginning and at the end (24 hours) in the apical compartment media. IL-8 was measured using a U-PLEX assay plate (MSD). The height of the bar indicates average measurements (n=2). IL-8 is expressed as pg/ml, by accounting for the volumes of the two compartments (250 µl for the apical compartment, 750 µl for the basolateral compartment). No statistical analysis was carried out due to the insufficient number of replicates (n=2).

4.7. Beneficial effects of bifidobacterial metabolites during short-term induced inflammation

4.7.1. Bifidobacterial metabolites increase barrier function, and partially protect against inflammation-induced loss of epithelial barrier

To evaluate the protective effects of bifidobacterial metabolites on barrier function during long-term inflammation, TEER was measured at baseline, before PMA-treatment (20 hours) and at the end (24 hours). In the first 20 hours of the experiment, TEER values slightly decreased across all conditions, with or without the exposure to bifidobacterial metabolites or rapamycin. This observation could be due to an issue with the instrument used for collection of the TEER measurements (**Figure 3.11**).

Between 20 and 24 hours, TEER remained stable in PMA-treated samples or untreated ones (RPMI), while it decreased further in DMSO-treated samples (**Figure 3.11**). Conversely, TEER values increased in all samples that were pre-exposed to bifidobacterial metabolites or rapamycin, independent of whether inflammation was induced with PMA or not (**Figure 3.11**). However, the increase in TEER was higher for samples that were pre-exposed to bifidobacterial metabolites and where no inflammation was induced, with similar effects observed for *B. breve* UCC2003 and *B. longum* LH206 supernatants (**Figure 3.11**).

Overall, these results point towards the ability of bifidobacterial metabolites to increase epithelial barrier in the absence of inflammation, and to partially rescue the loss of barrier integrity resulting from induction of short-term inflammation in Caco-2 cells.

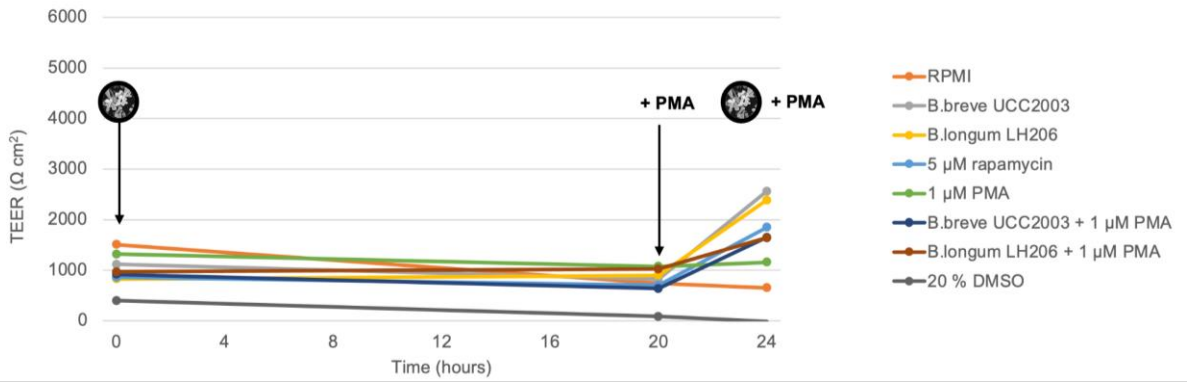

Figure 3.11. Changes in TEER measurements of Caco-2 monolayers on Transwells upon bifidobacterial metabolite exposure and short-term PMA-induced inflammation. Line graph showing changes in TEER over time. TEER measurements were taken at the beginning (0 hours), after

bifidobacterial exposure (20 hours) and at the end (24 hours) in all conditions. TEER measurements were collected prior to medium removal using an Epithelial Tissue Volt Ohmmeter 2 (EVOM2) and STX-100 electrodes. TEER measurements are expressed as Ω cm^2 by adjusting the measured TEER for the surface area of the Transwell used (0.96 cm^2). Average values are shown (n=3).

4.7.2. Bifidobacterial metabolites do not protect against inflammation-induced decrease in epithelial cell viability

Next, to assess the protective effect of bifidobacterial metabolites exposure against cytotoxicity induced by short-term inflammation, Caco-2 cell viability was measured in the media in the absence or presence of bifidobacterial metabolites and inflammation. Cytotoxicity levels were evaluated in the apical and basolateral compartments of Transwells at the beginning, before PMA-treatment (20 hours), and at the end (24 hours). In the absence of inflammation, cytotoxicity levels remained stable in both the apical and basolateral compartment for all samples, with only a small decrease recorded in the basolateral compartment for samples exposed to *B. longum* LH206 supernatant (**Figure 3.12**).

Between 20 and 24 hours, cytotoxicity increased in all conditions, which could be due to an issue with the measuring instrument (**Figure 3.12)**. However, this increase was higher for PMA-treated samples compared to untreated ones (RPMI). Additionally, at the end of the experiment, the measured cytotoxicity was higher in PMA-treated samples that had been pre-exposed to bifidobacterial metabolites, especially those from *B. longum* LH206 (**Figure 3.12**).

Overall, these observations support an inflammation-induced decrease in cell viability, which is further increased by pre-exposure with bifidobacterial metabolites, especially those from *B. longum* LH206.

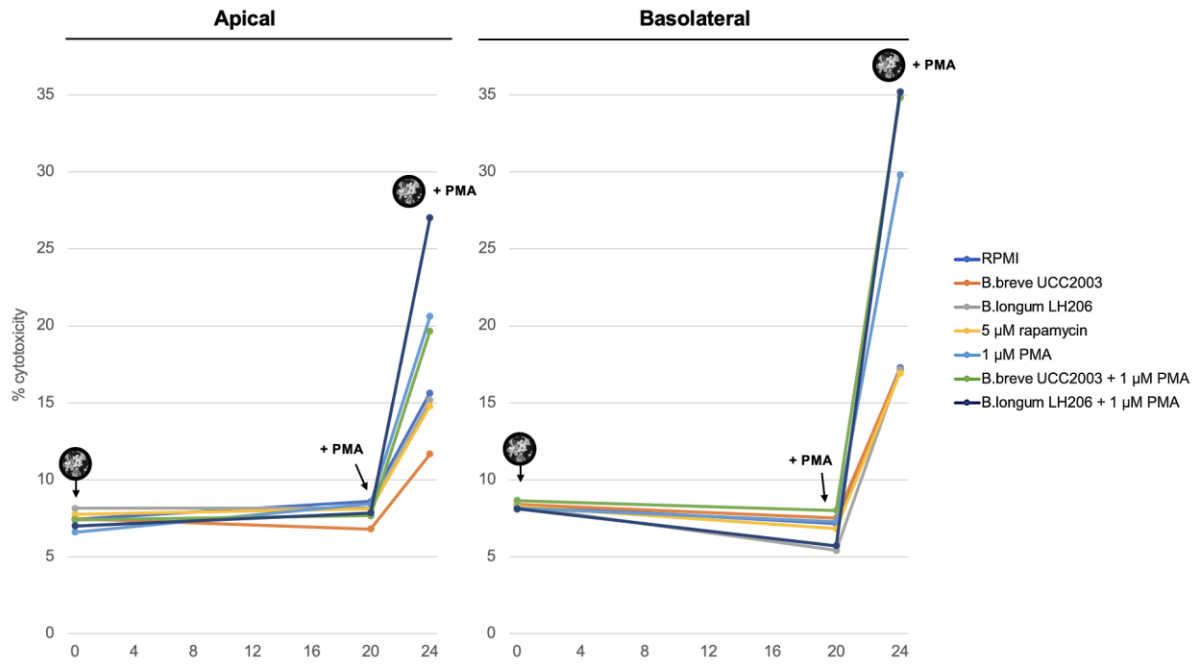

Figure 3.12. Changes in epithelial cell cytotoxicity of Caco-2 monolayers on Transwells upon bifidobacterial metabolite exposure and short-term PMA-induced inflammation. Line graphs indicating average cytotoxicity measurements relative to the short-term inflammation set-up for all conditions. Measurements for the apical (left) and basolateral (right) compartments are shown separately. Cytotoxicity measurements were taken at the beginning, after bifidobacterial exposure (20 hours) and at the end (24 hours). Line graphs show average measurements (n=3) of percent (%) cytotoxicity, which was calculated relative to the maximum cytotoxicity obtained for Caco-2 cells treated with 20% DMSO for 24 hours.

4.7.3. Bifidobacterial metabolites do not protect against inflammation-induced increase in IL-8 production

To assess the protective effects of bifidobacterial metabolites against short-term inflammation-induced cytokine release, we measured the amount of pro-inflammatory cytokine IL-8 released by Caco-2 cells in the basolateral compartment of the Transwells.

Exposure to bifidobacterial metabolites did not result in the accumulation of IL-8 in the basolateral compartment, similar to what was observed in the short-term inflammatory set-up (**Figure 3.10, 3.13**). Furthermore, the induction of short-term inflammation resulted in a sharp increase in IL-8 levels, which could not be rescued by bifidobacterial supernatant exposure prior to induction of inflammation (**Figure 3.13**). However, contrary to what was observed in the short-term inflammation set-up, no significant difference in measured IL-8 levels was

observed at the end of the experiment between PMA-treated samples in the presence or absence of bifidobacterial supernatant prior to inflammation induction (**Figure 3.10, 3.13**).

Overall, these results suggest that there are no protective effects of bifidobacterial metabolites against IL-8-induced release upon long-term inflammation. Again, these results may be due to other cytokines than IL-8 being released during inflammation, which could mediate the anti-inflammatory effects of bifidobacterial-derived metabolites.

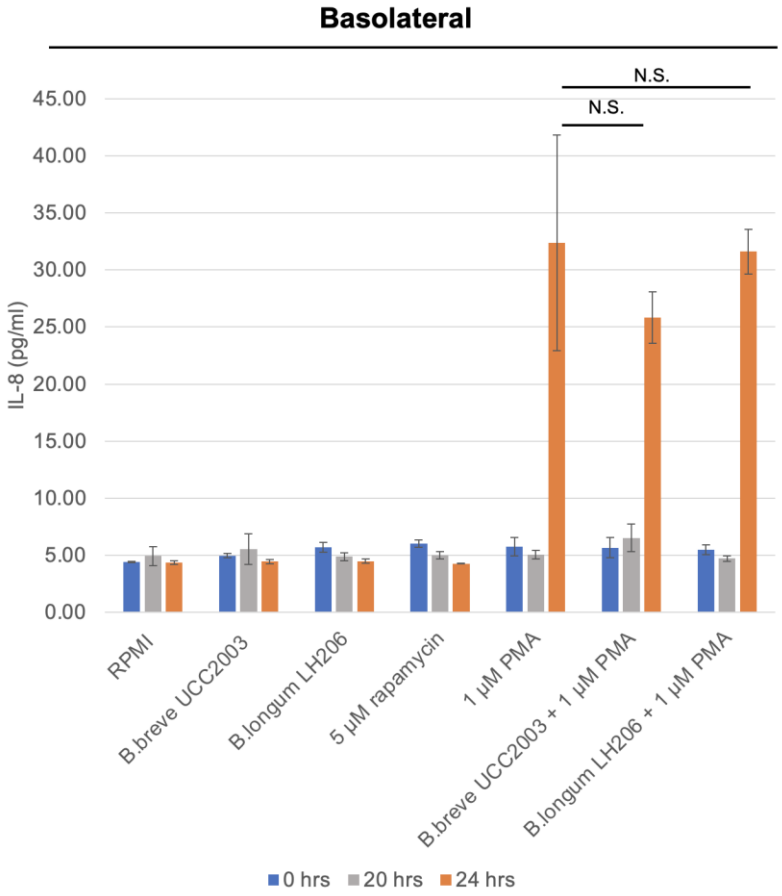

Figure 3.13. **IL-8 accumulation in the basolateral compartment of Caco-2 cell monolayers on Transwells upon bifidobacterial metabolite exposure and short-term induced inflammation.** Bar graph showing the amount of IL-8 released in the media by Caco-2 cells. IL-8 was measured in the basolateral compartment only by ELISA. IL-8 was quantified at the beginning (0 hours), after bifidobacterial exposure (20 hours) and at the end (24 hours). Height of the bar indicates average measurements ± SD (n=3), expressed as pg/ml, by accounting for the volumes of the two compartments (250 µl for the apical, 750 µl for the basolateral). Statistical significance was calculated relative to the media control (RPMI 1640) or inflammatory control (PMA) by performing a Student t-test. All comparisons tested were not-significant (N.S.), therefore they were not reported on the graph, apart from at 24 hours for the PMA-treated samples.

4.8. Bifidobacterial-derived metabolites regulate autophagy processes in intestinal epithelial cells

To evaluate whether bifidobacterial metabolites regulate autophagy in intestinal epithelial cells, uninflamed Caco-2 monolayers were stained for autophagy proteins LC3 and p62, and autophagy flux was evaluated by immunofluorescence staining and quantification of LC3 and p62 puncta (**Figure 3.14**). Quantification of lipidated LC3 puncta represents the gold-standard measure for the numbers of autophagosomes in cells, while p62 dot intensity can be used as indication of autolysosomes formation (see **Chapter 1**). To quantify the number of puncta and signal intensity within intestinal cells in Caco-2 monolayers, representative images of LC3 and p62 immunostaining were collected by confocal microscopy and further analysed using the Imaris cell imaging software. First, a pipeline was built to first identify/segment epithelial cells within organoids based on membrane immunostaining (**Figure 3.14A**). Subsequently, LC3 or p62 puncta were identified based on LC3 or p62 proteins immunostaining (**Figure 3.14B**). Finally, the number of puncta and average intensity per cell for each set of images was computed to quantify autophagy processes (**Figure 3.14C**).

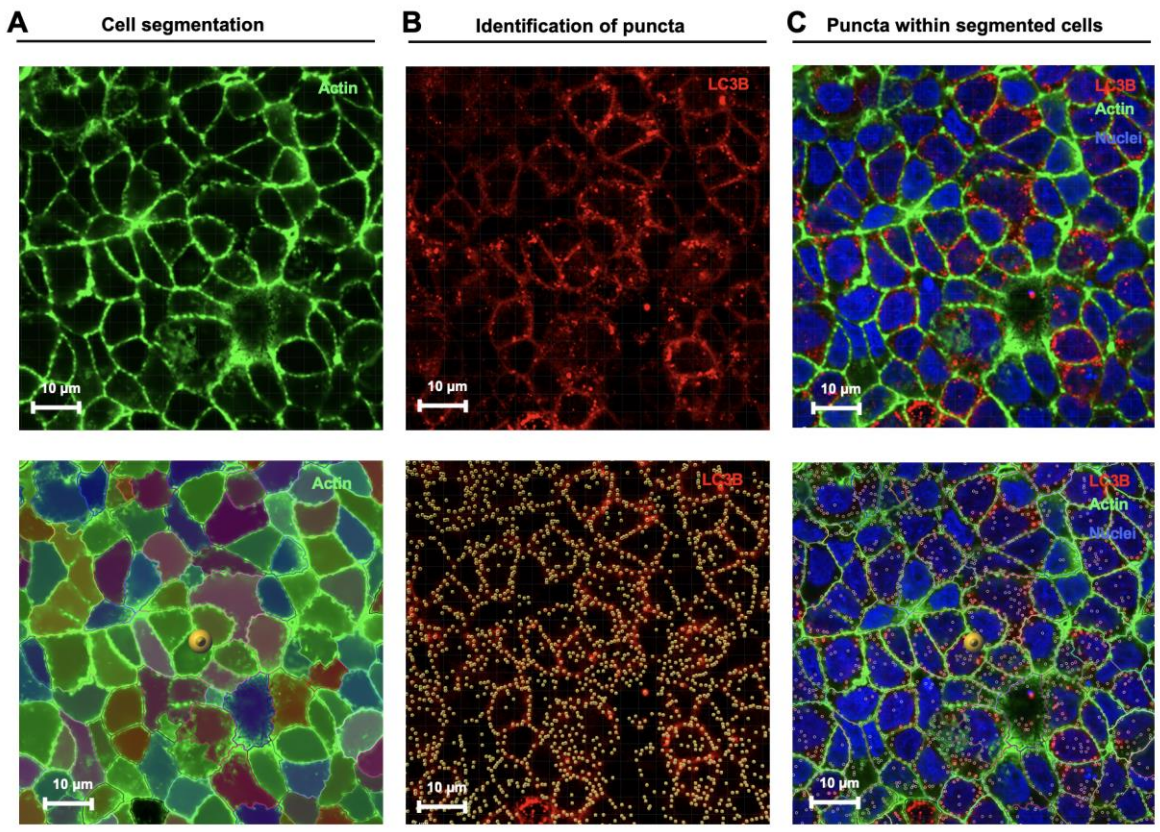

Figure 3.14. Analysis and quantification of LC3 and p62 puncta in Caco-2 cell monolayers. A) Cell segmentation; single cells within Caco-2 monolayers were identified using the cell membrane

identification function within the 'Cell module'. Segmentation was based on green actin immunostaining (phalloidin-iFluor488). The following parameters were used: cell size 7 µm, membrane thickness 0.1 µm, and local contrast method was applied. **B)** Identification of puncta; the number of LC3/p62 puncta in each cell was identified based on the LC3/p62 red channel (Alexa Fluor 594) using the spot identification function within the 'Cell module'. The following parameters were used: 0.9 µm as puncta diameter, and background subtraction method was applied. **C)** Puncta within segmented cells; the number of p62/LC3 puncta and average intensity of puncta per cell were identified by combining the identification of spots and cell segmentation layers. **A, B, C)** Caco-2 monolayers were stained for nuclei (blue, DAPI), actin brush border (green, phalloidin-iFluor488) and p62/LC3 proteins (red, Alexa Fluor 594). Images were collected using a LSM880 confocal microscope with AiryScan (Zeiss), using 63x oil immersion lens. Image analysis was performed using the Imaris cell imaging software (Oxford Instruments). A separate plate of Caco-2 cells was used for LC3B and p62 staining due to the anti-LC3 and anti-p62 primary antibodies used being raised in the same species.

To evaluate the effects of bifidobacterial metabolites (*B. breve* UCC2003 and *B. longum* LH206), the number and signal intensity of LC3 and p62 puncta in Caco-2 monolayers exposed to *Bifidobacterium* metabolites was compared to those treated with rapamycin, a potent autophagy activator, or left untreated (RPMI). Uninflamed monolayers in the long-term ("set-up 1") and short-term ("set-up 2") inflammatory set-ups were used for this analysis as a starting point to decipher the direct effects of bifidobacterial metabolites on autophagy flux, without the confounding factor of inflammation, where autophagy also plays a role (Netea-Maier et al., 2016).

In both set-ups, rapamycin treatment increased the number and mean intensity of LC3 puncta compared to control (**Figure 3.15A, 3.16A**). This could also be observed by the marked presence of bright puncta observed especially in the set-up 1, suggesting the presence of a higher number of autophagosomes (**Figure 3.15B**). In set-up 2, the difference was visually less marked, as indicated by the non-significant increase in both number and mean intensity of LC3 puncta compared to control, which could be due to a less successful staining or loss of signal when capturing confocal images (**Figure 3.16A, B**). Conversely, rapamycin treatment significantly decreased both the number and signal intensity of p62 puncta compared to control, suggesting the presence of a lower number of autolysosomes (**Figure 3.16C, D**). This observation could be made for set-up 2 only, as the p62 immunostaining was not available for the control condition in set-up 1, as the only set of samples available was used for LC3 staining (**Figure 3.15C, D**).

Furthermore, exposure to bifidobacterial metabolites resulted in a statistically significant increase in set-up 1 (**Figure 3.15A, B**), and a significant decrease or no change in set-up 2

(**Figure 3.16A, B**) of the number and signal intensity of LC3 puncta compared to control. In set-up 1, this increase was less pronounced compared to rapamycin-treated cells, and it was higher (or more significant) for *B. breve* UCC2003 than for *B. longum* LH206-derived metabolites compared to control, suggesting the presence of a higher number of autophagosomes (**Figure 3.15A, B**). Conversely, exposure to bifidobacterial metabolites resulted in a significant decrease in the number and signal intensity of p62 puncta compared to control, suggesting the presence of a lower number of autolysosomes (**Figure 3.16C, D**). In particular, this decrease was comparable to that observed in rapamycin-treated samples, and it was higher samples exposed to *B. breve* UCC2003 than for *B. longum* LH206-derived metabolites compared to control (**Figure 3.16C**). Again, this observation could be made for set-up 2 only, as the p62 immunostaining was not available for the control condition in set-up 1 (**Figure 3.15C, D**). In set-up 2, the inconsistency between changes in LC3 and p62 signal upon bifidobacterial supernatant exposure could be possibly attributed to the low quality and more diffused signal, as it can be observed for the confocal images of Caco-2 monolayers (**Figure 3.16B, D**). In general, the staining used for cell segmentation was less defined than in set-up 1, which might have created problems during the segmentation step.

Overall, results showed that quantification of LC3 and p62 puncta can be used to monitor changes in autophagy fluxes in Caco-2 cells, as indicated by the observed higher number of autophagosomes and lower number of autolysosomes upon rapamycin treatment. Furthermore, these results suggest an activation of autophagy flux in epithelial cells upon exposure to bifidobacterial metabolites, particularly those produced by *B. breve* UCC2003.

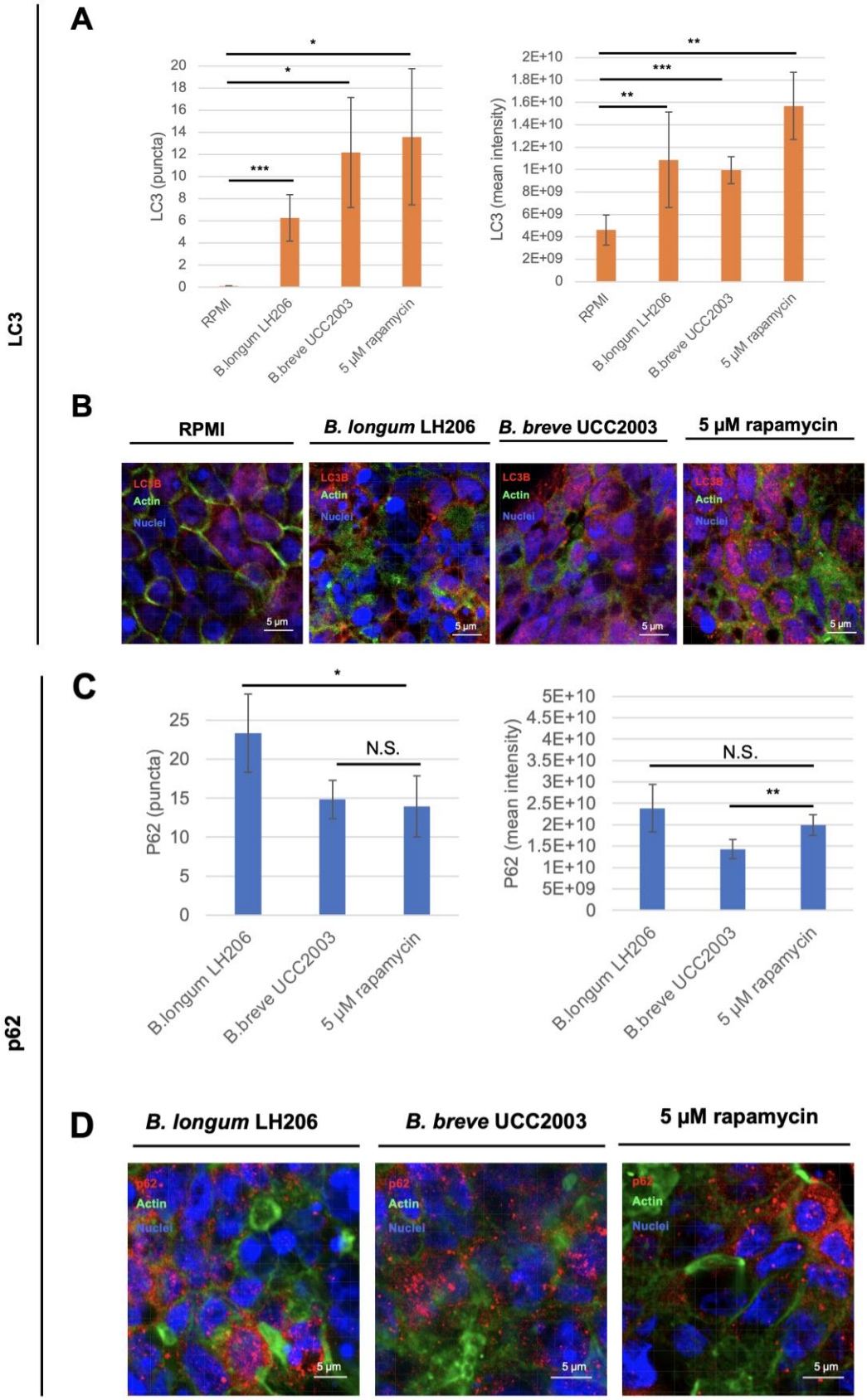

Figure 3.15. Quantification of p62 and LC3 puncta in Caco-2 cell monolayers exposed to bifidobacterial metabolites upon long-term inflammation. A, C) Bar chart indicating the mean

number of puncta per cell and the average signal intensity of LC3 staining (A) or p62 staining (C) for all conditions. Error bars indicate standard deviations (n=4). **B, D)** Immunostaining of LC3 (B) and p62 (D) proteins of Caco-2 monolayers on Transwells either left untreated (RPMI), treated with 5 µM rapamycin, or exposed to 20% *B. longum* LH206 or *B. breve* UCC2003 supernatant for 24 hours. Caco-2 cell monolayers were stained for nuclei (blue, DAPI), actin brush border (green, phalloidin-iFluor488) and p62/LC3 (red, Alexa Fluor 594). Confocal images were obtained using a LSM880 confocal microscope with AiryScan (Zeiss), using a 63x oil immersion lens. Image analysis was carried out using IMARIS. Image analysis was performed using the Imaris cell imaging software (Oxford Instruments). Statistical significance was calculated relative to the media control (RPMI) (A) or relative to the positive control rapamycin when the media control was not available (C) by performing a Student t-test. N.S., non-significant (p-value > 0.05); * p-value < 0.05; **p-value < 0.01; *** p-value < 0.001.

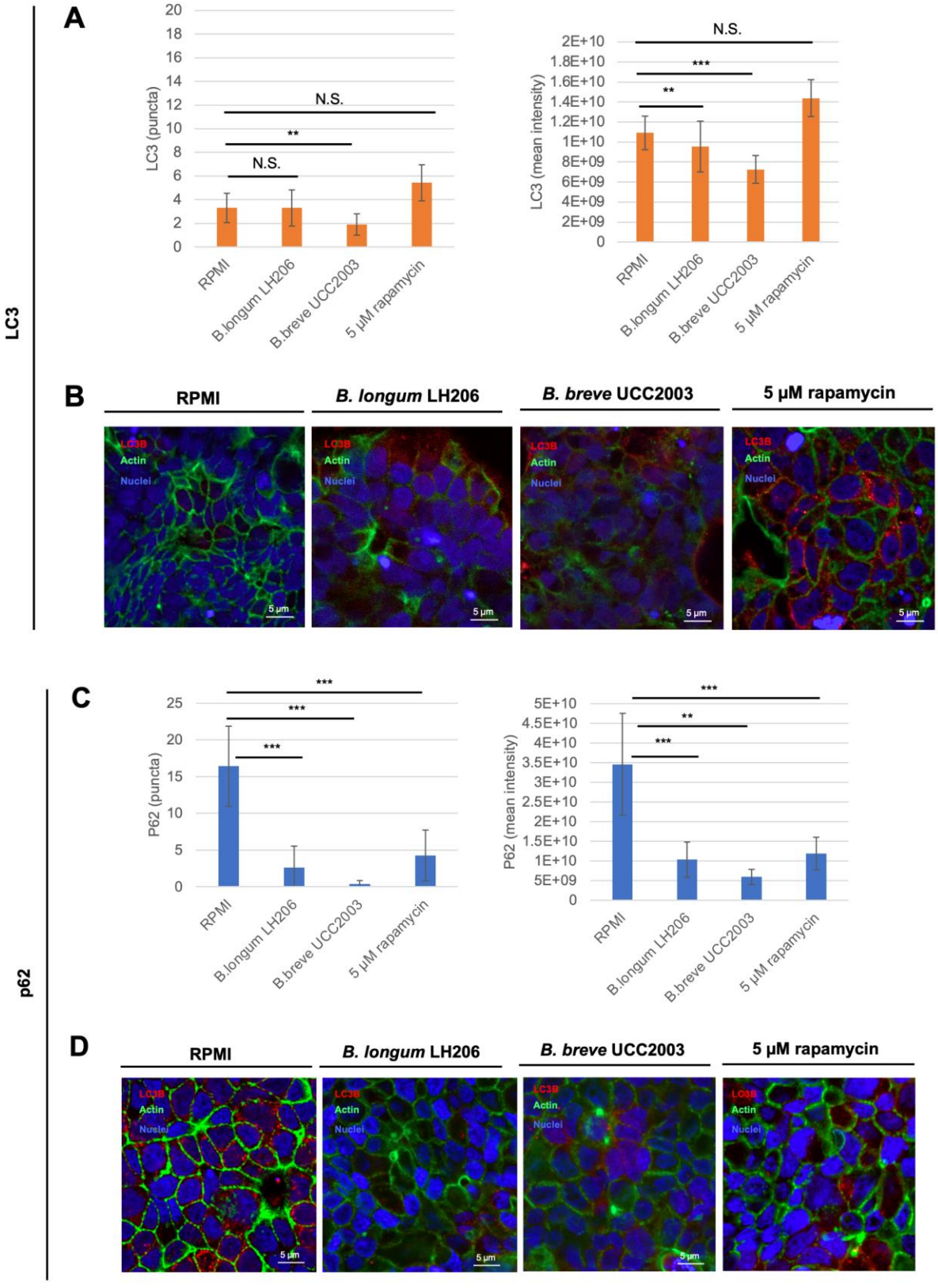

Figure 3.16. Quantification of p62 and LC3 puncta in Caco-2 monolayers exposed to bifidobacterial metabolites upon short-term inflammation. A, C) Bar chart indicating the mean number of puncta per cell and the average signal intensity of LC3 staining (A) or p62 staining (C) for all

conditions. Error bars indicate standard deviation (n=4). **B, D)** Immunostaining of LC3 (B) and p62 (D) proteins of Caco-2 monolayers on Transwells either left untreated (RPMI), treated with 5 µM rapamycin, or exposed to 20% *B. longum* LH206 or *B. breve* UCC2003 supernatant for 24 hours. Caco-2 monolayers were stained for nuclei (blue, DAPI), actin brush border (green, phalloidin-iFluor488) and p62/LC3 (red, Alexa Fluor 594). Confocal images were obtained using a LSM880 confocal microscope with AiryScan (Zeiss), using a 63x oil immersion lens. Image analysis was performed using the Imaris cell imaging software (Oxford Instruments). Statistical significance was calculated relative to the media control (RPMI) by performing a Student t-test. N.S., non-significant (p-value > 0.05); * p-value < 0.05; **p-value < 0.01; *** p-value < 0.001.

4. Discussion

The goal of this project was to assess the beneficial effects of exposure to bifidobacterial metabolites on loss of barrier integrity, cell viability and secretion of pro-inflammatory cytokine release during short-term and long-term induced inflammation. Additionally, the role of autophagy modulation in mediating these effects was evaluated.

To do so, I first identified the ideal concentration of bacterial medium BHI that could be used to expose Caco-2 cells to bacterial metabolites without decreasing cell viability. All concentrations up to 20% did not significantly increase cytotoxicity compared to the control, and therefore 20% was chosen as the concentration for exposure (**Figure 3.2**). Furthermore, I confirmed that bifidobacterial strains selected for the analysis could grow in this media, reaching the late exponential phase of growth after 9 hours, the time point where supernatants were collected **(Figure 3.3).** BHI is a rich media and does not represent the environment found in the gut including the presence of dietary substrates and other bacterial metabolites derived from cross-feeding. Therefore, metabolites produced by bifidobacteria in this environment may not fully reflect what is present *in vivo.* Indeed, a study comparing the effect of four different media on microbial metabolites, found that BHI promoted the selective growth of *Bacteroides*, while a gut-microbiota specific medium (GMM) resulted in a significant increase in *Actinobacteria* including *Bifidobacterium* spp. (Yousi et al., 2019). Hence, future experiments should consider the media composition where *Bifidobacterium* spp. are grown prior to metabolites extraction and use such media that better reflects the environment of the gut.

To induce inflammation in Caco-2 cell monolayers, PMA was employed, and the maximum concentration that could be added without significantly decreasing cell viability was determined. Because 24 hours treatment with up to 1 µM PMA did not further decrease cell viability compared to the media control, this concentration was chosen forward to induce short-term and long-term inflammation in Caco-2 cells (**Figure 3.6**). Surprisingly, in both experimental set-ups used, 1 µM PMA treatment resulted to be cytotoxic for Caco-2 monolayers, with a higher cytotoxicity observed after 4 hours compared to 20 hours (**Figure 3.9, Figure 3.12**). This discrepancy in results is hard to explain, but could be due to the different set-up used for inflammation, which was represented by 7-day old Caco-2 grown on flat-bottom 96 well plates in the dose-response experiment (**Figure 3.6)**, compared to differentiated (13-24 days) Caco-2 cell monolayers grown on Transwells in the final experiments (**Figure 3.9, 3.12**).

Overall, in both short-term and long-term induced inflammation set-ups, PMA-treatment resulted in a loss of epithelial barrier, reduced cell viability and accumulation of pro-inflammatory IL-8 in the media. This suggests that the inflammation was correctly modelled using the Caco-2 monolayer system (**Figures 3.8-13**). When comparing short-term and long-term induced inflammation, the total amount of cytotoxicity levels and secreted IL-8 measured in the basolateral compartment were higher in the long-term inflammation set-up (**Figures 3.9, 3.10**) compared to the short-term one (**Figures 3.12, 3.13**), in line with the longer PMA treatment used (20 hours vs 4 hours) (**Figure 3.7**). The loss in epithelial barrier as measured by TEER was also higher when long-term inflammation was induced (**Figure 3.8**) compared to short-term inflammation (**Figure 3.11**). However, it was more difficult to make any solid conclusions here due to the unreliable TEER measurements taken during the short-term inflammatory set-up, probably attributable to an issue with the measurement instrument.

When assessing the beneficial effects of bifidobacteria metabolites (*B. breve* UCC2003, *B. longum* LH206) in the absence of inflammation, a 24-hours exposure to bifidobacterial metabolites resulted in an increased epithelial barrier for both strains (**Figures 3.8, 3.11**), while no clear effects could be identified for cell viability measurements (**Figure 3.9, 3.12**). At the same time, 24 hours exposure resulted in a small apical accumulation of IL-8 in the short-term inflammation set-up, which was higher for *B. breve* UCC2003-derived metabolites compared to *B. longum* LH206 (**Figure 3.10**). However, this could not be confirmed in the long-term set-up, as these samples were not collected (**Figure 3.13**). The accumulation of IL-8 elicited by exposure to *Bifidobacterium* metabolites could be due to the recognition of bacterial components by epithelial cells. IL-8 release is dependent on the activation of NF-κB signalling, which can be in turn regulated by TLRs or EGFRs (Claud et al., 2003**).** Interestingly, *B. breve* UCC2003-derived EPS was shown to be recognised as MAMPs *via* specific PRRs including TLR1, TLR2, and TLR6, leading to the production of various cytokines (Hidalgo-Cantabrana et al., 2012). Indeed, the EPS-dependent NF-KB activation *via* TLRs may represent one of the mechanisms involved in the observed increase in IL-8 secretion upon exposure of Caco-2 cells to *Bifidobacterium*-derived metabolites.

When assessing the beneficial effects of bifidobacterial supernatant during long-term and short-term inflammation, exposure to *Bifidobacterium*-derived metabolites protected against the loss of barrier integrity during short-term inflammation only, but not long-term inflammation **(Figure 3.8, 3.11).** Additionally, effect of bifidobacterial metabolites exposure on cell viability during inflammation were ambiguous, as increase in cytotoxicity could be partially restored in the long-term inflammation (especially by *B. longum* LH206-derived metabolites) (**Figure 3.9**),

while it was further increased in the short-term set-up (**Figure 3.12**). However, it needs to be considered that the differences recorded were very small, and these ambiguous results could be simply due the initial quality of the Caco-2 monolayer, or to the number of technical replicates used (two in the long-term inflammation and three in the short-term inflammation set-ups).

Surprisingly, no protective effects of bifidobacterial metabolites were observed against IL-8-induced release upon either short-term or long-term inflammation (**Figure 3.10, 3.13**). Previously, *in vitro* and *in vivo* studies have shown the anti-inflammatory properties of selected bifidobacterial strains (Riedel et al., 2006; Singh et al., 2020; Wu et al., 2016; Yu et al., 2019). However, IL-8 was not measured in these studies, suggesting that the beneficial effects of bifidobacterial metabolites may be mediated *via* another pathway than the one upstream of IL-8 production. Mechanisms behind the inflammatory effects of bifidobacterial metabolites are still unclear, and further work will be needed to clarify the molecular mechanisms behind these beneficial effects.

In this project, I aimed to unravel effects of bifidobacterial metabolites on autophagy modulation, and results showed a trend towards the activation of autophagy flux upon exposure to bifidobacterial metabolites, particularly those produced by *B. breve* UCC2003 (**Figure 3.15, 3.16**). However, changes observed were not always statistically significant. Generally, Caco-2 cell models represent a good model to study autophagy, as they can respond to various stimuli activating the autophagy flux, compared to other colorectal cancer (CRC) cell lines (Lauzier et al., 2019). Furthermore, quantification of lipidated LC3 puncta and p62 dots, represents the golden standard for autophagy assessment in mammalian cells (Seranova et al., 2019). Hence, the current results could be due to other limitations associated with the specific experimental execution. First, a uniform antibody staining for both LC3 and p62 was not achieved, especially in set-up 2, probably due to technical issues in the staining protocol. This is crucial to properly compare across conditions, and can introduce variability in the results. Second, LC3 and p62 puncta are very small objects to identify, and collect a sharp image of, which is a requirement for numbers per cell and mean signal quantification. Here, due to the high number of conditions, single plane images were collected based on a fixed focus on nuclei staining (to allow comparability across conditions). Although time-effective, this method, together with the non-homogeneous staining, led to a high variability in the intensity of the p62/LC3 puncta signal based on the location on the slide, biassing the quantification of the signal. To improve resolution and obtain more defined puncta, collecting z-stacks of different areas of the monolayers using high-throughput imaging systems, could be used to increase the resolution while maintaining a sustainable collection time frame.

With this study, we used a simplified model to study the beneficial effects of bifidobacterial metabolites on the epithelium during intestinal inflammation. However, this set-up presented some limitations, including how inflammation was induced, the use of metabolites instead of whole bacteria, the presence of static co-culture conditions, and the use of Caco-2 cells. One limitation can be identified in the type of inflammatory agent used, its concentration, or length of treatment. In both set-ups, PMA treatment resulted in a relatively high decrease in epithelial cell viability, which was proportional to the treatment time (4 hours vs 20 hours) (**Figure 3.9, 3.12**), and in line with a sharp increase in pro-inflammatory IL-8 release and decrease in epithelial barrier integrity (**Figure 3.10, 3.13**). In the future, a milder treatment to induce inflammation, such as a cocktail of cytokines (TNF, flagellin, IL1β) could better mimic the effect of chronic inflammation observed in conditions such as IBD, and better highlight the possible protective effects of bifidobacterial-derived metabolites.

Another limitation is that *Bifidobacterium*-derived metabolites were studied instead of whole bacteria - a choice that was made for several reasons: (i) to eliminate the effects of an aerobic environment on bifidobacterial metabolism; (ii) to remove biases resulting from the presence of bacterial and epithelial-derived molecules impacting on each other's function; (iii) to avoid the need for different media and environmental requirements for bacterial and epithelial cells. Bacterial-derived molecules (SCFAs, bile acids, tryptophan metabolites) are becoming increasingly important to treat a series of diseases including IBD (Agus et al., 2021; Lavelle and Sokol, 2020), and have been proposed as a better treatment solution compared to whole probiotics (Cunningham et al., 2021). *Bifidobacterium* metabolites, in particular SCFAs, were shown to benefit the host by promoting GC differentiation and mucus production (Wrzosek et al., 2013), barrier integrity (den Besten et al., 2013; Ríos-Covián et al., 2016) and the anti-inflammatory response (Furusawa et al., 2013; Zhang et al., 2016). However, other membrane-bound molecules could also be involved in mediating the effects of bifidobacterial metabolites (Fanning et al., 2012).

Furthermore, exposure to bacterial metabolites was static, with all metabolites isolated at a specific time of the bacterial growth curve (**Figure 3.3**), and subsequently applied to the Caco-2 cell monolayer. However, to properly mimic the real-time effects of host-microbiome interactions *in vitro*, viable and functional intestinal and bacterial cells should be in contact for a certain amount of time within the same space (Kim et al., 2012; Park et al., 2017). To overcome some of the challenges associated with this, microfluidic devices could be used including HuMiX (see **Chapter 1**).

Finally, another limitation was the use of Caco-2 cell monolayers to model the intestinal epithelium. Caco-2 have been shown to not always respond to inflammatory stimuli (Grouls et al., 2022), which highlights the need for better *in vitro* models when looking at the immunomodulatory effects of bifidobacterial metabolites on the intestinal epithelium. Furthermore, Caco-2 cells do not fully represent the tissue heterogeneity or location-specific characteristics (duodenum, colon, etc) of the epithelium. Bifidobacteria reach their highest proportion (up to 90%) in the colon during early life, followed by a sharp decrease in adulthood (Turroni et al., 2012). Despite their low abundance in the human colon, they can have a large health impact, as their decrease in relative abundance has been associated with several diseases including diarrhoea, IBD, obesity, and obesity (Di Gioia et al., 2014; Grimm et al., 2014). To this regard, more representative models such as organoids would help to better mimic the different cell types and location-specific differences (such as colon versus ileum) of the epithelium, and better respond to microbial challenges such as exposure to *Bifidobacterium*-derived metabolites.

5. Future research directions

Overall, this study represents a starting point for the evaluation of the protective effects of bifidobacterial metabolites on barrier integrity, cell viability and pro-inflammatory cytokine release in the context of inflammation, as well as the modulation of autophagy processes. In the future, a similar set-up could be envisioned using more representative models such as organoids, which better mimic the different cell types and location specific differences of the epithelium. For instance, the use of organoid-derived monolayers would allow better study of the impact of bifidobacterial metabolites on different populations of epithelial cells (goblet, Paneth cells) in specific locations of the epithelium (ileum, colon). Additionally, the use of patient-derived organoids, for instance from IBD patients, could also help to better mimic not only the environmental but also genetic background triggering inflammatory diseases of the gut, which could help decipher the role of probiotics-host interactions in IBD.

Furthermore, based on the results of the preliminary experiment, the same set-up could be repeated using microfluidics devices such as HuMiX device, where whole bacteria can be separated from the epithelial layer, and the effect of real-time production of metabolites can be evaluated. Adding immune cells to the inflammatory epithelial model would also be important, to understand how the beneficial effects of bifidobacterial metabolites on the epithelium are mediated. As explained in **Chapter 1**, immune cells can communicate with IECs in response to signals deriving from microbes through several mechanisms (endocytosis, antigen presentation, cytokines secretion) (Bui et al., 2018; Ho et al., 2020; Luissint et al.,

2019). Several efforts are being made to advance currently available microfluidics models, for instance with the development of so called “immuno-HuMiX”, which would allow the coexistence of microbial, epithelial, and immune cells in three separate compartments (Shah et al., 2016). Such systems could be used in the future to understand the role of resident immune cells in mediating the beneficial effects of bifidobacterial metabolites on the intestinal epithelium during inflammation. Finally, within this system, several outcome measures could be collected in the same set-up including microscopy, host transcriptomics and proteomics and bacterial metabolomics. Integration of these measures would allow better insights into the molecular mechanisms behind these beneficial effects.

Because autophagy is not a static process, quantifying the number of p62/LC3 puncta over time would allow a more accurate representation of autophagy flux in the cell. For instance, it would be important to better understand the timing of autophagy activation/inhibition by different bacterial strains, as well as in different epithelial cell types. For this purpose, the use of autophagy reporters in combination with live cell imaging will be key for future studies looking at autophagy modulation in intestinal epithelial cells. As mentioned in **Chapter 2**, the use of human healthy colonic organoid autophagy reporter lines combined with high-throughput live imaging, could help identify autophagy modulation in a time-dependent and cell-dependent manner.

In conclusion, in this chapter I successfully set-up a co-culture model to study the protective effects of bifidobacterial metabolites on intestinal barrier integrity, epithelial cell viability and pro-inflammatory cytokine release, and autophagy processes. Results showed beneficial effects upon bifidobacterial metabolites exposure towards an increased barrier function and autophagy flux in the absence of inflammation, as well as a reduction of loss of cell viability and barrier function in the presence of inflammation, although results were relatively small. In the future, by implementing a better set-up to mimic inflammation of the epithelium, co-culturing the whole bacteria and using more representative models such as organoids could help unravel the beneficial effects of bifidobacterial metabolites on the gut, possibly highlighting specific strains that can be used to manage detrimental effects on the gut epithelium observed in inflammatory diseases such as IBD.

Chapter 4: Effect of bifidobacterial metabolites on epithelial cell function and differentiation in the healthy colon using human organoids

1. Introduction

B. breve UCC2003, which was originally isolated from a nursing stool (O'Connell Motherway et al., 2011), has gained interest for their potential beneficial effects in the gut. Indeed, previous studies have shown its ability to reduce epithelial cell shedding and increase epithelial proliferation (Hughes et al., 2017; O'Connell Motherway et al., 2019). Furthermore, it has been shown to protect mice against infection and to modulate the gut microbiota composition through EPS cross feeding (Christiaen et al., 2014; Fanning et al., 2012a; Fanning et al., 2012b; Püngel et al., 2020). A recent transcriptomics study also highlighted the ability of *B. breve* UCC2003 to alter key genes involved in cell differentiation (including stem cell proliferation) and barrier function in neonatal murine IECs, suggesting its ability to modulate epithelial homeostasis and regeneration under stress conditions (Kiu et al., 2020). In **Chapter 3,** *B. breve* UCC2003-derived metabolites increased epithelial barrier in the absence of inflammation and had a small protective effect against loss of epithelial barrier and cell viability in the presence of inflammation in a Caco-2 cell model.

One important mechanism playing a key role in intestinal barrier function, homeostasis and inflammation by IEC function is represented by autophagy. Because defective autophagy processes are associated with onset of diseases such as IBD (Matsuzawa-Ishimoto et al., 2018), probiotic supplementation strategies have been explored to enhance autophagy in the gut. In recent works, *B. dentium* supplementation was shown to enhance goblet cell function, including mucin production and secretion, *via* the upregulation of autophagy (Engevik et al., 2019), while *B. longum* suppressed inflammatory IL-1β expression *via* autophagy related ATG16L1 protein in a *Salmonella*-infected Caco-2 cell model (Lai and Huang, 2019). Furthermore, results from **Chapter 3** suggested that *B. breve* UCC2003 activates autophagy processes in Caco-2 cells, as identified by immunostaining and quantification of LC3 and p62 puncta.

However, most of these studies were carried out using mouse models or cell lines that do not reflect tissue heterogeneity and location specific characteristics (duodenum, colon, etc) of the human intestinal epithelium (May et al., 2017). Hence, additional studies are needed to understand the beneficial effects of *B. breve* UCC2003-derived metabolites on the human

IECs and the molecular mechanisms. To this regard, human intestinal organoids represent a good model to study the effects of *Bifidobacterium*-derived metabolites on the epithelium. Organoids maintain the crypt-villi structure of the intestine, contain the majority of intestinal cell types and retain the genetic, transcriptional and epigenetic characteristics of the donor and intestinal segment (duodenum, jejunum, ileum) they were derived from(Cramer et al., 2015; Dekkers et al., 2016; Kraiczy et al., 2019; Middendorp et al., 2014). In **Chapter 2**, I presented the outcome of several optimization experiments where I established human colonic organoid models, and optimised the co-culture conditions, and RNA extraction methods to study the effects of exposure of epithelial cells to *Bifidobacterium*-derived metabolites *in vitro*.

This chapter presents a study investigating the effect of *B. breve* UCC2003 metabolites on intestinal epithelial cell function during intestinal differentiation. To do so, human colonic organoids from two healthy donors were differentiated for 3 days, while being exposed to *B. breve* UCC2003 supernatant, *L. rhamnosus* supernatant (positive bacterial control, previously known to regulate host function including autophagy (Zaylaa et al., 2019) or media control. Changes in gene expression profiles upon bacterial metabolite exposure were measured and further analysed to investigate modulated transcriptional changes, biological functions and transcriptional regulators modulated by *B. breve* UCC2003 metabolites. Prior information about cell markers of epithelial cell type populations from the Gut Cell Atlas was also integrated with the transcriptomics data to elucidate the role of *B. breve* UCC2003 metabolites in modulating the shift of specific epithelial populations during differentiation. Furthermore, information about proteins playing a role in autophagy from the Autophagy Regulatory Network (ARN) resource (Türei et al., 2015) was integrated with the results, to unravel the effect of bifidobacteria metabolites in modulating autophagy processes. Finally, metabolomics data from *B. breve* UCC2003 was integrated with the results to understand which specific bacterial metabolites.

The outcome of this study revealed that *B. breve* UCC2003 supernatant modulates genes involved in epithelial cell growth and differentiation, shifting the growth of stem cells towards more progenitor cells and absorptive enterocytes, and upregulating genes involved in barrier function. Overall, these effects could be beneficial to obtain a more mature epithelium and better barrier integrity, which is often dysregulated in diseases such as IBD. Furthermore, additional mechanisms were found to mediate the effects of bifidobacterial metabolites on the epithelium, including the downregulation of WNT signalling *via* epigenetic mechanisms, and downregulation cholesterol biosynthesis. Finally, bacterial metabolites succinate, acetate, butyrate, and propionate were predicted to mediate several of these effects, *via* the activation *NFKB1, JUN* and *FOS* transcription factors, findings that could be further tested and validated in the future.

2. Aims & Objectives

The main aims of this study are:

1) Study the regulation of gene expression profiles in human colonic epithelial cells exposed to *B. breve* UCC2003 metabolites.

2) Assess the added effect of *B. breve* UCC2003 metabolites on epithelial gene expression profiles compared to *L. rhamnosus* metabolites and media control.

3) Study the modulation of autophagy by identifying specific autophagy genes and their direct regulators regulated upon *B. breve* UCC2003 metabolites exposure.

4) Study the regulation of markers of specific intestinal epithelial cell populations.

5) Predict which bacterial metabolites are involved in the observed effects on epithelial cells.

3. Methods

3.1. Establishment of human colonic organoid cultures

Two human colonic organoids lines from healthy donors were obtained from collaborators at King's College London (KCL) (organoid line 1), or purchased from the Hubrecht Organoid Technology (HUB) biobank (organoid line 2). Characteristics of these two organoid lines are described in **Table 4.1**.

Organoid line 1 was obtained through an approved Material Transfer Agreement (MTA) in place between the two institutions. Generation of this line was performed under the approved ethics procedures in place in the supplier institution. Organoid line 2 was purchased by the HUB (reference: HUB-02-D2-089), hence generation of this line followed the ethics procedures in place in the supplier country and institution.

Organoids were expanded from frozen stocks in Matrigel bubbles (40 µl) using 24-well plates at 37^0C, 5% CO_2, as described in **Chapter 2**. Organoids were fed with 500 µl human OGM (Intesticult, StemCell Technologies), supplemented with 100 U/mL penicillin (P)/100 µg/mL streptomycin (S) and 10 µM Y-27632 (ROCK inhibitor; Tocris) per well every 2-3 days. Organoids were split every 7-10 days approximately. Y-27632 was only added after splitting and removed at the subsequent feeding. Media was replaced every 2 days.

Table 4.1. Human colonic organoid lines. Abbreviations: KCL, King's College London; HUB, Hubrecht Organoid Technology

	Organoid line 1	**Organoid line 2**
Gender	Male	Female
Background	Healthy	Healthy
Tissue of origin	Colon	Ascending colon
Morphology	Cystic	Cystic
Received from	KCL (collaborators)	HUB (purchased)

2.2. Extraction of bacterial metabolites

Frozen bacterial stocks of *B. breve* UCC2003 and *L. rhamnosus* were streaked onto BHI and MRS agar plates (supplemented with 0.05% (wt/vol) L-cysteine HCl), respectively, which had previously been pre-reduced in the anaerobic cabinet for at least 48 hours. Once inoculated, plates were incubated in anaerobiosis for 2-3 days at 37^0C. 3-4 isolated colonies were picked to make bacterial liquid cultures into BHI and MRS liquid media (supplemented with 0.05% (wt/vol) L-cysteine HCl). Cultures were grown for 2 days in the anaerobic cabinet at 37^0C, after which they were diluted 1:50 into BHI broth. ΔOD_{600} of the culture was measured over time. Bacterial supernatants were collected at the late exponential phase (see details in **Chapter 2**) by spinning down the cultures for 10 minutes at 37^0C at 10,000 rpm. Subsequently, supernatants were removed and filter-sterilised using a 0.22 µm sterile filter. Supernatants were stored at -20^0C until further use.

3.3. Exposure to bacterial metabolites

Human healthy colonic organoid lines 1 and 2 were expanded in 500 µl human OGM (Intesticult, StemCell Technologies) (supplemented with 100 U/mL/100 µg/mL P/S) in each well of a 24-well plate. Each organoid line was expanded on a separate set of plates. When enough material was obtained, media was removed, organoid domes were washed with PBS and 500 µl of different media combinations were added to each well to study the effects of exposure to bacterial metabolites on organoid differentiation and epithelial cell function (**Figure 4.1**). In particular, organoids were exposed to either human ODM (supplemented with 100 U/mL/100 µg/mL P/S) alone (media control), supplemented with 10% *B. breve* UCC2003 or with 10% *L. rhamnosus* supernatants in BHI (positive bacterial control). Four technical replicates for each condition (8 organoid wells, pulled together by 2 for RNA extraction), and 2 biological replicates (organoid lines) were used. RNA was extracted at day 3 and day 5, at the beginning (pre-differentiation) and 24 hours (post-differentiation) post-bifidobacteria exposure. Media was replaced every day during the 3-day experimental period. Growth medium was collected all time points for additional measurements.

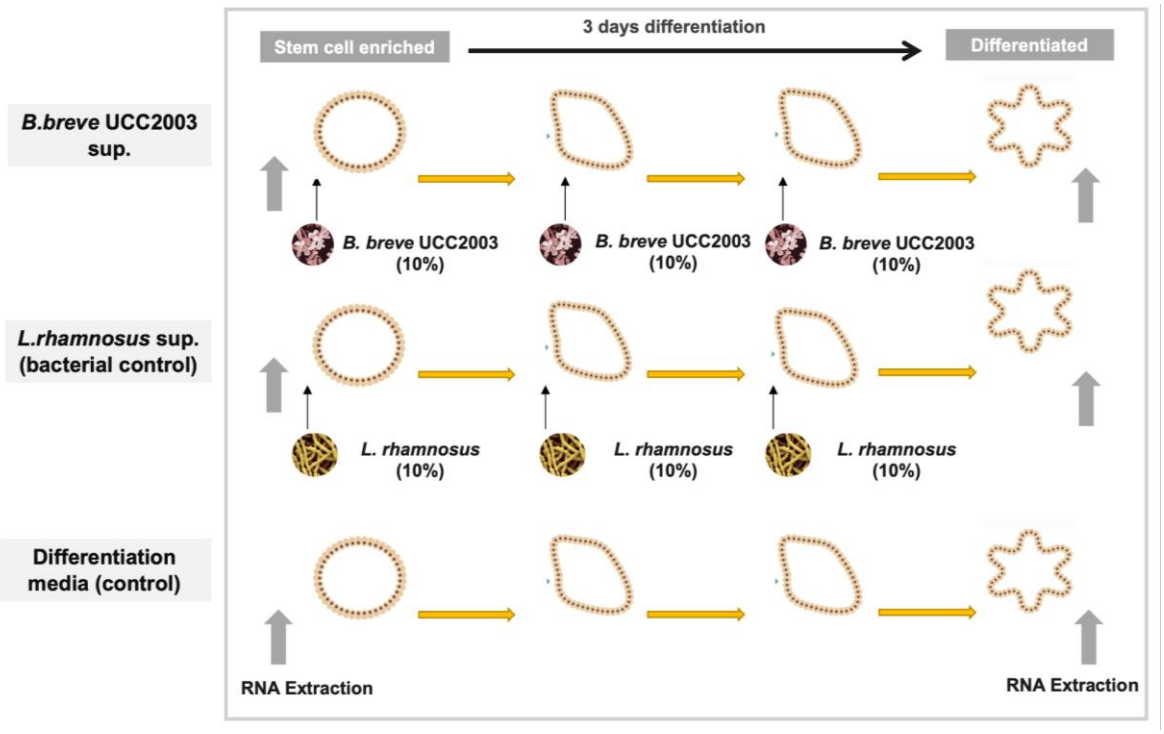

Figure 4.1. Schematic representation of the experimental set-up for the transcriptomics experiment. (3D) colonic organoid cultures from two healthy donors (organoid line 1, organoid line 2) were grown in human OGM, following which they were differentiated for 3 days in human ODM either alone or with 10% *B. breve* UCC2003 or 10% *L. rhamnosus* supernatants (sup.). Media was refreshed every day (including metabolites) during the 3 days differentiation and total RNA was extracted before the differentiation (t = 0 hours) and after (t = 72 hours). Four technical replicates/wells were prepared for each condition and organoid line.

3.4. RNA extraction, preparation, and sequencing

For total RNA extraction, 500 µl of Cell Recovery Solution (Corning) was added to each well, and plates incubated on ice for 20 minutes on a shaking platform (70 rpm). Using a pre-coated P1000 tip (2% FBS in PBS), organoids were transferred into a 15 ml LoBind tube (Merck), pooling two wells of the same technical replicates together. Organoid suspensions were collected by centrifugation for 3 min at 300x g, and washed once with 1 ml PBS. Cells were lysed with 350 µl of lysis buffer (provided by the RNA extraction kit) supplemented with with 0.1 mM 2-mercaptoethanol (2-ME), vortexed and stored at -20^{0}C for at least 2 hours prior to RNA isolation. RNA was extracted using commercially available kits RNAesy (QIAGEN) following manufacturer's instructions. To further concentrate and de-salt the isolated RNA samples, an additional ethanol precipitation step was performed. The quality and quantity of RNA was measured on a Nanodrop using the RNA50 for Nucleic acids program. In parallel, RNA was also quantified using the Qubit kit and Qubit 3 instrument following the standard kit

instructions. More detailed steps about the RNA isolation are explained in **Chapter 2**. Stranded RNA Libraries were constructed using the NEXTflex™ Rapid Directional RNA-Seq Kit (PerkinElmer, 5138-07) using the polyA pull down beads from Illumina TruSeq RNA v2 library construction kit (Illumina, RS-122-2001). Stranded RNA was sequenced on the Illumina NovaSeq 6000 instrument to obtain 100 base paired end reads.

3.5. Quality control, pre-processing, alignment

Quality control (QC), processing, sequence alignment and computation of raw read counts was performed by myself using the in-house TranscriptOmiX pipeline, developed by Matthew Madgwick (PhD student in the Korcsmaros group, EI). The quality of stranded reads was assessed using FastQC (Wingett and Andrews, 2018). Reference Human genome reads and annotation files were downloaded from Ensembl (version GRCh38.105). Reads were aligned using the Spliced Transcripts Alignment to a Reference (STAR) method (Dobin et al., 2013). Post-aligned quality control was performed using FastQC (Wingett and Andrews, 2018). Raw read counts were computed using a custom-made script as part of the TranscriptOmix pipeline.

3.6. Transcriptomics data processing

Count normalisation was performed using the median of ratios method (estimation of size factors) and transformation was performed using regularised log (log2) transformation as part of the R package DESeq2 (Love et al., 2014). Visualisation of the normalised data was carried out using dimensionality reduction methods principal component analysis (PCA) using R.

3.7. Differential expression analysis

Differential expression analysis was performed on normalised count data using EdgeR (McCarthy et al., 2012; Robinson et al., 2010) and the DeSeq2 packages in R (Love et al., 2014). DIfferentially expressed genes (DEGs) were calculated by comparing gene expression profiles of bifidobacteria-treated organoids at the end of the experiment (t=72 hours) to either undifferentiated organoid controls at baseline (t = 0 hours) or differentiated organoid exposed to media control (t = 72 hours). Correction for multiple comparisons was also applied using the Holm–Bonferroni method (FDR < 0.05). Shrinkage of Log2FoldChanges was performed using the apeglm method. DEGs were further filtered for for adjusted p-value < 0.05 and |Log2FoldChange| > 0.5 or 1 (based on the specific analysis) to obtain a list of significant DEGs.

3.8. Epithelial cell marker analysis

A list of epithelial cell marker genes was retrieved for each cluster/each epithelial cell population identified in the Gut Cell Atlas adult healthy colonic dataset (www.gutcellatlas.org). For the analysis, the following epithelial cell types were used: transit-amplifying (TA), Tuft, colonocytes, goblet cells (GCs), stem cells (SCs), Microfold (M) cells and Paneth cells (PCs). For each marker gene within a cluster, z-scores, Log2FoldChanges, p-values and adjusted p-values were retrieved from the original dataset. Subsequently, top epithelial markers were obtained by filtering genes with |Log2FoldChange| > 1 and adjusted p-value < 0.01. Subsequently, epithelial cell markers were filtered for significant DEGs in *B. breve* UCC2003 or *L. rhamnosus* metabolites compared to control (adjusted p-value < 0.05) in both organoid lines. Separate analyses were carried out to compare DEGs in differentiated organoids (t = 72 hours) compared to undifferentiated (t=0 hours) or differentiated organoid controls (t = 72 hrs). For the former comparison, only unique DEGs in differentiated organoids exposed to *B. breve* UCC2003 or *L. rhamnosus* metabolites compared to the undifferentiated controls were used.

3.9. First neighbour of DEGs networks generation

Intermediary signalling protein interactions known to occur in humans were obtained from the core protein-protein interaction (PPI) layer of the OmniPath resource using the 'OmnipathR' R package (Türei et al., 2016). A list of expressed genes in differentiated organoids, exposed to *B. breve* UCC2003 or *L. rhamnosus* supernatants, was generated from the log2 normalised count table by fitting a gaussian kernel (Beal, 2017). All genes with expression values above mean minus three SDs were considered as expressed genes for the given cell type in the given intestinal location. Subsequently, the list of *a priori* PPI interactions was filtered to obtain contextualised PPI networks, whereby both source and target nodes were expressed in differentiated organoids exposed to *B. breve* UCC3003 or *L. rhamnosus* supernatants compared to differentiated organoid controls. Contextualised PPI networks were further filtered for DEGs in organoids exposed to *B. breve* UCC2003 or *L. rhamnosus* metabolites compared to differentiated organoid controls (|Log2FoldChange| > 1, adjusted p-value <0.05) and their direct interactors to generate signalling networks of DEGs and their interacting partner ("first neighbour of DEGs networks). The analysis of first neighbour networks can help identify connections between (translated genes) which work closely together and therefore are likely to have similar functions. Furthermore, it can help annotate functional associations through the identification of additional biologically relevant proteins (Módos et al., 2017).

3.10. Autophagy analysis

To identify which DEGs or their direct interactors that were involved in autophagy upon bifidobacteria exposure, the Autophagy Regulatory Network (ARN) resource (Türei et al., 2015) was used to obtain a list of all the possible proteins either directly playing a role in autophagy (autophagy proteins) or regulating autophagy proteins (direct autophagy regulators). Subsequently, this *a priori* list was further filtered to identify DEGs alone or DEGs and their direct interactors involved in autophagy processes (**Figure 4.2**). To do so, the *a priori* list of autophagy proteins and their regulators was filtered for DEGs in organoids exposed *B. breve* UCC2003 or *L. rhamnosus* supernatants compared to differentiated or undifferentiated controls (adjusted p-value <0.05, Log2FoldChange > 1). Alternatively, the same list was filtered for DEGs and their direct interactors, identified previously through the generation of first neighbour networks of DEGs (**Figure 4.2**).

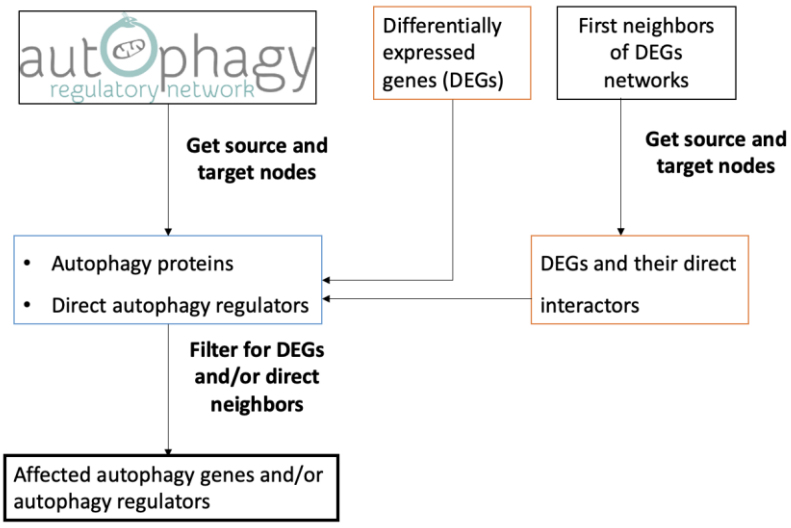

Figure 4.2. Schematic overview of the workflow to identify autophagy related DEGs and their direct interactors modulated upon *Bifidobacterium* metabolites exposure.

3.11. Pathway and Transcription Factor analyses

Signalling pathway and upstream Transcription Factors (TFs) analyses were performed using PROGENy (Schubert et al., 2018) to infer signalling pathway activity, and DoRoThEA (Garcia-Alonso et al., 2019) and VIPER (Alvarez et al., 2016) to infer upstream transcription factor activity using R.

Signalling pathway activity was inferred using PROGENy from the log2FoldChange of DEGs in organoids exposed to *B. breve* UCC2003 or *L. rhamnosus* metabolites compared to

undifferentiated or differentiated controls (Schubert et al., 2018). For the TF analysis, a *priori* knowledge of interactions between human TFs and their target genes (TG) were obtained from the DoRothEA collection using the DoRothEA R package (Garcia-Alonso et al., 2019). Only signed interactions of the top three confidence levels (A, B, C) were used, which include interactions from all resources analysed except those present in one resource only, or those derived from computational predictions, which are characterised by a low confidence level (Garcia-Alonso et al., 2019). Next, VIPER was used to score the TF activity based on enriched regulon analysis (Alvarez et al., 2016) using the TF-TGs interactions (from DoRothEA) and the differential expression data from organoids exposed to *B. breve* UCC2003 or *L. rhamnosus* supernatants compared to differentiated or undifferentiated controls. VIPER infers a quantification of the differential protein activity for each TF, which is expressed as Normalised Enrichment Score (NES). Next, a correction for pleiotropic regulation is applied to adjust the NES of a given TF to take into account the presence of regulation of genes that are also co-regulated by another TF. For visualisation purposes, only TFs with |NES| > 2 after correction for pleiotropic regulation was applied, and regulating at least 15 targets were considered.

3.12. Transcription factor-target genes network generation

A *priori* TF-TG interactions obtained from DoRothEA (Garcia-Alonso et al., 2019) were filtered for TGs and TFs that were expressed in differentiated organoid line 1 or 2 exposed to *B. breve* UCC2003 or *L. rhamnosus* supernatants. For visualisation purposes, only TFs regulating the highest number of genes were shown. In particular, TF-TGs networks were filtered for TFs targeting at least 3 DEGs for organoid line 1 or 6 DEGs for organoid line 2 (since more DEGs were regulated in this organoid line), using the |Log2FoldChange| > 0.5, and adjusted p-value < 0.05 cut-offs. TF-TG networks for each condition and organoid line were visualised using Cytoscape (version 3.9) (Shannon et al., 2003).

3.13. Gene Ontology enrichment analysis

Gene Set Enrichment Analysis (GSEA) of DEGs and functional overrepresentation analysis of (i) TF-TG interaction networks and (ii) first neighbours of DEGs networks were performed using the R packages ‘ClusterProfiler’ (Wu et al., 2021; Yu et al., 2012) and Gene Ontology (GO) annotations (Ashburner et al., 2000). For the GSEA analysis of DEGs, DEGs in organoids exposed to bacterial metabolites compared to differentiated or undifferentiated controls were used as a test list. For this analysis, no background list was required. Additionally, top enriched functions were filtered for those with q-value < 0.0001 and |NES| > 1.5. For the functional overrepresentation analysis of TF-TG networks, source and target nodes of TF-TG networks in organoids exposed to bacterial metabolites compared to

differentiated or undifferentiated controls were used as test list. For the functional overrepresentation analysis of first neighbours of DEGs networks, a list of source and target nodes in the first neighbours of DEG networks of organoids exposed to bacterial metabolites compared to differentiated controls was used as a test list. Additionally, the list of source and target nodes in the contextualised PPI network of organoids exposed to bacterial metabolites was used as a background list. The top overrepresented functions were selected when they had at least 5 contributing genes and with a significance of q-value < 0.05.

3.14. Metabolite-host gene networks generation

Metagenomics (16S rRNA sequencing) and metabolomics (1H-NMR) data was obtained from a published experiment carried out by members of the Hall group, where model colon vessels were inoculated with *B. breve* UCC2003 and microbiome dynamics was monitored over time (0-408 hours) (Püngel et al., 2020). In particular, a list of metabolites (and their concentration) and 16S rRNA raw reads of the vessel inoculated with *B. breve* UCC2003 were used. Spearman correlation between 16S reads of *B. breve* UCC2003 and identified bacterial metabolites over time were also used to identify which of the measured metabolites could be produced by *B. breve* UCC2003. Here, calculated p-values were adjusted for multiple comparisons using Benjamini & Hochberg correction. Next, a list of manually curated relationships between bacterial metabolites and human host target genes was downloaded from the GutM Gene database (version 1.0) (Cheng et al., 2022). To build metabolite-host gene networks, the *a priori* metabolite-target gene network was filtered for target genes that were either DEGs (|Log2FoldChange > 0.5, adjusted p-value < 0.05) or TFs inferred by PROGENy analysis in organoids exposed to *B. breve* UCC2003 supernatant compared to differentiated controls. Metabolite-host gene networks were expanded one step further from affected TFs by adding all their possible target genes, which previously identified by building TF-TG networks of organoids exposed to *B. breve* UCC2003 supernatant compared to differentiated controls. Bacterial metabolite-host gene networks were visualised separately for each organoid line in Cytoscape (version 3.9) (Shannon et al., 2003).

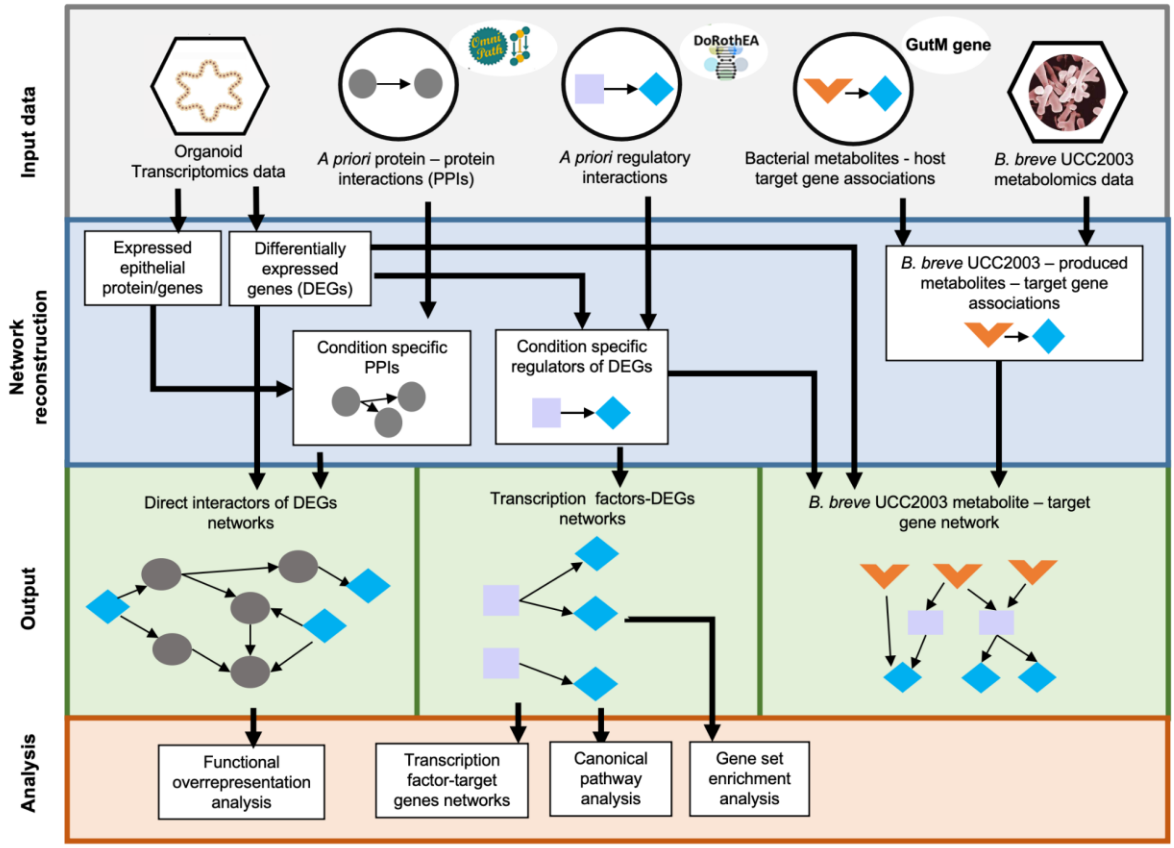

Figure 4.3. **Schematic representation of the bioinformatics analysis. Input data**; transcriptomics data of healthy human colonic organoids exposed to bifidobacterial metabolites was integrated with *a priori* knowledge on human PPI or regulatory interactions from OmniPath and Dorothea databases, respectively. Alternatively, transcriptomics data and metabolomics data of *B. breve* UCC2003 was integrated with *a priori* knowledge on associations between bacterial metabolites and human host target genes from the GutM Gene database ("input data"). **Network reconstruction**; integration of these datasets allows to build molecular interaction networks, illustrating host condition-specific PPIs and regulators of DEGs, as well as bifidobacterial metabolite - host target gene association networks. **Output;** host condition-specific PPIs can be useful to reproduce interactions between DEGs upon bifidobacterial-metabolite exposure and their direct interactors, while condition-specific regulatory networks can be further developed to build regulatory networks showing the master regulators of DEGs upon bifidobacteria exposure. Finally, metabolite-host target gene networks can be used to visualise associations between *B. breve* UCC2003-produced metabolites and affected genes and TFs in host epithelial cells. **Analysis**; further analysis of these networks can help unravel the main modulated canonical pathways and gene sets, functional changes and upstream regulators in the host by bifidobacteria.

4. Results

4.1. Exposure to *B. breve* or *L. rhamnosus* metabolites has no phenotypic impact on organoids during differentiation

At the beginning of the experiment, the two organoid lines were kept in a medium to enrich the stem-cell compartment. Upon microscopic observations, the two lines appeared different, with organoid line 1 characterised by thicker cell membranes compared to line 2 (**Figure 4.4**). Both lines successfully differentiated over the 3 days period, and were both characterised by thicker cell borders and the presence of budding, indicating the formation of crypt-villi structures typical of differentiated epithelium. Interestingly, these characteristics were more evident in organoid line 1 compared to line 2, in line with the more differentiated status at the beginning of the experiment **(Figure 4.4)**.

Upon microbial metabolite exposure (*B. breve* UCC2003 and *L. rhamnosus*), no clear morphological changes could be identified compared to organoids fed with just media control for 3 days **(Figure 4.4).** Additionally, there were no clear differences in terms of size and number of organoids across different wells for organoids treated with metabolites compared to those untreated for both organoid lines **(Figure 4).**

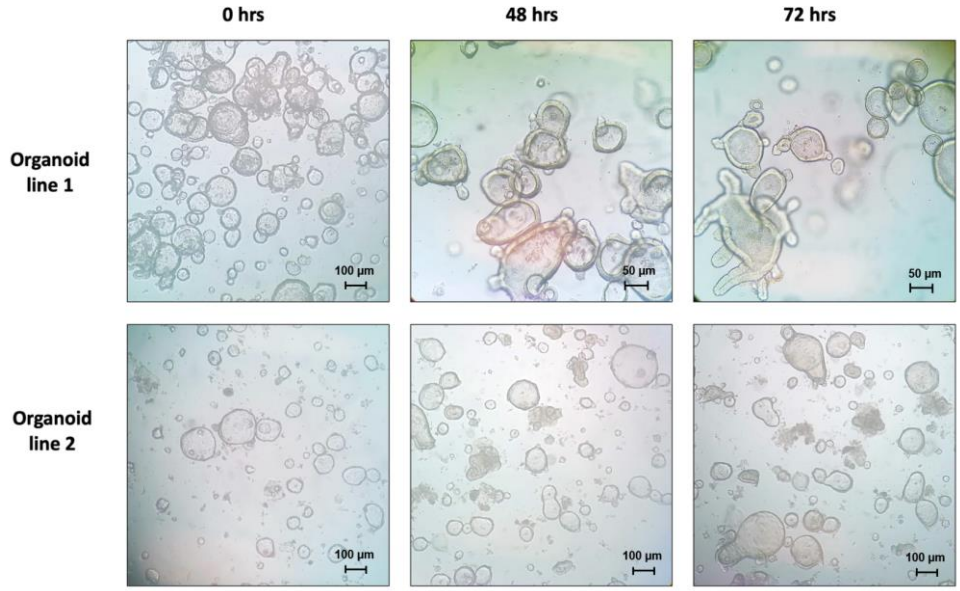

Figure 4.4. Differentiation of healthy human colonic organoids during 3 days. Representative brightfield microscope images of human colonic organoids. Images are shown for each organoid line (1 and 2) at the beginning of the experiment (t = 0 hours), after 2 days (t = 48 hours) and at the end of the experiment (t = 72 hours). No difference was identified between treated and untreated organoids, so images of organoids exposed to bacterial metabolites (*B. breve* UCC2003 and *L. rhamnosus*) are not shown.

4.2. Exposure to *B. breve* or *L. rhamnosus* metabolites has a modest effect on gene expression profiles of intestinal epithelial cells

Following bulk RNA sequencing of human colonic organoids exposed to *B. breve* UCC2003, *L. rhamnosus* metabolites or media control during differentiation, I carried out a visualisation of the (log2 transformed) transcriptomics data using principal component analysis (PCA). Results showed that the bigger differences in transcriptomics profiles (PC1, 41.61% variation and PC2, 30.8% variation) (**Figure 4.5A**) were dependent on the differentiation status of the organoid (undifferentiated or differentiated, as well as organoid line (organoid line 1 or 2) (**Figure 4.5B**). Conversely, only a small part of the variation in transcriptomics profiles could be attributed to the treatment (control, or bacterial supernatants) (**Figure 4.5B**). This suggested that, at least based on all genes of the genome, exposure to bacterial metabolites did not result in any detectable differences in gene expression profiles of epithelial cells. Similar results were obtained using a non-linear dimensionality reduction approach, namely uniform manifold approximation and projection (UMAP) (McInnes et al., 2018) (**Supplementary Figure 4.1**).

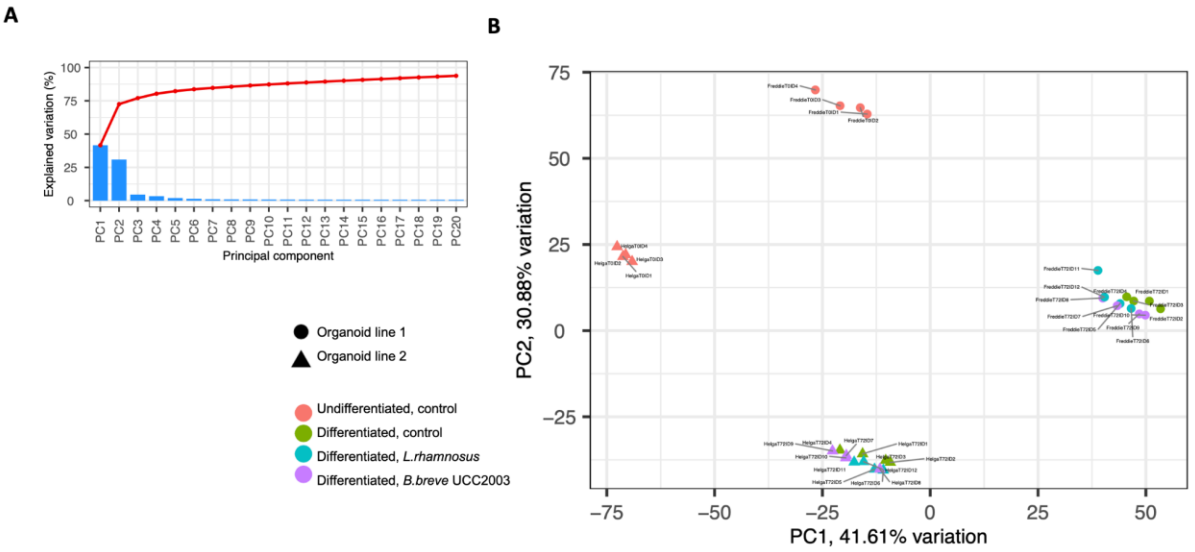

Figure 4.5. PCA plot of normalised counts data. A) Bar plot of ranked principal components by percent (%) of explained variation. B) PCA plot showing all samples where point shape indicates Organoid line (1 and 2) and colour indicates the condition (differentiation state and treatment). Undifferentiated organoid (t = 0 hours) or differentiated for 3 days (t = 72 hours), treated with bacterial supernatants (*L. rhamnosus, B. breve* UCC2003) or untreated (control). Plots were created using R.

4.3. Organoid differentiation affects gene expression profiles of epithelial cells

Next, I carried out differential expression analysis to compare gene expression profiles between organoids exposed to bacterial metabolites and media control. Because exposure to bacterial metabolites was carried out during organoid differentiation, I made two different comparisons for each organoid line used. In particular, organoids exposed to bacterial metabolites (*B. breve* UCC2003, *L. rhamnosus* supernatants) at the end of the experiment (t = 72 hrs) were either compared to (i) differentiated organoid controls (exposed to media alone) (t = 72 hours) or (ii) undifferentiated organoid controls (t = 0 hours) (**Figure 4.6**).

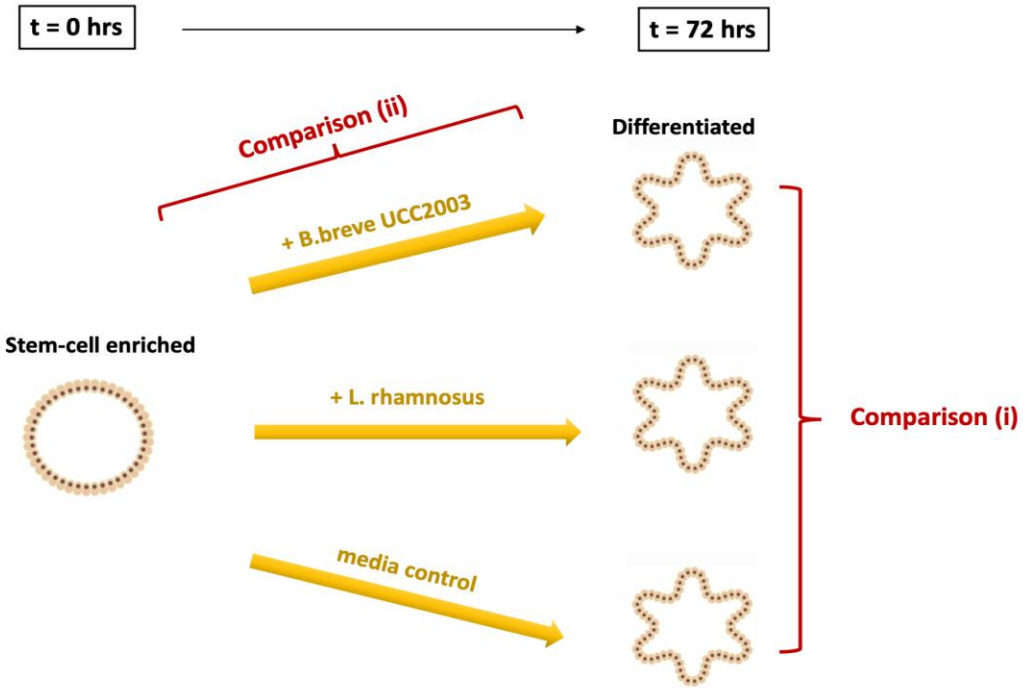

Figure 4.6. Schematic representation of the differential expression analysis set-up. The effect of bacterial metabolites on gene expression profiles in epithelial cells was assessed by comparing organoids exposed to *B. breve* UCC2003 or *L. rhamnosus* sup. to differentiated controls (grown in media only) (t = 72 hrs). Alternatively, the effect of bifidobacteria was assessed by comparing organoids exposed to *B. breve* UCC2003 or *L. rhamnosus* sup. (t = 72 hours) to undifferentiated controls (t = 0 hours), following the removal of the effect of organoid differentiation.

When comparing organoids exposed to bacterial supernatants compared to differentiated controls, 40 and 53 DEGs (|Log2FoldChange| > 1) were identified in organoid 1 and 2, respectively, upon *B. breve* UCC2003 sup. exposure (**Supplementary Figure 4.2A)**. Additionally, 18 and 24 DEGs (|log2FoldChange| > 1) were identified in organoid 1 and 2, respectively, upon *L. rhamnosus* sup. exposure **(Supplementary Figure 4.2A).** The number

of significant DEGs was relatively low, as most DEGs did not pass the log2FoldChange cut-off of 1. This could be observed when plotting all possible DEGs and their associated Log2FoldChange and adjusted p-value against the 1 cut-off **(Supplementary Figure 4.3)**. Hence, to expand the dataset used, further analyses were carried out using a lower cut-off of 0.5. With this new cut-off, 146 and 269 DEGs were identified upon *B. breve* UCC2003 sup. exposure, and 107 and 118 DEGs under *L. rhamnosus* sup. exposure in organoid line 1 and 2, respectively **(Figure 4.7A)**.

When comparing organoids exposed to bacterial supernatants to undifferentiated controls, 3376 and 2743 DEGs (|Log2FoldChange| > 1) were identified upon *B. breve* UCC2003 sup. exposure and 3131 and 2879 DEGs upon *L. rhamnosus* sup. exposure in organoid line 1 and 2 respectively (**Supplementary Figure 4.2B**). Additionally, growing organoids in differentiation media alone for 3 days, resulted in 3526 and 2956 DEGs (adjusted p-value < 0.05, |Log2FoldChange| > 1) in organoid line 1 and 2, respectively (**Supplementary Figure 4.2B**). Using a lower cut-off of 0.5, almost doubled the amount of DEGs identified, in particular 6482 and 5083 DEGs upon *B. breve* UCC2003 sup. exposure, and 5997 and 5338 DEGs upon *L. rhamnosus* sup. exposure in organoid line and 2, respectively **(Figure 4.7B).** Furthermore, upon organoid differentiation, 6743 and 5460 DEGs were identified in organoid line 1 and 2, respectively (**Figure 4.7B**).

In general, effects were comparable among bacteria, although *B. breve* UCC2003 sup. exposure resulted in a higher number of DEGs in both lines compared to the bacterial control *L. rhamnosus* (**Figure 4.7A**). Additionally, upon *B. breve* UCC2003 sup. exposure compared to differentiated controls, the number of DEGs in organoid line 2 was almost double than in organoid line 1, showing a bigger effect of bifidobacteria exposure, in a patient-specific manner (**Figure 4.7A**).

When comparing organoids exposed to bacterial supernatants to undifferentiated controls, both the differentiation effect and bacterial exposure were responsible for changes observed in the number of DEGs. Hence, to remove the effect given by the organoid differentiation over time and uniquely identify the effect given by bacterial metabolites, DEGs unique to *B. breve* UCC2003 or *L. rhamnosus* sup. exposure were calculated by removing overlapping DEGs of differentiated organoids exposed to media control alone (**Figure 4.7C**). Overlapping DEGs were considered when they had adjusted p-value < 0.05 and |Log2FoldChange|> 0.5, and where the change was in the same direction for both conditions. The majority of DEGs (5881 and 5415 in organoid line 1; 4506 and 4698 in organoid line 2) were overlapping between bacterial supernatants exposure (*B. breve* UCC2003 and *L. rhamnosus*) and control, showing

that the majority of gene expression changes were driven by organoid differentiation (not shown). After removal of these overlapping genes, 601 and 577 unique DEGs were found upon *B. breve* UCC2003, and 582 and 640 unique DEGs upon *L. rhamnosus* sup. exposure, in organoid line 1 and 2, respectively (**Figure 4.7C**).

A

Condition	Organoid line 1	Organoid line 2	Total n of DEGs (t=72 h vs t=72 h)
B.breve UCC2003	146	269	
L.rhamnosus	107	118	

B

Condition	Organoid line 1	Organoid line 2	Total n of DEGs (t=72 h vs t=0 h)
B.breve UCC2003	6482	5083	
L.rhamnosus	5997	5338	
Control	6743	5460	

C

Condition	Organoid line 1	Organoid line 2	Total n of DEGs *minus control overlap* (t=72 h vs t=0 h)
B.breve UCC2003 (minus control)	601	577	
L.rhamnosus (minus control)	582	640	

Figure 4.7. DEGs upon bacterial metabolites exposure compared to control. A) Total number of DEGs identified between organoids exposed to bacterial supernatants (t = 72 hours) and differentiated controls (t = 72 hours). **B)** Total number of DEGs identified between organoids exposed to bacterial supernatants (t=72 hrs) and undifferentiated controls (t = 0 hours). **C)** DEGs between organoids exposed to bacterial supernatants (t = 72 hours) and undifferentiated controls (t = 0 hours), where overlapping DEGs between bacterial treatment and control conditions have been removed ("minus control"). A, B, C) In all tables, significantly DEGs are shown where adjusted p-value < 0.05, |Log2FoldChange| > 0.5.

4.4. Impact of donor and bacterial treatment on gene expression changes upon organoid differentiation

In order to understand how similar or different was the response of the two healthy colonic organoid lines used in this study, the number of overlapping DEGs between the two organoid lines for the different conditions and comparisons was computed. When comparing differentiated organoid to undifferentiated organoid controls, indicating changes happening upon organoid differentiation, a high proportion of DEGs (4037) was shared between the two organoid lines (59.8% overlap for organoid line 1, and 73.9% overlap for line 2) (**Figure 4.8A**). This indicated a similar differentiation pattern, which could also be observed looking at the general transcriptional differences visualised by PCA or UMAP **(Figure 4.5** and **Supplementary Figure 4.1)**.

When comparing organoids exposed to bacterial supernatants to differentiated controls, a relatively small amount of DEGs (63 for *B. breve* UCC2003 and 14 for *L. rhamnosus*) was shared between the two organoid lines (23.4-43% for *B. breve* UCC2003, 13-11.8% for *L. rhamnosus*) (**Figure 4.8A**). When comparing organoids exposed to bacterial supernatants to undifferentiated controls, an even smaller amount of DEGs (81 for *B. breve* UCC2003 and 37 for *L. rhamnosus*) was shared between the two organoid lines (6.4-13.4% for *B. breve* UCC2003, 5.8-13.9% for *L. rhamnosus*) (**Figure 4.8A**). Overall, these findings highlighted organoid line-specific, and thus patient-specific differences in response to bacterial metabolites exposure.

In general, the number of DEGs upon *B. breve* UCC2003 exposure was higher than upon *L. rhamnosus* exposure, which is a well-established probiotic bacteria, in both organoid lines **(Figure 4.7A, C**). However, to decipher whether bifidobacteria exposure resulted in any added effects on epithelial cells transcriptomics profiles, the number of overlapping DEGs upon *B. breve* UCC2003 or *L. rhamnosus* sup. exposure for each comparison and organoid lines was calculated. When comparing organoids exposed to bacterial supernatants to differentiated controls, 25 and 68 DEGs were shared in organoid lines 1 and 2, respectively between treatment type (17.1-25.2% overlap for *B. breve* UCC2003, 23.4-57% for *L. rhamnosus*) (**Figure 4.8B**). Similarly, when comparing to undifferentiated controls, 260 and 308 DEGs were overlapping in organoid lines 1 and 2, respectively, between treatments (43.2-53.4% overlap for *B. breve* UCC2003, 44.7-48.1% overlap for *L. rhamnosus*) (**Figure 4.8B**). Overall, these numbers highlight a similar effect of the two bacterial strains, but also the presence of bifidobacteria-unique effects.

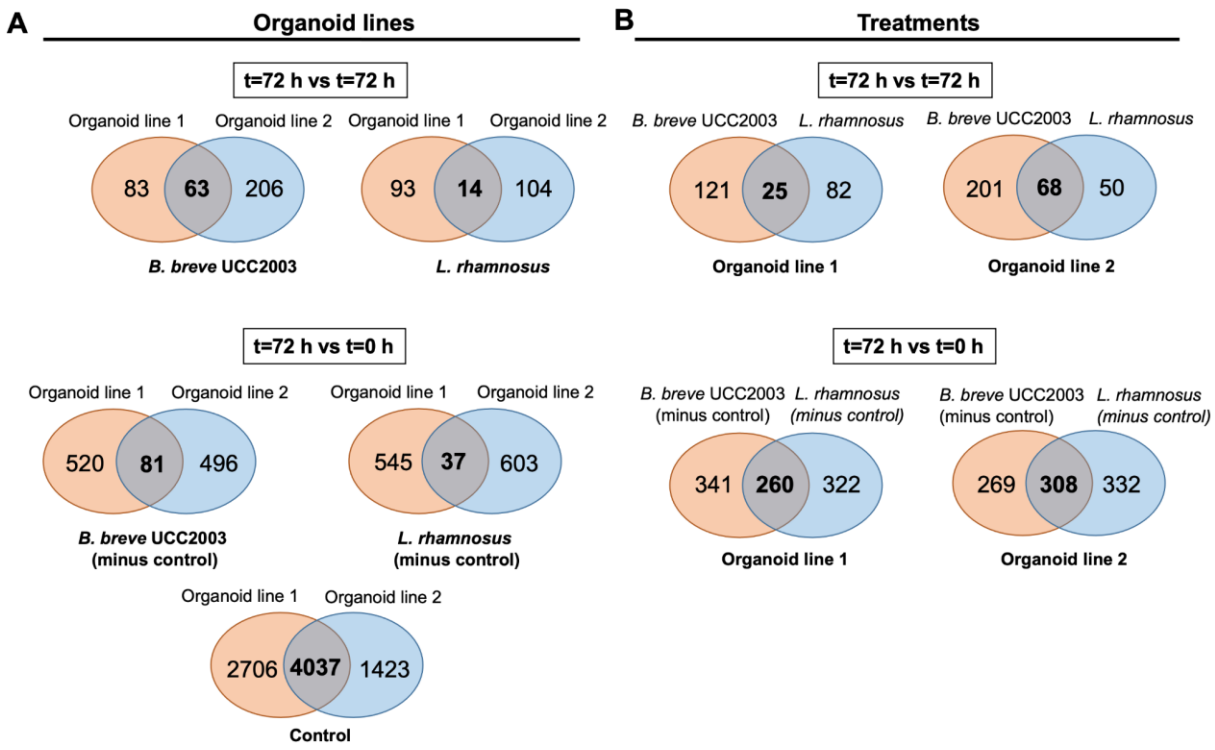

Figure 4.8. Unique and overlapping DEGs between organoid lines and bacterial treatment used. Venn diagrams showing overlapping DEGs between organoid lines (A) or bacterial treatments (B). DEGs were filtered for |Log2FoldChange| > 0.5 and adjusted p-value < 0.05.

4.5. Altered gene expression patterns and regulatory landscape upon organoid differentiation

To validate the successful differentiation of organoids over the 3 days period, signalling pathway and upstream TF inference were performed using PROGENy and DoRothEA, respectively. Upon organoid differentiation, top activated pathways in both lines were hypoxia and Janus kinase-signal transducer and activator of transcription (JAK-STAT), which mediates intestinal homeostasis in response to cytokines (Salas et al., 2020) (**Figure 4.9A**). Conversely, top inhibited pathways were mitogen-activated protein kinase (MAPK), WNT pathway and EGFR pathways (**Figure 4.9A**). Interestingly, the estrogen and androgen pathways were also inhibited upon differentiation in organoid line 1 and 2, respectively, probably reflecting the different sex type of the organoid donors (**Figure 4.9A**).

Furthermore, TF analysis found that, upon differentiation, the most activated TFs in both lines were involved in enterocyte fate (Hepatocyte Nuclear Factor 4 Alpha; HNF4A), terminal differentiation of the epithelium upstream of Notch (Hepatocyte Nuclear Factor 1 Alpha;

HNF1A and 1 Beta; HNF1B) and early intestinal differentiation (caudal-type homeobox 2; CDX2) (**Figure 4.9B**). Conversely, the most inhibited TFs were involved in embryonic development (SRY-Box Transcription Factor 2 (SOX2)) and WNT signalling (Transcription Factor 7 Like 2; TCF7L2, also known as ATF4) (**Figure 4.9B**). Regulation of these TFs upon organoid differentiation is indicative of the loss of stemness and early development phenotype and promotion of differentiation towards a more mature epithelium.

GSEA analysis also revealed that gene sets related to lipid metabolism were positively enriched (NES> 2, adjusted p-value < 0.05), while gene sets related to cell division, translation, transcription and post-translational events were negatively enriched (NES< 2, q value < 0.05) in both lines upon organoid differentiation (**Supplementary Figure 4.4**).

Finally, to investigate which epithelial cell populations were affected upon organoid differentiation, I carried out an epithelial cell marker gene analysis. Results revealed that markers for all major differentiated cell types (enterocytes, M cells, GCs) were significantly upregulated (|Log2FoldChange| > 1, adjusted p-value < 0.05) upon differentiation in both lines (**Supplementary Figure 4.5)**, further confirming the correct differentiation of colonic organoids over the 3-days period.

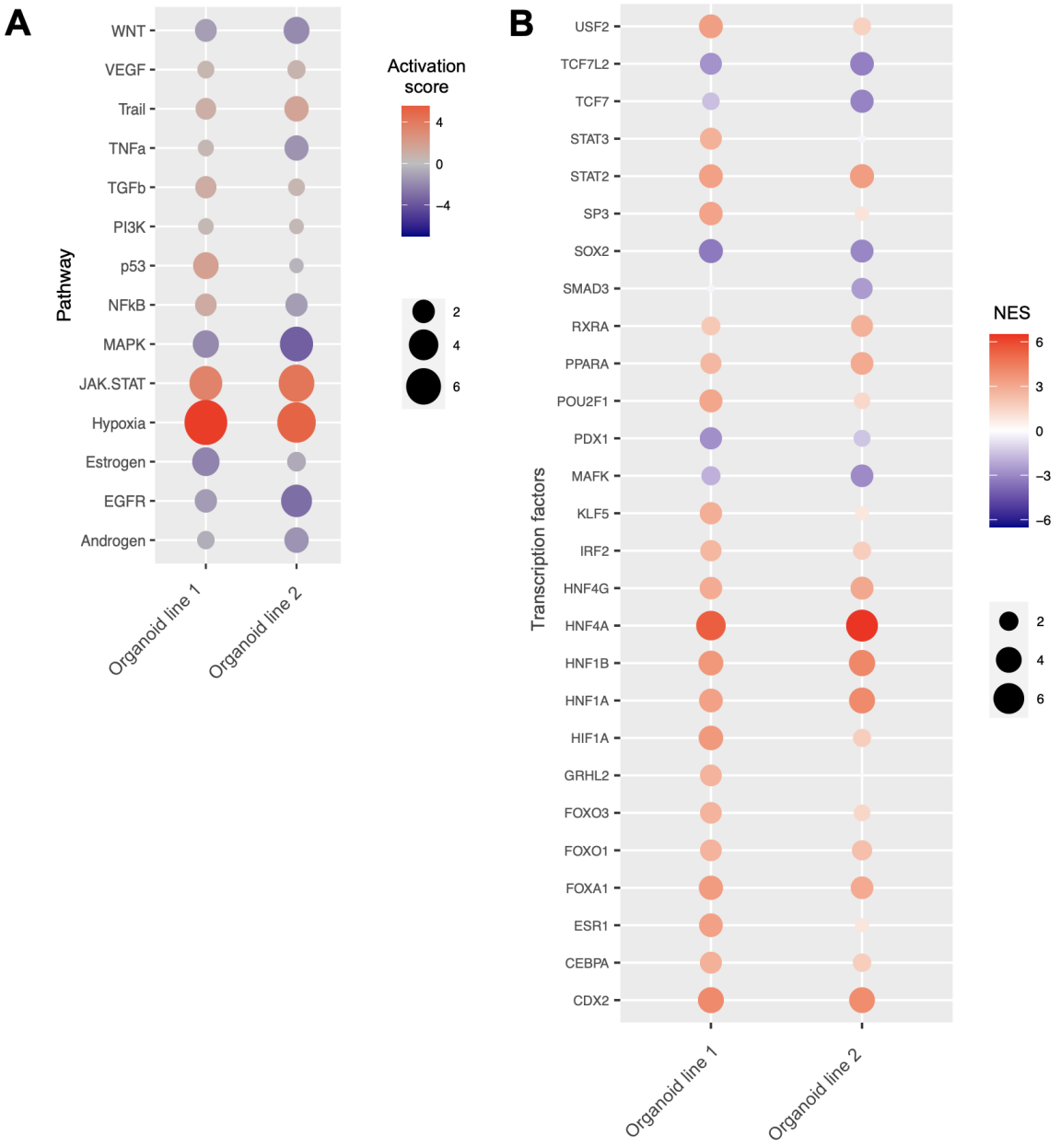

Figure 4.9. **Pathway and TF analyses of human colonic organoid lines upon differentiation. A)** Bubble chart indicating canonical pathways modulated upon organoid differentiation. Size of the bubble indicates the Progeny activation score and colour indicates the direction of the predicted change (red, activated; blue, inhibited). **B)** Bubble chart indicating TFs predicted to be modulated using Progeny and Dorothea. Size of the bubble indicates the NES and colour indicates the direction of the predicted change (red, activated; blue, inhibited). Pleiotropic correction for multiple regulation was applied, and only TFs regulating a minimum of 8 targets and with predicted |NES| > 2.5 in either organoid line 1 or 2 are shown. Plots were created using the ggplot2 package in R.

4.6. Bifidobacteria enhances epithelial markers of enterocytes and M cells populations

Upon *B. breve* UCC2003 sup. exposure of organoids compared to differentiated controls, markers of TA cells, enterocytes and M cells were upregulated, while markers of SCs, GCs and Tuft cell populations were mostly downregulated compared to differentiated organoid control (**Figure 4.10**). Similar results could also be observed upon *L. rhamnosus* exposure, although the number of differentially expressed markers was lower, supporting the presence of a bigger effect for *B. breve* UCC2003 sup. on epithelial differentiation (**Supplementary Figure 4.6**).

Furthermore, upon *B. breve* UCC2003 or *L. rhamnosus* sup. exposure of organoids compared to undifferentiated controls, only a few differentially expressed markers were identified compared to the total number of DEGs. Nevertheless these results pointed towards the similar conclusions for both bacteria and organoid lines (**Supplementary Figures 4.7, 4.8**).

Overall, results of the cell marker analysis seem to indicate the ability of bacterial metabolites to increase the differentiation of the epithelium by restricting the number of stem cells, while shifting the balance towards more progenitor cells and differentiated absorptive enterocytes. Additionally, the increase in antigen presenting M-cells supports the recognition of host-microbe interactions happening at the epithelial interface.

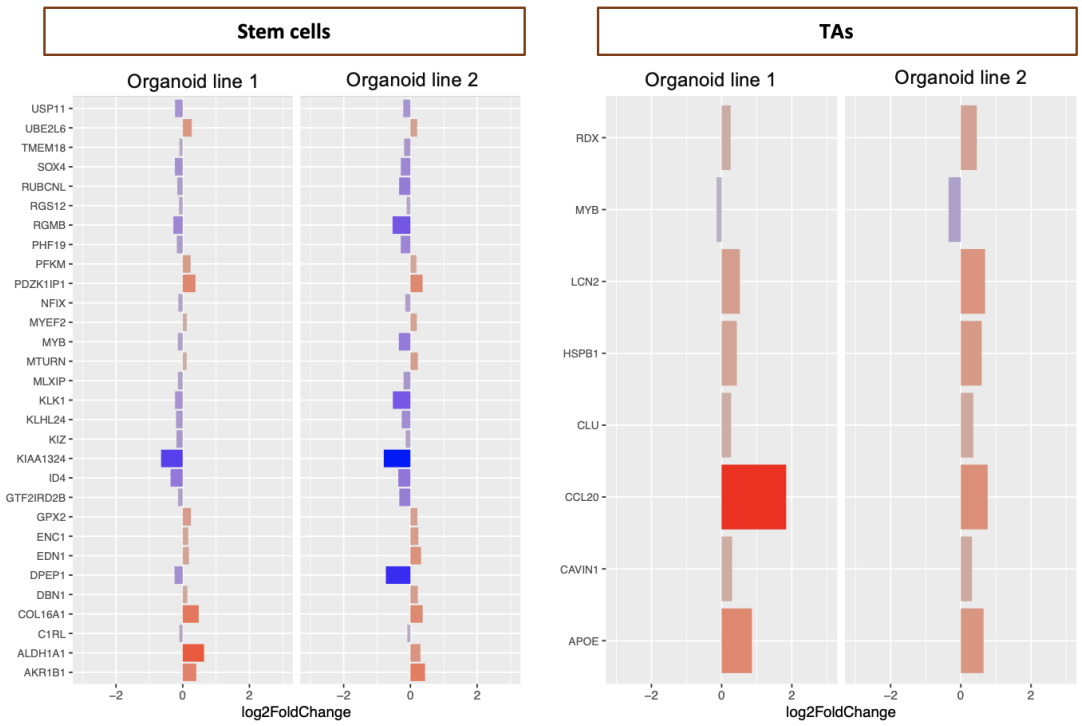

(Figure continues on the next page)

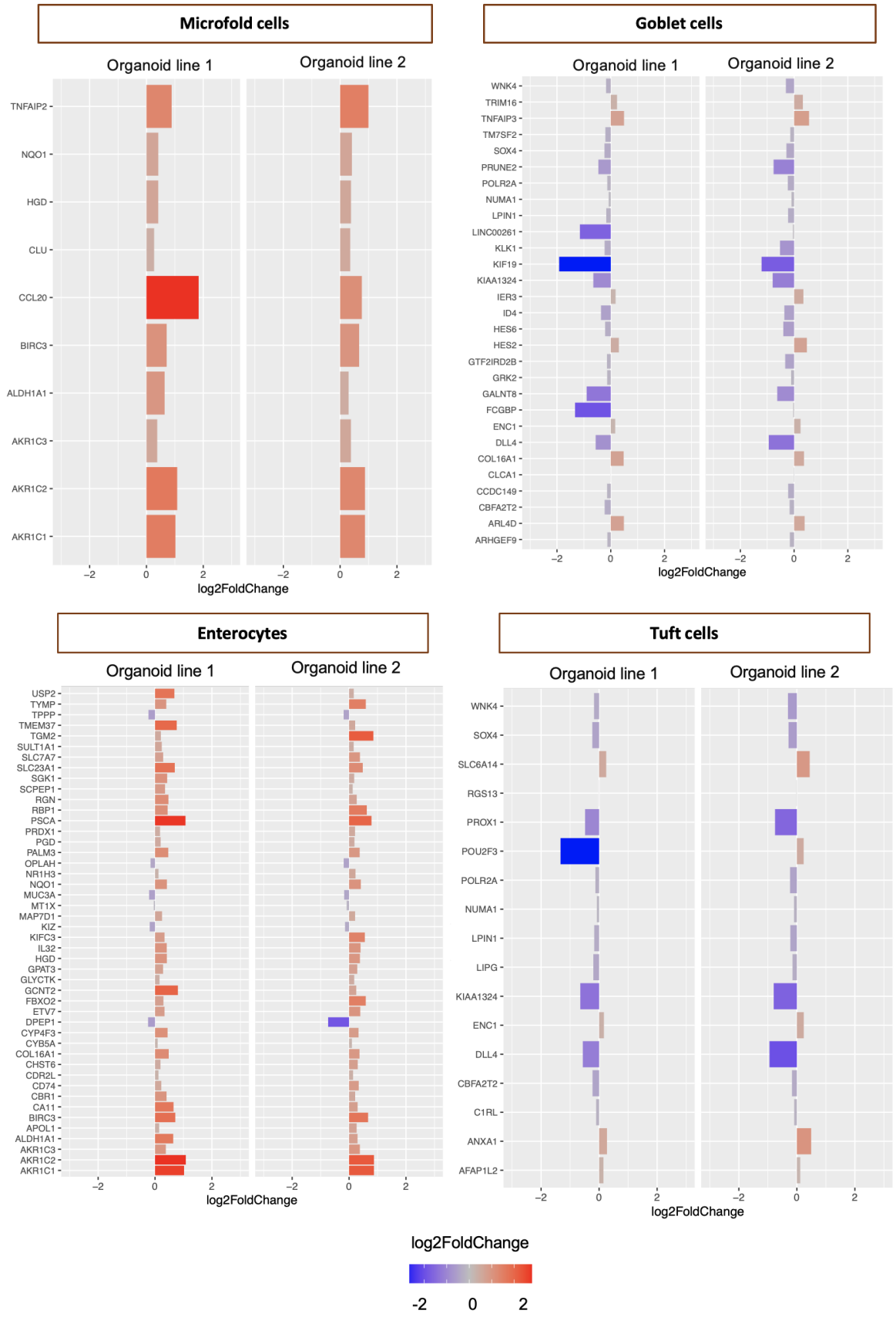

Figure 4.10. Top differentially expressed markers of epithelial cell populations upon *B. breve* UCC2003 exposure of organoids compared to differentiated controls. The height of the bar plot and colour gradient (red, positive; blue, negative) indicates the Log2FoldChange value in organoids

exposed to *B. breve* UCC2003 sup. compared differentiated controls (t = 72 hours) in organoid lines 1 and 2. DEGs in *B. breve* UCC2003 compared to control (adjusted p-value < 0.05) were filtered for markers of epithelial cells from the Gut Cell Atlas (adult healthy colon), (Log2FoldChange > 1, adjusted p-value < 0.01). Only markers that were significant in both organoid lines are shown. Bar plots were created using ggplot2 in R.

4.7. Pathway and functional analyses reveal the effects of *B. breve* UCC2003 metabolites on epithelial function

To investigate which pathways were modulated in intestinal epithelial cells upon bacterial exposure, I carried out a pathway analysis using PROGENy. Organoids exposed to *B. breve* UCC2003 sup., were characterised by pro-inflammatory NF-kB and TNF-α signalling being activated compared to differentiated controls (**Figure 4.11**). These pathways were predicted to be activated upon exposure to *L. rhamnosus* as well, although to a lower extent **(Figure 4.11**).

When comparing treated organoids to undifferentiated controls, after removing the effect of differentiation, pathway analysis confirmed similar observations for both *B. breve* UCC2003 and *L. rhamnosus* sup. (**Supplementary Figure 4.9**). In particular, the WNT pathway was found to be more activated upon *B. breve* UCC2003 sup. exposure in both lines, while this pathway was inhibited in the media control (during simple differentiation) (**Supplementary Figure 4.9**). Finally, upon both *B. breve* UCC2003 and *L. rhamnosus* sups. exposure, stress and cell-death pathways (trail, hypoxia) were inhibited, while activated in the control; MAPK pathway was more inhibited than in the control; JAK-STAT was less activated than in the control; and EGFR was activated, while inhibited in controls, in both organoid lines (**Supplementary Figure 4.9**).

Overall, these results suggest that bifidobacterial metabolites may initiate physiological immune responses in epithelial cells such as TNF-α, NF-kB, and JAK-STAT signalling, whilst decreasing other stress and cell-death related pathways (trail and hypoxia). Additionally, bifidobacterial metabolites were also able to promote intestinal homeostasis *via* WNT signalling, as well as enterocytes proliferation *via* EGFR signalling.

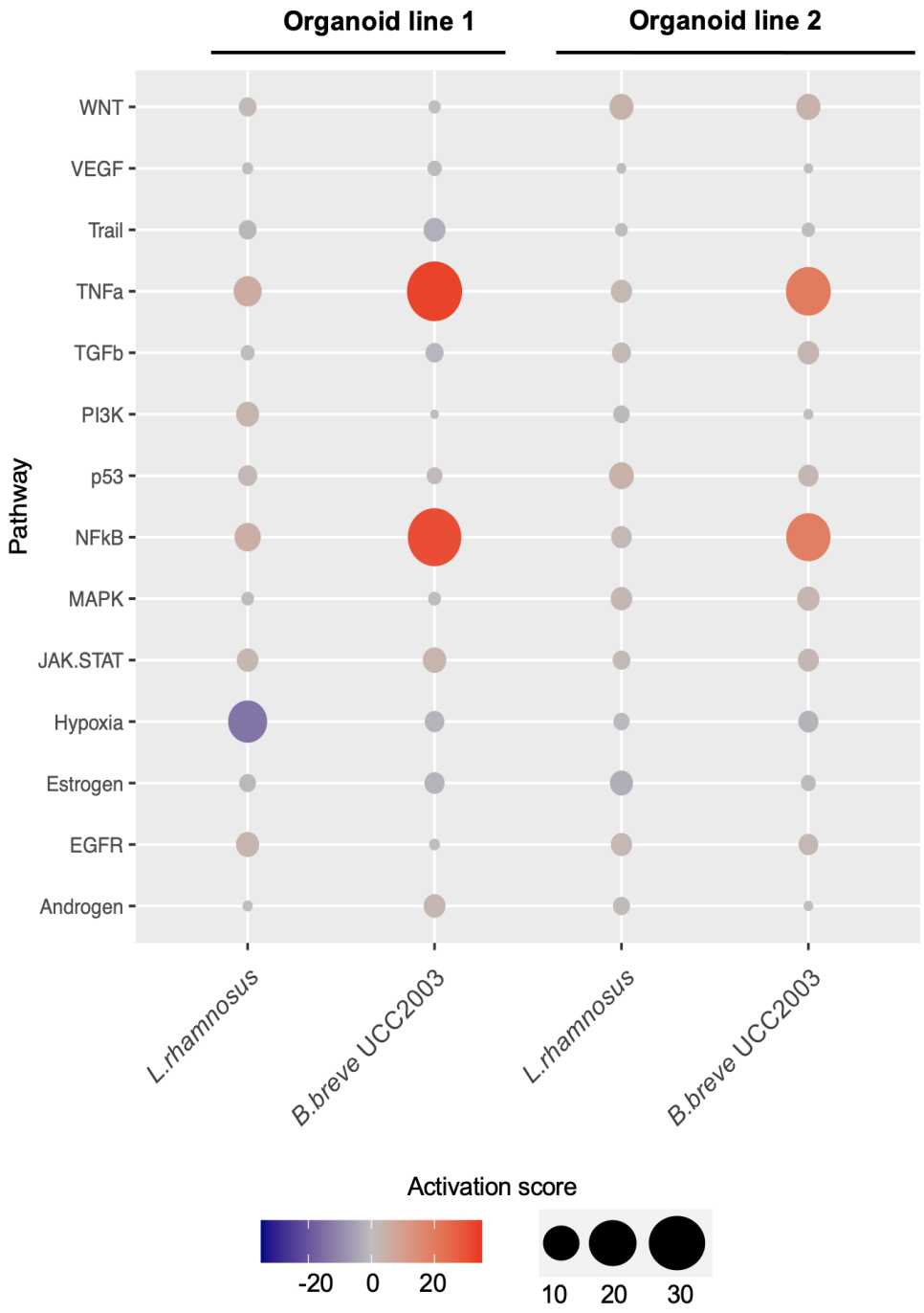

Figure 4.11. Pathway analysis of differentiated organoids exposed to bacterial metabolites compared differentiated controls. Bubble chart indicating canonical pathways modulated in organoids exposed to bacterial metabolites compared to differentiated controls (t = 72 hours). Size of the bubble indicates the Progeny activation score and colour indicates the direction of the predicted change (red, activated; blue, inhibited). Plots were created using the ggplot2 package in R.

GSEA was used to further investigate which functions were modulated by bifidobacterial metabolites in epithelial cells. Upon *B. breve* UCC2003 sup. exposure of organoids, when compared to differentiated controls, top activated functions were related to inflammation (neutrophil chemotaxis, neutrophil migration, response to interleukin-1, response to TNF-a) in both organoid lines, electron transport chain in organoid line 1 only, and extracellular matrix organisation, cell adhesion, epidermis development and nervous system processes (regulation of trans synaptic signalling) in organoid line 2 only (**Figure 4.12**). Furthermore, when compared to undifferentiated controls, no added information was provided, as activated functions were mainly related to general cellular processes such as localisation, transport, and metabolic processes (**Supplementary Figure 4.10**).

Conversely, downregulated functions upon *B. breve* UCC2003 exposure of organoids compared to differentiated controls, were mainly related to lipid metabolism (cholesterol biosynthetic process, sterol metabolic process) and chromatin modifications (line 1 and 2), as well as negative regulation of cell division and general cellular response to chemical stimulus in line 1 only (**Figure 4.12**). Similarly to the upregulated functions, the additional comparison to undifferentiated controls generally confirmed these findings, or added no relevant information (**Supplementary Figure 4.10**).

When looking at *L. rhamnosus* sup. exposure of organoids compared to differentiated controls, some functions were similarly activated, including those related to the nervous system (regulation of nervous system processes), epidermis development (keratinocyte differentiation, cornification, epidermis development), ECM organisation and cell-substrate adhesion (line 2) (**Supplementary Figure 4.11**). Interestingly, results showed some additional functions uniquely modulated by *L. rhamnosus*, including some related to ribosomal RNA processing, mitochondrial gene expression and ncRNA metabolic processes in organoid line 1 only (**Supplementary Figure 4.11**).

As for the inhibited functions, some were similar to those found upon *B. breve* UCC2003 sup exposure, including chromatin modifications and lipid metabolism (**FIgure 4.12, Supplementary Figure 4.11**). However, some additional functions that were inhibited included negative regulation of intracellular signalling transduction, and positive regulation of protein kinase activity, autophagy, and RNA processing (RNA splicing, ncRNA metabolic process) (**Supplementary Figure 4.11**). Similarly to *B. breve* UCC2003, comparing organoids exposed to *L. rhamnosus* sup. to undifferentiated controls did not provide any relevant additional information (**Supplementary Figure 4.12**).

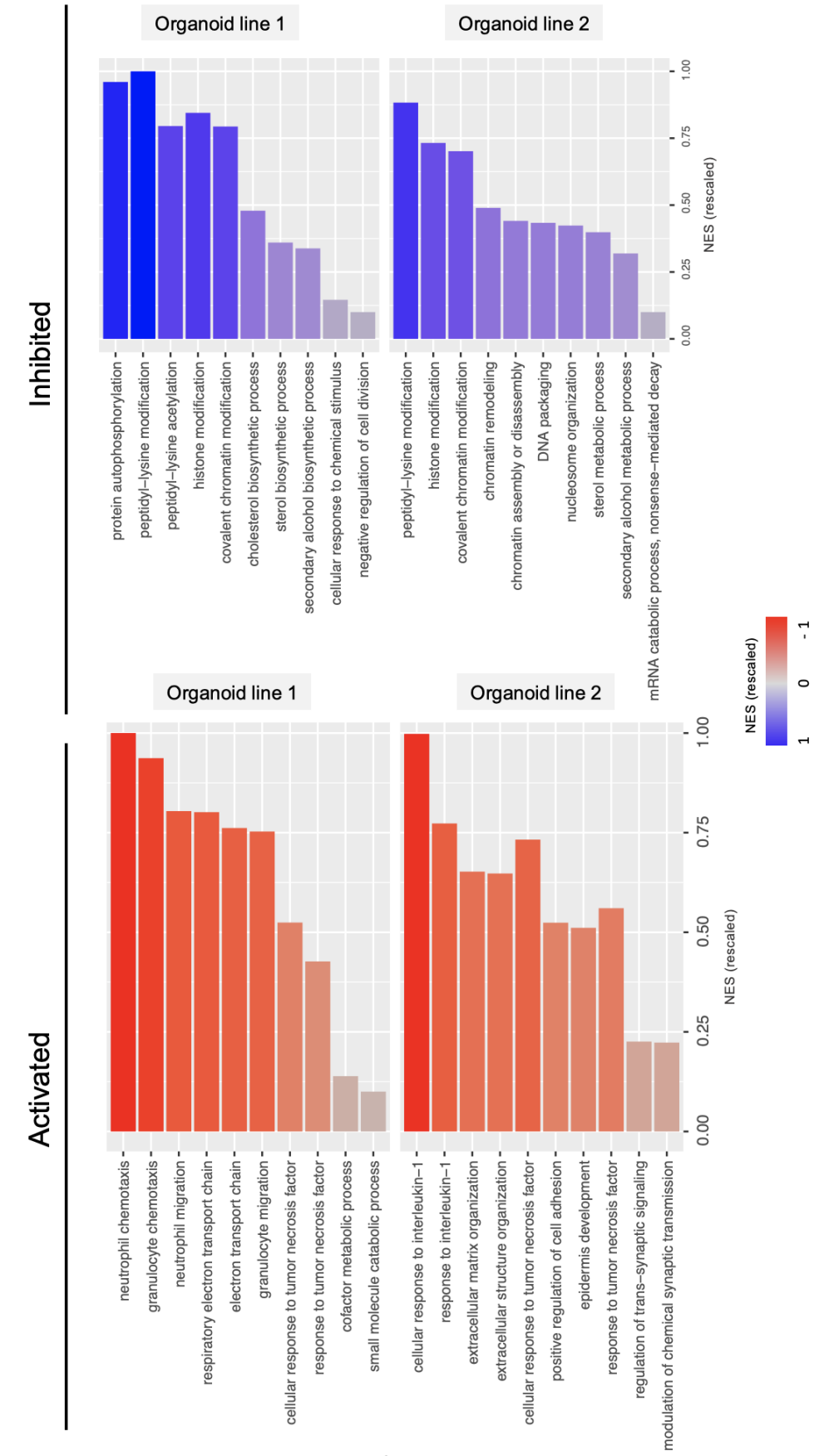

(Figure caption on the next page)

Figure 4.12. Top enriched functions identified by GSEA of DEGs upon *B. breve* UCC2003 bacterial exposure of organoids compared to differentiated controls. Top 10 GO activated and inhibited functions upon *B. breve* UCC2003 sup. exposure of organoids compared to differentiated controls (t = 72 hours) are shown. Activated functions are indicated when NES > 0, while inhibited functions when NES < 0. The length of the bar and colour (red, highest; blue, lowest) indicates the NES score. NES score was rescaled for visualisation purposes. Bar plots were created using the ggplot2 package in R.

4.8. Transcriptional regulators modulated by bifidobacterial metabolites

To understand upstream regulators modulating the observed changes in epithelial cells following bacterial supernatant exposure, TF activity was inferred from downstream gene expression changes using PROGENy and DoRoThEA.

TFs related to epithelial differentiation (*ETV4, NCOR1, FOXP1*), inflammation (*REL, NF-kB1*) and WNT signalling (*BACH1, HBP1*) were among the top activated in both organoid lines upon *B. breve* UCC2003 sup. exposure of organoids compared to differentiated controls (**Figure 4.13**). Conversely, TFs involved in the progression of the cell cycle and WNT signalling (*TAF1, KMT2A, ZNF384*), fatty acid/cholesterol biosynthesis *(SREBF1/2*), chromatin modifications (ARID2/3A/1B) and mucin expression (*NCOA3*) were among the top inhibited in both organoid lines upon *B. breve* UCC2003 sup. exposure compared to differentiated controls (**Figure 4.13**). Similar TFs were predicted upon *L. rhamnosus* exposure compared to differentiated controls (**Figure 4.13**).

Finally, when comparing bacterial exposure of organoids to undifferentiated controls, results were less marked (**Supplementary Figure 4.13**), and mainly involved the activation of *SP1, NF-KB1* (organoid line 1 only) and *ZNF263* (organoid line 1 and 2).

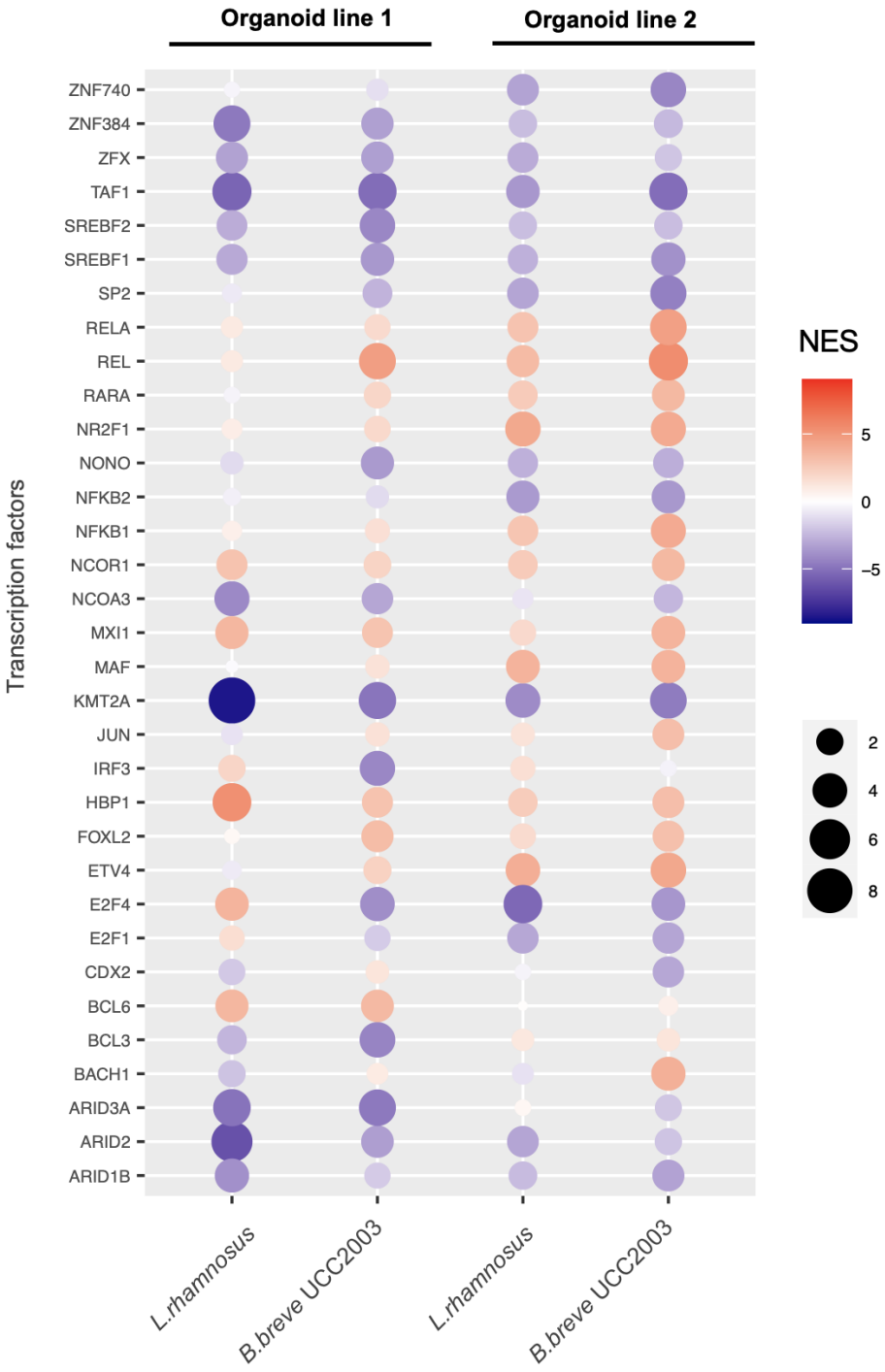

Figure 4.13. Predicted TFs regulating gene expression changes upon exposure of organoids to bacterial metabolites compared to differentiated controls. TFs upon bacterial exposure of organoids compared to differentiated control (t = 72 hours). TFs where pleiotropic correction for multiple regulation was applied, regulating a minimum 15 targets, and with |NES| > 3 in organoid line 1 or 2 are shown. Bubble plots were created using the ggplot2 package in R.

4.9. Transcription factor-target gene networks

To investigate how the predicted regulated TFs were affecting the DEGs upon bacterial metabolites exposure, regulatory networks were built connecting expressed TFs to their regulated DEGs upon *B. breve* UCC2003 or *L. rhamnosus* exposure compared to control in each organoid line.

These networks identified 14 and 33 regulated TFs upon *B. breve* UCC2003 sup. exposure compared to differentiated control in organoid line 1 and 2 respectively, out of which 13 were shared (**Figure 4.14A**). Furthermore, 12 and 6 regulated TFs were identified upon *L. rhamnosus* sup. exposure compared to differentiated controls in organoid line 1 and 2, respectively, out of which 5 were shared (**Figure 4.14A**). Overall, the number of regulated TFs was lower upon *L. rhamnosus* exposure, and a higher number of TFs regulated uniquely upon *B. breve* UCC2003 exposure was found (**Figure 4.14B**). In particular, TFs uniquely regulated by *B. breve* UCC2003 in both organoid lines included *STAT1/3, TEAD1, MYC*, and *FOXL2* (**Supplementary Table 4.1**).

Similar results were found in TF-DEG networks of organoids exposed to bacterial supernatants compared to undifferentiated controls. Here, 56 and 40 TFs were regulated in organoid line 1 and 2 upon *B. breve* UCC2003 sup. exposure, out of which 22 were shared (**Supplementary Figure 4.14A**). Furthermore, 21 and 49 TFs were regulated upon *L. rhamnosus* sup. exposure, out of which 16 were shared (**Supplementary Figure 4.14A**). Here, a large proportion of TFs was shared among the two bacteria, and a higher number of unique TFs was found upon *B. breve* UCC2003 sup. exposure in organoid line 1 (**Supplementary Figure 4.14B**). TFs uniquely regulated by *B. breve* UCC2003 in both organoid lines included *IRF4, POU2F2, CTCF, LYL1, BCL6, MEF2A, EGR1, BCL3, JUN, E2F4*, and *ZBTB7A* (**Supplementary Table 4.2**).

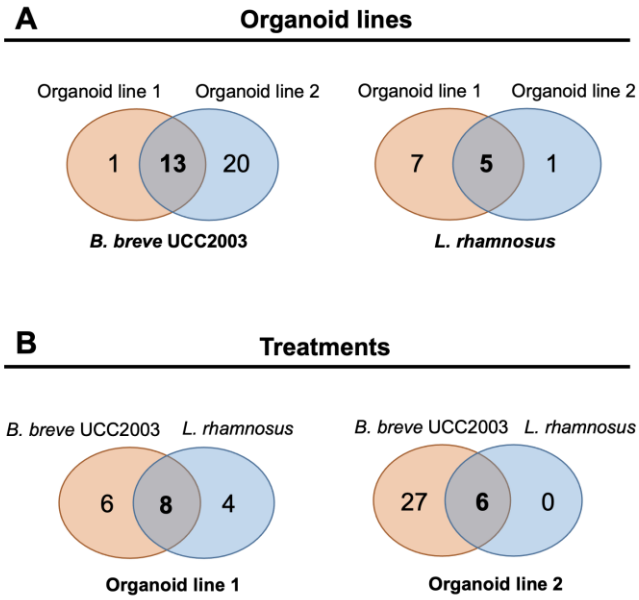

Figure 4.14. Transcription factors in TF-DEG networks of organoids exposed to bacterial supernatants compared to differentiated controls. Venn diagrams showing the unique and overlapping TFs identified in the TF-TG regulatory networks for each organoid line and bacterial exposure type. A) Comparison between organoid lines for each bacterial treatment. B) Comparison between bacterial treatment for each organoid line.

By further filtering the TF-TG networks for TFs regulating the highest amount of DEGs, and including the TF activity, master regulators by which bacterial metabolites affect a high number of genes could be identified. Upon *B. breve* UCC2003 sup. exposure of organoids compared to differentiated controls, master regulators that were activated in both lines included *JUN, NFKB1,* and *RELA* (**Figure 4.15**). These TFs were regulating genes involved in immune response (*CXCL2, CCL20, CXCL3, TNF, CXCL8, CXCL1, CXCL5, MMP7*); *ZNF263* regulating genes involved in chromatin remodelling (*CDH5*) and positive regulation of WNT signalling (*RET*), brush border establishment (*SORCS2*), and receptor tyrosine kinases signalling (PLCG2) (**Figure 4.15**). Additionally, the main master regulator inhibited upon *B. breve* UCC2003 sup. exposure included *SP1*, regulating genes involved in oxidative stress (*CYP1B1, APOE*) and ***MYC*** regulating EECs marker gene (*INSM1*), cell proliferation and differentiation (*TGFB3*), WNT target gene (*ASCL2*), and (*LTB/TNF*-C) (**Figure 4.15**).

Most of these TFs, apart from *MYC*, were also predicted to be regulated upon *L. rhamnosus* sup. exposure of organoids compared to differentiated controls **(Supplementary Figure 4.15).** This potentially highlights a bifidobacteria-specific effect on epithelial proliferation and differentiation mediated by the inhibition of *MYC.*

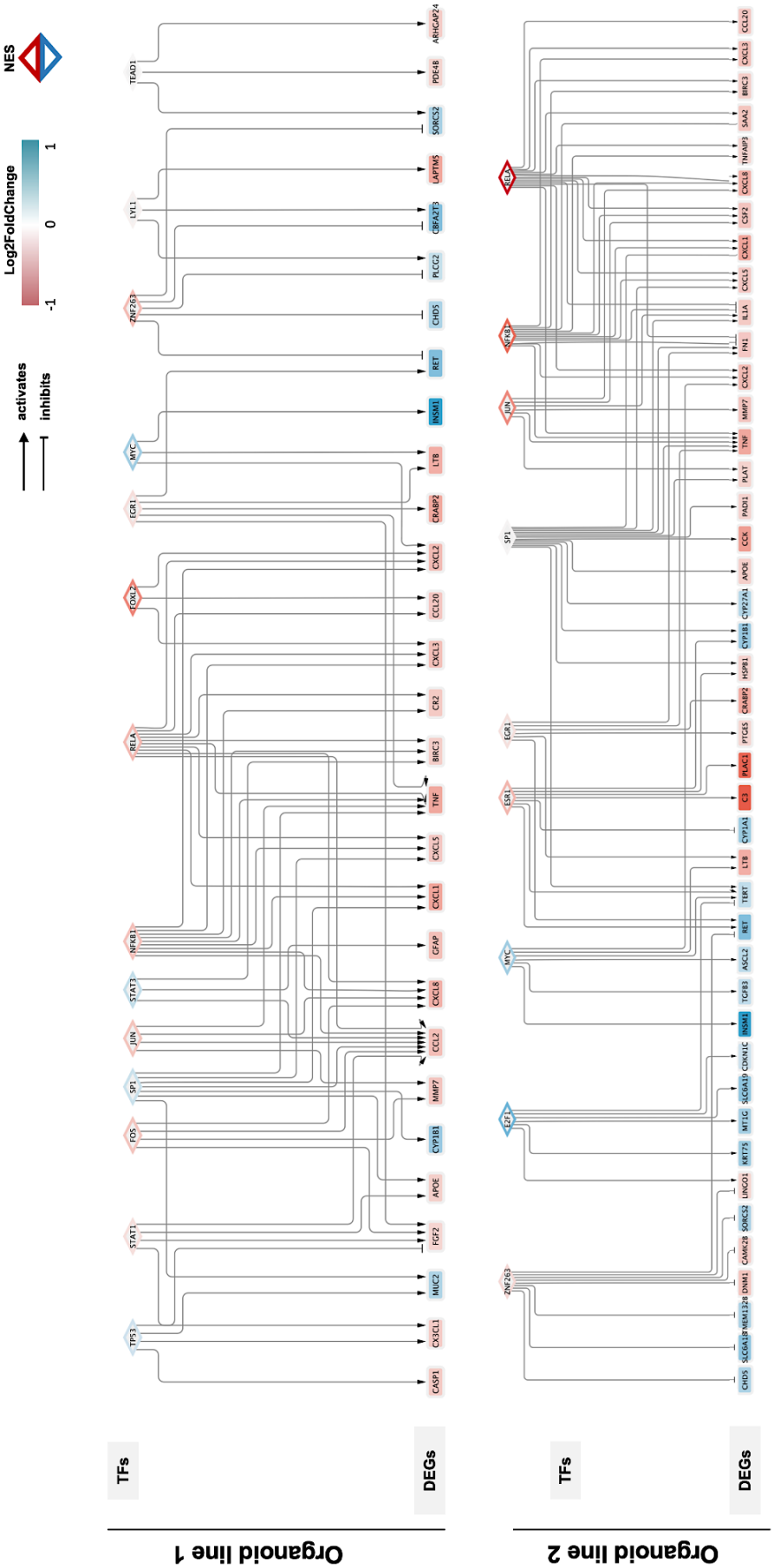

(Figure caption on the next page)

Figure 4.15. TF-TG networks upon *B. breve* UCC2003 exposure of organoids compared to differentiated controls. Regulatory networks showing top TFs (regulating at least 3 DEGs, except in organoid line 2 where at least 6 DEGs are shown) and the corresponding regulated DEGs in organoid lines exposed to *B. breve* UCC2003 sup. compared to differentiated controls. The edge colour indicates the NES of the TF (red, activated (NES>0); blue, inhibited (NES < 0), while the colour gradient of the node indicates the Log2FoldChange of the DEG (red, upregulated; blue, downregulated). Arrows indicate the direction of the regulation, either activation (pointed arrow) or inhibition (T arrow). Networks were created in Cytoscape (version 3.8.2).

Functional analysis of regulatory networks upon *B. breve* UCC2003 exposure of organoids compared to differentiated controls also confirmed many of these regulated functions, such as genes involved in humoral immune response and response to molecules of bacterial origin (including regulation of peptide secretion), response to oxidative stress and apoptosis, epithelial cell proliferation and differentiation, immune cell homeostasis and differentiation, and transcription of miRNAs in both organoid lines (**Figures 4.16A, B**).

Similar functions were regulated upon *L. rhamnosus* exposure as well in both organoid lines, with additional functions involved in hormone biosynthesis (**Supplementary Figures 4.16A, B**). When analysing regulatory networks of organoids exposed to bacterial supernatants compared to undifferentiated controls, similar results were also found (**Supplementary Figures 4.17A, B** and **Supplementary Figures 4.18A, B)**.

Figure 4.16. Functional analysis of TF-TG networks upon *B. breve* UCC2003 exposure of organoids compared to differentiated controls. A) Revigo analysis of GO enriched functions of TF-DEG networks upon *B. breve UCC2003* exposure of organoids compared to differentiated controls (t = 72 hours). Results are split in different boxes based on the organoid line and treatment. **B)** Bubble plot showing the 15 top enriched GO functions of TF-DEG networks upon *B. breve UCC2003* exposure of organoids compared to differentiated controls (t = 72 hours). The colour of the bubble indicates the q-value of the enriched function (lowest, blue; highest, red), while the size indicates the number of elements contributing to the enriched function indicated. Functions are split in different boxes based on whether they are enriched in organoid line 1 only, line 2 only or both lines. Plots were created using the ClusterProfiler package in R.

(Figure shown on the next page)

A

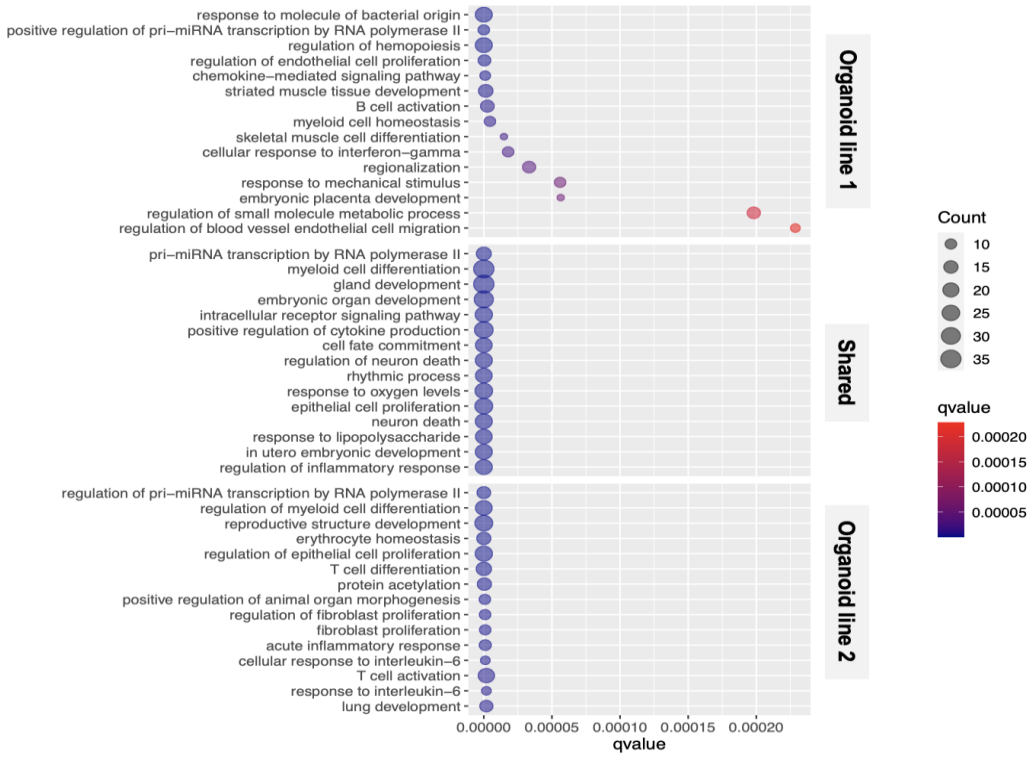
response to molecule of bacterial origin
positive regulation of pri−miRNA transcription by RNA polymerase II
regulation of hemopoiesis
regulation of endothelial cell proliferation
chemokine−mediated signaling pathway
striated muscle tissue development
B cell activation
myeloid cell homeostasis
skeletal muscle cell differentiation
cellular response to interferon−gamma
regionalization
response to mechanical stimulus
embryonic placenta development
regulation of small molecule metabolic process
regulation of blood vessel endothelial cell migration
Organoid line 1
pri−miRNA transcription by RNA polymerase II
myeloid cell differentiation
gland development
embryonic organ development
intracellular receptor signaling pathway
positive regulation of cytokine production
cell fate commitment
regulation of neuron death
rhythmic process
response to oxygen levels
epithelial cell proliferation
neuron death
response to lipopolysaccharide
in utero embryonic development
regulation of inflammatory response
Shared
regulation of pri−miRNA transcription by RNA polymerase II
regulation of myeloid cell differentiation
reproductive structure development
erythrocyte homeostasis
regulation of epithelial cell proliferation
T cell differentiation
protein acetylation
positive regulation of animal organ morphogenesis
regulation of fibroblast proliferation
fibroblast proliferation
acute inflammatory response
cellular response to interleukin−6
T cell activation
response to interleukin−6
lung development
Organoid line 2
0.00000
0.00005
0.00010
0.00015
0.00020
qvalue
Count
10
15
20
25
30
35
qvalue
0.00020
0.00015
0.00010
0.00005

B

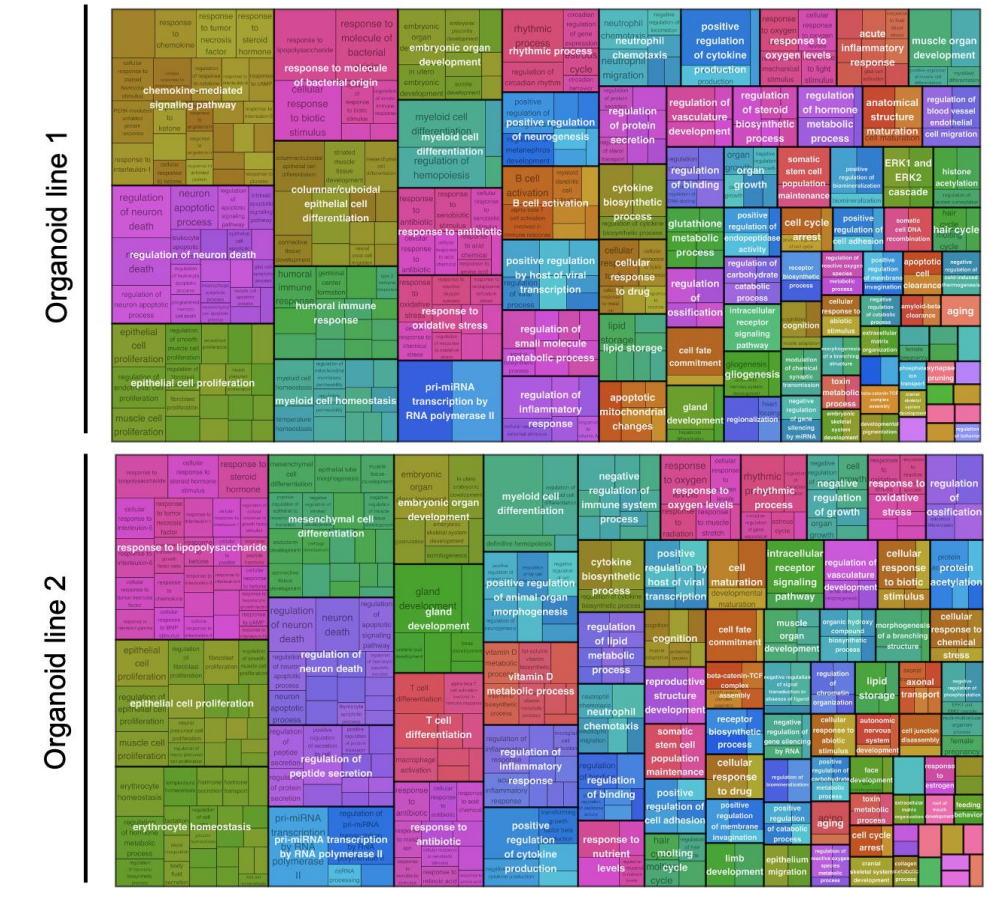
Organoid line 1
chemokine−mediated signaling pathway
response to molecule of bacterial origin
embryonic organ development
rhythmic process
neutrophil chemotaxis
positive regulation of cytokine production
response to oxygen levels
acute inflammatory response
muscle organ development
regulation of neuron death
neuron apoptotic process
columnar/cuboidal epithelial cell differentiation
myeloid cell differentiation
positive regulation of neurogenesis
regulation of protein secretion
regulation of vasculature development
regulation of steroid biosynthetic process
regulation of hormone metabolic process
anatomical structure maturation
regulation of blood vessel endothelial cell migration
regulation of binding
somatic stem cell population maintenance
ERK1 and ERK2 cascade
histone acetylation
B cell activation
cytokine biosynthetic process
glutathione metabolic process
cell cycle arrest
hair cycle
response to antibiotic
positive regulation by host of viral transcription
cellular response to drug
regulation of carbohydrate catabolic process
apoptotic cell clearance
regulation of ossification
response to oxidative stress
lipid storage
cell fate commitment
intracellular receptor signaling pathway
cognition
aging
humoral immune response
regulation of small molecule metabolic process
gliogenesis
epithelial cell proliferation
pri−miRNA transcription by RNA polymerase II
apoptotic mitochondrial changes
gland development
regionalization
myeloid cell homeostasis
regulation of inflammatory response
Organoid line 2
mesenchymal cell differentiation
embryonic organ development
myeloid cell differentiation
negative regulation of immune system process
response to oxygen levels
rhythmic process
negative regulation of growth
response to oxidative stress
regulation of ossification
response to lipopolysaccharide
gland development
positive regulation of animal organ morphogenesis
cytokine biosynthetic process
positive regulation by host of viral transcription
cell maturation
intracellular receptor signaling pathway
regulation of vasculature development
cellular response to biotic stimulus
protein acetylation
regulation of neuron death
T cell differentiation
vitamin D metabolic process
regulation of lipid metabolic process
cognition
muscle organ development
cellular response to chemical stress
epithelial cell proliferation
regulation of peptide secretion
neutrophil chemotaxis
cell fate commitment
reproductive structure development
lipid storage
axonal transport
somatic stem cell population maintenance
receptor biosynthetic process
cellular response to drug
regulation of inflammatory response
regulation of binding
positive regulation of cell adhesion
erythrocyte homeostasis
response to antibiotic
positive regulation of cytokine production
response to nutrient levels
limb development
epithelium migration
aging
cell cycle arrest
pri−miRNA transcription by RNA polymerase II

4.10. Analysis of direct interactors of DEGs reveals rewiring of several functions involved in immune responses, epithelial differentiation and stem cell proliferation

To expand the functional analysis, I built molecular networks connecting DEGs of organoids exposed to bacterial supernatants compared to differentiated controls with their direct interactors ("first neighbour of DEGs"). Networks generated from DEGs upon *B. breve* UCC2003 were bigger in size and more connected (77 nodes and 203 edges, line 1; 109 nodes and 232 edges, line 2) compared to those generated from DEGs upon *L. rhamnosus* exposure (56 nodes and 108 edges, line 1; 9 nodes and 7 edges, line 2) (**Figure 4.17 and Supplementary Figure 4.19**). These observations seem to suggest a bigger impact of *B. breve* UCC2003 compared to *L. rhamnosus* on the intermediary PPI signalling networks in IECs during differentiation.

Functional overrepresentation analysis of GO terms for this network upon *B. breve* UCC2003 sup. exposure revealed several enriched functions in both organoid lines, including those related to regulation of immune processes in response to bacteria, regulation of DNA-binding factor activity, epithelial morphogenesis and differentiation, positive regulation of stem cell proliferation, peptidyl-tyrosine modifications (**Figure 4.17** and **Supplementary Figure 4.20**). Furthermore, functions related to EGF(R) signalling, JAK-STAT signalling and adaptive thermogenesis, in organoid line 1, as well as the regulation of ERBB signalling pathway and cell junction assembly in organoid line 2 were also found to be enriched upon *B. breve* UCC2003 sup. exposure (**Figure 4.17 and Supplementary Figure 4.20**).

Most of these functions were also enriched upon *L. rhamnosus* sup. exposure, including those related to peptidyl-tyrosine modifications, regulation of (epithelial) cell morphogenesis, JAK-STAT signalling and immune processes related to bacterial entry (**Supplementary Figure 4.19, 4.21**). However, functions such as stem cell proliferation, EGFR signalling and cell junctions assembly were modulated uniquely by *B. breve* UCC2003 (**Figure 4.17 and Supplementary Figure 4.20**). Conversely, additional functions were found to be modulated by *L. rhamnosus* only, including positive regulation of cell adhesion, ECM organisation, and haemostasis, although the number of proteins found to participate in these functions was much lower (**Supplementary Figures 4.19, 4.21**).

Enriched functions

- EGF(R) signalling
- GPCR signalling
- JAK-STAT signalling
- Adaptive thermogenesis

- peptidyl-tyrosine modifications
- Positive regulation of DNA-binding factor activity
- regulation of immune processes in response to bacteria
- Regulation of epithelial morphogenesis and differentiation
- positive regulation of stem cell proliferation

- ERBB signalling pathway
- Junction assembly

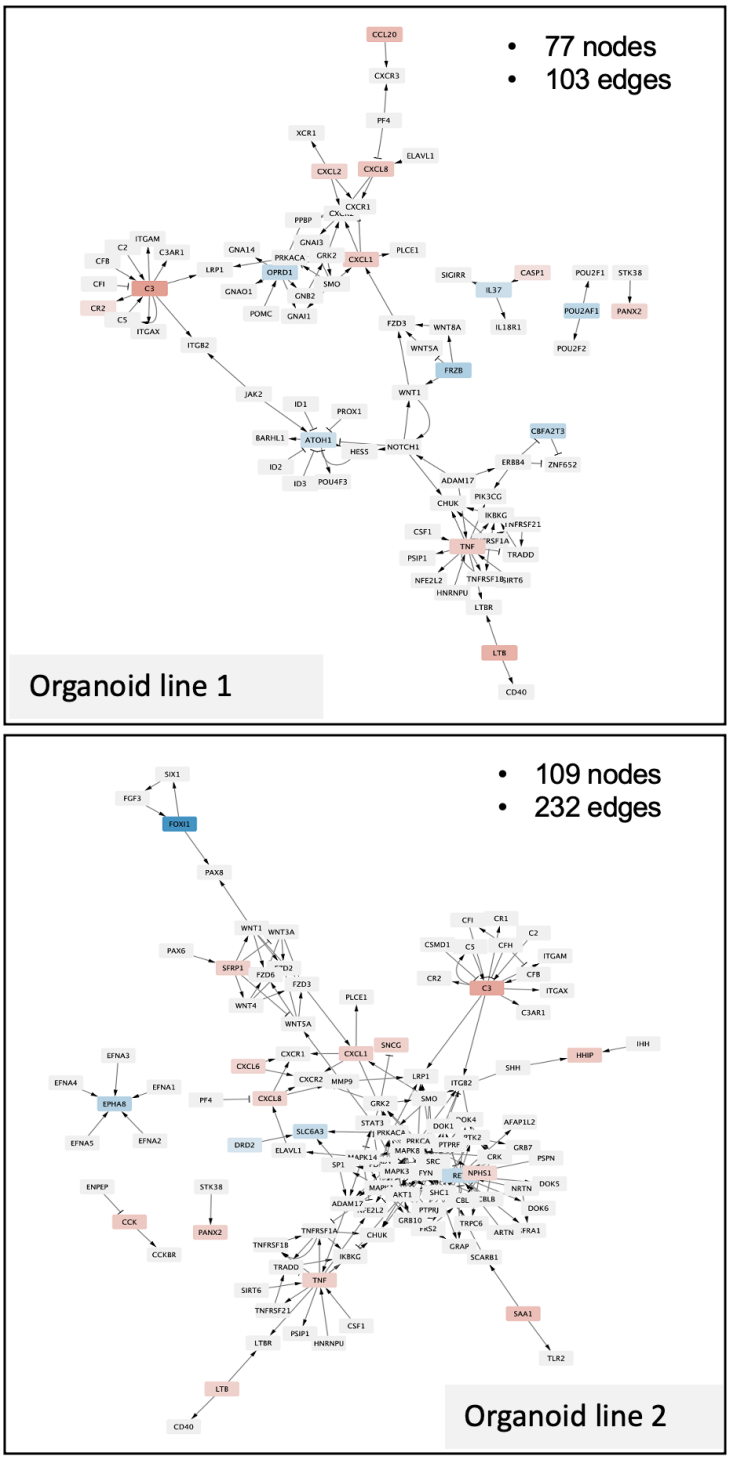

Figure 4.17. Interaction networks of DEGs and their direct interactors upon *B. breve* UCC2003 exposure. Networks: colour of the nodes indicates Log2FoldChange of DEGs (|Log2Foldchange| > 1, adjusted p-value < 0.05) in organoids exposed to *B. breve* UCC2003 sup. compared to differentiated controls (t = 72 hours) in organoid line 1 (top) and 2 (bottom). Enriched functions: Top enriched functions in organoids exposed to *B. breve* UCC2003 sup. compared to differentiated controls in organoid line 1 or 2 identified by GO overrepresentation analysis of first neighbour networks of DEGs (|Log2Foldchange| > 1, adjusted p-value < 0.05). Networks were created in Cytoscape (version 3.8.2).

4.11. Autophagy is modestly modulated by bifidobacterial metabolites

To study the effect of bifidobacterial exposure on autophagy processes, the Autophagy Regulatory Network (ARN) resource was used to identify DEGs (or their interactors) that could play either a direct role (autophagy proteins) or regulate autophagy proteins (direct autophagy regulators).

Upon exposure of organoids to *B. breve UCC2003* sup. compared to differentiated controls, only two DEGs were found to be involved in autophagy regulation. These included keratin 4 (*KRT4*) (line 1, upregulated), a cytoskeleton protein expressed in differentiated layers of the epithelium, and Microtubule Associated Protein 1A *(MAP1A*) (line 2, downregulated) involved in microtubule assembly. Interestingly, both MAP1A and KRT4 were also modulated by *L. rhamnosus* in both organoid lines. Additionally, Asparagine Synthetase (Glutamine-Hydrolyzing) *(ASNS),* an enzyme activated following amino acid deprivation (Lin et al., 2018), was downregulated *L. rhamnosus* sup. exposure in organoid line 1 only.

When comparing organoids exposed to bacterial supernatants to undifferentiated controls, an additionally 5-5 autophagy-related DEGs were found to be uniquely modulated in organoid line 1 (*ANXA1, HK1, RCN2, SESN1, MAP1LC3B2*) and in organoid line 2 (*NCOA7, TKT, CBR1, ESR2, GABARAPL1*). Additionally, two autophagy-related DEGs were modulated in both lines. These included Hydroxyacyl-CoA Dehydrogenase Trifunctional (*HADHA)* (upregulated) and ubiquitin specific protease 11 (*USP11)* (downregulated). Upon *L. rhamnosus* exposure, a similar number of autophagy related DEGs was modulated, including 5 in organoid line 1 only (*NEDD4, ULK2, RCN2, HK1, ANXA1*), and 5 in organoid line 2 only (*ESR2, HADHA, PRKAB2, CTNNB1, PTK2B*) with none of them being shared among the two lines.

Overall, these results indicate that bifidobacteria only has a modest effect on the direct regulation of autophagy, therefore other signalling pathways, either unrelated or indirectly related to autophagy could play a role in mediating its effects on the epithelium.

4.12. Short chain fatty acids produced by *B. breve* UCC2003 predict the modulation of inflammatory-related genes in intestinal epithelial cells

To identify which *B. breve* UCC2003-derived metabolites could be responsible for the effects on epithelial cell function, I used metagenomics (16S) and metabolomics data (1H-NMR) from a model colon vessel (containing complex microbiota) exposed to *B. breve* UCC2003 during

a period of 0-408 hours. Upon exposure to *B. breve* UCC2003, the main metabolites measured were acetate, butyrate, ethanol, formate, lactate, propionate, and succinate (**Supplementary Table 4.3**). Of these, ethanol, succinate, formate and lactate were positively correlated with *B. breve* UCC2003 raw reads; propionate and butyrate were negatively correlated, and no correlation was found for acetate (**Supplementary Table 4.4**).

Next, I used *a priori* associations between bifidobacterial metabolites and human target genes (from the GutM database) to construct molecular networks connecting measured metabolites in the model colon vessel inoculated with *B. breve* UCC2003 to affected TFs or DEGs in treated organoids compared to either differentiated or undifferentiated controls (**Figure 4.18, Supplementary Figure 4.22**). No information about ethanol, formate, and lactate were found, hence these metabolites were excluded from the analysis.

When comparing treated organoids to differentiated controls, associations between metabolites and affected host genes (DEGs or TFs) were found for butyrate and propionate for organoid line 1, and for butyrate, succinate and acetate for organoid line 2 (**Figure 4.18**). The analysis of these networks revealed that, in both lines, the presence of these metabolites was associated with a change in *NFKB1, JUN* and *FOS* transcription factors activity. These TFs had been previously predicted to be activated upon *B. breve* UCC2003 sup. exposure by inferring their activity using VIPER (**Figure 4.13, 15**). Furthermore, the most affected genes, either directly or indirectly (through the modulation of transcription factor activity) were related to inflammation (*TNF, CR2, CXCL1/2/3/5/8, CCL2, MMP7*) and anti-apoptotic effects (*BIRC3*). Interestingly, *BIRC3* has been shown to be a key target for the anti-apoptotic protection mediated by inflammatory cytokines in peripheral nerves, highlighting the possibility for a similar mechanism to contribute to the beneficial effects of bifidobacterial metabolites on the intestinal epithelium (Wang et al., 2012).

Similar findings were also found for associations between measured metabolites and affected host genes in treated organoids compared to undifferentiated controls, although the number of affected genes was slightly higher (**Supplementary Figure 4.22**). Here, butyrate, propionate, succinate and acetate were found to affect host target genes in both organoid lines (**Supplementary Figure 4.22**). Similarly to the comparison with differentiated controls, *NFKB1, JUN* and *FOS* were among the affected TFs, which were predicted to be activated, in organoid line 1, while no affected TF were found in organoid line 2. In addition to the inflammatory-related genes already found, the analysis of these networks highlighted several additional affected genes involved in histone modifications (*HDAC1/5/9*) which were mostly

downregulated, tight junctions (*CLDN3*) and antimicrobial peptides (*DEFB1*), which were mostly upregulated (**Supplementary Figure 4.22**).

Overall, the analysis of metabolite-host networks further confirmed several effects of bifidobacterial metabolites on the epithelium, *via* the activation of *NFKB1, JUN* and *FOS* transcription factors, and highlighted a possible role of succinate, acetate, butyrate and propionate in mediating these effects. These included the upregulation of genes involved in the immune response (including antimicrobial peptide release), barrier function, and epigenetics effects mediated by downregulation of histone deacetylates.

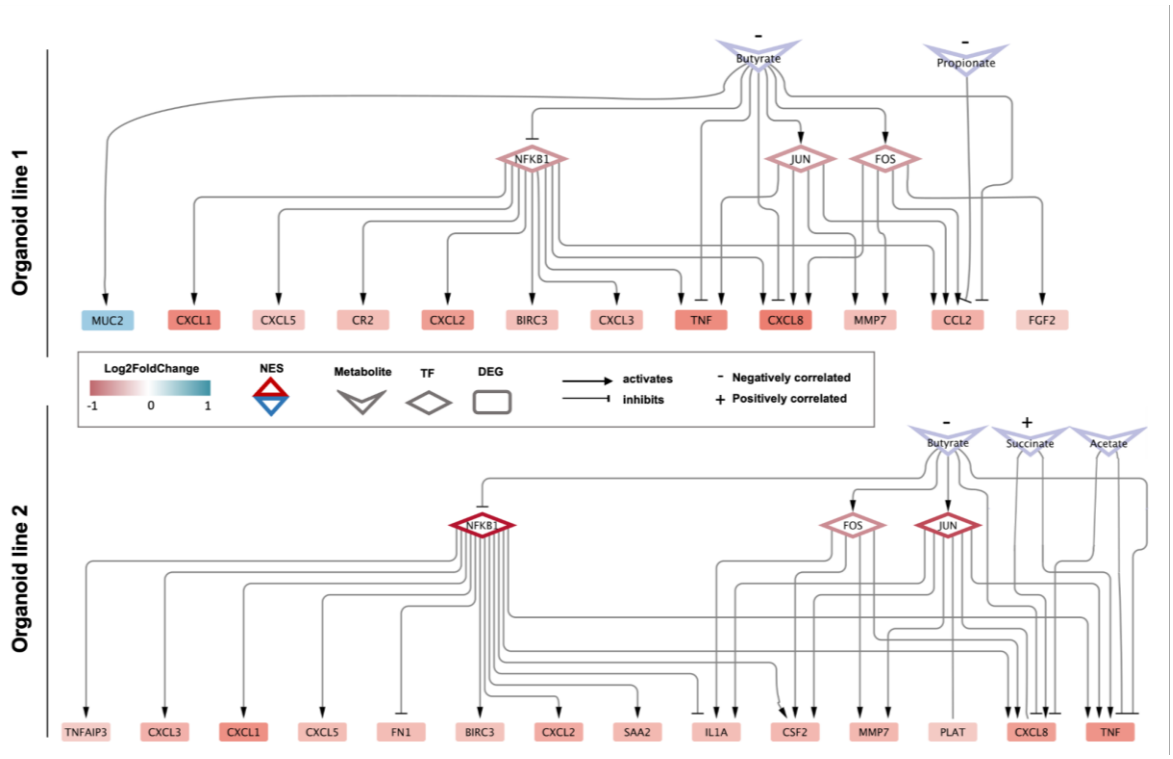

Figure 4.18. Metabolite-host gene networks upon *B. breve* UCC2003 sup. exposure of organoids compared to differentiated controls. Metabolite-host gene networks showing *B. breve* UCC2003-produced metabolites and their affected target genes. Affected host genes are either predicted TFs or affected DEGs (|Log2FoldChange| > 0.5, adjusted p-value < 0.05) in organoids exposed to *B. breve* UCC2003 compared to differentiated controls (t = 72 hours). The edge colour indicates the NES of the TF (red, activated (NES>0); blue, inhibited (NES < 0), while the colour gradient of the node indicates the Log2FoldChange of the DEG (red, upregulated; blue, downregulated). Arrows indicate the direction of the regulation, either activation (pointed arrow) or inhibition (T arrow). The shape indicates whether the node is a metabolite (arrow), TF (rhombus) or DEG (rectangle). Networks were created in Cytoscape (version 3.8.2).

5. Discussion

Previous research has highlighted the role of bifidobacteria in modulating different host processes in the gut. For instance, a previous study in infant mice found that *B. breve* UCC2003 affected genes involved in stem cell proliferation and barrier function (Kiu et al., 2020). However, the specific modulating factors and mechanisms involved in regulating these effects in the human gut are not known. Hence, I set-up this study to investigate *B. breve* UCC2003-derived metabolites on intestinal epithelial cell gene expression profiles of human colonic organoids during epithelial differentiation. Results revealed that *B. breve* UCC2003 supplementation was able to shift the differentiation of stem cells towards more transit-amplifying cells and absorptive enterocytes. Meanwhile, it resulted in the upregulation of genes involved in epithelial cell growth, differentiation, and barrier function, possibly *via* the regulation of transcription factors acting as epigenetic modulators on WNT-dependent pathways **(Figure 4.19)**. Overall, these effects could be beneficial to obtain a more mature epithelium and enhanced epithelial barrier, which is often dysregulated in diseases such as IBD (Martini et al., 2017). Furthermore, *B. breve* UCC2003 exposure resulted in the downregulation of cholesterol biosynthesis through inhibition of SREBF1/2-regulated genes, which could represent a novel mechanism by which bifidobacteria exert their cholesterol-lowering beneficial effects on the epithelium **(Figure 4.19)**.

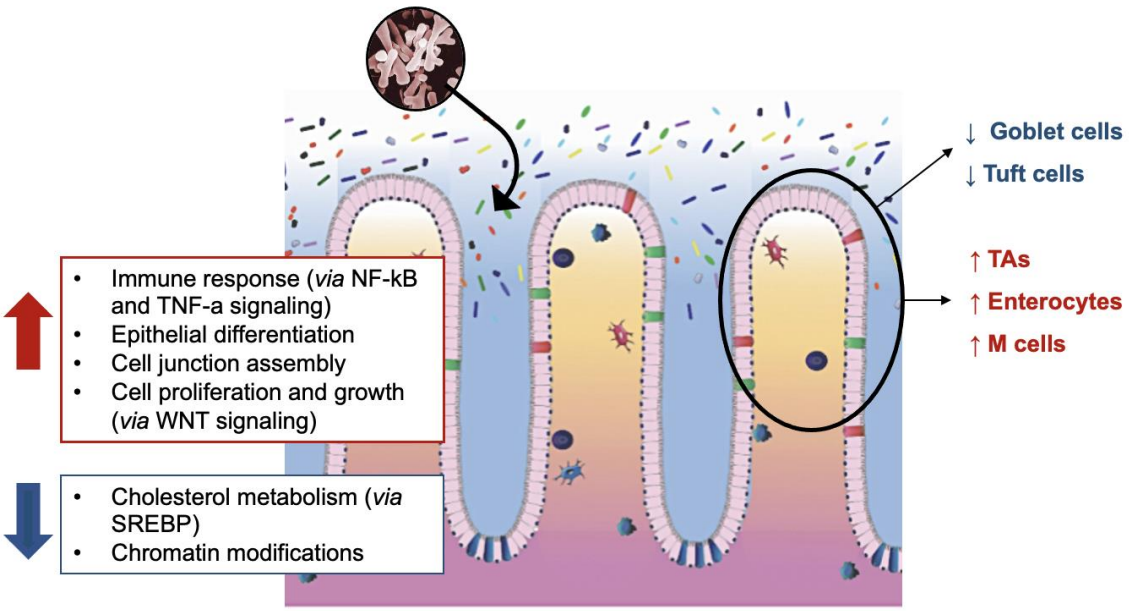

Figure 4.19. Overview of predicted mechanisms of action of *B. breve* UCC2003-derived metabolites on human colonic epithelial cells during differentiation.

In this study, we looked at the effect of organoid differentiation of a period of 3 days, as this would reflect in organoids the life span of gut regeneration *in vivo*, which is around 4-5 days (Sprangers et al., 2021). During this period, we observed the differentiation of organoids by observing organoid morphology under a brightfield microscope (**Figure 4.4**). Upon exposure to *B. breve* UCC2003 and *L. rhamnosus*-derived metabolites, no clear morphologic differences in terms of size and number of organoids were observed compared to the organoids exposed to differentiation media only (**Figure 4.4**).

When looking at gene expression changes upon bacterial metabolites treatment, most of the variation was driven by the organoid line and differentiation status, while only a minor difference could be attributed to the treatment type (bacterial metabolites) (**Figure 4.5B**). This was also in line with the relatively low number of differentially expressed genes found when comparing treated differentiated organoids to the untreated differentiated controls in both organoid lines (**Figure 4.7**). The low number of DEGs could be mainly attributed to the small Log2FoldChange, which made most of them not pass the generally used threshold for significance of |Log2FoldChange| > 1. Likely, the expected effect of bacterial-derived metabolites on a healthy epithelium should be relatively small compared to other treatment such as exposure to a pathogen or specific drug, which may explain the small effect size. Furthermore, as shown by the epithelial cell marker analysis, *B. breve* UCC2003 metabolites might have a different effect on specific epithelial cell populations in the colonic epithelium, which could lead to the averaging out of opposite cell-specific effects of bifidobacteria when a bulk RNAseq approach is employed. These observations, together with the presence of high interindividual variation, may explain the modest effect observed, and future studies should include a higher number of organoid donors to account for this issue.

When looking at gene expression profiles upon differentiation, a similar differentiation pattern was observed for both organoid lines, as indicated by the similar trend when looking at overall transcriptional differences using a PCA or UMAP plot **(Figure 4.8).** Furthermore, this similarity was also confirmed by the number of DEGs shared upon differentiation between the two organoid lines (**Figure 4.8**). Upon organoid differentiation, several pathways involved in SCs and TAs cell proliferation and maintenance of pluripotency, including WNT pathway (Nusse, 2008), EGFR signalling (Qin et al., 2020; Sanman et al., 2021) and MAPK signalling (Wei et al., 2020), were downregulated. At the transcription factor level, these changes were regulated by a general inhibition of transcription factors *SOX2* and *TCF7L2,* involved in the regulation of early embryonic development (Raghoebir et al., 2012) and WNT pathway (van Es et al., 2012), respectively. Conversely, pathways involved in intestinal cell differentiation were upregulated upon organoid differentiation in both lines. These effects seem to be dependent on the activation of transcription factor *CDX2*, a master regulator of early intestinal differentiation

(Coskun et al., 2011), as well as HNFs, involved in determining enterocyte fate (*HNF4A*) (Chen et al., 2019) and terminal differentiation of the epithelium (*HNF1A, HNF1B*) by acting upstream of Notch (D'Angelo et al., 2010). Overall, these findings confirm at the molecular level the successful differentiation of intestinal organoids over the experimental 3-day period.

Despite mild differences in gene expression profiles upon exposure to bacterial metabolites, specific changes could be observed upon *B. breve* UCC2003 and *L. rhamnosus* exposure. Overall, response to bacterial metabolites was mainly organoid line-specific, and thus patient-specific (**Figure 4.8A**). This is an interesting finding, as it highlights the need for personalised probiotics treatment tailored to each individual. Nevertheless, shared patterns could be observed in both lines, as demonstrated by a relatively large amount of shared DEGs and predicted TFs (**Figure 4.8A, 4.14A**). The effect of the two probiotic bacterial strains was also partially shared (**Figure 4.8B, 4.14B).** Yet, a bigger effect for *B. breve* UCC2003 compared to *L. rhamnosus* and the presence of several bifidobacteria-unique effects were found, based on the number of unique DEGs, indicating a potential added beneficial effect brought by this particular strain on epithelial cell modulation (**Figure 4.8B**).

Analysis of epithelial cell markers identified that upon exposure to *Bifidobacterium*-derived metabolites, markers of enterocytes, TAs, and M cells were upregulated, while markers of goblet cells and tuft cells were downregulated during organoid differentiation (**Figure 4.10**). M cells play a central role in the initiation of mucosal immune responses by transporting antigens and microorganisms to the underlying lymphoid tissue (Nicoletti, 2000). Interestingly, an increase in M cell numbers and cell markers was observed in organoids infected with *Salmonella enterica* serovar Typhimurium (Rouch et al., 2016). However, the downstream effects of the interaction between these cell types and commensal/pathogen bacteria in the gut are not completely clear, making it difficult to speculate about the overall effect of *Bifidobacterium*-derived metabolites in upregulating markers of this cell type. Interestingly, *Bifidobacterium* spp. improved vaccine efficacy by modulating the immune response, and M cells may play a role in these observed effects (Jordan et al., 2022).

Upon exposure of differentiating human colonic organoids to bifidobacterial metabolites, genes involved in adhesion to the epithelium and immune signalling (e.g. NF-kB and TNF-α) were upregulated (**Figure 4.11, 4.12).** The organoid cultures were virtually microbe-free and introducing bacterial metabolites should result in the activation of specific signalling due to the recognition of microbial-derived molecules (PAMPs). Hence, these results indicate the successful communication interactions between microbial metabolites and receptors on IECs.

Furthermore, exposure to *B. breve* UCC2003 upregulated genes involved in intestinal development and cell junction assembly (**Figure 4.12, 4.16**). As previously mentioned, this was also accompanied by an upregulation of cell markers for TAs cells and enterocytes, suggesting an increased differentiation towards these cell types (**Figure 4.10**). These results are in line with a previous study, where a 3-day gavage with *B. breve* UCC2003 upregulated key genes linked with epithelial barrier function in neonatal murine IECs (Kiu et al., 2020). The ability of bifidobacterial metabolites to shift the differentiation of SCs towards more TAs and mature enterocyte cell populations, and enhance epithelial maturation, could be important in early life, for instance for premature infants, characterised by an immature epithelial layer (Demers-Mathieu, 2022).

Upon bifidobacteria exposure, genes involved in cholesterol biosynthesis were downregulated in both organoid lines, together with the predicted inhibition of transcription factors *SREBF1/2* regulating fatty acid and cholesterol biosynthesis (**Figure 4.12, 4.13)**. Previous studies have shown the ability of the gut microbiota to regulate cholesterol metabolism, and the interplay with bile acid production (Molinero et al., 2019), which are gaining increasing attention for their role in IBD pathogenesis (Bromke and Krzystek-Korpacka, 2021). So far, only a few studies have highlighted the ability of specific probiotics to modulate cholesterol metabolism (Wa et al., 2019). These findings mainly involved the upregulation of liver X receptor (LXRs) and peroxisome proliferator-activated receptor (PPARs) genes, together with the inhibition of carbohydrate response element (ChRE)-binding protein (ChREBP) genes (Wa et al., 2019)**.** Here, the downregulation of cholesterol biosynthesis through inhibition of SREBF1/2-regulated genes could represent a novel mechanism by which bifidobacteria exert their cholesterol-lowering beneficial effects on the epithelium, possibly via SCFAs production such as butyrate.

Genes involved in chromatin modifications were downregulated in IECs exposed to *B. breve* UCC2003 metabolites (**Figure 4.12**). Chromatin modifications, in particular DNA demethylation and protein lysine modification, play an important role in the regulation of WNT signalling (Sharma et al., 2021; You et al., 2022). Interestingly, among TFs predicted to be regulated upon *Bifidobacterium* metabolites exposure (*SP1, EGR1, ZNF263*) are known regulators of WNT signalling via histone modification mechanisms (**Figure 4.13, 4.15**). In particular, *SP1* reduces oxidative stress and inflammatory-related intestinal injury by interacting with WNT signalling (Liu et al., 2022), while the *EGR1/MAPK/ZNF263* axis has been found to promote WNT signalling through the epigenetic silencing of SIX3 promoter (Yu et al., 2020). Interestingly, canonical pathway analysis confirmed that WNT signalling was mildly upregulated in both lines upon *B. breve* UCC2003 metabolites exposure (**Figure 4.11**).

Overall, these results suggest the ability of *B. breve UCC2003 to* contribute to WNT signalling activation through a generalised inhibition of epigenetic modifications in IECs.

One of the goals of this study was to assess the effect of *B. breve* UCC2003 on goblet cell function and the role of autophagy modulation. Indeed, previous work found that some bifidobacterial strains, such as *B. dentium* were able to increase goblet cell numbers and mucus production *via* modulation of autophagy (Engevik et al., 2019). In this study, both GC-specific markers and genes involved in mucus production (e.g. *MUC2*) were downregulated following exposure to *B. breve* UCC2003 (**Figure 4.10, 4.15**). Furthermore, when looking at the modulation of autophagy-related genes in relation to these effects, results observed were very small and sometimes pointed to an opposite effect. For instance, one of the autophagy proteins found to be downregulated upon *B. breve* UCC2003 exposure is involved in the degradation of KLF4, a key marker for GC terminal differentiation, thus promoting intestinal cell proliferation (Meng et al., 2021). One possible explanation is that bifidobacteria were added to the basolateral side of the epithelium, resulting in the activation of different pathways, which could have resulted in downregulation of GCs. Furthermore, only core autophagy genes and their direct regulators were included in this analysis, but indirect regulators or associated pathways could also play a role. Future studies could expand this analysis by considering other layers of the autophagy regulatory network (Türei et al., 2015).

Finally, integrating metabolomics information about *B. breve* UCC2003-produced metabolites within a model colon vessel to build metabolite-host networks, helped to confirm several of the previously observed effects. These included the role of *NFKB1, JUN* and *FOS* transcription factors, upregulation of genes involved in the immune response (including antimicrobial peptide release) and barrier function, and epigenetics effects resulting in the downregulation of genes related to chromatin modifications (**Figure 4.18**). Furthermore, a possible role for succinate, acetate, butyrate and propionate in mediating these effects was found (**Figure 4.18**). These results are in line with previous studies indicating a role for butyrate in reducing SC proliferation and promoting intestinal differentiation and tight junctions (den Besten et al., 2013; Ríos-Covián et al., 2016), and of propionate in regulating intestinal homeostasis through immunomodulatory and anti-carcinogenic effects (Bunesova et al., 2018; Kaiko et al., 2016; Reichardt et al., 2014; Sun et al., 2018). Furthermore, acetate, propionate, and butyrate have been shown to mediate epigenetic effects, resulting in the inhibition of histone deacetylase, confirming some of our findings (Krautkramer et al., 2016).

As explained in **Chapter 1**, *Bifidobacterium* spp. can produce acetate and lactate by degrading mucin or diet-derived, non-digestible carbohydrates, but not butyrate and propionate. These SCFAs can instead be produced by other microbes following the fermentation of bifidobacterial products (Flint et al., 2015). Not much is known about succinate production, as it is an intermediate of bacterial carbohydrate metabolism and does not typically accumulate in the human gut (Nagpal et al., 2017). These observations suggest that predicted effects can be a result of the indirect or direct production of these metabolites by bifidobacteria. It is important to stress that metabolites produced by *B. breve* UCC2003 grown in BHI, which were used for organoid exposure in the transcriptomics study, may be different from those produced in a complex microbiota community such as the model colon vessel, which were assessed in the metabolomics study. Unfortunately, although collecting aliquots of *B. breve* UCC2003 supernatants in BHI for a subsequent metabolomics study, measurements of these samples was not performed during my PhD due to time and financial reasons. In the future, the type of metabolites produced in BHI and in the colon vessel (containing complex microbiota) should be compared to assess any differences or similarities between the used set-ups.

This study presents some limitations, including the use of bulk transcriptomics, the type of media used for the exposure, and the basolateral exposure. First, bulk transcriptomics was used to understand the effect of *Bifidobacterium* metabolites exposure on gene expression changes. However, this method does not allow to detect shifts in the proportion of IEC populations upon bacterial exposure. To overcome this limitation, a cell marker analysis was performed, which found that markers of TAs, enterocytes, and M cells were upregulated, while markers of stem cells, goblet cells and Paneth cells were downregulated following *Bifidobacterium* metabolites exposure. For this analysis, top cell markers from the Gut Cell Atlas were used to distinguish epithelial cell populations. However, a fraction of these markers might also be expressed by other cell types. In this context, M cells are not generally found in organoids, unless special stimuli are present (e.g. RANKL). In this context, the increase in M cells found upon bifidobacterial exposure might instead suggest that other cell types expressing M cell markers are being regulated.

Given the observed shifts in markers of intestinal epithelial cell populations, the measured changes in epithelial gene expression profiles could be simply due to different gene expression signatures of specific IEC populations. Indeed, a scRNAseq study highlighted the presence of specific pathway signatures in different IECs, such as enrichment in WNT pathway in stem cells, and NF-kB and TNF-α pathway in enterocytes (Mead et al., 2022). Consequently, upregulation of NF-kB and TNF-α pathways upon *B. breve* UCC2003 exposure could be explained by a shift towards the enterocyte population, as evidenced by the concomitant

upregulation of cell markers of enterocytes upon bacterial exposure. Likewise, upregulation of WNT signalling upon *B. breve* UCC2003 exposure is not in line with the downregulation of SC markers, a population where WNT signalling is the most active (Mead et al., 2022). These results could be simply due to WNT-related genes being regulated differently in IECs populations (e.g. stem cells and enterocytes), and further experiments are needed to clarify these findings.

Another limitation is represented by the media used to collect *B. breve* UCC2003 metabolites, BHI, is not reflective of the gut environment, and could therefore have impacted on the type of metabolites such as SCFAs produced *in vitro*. As discussed in **Chapter 2 and 3,** future experiments should consider using such media that better reflects the environment of the gut.

Finally, exposure of organoids to bacterial metabolites was performed on the basolateral side of the epithelium, as metabolites were directly added to the culture medium. However, most bacterial-host interactions happen at the apical side. In **Chapter 2**, I presented different optimization experiments with the goal of establishing human colonic organoids with reversed polarity. Using these models, metabolites could be added directly to the medium to study the apical interaction between bacteria and epithelial cells. Yet, more time would have been needed to optimise these models for such transcriptomics experiments. In the future, further characterisation of these models and their use in similar co-culture experiments would help achieve a better modelling of bifidobacteria-host interactions happening *in vivo* in the gut.

6. Future research directions

Overall, this study was a starting point to investigate the effects of *B. breve* UCC2003-derived metabolites on intestinal epithelial cell function and differentiation using patient-derived colonic organoid models. Results highlighted patient specific differences in the response to bacterial supplementation, and bifidobacterial-specific effects on the epithelium, which were not observed upon exposure to other probiotic strains such as *L. rhamnosus*. Overall, these effects resulted in enhanced epithelial differentiation and barrier function *via r*egulation of WNT and epigenetics mechanisms, and downregulation of cholesterol biosynthesis, which could represent a novel mechanism by which bifidobacteria exert beneficial cholesterol-lowering effects.

This study was carried out using bacterial metabolites instead of live bacteria, thereby excluding the two-sided real-time interaction between bifidobacterium and colonic IECs over time. In a real *in vivo* setup, *Bifidobacterium*-derived metabolites would influence IECs modulating their function, with epithelial cells interacting with bifidobacteria to change their metabolism. In this study, metabolites were extracted and kept frozen prior to organoid treatment, exposing epithelial cells to the same original mix each day of the 3-day differentiation period. This simplified set-up was chosen due to the unavailability and associated cost of set-ups allowing to keep bacterial cells in an oxygen-free environment while keeping epithelial cells in the presence of oxygen such as the anaerobic organoid-on-chip or the HuMiX module (Jalili-Firoozinezhad et al., 2019; Shah et al., 2016). In the future, these more sophisticated set-ups could be used to make better predictions about the real-time effect of the two way communication between bifidobacteria and IECs, as explained in my published review (Poletti et al., 2021).

In this presented study, the effect of one strain of bifidobacteria on two separate organoid donors was tested, given the time and cost-associated constraints. However, as shown by the organoid-specific response to bacterial metabolites, more organoid donors should be considered to account for the interindividual response to probiotics treatments. Furthermore, distinct bifidobacterial strains may exert a different effect on the host, highlighting the need to set-up a system to test many different bacterial strains (Beck et al., 2022). Hence, in alternative to the use of organoid-based microfluidics devices for more detailed mechanistic studies, a follow-up experiment could envision the use of organoids (e.g. apical out) in combination with a high-throughput platform, to assess the effect of multiple bifidobacterial strains (and/or their metabolites) on several different patient-derived organoids (Brandenberg et al., 2020; Co et al., 2021; Mead et al., 2022).

Further studies should employ scRNAseq or fluorescence-activated single cell sorting (FACS) of IECs prior to low-input sequencing to understand the transcriptomics regulation by bifidobacteria in a cell-type specific manner. Despite working during my PhD on the optimization of FACS protocols to identify different cell type populations in the gut, I could not develop them well enough to use to measure the shift in epithelial cell populations in this experiment. Hence, further optimisations will be needed in the future for the application of this methodology to organoids. Eventually, the application of these methods or use of scRNAseq will help elucidate the cell type-specific effect of bifidobacteria on intestinal epithelial populations.

Finally, due to the lack of time, it was not possible to validate the bioinformatics predictions made from the RNAseq dataset using experimental models such as organoid. Future studies could assess the effect on increased barrier function or intestinal differentiation using immunofluorescence staining for tight junctions (ZO-1) and cell proliferation (KI67). Additionally, the ability of bifidobacteria to promote differentiation of the epithelium towards enterocytes could be studied using cell-specific marker stains and IEC populations quantified using FACS or immunofluorescence staining.

To conclude with, this study was useful to understand how human colonic organoids can be used to assess the effect of candidate probiotic strains, including bifidobacteria, on intestinal epithelial cell function during intestinal differentiation. Furthermore, analysis of transcriptomics changes upon bacterial metabolites exposure, elucidated possible mechanisms of action of *B. breve* UCC2003, which could be further tested and validated. Implementation of more sophisticated organoid-based systems to study the real-time interaction between whole bacteria and their metabolites and epithelial cells, the use of single cell technologies or other methods to identify the effect on specific cell populations, and further validation of the bioinformatics prediction will help achieving a better understanding of the mechanisms involved in the beneficial effects of bifidobacteria on the epithelium. Eventually, this understanding could lead to more targeted microbial therapies to target or prevent inflammatory diseases of the gut such as IBD.

Chapter 5: Mapping the epithelial–immune cell interactome upon SARS-CoV-2 infection in the gut and the upper airways

1. Introduction

The recent COVID-19 pandemic is caused by infection with the severe acute respiratory syndrome coronavirus 2 (SARS-CoV-2). While SARS-CoV-2 mainly targets the lung and upper airways (Mick et al., 2020; Peacock et al., 2022; Tay et al., 2020), other organs can be infected too, including the heart, kidney, brain, and the intestine (Gupta et al., 2020). In addition to directly infecting key organs, SARS-CoV-2 infection is characterised by an excessive inflammatory response mediated by both the innate and adaptive immune systems (Olbei et al., 2021; Tay et al., 2020). This overactivated inflammatory response, also known as cytokine release syndrome (CRS) or cytokine storm, is a consequence of high levels of circulating cytokines and chemokines, and it is thought to be responsible for the severe COVID-19 symptoms some patients experience (Arunachalam et al., 2020). To our knowledge, there is no clear understanding of which particular inflammatory pathways and cell types are responsible for driving this process, and the role played by specific organs in initiating and maintaining this process (Stone et al., 2020). To this regard, the GI tract seems to be quite important, and the causal role of SARS-CoV-2 on intestinal damage and of the small intestine in contributing to CRS was recently highlighted (Kale et al., 2020; Martin-Cardona et al., 2021). In particular, severe intestinal complications were reported in the presence of SARS-CoV-2 intestinal infection (Martin-Cardona et al., 2021), with small intestinal immunopathology identified as the major contributor to mortality in CRS (Kale et al., 2020).

The intestinal epithelium of the GI tract forms the primary line of defence against external stimuli, and together with resident immune cells, helps maintain homeostasis and defend the body from infections. Human intestinal organoids have been used as a tool to study SARS-CoV-2 infection in the gut and the inflammatory responses of specific intestinal epithelial cell types (Lamers et al., 2020; Stanifer et al., 2020; Triana et al., 2021b; Zang et al., 2020). These studies provided evidence that SARS-CoV-2 is able to infect and actively replicate in human intestinal cells, in particular in enterocytes (Lamers et al., 2020; Triana et al., 2021b). These

studies also revealed that, contrary to the limited type I and type III interferon (IFN) immune response observed in the lungs (Blanco-Melo et al., 2020; Hadjadj et al., 2020), the response to SARS-CoV-2 infection in the gut is characterised by a cell-type specific inflammatory response that is important in the development of systemic reactions (Stanifer et al., 2020). Examination of human intestinal samples has also shown that infection of gut epithelial cells results in the activation of local immune populations (Guo et al., 2021). Yet, the exact effects of viral infection in the gut and the role of epithelial cell–immune cell interaction in mediating the inflammatory response of the body are not known. This information could ultimately aid the development of treatments and strategies to optimise the level and type of immune response, as we would understand better the viral strategies dysregulating our immune system.

One of the main challenges associated with the study of the role of the epithelium and resident immune cells in the gut during COVID-19 infection is that the contribution of these components has been highlighted separately. Due to the lack of adequate and complex experimental systems to model and analyse these interactions, to the best of our knowledge, no study has been carried out so far to analyse epithelial–immune crosstalk in the GI tract upon SARS-CoV-2 infection. Instead, large-scale, integrative models are needed to address key questions that cannot yet be solved with available experimental models.

The main goal of this project was to develop a computational framework to model the effect of SARS-CoV-2 on epithelial cells and epithelial–immune cell-cell interactions during COVID-19 infection. To achieve this, I used two intracellular modelling tools (ViralLink and CARNIVAL) with intercellular network approaches (from OmniPath) (Liu et al., 2019; Treveil et al., 2021; Türei et al., 2021), together with available data on SARS-CoV-2–human miRNA-protein or protein–protein interactions predictions and scRNAseq datasets of SARS-CoV-2 infected intestinal epithelial cells to model the effect of viral infection on intracellular and intercellular signalling networks in gut. By using this model, I was able to improve the understanding of the effect of viral infection on ileal and colonic epithelial cells, and the role of epithelial–immune cell crosstalk during SARS-CoV-2 infection. Additionally, I identified key intercellular inflammatory pathways involved in the epithelial-immune crosstalk that could pave the way for potential successful strategies against the cytokine release syndrome associated-symptoms observed in severe cases of COVID-19. This chapter is based on a peer-reviewed article published in NPJ Systems Biology and Applications, in which I am the first author (Poletti et al., 2022). The published article is reproduced in **Appendix 3**. Furthermore, the methodology used for the analysis has been published in PLOS Computational Biology by Dr. Agatha Treveil (former postdoc, EI & QIB), in which I am the 7th author (Treveil et al., 2021).

2. Aims and objectives

This project was initiated during the COVID-19 pandemic, mainly driven by curiosity in understanding more about the SARS-CoV-2 infection in the gut. Due to the inaccessibility of the laboratories during that period, I joined the efforts of other members of the groups to reutilise computational approaches to study this disease.

In particular, the prime goal of this work was to understand the role played by the gut during SARS-CoV-2 infection, and to decipher whether signalling stemming from the gut could be contributing to the overactivated immune response observed in severe COVID-19 cases. Hence, we hypothesised that SARS-CoV-2 proteins or miRNA were able to modulate the intracellular and intercellular communication signalling in the gut, and that this altered signalling was leading to modified epithelial-immune cell crosstalk, which could be linked to increased inflammatory signalling of severe COVID-19 cases. As a broader proof of concept, we also applied this analysis to the upper airways. However, this work will not be presented in the context of this thesis.

Our aim was three-fold:

1) Characterise how SARS-CoV-2 proteins and miRNAs drive an alteration in the intracellular signalling of epithelial cells in the gut (colon, ileum), leading to modified ligand expression.
2) Characterise the SARS-CoV-2 dependent alteration in intercellular signalling between infected epithelial cells and resident immune cells driven by altered ligands.
3) Assess ligands that could be responsible for inflammation observed in severe COVID-19 patients.

In order to achieve these goals, we set-up a team of people working on each of the goals. The study was planned by myself, Dr. Agatha Treveil (postdoc, EI, QIB), Dr. Dezso Modos (postdoc, QIB, EI), Dr. Leila Gul (PhD student, EI) and Luca Csabai (PhD student, Eotvos Lorand University, Hungary). The initial analyses for the intracellular part were performed by myself (viral proteins) and Luca Csabai (viral miRNAs), while Dr. Agatha Treveil and Dr. Leila Gul performed the intercellular analysis, under the supervision of Dr. Dezso Modos. The final analyses were re-done by myself for both intracellular and intercellular gut analysis and upper airways (not presented in this thesis), while the ligand analysis of the gut was done by Dr. Agatha Treveil. The published manuscript was also written by myself, and reviewed by Dr. Agatha Treveil.

3. Methods

3.1. Overview of the integrated computational workflow

To investigate the effect of SARS-CoV-2 infection in the gut, I created an integrated bioinformatics framework (**Figure 5.1**) that allowed me to model:

1) How SARS-CoV-2 proteins and miRNAs affect intracellular signalling networks of infected intestinal (colonic and ileal) epithelial cells leading to modified secreted ligands expression **(intracellular analysis).**
2) How altered epithelial ligands in the gut (colon, ileum) drive modified intercellular communication networks between infected epithelial cells and resident immune cells **(intercellular analysis).**
3) Which altered epithelial ligands upon infection in the gut (colon, ileum) are likely to drive the overactive immune response observed in severed COVID-19 patients (**ligands analysis).**

In order to build intracellular and intercellular networks, I used various types of data:

- scRNAseq of SARS-CoV-2 infected intestinal organoids from (Triana et al., 2021a);
- scRNAseq of resident immune cells in the healthy colon and ileum (Martin et al., 2019; Smillie et al., 2019);
- Predictions about SARS-CoV-2 proteins and miRNAs interacting with human proteins from IntAct (Hermjakob et al., 2004; Orchard et al., 2014) and from (Saçar Demirci and Adan, 2020), respectively;
- *A priori* knowledge on intracellular protein-protein interactions from OmniPath (Türei et al., 2021);
- *A priori* knowledge on transcription factor-target genes interactions from DoRothEA (Garcia-Alonso et al., 2019);
- *A priori* knowledge on secreted ligands-receptor interactions from OmniPath (Türei et al., 2021).

Intracellular and intercellular networks were subsequently integrated and functional analyses carried out on the PPI layer (intracellular network) and ligands-receptor layers (intercellular network) to understand the impacted intracellular and intercellular epithelial functions upon SARS-CoV-2 infection. Additionally, ligands and receptors participating in epithelial-immune crosstalk during infection were scored by importance based on the number of intercellular interactions and immune cell targeted in which they were involved. Finally, altered epithelial ligands were compared to previous literature information on inflammatory processes in severe

COVID-19 patients to point out specific epithelial-derived ligands that could be driving the inflammatory process upon SARS-CoV-2 infection.

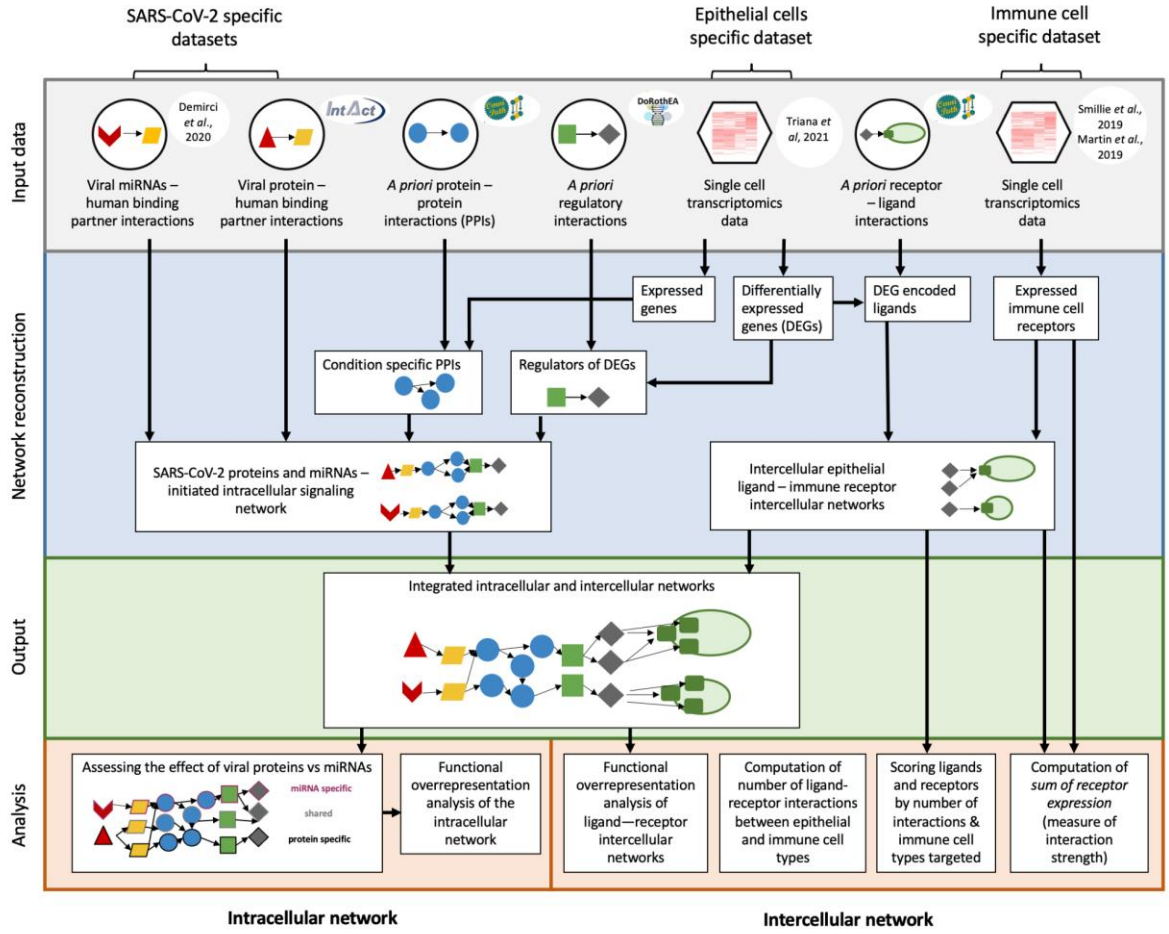

Figure 5.1. Integrated workflow to analyse the intracellular and intercellular effect of SARS-CoV-2 in the gut. Schematic workflow illustrating the different analytical steps used to construct the intracellular and intercellular signalling networks between epithelial cells in SARS-CoV-2 infected intestinal organoids (ileal and colonic organoids, 24 hours infection) and immune cell types.

3.2. Intercellular networks

3.2.1. Input data

3.2.1.1. Intestinal epithelial cells

Single cell transcriptomics data of intestinal (colonic and ileal) organoids infected with SARS-CoV-2 (BavPat1/2020 strain) was obtained from (Triana et al., 2021a). Differentially expressed genes upon SARS-CoV-2 infection were identified for each epithelial cell type using R packages ‘Mast’ and ‘Seurat’ (Hao et al., 2021; McDavid et al., 2021). Data of directly infected

or bystander epithelial cells from intestinal organoids infected with SARS-CoV-2 for 24 hours were compared with the equivalent cell type from uninfected organoids. Any genes with adjusted p-value ≤ 0.05 and |log2 fold change (FC)| ≥ 0.5 were considered significantly differentially expressed. Differential expression could only be calculated for cell types within a condition where data was available from ≥ 3 individual cells.

3.2.1.2. Intestinal resident immune cells

Single cell expression data from ileal and colonic resident immune cells was obtained from (Martin et al., 2019) and (Smillie et al., 2019), respectively. In particular, data from healthy samples and uninflamed Crohn's disease samples was used for colonic and ileal immune cell populations, respectively. Immune cell populations were identified through annotated clustering from (Chua et al., 2020; Martin et al., 2019; Smillie et al., 2019). Cell type labels were maintained as originally published. Following removal of all genes with count = 0, normalised log2 counts across all samples (separately for each cell type) were fitted to a gaussian kernel (Beal, 2017). All genes with expression values above mean minus three standard deviations were considered as expressed genes for the given cell type in the given intestinal location. For the ligand-receptor predictions (intercellular analysis), a representative collection of immune cells relevant in gut inflammation and SARS-CoV-2 infection based on previous literature was selected, which included all macrophages, T cells, B cells, plasma cells, Innate Lymphoid Cells (ILCs), mast cells and a representative group of dendritic cells (DCs) (Filbin et al., 2020; Martin et al., 2019; Schultze and Aschenbrenner, 2021; Sette and Crotty, 2021; Smillie et al., 2019).

3.2.2. Defining ligand-receptor interactions between cell types

A list of ligand-receptor interactions was obtained from OmniPath on 23 September 2020 using the 'OmnipathR' R package (Türei et al., 2021). Source databases used to retrieve the ligand-receptor interactions through OmnipathR included six independent resources (CellPhoneDB, HPMR, Ramilowski 2015, Guide2Pharma, Kirouac 2010, Gene Ontology) (Ashburner et al., 2000; Ben-Shlomo et al., 2003; Kirouac et al., 2010; Pawson et al., 2014; Ramilowski et al., 2015; Vento-Tormo et al., 2018). No weighing was performed on ligand-receptor interactions, and protein complexes were dealt with by including each of their individual proteins in the list.

Ligand-receptor interactions (intercellular interactions) were predicted between epithelial cells types and resident immune cells according to the following conditions:

1) The ligand is differentially expressed in the epithelial cell (upon SARS-CoV-2 infection, in directly infected or bystander cells of the colon and ileum);

2) The receptor is expressed in the immune cell in the relevant dataset (i.e., ileal or colonic immune cells);
3) The ligand-receptor interaction is present in the OmniPath *a priori* ligand-receptor network.

For the gut analysis, intercellular interactions were defined separately for directly infected epithelial cells and bystander epithelial cell populations in the ileum and in the colon. Enteroid epithelial data was paired with ileal immune cell data (Martin et al., 2019), while colonoid epithelial data was paired with colonic immune cell data (Smillie et al., 2019). Intercellular interactions were defined between every possible pair of epithelial cells and immune cells for each condition. Interactions derived from upregulated ligands ("upregulated interactions") were evaluated separately from interactions derived from downregulated ligands ("downregulated interactions").

3.2.3. Scoring of ligands, receptors and immune cell types involved in ligand-receptor interactions

To assess the importance of specific ligands, receptors and immune cell types, additional parameters were computed using the ligand-receptor network. First, the number of interactions between each epithelial and immune cell type was computed by summing up all the possible interactions between each differentially expressed epithelial ligand and each of the receptors expressed by the specific immune cell type. Second, the number of immune cell types involved in each ligand-receptor pair was computed by counting the number of different immune cell types which were expressing the receiving receptor. Third, for each ligand, a "sum of receptor expression value" was computed for each interacting immune cell type, based on the number of interacting receptors and the mean expression level of the interacting receptors.

3.2.4. Data visualisation

Venn diagrams were generated using the 'gplots' R package. Heatmaps were generated using the 'ggplot2' and 'pheatmap' packages (Kolde, 2012; Wickham, 2016). Barplots were generated with the 'ggplot2' package. Network visualisations were done using Cytoscape (version 3.8.2) (Shannon et al. 2003; Su et al. 2014).

3.3. Intracellular networks

Two previously established tools were employed to predict the effect of SARS-CoV-2 infection on epithelial cells: ViralLink and CARNIVAL (Liu et al., 2019; Treveil et al., 2021). Both tools, using related but distinct methods, infer causal molecular interaction networks. These networks link perturbed human proteins predicted to interact with SARS-CoV-2 viral proteins

or miRNAs, to transcription factors known to regulate the observed differentially expressed ligands in infected epithelial cells.

3.3.1. Input data

To reconstruct the intracellular causal networks, three different *a priori* interactions datasets were used. Information on viral proteins and their interacting human binding partners was obtained from the SARS-CoV-2 collection of the IntAct database on 1st October 2020 (Hermjakob et al., 2004; Orchard et al., 2014). Predicted SARS-CoV-2 miRNAs and their putative human binding partners were obtained from (Saçar Demirci and Adan, 2020). Intermediary signalling protein interactions known to occur in humans were obtained from the core PPI layer of the OmniPath collection using the 'OmnipathR' R package on 7th October 2020 (Türei et al., 2016). Only directed and signed interactions were included. Interactions between human transcription factors (TFs) and their target genes (TG) were obtained from the DoRothEA collection using the DoRothEA R package on 7th October 2020 (Garcia-Alonso et al., 2019). Only signed interactions of the top three confidence levels (A, B, C) were used. These include interactions from all resources analysed except those present in one resource only, or derived from computational predictions, characterised by a low confidence level (Garcia-Alonso et al., 2019).

Normalised transcript counts and differentially expressed ligands were obtained from single cell transcriptomics data of (i) colonoids and enteroids infected with SARS-CoV-2 obtained from (Triana et al., 2021b), as previously described.

3.3.2. ViralLink pipeline

Intracellular causal networks were inferred using the ViralLink pipeline, which was previously built by Dr. Agatha Treveil (former postdoc, EI, QIB) and described in (Treveil et al., 2021). Briefly, the list of expressed genes in infected immature enterocytes (originally known as "immature enterocytes 2" (MMP7+, MUC1+, CXCL1+)) from SARS-CoV-2-infected ileal and colonic organoids (Triana et al., 2021b) was used to filter the *a priori* molecular interactions from OmniPath and DoRothEA, to obtain PPI and TF-TG sub-networks where both interacting molecules are expressed (described as "contextualised" networks). Transcription factors regulating the differentially expressed ligands were predicted using the contextualised DoRothEA TF—TG interactions and scored as described in (Treveil et al., 2021). Human binding proteins of viral proteins and viral miRNAs obtained from the IntAct database (Hermjakob et al., 2004; Orchard et al., 2014) and (Saçar Demirci and Adan, 2020), respectively, were connected to the listed TFs through the contextualised PPIs using a network diffusion approach called Tied Diffusion Through Interacting Events (TieDIE) (Paull

et al., 2013). In this model, all viral protein—human binding protein interactions were assumed to be inhibitory in action, based on likely biological function, and given a lack of clear literature evidence of proven action. All viral miRNA—human binding protein interactions were set as inhibitory based on biological action of miRNAs (Huang et al., 2011). The final reconstructed network contains “nodes”, which refers to the interacting partners, and “edges”, which refers to the interaction between nodes. Nodes include viral proteins and miRNAs, human binding proteins, intermediary signalling proteins, TFs and differentially expressed ligands. Edges include activatory or inhibitory interactions.

For ileal and colonic data, separate networks were generated using the viral miRNA and viral protein as perturbations, and subsequently joined using the “Merge” function within Cytoscape to generate the final intracellular network. Nodes and edges were annotated according to their involvement in networks downstream of viral miRNAs or proteins. Further analyses were performed separately on the different layers of the network: miRNA specific, protein specific or shared nodes.

3.3.3. CARNIVAL pipeline

Intracellular causal networks were inferred using CARNIVAL and associated tools for analyses of expression data as described in (Liu et al., 2019). For simplicity, we refer to the pipeline as described in (Liu et al., 2019) as the CARNIVAL pipeline. Briefly, PROGENy was used to infer pathway activity from the Log2FoldChange of the infected immature enterocytes 2 gene expression data (Schubert et al., 2018). Next, using the TF-TGs interactions (from DoRothEA) and the differential expression data from infected organoids, VIPER was used to score TF activity based on enriched regulon analysis (Alvarez et al., 2016). Here, only the top 25 TFs regulating at least 15 target genes were taken forward, and a correction for pleiotropic regulation was included. Finally, CARNIVAL applied an integer linear programming approach to identify the most likely paths between human interaction partners of viral proteins or miRNAs and the selected TFs, through PPIs from OmniPath, considering the activity scores from PROGENy and VIPER. Viral protein—human binding protein interactions signs were specified to CARNIVAL as ‘inhibitory’, based on likely biological function, and given a lack of clear literature evidence of proven action. All viral miRNA—human binding protein interactions were also set as inhibitory based on biological action of miRNAs (Huang et al., 2011).

3.4. Network functional analysis

Functional overrepresentation analysis was performed on the networks constructed as above-mentioned using the R packages ‘ClusterProfiler’ and ‘ReactomePA’, for Gene Ontology (GO) (Ashburner et al., 2000) and for Reactome (Fabregat et al., 2018; Yu and He, 2016; Yu et al.,

2012) annotations, respectively. For the intercellular network, the analysis was carried out separately for ligand-receptor intercellular interactions driven by either upregulated or downregulated ligands. For the upregulated interactions, a list of upregulated ligands and their connecting immune receptors was used as the test. For the downregulated interactions, a list of downregulated ligands and their connecting immune receptors was used. Where a list of ligands plus receptors contained <5 genes, it was excluded from the analysis. All ligands and receptors from the original ligand-receptor network used as prior knowledge input for the intercellular analysis was used as the statistical background.

For the intracellular network, the analysis was done separately for each of the sub-networks (viral protein specific, viral miRNA specific, or shared). For each sub-network, a set of genes that were human binding proteins, intermediary proteins and TFs in the network ("PPI layer") was used as a test list, and a set of all nodes from the original OmniPath PPI interaction network used as prior knowledge input for the intracellular analysis was used as the statistical background. For the Reactome pathway enrichment analysis the IDs were converted to Entrez Gene ID within the 'ReactomePA' package. Functional categories with adjusted p value ≤ 0.05 and with gene count > 3 were considered significantly overrepresented.

3.5. Selection of ligands involved in the inflammatory process

To show how our approach could help point out specific epithelial-derived ligands driving the inflammatory process upon SARS-CoV-2 infection, the list of differentially expressed ligands in infected immature enterocytes in both colon and ileum was validated using independent data from three previously published studies.

This analysis was mainly performed by Dr. Agatha Treveil (former postdoc, EI, QIB). More specifically, to identify ligands whose expression was induced by cytokines, ligands were compared to DEGs in human colonic organoids exposed to cytokines from (Pavlidis et al., 2021). Next, to identify ligands already known to influence immune cell population, ligands were compared to two databases: ImmunoGlobe, a manually curated intercellular immune interaction network (Atallah et al., 2020), and ImmunoeXpresso, a collection of cell–cytokine interactions generated through text mining (Kveler et al., 2018). Finally, to identify ligands that could directly explain blood cytokine level changes in COVID-19 patients via direct immune cell regulation, ligands were compared to the data from a large dataset we recently manually compiled using COVID-19 patient publications (Olbei et al., 2021).

4. Results

4.1. Epithelial–immune interactome in the gut

First, to assess which epithelial cell type could drive the response to SARS-CoV-2 infection, we looked at the epithelial cell population in both directly infected and bystander cells which had the highest number of ligands among the DEGs upon infection. In general, epithelial cell populations in directly infected cells presented a higher number of altered ligands compared to bystander cells in both ileum and colon (**Figure 5.2**). Additionally, immature enterocytes 2 (enterocyte subpopulation characterised by MMP7+, MUC1+, CXCL1+) had the highest number of differentially expressed ligands upon infection in both directly infected and bystander cells in the ileum and colon, although the number of ligands was higher in directly infected cells (**Figure 5.2**). In directly infected cells, the second most impacted epithelial cell population was TAs in the colon and cycling TAs and TAs in the ileum (**Figure 5.2**).

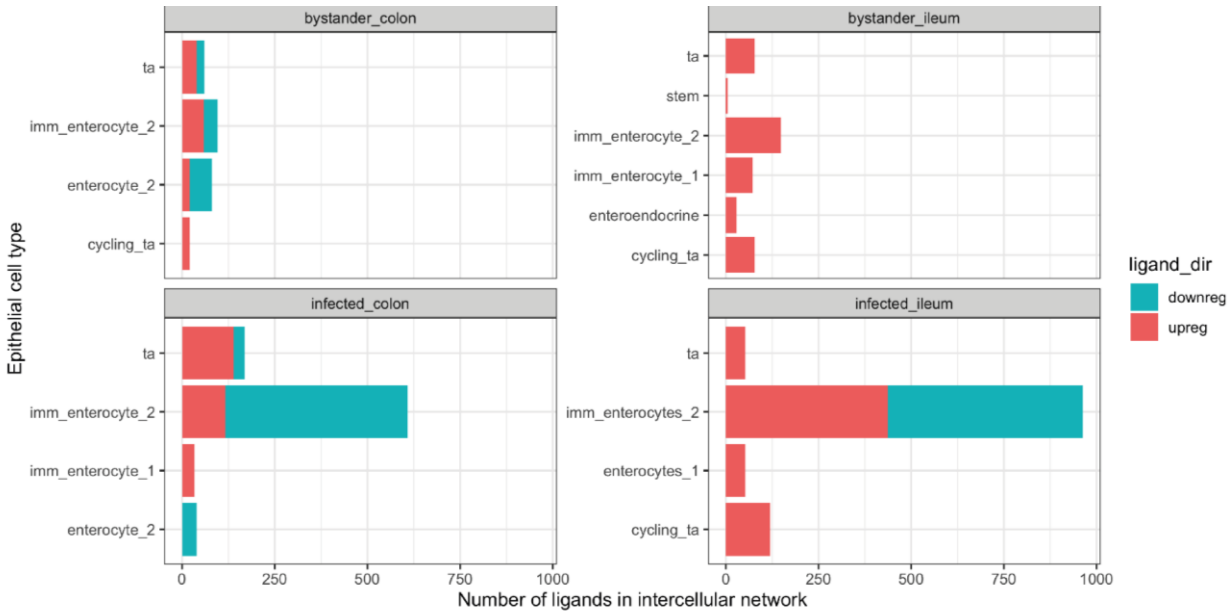

Figure 5.2. Differentially expressed ligands upon SARS-CoV-2 infection in infected or bystander epithelial sub-populations. Bar chart indicating the number of differentially expressed ligands in the intercellular network in each epithelial sub-populations, either bystander or infected, in ileal or colonic organoids infected with SARS-CoV-2 vs control (24 hours). Differentially expressed ligands are those DEGs found in(Lamers et al., 2020; Stanifer et al., 2020; Triana et al., 2021b; Zang et al., 2020), for which at least one binding receptor was found on immune cell populations. The colour of the bar indicates the direction of regulation (red, upregulated; blue: downregulated).

Because immature enterocytes were the most impacted population in both infected and bystander cells, I focused on this cell type to study the effect of SARS-CoV-2 on the gut. To build the intercellular network, differentially expressed ligands of colonic and ileal immature enterocytes were connected to their binding receptors on immune cell populations. More specifically, this was done by computing all the possible interactions between each set of up or downregulated epithelial ligands upon infection and each of the receptors expressed by the specific immune cell type were identified. Additionally, statistics were generated about the number of interactions between each ligand-receptor pair (ligand-receptor level), but also between each epithelial-immune cell pair (cell level).

When looking at the number of ligand–receptor interactions between each epithelial–immune cell type pair (cell level), directly infected intestinal cell populations had a higher number of predicted interactions with immune cells compared to bystander cell populations in both colon and ileum, supporting a role for direct viral infection in altering intercellular signalling in the gut (**Figure 5.3A, B**).

In infected immature enterocytes, interactions with immune cells were driven mostly by downregulated ligands in the colon, and by upregulated ligands in the ileum (**Figure 5.3A, B**). Additionally, the highest number of epithelial–immune interactions was identified between downregulated ligands and plasma cells, as well as CD4+/CD8+ T cells, macrophages and dendritic cells (DCs) to a lesser extent in the colon **(Figure 5.3A**). Conversely, in the ileum, the highest number of interactions was identified between upregulated ligands and IgA plasma cells, T resident memory (Trm) cells, DCs and resident macrophages (**Figure 5.3B**). Interestingly, it seemed that the higher number of interactions in the ileum compared to the colon was not a result of a higher number of upregulated ligands (20), as this was similar to the number of downregulated ones (24) (**Figure 5.3A, B**). Instead, the higher number of interactions was driven by upregulated ligands binding to multiple receptors on each immune cell targeted (not shown).

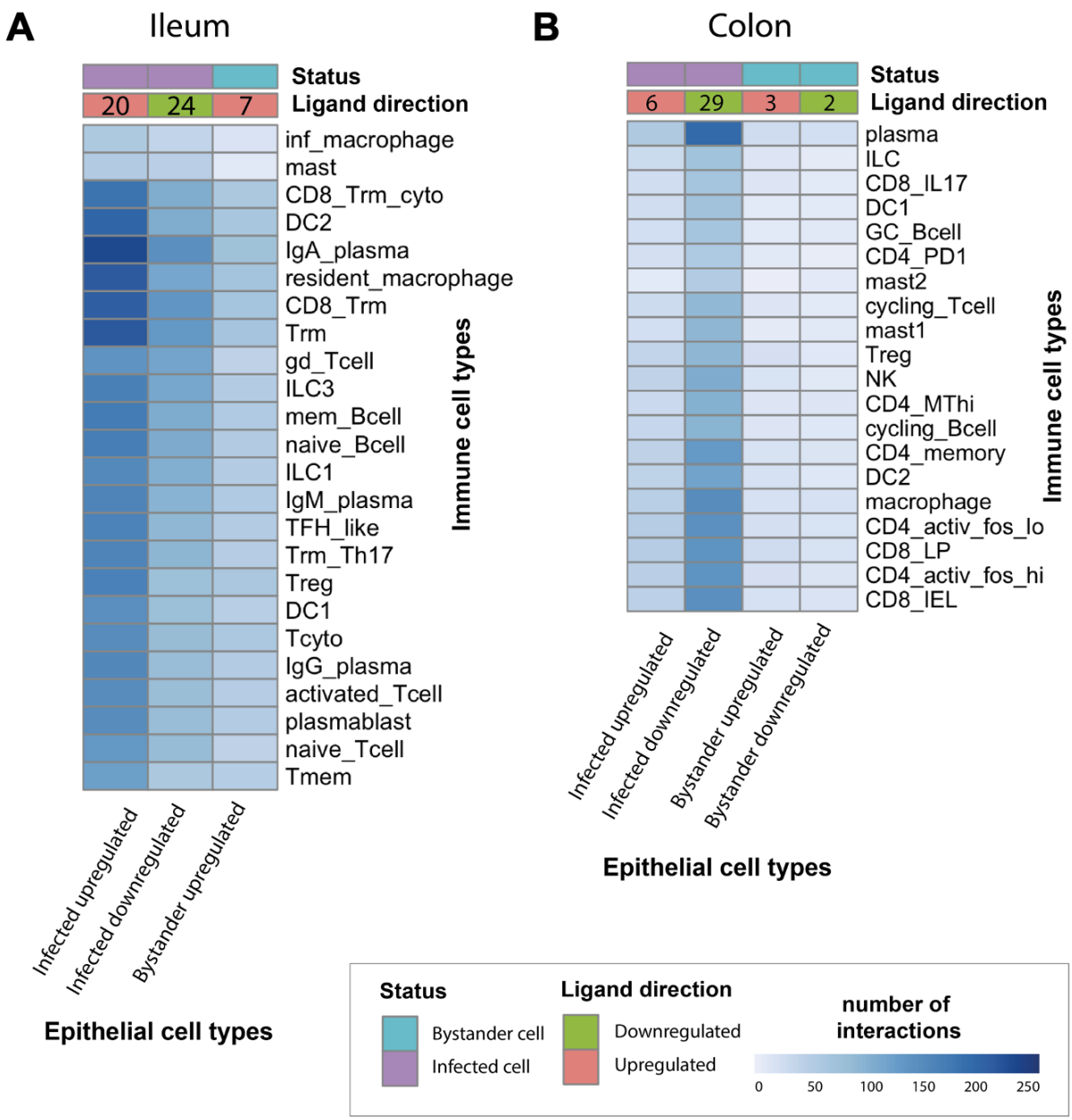

Figure 5.3: Upregulated and downregulated intercellular interactions between colonic and ileal infected immature enterocytes and resident immune cells upon infection in the colon and ileum. A, B) Heatmap showing the number of interactions between immature enterocytes and resident immune cells in the colon (A) and ileum (B). Interactions driven by upregulated and downregulated ligands (ligand direction) are shown separately for infected and bystander cells (status), and for ileum and colonic organoids. The intensity of the colour indicates the number of interactions with the immune cell types whose receptor is targeted by the epithelial cell ligands. The numbers on the ligand direction row refer to the number of upregulated or downregulated ligands driving the indicated interactions with immune cells for the different groups/conditions.

4.2. Intracellular signalling

To further understand how SARS-CoV-2 infection drives altered ligand expression in infected intestinal epithelial cells, I used bioinformatics tools to reconstruct the altered intracellular signalling in the directly infected immature enterocyte population driven by SARS-CoV-2. In particular, ViralLink and CARNIVAL were used to construct a causal network linking perturbed human proteins binding with SARS-CoV-2 viral proteins or miRNAs to activated TFs regulating the differentially expressed ligands upon infection, through altered intracellular protein-protein signalling cascades **(Figure 5.1)**. By integrating this network with tissue-specific epithelial data, I was able to construct two separate causal networks for infected immature enterocytes of the ileum and colon, which allowed me to look at differences in response between these two tissues (**Figure 5.1**). Finally, because *a priori* information on SARS-CoV-2 miRNAs/proteins - human protein interactions was used to build these networks, separate sublayers representing altered signalling stemming from upstream perturbations caused by SARS-CoV-2 miRNAs, proteins or both were constructed. The analysis of these sublayers would enable us to assess the contribution of each of these viral factors in altering the intracellular signalling cascade (**Figure 5.1**).

4.2.1. Network characteristics

When looking at network characteristics between the intracellular signalling networks generated with ViralLink vs CARNIVAL, networks generated using CARNIVAL were of much smaller sizes compared to those built with ViralLink (274 nodes and 479 nodes compared to 1423 and 1316 nodes for the colonic and ileal networks) (**Supplementary Figure 5.1A, B**). This result is linked to the property of CARNIVAL to find the most optimal paths based on the given input constraints compared to ViralLink where all possible interactions are explored. Hence, CARNIVAL networks are useful to understand specific molecular mechanisms and modulators upon SARS-CoV-2 infection.

When looking at networks generated with ViralLink, networks were similar in terms of size and network characteristics between colon and ileum, including diameter, characteristic path length, average number of neighbours, and number of molecular entities (nodes, miRNAs, genes or proteins) and molecular interactions (edges, activatory or inhibitory). The colonic network was made of 1423 nodes and 9971 edges, and had a network diameter of 10, characteristic path length of 4 and average number of neighbours of 14 (**Supplementary Figure 5.1A**). Additionally, the ileal network was made of 1316 nodes and 7935 edges, and had a network diameter of 9, characteristic path length of 4 and average number of neighbours of 12 (**Supplementary Figure 5.1A**). In the colon, there were 47 viral proteins/miRNAs, 409

human binding proteins, 908 intermediary signalling proteins, 37 TFs and 22 differentially expressed ligands, while in the ileum 47 viral proteins or miRNAs, 394 human binding proteins, 810 intermediary signalling proteins, 37 TFs and 28 differentially expressed ligands (**Supplementary Figure 5.1A**)**.**

When looking at networks generated with CARNIVAL, the ileal and colonic networks differed in terms of both size and network characteristics. In particular, the ileal network was bigger in size and had more connections compared to the colonic one: while the ileal network had 274 nodes and 479 edges, the colonic network had 147 nodes and 279 edges (**Supplementary Figure 5.1B**). Additionally, network diameter and path length were bigger in the colon compared to the ileum. The colonic network had a network diameter of 15 and a path length of 6.3, while the ileal network had diameter of 9 and a path length of 3.3, showing higher number and more connected nodes in the ileal network. (**Supplementary Figure 5.1B**). In the colon, there were 20 viral proteins/miRNAs, 27 human binding proteins, 36 intermediary signalling proteins, 43 TFs and 21 differentially expressed ligands, while in the ileum we found 21 viral proteins or miRNAs, 31 human binding proteins, 169 intermediary signalling proteins, 26 TFs and 25 differentially expressed ligands (**Supplementary Figure 5.1B**)**.** Hence, size and characteristics differences observed between the ileal and colonic networks could be mainly due to the higher number and highly interconnected intermediary signalling proteins identified in the ileal network (**Supplementary Figure 5.1B, 5.2, 5.3**).

To note, for ViralLink intracellular networks, upstream signalling was predicted for 22 out of the initial 35 differentially expressed ligands (29 down- and 6 up-regulated) in the colon, and for 28 out of 44 differentially expressed ligands (24 down- and 20 up-regulated) for the ileum (**Figure 5.2 and Supplementary Figure 5.1A**). These numbers are lower than those predicted to be differentially expressed upon infection by (Triana et al., 2021b), indicating that some ligands are not affected by direct upstream signalling changes but by more complex mechanisms, or the original knowledge network used as input for the analysis did not contain information about such ligands (Menche et al., 2015) (**Figure 5.2 and Supplementary Figure 5.1A**). For CARNIVAL, the number of differentially expressed ligands in the network is smaller than the original one, due to the nature of the algorithm, which identifies the most optimal path based on the given input constraints, compared to ViralLink where all possible interactions are explored (**Supplementary Figure 5.1B and Methods**).

4.2.2. Functional analysis

To understand how SARS-CoV-2 infection in immature enterocytes affects their function through the modulation of intracellular signalling, I carried out a functional analysis on the

intracellular networks generated with ViralLink and CARNIVAL. More specifically, a functional overrepresentation analysis (GO and Reactome) of the PPI layer of each intracellular causal sub-network (stemming from viral proteins, miRNAs, or both) was performed to assess the contributions of SARS-CoV-2 miRNAs or proteins to the changes observed (**Figure 5.1 and Methods**).

For the **ViralLink** networks, functional analysis revealed an overrepresentation of pathways related to inflammation and chemotaxis NF-kB signalling, interleukin signalling, chemokine signalling) in both ileum and colon (**Figure 5.4A, B**). Additionally, there was an overrepresentation of functions related to interferon (IFN) signalling and Mitogen-Activated Protein Kinase (MAPK) signalling being overrepresented uniquely in the ileum in both viral protein and miRNA intracellular networks (**Figure 5.4B**). An overrepresentation of laminin-driven interaction pathways, which I observed uniquely for viral miRNA intracellular network in both ileum and colon, could be indicative of an increased recruitment and adhesion of immune cells following infection (**Figure 5.4A, B**). Furthermore, an overrepresentation of pathways related to negative regulation of apoptosis, cell cycle, cell proliferation and growth was observed in both ileal and colonic networks, suggesting an effect of SARS-CoV-2 on epithelial cell tissue renewal (**Figure 5.4A, B**). Interestingly, an overrepresentation of the WNT signalling pathway, which is a key pathway for stem cell renewal, was found uniquely in the viral protein sub-network in both tissues. Conversely, pathways related to the establishment of cell and tissue polarity were found uniquely in the colon, possibly indicating an attempt for tissue healing following viral infection (**Figure 5.4**).

For the CARNIVAL networks, functional analysis confirmed similar affected functions upon infection as those found in the ViralLink networks such as senescence or inflammation, suggesting functional overlap between networks obtained using these two methods **(Figure 5.4 and Supplementary Figure 5.2, 5.3)**. In this context, the choice of which tool (ViralLink or CARNIVAL) to be used to build the intracellular network for a particular study should be driven by the specific study aims and biological questions.

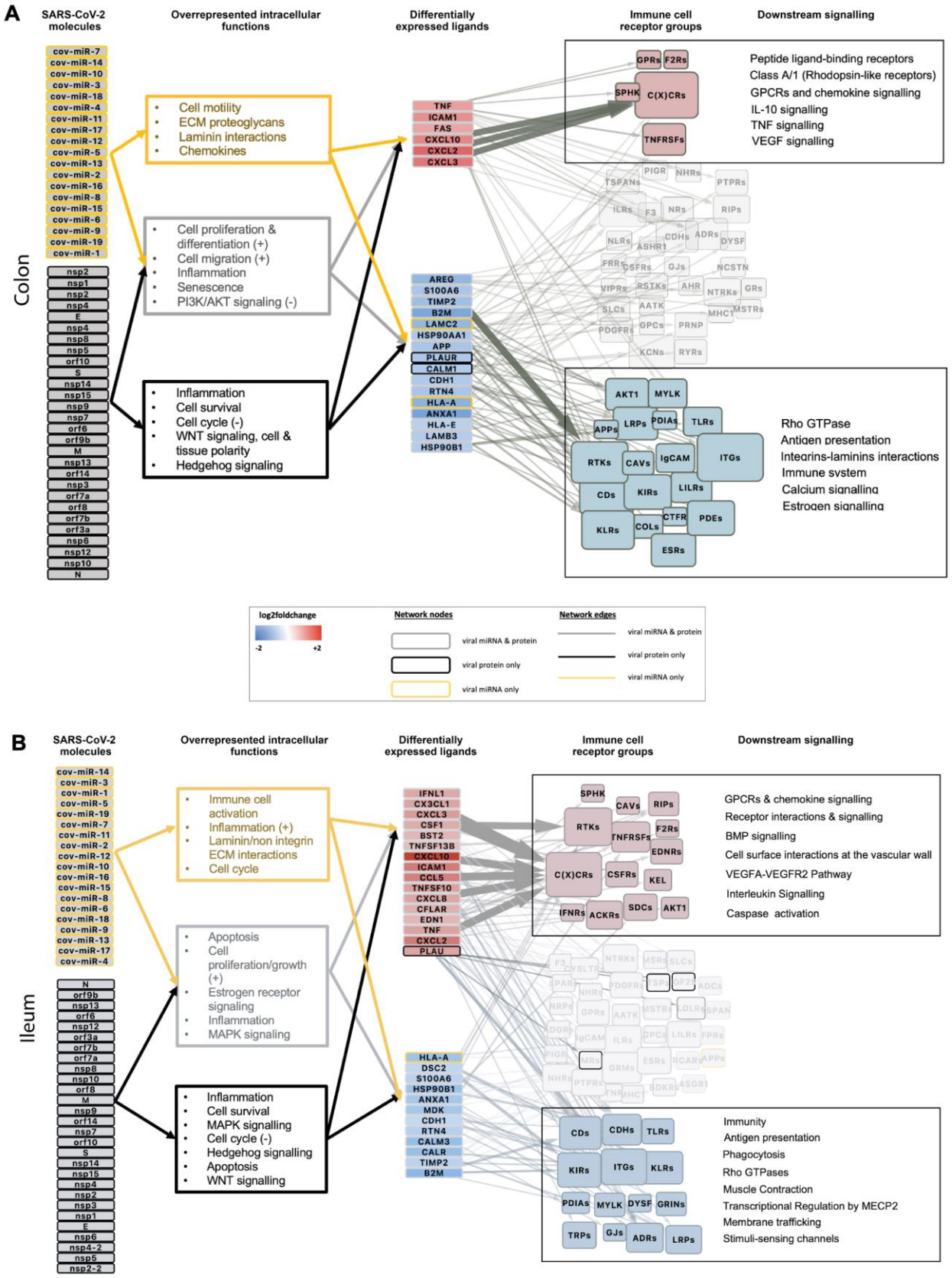

Figure 5.4: Overview of intracellular and intercellular signalling of colonic and ileal infected immature enterocytes upon SARS-CoV-2 infection. A, B) Overview of intracellular and intercellular

signalling upon SARS-CoV-2 infection in colonic (A) and ileal (B) infected immature enterocytes and immune cell populations. From left to right: signalling cascade going from SARS-CoV-2 molecules (proteins or miRNAs) to differentially expressed ligands on immature enterocytes and binding receptor groups on immune cells. Intracellular network: SARS-COV-2 molecules are grouped separately if they are viral proteins (bottom) or miRNAs (top). Differentially expressed ligands for which no upstream signalling was identified, but downstream intercellular connections were predicted are excluded from this figure. Differentially expressed ligands are grouped based on the direction of regulation, which is indicated with blue when downregulated (bottom) and red when upregulated (top) when comparing SARS-CoV-2 infected vs uninfected conditions. Colours of the nodes and of the functional analysis indicate if the original network was a miRNA only (yellow), viral protein only (black) or both viral protein and miRNA (grey). Functional overrepresentation analysis was carried out for the "PPI layer" of the intracellular network which includes human binding proteins, intermediary signalling proteins and TFs (adjusted p-value < 0.05, $n > 3$). Intercellular network: Size of the receptor node represents the sum of receptors within the group targeted by each incoming ligand. Functional analysis is indicated for ligand–receptor groups. Receptor groups layout is based on whether they contributed to the functional analysis of upregulated interactions (red) or downregulated interactions (blue). Receptor groups not contributing to any functions are indicated in light grey.

4.2.3. Transcription factors and central nodes

Further analysis of these networks can help predict key transcription factors responsible for the upstream regulation of altered ligands upon infection. In particular, the main TFs predicted to regulate the intracellular signalling upon infection were *ATF2/3, FOS, JUN, STAT1*, and NFKB1 in both colon and ileum, which were upregulated upon infection **(Supplementary Figure 5.2, 5.3).** These transcription factors play a role in interferon response (*STAT1*), and inflammation (*NFKB1*), anti-apoptosis and cell growth (*ATF2/3*), cell proliferation and differentiation (*JUN, FOS*), suggesting an increase in these functions upon SARS-CoV-2 infection in both tissues.

Interestingly, viral miRNAs were predicted to target different intracellular signalling processes between colon and ileum (miR_10,11,16,18 in the colon and miR_4,5,6,18 in the ileum) **(Supplementary Figure 5.2, 5.3)**. Additionally, by analysing these networks, we observed that *NOTCH1* and *SMAD4*, seem to be central TFs to the intracellular signalling cascade in the colon, by receiving several signals driven by viral miRNAs (*NOTCH1*) and viral proteins (*SMAD4*), respectively **(Supplementary Figure 5.2, 5.3)**. Interestingly, both the Notch and TGF-β SMAD-dependent signalling pathways are involved in intestinal epithelial cell homeostasis, including stem cell maintenance, progenitor cell proliferation and maintenance of cell differentiation, suggesting a modulation of these pathways upon infection. In the ileal network, *JAK2* and cAMP response element-binding protein (*CREB1)*, as well as *SMAD2,*

SMAD3 and *ERK2/MAPK1* seem to play a central role in the intracellular PPI signalling driven by viral miRNAs and viral proteins, respectively, and *JAK2* and both *SMAD2* and *SMAD3* were also upregulated upon infection **(Supplementary Figure 5.2, 5.3)**. These transcription factors play a key role in the regulation of immunity (*JAK2, CREB1)*, cell proliferation and differentiation (*MAPK1*) and plasticity (*SMAD2/3*), suggesting a positive regulation of these functions uniquely in the ileum upon infection.

4.3. Intercellular signalling

To understand the functional impact of epithelial infection on the epithelial–immune interactome, I linked upregulated and downregulated epithelial ligands of colonic and ileal immature enterocytes (infected or bystander) upon infection to their binding receptors on immune cells, hereby building intercellular epithelial-immune networks (**Figure 5.1 and Methods**). Next, for each set of up and downregulated intercellular interactions, I looked at which ligands, receptors and immune cell types were involved in these intercellular interactions, also looking at any similarities or differences between the colon and ileum (**Figure 5.1 and Methods**). For the purpose of this thesis, only results relative to directly infected immature enterocytes will be presented, while those relative to bystander cells can be found in the published article (see **Appendix 3**).

4.3.1. Upregulated intercellular interactions

Upregulated ligands of infected immature enterocytes upon infection as well as binding receptors on immune cells were mainly shared among colon and ileum (**Supplementary Figure 5.4, 5.5**). Shared upregulated ligands included mainly cytokines and chemokines (CXCL2/3/10 and TNF-α) and the adhesion factor intercellular adhesion molecule 1 (ICAM1). Interestingly, additional ligands were upregulated in the ileum upon infection but not in the colon, including several chemokines (colony stimulating factor 1 (CSF1), CXCLs, TNF superfamily (TNFSFs)) and adhesion factors (Plasminogen Activator (PLAU), Ephrin A1 (EFNA1)) (**Supplementary Figure 5.4**). Additionally, of the 38 receptors targeted by upregulated ligands in the colon, all were targeted in the ileum too, and they were mainly represented by chemokine receptors (CXCRs, CCRs) (**Supplementary Figure 5.5**). Because of the large overlap between ligands and receptors, most epithelial–immune interactions driven by upregulated ligands were also similar in both tissues (one unique to colon, 219 unique to ileum, 66 shared), and were represented mainly by chemokine-chemokine receptors interactions (**Supplementary Figure 5.6**). Nevertheless, some tissue-specific interactions could be found. These included ileal-specific upregulated interactions driven by PLAU, EFNA1 and colony stimulating factor 1 (CSF1), binding to various receptors on immune cells, pointing

towards an increased immune cell recruitment and adhesion **(Supplementary Figure 5.6).** Additionally, I found one colon-specific upregulated interaction between epithelial Fas Cell Surface Death Receptor (FAS) binding to receptor-interacting serine/threonine-protein kinase 1 (RIPK), pointing towards increased cell death upon infection (**Supplementary Figure 5.6**).

To understand which epithelial ligands and immune cell receptors were driving most epithelial–immune cell interactions, I scored ligands and receptors based on the number of interactions they were involved in. When doing so, interactions driven by upregulated ligands ("upregulated interactions"), and those driven by downregulated ligands upon infection (downregulated interactions) were studied separately (**Figure 5.1 and Methods**). In both tissues, the highest number of upregulated interactions was driven by chemokines (CXCLs) and TNF-α as ligands (**Figure 5.5A, B**) and chemokine receptors (CXCR 3,4,5,6 and CCR 1,2,5,7,9,10) as receptors on immune cells (**Figure 5.6A, B**), overall pointing towards an increased immune cell recruitment upon infection. The high number of upregulated interactions driven by chemokines could be attributable to the widespread presence of several different chemokine receptors on immune cells (not shown).

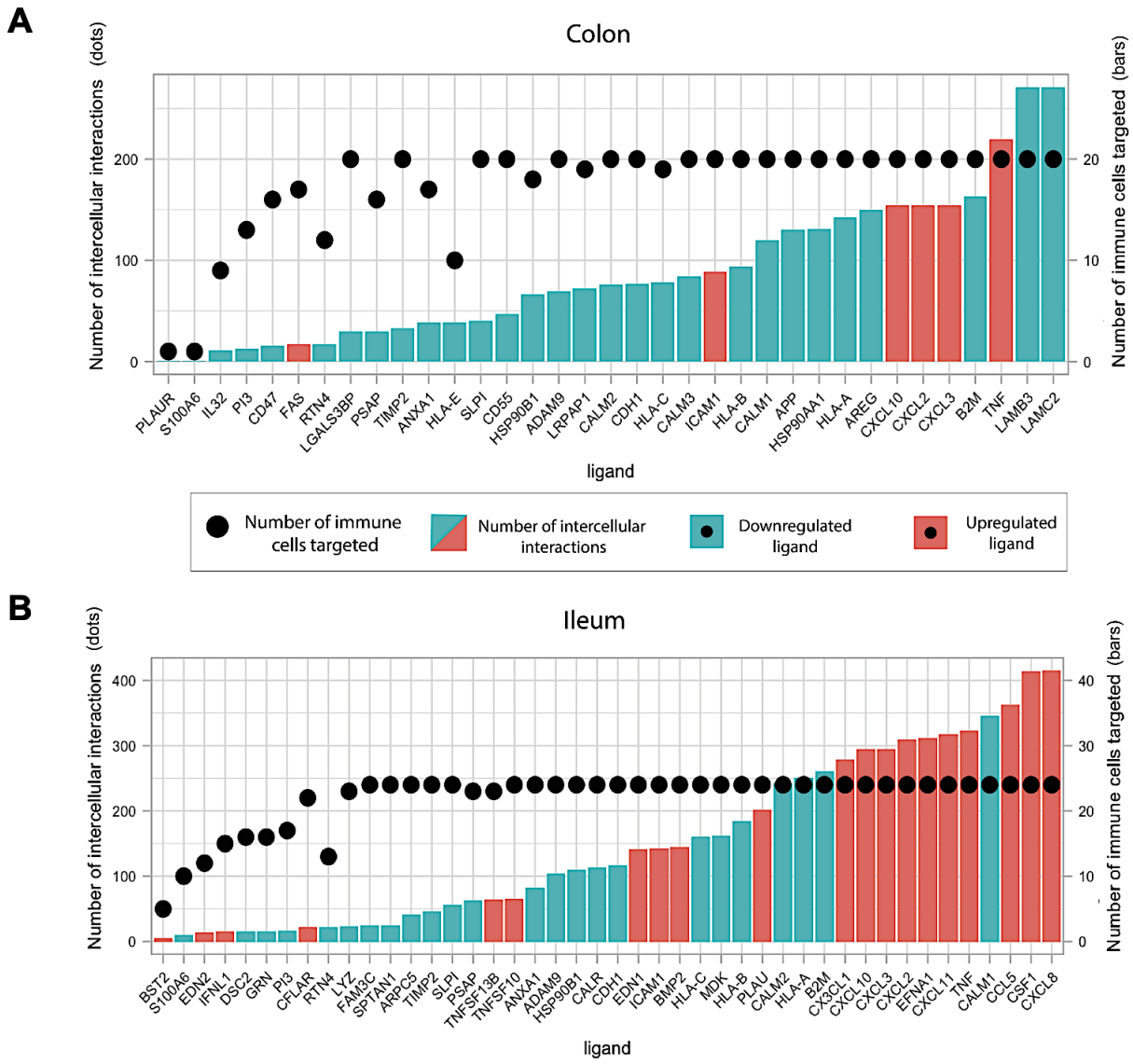

Figure 5.5: Ligands participating in ligand–receptor interactions between infected immature enterocytes and resident immune cells upon infection in the colon and ileum. **A, B)** Bar plot showing the upregulated and downregulated ligands in the colonic (A) and ileal (B) infected immature enterocytes–immune cell network scored by number of interactions (height of the bar plot) and number of immune cells targeted (black dots). Upregulated ligands are shown in red and downregulated ligands in blue.

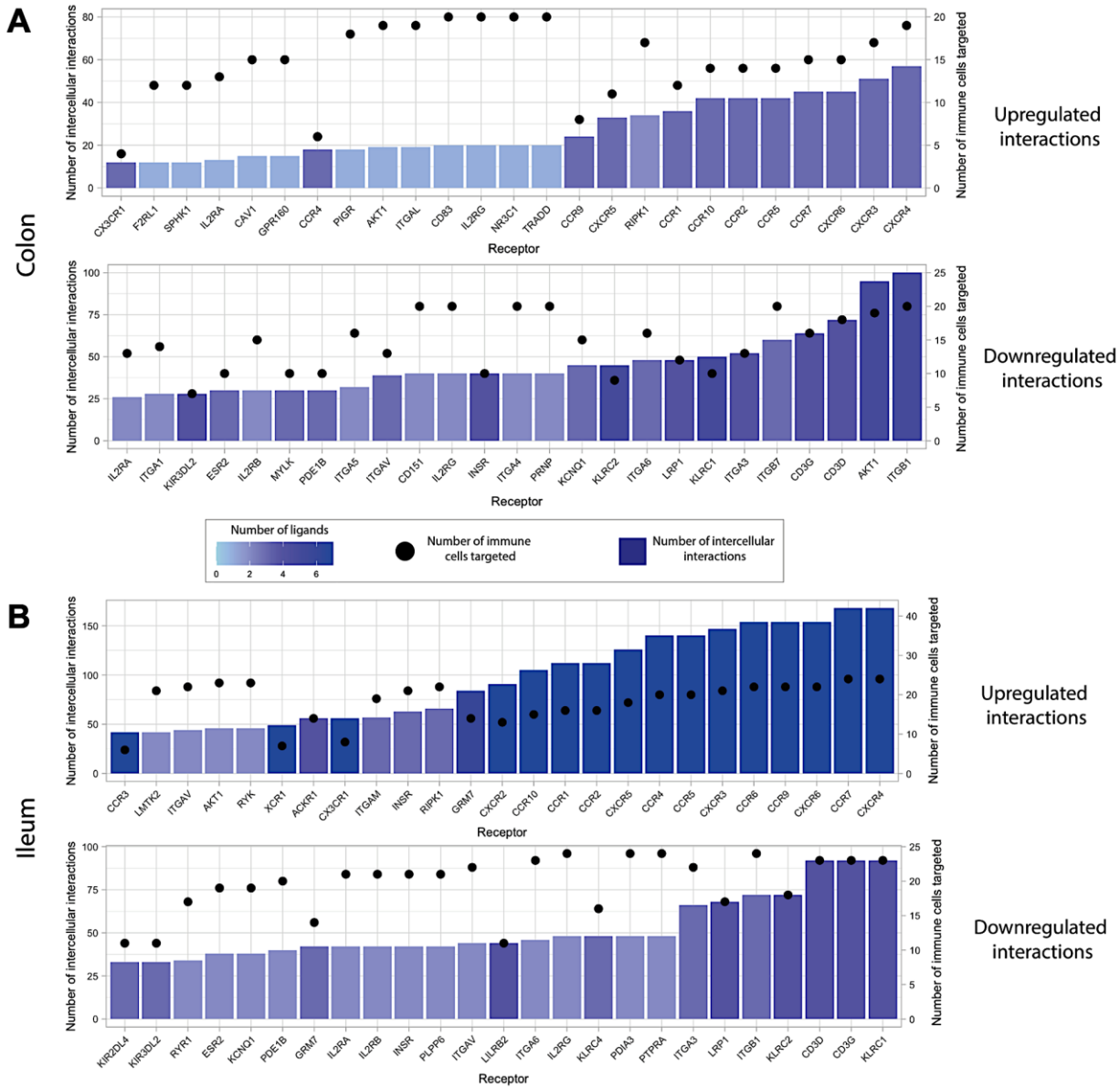

Figure 5.6. Receptors involved in intercellular interactions between colonic and ileal infected immature enterocytes and resident immune cells. A, B) Bar plot showing the immune receptors targeted by upregulated (top graph) and downregulated (bottom graph) ligands in colonic (A) and ileal (B) infected immature enterocytes, scored by number of interactions (height of the bar plot) and number of immune cells targeted (black dots). The colour of the bar plots indicates the number of ligands targeting each of the receptors indicated.

In addition to the number of interactions driven, I wanted to understand which epithelial ligands and immune receptors were driving the strongest epithelial–immune cell interactions. For this purpose, I scored all ligands and receptors based on the “sum of receptor expression” value, which considers the number of interacting receptors and the level of receptor expression in each immune cell type (**Figure 5.1 and Methods**). In the colon, the strongest upregulated interactions involved the epithelial TNF-α binding to B cells, T cells (CD4/CD8+), NK cells,

macrophages and DCs, as well as epithelial chemokines (CXCL2,3, 10) binding to T cells (CD4/CD8+) and NK cells (**Figure 5.7A**). Similarly, in the ileum the strongest upregulated interactions involved epithelial chemokines binding to T cells populations (regulatory (Treg), cytotoxic (Tcyto), memory (Tmem) and cytotoxic CD8+ resident memory (CD8 Trm cyto) T cells), as well as TNF-α and CSF1 binding to macrophages and DCs (**Figure 5.7B**). Receptors driving the strongest upregulated interactions were mainly chemokine receptors (CXCRs, CCRs) in both colon and ileum, and RIPK1 in the colon only (**Figure 5.8A, B**).

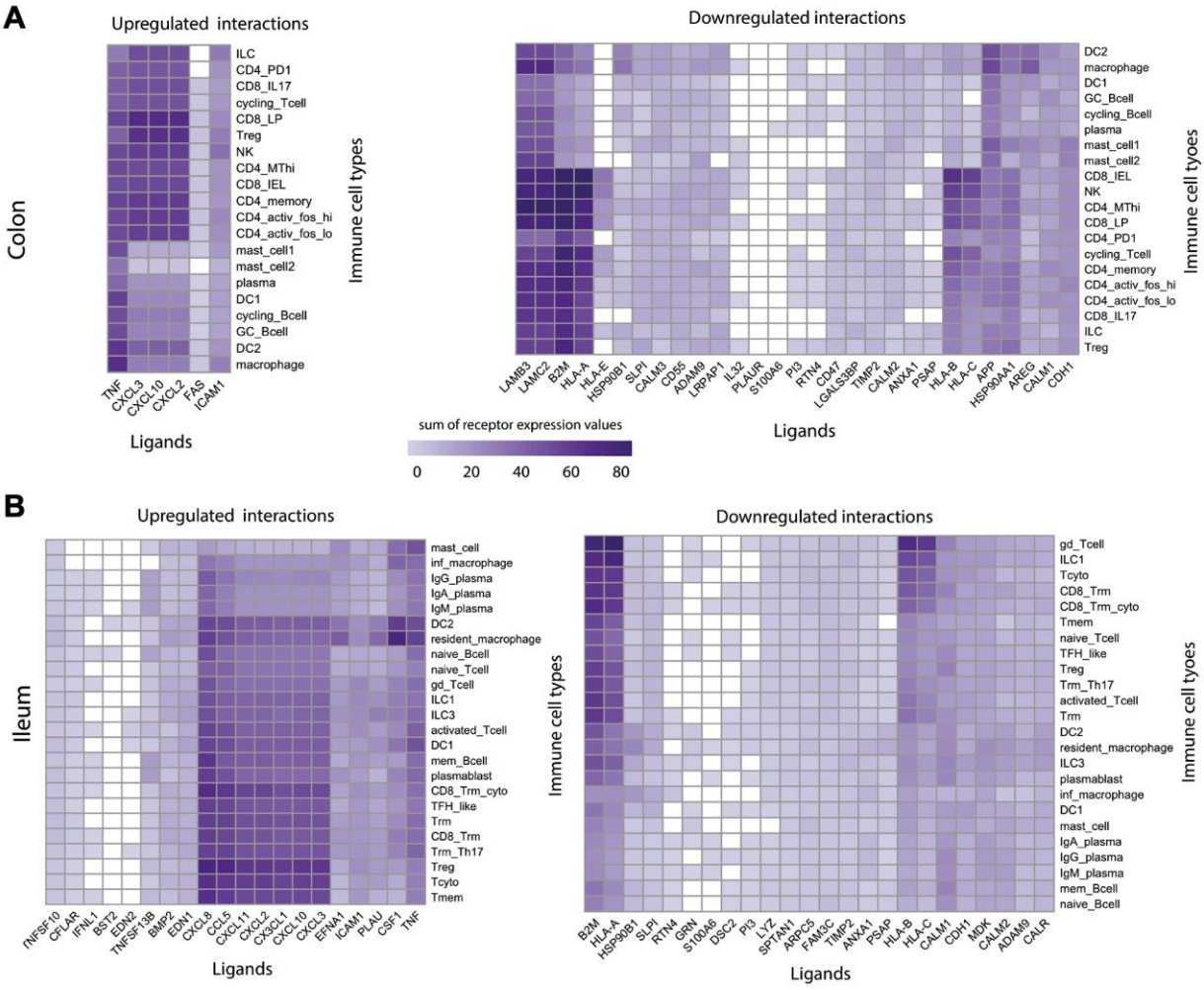

Figure 5.7. Ligands of infected immature enterocytes involved in the strongest up and downregulated interactions upon SARS-CoV-2 infection in the colon and ileum. A, B) Heatmap showing the upregulated and downregulated interactions in the colon (A) and ileum (B) between intestinal epithelial ligands and resident immune cells upon infection of immature enterocytes with SARS-CoV-2. The strength of the interaction is expressed by accounting for the number of interactions between epithelial ligands and immune receptors and the level of receptor expression of immune cells. The strength of the interaction, named “sum of expression values”, is visualised using a colour gradient from white (weakest interactions) to purple (strongest interactions).

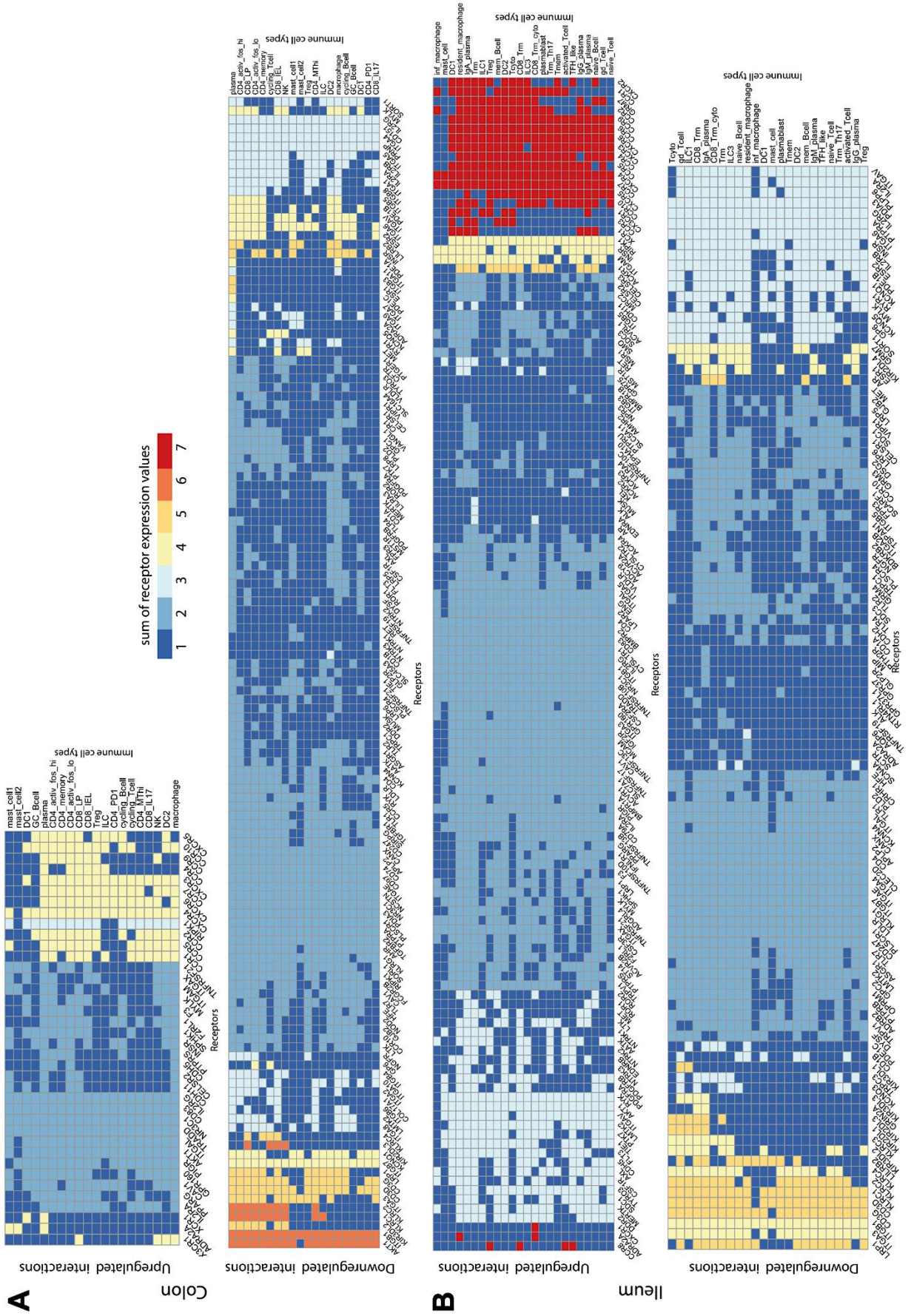

(Figure caption on the next page)

Figure 5.8. Receptors on immune cell types involved in the strongest up and downregulated interactions upon SARS-CoV-2 infection in the colon and ileum. A, B) Heatmap showing the upregulated and downregulated interactions in the colon (A) and ileum (A) between receptors and resident immune cell types upon infection of immature enterocytes with SARS-CoV-2. The number of interactions in which each receiving receptor on immune cell types is involved is visualised using a colour gradient from blue (weakest interactions) to red (strongest interactions).

Finally, to better understand the role of epithelial–immune interactions in driving infection, I ran a functional overrepresentation analysis of each ligand-receptor pair involved in upregulated and downregulated intercellular interactions (**Figure 5.1 and Methods**). In line with the major overlap in upregulated intercellular interactions between colon and ileum, results showed that most enriched functions were shared and included chemotaxis (GPCR signalling, chemokine signalling), immunity (interleukin signalling), apoptosis (caspase activation) and angiogenesis (Vascular endothelial growth factor (VEGF) A-receptor 2 (VEGFR2) pathway) (**Figure 5.9A, B and Supplementary Figure 5.7**). I found only some limited tissue-specific functions, including one colonic-specific function related to pro-inflammatory responses (TNF signalling) (**Figure 5.9A**) and one ileal-specific function related to stem cell renewal (BMP signalling) (**Figure 5.9B**).

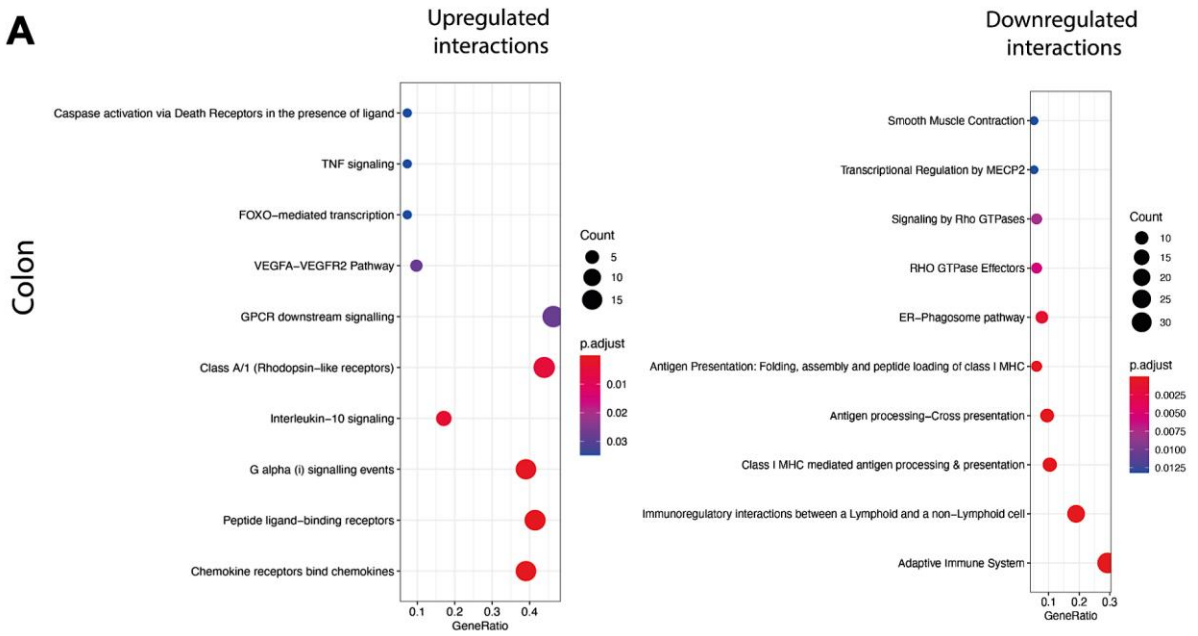

(Figure continues on the next page)

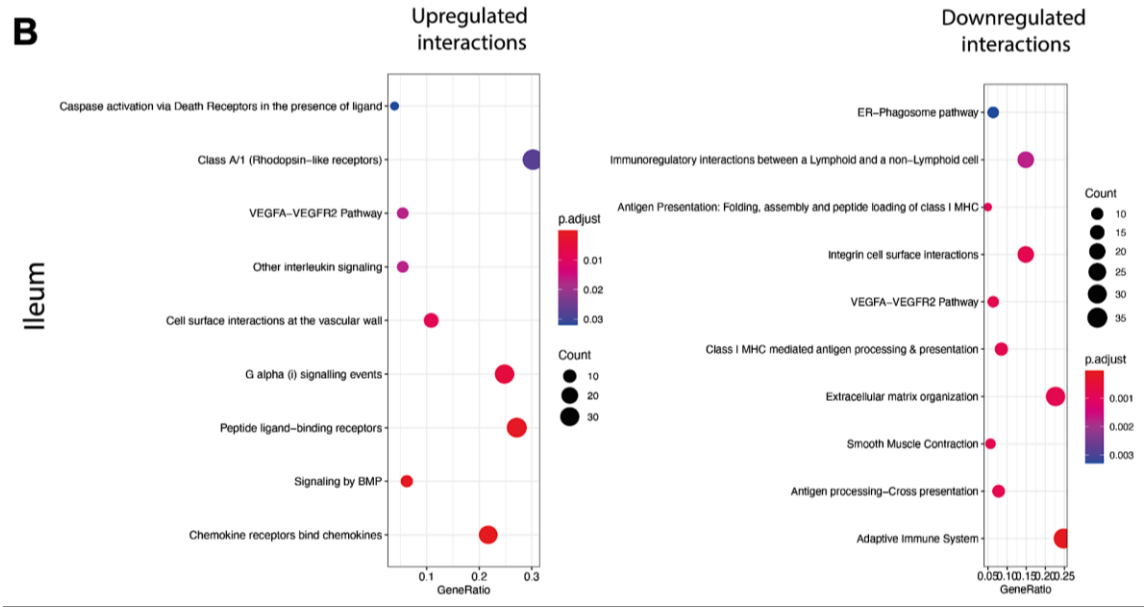

Figure 5.9. Functional analysis of ligand-receptor interactions between ileal and colonic immature enterocytes and resident immune cells upon SARS-CoV-2. A, B) Reactome functional overrepresentation analysis carried out a list of all upregulated ligands and receptors for interactions of a specific condition. There was no weighting for the number of interactions of each ligand/receptor. Analyses relative to interactions driven by upregulated and downregulated ligands in the colon (A) and ileum (B) are shown separately.

4.3.2. Downregulated intercellular interactions

Downregulated ligands in infected immature enterocytes upon infection as well as targeted receptors on immune cells were tissue-specific to a large extent, resulting in a large proportion of downregulated interactions being tissue-specific as well (73 unique to ileum, 125 to colon) (**Supplementary Figure 5.4, 5.5, 5.6**).

In both tissues, the highest number of downregulated interactions was driven by the epithelial ligands human leukocyte antigens (HLA-A/B/C), beta-2-microglobulin (B2M) and calmodulin (CALM1/2) (**Figures 5.5A, B**), and integrins (ITGs), Killer Cell Lectin Like Receptors C (KLRCs) and LDL Receptor Related Protein 1 (LRP1) as receptors on immune cells in both colon and ileum (**Figure 5.6A, B**). Additionally, uniquely in the colon, the highest number of downregulated interactions was driven by two epithelial-derived laminins (LAMC2, LAMB3) (**Figure 5.5A**), and by AKT1 (Protein kinase B, PKB) present on immune cell types (**Figure 5.6A**).

When investigating the strength of these intercellular interactions, we found that HLAs (HLA-A, B, C) and B2M targeting T cells (colon: CD4/CD8+, Tregs; ileum: Trm, Tregs, cytotoxic T cells), NK cells (colon only), ILCs and macrophages (ileum only) represented the strongest downregulated interactions in both colon and ileum (**Figure 5.7A, B**). Additionally, uniquely in the colon, laminins (LAMB3, LAMC2) targeting T cells and macrophages represented the strongest downregulated interactions (**Figure 5.7A**). Receptors driving the strongest downregulated interactions were AKT1 uniquely in the colon (**Figure 5.8A**) as well as integrins, KLRCs and LRP1 in both colon and ileum (**Figures 5.8A, B**).

By running a functional overrepresentation analysis of ligands and receptors participating in downregulated interactions (**Supplementary Figure 5.7**), I found shared enriched functions related to antigen processing and cross-presentation (MHC class I–mediated), phagocytosis (endoplasmic reticulum (ER) phagosome pathway, signalling by RHO GTPases) and cell–cell communication (immunoregulatory interactions between a lymphoid and non-lymphoid cell) in both tissues, possibly suggesting decreased epithelial–immune cell crosstalk functions related to the activation of the innate and adaptive immune response (**Figure 5.9A, B**). Furthermore, I found several colon-specific enriched functions related to the ECM organisation and integrin cell surface interactions, which play an important role in processes critical to inflammation, infection, and angiogenesis, thereby suggesting a negative regulation of these vital interactions uniquely in the colon (**Figure 5.9A**). The only function uniquely overrepresented in the ileum was transcriptional regulation by MECP2, whose expression has been shown to play a role in intestinal morphology and function (**Figure 5.9B**).

4.4. Implication of epithelial ligands in the inflammatory process

By analysing the altered intracellular and intercellular signalling networks in intestinal epithelial cells upon infection, I identified several differentially expressed ligands which could potentially play a role in driving inflammatory processes upon SARS-CoV-2 infection. To validate the importance and role these ligands could play during immune responses to SARS-CoV-2, I integrated this information with independent data from three previously published studies (**Figure 5.1 and Methods**).

First, I compared differentially expressed ligands upon SARS-CoV-2 infection to DEGs in human colonic organoids exposed to inflammatory cytokines (Pavlidis et al., 2021). By doing so, I identified 24 ligands whose expression change was regulated by cytokines during intestinal inflammation, thereby which are likely to contribute to the inflammatory responses

upon infection **(Table 5.1)**. Second, I compared ileal and colonic ligands to data from ImmunoGlobe, a manually curated intercellular immune interaction network (Atallah et al., 2020) and ImmunoeXpresso, a collection of cell–cytokine interactions generated through text mining (Kveler et al., 2018). By doing so, I identified an additional 12 ligands that are previously known to influence immune cell populations (**Table 5.1**). The full list of affected immune cell types for each epithelial ligand is available in **Table 5.1**. Finally, to understand which ileal and colonic ligands could explain blood cytokine level changes of COVID-19 patients via direct immune cell regulation, I used data previously published by our group (Olbei et al., 2021), and was able to identify 6 ligands capable of creating the detected blood cytokine levels during infection (**Table 5.1**).

These three lists of ligands were used to rank the differentially expressed ligands which were likely to play an important role in the inflammatory process. Criteria used for the ranking included: based on a series of criteria, including whether they were found in any of the three studies above-mentioned, they were tissue-specific, and they had the highest number of targets. In this way, I could draw a list of 18 highly ranked ligands, for which there is strong evidence of their role in epithelial–immune cell interactions during the inflammatory SARS-CoV-2 disease response (**Table 5.1**). These ligands included CSF1, various chemokines (CXCL10, CXCL11, CXCL2, CXCL3, CCL5, CX3CL1, CXCL8), TNF-α & TNFSF13b, and ICAM1 among the upregulated ones; and various laminins (LAMC2, LAMB3), AREG, B2M), human leukocyte antigens (HLAs) (HLA-A, HLA-B) and IL32 among the downregulated ones.

Table 5.1. Key differentially expressed ligands produced by infected immature enterocytes drive the inflammatory process upon SARS-CoV-2 infection. Table showing a list of top-ranked differentially expressed ligands in infected immature enterocytes which were identified to drive inflammation upon SARS-CoV-2 infection. The ranking of the ligands was performed using multiple criteria as explained in the **Methods**. 'Organoid type' indicates whether the expression change of the ligand was found in ileal or colonic infected immature enterocytes upon SARS-CoV-2 infection, respectively. 'Expression change upon SARS-CoV-2 infection' indicates the direction of expression change of the ligand in infected immature enterocytes upon SARS-CoV-2 infection. 'Regulation by cytokines' indicates whether ligand expression was found to be regulated by cytokines during inflammation based on results from (Pavlidis et al., 2021). Ileal data was not available (n.d.) in this study, so no conclusions could be drawn for ileal ligands. 'Known to affect immune cells' indicates whether the ligand was found to be regulated by immune cells using data from ImmunoGlobe (1) and ImmuneXpresso (2) databases. 'Directly explain patient blood cytokine levels' indicates whether the ligand was found to directly regulate blood cytokine levels in COVID-19 patients from (Olbei et al., 2021).

(Table shown on the next page)

Ranking	Ligand	Ligand description	Organoid type	Expression changes upon SARS-CoV-2 infection	Regulation by cytokines	Known to affect immune cells	Directly explain patients' blood cytokine levels
1	CXCL2	C-X-C Motif Chemokine Ligand 2	Colonic, Ileal	Up	IFNG, TNF, IL-17, IL-22 (up)	Neutrophils (1,2), fibroblasts, T cells, NK cell and CD8a+ DCs (1), leukocytes (2)	✓
1	CXCL3	C-X-C Motif Chemokine Ligand 3	Colonic, Ileal	Up	TNF, IL-22 (up)	Neutrophils, fibroblasts (1), T cells (2)	✓
1	CXCL10	C-X-C Motif Chemokine Ligand 10	Colonic, Ileal	Up	IFNG, TNF (up)	DC, Th1, NK cells, B cells, monocytes (1), and 29 additional immune cell types (2)	✓
1	CSF1	Colony stimulating factor 1	Colonic	Up		35 immune cell types (2)	✓
1	CXCL11	C-X-C Motif Chemokine Ligand 11	Ileal	Up	n.d. (3)	DC (1,2), B cells, NK cells, Th1, monocytes, macrophages (1), lymphocytes, T cells, CD8+ alpha/beta T cell (2)	✓
2	TNFSF13B	TNF Superfamily Member 13b	Ileal	Up	n.d.	B cell, T cell, follicular B cell, naïve B cell, Th17, neutrophils, monocytes (2)	✓
2	LAMC2	Laminin Subunit Gamma 2	Colonic	Down	TNF, IL-22 (up)		
2	CCL5	C-C Motif Chemokine Ligand 5	Ileal	Up	n.d. (3)	T cells, basophils, eosinophils, macrophages, monocytes, NK cells, DC, Memory T cells, Th1 and Th2 (1), and 23 additional immune cell types (2)	
2	CX3CL1	C-X3-C Motif Chemokine Ligand 1	Ileal	Up	n.d. (3)	Monocytes, T cells, neutrophil, NK, DC, Mast cells and microglia (1), and 19 additional immune cell types (2)	
2	CXCL8	C-X-C Motif Chemokine Ligand 8	Ileal	Up	n.d. (3)	Neutrophils, macrophages, basophils, naïve T cells, CD8+ T cells, monocytes (1), and 44 additional immune cell types (2)	
3	ICAM1	Intercellular Adhesion Molecule 1	Colonic, Ileal	Up	IFNG, TNF, IL-22 (up)		
3	IL32	Interleukin 32	Colonic	Down	IFNG, TNF (up)		
3	AREG	Amphiregulin	Colonic	Down	IFNG (up), IL-13 (down)		
3	TNF	Tumour Necrosis Factor	Colonic, Ileal	Up	TNF, IL-22 (+)	Non-specific: 129 immune cell types (2)	
3	B2M	Beta-2-immunoglobulin	Colonic, Ileal	Down	IFNG (up)		
3	HLA-A	Major Histocompatibility Complex, Class I, A	Colonic, Ileal	Down	IFNG (up)		
3	HLA-B	Major histocompatibility complex, class I, B	Colonic, Ileal	Down	IFNG (up)		
3	LAMB3	Laminin Subunit Beta 3	Colonic	Down			

5. Discussion

In this work, we have developed an integrated framework to model how altered intracellular signalling in epithelial cells drives a different epithelial-immune interactome upon infection. As a proof-of-concept study, we first applied this model to highlight the putative role of the gut during the immune response following SARS-CoV-2 infection, showing how several intracellular and intercellular mechanisms are affected, with key differences between colon and ileum. A visual schematic of our key findings can be found in **Figure 5.10**. Additionally, we proved the applicability of this framework to other tissues of interest by analysing intra and intercellular interactions of the upper airway epithelium in moderate COVID-19 patients (not presented in this thesis), confirming many of the findings highlighted in the literature, and pointing out key cell-cell interactions of interest.

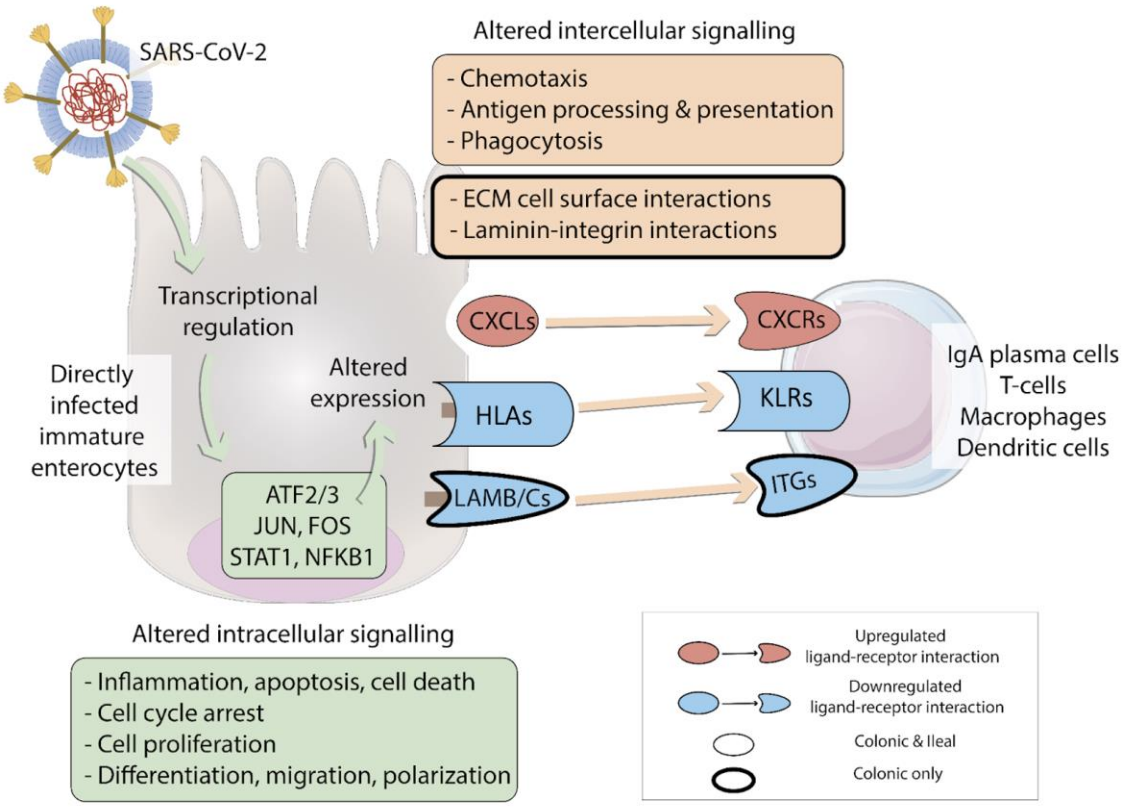

Figure 5.10: Overview of intracellular and intercellular signalling upon SARS-CoV-2 infection of colonic and ileal immature enterocytes and resident immune cells. SARS-CoV-2 directly infects colonic and ileal immature enterocytes. Upon infection, transcription factors ATF2/3, JUN, FOS, STAT1 and NFKB1 are modulated, resulting in altered intracellular signalling pathways and altered ligands expression, including upregulation of chemokines (CXCLs) and human leukocyte antigens (HLAs), and downregulation of laminins (LAMB/Cs). Altered ligands expression drives differential intercellular interactions between epithelial ligands and immune cell receptors (chemokine receptors (CXCRs), killer cell lectin-like receptors (KLRs) and integrins (ITGs)) expressed on immune cells.

SARS-CoV-2 has been shown to actively infect and reproduce in the human gut and in human gastro-intestinal organoids (Lamers et al., 2020; Stanifer et al., 2020; Triana et al., 2021b). However, the exact effect of intestinal inflammation and the role of epithelial-immune interactions in the hyperinflammatory immune response ("cytokine storm") characterising many COVID-19 patients are not known (Arunachalam et al., 2020; Olbei et al., 2021). Accurately modelling these interactions could help identify potential targets that are key to selectively disrupt such cell-cell interactions underlying extreme inflammatory conditions during SARS-CoV-2 infection. This would be extremely important given the failure of most randomised control trials associated with pro-inflammatory drug candidates for COVID-19 (Abubakar et al., 2020).

The altered epithelial-immune cell crosstalk during SARS-CoV-2 infection has been explored within the nasopharynx and lungs using scRNA seq data (Chua et al., 2020). This study found stronger epithelial-immune cell interactions in critically ill patients based on ligand-receptor expression profiles, highlighting the importance of the crosstalk between infected cells and local immune cells in the disease course. However, to our knowledge, no prior study has been carried out so far to investigate the effect of viral infection in host intestinal cells, and the role and contribution of intestinal epithelial cell–immune cell crosstalk during SARS-CoV-2 infection.

In this work, we developed an integrated pipeline to model the effect of intracellular signalling perturbation in epithelial cells on the epithelial-immune interactome in the gut. As a proof-of-concept, we exploited previously published data on SARS-CoV-2 (BavPat1/2020) infection in intestinal organoids (Triana et al., 2021b) to investigate the effect of SARS-CoV-2 proteins and potential miRNAs on ileal and colonic epithelial cell intracellular signalling and function (**Figure 5.1**). Analysis of these potential miRNAs encoded by SARS-CoV-2 was also included, as previous studies highlighted the regulatory role of similar miRNAs produced by RNA viruses and their ability to downregulate host genes and affecting host functions (Bruscella et al., 2017; Griffiths-Jones et al., 2008; Saçar Demirci and Adan, 2020). Furthermore, we modelled how specific epithelial ligands, whose expression was altered upon infection, were driving specific epithelial-immune interactions *via* their altered binding to receptors expressed on resident immune cell populations (**Figure 5.1**) (Martin et al., 2019; Smillie et al., 2019).

While our previous data pointed towards immature enterocytes as the prime target of SARS-CoV-2 infection, the application of our integrated pipeline allowed us to model how this epithelial population, when directly infected, also drives the majority of interactions with gut

resident immune cells stemming from their differentially regulated ligands by SARS-CoV-2 (**Figure 5.2, 5.3**). Upon infection of immature enterocytes, intracellular signalling pathways were altered, with a direct effect on pathways of inflammation, apoptosis, cell survival and cell death (**Figure 5.4A, B**). Pathways related to cell cycle (negative regulation of G2/M transition) and cell proliferation were also altered upon infection (**Figure 5.4A, B**), in line with a previous phosphoproteomics study finding a correlation with cell cycle arrest upon SARS-CoV-2 infection (Bouhaddou et al., 2020). Finally, pathways involved in cell differentiation, cell migration and epithelial polarisation were also modulated upon infection (**Figure 5.4A, B**), which to our knowledge no other study had highlighted before.

By using available ligand-receptor interaction data, we aimed to understand how infected gut epithelial cells recruit resident immune cell populations to find key interactions driving the immune response during infection. Our analysis revealed that IgA plasma cells were the immune cell population with the highest number of cell-cell interactions upon infection in both colon and ileum, with the highest number of epithelial-immune interactions driven by downregulated epithelial ligands (29) in the colon, and upregulated epithelial ligands (20) in the ileum (**Figure 5.3A, B**). Previous studies suggests that IgA is indeed the main type of immunoglobulin induced by mucosal infection of SARS-CoV-2, stressing the importance of the crucial role played by IgA-mediated mucosal immunity in anti-SARS-CoV-2 infection (Sterlin et al., 2021).

Our analysis revealed that in the colon, the highest epithelial-immune interactions were driven by downregulated epithelial ligands (29) (**Figure 5.3A**), with the strongest driven by laminins, HLAs and calmodulins, possibly suggesting a decreased antigen presentation and calcium-dependent activation of these cell types (**Figure 5.5A, 5.7A**). Conversely, in the ileum these interactions were driven by upregulated epithelial ligands (20) (**Figure 5.3B**), with the strongest driven by cytokines/chemokines (TNF-a, CXCLs, CSF1) and adhesion factors (ICAM1, PLAU), possibly suggesting increased recruitment of these cell types to the epithelium (**Figure 5.5B, 5.7B)**. Interestingly, the number of interactions with immune cells was not simply driven by the overall number of SARS-CoV-2 regulated ligands but by a few ligands presenting many different receptors on immune cells, and their relative expression change following infection (**Supplementary Figure 5.7**). Of note, the size of each immune cell population was not taken into account in this analysis (see **Methods**).

By further analysing the specific ligand-receptor interactions driving epithelial-immune crosstalk upon SARS-CoV-2 infection, we could observe that strong upregulated interactions upon infection were mostly shared by both colon and ileum, and were represented by

chemokine and TNF-α driven interactions, possibly reflecting a general effect of the inflammation process (**Figure 5.12A, B and Supplementary Figure 5.6**). Functional analysis highlighted a relation to proinflammatory signalling pathways, including TNF-α signalling, interleukin signalling and chemotaxis *via* GPCR signalling, overall suggesting an increasing recruitment and cell adhesion of these immune cell populations upon infection (**Figure 5.13A, B**). Notably, four chemokine receptors identified by our study (CXCR6 in the ileum, CCR1/2 and CCR9 in both ileum and colon) are coded in a genomic region found to be a COVID-19 risk locus on chromosome 3, further validating our predictions (Schultze and Aschenbrenner, 2021).

Conversely, we could observe that strong downregulated interactions were driven by epithelial HLAs (HLA-A, B, C) and B2M, a subcomponent of the major histocompatibility complex I (MHC I) in both tissues (**Figure 5.5**). According to our analysis, these ligands were mainly binding to KLR receptors, which are mainly presented on NK cells (**Figure 5.6 and 5.7**). Downregulation of HLA-KLR interactions may represent an immune evasion mechanism (Koutsakos et al., 2019) that a recent study proposed as a way SARS-CoV-2 protein ORF8 uses to escape host immune surveillance (Park, 2020).

Uniquely in the colon, strong downregulated interactions were driven by epithelial laminins (LAMB3 and LAMC2) and integrins on immune cells (**Figure 5.5 and 5.6**), with T cells and macrophages as the main immune cell types targeted upon infection (**Figure 5.7**). Laminin-integrin binding contributes to focal adhesion of immune cells to the inflamed tissue (Simon and Bromberg, 2017), and downregulation of laminins could represent an additional strategy for immune evasion following viral infection uniquely in the colon. Furthermore, laminins are known to play a role in shaping the architecture of intestinal mucosa, and an altered expression has been observed in Crohn's disease, a type of IBD, driven by pro-inflammatory cytokines TNF-α and IFN-γ (Bouatrouss et al., 2000; Francoeur et al., 2004; Mahoney et al., 2008).

Finally, calmodulin genes (*CALM1, CALM2, CALM2*) were predicted to drive several downregulated ligand-receptor interactions in both tissues (**Figure 5.5A, B**), mainly binding to cyclic AMP-specific phosphodiesterases (PDEs) (PDE1A, PDE1B, PDE1C) on immune cells in both tissues upon infection (**Figure 5.6A, B and Supplementary Figure 5.7**). PDEs, whose activation is calcium/calmodulin dependent, are responsible for cyclic AMP (cAMP) degradation in T cells, which is a potent inhibitor of T-cell activation (Bjørgo et al., 2011). Hence, the downregulation of CALM-PDEs interactions following SARS-CoV-2 infection implies an increase in intracellular cAMP in T cells, and consequently an inhibition of their

activity. Thus, downregulation of calmodulin-phosphodiesterases could represent another way during SARS-CoV-2 infection to evade the immune activation and viral clearance.

With our integrated framework, we provided a key tool to study the effect of intracellular signalling perturbation in gut epithelial cells driving differential epithelial-immune interactions. By applying this workflow on SARS-CoV-2 infected organoids scRNA seq data, we confirmed many of the previous findings about SARS-CoV-2 infection, including the induced pro-inflammatory responses driven by chemokines and the role played by T cells **(Figure 5.10)**. Additionally, we uncovered mechanisms by which SARS-CoV-2 may evade the immune responses by interfering with epithelial-immune cell connections. Such mechanisms include downregulation of antigen presentation mediated by HLAs-KLR interactions and of focal adhesion pathways mediated by laminin-integrins interactions **(Figure 5.10).** Finally, I highlighted a set of intestinal epithelial ligands and immune cell populations implicated in altered epithelial-immune interactions during SARS-CoV-2 infection, which could potentially drive the excessive inflammatory processes seen in severe COVID-19 patients **(Table 5.1).**

Despite the interesting findings, the presented analysis presents some limitations. When constructing the intracellular causal network, the effect of SARS-CoV-2 proteins towards human binding partners was always considered as inhibitory. However, this is not always the case. Furthermore, two different single cell transcriptomics datasets were used for colonic and ileal immune cell populations, due to the unavailability of both datasets from the same experiment. Similarly, IBD uninflamed data and healthy data were used for the ileum and colon respectively, as healthy control scRNAseq immune cell data for both tissues was not available at the time of the analysis. Finally, the *a priori* resources used to infer the intracellular and intercellular interaction networks may have some intrinsic limitations associated with them (Dimitrov et al., 2022).

6. Future research directions

With our integrated workflow, we established a computational method to evaluate the effect of viral infection on host intestinal epithelial cell functions and how this consequently modulates the epithelial-immune crosstalk and immune activation during SARS-CoV-2 infection. Although not included in this thesis, I further demonstrated the applicability of this workflow to other tissues by modelling the intracellular and intercellular signalling of upper airway epithelial cells in moderate COVID-19 cases. Results of this analysis confirmed several findings

previously highlighted in the literature, and more details can be found in the published article (see **Appendix 3**).

Our analysis presented some limitations, mainly related to the data availability when the analysis was carried out, as presented in the discussion. For instance, the effect of SARS-CoV-2 proteins on human binding partners has always been considered as inhibitory due to the lack of available information. Furthermore, a scRNAseq of immune cells from a healthy donor was used, instead of a SARS-CoV-2 infected one. Since the beginning of the COVID-19 pandemic, several more studies have been published, further assessing the effect of SARS-CoV-2 on the host. In the future, adding increasingly available datasets to this presented workflow, could help refine predictions about upstream perturbations as well as targeted immune cell types, overall resulting in a more accurate model.

In addition to the input datasets used, the motivation to make these analyses available to the community in the shortest time possible, resulted in the use of a limited selection of *a priori* network resources and methods to infer intracellular and intercellular interaction networks. However, each of these resources has intrinsic limitations associated with them (Dimitrov et al., 2022). In future studies, this integrated analysis could be repeated by including other resources available in the community, and using specific tools such as the LIgand-receptor ANalysis frAmework (LIANA) to compare across several resources available, helping to choose the one(s) providing the best overall prediction (Dimitrov et al., 2022).

Other changes to the model could also be implemented to further refine the presented bioinformatics predictions. For instance, the overall size of immune cell populations was not considered. Future analyses could improve our predictions by obtaining the information about different proportions of immune cells from the scRNAseq dataset used, and use it to normalise the identified intercellular interactions. Hence, extension of the study in this way could refine the importance of each type of ligand-receptor communication in mediating the overall downstream functional changes, leading to a better prediction of the effect size for each ligand-receptor combination.

Finally, future studies should be done to experimentally validate the bioinformatics predictions, to confirm the main processes, molecules and cell types involved. For this purpose, the presented immune evasion mechanisms including the downregulation of antigen-presentation interactions and calcium signalling could be an interesting mechanisms to start with. To enable such validations, intestinal organoids represent an excellent *in vitro* model (Kim et al., 2020). Currently, introduction of immune cells to an organoid system is a challenging task. Yet, a

recent study where human intestinal CD4+ T cells have been co-cultured with human intestinal organoids (Schreurs et al., 2021), may represent a promising set-up for future studies to investigate epithelial-immune cell interactions during SARS-CoV-2 induced inflammation in the gut. As explained in my published review on organoids (see **Appendix 3**) or reviewed elsewhere (Min et al., 2020), such co-culture systems could be excellent to study intestinal host-microbe interactions, including the detailed experimental analysis of SARS-CoV-2 infection.

To conclude with, our analysis was a starting point to decipher the effects of SARS-CoV-2 on intestinal epithelial cell function in the colon and ileum, and the role of the gut in propagating inflammation during infection. In the future, the increasing availability of scRNAseq datasets, a more detailed analysis encompassing other developed resources to infer signalling networks, and the experimental validation of bioinformatics prediction using organoids co-cultured with immune cells, will allow further elucidation of the key role played by the gut during COVID-19 (or other infectious diseases), including description of the main cell types and mechanisms involved. Eventually, we hope that this will lead to better understanding of the patho-mechanism of the disease and possibly improved treatment strategies.

Chapter 6: Integrated Discussion

Maintenance of gut homeostasis relies on a complex interplay between the gut microbiota, the intestinal epithelium, and immune cells. The intestinal microbiota, by interacting with the epithelium of the gut through metabolites or other released factors (Earle et al., 2015; Geva-Zatorsky et al., 2015; Peterson and Artis, 2014), takes part in various processes including the maintenance of intestinal barrier functions and integrity (Earle et al., 2015; Geva-Zatorsky et al., 2015), modulation of the host immune system (Zelante et al., 2013), and prevention of colonisation from pathogens (Zelante et al., 2013). Conversely, the intestinal epithelium also plays a key role by acting as a physical barrier as well as coordinating the immune defence and crosstalk between bacterial and immune cells (Allaire et al., 2018). Understanding the mechanisms behind the crosstalk between gut microbiota members and host epithelial cells is therefore crucial to maintain health.

Among gut microbiota members, *Bifidobacterium* has shown promising results towards the protection against a range of diseases, including IBD. Evidence suggests that this probiotic bacterium can affect several cellular processes in intestinal epithelial cells, thereby promoting health. However, the specific bacterial modulating factors as well as the specific mechanisms and host targets involved in these effects are largely unknown. Hence, investigating the interactions between bifidobacteria and epithelial cells in the gut is key to understanding the mechanisms behind the beneficial effects of bifidobacteria on gut health.

However, studying host-microbe interactions *in vitro* can be challenging. To this regard, organoid models have been proposed as a key tool allowing to investigate interactions between microbes and epithelial cells in a physiological relevant manner. Organoid models are still in their infancy, and several optimisations are required for their exposure to anaerobic microbes such as bifidobacteria, and to allow molecular applications to decipher mechanisms involved in bifidobacteria-host interactions.

Throughout my thesis, several outcomes were achieved to address these research gaps:

- In **Chapter 1,** in addition to the already existing literature, I provided the community with a comprehensive review of organoid-based *ex vivo* models available to investigate the effect of microbiota on the intestinal epithelium, and discover novel microbial therapies, with a special focus on IBD (see **Appendix 3**). Several downstream applications such as high-throughput microbial screening and 'omics technologies

were presented, highlighting their potential to gain better mechanistic insights into the microbial-host crosstalk in the gut.

- In **Chapter 2**, I developed or optimised protocols and culture conditions for the establishment of organoid-microbe co-cultures, with a focus on bifidobacteria. Furthermore, protocols for downstream applications such as immunostaining and RNA sequencing were optimised for their use to decipher molecular mechanisms behind the beneficial effects of bifidobacteria on the epithelium, in particular autophagy.

- In **Chapter 3,** a Caco-2 monolayer co-culture system was set up to study the protective effects of *B. breve* UCC2003 and *B. longum* LH206-derived metabolites on intestinal barrier integrity, epithelial cell viability and pro-inflammatory cytokine release, as well as autophagy processes. Results demonstrated small beneficial effects towards an increase in barrier function and autophagy flux in the absence of inflammation, and reduction of loss of cell viability and barrier function in the presence of inflammation.

- In **Chapter 4,** a patient colonic organoid co-culture system was established to investigate the effects of *B. breve* UCC2003-derived metabolites on intestinal epithelial cell function during epithelial differentiation. Results highlighted patient-specific differences to bacterial treatment, and found *Bifidobacterium*-specific effects, including an enhanced epithelial differentiation and barrier function *via* epigenetics mechanisms, and downregulation of cholesterol biosynthesis.

- In **Chapter 5,** as an additional COVID-related project outside my PhD scope, I have provided the scientific community with integrated computational method to evaluate the effect of SARS-CoV-2 viral infection on host epithelial cell function in the gut, and how this consequently modulates the epithelial-immune crosstalk during infection (see **Appendix 3**). Results pointed out tissue-specific differences in response to infection, as well as several pro-inflammatory pathways modulated in epithelial cells. Furthermore, modified intercellular interactions driven by altered epithelial ligand expression were identified, possibly driving systemic inflammatory responses, and representing a way SARS-CoV-2 may use to evade the immune system.

One goal of my PhD was to advance the use of organoids to study microbe-host interactions in the gut. In **Chapter 2**, I described methods developed to establish mouse and human organoid models and generate readouts that could be used to investigate host-microbe interactions, including apical out organoids and organoid-derived monolayers. In **Chapter 4,** I built on this work and showed how (3D) organoid models can be used to investigate the effects of bifidobacteria on intestinal epithelial cell function. One limitation of the 3D organoid model

used is that only basolateral interactions could be evaluated, while bacteria-host interactions generally happen at the apical surface. In the future, apical out organoids and organoid-derived monolayers could be used to evaluate apical interactions. In **Chapter 2,** I worked on improving the establishment and characterisation of these models, yet I did not manage to employ them for the mechanistic study presented in **Chapter 4,** due to several associated limitations. For apical-out organoids, the reversion process is not always complete, and further characterisation is needed to assess whether all the cell types and tissue architecture are present as *in vivo* tissue (Co et al., 2019; Stroulios et al., 2021). While organoid-derived monolayers represent a much better characterised model, a high quantity of starting organoid material is required for their establishment, and these models are not fully differentiated, which made it more difficult to look at the effect of bifidobacterial-derived metabolites during epithelial maturation (Poletti et al., 2021).

One of the hypotheses behind my PhD was that *Bifidobacterium* spp. affected cellular processes in intestinal epithelial cells, thus exerting a beneficial effect on the host. In **Chapter 3**, I found using Caco-2 monolayer model that two strains of bifidobacteria, *B. breve* UCC2003 and *B. longum* LH206 had a beneficial effect against loss of epithelial barrier during inflammation. Furthermore, in **Chapter 4**, using human colonic organoid models, I elucidated mechanisms of action behind the beneficial effects of *B. breve* UCC2003 on intestinal epithelial cell function during epithelial differentiation. In particular, I highlighted its role in affecting epithelial cell differentiation *via* epigenetic regulation of WNT-dependent pathways, thereby contributing to enhanced intestinal maturation. Furthermore, I elucidated a previously unknown mechanism by which bifidobacteria may exert their cholesterol-lowering effects by the downregulation of cholesterol biosynthesis *via* the inhibition of SREBF1/2-target genes.

In this thesis, I studied the effect of bifidobacterial-derived metabolites on the whole epithelium. However, future studies should also focus on the cell-type specific effect of bifidobacterial metabolites. In **Chapter 4**, I found that exposure with *B. breve* UCC2003-derived metabolites upregulated markers of enterocytes, transit-amplifying and M cells, while downregulating markers of goblet and tuft cells in healthy colonic organoids during differentiation. Because of the bulk transcriptomics, we could not identify the effect on the transcriptomics profiles of specific cell types. However, as indicated throughout the thesis, many methods exist to study the effect on specific cell types. These include the use of cell-type enriched organoids and fluorescence activated cell sorting (Fujii et al., 2018; Jones et al., 2019; Park et al., 2018), or single cell technologies (Tang et al., 2019). During my PhD, I worked on developing a methodology to quantify epithelial cells from mouse ileal organoids based on specific

intracellular and cell membrane markers. Yet, results were not satisfactory enough and the used markers would need to be optimised to use this methodology in the future.

One important mechanism to maintain gut homeostasis and intestinal cell function is represented by autophagy, a cellular degradation mechanism important for intestinal homeostasis and maintenance of barrier function. **In Chapter 4**, I found that *B. breve* UCC2003 and *B. longum* LH206 had a small effect on the autophagy flux, quantified by looking at p62 and LC3 puncta in a Caco-2 cell model. Furthermore, when studying the effect of *B. breve* UCC2003 on autophagy-related genes using human colonic organoids, a very small effect was found. These results could be due to autophagy being regulated at the post-transcriptional and post-translational level, rather than the measured transcriptional level. Further studies using proteomics and phosphoproteomics data could help elucidate the effect of these strains on autophagy processes. Furthermore, autophagy is not a static process and the use of autophagy reporter lines in combination with live cell imaging will be key to monitor autophagy flux over time within epithelial cells.

Throughout this thesis, I looked at the effect of bifidobacterial-derived metabolites on the epithelium only, instead of looking at the effect of the whole bacteria. This approach could involve some limitations, as *B. breve* UCC2003 membrane components such as the EPS could be responsible for its effects on intestinal cells, as described in **Chapter 1**. Furthermore, the effect of metabolites and their change was not evaluated during the co-culture period, as metabolites were collected in bacterial media before the experiment. To study the effect of whole bacteria and/or real-time metabolite production, microfluidics devices such as the gut-on-chip or HuMiX could be used, respectively (Kasendra et al., 2018; Shah et al., 2016). Yet, both systems bring along some limitations including the high initial material required, high-associated cost, and reduced application for high-throughput experiments. In the future, easier accessibility to these devices could allow their use for bifidobacteria-host interaction studies, resulting in better evaluation of the effect of bacterial components and real-time metabolite production on host intestinal epithelial cells.

In this thesis, the effect of *Bifidobacterium* metabolites in the context of inflammation using Caco-2 models, or without the presence of inflammation using organoids was evaluated (**Chapter 3, 4**). Previous studies have shown a differential response of epithelial cells to bacterial-derived SCFAs in the presence/absence of inflammation (Vancamelbeke et al., 2019), showing the need to compare the role of host-microbe interactions with and without an inflammatory state. For instance, this may be important when looking at the effect of bifidobacteria during inflammatory gut diseases such as IBD. Interestingly, a recent study has

shown that exposure of organoids to a defined inflammatory mix is able to re-induce the inflammatory phenotype while maintaining organoid patient specificity (Arnauts et al., 2020). Hence, future studies looking at the beneficial effects of bifidobacteria should introduce an inflammatory condition in their work to obtain more valid results. Furthermore, in both studies, immune cells were absent. As seen in **Chapter 5**, resident immune populations are crucial to mediate the signal from viral components in the gut, and a similar conclusion could be made for bacterial-derived metabolites. Hence, introducing resident immune populations within a Transwell model or microfluidics device would be crucial for future studies elucidating the role of microbiota-host interactions.

In addition to the biological findings, I have shown through two projects how molecular networks can be used to extract biological insights from transcriptomics datasets. In **Chapter 4**, I reconstructed regulatory networks and protein-protein interaction networks to study the effect on upstream transcriptional regulators and first neighbours of altered proteins upon *B. breve* UCC2003-derived metabolites. Furthermore, I predicted which bifidobacterial-derived metabolites are responsible for these effects. For prediction of bacterial metabolites, I used the GutMGene database, collecting validated relationships between gut microbial metabolites and their host mammalian target genes (Cheng et al., 2022). However, the number of metabolites collected in this database is very limited, and mainly consists of association relationships, rather than predictions or validation of direct interactions between a specific metabolite and its receptor in intestinal cells. For bacterial proteins, databases generally exist collating information about domain-domain (DDIs) or domain-motifs interactions (DMIs) between bacterial and human proteins such as DOMINE for DDIs (Raghavachari et al., 2008; Yellaboina et al., 2011) and Eukaryotic Linear Motif (ELM) database for DMIs (Dinkel et al., 2016; Korcsmaros et al., 2013; Puntervoll et al., 2003). However, not enough information is present in these databases on *B. breve* UCC2003 or related bacterial species. Alternatively, computational predictions can also be used to infer DDIs (Raghavachari et al., 2008, Yellaboina et al., 2011) and DMIs (Gibson et al., 2015) using the structural information of interacting proteins. For the work of this thesis, not enough structural information about *B. breve* UCC2003 proteins was available to carry out such predictions. Yet, the increasing efforts being made by companies such as DeepMind and Meta to predict structures of uncharacterised bacterial proteins using artificial-intelligence will make these types of predictions more accessible in the future (Jumper et al., 2021; Lin et al., 2022; Varadi et al., 2022).

In **Chapter 5**, I further extended the study of PPI and regulatory interactions in healthy colonic cells and microbes by reconstructing causal networks linking the binding of SARS-CoV

proteins or miRNAs to human receptors and transcriptional changes happening during SARS-CoV-2 infection. Due to time constraints, only two network propagation tools, ViralLink and CARNIVAL, were used. However, many more tools exist to build these molecular networks, with associated limitations, and future studies should include a broader number of tools and compare the results obtained to choose the most optimised solution (Garrido-Rodriguez et al., 2022; Picart-Armada et al., 2019). Additionally, intercellular interaction networks were constructed to connect altered ligands in immature enterocytes during infection to their corresponding receptors on immune cell populations using the OmniPath database (Turei et al., 2021; Türei et al., 2016). Limitations of this analysis include the use of two distinct datasets for colon and ileum, the use of a healthy immune cell data instead of infected one, and not considering the size of the immune population when studying epithelial-immune interactions. Future analyses should improve the type of input data used, and diversify the method used to infer the intercellular interactions, including their normalisation for the size of target cell populations (Dimitrov et al., 2022)**.**

Through the work covered in this thesis, I developed experimental models and techniques to characterise different parameters in organoids that will continue to be used in the research groups for future projects. Furthermore, following the methodology used in **Chapter 4** and the publication of **Chapter 5**, I hope that more and more researchers will use a combination of experimental and computational approaches with network-based methods in their work. In particular, the research presented in this PhD highlights the benefits and accessibility of these methods to unravel mechanisms of action and the role in the gut of probiotic bacteria such as *Bifidobacterium* during health and disease.

In conclusion, this PhD research has contributed to the optimisation of intestinal organoid model for host-microbe interactions studies and the mechanistic understanding of the effect of bifidobacteria on the colonic epithelium during health and inflammation, as well as the interplay between SARS-CoV-2, the intestinal epithelium, and immune cells during viral infection. At the same time, it contributed to the use of network biology for the interpretation of transcriptomics data and the study of host-microbe interactions in the gut. Findings highlighted in this thesis represent a starting point for future in depth mechanistic and experimental validation studies. Ultimately, this research will lead to a better understanding of the beneficial effects of bifidobacteria in the gut and the mechanisms behind these effects, which will drive targeted approaches for their use for prevention and treatment of gut diseases such as IBD.

References

Abubakar, A. R., Sani, I. H., Godman, B., Kumar, S., Islam, S., Jahan, I. and Haque, M. (2020). Systematic Review on the Therapeutic Options for COVID-19: Clinical Evidence of Drug Efficacy and Implications. *Infect. Drug Resist.* 13, 4673–4695.

Aden, K., Tran, F., Ito, G., Sheibani-Tezerji, R., Lipinski, S., Kuiper, J. W., Tschurtschenthaler, M., Saveljeva, S., Bhattacharyya, J., Häsler, R., et al. (2018). ATG16L1 orchestrates interleukin-22 signaling in the intestinal epithelium via cGAS-STING. *J. Exp. Med.* 215, 2868–2886.

Adolph, T. E., Tomczak, M. F., Niederreiter, L., Ko, H.-J., Böck, J., Martinez-Naves, E., Glickman, J. N., Tschurtschenthaler, M., Hartwig, J., Hosomi, S., et al. (2013). Paneth cells as a site of origin for intestinal inflammation. *Nature* 503, 272–276.

Agus, A., Clément, K. and Sokol, H. (2021). Gut microbiota-derived metabolites as central regulators in metabolic disorders. *Gut* 70, 1174–1182.

Akay, H. K., Bahar Tokman, H., Hatipoglu, N., Hatipoglu, H., Siraneci, R., Demirci, M., Borsa, B. A., Yuksel, P., Karakullukcu, A., Kangaba, A. A., et al. (2014). The relationship between bifidobacteria and allergic asthma and/or allergic dermatitis: a prospective study of 0-3 years-old children in Turkey. *Anaerobe* 28, 98–103.

Alessandri, G., Ossiprandi, M. C., MacSharry, J., van Sinderen, D. and Ventura, M. (2019). Bifidobacterial dialogue with its human host and consequent modulation of the immune system. *Front. Immunol.* 10, 2348.

All-in-one approach to culture, image and quantify large numbers of organoids at all scales. (2022). *Nat. Methods* 19, 799–800.

Allaire, J. M., Crowley, S. M., Law, H. T., Chang, S.-Y., Ko, H.-J. and Vallance, B. A. (2018). The intestinal epithelium: central coordinator of mucosal immunity. *Trends Immunol.* 39, 677–696.

Allen-Vercoe, E. (2013). Bringing the gut microbiota into focus through microbial culture: recent progress and future perspective. *Curr. Opin. Microbiol.* 16, 625–629.

Alsehli, H., Mosis, F., Thompson, C., Hamrud, E., Wiseman, E., Gentleman, E. and Danovi, D. (2020). An integrated pipeline for high-throughput screening and profiling of spheroids using simple live image analysis of frame to frame variations. *Methods*.

Alvarez-Martin, P., O'Connell Motherway, M., Turroni, F., Foroni, E., Ventura, M. and van Sinderen, D. (2012). A two-component regulatory system controls autoregulated serpin expression in Bifidobacterium breve UCC2003. *Appl. Environ. Microbiol.* 78, 7032–7041.

Alvarez, M. J., Shen, Y., Giorgi, F. M., Lachmann, A., Ding, B. B., Ye, B. H. and Califano, A. (2016). Functional characterization of somatic mutations in cancer using network-based inference of protein activity. *Nat. Genet.* 48, 838–847.

Arboleya, S., Watkins, C., Stanton, C. and Ross, R. P. (2016). Gut bifidobacteria populations in human health and aging. *Front. Microbiol.* 7, 1204.

Arenas-Padilla, M., González-Rascón, A., Hernández-Mendoza, A., Calderón de la Barca, A. M., Hernández, J. and Mata-Haro, V. (2022). Immunomodulation by Bifidobacterium

animalis subsp. lactis Bb12: Integrative Analysis of miRNA Expression and TLR2 Pathway-Related Target Proteins in Swine Monocytes. *Probiotics Antimicrob. Proteins* 14, 510–522.

Arnauts, K., Verstockt, B., Santo Ramalho, A., Vermeire, S., Verfaillie, C. and Ferrante, M. (2020). Ex vivo mimicking of inflammation in organoids derived from patients with ulcerative colitis. *Gastroenterology*.

Arunachalam, P. S., Wimmers, F., Mok, C. K. P., Perera, R. A. P. M., Scott, M., Hagan, T., Sigal, N., Feng, Y., Bristow, L., Tak-Yin Tsang, O., et al. (2020). Systems biological assessment of immunity to mild versus severe COVID-19 infection in humans. *Science* 369, 1210–1220.

Ashburner, M., Ball, C. A., Blake, J. A., Botstein, D., Butler, H., Cherry, J. M., Davis, A. P., Dolinski, K., Dwight, S. S., Eppig, J. T., et al. (2000). Gene Ontology: tool for the unification of biology. *Nat. Genet.* 25, 25–29.

Astolfi, M., Péant, B., Lateef, M. A., Rousset, N., Kendall-Dupont, J., Carmona, E., Monet, F., Saad, F., Provencher, D., Mes-Masson, A. M., et al. (2016). Micro-dissected tumor tissues on chip: an ex vivo method for drug testing and personalized therapy. *Lab Chip* 16, 312–325.

Atallah, M. B., Tandon, V., Hiam, K. J., Boyce, H., Hori, M., Atallah, W., Spitzer, M. H., Engleman, E. and Mallick, P. (2020). ImmunoGlobe: enabling systems immunology with a manually curated intercellular immune interaction network. *BMC Bioinformatics* 21, 346.

Auclair, B. A., Benoit, Y. D., Rivard, N., Mishina, Y. and Perreault, N. (2007). Bone morphogenetic protein signaling is essential for terminal differentiation of the intestinal secretory cell lineage. *Gastroenterology* 133, 887–896.

Azcárate-Peril, M. A., Sikes, M. and Bruno-Bárcena, J. M. (2011). The intestinal microbiota, gastrointestinal environment and colorectal cancer: a putative role for probiotics in prevention of colorectal cancer? *Am. J. Physiol. Gastrointest. Liver Physiol.* 301, G401-24.

Bäckhed, F., Ley, R. E., Sonnenburg, J. L., Peterson, D. A. and Gordon, J. I. (2005). Host-bacterial mutualism in the human intestine. *Science* 307, 1915–1920.

Banerjee, A., McKinley, E. T., von Moltke, J., Coffey, R. J. and Lau, K. S. (2018). Interpreting heterogeneity in intestinal tuft cell structure and function. *J. Clin. Invest.* 128, 1711–1719.

Barker, N. (2014). Adult intestinal stem cells: critical drivers of epithelial homeostasis and regeneration. *Nat. Rev. Mol. Cell Biol.* 15, 19–33.

Barker, N., Huch, M., Kujala, P., van de Wetering, M., Snippert, H. J., van Es, J. H., Sato, T., Stange, D. E., Begthel, H., van den Born, M., et al. (2010). Lgr5(+ve) stem cells drive self-renewal in the stomach and build long-lived gastric units in vitro. *Cell Stem Cell* 6, 25–36.

Barker, N., van de Wetering, M. and Clevers, H. (2008). The intestinal stem cell. *Genes Dev.* 22, 1856–1864.

Barker, N., van Es, J. H., Kuipers, J., Kujala, P., van den Born, M., Cozijnsen, M., Haegebarth, A., Korving, J., Begthel, H., Peters, P. J., et al. (2007). Identification of stem cells in small intestine and colon by marker gene Lgr5. *Nature* 449, 1003–1007.

Bartel, D. P. (2018). Metazoan MicroRNAs. *Cell* 173, 20–51.

Bartfeld, S. (2016). Modeling infectious diseases and host-microbe interactions in gastrointestinal organoids. *Dev. Biol.* 420, 262–270.

Bartfeld, S. and Clevers, H. (2015). Organoids as model for infectious diseases: culture of human and murine stomach organoids and microinjection of helicobacter pylori. *J. Vis. Exp.*

Bartfeld, S., Bayram, T., van de Wetering, M., Huch, M., Begthel, H., Kujala, P., Vries, R., Peters, P. J. and Clevers, H. (2015). In vitro expansion of human gastric epithelial stem cells and their responses to bacterial infection. *Gastroenterology* 148, 126-136.e6.

Basak, O., Beumer, J., Wiebrands, K., Seno, H., van Oudenaarden, A. and Clevers, H. (2017). Induced Quiescence of Lgr5+ Stem Cells in Intestinal Organoids Enables Differentiation of Hormone-Producing Enteroendocrine Cells. *Cell Stem Cell* 20, 177-190.e4.

Beal, J. (2017). Biochemical complexity drives log-normal variation in genetic expression. *Eng. biol.* 1, 55–60.

Beck, L. C., Masi, A. C., Young, G. R., Vatanen, T., Lamb, C. A., Smith, R., Coxhead, J., Butler, A., Marsland, B. J., Embleton, N. D., et al. (2022). Strain-specific impacts of probiotics are a significant driver of gut microbiome development in very preterm infants. *Nat. Microbiol.* 7, 1525–1535.

Becker, S., Oelschlaeger, T. A., Wullaert, A., Vlantis, K., Pasparakis, M., Wehkamp, J., Stange, E. F. and Gersemann, M. (2013). Bacteria regulate intestinal epithelial cell differentiation factors both in vitro and in vivo. *PLoS ONE* 8, e55620.

Bel, S., Pendse, M., Wang, Y., Li, Y., Ruhn, K. A., Hassell, B., Leal, T., Winter, S. E., Xavier, R. J. and Hooper, L. V. (2017). Paneth cells secrete lysozyme via secretory autophagy during bacterial infection of the intestine. *Science* 357, 1047–1052.

Ben-Shlomo, I., Yu Hsu, S., Rauch, R., Kowalski, H. W. and Hsueh, A. J. W. (2003). Signaling receptome: a genomic and evolutionary perspective of plasma membrane receptors involved in signal transduction. *Sci. STKE* 2003, RE9.

Beumer, J., Artegiani, B., Post, Y., Reimann, F., Gribble, F., Nguyen, T. N., Zeng, H., Van den Born, M., Van Es, J. H. and Clevers, H. (2018). Enteroendocrine cells switch hormone expression along the crypt-to-villus BMP signalling gradient. *Nat. Cell Biol.* 20, 909–916.

Bevins, C. L. and Salzman, N. H. (2011). Paneth cells, antimicrobial peptides and maintenance of intestinal homeostasis. *Nat. Rev. Microbiol.* 9, 356–368.

Bezirtzoglou, E., Tsiotsias, A. and Welling, G. W. (2011). Microbiota profile in feces of breast- and formula-fed newborns by using fluorescence in situ hybridization (FISH). *Anaerobe* 17, 478–482.

Bhat, S. A., Ahmad, S. M., Mumtaz, P. T., Malik, A. A., Dar, M. A., Urwat, U., Shah, R. A. and Ganai, N. A. (2016). Long non-coding RNAs: Mechanism of action and functional utility. *Noncoding RNA Res* 1, 43–50.

Bjerknes, M. and Cheng, H. (2006). Intestinal epithelial stem cells and progenitors. *Meth. Enzymol.* 419, 337–383.

Bjørgo, E., Moltu, K. and Taskén, K. (2011). Phosphodiesterases as targets for modulating T-cell responses. *Handb. Exp. Pharmacol.* 345–363.

Blanco-Melo, D., Nilsson-Payant, B. E., Liu, W.-C., Uhl, S., Hoagland, D., Møller, R., Jordan, T. X., Oishi, K., Panis, M., Sachs, D., et al. (2020). Imbalanced Host Response to SARS-CoV-2 Drives Development of COVID-19. *Cell* 181, 1036-1045.e9.

Bouatrouss, Y., Herring-Gillam, F. E., Gosselin, J., Poisson, J. and Beaulieu, J. F. (2000). Altered expression of laminins in Crohn's disease small intestinal mucosa. *Am. J. Pathol.* 156, 45–50.

Bouhaddou, M., Memon, D., Meyer, B., White, K. M., Rezelj, V. V., Correa Marrero, M., Polacco, B. J., Melnyk, J. E., Ulferts, S., Kaake, R. M., et al. (2020). The Global Phosphorylation Landscape of SARS-CoV-2 Infection. *Cell* 182, 685-712.e19.

Bovolenta, L. A., Acencio, M. L. and Lemke, N. (2012). HTRIdb: an open-access database for experimentally verified human transcriptional regulation interactions. *BMC Genomics* 13, 405.

Bozzetti, V. and Senger, S. (2022). Organoid technologies for the study of intestinal microbiota-host interactions. *Trends Mol. Med.* 28, 290–303.

Brandenberg, N., Hoehnel, S., Kuttler, F., Homicsko, K., Ceroni, C., Ringel, T., Gjorevski, N., Schwank, G., Coukos, G., Turcatti, G., et al. (2020). High-throughput automated organoid culture via stem-cell aggregation in microcavity arrays. *Nat. Biomed. Eng.* 4, 863–874.

Brandtzaeg, P. (2017). Role of the intestinal immune system in health. In *Crohn's disease and ulcerative colitis* (ed. Baumgart, D. C.), pp. 23–56. Cham: Springer International Publishing.

Brattås, P. L., Hersbach, B. A., Madsen, S., Petri, R., Jakobsson, J. and Pircs, K. (2021). Impact of differential and time-dependent autophagy activation on therapeutic efficacy in a model of Huntington disease. *Autophagy* 17, 1316–1329.

Braverman, J. and Yilmaz, Ö. H. (2018). From 3D Organoids back to 2D Enteroids. *Dev. Cell* 44, 533–534.

Brazovskaja, A., Treutlein, B. and Camp, J. G. (2019). High-throughput single-cell transcriptomics on organoids. *Curr. Opin. Biotechnol.* 55, 167–171.

Bromke, M. A. and Krzystek-Korpacka, M. (2021). Bile acid signaling in inflammatory bowel disease. *Int. J. Mol. Sci.* 22,.

Brückner, A., Polge, C., Lentze, N., Auerbach, D. and Schlattner, U. (2009). Yeast two-hybrid, a powerful tool for systems biology. *Int. J. Mol. Sci.* 10, 2763–2788.

Bruscella, P., Bottini, S., Baudesson, C., Pawlotsky, J.-M., Feray, C. and Trabucchi, M. (2017). Viruses and miRNAs: More friends than foes. *Front. Microbiol.* 8, 824.

Buchanan, M., Caldarelli, G., De Los Rios, P., Rao, F. and Vendruscolo, M. eds. (2010). *Networks in cell biology*. Cambridge University Press.

Bues, J., Biočanin, M., Pezoldt, J., Dainese, R., Chrisnandy, A., Rezakhani, S., Saelens, W., Gardeux, V., Gupta, R., Sarkis, R., et al. (2022). Deterministic scRNA-seq captures variation in intestinal crypt and organoid composition. *Nat. Methods* 19, 323–330.

Bui, T. M., Mascarenhas, L. A. and Sumagin, R. (2018). Extracellular vesicles regulate immune responses and cellular function in intestinal inflammation and repair. *Tissue Barriers* 6, e1431038.

Bui, T. M., Mascarenhas, L. A. and Sumagin, R. (2018). Extracellular vesicles regulate immune responses and cellular function in intestinal inflammation and repair. *Tissue Barriers* 6, e1431038.

Bunesova, V., Lacroix, C. and Schwab, C. (2018). Mucin Cross-Feeding of Infant Bifidobacteria and Eubacterium hallii. *Microb. Ecol.* 75, 228–238.

Caballero-Franco, C., Keller, K., De Simone, C. and Chadee, K. (2007). The VSL#3 probiotic formula induces mucin gene expression and secretion in colonic epithelial cells. *Am. J. Physiol. Gastrointest. Liver Physiol.* 292, G315-22.

Cabrera, S., Maciel, M., Herrera, I., Nava, T., Vergara, F., Gaxiola, M., López-Otín, C., Selman, M. and Pardo, A. (2015). Essential role for the ATG4B protease and autophagy in bleomycin-induced pulmonary fibrosis. *Autophagy* 11, 670–684.

Cadwell, K., Liu, J. Y., Brown, S. L., Miyoshi, H., Loh, J., Lennerz, J. K., Kishi, C., Kc, W., Carrero, J. A., Hunt, S., et al. (2008). A key role for autophagy and the autophagy gene Atg16l1 in mouse and human intestinal Paneth cells. *Nature* 456, 259–263.

Cadwell, K., Patel, K. K., Komatsu, M., Virgin, H. W. and Stappenbeck, T. S. (2009). A common role for Atg16L1, Atg5 and Atg7 in small intestinal Paneth cells and Crohn disease. *Autophagy* 5, 250–252.

Cadwell, K., Patel, K. K., Maloney, N. S., Liu, T.-C., Ng, A. C. Y., Storer, C. E., Head, R. D., Xavier, R., Stappenbeck, T. S. and Virgin, H. W. (2010). Virus-plus-susceptibility gene interaction determines Crohn's disease gene Atg16L1 phenotypes in intestine. *Cell* 141, 1135–1145.

Campbell, N. A., Reece, J. B., Urry, L. A., Cain, M. L., Wasserman, S. A., Minorsky, P. V. and Jackson, R. B. *Biology, 8th Edition*.

Castro-Bravo, N., Margolles, A., Wells, J. M. and Ruas-Madiedo, P. (2019). Exopolysaccharides synthesized by Bifidobacterium animalis subsp. lactis interact with TLR4 in intestinal epithelial cells. *Anaerobe* 56, 98–101.

Castro, D. M., de Veaux, N. R., Miraldi, E. R. and Bonneau, R. (2019). Multi-study inference of regulatory networks for more accurate models of gene regulation. *PLoS Comput. Biol.* 15, e1006591.

Chai, L. E., Loh, S. K., Low, S. T., Mohamad, M. S., Deris, S. and Zakaria, Z. (2014). A review on the computational approaches for gene regulatory network construction. *Comput. Biol. Med.* 48, 55–65.

Chan, T. E., Stumpf, M. P. H. and Babtie, A. C. (2017). Gene Regulatory Network Inference from Single-Cell Data Using Multivariate Information Measures. *Cell Syst.* 5, 251-267.e3.

Chang, M.-S., Chen, B.-C., Yu, M.-T., Sheu, J.-R., Chen, T.-F. and Lin, C.-H. (2005). Phorbol 12-myristate 13-acetate upregulates cyclooxygenase-2 expression in human pulmonary epithelial cells via Ras, Raf-1, ERK, and NF-kappaB, but not p38 MAPK, pathways. *Cell. Signal.* 17, 299–310.

Chapman, C. G. and Pekow, J. (2015). The emerging role of miRNAs in inflammatory bowel disease: a review. *Therap. Adv. Gastroenterol.* 8, 4–22.

Chen, L., Toke, N. H., Luo, S., Vasoya, R. P., Fullem, R. L., Parthasarathy, A., Perekatt, A. O. and Verzi, M. P. (2019). A reinforcing HNF4-SMAD4 feed-forward module stabilizes enterocyte identity. *Nat. Genet.* 51, 777–785.

Chen, Y.-M., Chang, C.-Y., Chen, H.-H., Hsieh, C.-W., Tang, K.-T., Yang, M.-C., Lan, J.-L. and Chen, D.-Y. (2018). Association between autophagy and inflammation in patients with rheumatoid arthritis receiving biologic therapy. *Arthritis Res. Ther.* 20, 268.

Cheng, H. and Leblond, C. P. (1974). Origin, differentiation and renewal of the four main epithelial cell types in the mouse small intestine. V. Unitarian Theory of the origin of the four epithelial cell types. *Am. J. Anat.* 141, 537–561.

Cheng, L., Qi, C., Yang, H., Lu, M., Cai, Y., Fu, T., Ren, J., Jin, Q. and Zhang, X. (2022). gutMGene: a comprehensive database for target genes of gut microbes and microbial metabolites. *Nucleic Acids Res.* 50, D795–D800.

Chi, S. W., Zang, J. B., Mele, A. and Darnell, R. B. (2009). Argonaute HITS-CLIP decodes microRNA-mRNA interaction maps. *Nature* 460, 479–486.

Christiaen, S. E. A., O'Connell Motherway, M., Bottacini, F., Lanigan, N., Casey, P. G., Huys, G., Nelis, H. J., van Sinderen, D. and Coenye, T. (2014). Autoinducer-2 plays a crucial role in gut colonization and probiotic functionality of Bifidobacterium breve UCC2003. *PLoS ONE* 9, e98111.

Chua, R. L., Lukassen, S., Trump, S., Hennig, B. P., Wendisch, D., Pott, F., Debnath, O., Thürmann, L., Kurth, F., Völker, M. T., et al. (2020). COVID-19 severity correlates with airway epithelium-immune cell interactions identified by single-cell analysis. *Nat. Biotechnol.* 38, 970–979.

Claud, E. C., Savidge, T. and Walker, W. A. (2003). Modulation of human intestinal epithelial cell IL-8 secretion by human milk factors. *Pediatr. Res.* 53, 419–425.

Clevers, H. (2013). The intestinal crypt, a prototype stem cell compartment. *Cell* 154, 274–284.

Clevers, H. C. and Bevins, C. L. (2013). Paneth cells: maestros of the small intestinal crypts. *Annu. Rev. Physiol.* 75, 289–311.

Co, J. Y., Margalef-Català, M., Li, X., Mah, A. T., Kuo, C. J., Monack, D. M. and Amieva, M. R. (2019). Controlling Epithelial Polarity: A Human Enteroid Model for Host-Pathogen Interactions. *Cell Rep.* 26, 2509-2520.e4.

Co, J. Y., Margalef-Català, M., Monack, D. M. and Amieva, M. R. (2021). Controlling the polarity of human gastrointestinal organoids to investigate epithelial biology and infectious diseases. *Nat. Protoc.* 16, 5171–5192.

Cohen, L. J., Esterhazy, D., Kim, S.-H., Lemetre, C., Aguilar, R. R., Gordon, E. A., Pickard, A. J., Cross, J. R., Emiliano, A. B., Han, S. M., et al. (2017). Commensal bacteria make GPCR ligands that mimic human signalling molecules. *Nature* 549, 48–53.

Collado, M. C., Donat, E., Ribes-Koninckx, C., Calabuig, M. and Sanz, Y. (2008). Imbalances in faecal and duodenal Bifidobacterium species composition in active and non-active coeliac disease. *BMC Microbiol.* 8, 232.

Coskun, M. (2014). Intestinal epithelium in inflammatory bowel disease. *Front Med (Lausanne)* 1, 24.

Coskun, M., Troelsen, J. T. and Nielsen, O. H. (2011). The role of CDX2 in intestinal homeostasis and inflammation. *Biochim. Biophys. Acta* 1812, 283–289.

Costello, S. P., Hughes, P. A., Waters, O., Bryant, R. V., Vincent, A. D., Blatchford, P., Katsikeros, R., Makanyanga, J., Campaniello, M. A., Mavrangelos, C., et al. (2019). Effect of Fecal Microbiota Transplantation on 8-Week Remission in Patients With Ulcerative Colitis: A Randomized Clinical Trial. *JAMA* 321, 156–164.

Cramer, J. M., Thompson, T., Geskin, A., LaFramboise, W. and Lagasse, E. (2015). Distinct human stem cell populations in small and large intestine. *PLoS ONE* 10, e0118792.

Cronin, M., Ventura, M., Fitzgerald, G. F. and van Sinderen, D. (2011). Progress in genomics, metabolism and biotechnology of bifidobacteria. *Int. J. Food Microbiol.* 149, 4–18.

Crosnier, C., Stamataki, D. and Lewis, J. (2006). Organizing cell renewal in the intestine: stem cells, signals and combinatorial control. *Nat. Rev. Genet.* 7, 349–359.

Csabai, L., Fazekas, D., Kadlecsik, T., Szalay-Bekő, M., Bohár, B., Madgwick, M., Módos, D., Ölbei, M., Gul, L., Sudhakar, P., et al. (2022). SignaLink3: a multi-layered resource to uncover tissue-specific signaling networks. *Nucleic Acids Res.* 50, D701–D709.

Cunningham, M., Azcarate-Peril, M. A., Barnard, A., Benoit, V., Grimaldi, R., Guyonnet, D., Holscher, H. D., Hunter, K., Manurung, S., Obis, D., et al. (2021). Shaping the future of probiotics and prebiotics. *Trends Microbiol.* 29, 667–685.

D'Angelo, A., Bluteau, O., Garcia-Gonzalez, M. A., Gresh, L., Doyen, A., Garbay, S., Robine, S. and Pontoglio, M. (2010). Hepatocyte nuclear factor 1alpha and beta control terminal differentiation and cell fate commitment in the gut epithelium. *Development* 137, 1573–1582.

D'Haens, G. R., Geboes, K., Peeters, M., Baert, F., Penninckx, F. and Rutgeerts, P. (1998). Early lesions of recurrent Crohn's disease caused by infusion of intestinal contents in excluded ileum. *Gastroenterology* 114, 262–267.

Dan, L., Liu, S., Shang, S., Zhang, H., Zhang, R. and Li, N. (2018). Expression of recombinant human lysozyme in bacterial artificial chromosome transgenic mice promotes the growth of Bifidobacterium and inhibits the growth of Salmonella in the intestine. *J. Biotechnol.* 272–273, 33–39.

Dave, M., Higgins, P. D., Middha, S. and Rioux, K. P. (2012). The human gut microbiome: current knowledge, challenges, and future directions. *Transl. Res.* 160, 246–257.

de Lau, W., Kujala, P., Schneeberger, K., Middendorp, S., Li, V. S. W., Barker, N., Martens, A., Hofhuis, F., DeKoter, R. P., Peters, P. J., et al. (2012). Peyer's patch M cells derived from Lgr5(+) stem cells require SpiB and are induced by RankL in cultured "miniguts". *Mol. Cell. Biol.* 32, 3639–3647.

de Vos, W. M. and de Vos, E. A. J. (2012). Role of the intestinal microbiome in health and disease: from correlation to causation. *Nutr. Rev.* 70 Suppl 1, S45-56.

Dekkers, J. F., Alieva, M., Wellens, L. M., Ariese, H. C. R., Jamieson, P. R., Vonk, A. M., Amatngalim, G. D., Hu, H., Oost, K. C., Snippert, H. J. G., et al. (2019). High-resolution 3D imaging of fixed and cleared organoids. *Nat. Protoc.* 14, 1756–1771.

Dekkers, J. F., Berkers, G., Kruisselbrink, E., Vonk, A., de Jonge, H. R., Janssens, H. M., Bronsveld, I., van de Graaf, E. A., Nieuwenhuis, E. E. S., Houwen, R. H. J., et al. (2016). Characterizing responses to CFTR-modulating drugs using rectal organoids derived from subjects with cystic fibrosis. *Sci. Transl. Med.* 8, 344ra84.

Demers-Mathieu, V. (2022). The immature intestinal epithelial cells in preterm infants play a role in the necrotizing enterocolitis pathogenesis: A review. *Health Sciences Review* 4, 100033.

den Besten, G., van Eunen, K., Groen, A. K., Venema, K., Reijngoud, D.-J. and Bakker, B. M. (2013). The role of short-chain fatty acids in the interplay between diet, gut microbiota, and host energy metabolism. *J. Lipid Res.* 54, 2325–2340.

Deretic, V. and Levine, B. (2018). Autophagy balances inflammation in innate immunity. *Autophagy* 14, 243–251.

Dharmani, P., Srivastava, V., Kissoon-Singh, V. and Chadee, K. (2009). Role of intestinal mucins in innate host defense mechanisms against pathogens. *J. Innate Immun.* 1, 123–135.

Di Gioia, D., Aloisio, I., Mazzola, G. and Biavati, B. (2014). Bifidobacteria: their impact on gut microbiota composition and their applications as probiotics in infants. *Appl. Microbiol. Biotechnol.* 98, 563–577.

Dikic, I. and Elazar, Z. (2018). Mechanism and medical implications of mammalian autophagy. *Nat. Rev. Mol. Cell Biol.* 19, 349–364.

Dimitrov, D., Türei, D., Garrido-Rodriguez, M., Burmedi, P. L., Nagai, J. S., Boys, C., Ramirez Flores, R. O., Kim, H., Szalai, B., Costa, I. G., et al. (2022). Comparison of methods and resources for cell-cell communication inference from single-cell RNA-Seq data. *Nat. Commun.* 13, 3224.

Din, A. U., Hassan, A., Zhu, Y., Zhang, K., Wang, Y., Li, T., Wang, Y. and Wang, G. (2020). Inhibitory effect of Bifidobacterium bifidum ATCC 29521 on colitis and its mechanism. *J. Nutr. Biochem.* 79, 108353.

Dinkel, H., Van Roey, K., Michael, S., Kumar, M., Uyar, B., Altenberg, B., Milchevskaya, V., Schneider, M., Kühn, H., Behrendt, A., et al. (2016). ELM 2016--data update and new functionality of the eukaryotic linear motif resource. *Nucleic Acids Res.* 44, D294-300.

Dobin, A., Davis, C. A., Schlesinger, F., Drenkow, J., Zaleski, C., Jha, S., Batut, P., Chaisson, M. and Gingeras, T. R. (2013). STAR: ultrafast universal RNA-seq aligner. *Bioinformatics* 29, 15–21.

Dotti, I. and Salas, A. (2018). Potential Use of Human Stem Cell-Derived Intestinal Organoids to Study Inflammatory Bowel Diseases. *Inflamm. Bowel Dis.* 24, 2501–2509.

Doxey, A. C. and McConkey, B. J. (2013). Prediction of molecular mimicry candidates in human pathogenic bacteria. *Virulence* 4, 453–466.

Drost, J., Artegiani, B. and Clevers, H. (2016). The generation of organoids for studying wnt signaling. *Methods Mol. Biol.* 1481, 141–159.

Drost, J., van Jaarsveld, R. H., Ponsioen, B., Zimberlin, C., van Boxtel, R., Buijs, A., Sachs, N., Overmeer, R. M., Offerhaus, G. J., Begthel, H., et al. (2015). Sequential cancer mutations in cultured human intestinal stem cells. *Nature* 521, 43–47.

Duell, B. L., Cripps, A. W., Schembri, M. A. and Ulett, G. C. (2011). Epithelial cell coculture models for studying infectious diseases: benefits and limitations. *J. Biomed. Biotechnol.* 2011, 852419.

Dugourd, A. and Saez-Rodriguez, J. (2019). Footprint-based functional analysis of multiomic data. *Current Opinion in Systems Biology* 15, 82–90.

Dutta, D., Heo, I. and Clevers, H. (2017). Disease Modeling in Stem Cell-Derived 3D Organoid Systems. *Trends Mol. Med.* 23, 393–410.

Eain, M. M. G., Baginska, J., Greenhalgh, K., Fritz, J. V., Zenhausern, F. and Wilmes, P. (2017). Engineering Solutions for Representative Models of the Gastrointestinal Human-Microbe Interface. *Engineering* 3, 60–65.

Earle, K. A., Billings, G., Sigal, M., Lichtman, J. S., Hansson, G. C., Elias, J. E., Amieva, M. R., Huang, K. C. and Sonnenburg, J. L. (2015). Quantitative imaging of gut microbiota spatial organization. *Cell Host Microbe* 18, 478–488.

Elbialy, A. (2021). In vivo autophagy quantification: Measuring LC3 and P62 puncta in 3D image system from zebrafish larvae. *J. Cell. Biochem.* 122, 1435–1444.

Elinav, E., Strowig, T., Kau, A. L., Henao-Mejia, J., Thaiss, C. A., Booth, C. J., Peaper, D. R., Bertin, J., Eisenbarth, S. C., Gordon, J. I., et al. (2011). NLRP6 inflammasome regulates colonic microbial ecology and risk for colitis. *Cell* 145, 745–757.

Engevik, M. A., Luk, B., Chang-Graham, A. L., Hall, A., Herrmann, B., Ruan, W., Endres, B. T., Shi, Z., Garey, K. W., Hyser, J. M., et al. (2019). Bifidobacterium dentium Fortifies the Intestinal Mucus Layer via Autophagy and Calcium Signaling Pathways. *MBio* 10,.

Esch, E. W., Bahinski, A. and Huh, D. (2015). Organs-on-chips at the frontiers of drug discovery. *Nat. Rev. Drug Discov.* 14, 248–260.

Ettayebi, K., Crawford, S. E., Murakami, K., Broughman, J. R., Karandikar, U., Tenge, V. R., Neill, F. H., Blutt, S. E., Zeng, X.-L., Qu, L., et al. (2016). Replication of human noroviruses in stem cell-derived human enteroids. *Science* 353, 1387–1393.

Fabregat, A., Jupe, S., Matthews, L., Sidiropoulos, K., Gillespie, M., Garapati, P., Haw, R., Jassal, B., Korninger, F., May, B., et al. (2018). The Reactome Pathway Knowledgebase. *Nucleic Acids Res.* 46, D649–D655.

Faith, J. J., Ahern, P. P., Ridaura, V. K., Cheng, J. and Gordon, J. I. (2014). Identifying gut microbe-host phenotype relationships using combinatorial communities in gnotobiotic mice. *Sci. Transl. Med.* 6, 220ra11.

Fallani, M., Young, D., Scott, J., Norin, E., Amarri, S., Adam, R., Aguilera, M., Khanna, S., Gil, A., Edwards, C. A., et al. (2010). Intestinal microbiota of 6-week-old infants across Europe: geographic influence beyond delivery mode, breast-feeding, and antibiotics. *J. Pediatr. Gastroenterol. Nutr.* 51, 77–84.

Fang, H., Fu, L. and Wang, J. (2018). Protocol for Fecal Microbiota Transplantation in Inflammatory Bowel Disease: A Systematic Review and Meta-Analysis. *Biomed Res. Int.* 2018, 8941340.

Fanning, S., Hall, L. J., Cronin, M., Zomer, A., MacSharry, J., Goulding, D., Motherway, M. O., Shanahan, F., Nally, K., Dougan, G., et al. (2012a). Bifidobacterial surface-exopolysaccharide facilitates commensal-host interaction through immune modulation and pathogen protection. *Proc Natl Acad Sci USA* 109, 2108–2113.

Fanning, S., Hall, L. J. and van Sinderen, D. (2012b). Bifidobacterium breve UCC2003 surface exopolysaccharide production is a beneficial trait mediating commensal-host interaction through immune modulation and pathogen protection. *Gut Microbes* 3, 420–425.

Fatehullah, A., Tan, S. H. and Barker, N. (2016). Organoids as an in vitro model of human development and disease. *Nat. Cell Biol.* 18, 246–254.

Fazekas, D., Koltai, M., Türei, D., Módos, D., Pálfy, M., Dúl, Z., Zsákai, L., Szalay-Bekő, M., Lenti, K., Farkas, I. J., et al. (2013). SignaLink 2 - a signaling pathway resource with multi-layered regulatory networks. *BMC Syst. Biol.* 7, 7.

Ferrario, C., Milani, C., Mancabelli, L., Lugli, G. A., Duranti, S., Mangifesta, M., Viappiani, A., Turroni, F., Margolles, A., Ruas-Madiedo, P., et al. (2016). Modulation of the eps-ome transcription of bifidobacteria through simulation of human intestinal environment. *FEMS Microbiol. Ecol.* 92, fiw056.

Filbin, M. R., Mehta, A., Schneider, A. M., Kays, K. R., Guess, J. R., Gentili, M., Fenyves, B. G., Charland, N. C., Gonye, A. L. K., Gushterova, I., et al. (2020). Plasma proteomics reveals tissue-specific cell death and mediators of cell-cell interactions in severe COVID-19 patients. *BioRxiv*.

Flint, H. J., Duncan, S. H., Scott, K. P. and Louis, P. (2015). Links between Diet, Gut Microbiota Composition and Gut Metabolism. *Proc. Nutr. Soc.* 74, 13–22.

Foerster, E. G., Mukherjee, T., Cabral-Fernandes, L., Rocha, J. D. B., Girardin, S. E. and Philpott, D. J. (2022). How autophagy controls the intestinal epithelial barrier. *Autophagy* 18, 86–103.

Fofanova, T. Y., Stewart, C., Auchtung, J. M., Wilson, R. L., Britton, R. A., Grande-Allen, K. J., Estes, M. K. and Petrosino, J. F. (2019). A novel human enteroid-anaerobe co-culture system to study microbial-host interaction under physiological hypoxia. *BioRxiv*.

Forbester, J. L., Goulding, D., Vallier, L., Hannan, N., Hale, C., Pickard, D., Mukhopadhyay, S. and Dougan, G. (2015). Interaction of Salmonella enterica Serovar Typhimurium with Intestinal Organoids Derived from Human Induced Pluripotent Stem Cells. *Infect. Immun.* 83, 2926–2934.

Foroni, E., Serafini, F., Amidani, D., Turroni, F., He, F., Bottacini, F., O'Connell Motherway, M., Viappiani, A., Zhang, Z., Rivetti, C., et al. (2011). Genetic analysis and morphological identification of pilus-like structures in members of the genus Bifidobacterium. *Microb. Cell Fact.* 10 Suppl 1, S16.

Foulke-Abel, J., In, J., Kovbasnjuk, O., Zachos, N. C., Ettayebi, K., Blutt, S. E., Hyser, J. M., Zeng, X.-L., Crawford, S. E., Broughman, J. R., et al. (2014). Human enteroids as an ex-vivo model of host-pathogen interactions in the gastrointestinal tract. *Exp Biol Med (Maywood)* 239, 1124–1134.

Francies, H. E., Barthorpe, A., McLaren-Douglas, A., Barendt, W. J. and Garnett, M. J. (2019). Drug sensitivity assays of human cancer organoid cultures. *Methods Mol. Biol.* 1576, 339–351.

Francoeur, C., Escaffit, F., Vachon, P. H. and Beaulieu, J.-F. (2004). Proinflammatory cytokines TNF-alpha and IFN-gamma alter laminin expression under an apoptosis-independent mechanism in human intestinal epithelial cells. *Am. J. Physiol. Gastrointest. Liver Physiol.* 287, G592-8.

Friedrich, M., Pohin, M. and Powrie, F. (2019). Cytokine networks in the pathophysiology of inflammatory bowel disease. *Immunity* 50, 992–1006.

Fujii, M., Matano, M., Nanki, K. and Sato, T. (2015). Efficient genetic engineering of human intestinal organoids using electroporation. *Nat. Protoc.* 10, 1474–1485.

Fujii, M., Matano, M., Toshimitsu, K., Takano, A., Mikami, Y., Nishikori, S., Sugimoto, S. and Sato, T. (2018). Human Intestinal Organoids Maintain Self-Renewal Capacity and Cellular Diversity in Niche-Inspired Culture Condition. *Cell Stem Cell* 23, 787-793.e6.

Fujii, M., Shimokawa, M., Date, S., Takano, A., Matano, M., Nanki, K., Ohta, Y., Toshimitsu, K., Nakazato, Y., Kawasaki, K., et al. (2016). A Colorectal Tumor Organoid Library Demonstrates Progressive Loss of Niche Factor Requirements during Tumorigenesis. *Cell Stem Cell* 18, 827–838.

Fujimichi, Y., Otsuka, K., Tomita, M. and Iwasaki, T. (2019). An efficient intestinal organoid system of direct sorting to evaluate stem cell competition in vitro. *Sci. Rep.* 9, 20297.

Fujimori, S., Gudis, K., Mitsui, K., Seo, T., Yonezawa, M., Tanaka, S., Tatsuguchi, A. and Sakamoto, C. (2009). A randomized controlled trial on the efficacy of synbiotic versus probiotic or prebiotic treatment to improve the quality of life in patients with ulcerative colitis. *Nutrition* 25, 520–525.

Furey, T. S. (2012). ChIP-seq and beyond: new and improved methodologies to detect and characterize protein-DNA interactions. *Nat. Rev. Genet.* 13, 840–852.

Furrie, E. (2005). Is Bifidobacterium a more effective probiotic therapy than Lactobacillus for patients with irritable bowel syndrome? *Nat. Clin. Pract. Gastroenterol. Hepatol.* 2, 304–305.

Furusawa, Y., Obata, Y., Fukuda, S., Endo, T. A., Nakato, G., Takahashi, D., Nakanishi, Y., Uetake, C., Kato, K., Kato, T., et al. (2013). Commensal microbe-derived butyrate induces the differentiation of colonic regulatory T cells. *Nature* 504, 446–450.

Galluzzi, L. and Green, D. R. (2019). Autophagy-Independent Functions of the Autophagy Machinery. *Cell* 177, 1682–1699.

Galluzzi, L., Baehrecke, E. H., Ballabio, A., Boya, P., Bravo-San Pedro, J. M., Cecconi, F., Choi, A. M., Chu, C. T., Codogno, P., Colombo, M. I., et al. (2017). Molecular definitions of autophagy and related processes. *EMBO J.* 36, 1811–1836.

Galvez, J., Rodríguez-Cabezas, M. E. and Zarzuelo, A. (2005). Effects of dietary fiber on inflammatory bowel disease. *Mol. Nutr. Food Res.* 49, 601–608.

Garcia-Alonso, L., Holland, C. H., Ibrahim, M. M., Turei, D. and Saez-Rodriguez, J. (2019). Benchmark and integration of resources for the estimation of human transcription factor activities. *Genome Res.* 29, 1363–1375.

Garrido-Rodriguez, M., Zirngibl, K., Ivanova, O., Lobentanzer, S. and Saez-Rodriguez, J. (2022). Integrating knowledge and omics to decipher mechanisms via large-scale models of signaling networks. *Mol. Syst. Biol.* 18, e11036.

Gehart, H. and Clevers, H. (2019). Tales from the crypt: new insights into intestinal stem cells. *Nat. Rev. Gastroenterol. Hepatol.* 16, 19–34.

Gehling, K., Parekh, S., Schneider, F., Kirchner, M., Kondylis, V., Nikopoulou, C. and Tessarz, P. (2021). Single organoid RNA-sequencing reveals high organoid-to-organoid variability. *BioRxiv*.

Gerbe, F., Brulin, B., Makrini, L., Legraverend, C. and Jay, P. (2009). DCAMKL-1 expression identifies Tuft cells rather than stem cells in the adult mouse intestinal epithelium. *Gastroenterology* 137, 2179–80; author reply 2180.

Gerbe, F., Sidot, E., Smyth, D. J., Ohmoto, M., Matsumoto, I., Dardalhon, V., Cesses, P., Garnier, L., Pouzolles, M., Brulin, B., et al. (2016). Intestinal epithelial tuft cells initiate type 2 mucosal immunity to helminth parasites. *Nature* 529, 226–230.

Geremia, A., Biancheri, P., Allan, P., Corazza, G. R. and Di Sabatino, A. (2014). Innate and adaptive immunity in inflammatory bowel disease. *Autoimmun. Rev.* 13, 3–10.

Geva-Zatorsky, N., Alvarez, D., Hudak, J. E., Reading, N. C., Erturk-Hasdemir, D., Dasgupta, S., von Andrian, U. H. and Kasper, D. L. (2015). In vivo imaging and tracking of host-microbiota interactions via metabolic labeling of gut anaerobic bacteria. *Nat. Med.* 21, 1091–1100.

Gevers, D., Kugathasan, S., Denson, L. A., Vázquez-Baeza, Y., Van Treuren, W., Ren, B., Schwager, E., Knights, D., Song, S. J., Yassour, M., et al. (2014). The treatment-naive microbiome in new-onset Crohn's disease. *Cell Host Microbe* 15, 382–392.

Gibson, T. J., Dinkel, H., Van Roey, K. and Diella, F. (2015). Experimental detection of short regulatory motifs in eukaryotic proteins: tips for good practice as well as for bad. *Cell Commun. Signal.* 13, 42.

Gill, S. R., Pop, M., Deboy, R. T., Eckburg, P. B., Turnbaugh, P. J., Samuel, B. S., Gordon, J. I., Relman, D. A., Fraser-Liggett, C. M. and Nelson, K. E. (2006). Metagenomic analysis of the human distal gut microbiome. *Science* 312, 1355–1359.

Gillespie, M., Jassal, B., Stephan, R., Milacic, M., Rothfels, K., Senff-Ribeiro, A., Griss, J., Sevilla, C., Matthews, L., Gong, C., et al. (2022). The reactome pathway knowledgebase 2022. *Nucleic Acids Res.* 50, D687–D692.

Gilmore, A. P. (2005). Anoikis. *Cell Death Differ.* 12 Suppl 2, 1473–1477.

Gjorevski, N., Sachs, N., Manfrin, A., Giger, S., Bragina, M. E., Ordóñez-Morán, P., Clevers, H. and Lutolf, M. P. (2016). Designer matrices for intestinal stem cell and organoid culture. *Nature* 539, 560–564.

Gkouskou, K. K., Deligianni, C., Tsatsanis, C. and Eliopoulos, A. G. (2014). The gut microbiota in mouse models of inflammatory bowel disease. *Front. Cell. Infect. Microbiol.* 4, 28.

Glover, J. S., Ticer, T. D. and Engevik, M. A. (2022). Characterizing the mucin-degrading capacity of the human gut microbiota. *Sci. Rep.* 12, 8456.

Godl, K., Johansson, M. E. V., Lidell, M. E., Mörgelin, M., Karlsson, H., Olson, F. J., Gum, J. R., Kim, Y. S. and Hansson, G. C. (2002). The N terminus of the MUC2 mucin forms trimers that are held together within a trypsin-resistant core fragment. *J. Biol. Chem.* 277, 47248–47256.

Goff, L. A. and Rinn, J. L. (2015). Linking RNA biology to lncRNAs. *Genome Res.* 25, 1456–1465.

Gohel, R., Kournoutis, A., Petridi, S. and Nezis, I. P. (2020). Molecular mechanisms of selective autophagy in Drosophila. *Int. Rev. Cell Mol. Biol.* 354, 63–105.

Gourbeyre, P., Berri, M., Lippi, Y., Meurens, F., Vincent-Naulleau, S., Laffitte, J., Rogel-Gaillard, C., Pinton, P. and Oswald, I. P. (2015). Pattern recognition receptors in the gut: analysis of their expression along the intestinal tract and the crypt/villus axis. *Physiol. Rep.* 3,.

Gracz, A. D., Williamson, I. A., Roche, K. C., Johnston, M. J., Wang, F., Wang, Y., Attayek, P. J., Balowski, J., Liu, X. F., Laurenza, R. J., et al. (2015). A high-throughput platform for stem cell niche co-cultures and downstream gene expression analysis. *Nat. Cell Biol.* 17, 340–349.

Gregorieff, A., Stange, D. E., Kujala, P., Begthel, H., van den Born, M., Korving, J., Peters, P. J. and Clevers, H. (2009). The ets-domain transcription factor Spdef promotes maturation of goblet and paneth cells in the intestinal epithelium. *Gastroenterology* 137, 1333–45.e1.

Gribble, F. M. and Reimann, F. (2016). Enteroendocrine cells: chemosensors in the intestinal epithelium. *Annu. Rev. Physiol.* 78, 277–299.

Griffiths-Jones, S., Saini, H. K., van Dongen, S. and Enright, A. J. (2008). miRBase: tools for microRNA genomics. *Nucleic Acids Res.* 36, D154-8.

Grimm, V., Westermann, C. and Riedel, C. U. (2014). Bifidobacteria-host interactions--an update on colonisation factors. *Biomed Res. Int.* 2014, 960826.

Groeger, D., O'Mahony, L., Murphy, E. F., Bourke, J. F., Dinan, T. G., Kiely, B., Shanahan, F. and Quigley, E. M. M. (2013). Bifidobacterium infantis 35624 modulates host inflammatory processes beyond the gut. *Gut Microbes* 4, 325–339.

Groschwitz, K. R. and Hogan, S. P. (2009). Intestinal barrier function: molecular regulation and disease pathogenesis. *J. Allergy Clin. Immunol.* 124, 3–20; quiz 21.

Grouls, M., van der Zande, M., de Haan, L. and Bouwmeester, H. (2022). Responses of increasingly complex intestinal epithelium in vitro models to bacterial toll-like receptor agonists. *Toxicol In Vitro* 79, 105280.

Guglielmetti, S., Balzaretti, S., Taverniti, V., Miriani, M., Milani, C., Scarafoni, A., Corona, S., Ciranna, A., Arioli, S., Santala, V., et al. (2014a). TgaA, a VirB1-like component belonging to a putative type IV secretion system of Bifidobacterium bifidum MIMBb75. *Appl. Environ. Microbiol.* 80, 5161–5169.

Guglielmetti, S., Zanoni, I., Balzaretti, S., Miriani, M., Taverniti, V., De Noni, I., Presti, I., Stuknyte, M., Scarafoni, A., Arioli, S., et al. (2014b). Murein lytic enzyme TgaA of Bifidobacterium bifidum MIMBb75 modulates dendritic cell maturation through its cysteine- and histidine-dependent amidohydrolase/peptidase (CHAP) amidase domain. *Appl. Environ. Microbiol.* 80, 5170–5177.

Guo, M., Tao, W., Flavell, R. A. and Zhu, S. (2021). Potential intestinal infection and faecal–oral transmission of SARS-CoV-2. *Nature Reviews Gastroenterology & Hepatology*.

Gupta, A., Madhavan, M. V., Sehgal, K., Nair, N., Mahajan, S., Sehrawat, T. S., Bikdeli, B., Ahluwalia, N., Ausiello, J. C., Wan, E. Y., et al. (2020). Extrapulmonary manifestations of COVID-19. *Nat. Med.* 26, 1017–1032.

Haber, A. L., Biton, M., Rogel, N., Herbst, R. H., Shekhar, K., Smillie, C., Burgin, G., Delorey, T. M., Howitt, M. R., Katz, Y., et al. (2017). A single-cell survey of the small intestinal epithelium. *Nature* 551, 333–339.

Hadjadj, J., Yatim, N., Barnabei, L., Corneau, A., Boussier, J., Smith, N., Péré, H., Charbit, B., Bondet, V., Chenevier-Gobeaux, C., et al. (2020). Impaired type I interferon activity and inflammatory responses in severe COVID-19 patients. *Science* 369, 718–724.

Halfvarson, J., Brislawn, C. J., Lamendella, R., Vázquez-Baeza, Y., Walters, W. A., Bramer, L. M., D'Amato, M., Bonfiglio, F., McDonald, D., Gonzalez, A., et al. (2017). Dynamics of the human gut microbiome in inflammatory bowel disease. *Nat. Microbiol.* 2, 17004.

Han, J.-D. J. (2008). Understanding biological functions through molecular networks. *Cell Res.* 18, 224–237.

Hao, Y., Hao, S., Andersen-Nissen, E., Mauck, W. M., Zheng, S., Butler, A., Lee, M. J., Wilk, A. J., Darby, C., Zager, M., et al. (2021). Integrated analysis of multimodal single-cell data. *Cell* 184, 3573-3587.e29.

Haramis, A.-P. G., Begthel, H., van den Born, M., van Es, J., Jonkheer, S., Offerhaus, G. J. A. and Clevers, H. (2004). De novo crypt formation and juvenile polyposis on BMP inhibition in mouse intestine. *Science* 303, 1684–1686.

Hart, A. L., Lammers, K., Brigidi, P., Vitali, B., Rizzello, F., Gionchetti, P., Campieri, M., Kamm, M. A., Knight, S. C. and Stagg, A. J. (2004). Modulation of human dendritic cell phenotype and function by probiotic bacteria. *Gut* 53, 1602–1609.

Hart, A. L., Stagg, A. J., Frame, M., Graffner, H., Glise, H., Falk, P. and Kamm, M. A. (2002). The role of the gut flora in health and disease, and its modification as therapy. *Aliment. Pharmacol. Ther.* 16, 1383–1393.

Hato, T. and Dagher, P. C. (2015). How the innate immune system senses trouble and causes trouble. *Clin. J. Am. Soc. Nephrol.* 10, 1459–1469.

Hautefort, I., Poletti, M., Papp, D. and Korcsmaros, T. (2022). Everything You Always Wanted to Know About Organoid-Based Models (and Never Dared to Ask). *Cell. Mol. Gastroenterol. Hepatol.* 14, 311–331.

Hayashi, F., Smith, K. D., Ozinsky, A., Hawn, T. R., Yi, E. C., Goodlett, D. R., Eng, J. K., Akira, S., Underhill, D. M. and Aderem, A. (2001). The innate immune response to bacterial flagellin is mediated by Toll-like receptor 5. *Nature* 410, 1099–1103.

He, C. and Klionsky, D. J. (2009). Regulation mechanisms and signaling pathways of autophagy. *Annu. Rev. Genet.* 43, 67–93.

He, T., Priebe, M. G., Zhong, Y., Huang, C., Harmsen, H. J. M., Raangs, G. C., Antoine, J. M., Welling, G. W. and Vonk, R. J. (2008). Effects of yogurt and bifidobacteria supplementation on the colonic microbiota in lactose-intolerant subjects. *J. Appl. Microbiol.* 104, 595–604.

Heel, K. A., McCauley, R. D., Papadimitriou, J. M. and Hall, J. C. (1997). Peyer's patches. *J. Gastroenterol. Hepatol.* 12, 122–136.

Heinz, M. C., Oost, K. C. and Snippert, H. J. G. (2020). Introducing the Stem Cell ASCL2 Reporter STAR into Intestinal Organoids. *STAR Protocols* 1, 100126.

Hellweg, C. E., Arenz, A., Bogner, S., Schmitz, C. and Baumstark-Khan, C. (2006). Activation of nuclear factor kappa B by different agents: influence of culture conditions in a cell-based assay. *Ann. N. Y. Acad. Sci.* 1091, 191–204.

Heppert, J. K., Davison, J. M., Kelly, C., Mercado, G. P., Lickwar, C. R. and Rawls, J. F. (2021). Transcriptional programmes underlying cellular identity and microbial responsiveness in the intestinal epithelium. *Nat. Rev. Gastroenterol. Hepatol.* 18, 7–23.

Hermjakob, H., Montecchi-Palazzi, L., Lewington, C., Mudali, S., Kerrien, S., Orchard, S., Vingron, M., Roechert, B., Roepstorff, P., Valencia, A., et al. (2004). IntAct: an open source molecular interaction database. *Nucleic Acids Res.* 32, D452-5.

Hidalgo-Cantabrana, C., López, P., Gueimonde, M., de Los Reyes-Gavilán, C. G., Suárez, A., Margolles, A. and Ruas-Madiedo, P. (2012). Immune modulation capability of exopolysaccharides synthesised by lactic acid bacteria and bifidobacteria. *Probiotics Antimicrob. Proteins* 4, 227–237.

Hidalgo-Cantabrana, C., Moro-García, M. A., Blanco-Míguez, A., Fdez-Riverola, F., Lourenço, A., Alonso-Arias, R. and Sánchez, B. (2017). In Silico Screening of the Human Gut Metaproteome Identifies Th17-Promoting Peptides Encrypted in Proteins of Commensal Bacteria. *Front. Microbiol.* 8, 1726.

Hidalgo-Cantabrana, C., Sánchez, B., Milani, C., Ventura, M., Margolles, A. and Ruas-Madiedo, P. (2014). Genomic overview and biological functions of exopolysaccharide biosynthesis in Bifidobacterium spp. *Appl. Environ. Microbiol.* 80, 9–18.

Hill, D. R., Huang, S., Nagy, M. S., Yadagiri, V. K., Fields, C., Mukherjee, D., Bons, B., Dedhia, P. H., Chin, A. M., Tsai, Y.-H., et al. (2017). Bacterial colonization stimulates a complex physiological response in the immature human intestinal epithelium. *eLife* 6,.

Ho, J., Chan, H., Liang, Y., Liu, X., Zhang, L., Li, Q., Zhang, Y., Zeng, J., Ugwu, F. N., Ho, I. H. T., et al. (2020). Cathelicidin preserves intestinal barrier function in polymicrobial sepsis. *Crit. Care* 24, 47.

Ho, J., Chan, H., Liang, Y., Liu, X., Zhang, L., Li, Q., Zhang, Y., Zeng, J., Ugwu, F. N., Ho, I. H. T., et al. (2020). Cathelicidin preserves intestinal barrier function in polymicrobial sepsis. *Crit. Care* 24, 47.

Hollins, A. J. and Parry, L. (2016). Long-Term Culture of Intestinal Cell Progenitors: An Overview of Their Development, Application, and Associated Technologies. *Curr. Pathobiol. Rep.* 4, 209–219.

Hooper, L. V. (2004). Bacterial contributions to mammalian gut development. *Trends Microbiol.* 12, 129–134.

Howitt, M. R., Lavoie, S., Michaud, M., Blum, A. M., Tran, S. V., Weinstock, J. V., Gallini, C. A., Redding, K., Margolskee, R. F., Osborne, L. C., et al. (2016). Tuft cells, taste-chemosensory cells, orchestrate parasite type 2 immunity in the gut. *Science* 351, 1329–1333.

Hsieh, C.-Y., Osaka, T., Moriyama, E., Date, Y., Kikuchi, J. and Tsuneda, S. (2015). Strengthening of the intestinal epithelial tight junction by Bifidobacterium bifidum. *Physiol. Rep.* 3,.

Huang, L., Liao, L. and Wu, C. H. (2016). Inference of protein-protein interaction networks from multiple heterogeneous data. *EURASIP J. Bioinform. Syst. Biol.* 2016, 8.

Huang, R. S., Gamazon, E. R., Ziliak, D., Wen, Y., Im, H. K., Zhang, W., Wing, C., Duan, S., Bleibel, W. K., Cox, N. J., et al. (2011). Population differences in microRNA expression and biological implications. *RNA Biol.* 8, 692–701.

Hughes, K. R., Harnisch, L. C., Alcon-Giner, C., Mitra, S., Wright, C. J., Ketskemety, J., van Sinderen, D., Watson, A. J. M. and Hall, L. J. (2017). Bifidobacterium breve reduces apoptotic epithelial cell shedding in an exopolysaccharide and MyD88-dependent manner. *Open Biol.* 7,.

Huh, D., Torisawa, Y., Hamilton, G. A., Kim, H. J. and Ingber, D. E. (2012). Microengineered physiological biomimicry: organs-on-chips. *Lab Chip* 12, 2156–2164.

Husted, A. S., Trauelsen, M., Rudenko, O., Hjorth, S. A. and Schwartz, T. W. (2017). GPCR-Mediated Signaling of Metabolites. *Cell Metab.* 25, 777–796.

Iheozor-Ejiofor, Z., Kaur, L., Gordon, M., Baines, P. A., Sinopoulou, V. and Akobeng, A. K. (2020). Probiotics for maintenance of remission in ulcerative colitis. *Cochrane Database Syst. Rev.* 3, CD007443.

Imdad, A., Nicholson, M. R., Tanner-Smith, E. E., Zackular, J. P., Gomez-Duarte, O. G., Beaulieu, D. B. and Acra, S. (2018). Fecal transplantation for treatment of inflammatory bowel disease. *Cochrane Database Syst. Rev.* 11, CD012774.

In, J., Foulke-Abel, J., Zachos, N. C., Hansen, A.-M., Kaper, J. B., Bernstein, H. D., Halushka, M., Blutt, S., Estes, M. K., Donowitz, M., et al. (2016). Enterohemorrhagic Escherichia coli reduce mucus and intermicrovillar bridges in human stem cell-derived colonoids. *Cell. Mol. Gastroenterol. Hepatol.* 2, 48-62.e3.

Inaba, Y., Ueno, N., Numata, M., Zhu, X., Messer, J. S., Boone, D. L., Fujiya, M., Kohgo, Y., Musch, M. W. and Chang, E. B. (2016). Soluble bioactive microbial mediators regulate proteasomal degradation and autophagy to protect against inflammation-induced stress. *Am. J. Physiol. Gastrointest. Liver Physiol.* 311, G634–G647.

Ivanov, D., Emonet, C., Foata, F., Affolter, M., Delley, M., Fisseha, M., Blum-Sperisen, S., Kochhar, S. and Arigoni, F. (2006). A serpin from the gut bacterium Bifidobacterium longum inhibits eukaryotic elastase-like serine proteases. *J. Biol. Chem.* 281, 17246–17252.

Jaks, V., Barker, N., Kasper, M., van Es, J. H., Snippert, H. J., Clevers, H. and Toftgård, R. (2008). Lgr5 marks cycling, yet long-lived, hair follicle stem cells. *Nat. Genet.* 40, 1291–1299.

Jakubczyk, D., Leszczyńska, K. and Górska, S. (2020). The Effectiveness of Probiotics in the Treatment of Inflammatory Bowel Disease (IBD)-A Critical Review. *Nutrients* 12,.

Jalali, S., Bhartiya, D., Lalwani, M. K., Sivasubbu, S. and Scaria, V. (2013). Systematic transcriptome wide analysis of lncRNA-miRNA interactions. *PLoS ONE* 8, e53823.

Jalili-Firoozinezhad, S., Gazzaniga, F. S., Calamari, E. L., Camacho, D. M., Fadel, C. W., Bein, A., Swenor, B., Nestor, B., Cronce, M. J., Tovaglieri, A., et al. (2019). A complex human gut microbiome cultured in an anaerobic intestine-on-a-chip. *Nat. Biomed. Eng.* 3, 520–531.

Johansson, M. E. V. and Hansson, G. C. (2016). Immunological aspects of intestinal mucus and mucins. *Nat. Rev. Immunol.* 16, 639–649.

Johansson, M. E. V., Gustafsson, J. K., Holmén-Larsson, J., Jabbar, K. S., Xia, L., Xu, H., Ghishan, F. K., Carvalho, F. A., Gewirtz, A. T., Sjövall, H., et al. (2014). Bacteria penetrate the normally impenetrable inner colon mucus layer in both murine colitis models and patients with ulcerative colitis. *Gut* 63, 281–291.

Jones, E. J., Matthews, Z. J., Gul, L., Sudhakar, P., Treveil, A., Divekar, D., Buck, J., Wrzesinski, T., Jefferson, M., Armstrong, S. D., et al. (2019). Integrative analysis of Paneth cell proteomic and transcriptomic data from intestinal organoids reveals functional processes dependent on autophagy. *Dis. Model. Mech.* 12,.

Joo, S.-S., Gu, B.-H., Park, Y.-J., Rim, C.-Y., Kim, M.-J., Kim, S.-H., Cho, J.-H., Kim, H.-B. and Kim, M. (2022). Porcine Intestinal Apical-Out Organoid Model for Gut Function Study. *Animals (Basel)* 12,.

Joossens, M., Huys, G., Cnockaert, M., De Preter, V., Verbeke, K., Rutgeerts, P., Vandamme, P. and Vermeire, S. (2011). Dysbiosis of the faecal microbiota in patients with Crohn's disease and their unaffected relatives. *Gut* 60, 631–637.

Jordan, A., Carding, S. R. and Hall, L. J. (2022). The early-life gut microbiome and vaccine efficacy. *Lancet Microbe* 3, e787–e794.

Jumper, J., Evans, R., Pritzel, A., Green, T., Figurnov, M., Ronneberger, O., Tunyasuvunakool, K., Bates, R., Žídek, A., Potapenko, A., et al. (2021). Highly accurate protein structure prediction with AlphaFold. *Nature* 596, 583–589.

Kaiko, G. E., Ryu, S. H., Koues, O. I., Collins, P. L., Solnica-Krezel, L., Pearce, E. J., Pearce, E. L., Oltz, E. M. and Stappenbeck, T. S. (2016). The Colonic Crypt Protects Stem Cells from Microbiota-Derived Metabolites. *Cell* 167, 1137.

Kakni, P., López-Iglesias, C., Truckenmüller, R., Habibović, P. and Giselbrecht, S. (2022). Reversing Epithelial Polarity in Pluripotent Stem Cell-Derived Intestinal Organoids. *Front. Bioeng. Biotechnol.* 10, 879024.

Kale, S. D., Mehrkens, B. N., Stegman, M. M., Kastelberg, B., Carnes, H., McNeill, R. J., Rizzo, A., Karyala, S. V., Coutermarsh-Ott, S., Fretz, J. A., et al. (2020). "Small" Intestinal Immunopathology Plays a "Big" Role in Lethal Cytokine Release Syndrome, and Its Modulation by Interferon-γ, IL-17A, and a Janus Kinase Inhibitor. *Front. Immunol.* 11, 1311.

Kang, R., Livesey, K. M., Zeh, H. J., Lotze, M. T. and Tang, D. (2011). HMGB1 as an autophagy sensor in oxidative stress. *Autophagy* 7, 904–906.

Karve, S. S., Pradhan, S., Ward, D. V. and Weiss, A. A. (2017). Intestinal organoids model human responses to infection by commensal and Shiga toxin producing Escherichia coli. *PLoS ONE* 12, e0178966.

Kasendra, M., Tovaglieri, A., Sontheimer-Phelps, A., Jalili-Firoozinezhad, S., Bein, A., Chalkiadaki, A., Scholl, W., Zhang, C., Rickner, H., Richmond, C. A., et al. (2018). Development of a primary human Small Intestine-on-a-Chip using biopsy-derived organoids. *Sci. Rep.* 8, 2871.

Kaser, A., Lee, A.-H., Franke, A., Glickman, J. N., Zeissig, S., Tilg, H., Nieuwenhuis, E. E. S., Higgins, D. E., Schreiber, S., Glimcher, L. H., et al. (2008). XBP1 links ER stress to intestinal inflammation and confers genetic risk for human inflammatory bowel disease. *Cell* 134, 743–756.

Kaushik, S. and Cuervo, A. M. (2018). The coming of age of chaperone-mediated autophagy. *Nat. Rev. Mol. Cell Biol.* 19, 365–381.

Kernbauer, E., Ding, Y. and Cadwell, K. (2014). An enteric virus can replace the beneficial function of commensal bacteria. *Nature* 516, 94–98.

Kerz, M., Folarin, A., Meleckyte, R., Watt, F. M., Dobson, R. J. and Danovi, D. (2016). A Novel Automated High-Content Analysis Workflow Capturing Cell Population Dynamics from Induced Pluripotent Stem Cell Live Imaging Data. *J. Biomol. Screen.* 21, 887–896.

Khalif, I. L., Quigley, E. M. M., Konovitch, E. A. and Maximova, I. D. (2005). Alterations in the colonic flora and intestinal permeability and evidence of immune activation in chronic constipation. *Dig. Liver Dis.* 37, 838–849.

Khandia, R., Dadar, M., Munjal, A., Dhama, K., Karthik, K., Tiwari, R., Yatoo, M. I., Iqbal, H. M. N., Singh, K. P., Joshi, S. K., et al. (2019). A Comprehensive Review of Autophagy and Its Various Roles in Infectious, Non-Infectious, and Lifestyle Diseases: Current Knowledge and Prospects for Disease Prevention, Novel Drug Design, and Therapy. *Cells* 8,.

Kim, D., Zeng, M. Y. and Núñez, G. (2017). The interplay between host immune cells and gut microbiota in chronic inflammatory diseases. *Exp. Mol. Med.* 49, e339.

Kim, H. J. and Ingber, D. E. (2013). Gut-on-a-Chip microenvironment induces human intestinal cells to undergo villus differentiation. *Integr Biol (Camb)* 5, 1130–1140.

Kim, H. J., Huh, D., Hamilton, G. and Ingber, D. E. (2012). Human gut-on-a-chip inhabited by microbial flora that experiences intestinal peristalsis-like motions and flow. *Lab Chip* 12, 2165–2174.

Kim, H. J., Li, H., Collins, J. J. and Ingber, D. E. (2016). Contributions of microbiome and mechanical deformation to intestinal bacterial overgrowth and inflammation in a human gut-on-a-chip. *Proc Natl Acad Sci USA* 113, E7-15.

Kim, J., Koo, B.-K. and Knoblich, J. A. (2020). Human organoids: model systems for human biology and medicine. *Nat. Rev. Mol. Cell Biol.* 21, 571–584.

Kim, K.-A., Kakitani, M., Zhao, J., Oshima, T., Tang, T., Binnerts, M., Liu, Y., Boyle, B., Park, E., Emtage, P., et al. (2005). Mitogenic influence of human R-spondin1 on the intestinal epithelium. *Science* 309, 1256–1259.

Kim, R., Attayek, P. J., Wang, Y., Furtado, K. L., Tamayo, R., Sims, C. E. and Allbritton, N. L. (2019). An in vitro intestinal platform with a self-sustaining oxygen gradient to study the human gut/microbiome interface. *Biofabrication* 12, 015006.

Kim, S.-E., Choi, S. C., Park, K. S., Park, M. I., Shin, J. E., Lee, T. H., Jung, K. W., Koo, H. S., Myung, S.-J. and Constipation Research group of Korean Society of Neurogastroenterology and Motility (2015). Change of Fecal Flora and Effectiveness of the Short-term VSL#3 Probiotic Treatment in Patients With Functional Constipation. *J. Neurogastroenterol. Motil.* 21, 111–120.

Kim, Y. S. and Ho, S. B. (2010). Intestinal goblet cells and mucins in health and disease: recent insights and progress. *Curr. Gastroenterol. Rep.* 12, 319–330.

Kin, T., Pelaez, D., R., V., Greenberg, J. and S., H. (2013). Pluripotent adult stem cells: A potential revolution in regenerative medicine and tissue engineering. In *Pluripotent Stem Cells* (ed. Bhartiya, D.), p. InTech.

Kinnebrew, M. A., Buffie, C. G., Diehl, G. E., Zenewicz, L. A., Leiner, I., Hohl, T. M., Flavell, R. A., Littman, D. R. and Pamer, E. G. (2012). Interleukin 23 production by intestinal CD103(+)CD11b(+) dendritic cells in response to bacterial flagellin enhances mucosal innate immune defense. *Immunity* 36, 276–287.

Kirouac, D. C., Ito, C., Csaszar, E., Roch, A., Yu, M., Sykes, E. A., Bader, G. D. and Zandstra, P. W. (2010). Dynamic interaction networks in a hierarchically organized tissue. *Mol. Syst. Biol.* 6, 417.

Kiu, R., Treveil, A., Harnisch, L. C., Caim, S., Leclaire, C., van Sinderen, D., Korcsmaros, T. and Hall, L. J. (2020). Bifidobacterium breve UCC2003 Induces a Distinct Global Transcriptomic Program in Neonatal Murine Intestinal Epithelial Cells. *iScience* 23, 101336.

Kline, K. A., Dodson, K. W., Caparon, M. G. and Hultgren, S. J. (2010). A tale of two pili: assembly and function of pili in bacteria. *Trends Microbiol.* 18, 224–232.

Koch, S. and Nusrat, A. (2012). The life and death of epithelia during inflammation: lessons learned from the gut. *Annu. Rev. Pathol.* 7, 35–60.

Kolde, R. (2012). Pheatmap: pretty heatmaps. *R package version 1.2* 1, 726.

Korcsmaros, T., Dunai, Z. A., Vellai, T. and Csermely, P. (2013). Teaching the bioinformatics of signaling networks: an integrated approach to facilitate multi-disciplinary learning. *Brief. Bioinformatics* 14, 618–632.

Korinek, V., Barker, N., Moerer, P., van Donselaar, E., Huls, G., Peters, P. J. and Clevers, H. (1998). Depletion of epithelial stem-cell compartments in the small intestine of mice lacking Tcf-4. *Nat. Genet.* 19, 379–383.

Kostic, A. D., Howitt, M. R. and Garrett, W. S. (2013). Exploring host-microbiota interactions in animal models and humans. *Genes Dev.* 27, 701–718.

Kostic, A. D., Xavier, R. J. and Gevers, D. (2014). The microbiome in inflammatory bowel disease: current status and the future ahead. *Gastroenterology* 146, 1489–1499.

Koutsakos, M., McWilliam, H. E. G., Aktepe, T. E., Fritzlar, S., Illing, P. T., Mifsud, N. A., Purcell, A. W., Rockman, S., Reading, P. C., Vivian, J. P., et al. (2019). Downregulation of MHC class I expression by influenza A and B viruses. *Front. Immunol.* 10, 1158.

Kozomara, A., Birgaoanu, M. and Griffiths-Jones, S. (2019). miRBase: from microRNA sequences to function. *Nucleic Acids Res.* 47, D155–D162.

Kraiczy, J., Nayak, K. M., Howell, K. J., Ross, A., Forbester, J., Salvestrini, C., Mustata, R., Perkins, S., Andersson-Rolf, A., Leenen, E., et al. (2019). DNA methylation defines regional identity of human intestinal epithelial organoids and undergoes dynamic changes during development. *Gut* 68, 49–61.

Kraiczy, J., Nayak, K. M., Howell, K. J., Ross, A., Forbester, J., Salvestrini, C., Mustata, R., Perkins, S., Andersson-Rolf, A., Leenen, E., et al. (2019). DNA methylation defines regional identity of human intestinal epithelial organoids and undergoes dynamic changes during development. *Gut* 68, 49–61.

Krautkramer, K. A., Kreznar, J. H., Romano, K. A., Vivas, E. I., Barrett-Wilt, G. A., Rabaglia, M. E., Keller, M. P., Attie, A. D., Rey, F. E. and Denu, J. M. (2016). Diet-Microbiota Interactions Mediate Global Epigenetic Programming in Multiple Host Tissues. *Mol. Cell* 64, 982–992.

Krishnan, M., Penrose, H. M., Shah, N. N., Marchelletta, R. R. and McCole, D. F. (2016). VSL#3 Probiotic Stimulates T-cell Protein Tyrosine Phosphatase-mediated Recovery of IFN-γ-induced Intestinal Epithelial Barrier Defects. *Inflamm. Bowel Dis.* 22, 2811–2823.

Kroemer, G., Mariño, G. and Levine, B. (2010). Autophagy and the integrated stress response. *Mol. Cell* 40, 280–293.

Kuhn, K. (2016). Altered colonic intraepithelial lymphocyte composition and function in Crohn's Disease. *The Journal of Immunology* 196, 54.10-54.10.

Kuma, A., Komatsu, M. and Mizushima, N. (2017). Autophagy-monitoring and autophagy-deficient mice. *Autophagy* 13, 1619–1628.

Kveler, K., Starosvetsky, E., Ziv-Kenet, A., Kalugny, Y., Gorelik, Y., Shalev-Malul, G., Aizenbud-Reshef, N., Dubovik, T., Briller, M., Campbell, J., et al. (2018). Immune-centric network of cytokines and cells in disease context identified by computational mining of PubMed. *Nat. Biotechnol.* 36, 651–659.

Lai, W. T. and Huang, F. C. (2019). Probiotics exert reciprocal effects on autophagy and interleukin-1β expression in Salmonella-infected intestinal epithelial cells via autophagy-related 16L1 protein. *Benef. Microbes* 10, 913–922.

Lamers, M. M., Beumer, J., van der Vaart, J., Knoops, K., Puschhof, J., Breugem, T. I., Ravelli, R. B. G., Paul van Schayck, J., Mykytyn, A. Z., Duimel, H. Q., et al. (2020). SARS-CoV-2 productively infects human gut enterocytes. *Science* 369, 50–54.

Lassen, K. G. and Xavier, R. J. (2018). Mechanisms and function of autophagy in intestinal disease. *Autophagy* 14, 216–220.

Lassen, K. G., Kuballa, P., Conway, K. L., Patel, K. K., Becker, C. E., Peloquin, J. M., Villablanca, E. J., Norman, J. M., Liu, T.-C., Heath, R. J., et al. (2014). Atg16L1 T300A variant decreases selective autophagy resulting in altered cytokine signaling and decreased antibacterial defense. *Proc Natl Acad Sci USA* 111, 7741–7746.

Lauzier, A., Normandeau-Guimond, J., Vaillancourt-Lavigueur, V., Boivin, V., Charbonneau, M., Rivard, N., Scott, M. S., Dubois, C. M. and Jean, S. (2019). Colorectal cancer cells respond differentially to autophagy inhibition in vivo. *Sci. Rep.* 9, 11316.

Lavelle, A. and Sokol, H. (2020). Gut microbiota-derived metabolites as key actors in inflammatory bowel disease. *Nat. Rev. Gastroenterol. Hepatol.* 17, 223–237.

Lawson, M. A. E., O'Neill, I. J., Kujawska, M., Gowrinadh Javvadi, S., Wijeyesekera, A., Flegg, Z., Chalklen, L. and Hall, L. J. (2020). Breast milk-derived human milk oligosaccharides promote Bifidobacterium interactions within a single ecosystem. *ISME J.* 14, 635–648.

Lee, Y.-S., Kim, T.-Y., Kim, Y., Lee, S.-H., Kim, S., Kang, S. W., Yang, J.-Y., Baek, I.-J., Sung, Y. H., Park, Y.-Y., et al. (2018). Microbiota-Derived Lactate Accelerates Intestinal Stem-Cell-Mediated Epithelial Development. *Cell Host Microbe* 24, 833-846.e6.

Leslie, J. L., Huang, S., Opp, J. S., Nagy, M. S., Kobayashi, M., Young, V. B. and Spence, J. R. (2015). Persistence and toxin production by Clostridium difficile within human intestinal organoids result in disruption of epithelial paracellular barrier function. *Infect. Immun.* 83, 138–145.

Levine, B. and Kroemer, G. (2019). Biological functions of autophagy genes: A disease perspective. *Cell* 176, 11–42.

Li, P., Chen, G., Zhang, J., Pei, C., Chen, Y., Gong, J., Deng, S., Cai, K., Li, H., Wang, D., et al. (2022a). Live Lactobacillus acidophilus alleviates ulcerative colitis via the SCFAs/mitophagy/NLRP3 inflammasome axis. *Food Funct.*

Li, X., Fu, G., Zhang, L., Guan, R., Tang, P., Zhang, J., Rao, X., Chen, S., Xu, X., Zhou, Y., et al. (2022b). Assay establishment and validation of a high-throughput organoid-based drug screening platform. *Stem Cell Res. Ther.* 13, 219.

Li, Y., Yang, N., Chen, J., Huang, X., Zhang, N., Yang, S., Liu, G. and Liu, G. (2020). Next-Generation Porcine Intestinal Organoids: an Apical-Out Organoid Model for Swine Enteric Virus Infection and Immune Response Investigations. *J. Virol.* 94,.

Limanskiy, V., Vyas, A., Chaturvedi, L. S. and Vyas, D. (2019). Harnessing the potential of gene editing technology using CRISPR in inflammatory bowel disease. *World J. Gastroenterol.* 25, 2177–2187.

Limketkai, B. N., Akobeng, A. K., Gordon, M. and Adepoju, A. A. (2020). Probiotics for induction of remission in Crohn's disease. *Cochrane Database Syst. Rev.* 7, CD006634.

Lin, H. H., Chung, Y., Cheng, C.-T., Ouyang, C., Fu, Y., Kuo, C.-Y., Chi, K. K., Sadeghi, M., Chu, P., Kung, H.-J., et al. (2018). Autophagic reliance promotes metabolic reprogramming in oncogenic KRAS-driven tumorigenesis. *Autophagy* 14, 1481–1498.

Lin, R., Jiang, Y., Zhao, X. Y., Guan, Y., Qian, W., Fu, X. C., Ren, H. Y. and Hou, X. H. (2014). Four types of Bifidobacteria trigger autophagy response in intestinal epithelial cells. *J. Dig. Dis.* 15, 597–605.

Lin, Z., Akin, H., Rao, R., Hie, B., Zhu, Z., Lu, W., dos Santos Costa, A., Fazel-Zarandi, M., Sercu, T., Candido, S., et al. (2022). Language models of protein sequences at the scale of evolution enable accurate structure prediction. *BioRxiv*.

Liu, A., Trairatphisan, P., Gjerga, E., Didangelos, A., Barratt, J. and Saez-Rodriguez, J. (2019). From expression footprints to causal pathways: contextualizing large signaling networks with CARNIVAL. *NPJ Syst. Biol. Appl.* 5, 40.

Liu, L., Saitz-Rojas, W., Smith, R., Gonyar, L., In, J. G., Kovbasnjuk, O., Zachos, N. C., Donowitz, M., Nataro, J. P. and Ruiz-Perez, F. (2020). Mucus layer modeling of human colonoids during infection with enteroaggragative E. coli. *Sci. Rep.* 10, 10533.

Liu, Z.-M., Wang, X., Li, C.-X., Liu, X.-Y., Guo, X.-J., Li, Y., Chen, Y.-L., Ye, H.-X. and Chen, H.-S. (2022). SP1 Promotes HDAC4 Expression and Inhibits HMGB1 Expression to Reduce Intestinal Barrier Dysfunction, Oxidative Stress, and Inflammatory Response after Sepsis. *J. Innate Immun.* 14, 366–379.

Lock, J. Y., Carlson, T. L. and Carrier, R. L. (2018). Mucus models to evaluate the diffusion of drugs and particles. *Adv. Drug Deliv. Rev.* 124, 34–49.

Long, Y., Wang, X., Youmans, D. T. and Cech, T. R. (2017). How do lncRNAs regulate transcription? *Sci. Adv.* 3, eaao2110.

López-Díaz, L., Jain, R. N., Keeley, T. M., VanDussen, K. L., Brunkan, C. S., Gumucio, D. L. and Samuelson, L. C. (2007). Intestinal Neurogenin 3 directs differentiation of a bipotential secretory progenitor to endocrine cell rather than goblet cell fate. *Dev. Biol.* 309, 298–305.

Love, M. I., Huber, W. and Anders, S. (2014). Moderated estimation of fold change and dispersion for RNA-seq data with DESeq2. *Genome Biol.* 15, 550.

Lu, R., Zhang, Y.-G., Xia, Y., Zhang, J., Kaser, A., Blumberg, R. and Sun, J. (2021). Paneth cell alertness to pathogens maintained by vitamin D receptors. *Gastroenterology* 160, 1269–1283.

Luissint, A.-C., Williams, H. C., Kim, W., Flemming, S., Azcutia, V., Hilgarth, R. S., Leary, M. N. O., Denning, T. L., Nusrat, A. and Parkos, C. A. (2019). Macrophage-dependent neutrophil recruitment is impaired under conditions of increased intestinal permeability in JAM-A-deficient mice. *Mucosal Immunol.* 12, 668–678.

Lukovac, S., Belzer, C., Pellis, L., Keijser, B. J., de Vos, W. M., Montijn, R. C. and Roeselers, G. (2014). Differential modulation by Akkermansia muciniphila and Faecalibacterium prausnitzii of host peripheral lipid metabolism and histone acetylation in mouse gut organoids. *MBio* 5,.

Macdonald, T. T. and Monteleone, G. (2005). Immunity, inflammation, and allergy in the gut. *Science* 307, 1920–1925.

Macfarlane, S., Furrie, E., Cummings, J. H. and Macfarlane, G. T. (2004). Chemotaxonomic analysis of bacterial populations colonizing the rectal mucosa in patients with ulcerative colitis. *Clin. Infect. Dis.* 38, 1690–1699.

Machiels, K., Joossens, M., Sabino, J., De Preter, V., Arijs, I., Eeckhaut, V., Ballet, V., Claes, K., Van Immerseel, F., Verbeke, K., et al. (2014). A decrease of the butyrate-producing species Roseburia hominis and Faecalibacterium prausnitzii defines dysbiosis in patients with ulcerative colitis. *Gut* 63, 1275–1283.

Mack, D. L., Guan, X., Wagoner, A., Walker, S. J. and Childers, M. K. (2014). Disease-in-a-dish: the contribution of patient-specific induced pluripotent stem cell technology to regenerative rehabilitation. *Am. J. Phys. Med. Rehabil.* 93, S155-68.

Mahoney, Z. X., Stappenbeck, T. S. and Miner, J. H. (2008). Laminin alpha 5 influences the architecture of the mouse small intestine mucosa. *J. Cell Sci.* 121, 2493–2502.

Makino, H. (2018). Bifidobacterial strains in the intestines of newborns originate from their mothers. *Biosci. Microbiota Food Health* 37, 79–85.

Makino, H., Martin, R., Ishikawa, E., Gawad, A., Kubota, H., Sakai, T., Oishi, K., Tanaka, R., Ben-Amor, K., Knol, J., et al. (2015). Multilocus sequence typing of bifidobacterial strains from infant's faeces and human milk: are bifidobacteria being sustainably shared during breastfeeding? *Benef. Microbes* 6, 563–572.

Mangin, I., Dossou-Yovo, F., Lévêque, C., Dessoy, M.-V., Sawoo, O., Suau, A. and Pochart, P. (2018). Oral administration of viable Bifidobacterium pseudolongum strain Patronus modified colonic microbiota and increased mucus layer thickness in rat. *FEMS Microbiol. Ecol.* 94,.

Mankertz, J. and Schulzke, J.-D. (2007). Altered permeability in inflammatory bowel disease: pathophysiology and clinical implications. *Curr. Opin. Gastroenterol.* 23, 379–383.

Marinov, G. K., Williams, B. A., McCue, K., Schroth, G. P., Gertz, J., Myers, R. M. and Wold, B. J. (2014). From single-cell to cell-pool transcriptomes: stochasticity in gene expression and RNA splicing. *Genome Res.* 24, 496–510.

Marteau, P., Cuillerier, E., Meance, S., Gerhardt, M. F., Myara, A., Bouvier, M., Bouley, C., Tondu, F., Bommelaer, G. and Grimaud, J. C. (2002). Bifidobacterium animalis strain DN-173 010 shortens the colonic transit time in healthy women: a double-blind, randomized, controlled study. *Aliment. Pharmacol. Ther.* 16, 587–593.

Martin-Cardona, A., Lloreta Trull, J., Albero-González, R., Paraira Beser, M., Andújar, X., Ruiz-Ramirez, P., Tur-Martínez, J., Ferrer, C., De Marcos Izquierdo, J. A., Pérez-Madrigal,

A., et al. (2021). SARS-CoV-2 identified by transmission electron microscopy in lymphoproliferative and ischaemic intestinal lesions of COVID-19 patients with acute abdominal pain: two case reports. *BMC Gastroenterol.* 21, 334.

Martin, J. C., Chang, C., Boschetti, G., Ungaro, R., Giri, M., Grout, J. A., Gettler, K., Chuang, L.-S., Nayar, S., Greenstein, A. J., et al. (2019). Single-Cell Analysis of Crohn's Disease Lesions Identifies a Pathogenic Cellular Module Associated with Resistance to Anti-TNF Therapy. *Cell* 178, 1493-1508.e20.

Martín, R., Chain, F., Miquel, S., Lu, J., Gratadoux, J.-J., Sokol, H., Verdu, E. F., Bercik, P., Bermúdez-Humarán, L. G. and Langella, P. (2014). The commensal bacterium Faecalibacterium prausnitzii is protective in DNBS-induced chronic moderate and severe colitis models. *Inflamm. Bowel Dis.* 20, 417–430.

Martín, R., Miquel, S., Benevides, L., Bridonneau, C., Robert, V., Hudault, S., Chain, F., Berteau, O., Azevedo, V., Chatel, J. M., et al. (2017). Functional Characterization of Novel Faecalibacterium prausnitzii Strains Isolated from Healthy Volunteers: A Step Forward in the Use of F. prausnitzii as a Next-Generation Probiotic. *Front. Microbiol.* 8, 1226.

Martini, E., Krug, S. M., Siegmund, B., Neurath, M. F. and Becker, C. (2017). Mend your fences: the epithelial barrier and its relationship with mucosal immunity in inflammatory bowel disease. *Cell. Mol. Gastroenterol. Hepatol.* 4, 33–46.

Martz, S. L., Guzman-Rodriguez, M., He, S.-M., Noordhof, C., Hurlbut, D. J., Gloor, G. B., Carlucci, C., Weese, S., Allen-Vercoe, E., Sun, J., et al. (2017). A human gut ecosystem protects against C. difficile disease by targeting TcdA. *J. Gastroenterol.* 52, 452–465.

Marzorati, M., Vanhoecke, B., De Ryck, T., Sadaghian Sadabad, M., Pinheiro, I., Possemiers, S., Van den Abbeele, P., Derycke, L., Bracke, M., Pieters, J., et al. (2014). The HMI™ module: a new tool to study the Host-Microbiota Interaction in the human gastrointestinal tract in vitro. *BMC Microbiol.* 14, 133.

Matano, M., Date, S., Shimokawa, M., Takano, A., Fujii, M., Ohta, Y., Watanabe, T., Kanai, T. and Sato, T. (2015). Modeling colorectal cancer using CRISPR-Cas9-mediated engineering of human intestinal organoids. *Nat. Med.* 21, 256–262.

Matsuzawa-Ishimoto, Y., Hine, A., Shono, Y., Rudensky, E., Lazrak, A., Yeung, F., Neil, J. A., Yao, X., Chen, Y.-H., Heaney, T., et al. (2020). An intestinal organoid-based platform that recreates susceptibility to T-cell-mediated tissue injury. *Blood* 135, 2388–2401.

Matsuzawa-Ishimoto, Y., Hwang, S. and Cadwell, K. (2018). Autophagy and Inflammation. *Annu. Rev. Immunol.* 36, 73–101.

Matsuzawa-Ishimoto, Y., Shono, Y., Gomez, L. E., Hubbard-Lucey, V. M., Cammer, M., Neil, J., Dewan, M. Z., Lieberman, S. R., Lazrak, A., Marinis, J. M., et al. (2017). Autophagy protein ATG16L1 prevents necroptosis in the intestinal epithelium. *J. Exp. Med.* 214, 3687–3705.

May, S., Evans, S. and Parry, L. (2017). Organoids, organs-on-chips and other systems, and microbiota. *Emerg. Top. Life Sci.* 1, 385–400.

Mazé, A., O'Connell-Motherway, M., Fitzgerald, G. F., Deutscher, J. and van Sinderen, D. (2007). Identification and characterization of a fructose phosphotransferase system in Bifidobacterium breve UCC2003. *Appl. Environ. Microbiol.* 73, 545–553.

McCarthy, D. J., Chen, Y. and Smyth, G. K. (2012). Differential expression analysis of multifactor RNA-Seq experiments with respect to biological variation. *Nucleic Acids Res.* 40, 4288–4297.

McCole, D. F. (2014). IBD candidate genes and intestinal barrier regulation. *Inflamm. Bowel Dis.* 20, 1829–1849.

McCracken, K. W., Catá, E. M., Crawford, C. M., Sinagoga, K. L., Schumacher, M., Rockich, B. E., Tsai, Y.-H., Mayhew, C. N., Spence, J. R., Zavros, Y., et al. (2014). Modelling human development and disease in pluripotent stem-cell-derived gastric organoids. *Nature* 516, 400–404.

McDavid, A., Finak, G. and Yajima, M. (2021). MAST: Tools and methods for analysis of single cell assay data in R. *R package version 1.18.0*.

McInnes, L., Healy, J., Saul, N. and Großberger, L. (2018). UMAP: uniform manifold approximation and projection. *JOSS* 3, 861.

Mead, B. E., Hattori, K., Levy, L., Imada, S., Goto, N., Vukovic, M., Sze, D., Kummerlowe, C., Matute, J. D., Duan, J., et al. (2022). Screening for modulators of the cellular composition of gut epithelia via organoid models of intestinal stem cell differentiation. *Nat. Biomed. Eng.* 6, 476–494.

Mehandru, S. and Colombel, J.-F. (2021). The intestinal barrier, an arbitrator turned provocateur in IBD. *Nat. Rev. Gastroenterol. Hepatol.* 18, 83–84.

Mehto, S., Jena, K. K., Nath, P., Chauhan, S., Kolapalli, S. P., Das, S. K., Sahoo, P. K., Jain, A., Taylor, G. A. and Chauhan, S. (2019). The crohn's disease risk factor IRGM limits NLRP3 inflammasome activation by impeding its assembly and by mediating its selective autophagy. *Mol. Cell* 73, 429-445.e7.

Mejlvang, J., Olsvik, H., Svenning, S., Bruun, J.-A., Abudu, Y. P., Larsen, K. B., Brech, A., Hansen, T. E., Brenne, H., Hansen, T., et al. (2018). Starvation induces rapid degradation of selective autophagy receptors by endosomal microautophagy. *J. Cell Biol.* 217, 3640–3655.

Menche, J., Sharma, A., Kitsak, M., Ghiassian, S. D., Vidal, M., Loscalzo, J. and Barabási, A.-L. (2015). Disease networks. Uncovering disease-disease relationships through the incomplete interactome. *Science* 347, 1257601.

Meng, C., Zhan, J., Chen, D., Shao, G., Zhang, H., Gu, W. and Luo, J. (2021). The deubiquitinase USP11 regulates cell proliferation and ferroptotic cell death via stabilization of NRF2 USP11 deubiquitinates and stabilizes NRF2. *Oncogene* 40, 1706–1720.

Micheel, C. M., Nass, S. J., Omenn, G. S., Committee on the Review of Omics-Based Tests for Predicting Patient Outcomes in Clinical Trials, Board on Health Care Services, Board on Health Sciences Policy and Medicine, I. of (2012). Omics-Based Clinical Discovery: Science, Technology, and Applications - Evolution of Translational Omics - NCBI Bookshelf.

Mick, E., Kamm, J., Pisco, A. O., Ratnasiri, K., Babik, J. M., Calfee, C. S., Castañeda, G., DeRisi, J. L., Detweiler, A. M., Hao, S., et al. (2020). Upper airway gene expression differentiates COVID-19 from other acute respiratory illnesses and reveals suppression of innate immune responses by SARS-CoV-2. *medRxiv*.

Middendorp, S., Schneeberger, K., Wiegerinck, C. L., Mokry, M., Akkerman, R. D. L., van Wijngaarden, S., Clevers, H. and Nieuwenhuis, E. E. S. (2014). Adult stem cells in the small

intestine are intrinsically programmed with their location-specific function. *Stem Cells* 32, 1083–1091.

Milani, C., Mangifesta, M., Mancabelli, L., Lugli, G. A., Mancino, W., Viappiani, A., Faccini, A., van Sinderen, D., Ventura, M. and Turroni, F. (2017). The Sortase-Dependent Fimbriome of the Genus Bifidobacterium: Extracellular Structures with Potential To Modulate Microbe-Host Dialogue. *Appl. Environ. Microbiol.* 83,.

Min, S., Kim, S. and Cho, S.-W. (2020). Gastrointestinal tract modeling using organoids engineered with cellular and microbiota niches. *Exp. Mol. Med.* 52, 227–237.

Mirsepasi-Lauridsen, H. C., Vrankx, K., Engberg, J., Friis-Møller, A., Brynskov, J., Nordgaard-Lassen, I., Petersen, A. M. and Krogfelt, K. A. (2018). Disease-Specific Enteric Microbiome Dysbiosis in Inflammatory Bowel Disease. *Front Med (Lausanne)* 5, 304.

Miryala, S. K., Anbarasu, A. and Ramaiah, S. (2018). Discerning molecular interactions: A comprehensive review on biomolecular interaction databases and network analysis tools. *Gene* 642, 84–94.

Mirza, A. H., Berthelsen, C. H., Seemann, S. E., Pan, X., Frederiksen, K. S., Vilien, M., Gorodkin, J. and Pociot, F. (2015). Transcriptomic landscape of lncRNAs in inflammatory bowel disease. *Genome Med.* 7, 39.

Mishra, J., Waters, C. M. and Kumar, N. (2012). Molecular mechanism of interleukin-2-induced mucosal homeostasis. *Am J Physiol, Cell Physiol* 302, C735-47.

Moayyedi, P., Surette, M. G., Kim, P. T., Libertucci, J., Wolfe, M., Onischi, C., Armstrong, D., Marshall, J. K., Kassam, Z., Reinisch, W., et al. (2015). Fecal microbiota transplantation induces remission in patients with active ulcerative colitis in a randomized controlled trial. *Gastroenterology* 149, 102-109.e6.

Módos, D., Bulusu, K. C., Fazekas, D., Kubisch, J., Brooks, J., Marczell, I., Szabó, P. M., Vellai, T., Csermely, P., Lenti, K., et al. (2017). Neighbours of cancer-related proteins have key influence on pathogenesis and could increase the drug target space for anticancer therapies. *NPJ Syst. Biol. Appl.* 3, 2.

Molinero, N., Ruiz, L., Sánchez, B., Margolles, A. and Delgado, S. (2019). Intestinal bacteria interplay with bile and cholesterol metabolism: implications on host physiology. *Front. Physiol.* 10, 185.

Montgomery, R. K., Carlone, D. L., Richmond, C. A., Farilla, L., Kranendonk, M. E. G., Henderson, D. E., Baffour-Awuah, N. Y., Ambruzs, D. M., Fogli, L. K., Algra, S., et al. (2011). Mouse telomerase reverse transcriptase (mTert) expression marks slowly cycling intestinal stem cells. *Proc Natl Acad Sci USA* 108, 179–184.

Moon, C., VanDussen, K. L., Miyoshi, H. and Stappenbeck, T. S. (2014). Development of a primary mouse intestinal epithelial cell monolayer culture system to evaluate factors that modulate IgA transcytosis. *Mucosal Immunol.* 7, 818–828.

Mowat, A. M., Donachie, A. M., Parker, L. A., Robson, N. C., Beacock-Sharp, H., McIntyre, L. J., Millington, O. and Chirdo, F. (2003). The role of dendritic cells in regulating mucosal immunity and tolerance. *Novartis Found. Symp.* 252, 291–302; discussion 302.

Muetze, T., Goenawan, I. H., Wiencko, H. L., Bernal-Llinares, M., Bryan, K. and Lynn, D. J. (2016). Contextual Hub Analysis Tool (CHAT): A Cytoscape app for identifying contextually

relevant hubs in biological networks. [version 2; peer review: 2 approved]. *F1000Res.* 5, 1745.

Muniz, L. R., Knosp, C. and Yeretssian, G. (2012). Intestinal antimicrobial peptides during homeostasis, infection, and disease. *Front. Immunol.* 3, 310.

Muñoz, J., Stange, D. E., Schepers, A. G., van de Wetering, M., Koo, B.-K., Itzkovitz, S., Volckmann, R., Kung, K. S., Koster, J., Radulescu, S., et al. (2012). The Lgr5 intestinal stem cell signature: robust expression of proposed quiescent “+4” cell markers. *EMBO J.* 31, 3079–3091.

Munoz, S., Guzman-Rodriguez, M., Sun, J., Zhang, Y.-G., Noordhof, C., He, S.-M., Allen-Vercoe, E., Claud, E. C. and Petrof, E. O. (2016). Rebooting the microbiome. *Gut Microbes* 7, 353–363.

Murthy, A., Li, Y., Peng, I., Reichelt, M., Katakam, A. K., Noubade, R., Roose-Girma, M., DeVoss, J., Diehl, L., Graham, R. R., et al. (2014). A Crohn’s disease variant in Atg16l1 enhances its degradation by caspase 3. *Nature* 506, 456–462.

Nagpal, R., Kurakawa, T., Tsuji, H., Takahashi, T., Kawashima, K., Nagata, S., Nomoto, K. and Yamashiro, Y. (2017). Evolution of gut Bifidobacterium population in healthy Japanese infants over the first three years of life: a quantitative assessment. *Sci. Rep.* 7, 10097.

Nalle, S. C. and Turner, J. R. (2015). Intestinal barrier loss as a critical pathogenic link between inflammatory bowel disease and graft-versus-host disease. *Mucosal Immunol.* 8, 720–730.

Naseer, M. I., Bibi, F., Alqahtani, M. H., Chaudhary, A. G., Azhar, E. I., Kamal, M. A. and Yasir, M. (2014). Role of gut microbiota in obesity, type 2 diabetes and Alzheimer’s disease. *CNS Neurol. Disord. Drug Targets* 13, 305–311.

Nash, T. J., Morris, K. M., Mabbott, N. A. and Vervelde, L. (2021). Inside-out chicken enteroids with leukocyte component as a model to study host-pathogen interactions. *Commun. Biol.* 4, 377.

Natividad, J. M. M., Hayes, C. L., Motta, J.-P., Jury, J., Galipeau, H. J., Philip, V., Garcia-Rodenas, C. L., Kiyama, H., Bercik, P. and Verdu, E. F. (2013). Differential induction of antimicrobial REGIII by the intestinal microbiota and Bifidobacterium breve NCC2950. *Appl. Environ. Microbiol.* 79, 7745–7754.

Netea-Maier, R. T., Plantinga, T. S., van de Veerdonk, F. L., Smit, J. W. and Netea, M. G. (2016). Modulation of inflammation by autophagy: Consequences for human disease. *Autophagy* 12, 245–260.

Neurath, M. F. (2019). Targeting immune cell circuits and trafficking in inflammatory bowel disease. *Nat. Immunol.* 20, 970–979.

Neurath, M. F. (2020). Host-microbiota interactions in inflammatory bowel disease. *Nat. Rev. Gastroenterol. Hepatol.* 17, 76–77.

Nguyen, T. L. A., Vieira-Silva, S., Liston, A. and Raes, J. (2015). How informative is the mouse for human gut microbiota research? *Dis. Model. Mech.* 8, 1–16.

Ni, J., Wu, G. D., Albenberg, L. and Tomov, V. T. (2017). Gut microbiota and IBD: causation or correlation? *Nat. Rev. Gastroenterol. Hepatol.* 14, 573–584.

Nicoletti, C. (2000). Unsolved mysteries of intestinal M cells. *Gut* 47, 735–739.

Noah, T. K., Donahue, B. and Shroyer, N. F. (2011). Intestinal development and differentiation. *Exp. Cell Res.* 317, 2702–2710.

Noel, G., Baetz, N. W., Staab, J. F., Donowitz, M., Kovbasnjuk, O., Pasetti, M. F. and Zachos, N. C. (2017). A primary human macrophage-enteroid co-culture model to investigate mucosal gut physiology and host-pathogen interactions. *Sci. Rep.* 7, 45270.

Nozaki, K., Mochizuki, W., Matsumoto, Y., Matsumoto, T., Fukuda, M., Mizutani, T., Watanabe, M. and Nakamura, T. (2016). Co-culture with intestinal epithelial organoids allows efficient expansion and motility analysis of intraepithelial lymphocytes. *J. Gastroenterol.* 51, 206–213.

Nuriel-Ohayon, M., Neuman, H. and Koren, O. (2016). Microbial Changes during Pregnancy, Birth, and Infancy. *Front. Microbiol.* 7, 1031.

Nusbaum, D. J., Sun, F., Ren, J., Zhu, Z., Ramsy, N., Pervolarakis, N., Kunde, S., England, W., Gao, B., Fiehn, O., et al. (2018). Gut microbial and metabolomic profiles after fecal microbiota transplantation in pediatric ulcerative colitis patients. *FEMS Microbiol. Ecol.* 94,.

Nusse, R. (2008). Wnt signaling and stem cell control. *Cell Res.* 18, 523–527.

O'Callaghan, A. and van Sinderen, D. (2016). Bifidobacteria and their role as members of the human gut microbiota. *Front. Microbiol.* 7, 925.

O'Connell Motherway, M., Houston, A., O'Callaghan, G., Reunanen, J., O'Brien, F., O'Driscoll, T., Casey, P. G., de Vos, W. M., van Sinderen, D. and Shanahan, F. (2019). A Bifidobacterial pilus-associated protein promotes colonic epithelial proliferation. *Mol. Microbiol.* 111, 287–301.

O'Connell Motherway, M., Zomer, A., Leahy, S. C., Reunanen, J., Bottacini, F., Claesson, M. J., O'Brien, F., Flynn, K., Casey, P. G., Munoz, J. A. M., et al. (2011). Functional genome analysis of Bifidobacterium breve UCC2003 reveals type IVb tight adherence (Tad) pili as an essential and conserved host-colonization factor. *Proc Natl Acad Sci USA* 108, 11217–11222.

O'Mahony, L., McCarthy, J., Kelly, P., Hurley, G., Luo, F., Chen, K., O'Sullivan, G. C., Kiely, B., Collins, J. K., Shanahan, F., et al. (2005). Lactobacillus and bifidobacterium in irritable bowel syndrome: symptom responses and relationship to cytokine profiles. *Gastroenterology* 128, 541–551.

O'Neill, I., Schofield, Z. and Hall, L. J. (2017). Exploring the role of the microbiota member Bifidobacterium in modulating immune-linked diseases. *Emerg. Top. Life Sci.* 1, 333–349.

O'Toole, P. W., Marchesi, J. R. and Hill, C. (2017). Next-generation probiotics: the spectrum from probiotics to live biotherapeutics. *Nat. Microbiol.* 2, 17057.

Oh, J. E. and Lee, H. K. (2014). Pattern recognition receptors and autophagy. *Front. Immunol.* 5, 300.

Ohno, H. (2016). Intestinal M cells. *J. Biochem.* 159, 151–160.

Olbei, M., Hautefort, I., Modos, D., Treveil, A., Poletti, M., Gul, L., Shannon-Lowe, C. D. and Korcsmaros, T. (2021). SARS-CoV-2 Causes a Different Cytokine Response Compared to Other Cytokine Storm-Causing Respiratory Viruses in Severely Ill Patients. *Front. Immunol.* 12, 629193.

Orchard, S., Ammari, M., Aranda, B., Breuza, L., Briganti, L., Broackes-Carter, F., Campbell, N. H., Chavali, G., Chen, C., del-Toro, N., et al. (2014). The MIntAct project - IntAct as a common curation platform for 11 molecular interaction databases. *Nucleic Acids Res.* 42, D358-63.

Ott, S. J., Musfeldt, M., Wenderoth, D. F., Hampe, J., Brant, O., Fölsch, U. R., Timmis, K. N. and Schreiber, S. (2004). Reduction in diversity of the colonic mucosa associated bacterial microflora in patients with active inflammatory bowel disease. *Gut* 53, 685–693.

Ouellette, A. J. (2011). Paneth cell α-defensins in enteric innate immunity. *Cell. Mol. Life Sci.* 68, 2215–2229.

Ouwehand, A. C., Isolauri, E., He, F., Hashimoto, H., Benno, Y. and Salminen, S. (2001). Differences in Bifidobacterium flora composition in allergic and healthy infants. *J. Allergy Clin. Immunol.* 108, 144–145.

Papin, J. A., Hunter, T., Palsson, B. O. and Subramaniam, S. (2005). Reconstruction of cellular signalling networks and analysis of their properties. *Nat. Rev. Mol. Cell Biol.* 6, 99–111.

Paramsothy, S., Kamm, M. A., Kaakoush, N. O., Walsh, A. J., van den Bogaerde, J., Samuel, D., Leong, R. W. L., Connor, S., Ng, W., Paramsothy, R., et al. (2017). Multidonor intensive faecal microbiota transplantation for active ulcerative colitis: a randomised placebo-controlled trial. *Lancet* 389, 1218–1228.

Paraskevopoulou, M. D. and Hatzigeorgiou, A. G. (2016). Analyzing MiRNA-LncRNA Interactions. *Methods Mol. Biol.* 1402, 271–286.

Park, G.-S., Park, M. H., Shin, W., Zhao, C., Sheikh, S., Oh, S. J. and Kim, H. J. (2017). Emulating Host-Microbiome Ecosystem of Human Gastrointestinal Tract in Vitro. *Stem Cell Rev and Rep* 13, 321–334.

Park, J.-H., Lee, J.-M., Lee, E.-J., Hwang, W.-B. and Kim, D.-J. (2018). Indole-3-Carbinol Promotes Goblet-Cell Differentiation Regulating Wnt and Notch Signaling Pathways AhR-Dependently. *Mol. Cells* 41, 290–300.

Park, M. D. (2020). Immune evasion via SARS-CoV-2 ORF8 protein? *Nat. Rev. Immunol.* 20, 408.

Parkes, G. C., Rayment, N. B., Hudspith, B. N., Petrovska, L., Lomer, M. C., Brostoff, J., Whelan, K. and Sanderson, J. D. (2012). Distinct microbial populations exist in the mucosa-associated microbiota of sub-groups of irritable bowel syndrome. *Neurogastroenterol. Motil.* 24, 31–39.

Parkes, M., Barrett, J. C., Prescott, N. J., Tremelling, M., Anderson, C. A., Fisher, S. A., Roberts, R. G., Nimmo, E. R., Cummings, F. R., Soars, D., et al. (2007). Sequence variants in the autophagy gene IRGM and multiple other replicating loci contribute to Crohn's disease susceptibility. *Nat. Genet.* 39, 830–832.

Parmar, N., Burrows, K., Vornewald, P. M., Lindholm, H. T., Zwiggelaar, R. T., Díez-Sánchez, A., Martín-Alonso, M., Fosslie, M., Vallance, B. A., Dahl, J. A., et al. (2021). Intestinal-epithelial LSD1 controls goblet cell maturation and effector responses required for gut immunity to bacterial and helminth infection. *PLoS Pathog.* 17, e1009476.

Pastuła, A., Middelhoff, M., Brandtner, A., Tobiasch, M., Höhl, B., Nuber, A. H., Demir, I. E., Neupert, S., Kollmann, P., Mazzuoli-Weber, G., et al. (2016). Three-Dimensional

Gastrointestinal Organoid Culture in Combination with Nerves or Fibroblasts: A Method to Characterize the Gastrointestinal Stem Cell Niche. *Stem Cells Int.* 2016, 3710836.

Patel, K. K., Miyoshi, H., Beatty, W. L., Head, R. D., Malvin, N. P., Cadwell, K., Guan, J.-L., Saitoh, T., Akira, S., Seglen, P. O., et al. (2013). Autophagy proteins control goblet cell function by potentiating reactive oxygen species production. *EMBO J.* 32, 3130–3144.

Patole, S. K., Rao, S. C., Keil, A. D., Nathan, L. A., Doherty, D. A., & Simmer, K. N. (2016). Benefits of bifidobacterium breve M-16V Supplementation in preterm neonates -A retrospective cohort study. *PLoS One*, 11.

Paull, E. O., Carlin, D. E., Niepel, M., Sorger, P. K., Haussler, D. and Stuart, J. M. (2013). Discovering causal pathways linking genomic events to transcriptional states using Tied Diffusion Through Interacting Events (TieDIE). *Bioinformatics* 29, 2757–2764.

Pavlidis, P., Tsakmaki, A., Treveil, A., Li, K., Cozzetto, D., Yang, F., Niazi, U., Hayee, B., Saqi, M., Friedman, J., et al. (2021). Cytokine responsive networks in human colonic epithelial organoids unveil a novel molecular stratification of inflammatory bowel disease. *SSRN Journal*.

Pawson, A. J., Sharman, J. L., Benson, H. E., Faccenda, E., Alexander, S. P. H., Buneman, O. P., Davenport, A. P., McGrath, J. C., Peters, J. A., Southan, C., et al. (2014). The IUPHAR/BPS Guide to PHARMACOLOGY: an expert-driven knowledgebase of drug targets and their ligands. *Nucleic Acids Res.* 42, D1098-106.

Payne, A. N., Zihler, A., Chassard, C. and Lacroix, C. (2012). Advances and perspectives in in vitro human gut fermentation modeling. *Trends Biotechnol.* 30, 17–25.

Peacock, T. P., Brown, J. C., Zhou, J., Thakur, N., Newman, J., Kugathasan, R., Sukhova, K., Kaforou, M., Bailey, D. and Barclay, W. S. (2022). The SARS-CoV-2 variant, Omicron, shows rapid replication in human primary nasal epithelial cultures and efficiently uses the endosomal route of entry. *BioRxiv*.

Peng, H., Yang, J., Li, G., You, Q., Han, W., Li, T., Gao, D., Xie, X., Lee, B.-H., Du, J., et al. (2017). Ubiquitylation of p62/sequestosome1 activates its autophagy receptor function and controls selective autophagy upon ubiquitin stress. *Cell Res.* 27, 657–674.

Peterson, L. W. and Artis, D. (2014). Intestinal epithelial cells: regulators of barrier function and immune homeostasis. *Nat. Rev. Immunol.* 14, 141–153.

Picart-Armada, S., Barrett, S. J., Willé, D. R., Perera-Lluna, A., Gutteridge, A. and Dessailly, B. H. (2019). Benchmarking network propagation methods for disease gene identification. *PLoS Comput. Biol.* 15, e1007276.

Pickert, G., Neufert, C., Leppkes, M., Zheng, Y., Wittkopf, N., Warntjen, M., Lehr, H.-A., Hirth, S., Weigmann, B., Wirtz, S., et al. (2009). STAT3 links IL-22 signaling in intestinal epithelial cells to mucosal wound healing. *J. Exp. Med.* 206, 1465–1472.

Pils, M. C., Bleich, A., Prinz, I., Fasnacht, N., Bollati-Fogolin, M., Schippers, A., Rozell, B. and Müller, W. (2011). Commensal gut flora reduces susceptibility to experimentally induced colitis via T-cell-derived interleukin-10. *Inflamm. Bowel Dis.* 17, 2038–2046.

Pinto-Sánchez, M. I., Smecuol, E. C., Temprano, M. P., Sugai, E., González, A., Moreno, M. L., Huang, X., Bercik, P., Cabanne, A., Vázquez, H., et al. (2017). Bifidobacterium infantis NLS Super Strain Reduces the Expression of α-Defensin-5, a Marker of Innate Immunity, in the Mucosa of Active Celiac Disease Patients. *J. Clin. Gastroenterol.* 51, 814–817.

Pleguezuelos-Manzano, C., Puschhof, J., van den Brink, S., Geurts, V., Beumer, J. and Clevers, H. (2020). Establishment and Culture of Human Intestinal Organoids Derived from Adult Stem Cells. *Curr. Protoc. Immunol.* 130, e106.

Poletti, M., Arnauts, K., Ferrante, M. and Korcsmaros, T. (2021). Organoid-based Models to Study the Role of Host-microbiota Interactions in IBD. *J Crohns Colitis* 15, 1222–1235.

Poletti, M., Treveil, A., Csabai, L., Gul, L., Modos, D., Madgwick, M., Olbei, M., Bohar, B., Valdeolivas, A., Turei, D., et al. (2022). Mapping the epithelial-immune cell interactome upon infection in the gut and the upper airways. *NPJ Syst. Biol. Appl.* 8, 15.

Pott, J., Kabat, A. M. and Maloy, K. J. (2018). Intestinal Epithelial Cell Autophagy Is Required to Protect against TNF-Induced Apoptosis during Chronic Colitis in Mice. *Cell Host Microbe* 23, 191-202.e4.

Potten, C. S., Kovacs, L. and Hamilton, E. (1974). Continuous labelling studies on mouse skin and intestine. *Cell Tissue Kinet.* 7, 271–283.

Powell, A. E., Wang, Y., Li, Y., Poulin, E. J., Means, A. L., Washington, M. K., Higginbotham, J. N., Juchheim, A., Prasad, N., Levy, S. E., et al. (2012). The pan-ErbB negative regulator Lrig1 is an intestinal stem cell marker that functions as a tumor suppressor. *Cell* 149, 146–158.

Pozo-Rubio, T., Mujico, J. R., Marcos, A., Puertollano, E., Nadal, I., Sanz, Y. and Nova, E. (2011). Immunostimulatory effect of faecal Bifidobacterium species of breast-fed and formula-fed infants in a peripheral blood mononuclear cell/Caco-2 co-culture system. *Br. J. Nutr.* 106, 1216–1223.

Püngel, D., Treveil, A., Dalby, M. J., Caim, S., Colquhoun, I. J., Booth, C., Ketskemety, J., Korcsmaros, T., van Sinderen, D., Lawson, M. A., et al. (2020). Bifidobacterium breve UCC2003 Exopolysaccharide Modulates the Early Life Microbiota by Acting as a Potential Dietary Substrate. *Nutrients* 12, 948.

Puntervoll, P., Linding, R., Gemünd, C., Chabanis-Davidson, S., Mattingsdal, M., Cameron, S., Martin, D. M. A., Ausiello, G., Brannetti, B., Costantini, A., et al. (2003). ELM server: A new resource for investigating short functional sites in modular eukaryotic proteins. *Nucleic Acids Res.* 31, 3625–3630.

Puschhof, J., Pleguezuelos-Manzano, C. and Clevers, H. (2021a). Organoids and organs-on-chips: Insights into human gut-microbe interactions. *Cell Host Microbe* 29, 867–878.

Puschhof, J., Pleguezuelos-Manzano, C., Martinez-Silgado, A., Akkerman, N., Saftien, A., Boot, C., de Waal, A., Beumer, J., Dutta, D., Heo, I., et al. (2021b). Intestinal organoid cocultures with microbes. *Nat. Protoc.* 16, 4633–4649.

Qi, Z., Li, Y., Zhao, B., Xu, C., Liu, Y., Li, H., Zhang, B., Wang, X., Yang, X., Xie, W., et al. (2017). BMP restricts stemness of intestinal Lgr5+ stem cells by directly suppressing their signature genes. *Nat. Commun.* 8, 13824.

Qian, X., Nguyen, H. N., Song, M. M., Hadiono, C., Ogden, S. C., Hammack, C., Yao, B., Hamersky, G. R., Jacob, F., Zhong, C., et al. (2016). Brain-Region-Specific Organoids Using Mini-bioreactors for Modeling ZIKV Exposure. *Cell* 165, 1238–1254.

Qin, X., Sufi, J., Vlckova, P., Kyriakidou, P., Acton, S. E., Li, V. S. W., Nitz, M. and Tape, C. J. (2020). Cell-type-specific signaling networks in heterocellular organoids. *Nat. Methods* 17, 335–342.

Raghavachari, B., Tasneem, A., Przytycka, T. M. and Jothi, R. (2008). DOMINE: a database of protein domain interactions. *Nucleic Acids Res.* 36, D656-61.

Raghoebir, L., Bakker, E. R. M., Mills, J. C., Swagemakers, S., Kempen, M. B., Munck, A. B., Driegen, S., Meijer, D., Grosveld, F., Tibboel, D., et al. (2012). SOX2 redirects the developmental fate of the intestinal epithelium toward a premature gastric phenotype. *J. Mol. Cell Biol.* 4, 377–385.

Ramilowski, J. A., Goldberg, T., Harshbarger, J., Kloppmann, E., Lizio, M., Satagopam, V. P., Itoh, M., Kawaji, H., Carninci, P., Rost, B., et al. (2015). A draft network of ligand-receptor-mediated multicellular signalling in human. *Nat. Commun.* 6, 7866.

Rashid, H.-O., Yadav, R. K., Kim, H.-R. and Chae, H.-J. (2015). ER stress: Autophagy induction, inhibition and selection. *Autophagy* 11, 1956–1977.

Ratajczak, W., Rył, A., Mizerski, A., Walczakiewicz, K., Sipak, O. and Laszczyńska, M. (2019). Immunomodulatory potential of gut microbiome-derived short-chain fatty acids (SCFAs). *Acta Biochim. Pol.* 66, 1–12.

Reichardt, N., Duncan, S. H., Young, P., Belenguer, A., McWilliam Leitch, C., Scott, K. P., Flint, H. J. and Louis, P. (2014). Phylogenetic distribution of three pathways for propionate production within the human gut microbiota. *ISME J.* 8, 1323–1335.

Riedel, C.-U., Foata, F., Philippe, D., Adolfsson, O., Eikmanns, B.-J. and Blum, S. (2006). Anti-inflammatory effects of bifidobacteria by inhibition of LPS-induced NF-kappaB activation. *World J. Gastroenterol.* 12, 3729–3735.

Ríos-Covián, D., Ruas-Madiedo, P., Margolles, A., Gueimonde, M., de Los Reyes-Gavilán, C. G. and Salazar, N. (2016). Intestinal Short Chain Fatty Acids and their Link with Diet and Human Health. *Front. Microbiol.* 7, 185.

Rioux, J. D., Xavier, R. J., Taylor, K. D., Silverberg, M. S., Goyette, P., Huett, A., Green, T., Kuballa, P., Barmada, M. M., Datta, L. W., et al. (2007). Genome-wide association study identifies new susceptibility loci for Crohn disease and implicates autophagy in disease pathogenesis. *Nat. Genet.* 39, 596–604.

Ro, S.-H., Fay, J., Cyuzuzo, C. I., Jang, Y., Lee, N., Song, H.-S. and Harris, E. N. (2020). SESTRINs: Emerging Dynamic Stress-Sensors in Metabolic and Environmental Health. *Front. Cell Dev. Biol.* 8, 603421.

Robinson, M. D., McCarthy, D. J. and Smyth, G. K. (2010). edgeR: a Bioconductor package for differential expression analysis of digital gene expression data. *Bioinformatics* 26, 139–140.

Rodríguez-Colman, M. J., Schewe, M., Meerlo, M., Stigter, E., Gerrits, J., Pras-Raves, M., Sacchetti, A., Hornsveld, M., Oost, K. C., Snippert, H. J., et al. (2017). Interplay between metabolic identities in the intestinal crypt supports stem cell function. *Nature* 543, 424–427.

Rogoz, A., Reis, B. S., Karssemeijer, R. A. and Mucida, D. (2015). A 3-D enteroid-based model to study T-cell and epithelial cell interaction. *J. Immunol. Methods* 421, 89–95.

Rouch, J. D., Scott, A., Lei, N. Y., Solorzano-Vargas, R. S., Wang, J., Hanson, E. M., Kobayashi, M., Lewis, M., Stelzner, M. G., Dunn, J. C. Y., et al. (2016). Development of Functional Microfold (M) Cells from Intestinal Stem Cells in Primary Human Enteroids. *PLoS ONE* 11, e0148216.

Ruiz, L., Delgado, S., Ruas-Madiedo, P., Sánchez, B. and Margolles, A. (2017). Bifidobacteria and Their Molecular Communication with the Immune System. *Front. Microbiol.* 8, 2345.

Ruiz, L., Ruas-Madiedo, P., Gueimonde, M., de Los Reyes-Gavilán, C. G., Margolles, A. and Sánchez, B. (2011). How do bifidobacteria counteract environmental challenges? Mechanisms involved and physiological consequences. *Genes Nutr.* 6, 307–318.

Runwal, G., Stamatakou, E., Siddiqi, F. H., Puri, C., Zhu, Y. and Rubinsztein, D. C. (2019). LC3-positive structures are prominent in autophagy-deficient cells. *Sci. Rep.* 9, 10147.

Russell, D. A., Ross, R. P., Fitzgerald, G. F. and Stanton, C. (2011). Metabolic activities and probiotic potential of bifidobacteria. *Int. J. Food Microbiol.* 149, 88–105.

Russo, E., Giudici, F., Fiorindi, C., Ficari, F., Scaringi, S. and Amedei, A. (2019). Immunomodulating Activity and Therapeutic Effects of Short Chain Fatty Acids and Tryptophan Post-biotics in Inflammatory Bowel Disease. *Front. Immunol.* 10, 2754.

Rutgeerts, P., Goboes, K., Peeters, M., Hiele, M., Penninckx, F., Aerts, R., Kerremans, R. and Vantrappen, G. (1991). Effect of faecal stream diversion on recurrence of Crohn's disease in the neoterminal ileum. *Lancet* 338, 771–774.

Saçar Demirci, M. D. and Adan, A. (2020). Computational analysis of microRNA-mediated interactions in SARS-CoV-2 infection. *PeerJ* 8, e9369.

Sahu, R., Kaushik, S., Clement, C. C., Cannizzo, E. S., Scharf, B., Follenzi, A., Potolicchio, I., Nieves, E., Cuervo, A. M. and Santambrogio, L. (2011). Microautophagy of cytosolic proteins by late endosomes. *Dev. Cell* 20, 131–139.

Sakurai, T., Hashikura, N., Minami, J., Yamada, A., Odamaki, T. and Xiao, J.-Z. (2017). Tolerance mechanisms of human-residential bifidobacteria against lysozyme. *Anaerobe* 47, 104–110.

Salas, A., Hernandez-Rocha, C., Duijvestein, M., Faubion, W., McGovern, D., Vermeire, S., Vetrano, S. and Vande Casteele, N. (2020). JAK-STAT pathway targeting for the treatment of inflammatory bowel disease. *Nat. Rev. Gastroenterol. Hepatol.* 17, 323–337.

Samara, J., Moossavi, S., Alshaikh, B., Ortega, V. A., Pettersen, V. K., Ferdous, T., Hoops, S. L., Soraisham, A., Vayalumkal, J., Dersch-Mills, D., et al. (2022). Supplementation with a probiotic mixture accelerates gut microbiome maturation and reduces intestinal inflammation in extremely preterm infants. *Cell Host Microbe* 30, 696-711.e5.

Sánchez, B., Delgado, S., Blanco-Míguez, A., Lourenço, A., Gueimonde, M. and Margolles, A. (2017). Probiotics, gut microbiota, and their influence on host health and disease. *Mol. Nutr. Food Res.* 61,.

Sanders, M. E., Merenstein, D. J., Reid, G., Gibson, G. R. and Rastall, R. A. (2019). Probiotics and prebiotics in intestinal health and disease: from biology to the clinic. *Nat. Rev. Gastroenterol. Hepatol.* 16, 605–616.

Sanderson, I. R. (2004). Short chain fatty acid regulation of signaling genes expressed by the intestinal epithelium. *J. Nutr.* 134, 2450S-2454S.

Sangiorgi, E. and Capecchi, M. R. (2008). Bmi1 is expressed in vivo in intestinal stem cells. *Nat. Genet.* 40, 915–920.

Sanman, L. E., Chen, I. W., Bieber, J. M., Steri, V., Trentesaux, C., Hann, B., Klein, O. D., Wu, L. F. and Altschuler, S. J. (2021). Transit-Amplifying Cells Coordinate Changes in Intestinal Epithelial Cell-Type Composition. *Dev. Cell* 56, 356-365.e9.

Sasaki, N., Miyamoto, K., Maslowski, K. M., Ohno, H., Kanai, T. and Sato, T. (2020). Development of a scalable coculture system for gut anaerobes and human colon epithelium. *Gastroenterology* 159, 388-390.e5.

Sato, T. and Clevers, H. (2013). Growing self-organizing mini-guts from a single intestinal stem cell: mechanism and applications. *Science* 340, 1190–1194.

Sato, T., Stange, D. E., Ferrante, M., Vries, R. G. J., Van Es, J. H., Van den Brink, S., Van Houdt, W. J., Pronk, A., Van Gorp, J., Siersema, P. D., et al. (2011). Long-term expansion of epithelial organoids from human colon, adenoma, adenocarcinoma, and Barrett's epithelium. *Gastroenterology* 141, 1762–1772.

Sato, T., van Es, J. H., Snippert, H. J., Stange, D. E., Vries, R. G., van den Born, M., Barker, N., Shroyer, N. F., van de Wetering, M. and Clevers, H. (2011a). Paneth cells constitute the niche for Lgr5 stem cells in intestinal crypts. *Nature* 469, 415–418.

Sato, T., Vries, R. G., Snippert, H. J., van de Wetering, M., Barker, N., Stange, D. E., van Es, J. H., Abo, A., Kujala, P., Peters, P. J., et al. (2009). Single Lgr5 stem cells build crypt-villus structures in vitro without a mesenchymal niche. *Nature* 459, 262–265.

Schiavi, E., Gleinser, M., Molloy, E., Groeger, D., Frei, R., Ferstl, R., Rodriguez-Perez, N., Ziegler, M., Grant, R., Moriarty, T. F., et al. (2016). The Surface-Associated Exopolysaccharide of Bifidobacterium longum 35624 Plays an Essential Role in Dampening Host Proinflammatory Responses and Repressing Local TH17 Responses. *Appl. Environ. Microbiol.* 82, 7185–7196.

Schlaermann, P., Toelle, B., Berger, H., Schmidt, S. C., Glanemann, M., Ordemann, J., Bartfeld, S., Mollenkopf, H. J. and Meyer, T. F. (2016). A novel human gastric primary cell culture system for modelling Helicobacter pylori infection in vitro. *Gut* 65, 202–213.

Schreurs, R. R. C. E., Baumdick, M. E., Drewniak, A. and Bunders, M. J. (2021). In vitro co-culture of human intestinal organoids and lamina propria-derived CD4+ T cells. *STAR Protocols* 2, 100519.

Schroeder, B. O. (2019). Fight them or feed them: how the intestinal mucus layer manages the gut microbiota. *Gastroenterol Rep (Oxf)* 7, 3–12.

Schroeder, B. O., Birchenough, G. M. H., Ståhlman, M., Arike, L., Johansson, M. E. V., Hansson, G. C. and Bäckhed, F. (2018). Bifidobacteria or Fiber Protects against Diet-Induced Microbiota-Mediated Colonic Mucus Deterioration. *Cell Host Microbe* 23, 27-40.e7.

Schubert, M., Klinger, B., Klünemann, M., Sieber, A., Uhlitz, F., Sauer, S., Garnett, M. J., Blüthgen, N. and Saez-Rodriguez, J. (2018). Perturbation-response genes reveal signaling footprints in cancer gene expression. *Nat. Commun.* 9, 20.

Schuijers, J., Junker, J. P., Mokry, M., Hatzis, P., Koo, B.-K., Sasselli, V., van der Flier, L. G., Cuppen, E., van Oudenaarden, A. and Clevers, H. (2015). Ascl2 acts as an R-spondin/Wnt-responsive switch to control stemness in intestinal crypts. *Cell Stem Cell* 16, 158–170.

Schultze, J. L. and Aschenbrenner, A. C. (2021). COVID-19 and the human innate immune system. *Cell* 184, 1671–1692.

Schwank, G., Koo, B.-K., Sasselli, V., Dekkers, J. F., Heo, I., Demircan, T., Sasaki, N., Boymans, S., Cuppen, E., van der Ent, C. K., et al. (2013). Functional repair of CFTR by CRISPR/Cas9 in intestinal stem cell organoids of cystic fibrosis patients. *Cell Stem Cell* 13, 653–658.

Scott, J. R. and Zähner, D. (2006). Pili with strong attachments: Gram-positive bacteria do it differently. *Mol. Microbiol.* 62, 320–330.

Sekiguchi, A., Kanno, H., Ozawa, H., Yamaya, S. and Itoi, E. (2012). Rapamycin promotes autophagy and reduces neural tissue damage and locomotor impairment after spinal cord injury in mice. *J. Neurotrauma* 29, 946–956.

Seok, J., Warren, H. S., Cuenca, A. G., Mindrinos, M. N., Baker, H. V., Xu, W., Richards, D. R., McDonald-Smith, G. P., Gao, H., Hennessy, L., et al. (2013). Genomic responses in mouse models poorly mimic human inflammatory diseases. *Proc Natl Acad Sci USA* 110, 3507–3512.

Seranova, E., Ward, C., Chipara, M., Rosenstock, T. R. and Sarkar, S. (2019). In vitro screening platforms for identifying autophagy modulators in mammalian cells. *Methods Mol. Biol.* 1880, 389–428.

Sette, A. and Crotty, S. (2021). Adaptive immunity to SARS-CoV-2 and COVID-19. *Cell* 184, 861–880.

Shah, P., Fritz, J. V., Glaab, E., Desai, M. S., Greenhalgh, K., Frachet, A., Niegowska, M., Estes, M., Jäger, C., Seguin-Devaux, C., et al. (2016). A microfluidics-based in vitro model of the gastrointestinal human-microbe interface. *Nat. Commun.* 7, 11535.

Shannon, P., Markiel, A., Ozier, O., Baliga, N. S., Wang, J. T., Ramage, D., Amin, N., Schwikowski, B. and Ideker, T. (2003). Cytoscape: a software environment for integrated models of biomolecular interaction networks. *Genome Res.* 13, 2498–2504.

Shao, B.-Z., Yao, Y., Zhai, J.-S., Zhu, J.-H., Li, J.-P. and Wu, K. (2021). The role of autophagy in inflammatory bowel disease. *Front. Physiol.* 12, 621132.

Sharma, A., Mir, R. and Galande, S. (2021). Epigenetic Regulation of the Wnt/β-Catenin Signaling Pathway in Cancer. *Front. Genet.* 12, 681053.

Sheil, B., Shanahan, F. and O'Mahony, L. (2007). Probiotic effects on inflammatory bowel disease. *J. Nutr.* 137, 819S–24S.

Shen, J., Obin, M. S. and Zhao, L. (2013). The gut microbiota, obesity and insulin resistance. *Mol. Aspects Med.* 34, 39–58.

Shroyer, N. F., Helmrath, M. A., Wang, V. Y.-C., Antalffy, B., Henning, S. J. and Zoghbi, H. Y. (2007). Intestine-specific ablation of mouse atonal homolog 1 (Math1) reveals a role in cellular homeostasis. *Gastroenterology* 132, 2478–2488.

Siahpirani, A. F. and Roy, S. (2017). A prior-based integrative framework for functional transcriptional regulatory network inference. *Nucleic Acids Res.* 45, e21.

Sica, V., Galluzzi, L., Bravo-San Pedro, J. M., Izzo, V., Maiuri, M. C. and Kroemer, G. (2015). Organelle-Specific Initiation of Autophagy. *Mol. Cell* 59, 522–539.

Sicard, J.-F., Le Bihan, G., Vogeleer, P., Jacques, M. and Harel, J. (2017). Interactions of Intestinal Bacteria with Components of the Intestinal Mucus. *Front. Cell. Infect. Microbiol.* 7, 387.

Silva, A. M., Barbosa, F. H. F., Duarte, R., Vieira, L. Q., Arantes, R. M. E. and Nicoli, J. R. (2004). Effect of Bifidobacterium longum ingestion on experimental salmonellosis in mice. *J. Appl. Microbiol.* 97, 29–37.

Simon, T. and Bromberg, J. S. (2017). Regulation of the immune system by laminins. *Trends Immunol.* 38, 858–871.

Singh, S., Bhatia, R., Khare, P., Sharma, S., Rajarammohan, S., Bishnoi, M., Bhadada, S. K., Sharma, S. S., Kaur, J. and Kondepudi, K. K. (2020). Anti-inflammatory Bifidobacterium strains prevent dextran sodium sulfate induced colitis and associated gut microbial dysbiosis in mice. *Sci. Rep.* 10, 18597.

Singh, V., Johnson, K., Yin, J., Lee, S., Lin, R., Yu, H., In, J., Foulke-Abel, J., Zachos, N. C., Donowitz, M., et al. (2022). Chronic Inflammation in Ulcerative Colitis Causes Long-Term Changes in Goblet Cell Function. *Cell. Mol. Gastroenterol. Hepatol.* 13, 219–232.

Sivan, A., Corrales, L., Hubert, N., Williams, J. B., Aquino-Michaels, K., Earley, Z. M., Benyamin, F. W., Lei, Y. M., Jabri, B., Alegre, M.-L., et al. (2015). Commensal Bifidobacterium promotes antitumor immunity and facilitates anti-PD-L1 efficacy. *Science* 350, 1084–1089.

Smillie, C. S., Biton, M., Ordovas-Montanes, J., Sullivan, K. M., Burgin, G., Graham, D. B., Herbst, R. H., Rogel, N., Slyper, M., Waldman, J., et al. (2019). Intra- and Inter-cellular Rewiring of the Human Colon during Ulcerative Colitis. *Cell* 178, 714-730.e22.

Smith, R. J., Rao-Bhatia, A. and Kim, T.-H. (2017). Signaling and epigenetic mechanisms of intestinal stem cells and progenitors: insight into crypt homeostasis, plasticity, and niches. *Wiley Interdiscip. Rev. Dev. Biol.* 6,.

Snippert, H. J., van der Flier, L. G., Sato, T., van Es, J. H., van den Born, M., Kroon-Veenboer, C., Barker, N., Klein, A. M., van Rheenen, J., Simons, B. D., et al. (2010). Intestinal crypt homeostasis results from neutral competition between symmetrically dividing Lgr5 stem cells. *Cell* 143, 134–144.

Soderholm, A. T. and Pedicord, V. A. (2019). Intestinal epithelial cells: at the interface of the microbiota and mucosal immunity. *Immunology* 158, 267–280.

Sontheimer-Phelps, A., Chou, D. B., Tovaglieri, A., Ferrante, T. C., Duckworth, T., Fadel, C., Frismantas, V., Sutherland, A. D., Jalili-Firoozinezhad, S., Kasendra, M., et al. (2020). Human Colon-on-a-Chip Enables Continuous In Vitro Analysis of Colon Mucus Layer Accumulation and Physiology. *Cell. Mol. Gastroenterol. Hepatol.* 9, 507–526.

Spence, J. R., Mayhew, C. N., Rankin, S. A., Kuhar, M. F., Vallance, J. E., Tolle, K., Hoskins, E. E., Kalinichenko, V. V., Wells, S. I., Zorn, A. M., et al. (2011). Directed differentiation of human pluripotent stem cells into intestinal tissue in vitro. *Nature* 470, 105–109.

Sperandio, B., Fischer, N., Joncquel Chevalier-Curt, M., Rossez, Y., Roux, P., Robbe Masselot, C. and Sansonetti, P. J. (2013). Virulent Shigella flexneri affects secretion, expression, and glycosylation of gel-forming mucins in mucus-producing cells. *Infect. Immun.* 81, 3632–3643.

Sprangers, J., Zaalberg, I. C. and Maurice, M. M. (2021). Organoid-based modeling of intestinal development, regeneration, and repair. *Cell Death Differ.* 28, 95–107.

Srutkova, D., Schwarzer, M., Hudcovic, T., Zakostelska, Z., Drab, V., Spanova, A., Rittich, B., Kozakova, H. and Schabussova, I. (2015). Bifidobacterium longum CCM 7952 Promotes Epithelial Barrier Function and Prevents Acute DSS-Induced Colitis in Strictly Strain-Specific Manner. *PLoS ONE* 10, e0134050.

Stamataki, D., Holder, M., Hodgetts, C., Jeffery, R., Nye, E., Spencer-Dene, B., Winton, D. J. and Lewis, J. (2011). Delta1 expression, cell cycle exit, and commitment to a specific secretory fate coincide within a few hours in the mouse intestinal stem cell system. *PLoS ONE* 6, e24484.

Stanifer, M. L., Kee, C., Cortese, M., Zumaran, C. M., Triana, S., Mukenhirn, M., Kraeusslich, H.-G., Alexandrov, T., Bartenschlager, R. and Boulant, S. (2020). Critical Role of Type III Interferon in Controlling SARS-CoV-2 Infection in Human Intestinal Epithelial Cells. *Cell Rep.* 32, 107863.

Steed, H., Macfarlane, G. T., Blackett, K. L., Bahrami, B., Reynolds, N., Walsh, S. V., Cummings, J. H. and Macfarlane, S. (2010). Clinical trial: the microbiological and immunological effects of synbiotic consumption - a randomized double-blind placebo-controlled study in active Crohn's disease. *Aliment. Pharmacol. Ther.* 32, 872–883.

Stelzner, M., Helmrath, M., Dunn, J. C. Y., Henning, S. J., Houchen, C. W., Kuo, C., Lynch, J., Li, L., Magness, S. T., Martin, M. G., et al. (2012). A nomenclature for intestinal in vitro cultures. *Am. J. Physiol. Gastrointest. Liver Physiol.* 302, G1359-63.

Sterlin, D., Mathian, A., Miyara, M., Mohr, A., Anna, F., Claër, L., Quentric, P., Fadlallah, J., Devilliers, H., Ghillani, P., et al. (2021). IgA dominates the early neutralizing antibody response to SARS-CoV-2. *Sci. Transl. Med.* 13,.

Stone, J. H., Frigault, M. J., Serling-Boyd, N. J., Fernandes, A. D., Harvey, L., Foulkes, A. S., Horick, N. K., Healy, B. C., Shah, R., Bensaci, A. M., et al. (2020). Efficacy of Tocilizumab in Patients Hospitalized with Covid-19. *N. Engl. J. Med.* 383, 2333–2344.

Stroulios, G., Brown, T., Moreni, G., Kondro, D., Dei, A., Eaves, A., Louis, S., Hou, J., Chang, W., Pajkrt, D., et al. (2022). Apical-out airway organoids as a platform for studying viral infections and screening for antiviral drugs. *Sci. Rep.* 12, 7673.

Stroulios, G., Stahl, M., Elstone, F., Chang, W., Louis, S., Eaves, A., Simmini, S. and Conder, R. K. (2021). Culture Methods to Study Apical-Specific Interactions using Intestinal Organoid Models. *J. Vis. Exp.*

Strugala, V., Dettmar, P. W. and Pearson, J. P. (2008). Thickness and continuity of the adherent colonic mucus barrier in active and quiescent ulcerative colitis and Crohn's disease. *Int. J. Clin. Pract.* 62, 762–769.

Sudhakar, P., Jacomin, A.-C., Hautefort, I., Samavedam, S., Fatemian, K., Ari, E., Gul, L., Demeter, A., Jones, E., Korcsmaros, T., et al. (2019). Targeted interplay between bacterial pathogens and host autophagy. *Autophagy* 15, 1620–1633.

Sudhakar, P., Machiels, K., Verstockt, B., Korcsmaros, T. and Vermeire, S. (2021). Computational Biology and Machine Learning Approaches to Understand Mechanistic Microbiome-Host Interactions. *Front. Microbiol.* 12, 618856.

Sufi, J., Qin, X., Rodriguez, F. C., Bu, Y. J., Vlckova, P., Zapatero, M. R., Nitz, M. and Tape, C. J. (2021). Multiplexed single-cell analysis of organoid signaling networks. *Nat. Protoc.* 16, 4897–4918.

Sun, J., Shen, X., Li, Y., Guo, Z., Zhu, W., Zuo, L., Zhao, J., Gu, L., Gong, J. and Li, J. (2016). Therapeutic potential to modify the mucus barrier in inflammatory bowel disease. *Nutrients* 8,.

Sun, M., Wu, W., Chen, L., Yang, W., Huang, X., Ma, C., Chen, F., Xiao, Y., Zhao, Y., Ma, C., et al. (2018). Microbiota-derived short-chain fatty acids promote Th1 cell IL-10 production to maintain intestinal homeostasis. *Nat. Commun.* 9, 3555.

Suzuki, K., Murano, T., Shimizu, H., Ito, G., Nakata, T., Fujii, S., Ishibashi, F., Kawamoto, A., Anzai, S., Kuno, R., et al. (2018). Single cell analysis of Crohn's disease patient-derived small intestinal organoids reveals disease activity-dependent modification of stem cell properties. *J. Gastroenterol.* 53, 1035–1047.

Swidsinski, A., Loening-Baucke, V., Theissig, F., Engelhardt, H., Bengmark, S., Koch, S., Lochs, H. and Dörffel, Y. (2007). Comparative study of the intestinal mucus barrier in normal and inflamed colon. *Gut* 56, 343–350.

Takahashi, Y., Sato, S., Kurashima, Y., Lai, C.-Y., Otsu, M., Hayashi, M., Yamaguchi, T. and Kiyono, H. (2017). Reciprocal inflammatory signaling between intestinal epithelial cells and adipocytes in the absence of immune cells. *EBioMedicine* 23, 34–45.

Takeda, N., Jain, R., LeBoeuf, M. R., Wang, Q., Lu, M. M. and Epstein, J. A. (2011). Interconversion between intestinal stem cell populations in distinct niches. *Science* 334, 1420–1424.

Tamaki, H., Nakase, H., Inoue, S., Kawanami, C., Itani, T., Ohana, M., Kusaka, T., Uose, S., Hisatsune, H., Tojo, M., et al. (2016). Efficacy of probiotic treatment with Bifidobacterium longum 536 for induction of remission in active ulcerative colitis: A randomized, double-blinded, placebo-controlled multicenter trial. *Dig. Endosc.* 28, 67–74.

Tan, J. K., McKenzie, C., Mariño, E., Macia, L. and Mackay, C. R. (2017). Metabolite-Sensing G Protein-Coupled Receptors-Facilitators of Diet-Related Immune Regulation. *Annu. Rev. Immunol.* 35, 371–402.

Tang, F., Lao, K. and Surani, M. A. (2011). Development and applications of single-cell transcriptome analysis. *Nat. Methods* 8, S6-11.

Tang, X., Huang, Y., Lei, J., Luo, H. and Zhu, X. (2019). The single-cell sequencing: new developments and medical applications. *Cell Biosci.* 9, 53.

Tay, M. Z., Poh, C. M., Rénia, L., MacAry, P. A. and Ng, L. F. P. (2020). The trinity of COVID-19: immunity, inflammation and intervention. *Nat. Rev. Immunol.* 20, 363–374.

Teague, B., Waterman, M. S., Goldstein, S., Potamousis, K., Zhou, S., Reslewic, S., Sarkar, D., Valouev, A., Churas, C., Kidd, J. M., et al. (2010). High-resolution human genome structure by single-molecule analysis. *Proc Natl Acad Sci USA* 107, 10848–10853.

Thomson, P., Medina, D. A. and Garrido, D. (2018). Human milk oligosaccharides and infant gut bifidobacteria: Molecular strategies for their utilization. *Food Microbiol.* 75, 37–46.

Thorne, C. A., Chen, I. W., Sanman, L. E., Cobb, M. H., Wu, L. F. and Altschuler, S. J. (2018). Enteroid monolayers reveal an autonomous WNT and BMP circuit controlling intestinal epithelial growth and organization. *Dev. Cell* 44, 624-633.e4.

Tian, H., Biehs, B., Warming, S., Leong, K. G., Rangell, L., Klein, O. D. and de Sauvage, F. J. (2011). A reserve stem cell population in small intestine renders Lgr5-positive cells dispensable. *Nature* 478, 255–259.

Tojo, R., Suárez, A., Clemente, M. G., de los Reyes-Gavilán, C. G., Margolles, A., Gueimonde, M. and Ruas-Madiedo, P. (2014). Intestinal microbiota in health and disease: role of bifidobacteria in gut homeostasis. *World J. Gastroenterol.* 20, 15163–15176.

Travassos, L. H., Carneiro, L. A. M., Ramjeet, M., Hussey, S., Kim, Y.-G., Magalhães, J. G., Yuan, L., Soares, F., Chea, E., Le Bourhis, L., et al. (2010). Nod1 and Nod2 direct autophagy by recruiting ATG16L1 to the plasma membrane at the site of bacterial entry. *Nat. Immunol.* 11, 55–62.

Treveil, A., Bohar, B., Sudhakar, P., Gul, L., Csabai, L., Olbei, M., Poletti, M., Madgwick, M., Andrighetti, T., Hautefort, I., et al. (2021). ViralLink: An integrated workflow to investigate the effect of SARS-CoV-2 on intracellular signalling and regulatory pathways. *PLoS Comput. Biol.* 17, e1008685.

Triana, S., Metz-Zumaran, C., Ramirez, C., Kee, C., Doldan, P., Shahraz, M., Schraivogel, D., Gschwind, A. R., Sharma, A. K., Steinmetz, L. M., et al. (2021b). Single-cell analyses reveal SARS-CoV-2 interference with intrinsic immune response in the human gut. *Mol. Syst. Biol.* 17, e10232.

Triana, S., Stanifer, M. L., Boulant, S. and Alexandrov, T. (2021a). COVID19_July.rda. *Figshare*.

Tripathi, S., Moutari, S., Dehmer, M. and Emmert-Streib, F. (2016). Comparison of module detection algorithms in protein networks and investigation of the biological meaning of predicted modules. *BMC Bioinformatics* 17, 129.

Tsuboi, K., Nishitani, M., Takakura, A., Imai, Y., Komatsu, M. and Kawashima, H. (2015). Autophagy Protects against Colitis by the Maintenance of Normal Gut Microflora and Secretion of Mucus. *J. Biol. Chem.* 290, 20511–20526.

Türei, D., Földvári-Nagy, L., Fazekas, D., Módos, D., Kubisch, J., Kadlecsik, T., Demeter, A., Lenti, K., Csermely, P., Vellai, T., et al. (2015). Autophagy Regulatory Network - a systems-level bioinformatics resource for studying the mechanism and regulation of autophagy. *Autophagy* 11, 155–165.

Türei, D., Korcsmáros, T. and Saez-Rodriguez, J. (2016). OmniPath: guidelines and gateway for literature-curated signaling pathway resources. *Nat. Methods* 13, 966–967.

Türei, D., Valdeolivas, A., Gul, L., Palacio-Escat, N., Klein, M., Ivanova, O., Ölbei, M., Gábor, A., Theis, F., Módos, D., et al. (2021). Integrated intra- and intercellular signaling knowledge for multicellular omics analysis. *Mol. Syst. Biol.* 17, e9923.

Turnbaugh, P. J., Ley, R. E., Hamady, M., Fraser-Liggett, C. M., Knight, R. and Gordon, J. I. (2007). The human microbiome project. *Nature* 449, 804–810.

Turroni, F., Bottacini, F., Foroni, E., Mulder, I., Kim, J.-H., Zomer, A., Sánchez, B., Bidossi, A., Ferrarini, A., Giubellini, V., et al. (2010b). Genome analysis of Bifidobacterium bifidum PRL2010 reveals metabolic pathways for host-derived glycan foraging. *Proc Natl Acad Sci USA* 107, 19514–19519.

Turroni, F., Foroni, E., O'Connell Motherway, M., Bottacini, F., Giubellini, V., Zomer, A., Ferrarini, A., Delledonne, M., Zhang, Z., van Sinderen, D., et al. (2010a). Characterization of the serpin-encoding gene of Bifidobacterium breve 210B. *Appl. Environ. Microbiol.* 76, 3206–3219.

Turroni, F., Peano, C., Pass, D. A., Foroni, E., Severgnini, M., Claesson, M. J., Kerr, C., Hourihane, J., Murray, D., Fuligni, F., et al. (2012). Diversity of bifidobacteria within the infant gut microbiota. *PLoS ONE* 7, e36957.

Turroni, F., Serafini, F., Foroni, E., Duranti, S., O'Connell Motherway, M., Taverniti, V., Mangifesta, M., Milani, C., Viappiani, A., Roversi, T., et al. (2013). Role of sortase-dependent pili of Bifidobacterium bifidum PRL2010 in modulating bacterium-host interactions. *Proc Natl Acad Sci USA* 110, 11151–11156.

Turroni, F., van Sinderen, D. and Ventura, M. (2011). Genomics and ecological overview of the genus Bifidobacterium. *Int. J. Food Microbiol.* 149, 37–44.

Underwood, M. A., Kananurak, A., Coursodon, C. F., Adkins-Reick, C. K., Chu, H., Bennett, S. H., Wehkamp, J., Castillo, P. A., Leonard, B. C., Tancredi, D. J., et al. (2012). Bifidobacterium bifidum in a rat model of necrotizing enterocolitis: antimicrobial peptide and protein responses. *Pediatr. Res.* 71, 546–551.

US National Library of Medicine (2019). 5-HTP in Patients With IBD in Clinical and Biologic Remission:Effect on Fatigue Scores.

Uytterhoeven, V., Lauwers, E., Maes, I., Miskiewicz, K., Melo, M. N., Swerts, J., Kuenen, S., Wittocx, R., Corthout, N., Marrink, S.-J., et al. (2015). Hsc70-4 Deforms Membranes to Promote Synaptic Protein Turnover by Endosomal Microautophagy. *Neuron* 88, 735–748.

Vaishnava, S., Behrendt, C. L., Ismail, A. S., Eckmann, L. and Hooper, L. V. (2008). Paneth cells directly sense gut commensals and maintain homeostasis at the intestinal host-microbial interface. *Proc Natl Acad Sci USA* 105, 20858–20863.

van de Wetering, M., Francies, H. E., Francis, J. M., Bounova, G., Iorio, F., Pronk, A., van Houdt, W., van Gorp, J., Taylor-Weiner, A., Kester, L., et al. (2015). Prospective derivation of a living organoid biobank of colorectal cancer patients. *Cell* 161, 933–945.

Van de Wiele, T., Van den Abbeele, P., Ossieur, W., Possemiers, S. and Marzorati, M. (2015). The simulator of the human intestinal microbial ecosystem (SHIME(R)). In *The impact of food bioactives on health* (ed. Verhoeckx, K.), Cotter, P.), Lopez-Exposito, I.), Kleiveland, C.), Lea, T.), Mackie, A.), Requena, T.), Swiatecka, D.), and Wichers, H.), pp. 305–317. Cham: Springer International Publishing.

van der Beek, C. M., Dejong, C. H. C., Troost, F. J., Masclee, A. A. M. and Lenaerts, K. (2017). Role of short-chain fatty acids in colonic inflammation, carcinogenesis, and mucosal protection and healing. *Nutr. Rev.* 75, 286–305.

van der Flier, L. G. and Clevers, H. (2009). Stem cells, self-renewal, and differentiation in the intestinal epithelium. *Annu. Rev. Physiol.* 71, 241–260.

van der Flier, L. G., van Gijn, M. E., Hatzis, P., Kujala, P., Haegebarth, A., Stange, D. E., Begthel, H., van den Born, M., Guryev, V., Oving, I., et al. (2009). Transcription factor achaete scute-like 2 controls intestinal stem cell fate. *Cell* 136, 903–912.

van Es, J. H. and Clevers, H. (2014). Paneth cells. *Curr. Biol.* 24, R547-8.

van Es, J. H., Haegebarth, A., Kujala, P., Itzkovitz, S., Koo, B.-K., Boj, S. F., Korving, J., van den Born, M., van Oudenaarden, A., Robine, S., et al. (2012). A critical role for the Wnt effector Tcf4 in adult intestinal homeostatic self-renewal. *Mol. Cell. Biol.* 32, 1918–1927.

Vancamelbeke, M. and Vermeire, S. (2017). The intestinal barrier: a fundamental role in health and disease. *Expert Rev. Gastroenterol. Hepatol.* 11, 821–834.

Vancamelbeke, M., Laeremans, T., Vanhove, W., Arnauts, K., Ramalho, A. S., Farré, R., Cleynen, I., Ferrante, M. and Vermeire, S. (2019). Butyrate Does Not Protect Against Inflammation-induced Loss of Epithelial Barrier Function and Cytokine Production in Primary Cell Monolayers From Patients With Ulcerative Colitis. *J Crohns Colitis* 13, 1351–1361.

VanDussen, K. L., Liu, T.-C., Li, D., Towfic, F., Modiano, N., Winter, R., Haritunians, T., Taylor, K. D., Dhall, D., Targan, S. R., et al. (2014). Genetic variants synthesize to produce paneth cell phenotypes that define subtypes of Crohn's disease. *Gastroenterology* 146, 200–209.

VanDussen, K. L., Marinshaw, J. M., Shaikh, N., Miyoshi, H., Moon, C., Tarr, P. I., Ciorba, M. A. and Stappenbeck, T. S. (2015). Development of an enhanced human gastrointestinal epithelial culture system to facilitate patient-based assays. *Gut* 64, 911–920.

Vanhove, W., Nys, K., Arijs, I., Cleynen, I., Noben, M., De Schepper, S., Van Assche, G., Ferrante, M. and Vermeire, S. (2018). Biopsy-derived Intestinal Epithelial Cell Cultures for Pathway-based Stratification of Patients With Inflammatory Bowel Disease. *J Crohns Colitis* 12, 178–187.

Varadi, M., Anyango, S., Deshpande, M., Nair, S., Natassia, C., Yordanova, G., Yuan, D., Stroe, O., Wood, G., Laydon, A., et al. (2022). AlphaFold Protein Structure Database: massively expanding the structural coverage of protein-sequence space with high-accuracy models. *Nucleic Acids Res.* 50, D439–D444.

Vaughan, E. E., Heilig, H. G. H. J., Ben-Amor, K. and de Vos, W. M. (2005). Diversity, vitality and activities of intestinal lactic acid bacteria and bifidobacteria assessed by molecular approaches. *FEMS Microbiol. Rev.* 29, 477–490.

Vento-Tormo, R., Efremova, M., Botting, R. A., Turco, M. Y., Vento-Tormo, M., Meyer, K. B., Park, J.-E., Stephenson, E., Polański, K., Goncalves, A., et al. (2018). Single-cell reconstruction of the early maternal-fetal interface in humans. *Nature* 563, 347–353.

Ventura, M., Canchaya, C., Tauch, A., Chandra, G., Fitzgerald, G. F., Chater, K. F. and van Sinderen, D. (2007). Genomics of Actinobacteria: tracing the evolutionary history of an ancient phylum. *Microbiol. Mol. Biol. Rev.* 71, 495–548.

Venturi, A., Gionchetti, P., Rizzello, F., Johansson, R., Zucconi, E., Brigidi, P., Matteuzzi, D. and Campieri, M. (1999). Impact on the composition of the faecal flora by a new probiotic preparation: preliminary data on maintenance treatment of patients with ulcerative colitis. *Aliment. Pharmacol. Ther.* 13, 1103–1108.

Villenave, R., Wales, S. Q., Hamkins-Indik, T., Papafragkou, E., Weaver, J. C., Ferrante, T. C., Bahinski, A., Elkins, C. A., Kulka, M. and Ingber, D. E. (2017). Human Gut-On-A-Chip Supports Polarized Infection of Coxsackie B1 Virus In Vitro. *PLoS ONE* 12, e0169412.

Vogel, C. and Marcotte, E. M. (2012). Insights into the regulation of protein abundance from proteomic and transcriptomic analyses. *Nat. Rev. Genet.* 13, 227–232.

von Martels, J. Z. H., Sadaghian Sadabad, M., Bourgonje, A. R., Blokzijl, T., Dijkstra, G., Faber, K. N. and Harmsen, H. J. M. (2017). The role of gut microbiota in health and disease: In vitro modeling of host-microbe interactions at the aerobe-anaerobe interphase of the human gut. *Anaerobe* 44, 3–12.

von Moltke, J., Ji, M., Liang, H.-E. and Locksley, R. M. (2016). Tuft-cell-derived IL-25 regulates an intestinal ILC2-epithelial response circuit. *Nature* 529, 221–225.

Voss, E., Wehkamp, J., Wehkamp, K., Stange, E. F., Schröder, J. M. and Harder, J. (2006). NOD2/CARD15 mediates induction of the antimicrobial peptide human beta-defensin-2. *J. Biol. Chem.* 281, 2005–2011.

Wa, Y., Yin, B., He, Y., Xi, W., Huang, Y., Wang, C., Guo, F. and Gu, R. (2019). Effects of Single Probiotic- and Combined Probiotic-Fermented Milk on Lipid Metabolism in Hyperlipidemic Rats. *Front. Microbiol.* 10, 1312.

Wacker, D., Stevens, R. C. and Roth, B. L. (2017). How ligands illuminate GPCR molecular pharmacology. *Cell* 170, 414–427.

Walsh, D. I., Dydek, E. V., Lock, J. Y., Carlson, T. L., Carrier, R. L., Kong, D. S., Cabrera, C. R. and Thorsen, T. (2018). Emulation of colonic oxygen gradients in a microdevice. *SLAS Technol.* 23, 164–171.

Wang, F., Scoville, D., He, X. C., Mahe, M. M., Box, A., Perry, J. M., Smith, N. R., Lei, N. Y., Davies, P. S., Fuller, M. K., et al. (2013). Isolation and characterization of intestinal stem cells based on surface marker combinations and colony-formation assay. *Gastroenterology* 145, 383–95.e1.

Wang, Y., DiSalvo, M., Gunasekara, D. B., Dutton, J., Proctor, A., Lebhar, M. S., Williamson, I. A., Speer, J., Howard, R. L., Smiddy, N. M., et al. (2017b). Self-renewing Monolayer of Primary Colonic or Rectal Epithelial Cells. *Cell. Mol. Gastroenterol. Hepatol.* 4, 165-182.e7.

Wang, Y., Gunasekara, D. B., Reed, M. I., DiSalvo, M., Bultman, S. J., Sims, C. E., Magness, S. T. and Allbritton, N. L. (2017a). A microengineered collagen scaffold for generating a polarized crypt-villus architecture of human small intestinal epithelium. *Biomaterials* 128, 44–55.

Wang, Y., Tang, X., Yu, B., Gu, Y., Yuan, Y., Yao, D., Ding, F. and Gu, X. (2012). Gene network revealed involvements of Birc2, Birc3 and Tnfrsf1a in anti-apoptosis of injured peripheral nerves. *PLoS ONE* 7, e43436.

Wei, G., Gao, N., Chen, J., Fan, L., Zeng, Z., Gao, G., Li, L., Fang, G., Hu, K., Pang, X., et al. (2020). Erk and MAPK signaling is essential for intestinal development through Wnt pathway modulation. *Development* 147,.

Wickham, H. ed. (2016). *ggplot2: Elegant Graphics for Data Analysis*. Springer-Verlag New York.

Williams, J. M., Duckworth, C. A., Burkitt, M. D., Watson, A. J. M., Campbell, B. J. and Pritchard, D. M. (2015). Epithelial cell shedding and barrier function: a matter of life and death at the small intestinal villus tip. *Vet. Pathol.* 52, 445–455.

Williamson, I. A., Arnold, J. W., Samsa, L. A., Gaynor, L., DiSalvo, M., Cocchiaro, J. L., Carroll, I., Azcarate-Peril, M. A., Rawls, J. F., Allbritton, N. L., et al. (2018). A High-Throughput Organoid Microinjection Platform to Study Gastrointestinal Microbiota and Luminal Physiology. *Cell. Mol. Gastroenterol. Hepatol.* 6, 301–319.

Wingett, S. W. and Andrews, S. (2018). FastQ Screen: A tool for multi-genome mapping and quality control. [version 2; peer review: 4 approved]. *F1000Res.* 7, 1338.

Winterbach, W., Van Mieghem, P., Reinders, M., Wang, H. and de Ridder, D. (2013). Topology of molecular interaction networks. *BMC Syst. Biol.* 7, 90.

Wittkopf, N., Neurath, M. F. and Becker, C. (2014). Immune-epithelial crosstalk at the intestinal surface. *J. Gastroenterol.* 49, 375–387.

Wlodarska, M., Thaiss, C. A., Nowarski, R., Henao-Mejia, J., Zhang, J.-P., Brown, E. M., Frankel, G., Levy, M., Katz, M. N., Philbrick, W. M., et al. (2014). NLRP6 inflammasome orchestrates the colonic host-microbial interface by regulating goblet cell mucus secretion. *Cell* 156, 1045–1059.

Wong, A. P., Bear, C. E., Chin, S., Pasceri, P., Thompson, T. O., Huan, L.-J., Ratjen, F., Ellis, J. and Rossant, J. (2012). Directed differentiation of human pluripotent stem cells into mature airway epithelia expressing functional CFTR protein. *Nat. Biotechnol.* 30, 876–882.

Workman, M. J., Mahe, M. M., Trisno, S., Poling, H. M., Watson, C. L., Sundaram, N., Chang, C.-F., Schiesser, J., Aubert, P., Stanley, E. G., et al. (2017). Engineered human pluripotent-stem-cell-derived intestinal tissues with a functional enteric nervous system. *Nat. Med.* 23, 49–59.

Worthington, J. J., Reimann, F. and Gribble, F. M. (2018). Enteroendocrine cells-sensory sentinels of the intestinal environment and orchestrators of mucosal immunity. *Mucosal Immunol.* 11, 3–20.

Wrzosek, L., Miquel, S., Noordine, M.-L., Bouet, S., Joncquel Chevalier-Curt, M., Robert, V., Philippe, C., Bridonneau, C., Cherbuy, C., Robbe-Masselot, C., et al. (2013). Bacteroides thetaiotaomicron and Faecalibacterium prausnitzii influence the production of mucus glycans and the development of goblet cells in the colonic epithelium of a gnotobiotic model rodent. *BMC Biol.* 11, 61.

Wu, B.-B., Yang, Y., Xu, X. and Wang, W.-P. (2016). Effects of Bifidobacterium supplementation on intestinal microbiota composition and the immune response in healthy infants. *World J. Pediatr.* 12, 177–182.

Wu, M.-H., Pan, T.-M., Wu, Y.-J., Chang, S.-J., Chang, M.-S. and Hu, C.-Y. (2010). Exopolysaccharide activities from probiotic bifidobacterium: Immunomodulatory effects (on J774A.1 macrophages) and antimicrobial properties. *Int. J. Food Microbiol.* 144, 104–110.

Wu, T., Hu, E., Xu, S., Chen, M., Guo, P., Dai, Z., Feng, T., Zhou, L., Tang, W., Zhan, L., et al. (2021). clusterProfiler 4.0: A universal enrichment tool for interpreting omics data. *Innovation (Camb)* 2, 100141.

Xie, Y., Zhao, Y., Shi, L., Li, W., Chen, K., Li, M., Chen, X., Zhang, H., Li, T., Matsuzawa-Ishimoto, Y., et al. (2020). Gut epithelial TSC1/mTOR controls RIPK3-dependent necroptosis in intestinal inflammation and cancer. *J. Clin. Invest.* 130, 2111–2128.

Yan, S., Yang, B., Zhao, J., Zhao, J., Stanton, C., Ross, R. P., Zhang, H. and Chen, W. (2019). A ropy exopolysaccharide producing strain Bifidobacterium longum subsp. longum YS108R alleviates DSS-induced colitis by maintenance of the mucosal barrier and gut microbiota modulation. *Food Funct.* 10, 1595–1608.

Yang, Q., Bermingham, N. A., Finegold, M. J. and Zoghbi, H. Y. (2001). Requirement of Math1 for secretory cell lineage commitment in the mouse intestine. *Science* 294, 2155–2158.

Yellaboina, S., Tasneem, A., Zaykin, D. V., Raghavachari, B. and Jothi, R. (2011). DOMINE: a comprehensive collection of known and predicted domain-domain interactions. *Nucleic Acids Res.* 39, D730-5.

You, H., Li, Q., Kong, D., Liu, X., Kong, F., Zheng, K. and Tang, R. (2022). The interaction of canonical Wnt/β-catenin signaling with protein lysine acetylation. *Cell. Mol. Biol. Lett.* 27, 7.

Young, C. N. J., Sinadinos, A., Lefebvre, A., Chan, P., Arkle, S., Vaudry, D. and Gorecki, D. C. (2015). A novel mechanism of autophagic cell death in dystrophic muscle regulated by P2RX7 receptor large-pore formation and HSP90. *Autophagy* 11, 113–130.

Yousi, F., Kainan, C., Junnan, Z., Chuanxing, X., Lina, F., Bangzhou, Z., Jianlin, R. and Baishan, F. (2019). Evaluation of the effects of four media on human intestinal microbiota culture in vitro. *AMB Express* 9, 69.

Yu, G. and He, Q.-Y. (2016). ReactomePA: an R/Bioconductor package for reactome pathway analysis and visualization. *Mol. Biosyst.* 12, 477–479.

Yu, G., Wang, L.-G., Han, Y. and He, Q.-Y. (2012b). clusterProfiler: an R package for comparing biological themes among gene clusters. *OMICS* 16, 284–287.

Yu, L. C.-H., Wang, J.-T., Wei, S.-C. and Ni, Y.-H. (2012a). Host-microbial interactions and regulation of intestinal epithelial barrier function: From physiology to pathology. *World J. Gastrointest. Pathophysiol.* 3, 27–43.

Yu, R., Zuo, F., Ma, H. and Chen, S. (2019). Exopolysaccharide-Producing Bifidobacterium adolescentis Strains with Similar Adhesion Property Induce Differential Regulation of Inflammatory Immune Response in Treg/Th17 Axis of DSS-Colitis Mice. *Nutrients* 11,.

Yu, Z., Feng, J., Wang, W., Deng, Z., Zhang, Y., Xiao, L., Wang, Z., Liu, C., Liu, Q., Chen, S., et al. (2020). The EGFR-ZNF263 signaling axis silences SIX3 in glioblastoma epigenetically. *Oncogene* 39, 3163–3178.

Zachos, N. C., Kovbasnjuk, O., Foulke-Abel, J., In, J., Blutt, S. E., de Jonge, H. R., Estes, M. K. and Donowitz, M. (2016). Human enteroids/colonoids and intestinal organoids functionally recapitulate normal intestinal physiology and pathophysiology. *J. Biol. Chem.* 291, 3759–3766.

Zang, R., Gomez Castro, M. F., McCune, B. T., Zeng, Q., Rothlauf, P. W., Sonnek, N. M., Liu, Z., Brulois, K. F., Wang, X., Greenberg, H. B., et al. (2020). TMPRSS2 and TMPRSS4 promote SARS-CoV-2 infection of human small intestinal enterocytes. *Sci. Immunol.* 5,.

Zaylaa, M., Alard, J., Kassaa, I. A., Peucelle, V., Boutillier, D., Desramaut, J., Rosenstiel, P., Nguyen, H. T. T., Dabboussi, F., Pot, B., et al. (2019). Autophagy: A Novel Mechanism Involved in the Anti-Inflammatory Abilities of Probiotics. *Cell. Physiol. Biochem.* 53, 774–793.

Zeissig, S., Bürgel, N., Günzel, D., Richter, J., Mankertz, J., Wahnschaffe, U., Kroesen, A. J., Zeitz, M., Fromm, M. and Schulzke, J. D. (2007). Changes in expression and distribution of claudin 2, 5 and 8 lead to discontinuous tight junctions and barrier dysfunction in active Crohn's disease. *Gut* 56, 61–72.

Zelante, T., Fric, J., Wong, A. Y. W. and Ricciardi-Castagnoli, P. (2012). Interleukin-2 production by dendritic cells and its immuno-regulatory functions. *Front. Immunol.* 3, 161.

Zelante, T., Iannitti, R. G., Cunha, C., De Luca, A., Giovannini, G., Pieraccini, G., Zecchi, R., D'Angelo, C., Massi-Benedetti, C., Fallarino, F., et al. (2013). Tryptophan catabolites from microbiota engage aryl hydrocarbon receptor and balance mucosal reactivity via interleukin-22. *Immunity* 39, 372–385.

Zeng, M. Y., Inohara, N. and Nuñez, G. (2017). Mechanisms of inflammation-driven bacterial dysbiosis in the gut. *Mucosal Immunol.* 10, 18–26.

Zeng, Z., Mukherjee, A., Varghese, A. P., Yang, X.-L., Chen, S. and Zhang, H. (2020). Roles of G protein-coupled receptors in inflammatory bowel disease. *World J. Gastroenterol.* 26, 1242–1261.

Zhang, M., Zhou, Q., Dorfman, R. G., Huang, X., Fan, T., Zhang, H., Zhang, J. and Yu, C. (2016). Butyrate inhibits interleukin-17 and generates Tregs to ameliorate colorectal colitis in rats. *BMC Gastroenterol.* 16, 84.

Zhang, Z. and Liu, Z. (2016). Paneth cells: the hub for sensing and regulating intestinal flora. *Sci. China Life Sci.* 59, 463–467.

Zhao, F., Edwards, R., Dizon, D., Afrasiabi, K., Mastroianni, J. R., Geyfman, M., Ouellette, A. J., Andersen, B. and Lipkin, S. M. (2010). Disruption of Paneth and goblet cell homeostasis and increased endoplasmic reticulum stress in Agr2-/- mice. *Dev. Biol.* 338, 270–279.

Zhou, J., Zhou, Z., Ji, P., Ma, M., Guo, J. and Jiang, S. (2019). Effect of fecal microbiota transplantation on experimental colitis in mice. *Exp. Ther. Med.* 17, 2581–2586.

Zierhut, C. and Funabiki, H. (2020). Regulation and Consequences of cGAS Activation by Self-DNA. *Trends Cell Biol.* 30, 594–605.

Zilbauer, M. and Kraiczy, J. (2017). Epigenetics in gastrointestinal health and disease: spotlight on DNA methylation in the intestinal epithelium. *Nestle Nutr. Inst. Workshop Ser.* 88, 35–44.

Appendix 1: Supplementary data for Chapter 4

This appendix contains all the supplementary material for **Chapter 4**.

These figures are mainly related to (i) comparison of organoids exposed to *B. breve* UCC2003 sup. compared to undifferentiated controls; (ii) analysis of organoids exposed to *L. rhamnosus* for both comparisons to differentiated and undifferentiated controls.

Supplementary Figures:

- **Supplementary Figure 4.1**. UMAP plots of normalised counts data.
- **Supplementary Figure 4.2.** Filtered DEGs table.
- **Supplementary Figure 4.3.** Volcano plots of DEGs upon bacterial exposure of organoids compared to differentiated controls.
- **Supplementary Figure 4.4**. Top GSEA functions identified in epithelial cell populations upon organoid differentiation.
- **Supplementary Figure 4.5**. Top differentially expressed markers of epithelial cell populations upon organoid differentiation.
- **Supplementary Figure 4.6.** Top differentially expressed markers of epithelial cell populations upon *L. rhamnosus* exposure of organoids compared to differentiated controls.
- **Supplementary Figure 4.7**. Bar plot showing top differentially expressed markers of epithelial cell populations upon *B. breve* UCC2003 exposure of organoids compared to undifferentiated controls.
- **Supplementary Figure 4.8**. Bar plot showing top differentially expressed markers of epithelial cell populations upon *L. rhamnosus* exposure of organoids compared to undifferentiated controls.
- **Supplementary Figure 4.9**. Pathway analysis of organoids exposed to bacterial metabolites compared undifferentiated controls.
- **Supplementary Figure 4.10.** Top enriched functions identified by GSEA of DEGs upon *B. breve* UCC2003 exposure of organoids compared to undifferentiated controls.
- **Supplementary Figure 4.11**. Top enriched functions identified by GSEA of DEGs upon *L. rhamnosus* exposure of organoids compared to differentiated controls.
- **Supplementary Figure 4.12**. Top enriched functions identified by GSEA of DEGs upon *L. rhamnosus* exposure of organoids compared to undifferentiated controls.

- **Supplementary Figure 4.13.** Predicted TFs regulating gene expression changes upon exposure of organoids to bacterial metabolites compared to undifferentiated controls.
- **Supplementary Figure 4.14.** Transcription factors in TF-DEG networks of organoids exposed to bacterial supernatants compared to undifferentiated controls.
- **Supplementary Figure 4.15.** TF-TG networks upon *L. rhamnosus* exposure of organoids compared to differentiated controls.
- **Supplementary Figure 4.16.** Functional analysis of TF-TG networks upon *L. rhamnosus* exposure of organoids compared to differentiated controls.
- **Supplementary Figure 4.17**. Functional analysis of TF-TG networks upon *B. breve* UCC2003 exposure of organoids compared to undifferentiated controls.
- **Supplementary Figure 4.18**. Functional analysis of TF-TG networks upon *L. rhamnosus* exposure of organoids compared to undifferentiated controls.
- **Supplementary Figure 4.19.** Interaction networks of DEGs and their direct interactors upon *L. rhamnosus* exposure.
- **Supplementary Figure 4.20**. Enriched GO functions in first neighbour networks of DEGs upon *B. breve UCC2003* exposure.
- **Supplementary Figure 4.21**. Enriched GO functions in first neighbour networks of DEGs upon *L. rhamnosus* exposure.
- **Supplementary Figure 4.22.** Metabolite-host gene networks upon *B. breve* UCC2003 sup. exposure of organoids compared to undifferentiated controls.

Supplementary Tables

- **Supplementary Table 4.1.** TFs regulated upon *B. breve* UCC2003 and *L. rhamnosus* sup. exposure of organoids compared to differentiated controls.
- **Supplementary Table 4.2.** TFs regulated upon *B. breve* UCC2003 and *L. rhamnosus* sup. exposure of organoids compared to undifferentiated controls.
- **Supplementary Table 4.3.** Raw metabolite concentration (in mM) for single metabolites in *B. breve* UCC2003 cultures over time as measured by 1H-NMR.
- **Supplementary Table 4.4.** Spearman correlation between 16S reads of *B. breve* UCC2003 and identified metabolites.

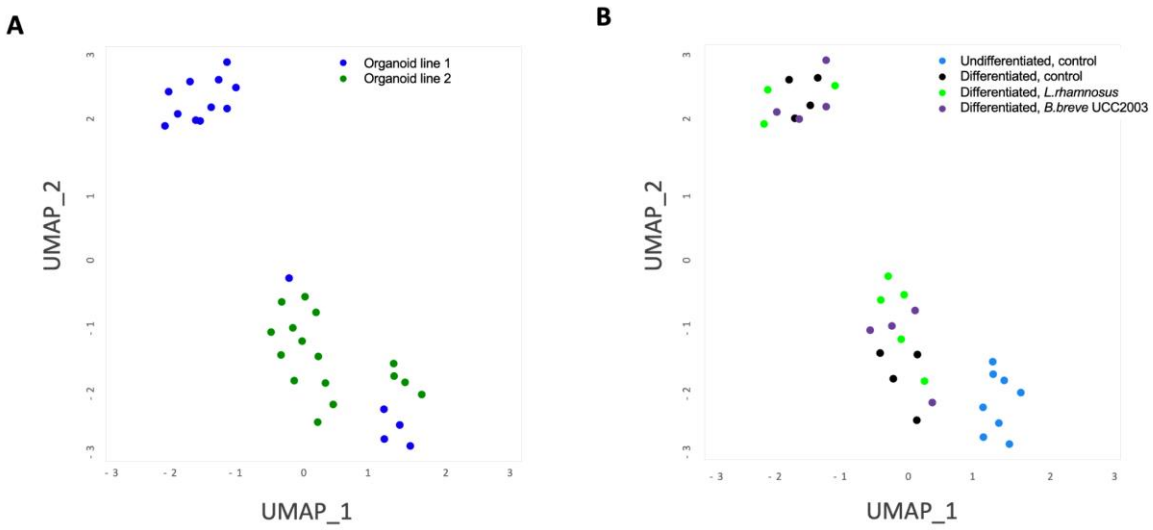

Supplementary Figure 4.1. UMAP plots of normalised counts data. A) Data colored by organoid line. B) Data colored by condition. Undifferentiated organoid (t = 0 hours) or differentiated for 3 days (t = 72 hours), treated with bacterial supernatants (*L. rhamnosus*, *B. breve* UCC2003) or untreated (media control). Plots were created in R.

A

Condition	Organoid line 1	Organoid line 2	Total n of DEGs (t=72 h vs t=72 h)
B.breve UCC2003	40	53	
L.rhamnosus	18	24	

B

Condition	Organoid line 1	Organoid line 2	Total n of DEGs (t=72 h vs t=0 h)
B.breve UCC2003	3376	2743	
L.rhamnosus	3131	2879	
Control	3526	2956	

Supplementary Figure 4.2. Filtered DEGs table. DEGs were filtered for |Log2FoldChange| > 1 and adjusted p-value < 0.05. For each organoid line, results are shown for comparisons between differentiated organoids exposed to *B. breve* UCC2003 and *L. rhamnosus* supernatants for 3 days (t = 72 hours) compared to control, which was either differentiated organoids (t = 72 hours) **(A)** or undifferentiated organoids (t = 0 hours) **(B).**

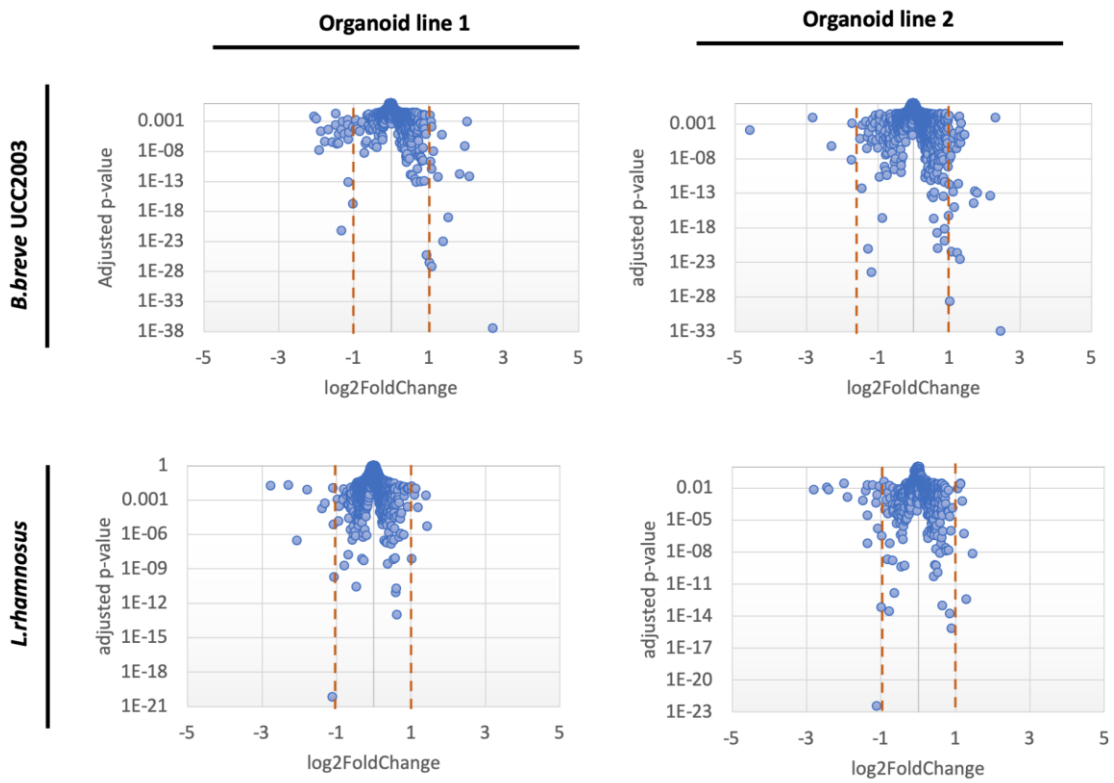

Supplementary Figure 4.3. **Volcano plots of DEGs upon bacterial exposure of organoids compared to differentiated controls.** Plots were created using Microsoft Excel (Office).

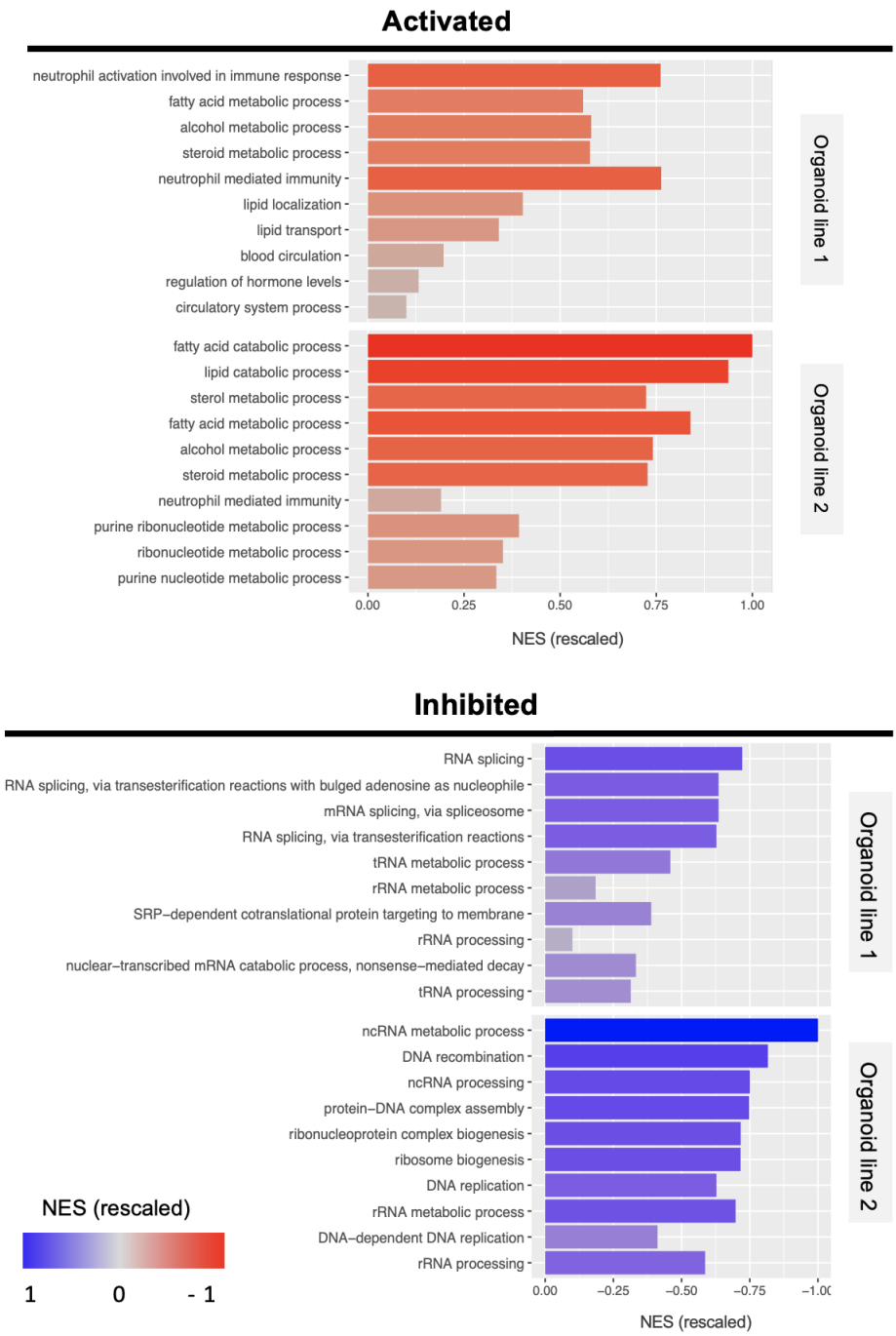

Supplementary Figure 4.4. **Top GSEA functions identified in epithelial cell populations upon organoid differentiation.** Top 10 GO activated and inhibited functions in untreated differentiated organoids (t = 72 hours) compared to undifferentiated controls (t = 0 hours) identified by GSEA analysis. Activated functions are indicated when NES > 0, while inhibited functions when NES < 0. The length of the bar and colour (red, highest; blue, lowest) indicates the NES score. NES score was rescaled (0,1) for visualisation purposes. Bar plots were created using the ggplot2 package in R.

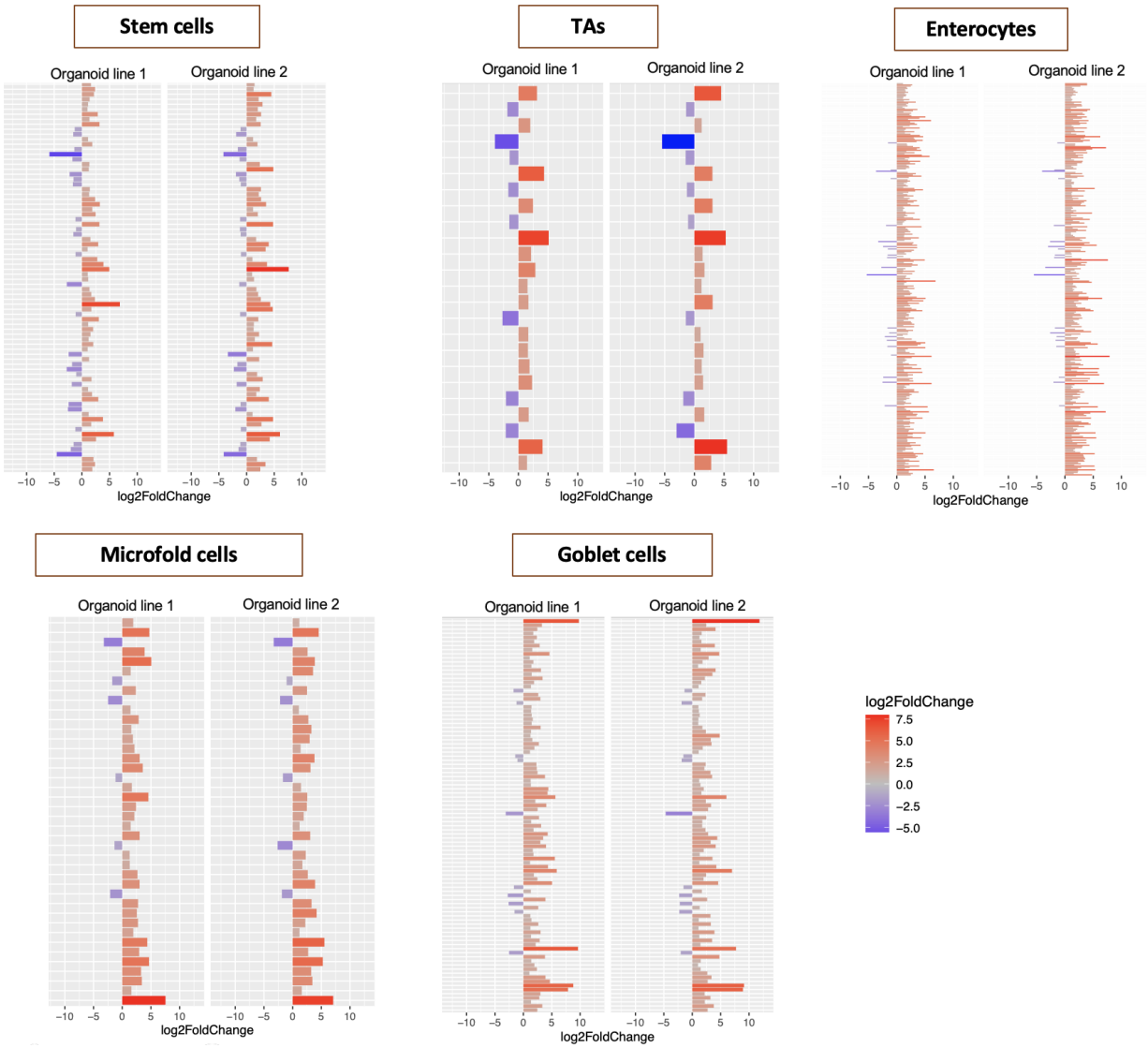

Supplementary Figure 4.5. Top differentially expressed markers of epithelial cell populations upon organoid differentiation. The height of the bar plot and colour gradient (red, positive; blue, negative) indicate the Log2FoldChange value in differentiated organoids (t = 72 hours) compared to undifferentiated control (t = 0 hours) in organoid lines 1 and 2. DEGs (Log2FoldChange > 1, adjusted p-value < 0.05) were filtered for markers of epithelial cells from the Gut Cell Atlas (adult healthy colon) (Log2FoldChange > 1, adjusted p-value < 0.01). Only markers that were significant in both organoid lines are shown. Bar plots were created using ggplot2 in R.

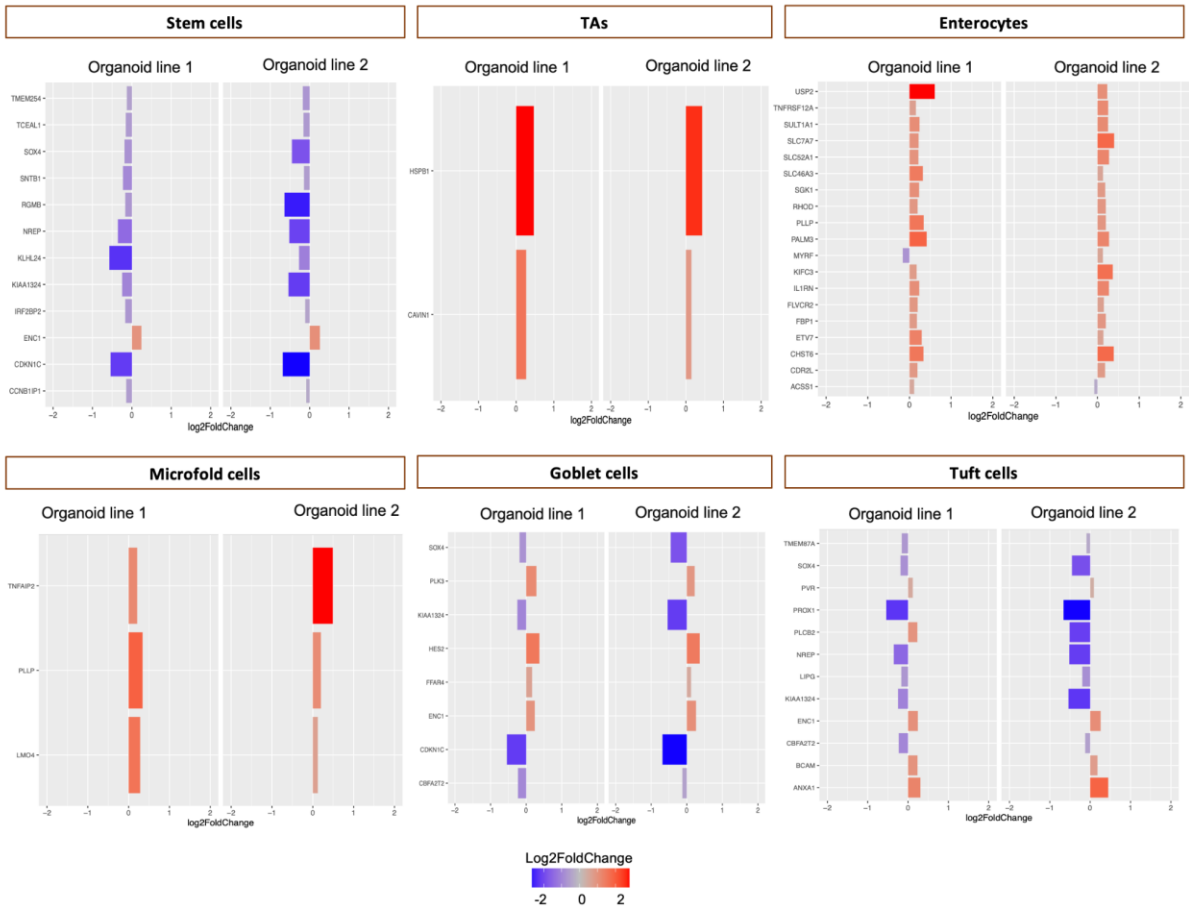

Supplementary Figure 4.6. Top differentially expressed markers of epithelial cell populations upon *L. rhamnosus* exposure of organoids compared to differentiated controls. The height of the bar plot and colour gradient (red, positive; blue, negative) indicates the Log2FoldChange value in organoids exposed to *L. rhamnosus* sup. compared to differentiated controls (t = 72 hours) in organoid lines 1 and 2. DEGs in *L. rhamnosus* compared to control (adjusted p-value < 0.05) were filtered for markers of epithelial cells from the Gut Cell Atlas (adult healthy colon) (Log2FoldChange > 1, adjusted p-value < 0.01). Only markers that were significant in both organoid lines are shown. Bar plots were created using ggplot2 in R.

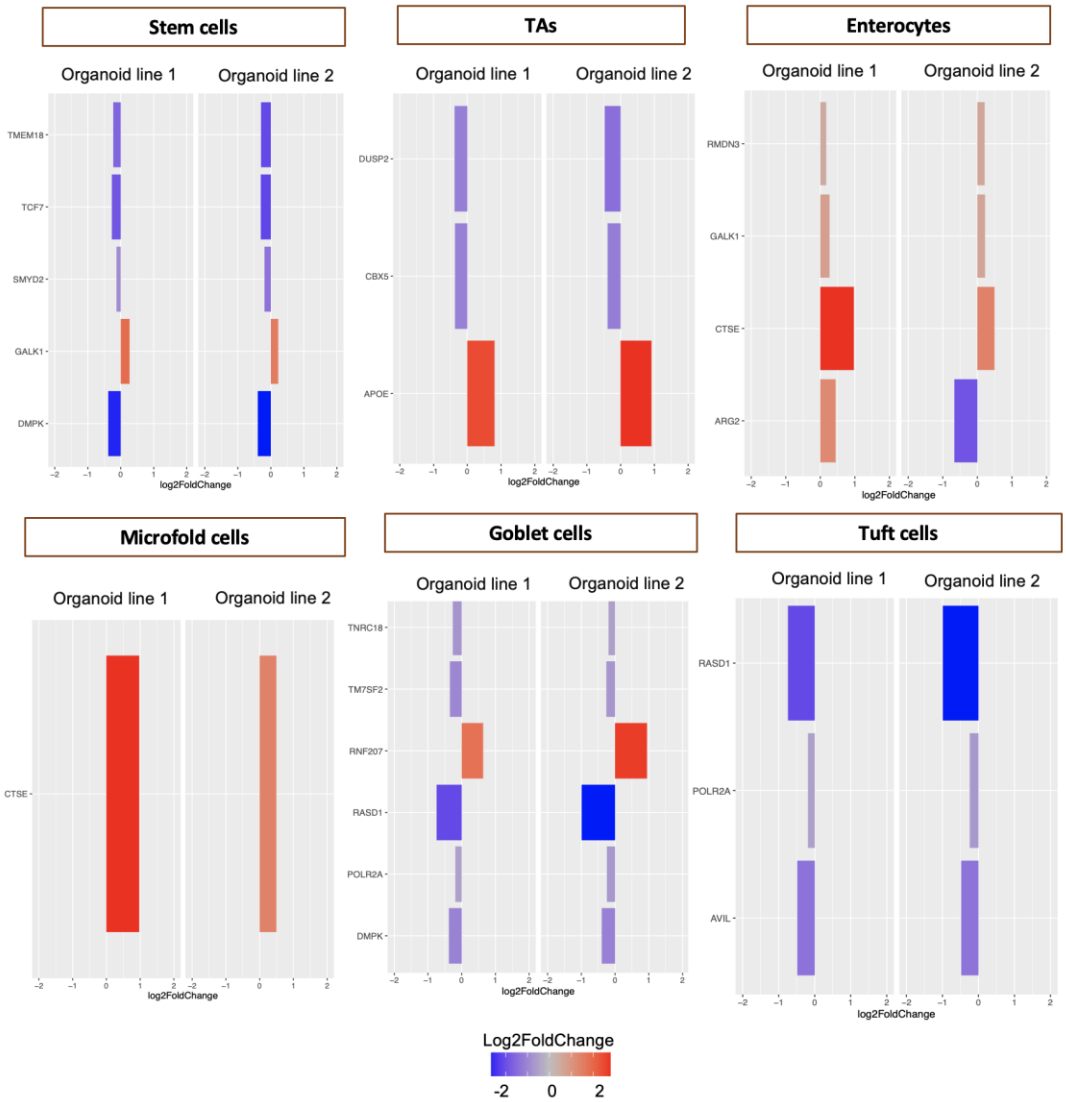

Supplementary Figure 4.7. Bar plot showing top differentially expressed markers of epithelial cell populations upon *B. breve* UCC2003 exposure of organoids compared to undifferentiated controls. The height of the bar plot and colour gradient (red, positive; blue, negative) indicates the Log2FoldChange in organoids exposed to *B.breve* UCC2003 sup. compared to differentiated controls in organoid line 1 and 2. DEGs in *B.breve* UCC2003 compared to control (adjusted p-value < 0.05) were filtered markers of epithelial cells from the Gut Cell Atlas (adult healthy colon), (|Log2Foldchange| > 1, adjusted p-value < 0.01). Only markers that were present in both organoid lines are shown. Bar plots were created using the ggplot2 package in R.

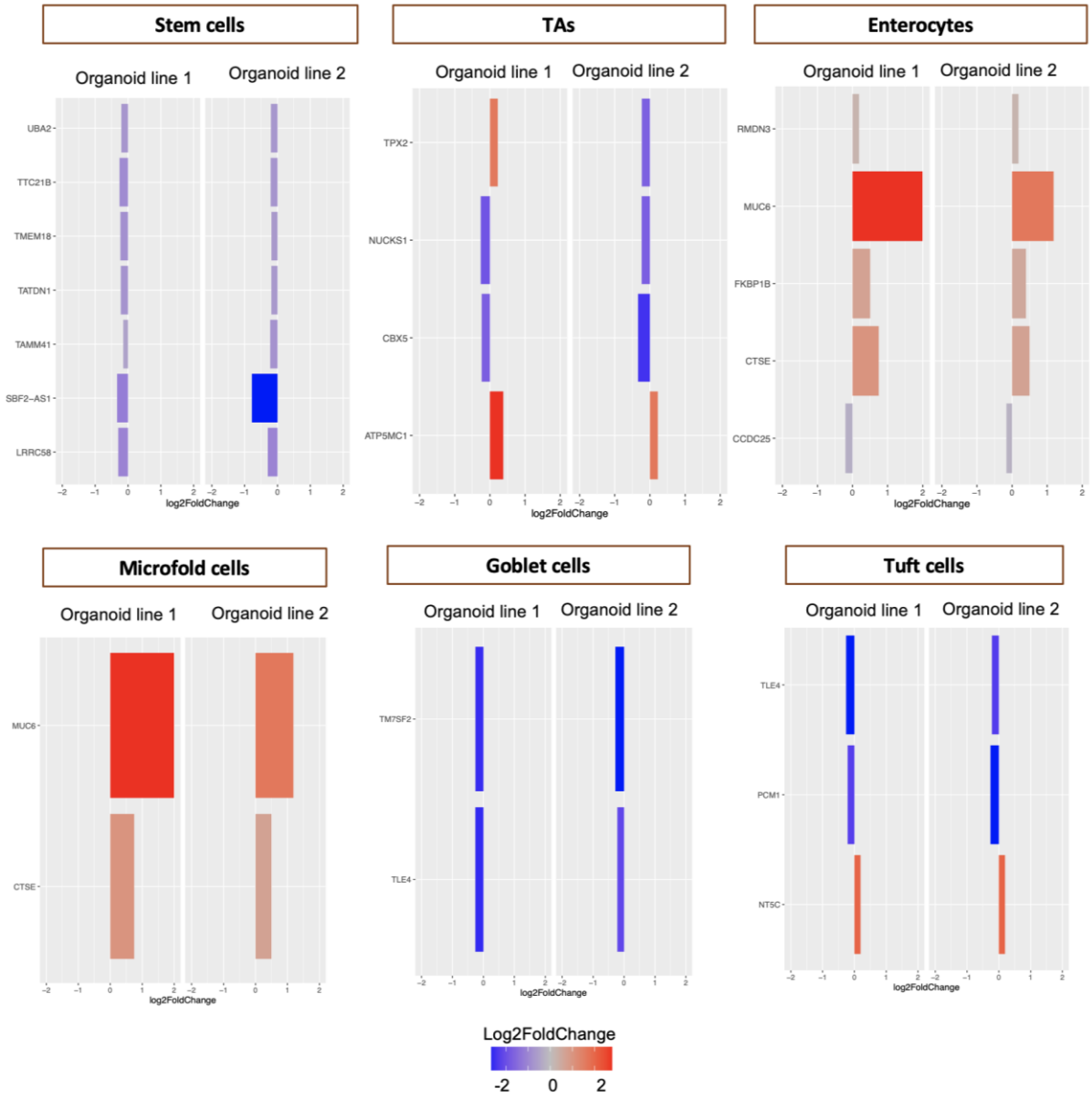

Supplementary Figure 4.8. Bar plot showing top differentially expressed markers of epithelial cell populations upon *L. rhamnosus* exposure of organoids compared to undifferentiated controls. The height of the bar plot and colour gradient (red, positive; blue, negative) indicates the Log2FoldChange in organoids exposed to *L.rhamnosus* sup. compared to undifferentiated controls in organoid line 1 and 2. DEGs in *L.rhamnosus* compared to control (adjusted p-value < 0.05) were filtered markers of epithelial cells from the Gut Cell Atlas (adult healthy colon) (|Log2Foldchange| > 1, adjusted p-value < 0.01). Only markers that were present in both organoid lines are shown. Plots were created using the ggplot2 package in R.

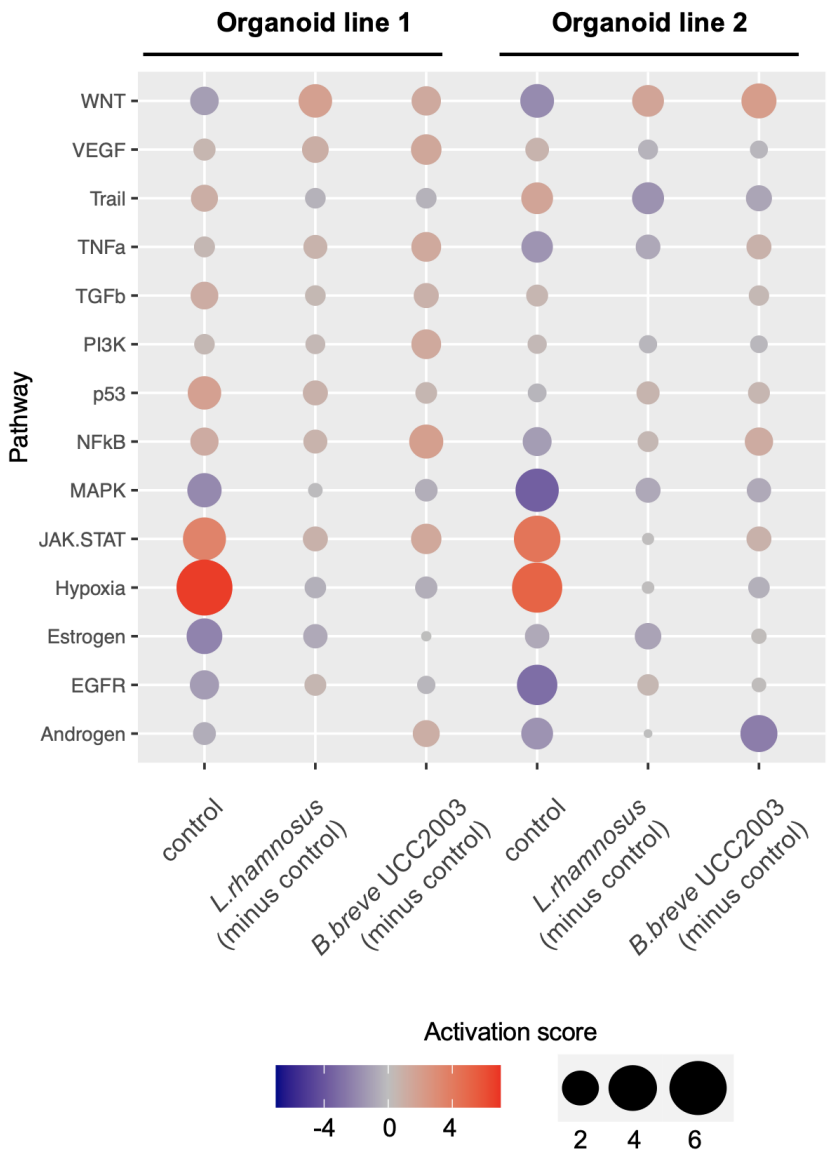

Supplementary Figure 4.9. Pathway analysis of organoids exposed to bacterial metabolites compared undifferentiated controls. Bubble chart indicating canonical pathways modulated in organoids exposed to bacterial metabolites compared to undifferentiated controls (t = 0 hours). Size of the bubble indicates the Progeny activation score and colour indicates the direction of the predicted change (red, activated; blue, inhibited). Plots were created using the ggplot2 package in R.

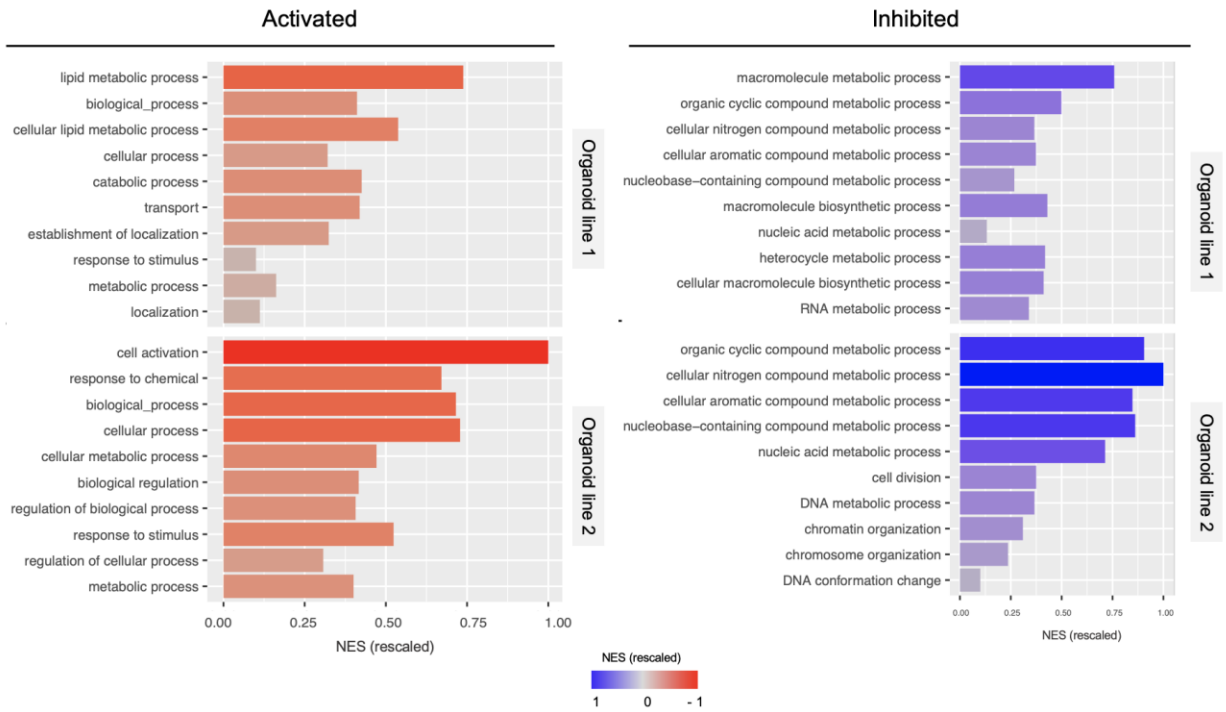

Supplementary Figure 4.10. Top enriched functions identified by GSEA of DEGs upon *B. breve* UCC2003 exposure of organoids compared to undifferentiated controls. Top 10 GO activated and inhibited functions upon *B. breve UCC2003* exposure of organoids compared to undifferentiated control (t = 0 hours) are shown. Activated functions are indicated when NES>0, while inhibited functions when NES <0. The length of the bar and colour (red, highest; blue, lowest) indicates the NES score. NES score was rescaled for visualisation purposes. Bar plots were created using the ggplot2 package in R.

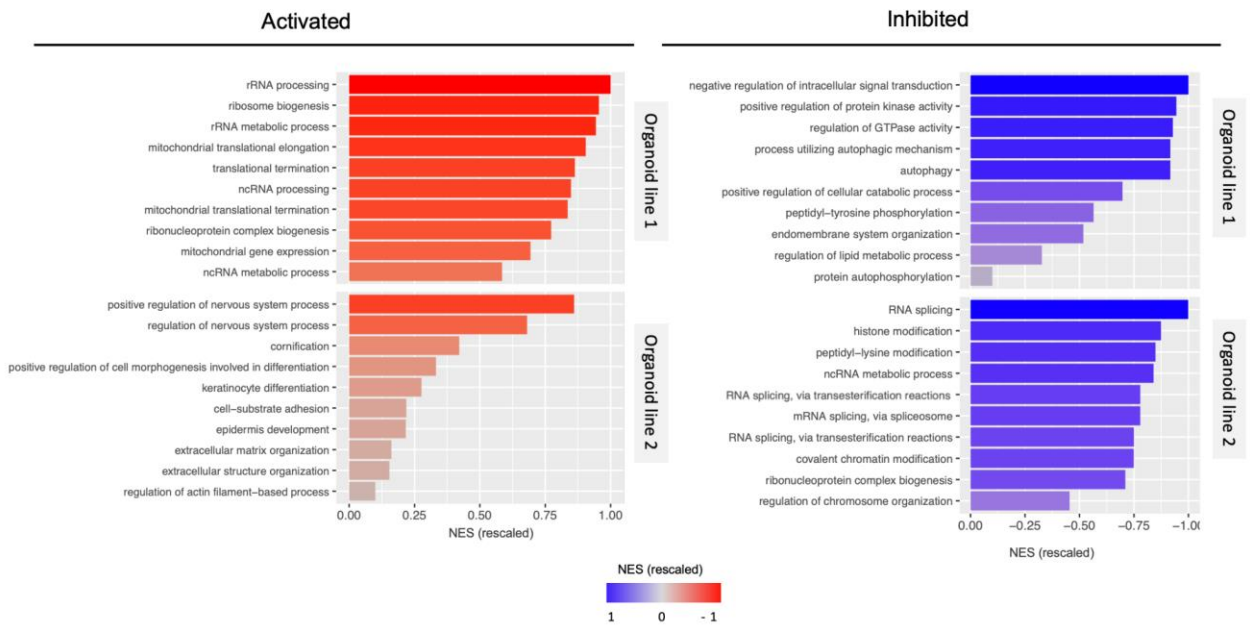

Supplementary Figure 4.11. Top enriched functions identified by GSEA of DEGs upon *L. rhamnosus* exposure of organoids compared to differentiated controls. Top 10 GO activated and inhibited functions upon *L. rhamnosus* exposure of organoids compared to differentiated control (t = 72 hours) are shown. Activated functions are indicated when NES>0, while inhibited functions when NES <0. The length of the bar and colour (red, highest; blue, lowest) indicates the NES score. NES score was rescaled for visualisation purposes. Bar plots were created using the ggplot2 package in R.

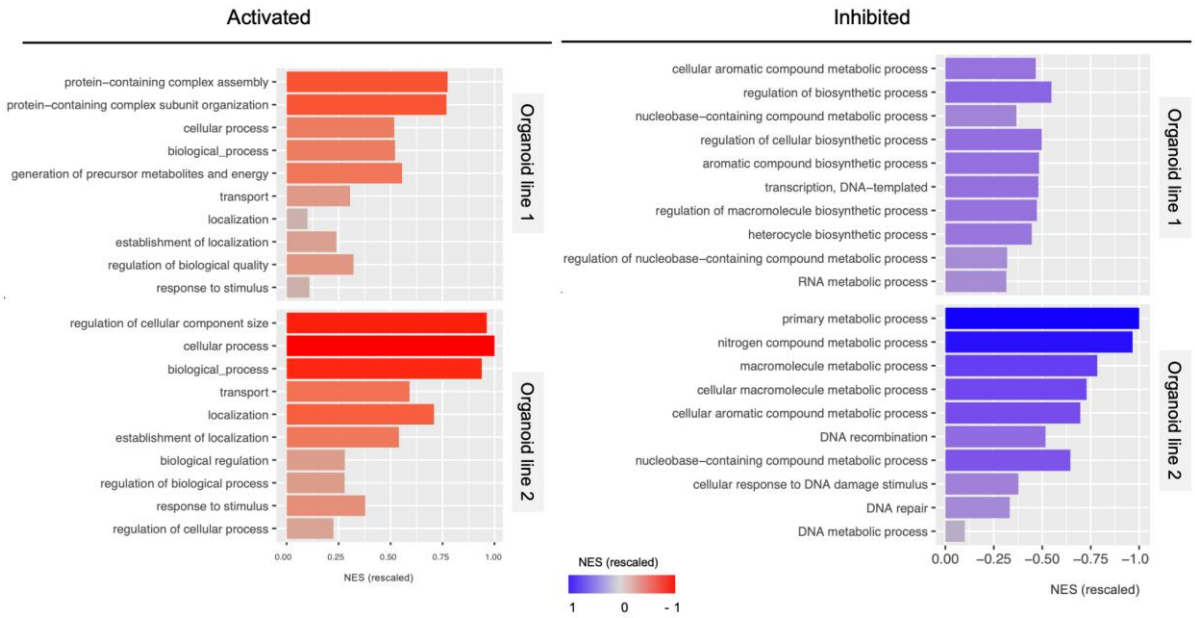

Supplementary Figure 4.12. Top enriched functions identified by GSEA of DEGs upon *L. rhamnosus* exposure of organoids compared to undifferentiated controls. Top 10 GO activated and inhibited functions upon *L.rhamnosus* exposure of organoids compared to undifferentiated control (t= 72 hours) are shown. Activated functions are indicated when NES>0, while inhibited functions when NES <0. The length of the bar and colour (red, highest; blue, lowest) indicates the NES score. NES score was rescaled for visualisation purposes. Bar plots were created using the ggplot2 package in R.

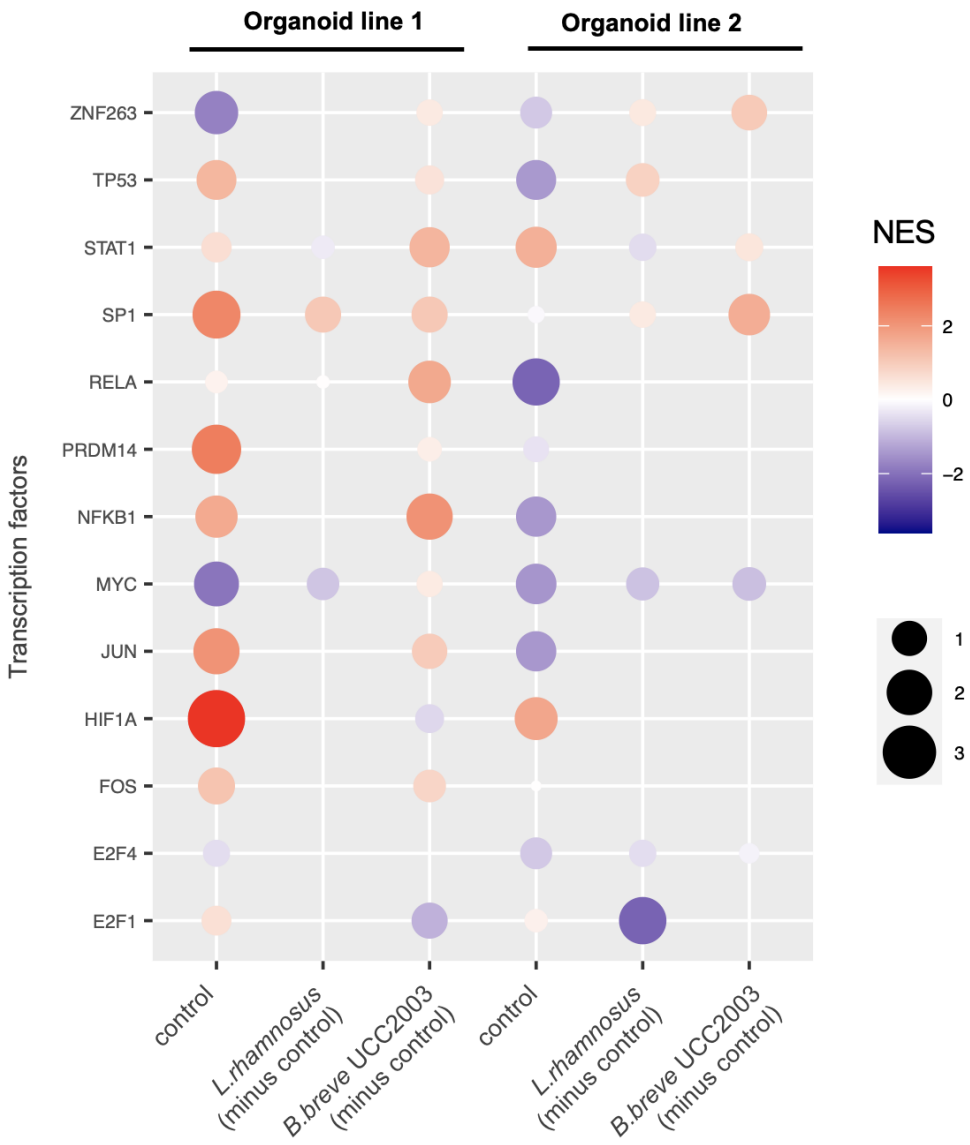

Supplementary Figure 4.13. Predicted TFs regulating gene expression changes upon exposure of organoids to bacterial metabolites compared to undifferentiated controls. TFs upon bacterial exposure of organoids compared to undifferentiated control (t = 0 hours). TFs where pleiotropic correction for multiple regulation, regulating a minimum 8 targets and with a |NES| > 0 in organoid line 1 or 2 are shown. A, B) The colour gradient (NES <0, blue; NES > 0, red) and size of the bubble indicate the Normalised Enrichment score (NES). NES > 0 indicates the TF is predicted to be activated, while a NES < 0 indicates the TF is predicted to be inhibited. Bubble plots were created using the ggplot2 package in R.

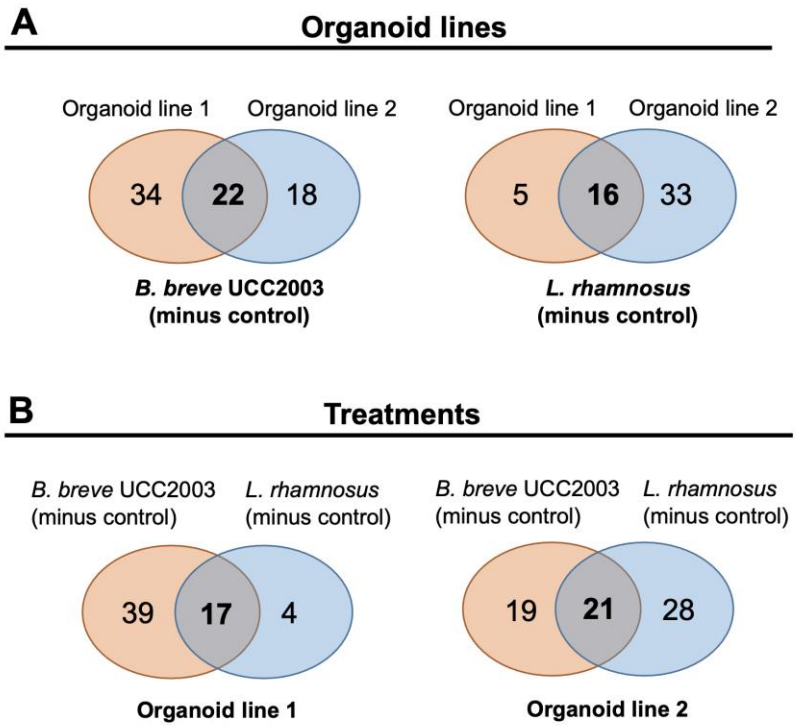

Supplementary Figure 4.14. Transcription factors in TF-DEG networks of organoids exposed to bacterial supernatants compared to undifferentiated controls. Venn diagrams showing the unique and overlapping TFs identified in the TF-TG regulatory networks for each organoid line and bacterial exposure type. A) Comparison between organoid lines for each bacterial treatment. B) Comparison between bacterial treatment for each organoid line.

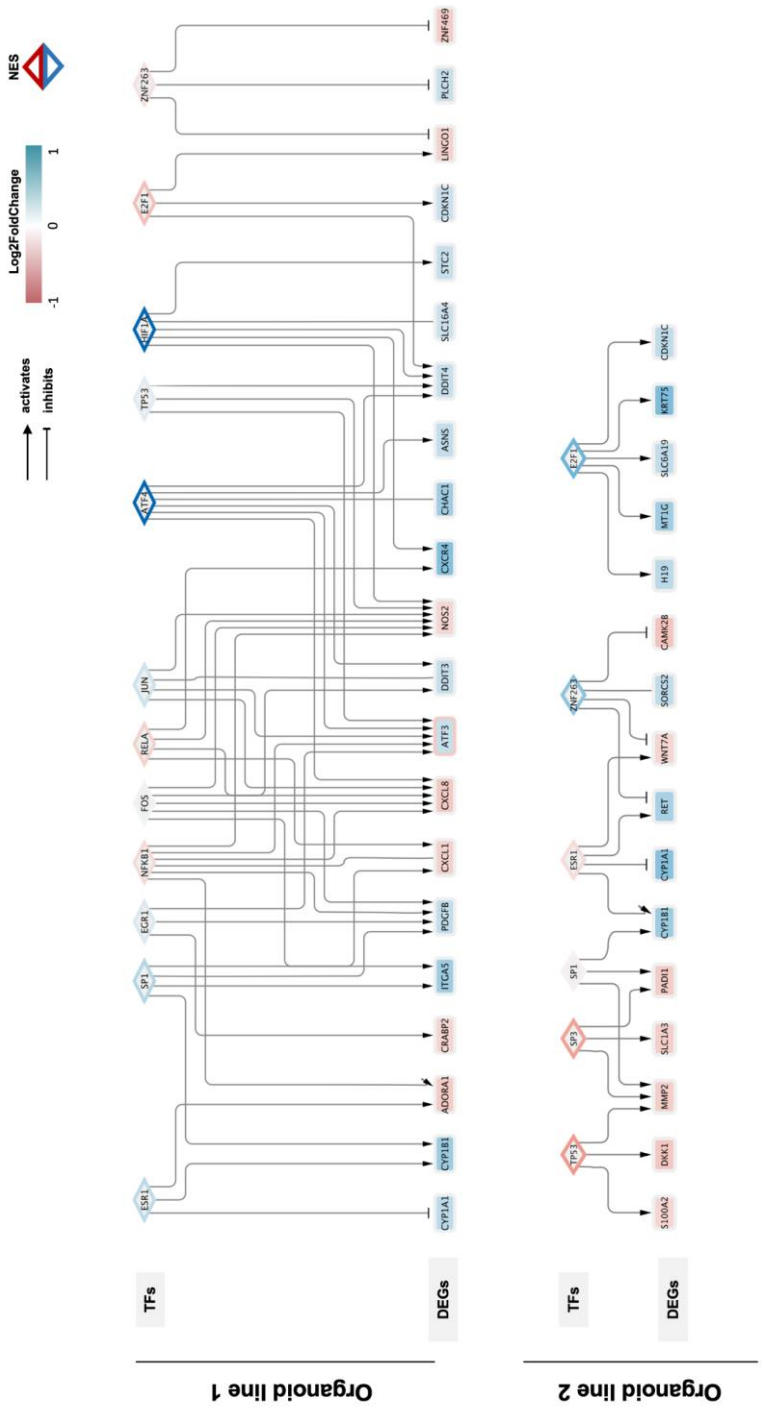

Supplementary Figure 4.15. TF-TG networks upon *L. rhamnosus* exposure of organoids compared to differentiated controls. Regulatory networks showing top TFs (regulating at least 3 DEGs) and the corresponding regulated DEGs in organoid lines exposed to *L. rhamnosus* sup. compared to differentiated controls. The edge colour indicates the NES of the TF (red, activated (NES > 0); blue, inhibited (NES < 0), while the colour gradient of the node indicates the Log2FoldChange of the DEG (red, upregulated; blue, downregulated). Arrows indicate the direction of the regulation, either activation (pointed arrow) or inhibition (T arrow). Networks were created in Cytoscape (version 3.8.2).

A

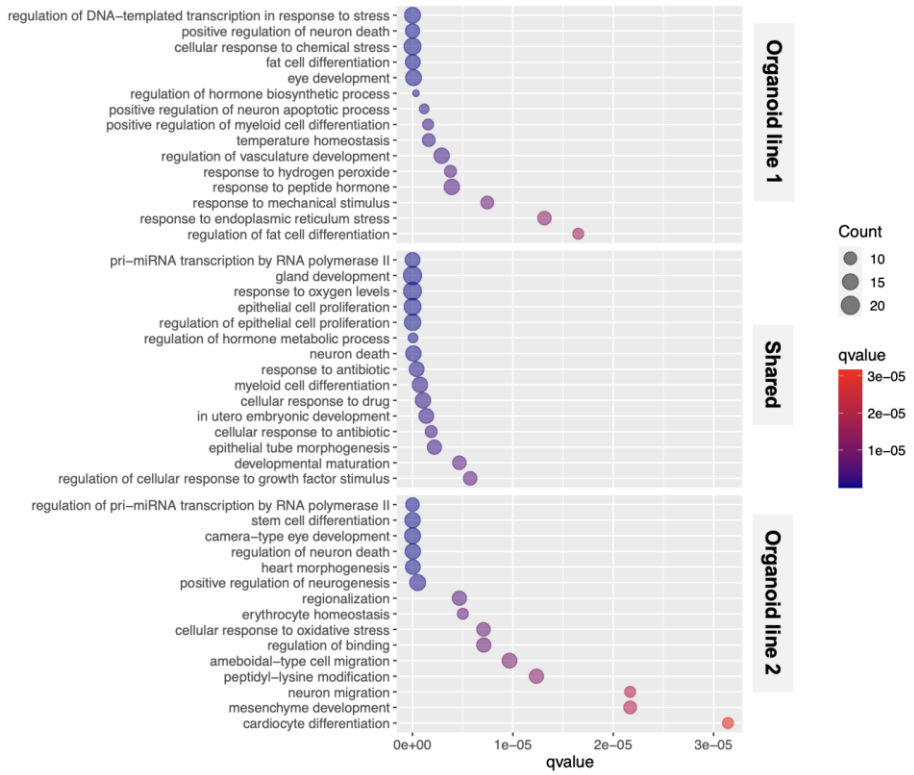

B

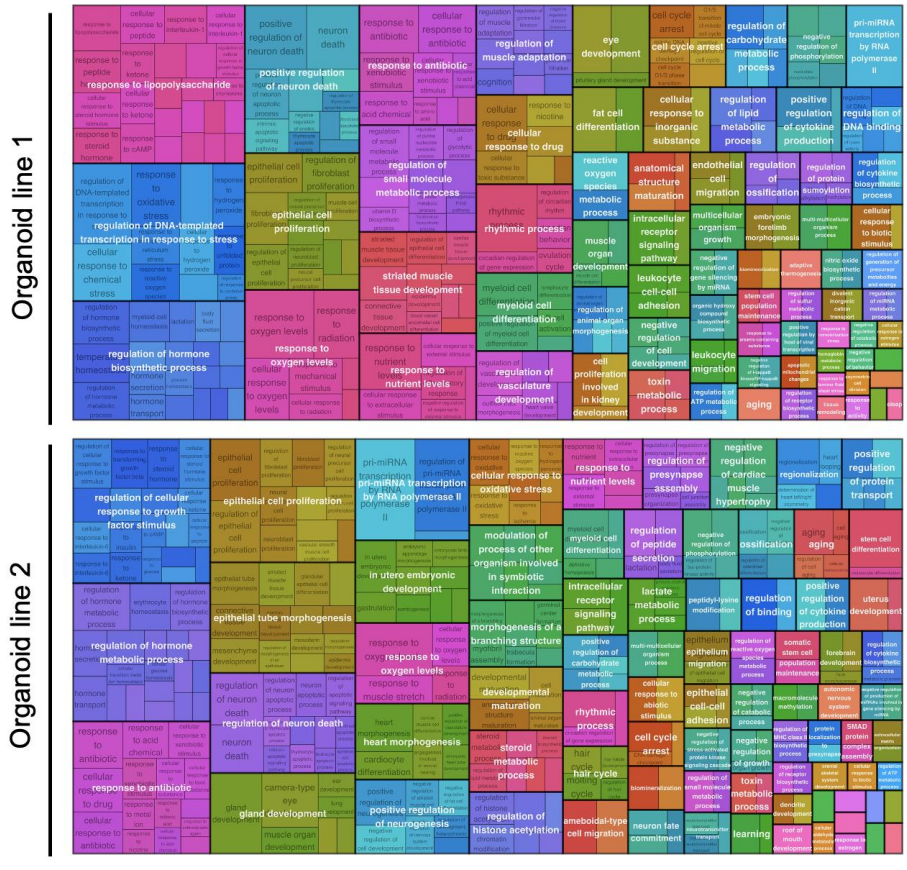

(Figure caption on the next page)

Supplementary Figure 4.16. Functional analysis of TF-TG networks upon *L. rhamnosus* exposure of organoids compared to differentiated controls. A) Revigo analysis of GO enriched functions of TF-DEG networks upon *L. rhamnosus* exposure of organoids compared to differentiated controls (t = 72 hours). Results are split in different boxes based on the organoid line. **B)** Bubble plot showing the 15 top enriched GO functions of TF-DEG networks upon *L. rhamnosus* exposure of organoids compared to differentiated controls (t = 72 hours). The colour of the bubble indicates the q-value of the enriched function (lowest, blue; highest, red), while the size indicates the number of elements contributing to the enriched function indicated. Functions are split in different boxes based on whether they are enriched in organoid line 1 only, line 2 only or both lines. Plots were created using the ClusterProfiler package in R.

A

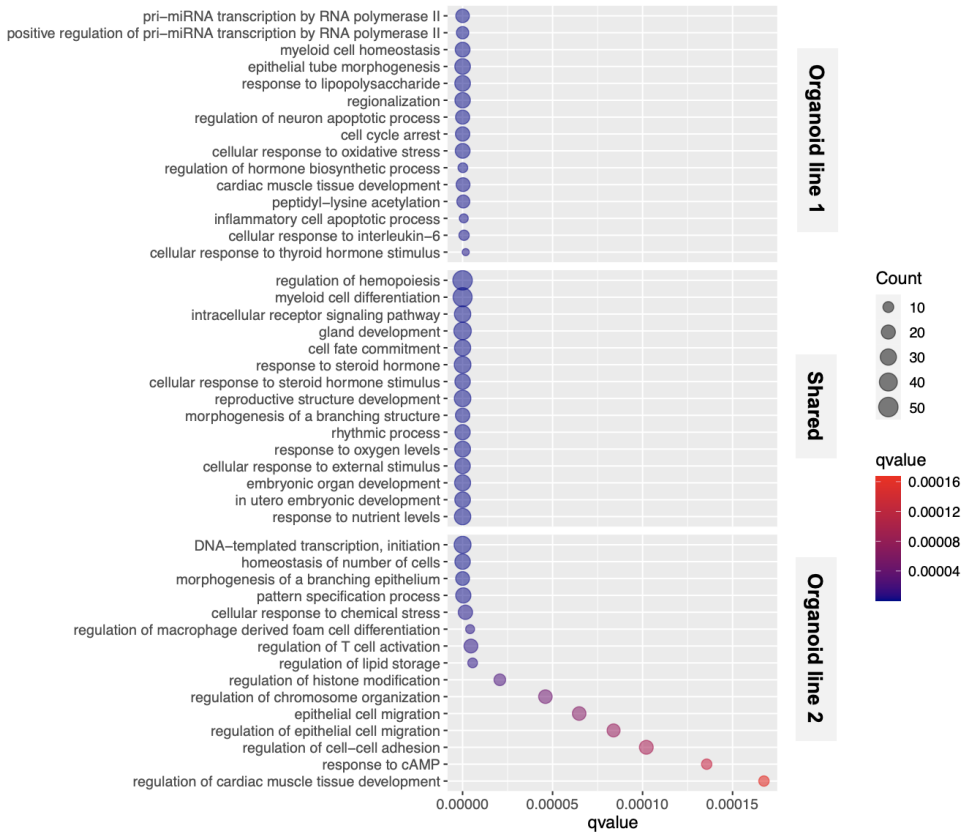

B

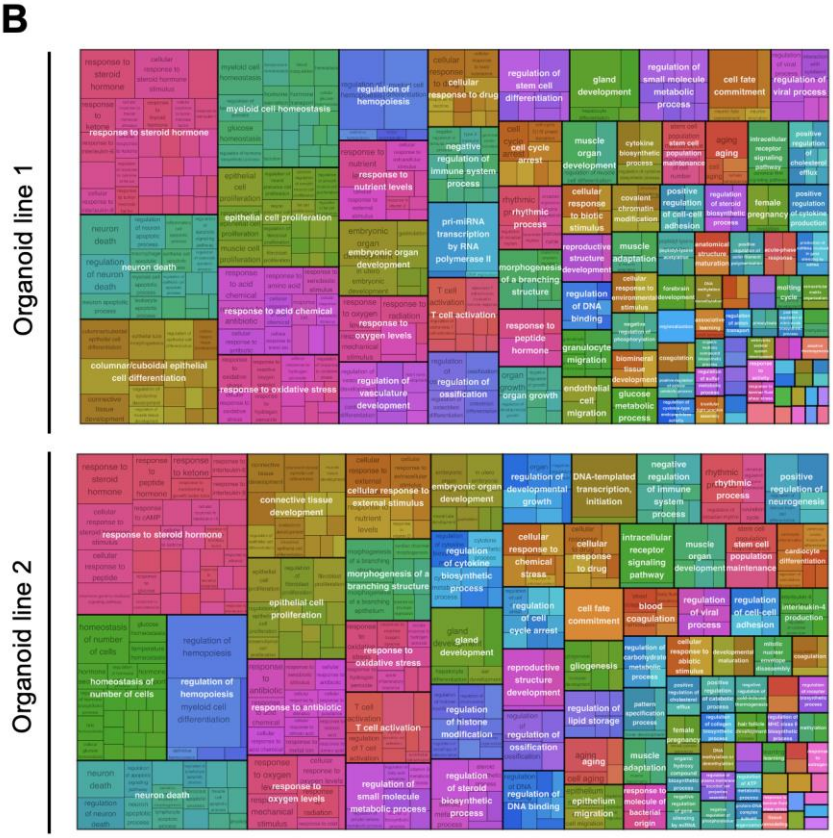

(Figure caption on the next page)

Supplementary Figure 4.17. Functional analysis of TF-TG networks upon *B. breve* UCC2003 exposure of organoids compared to undifferentiated controls. A) Revigo analysis of GO enriched functions of TF-DEG networks upon *B. breve UCC2003* exposure of organoids compared to undifferentiated controls (t = 0 hours). Results are split in different boxes based on the organoid line. **B)** Bubble plot showing the 15 top enriched GO functions of TF-DEG networks upon *B. breve UCC2003* exposure of organoids compared to undifferentiated controls (t = 0 hours). The colour of the bubble indicates the q-value of the enriched function (lowest, blue; highest, red), while the size indicates the number of elements contributing to the enriched function indicated. Functions are split in different boxes based on whether they are enriched in organoid line 1 only, line 2 only or both lines. Plots were created using the ClusterProfiler package in R.

A

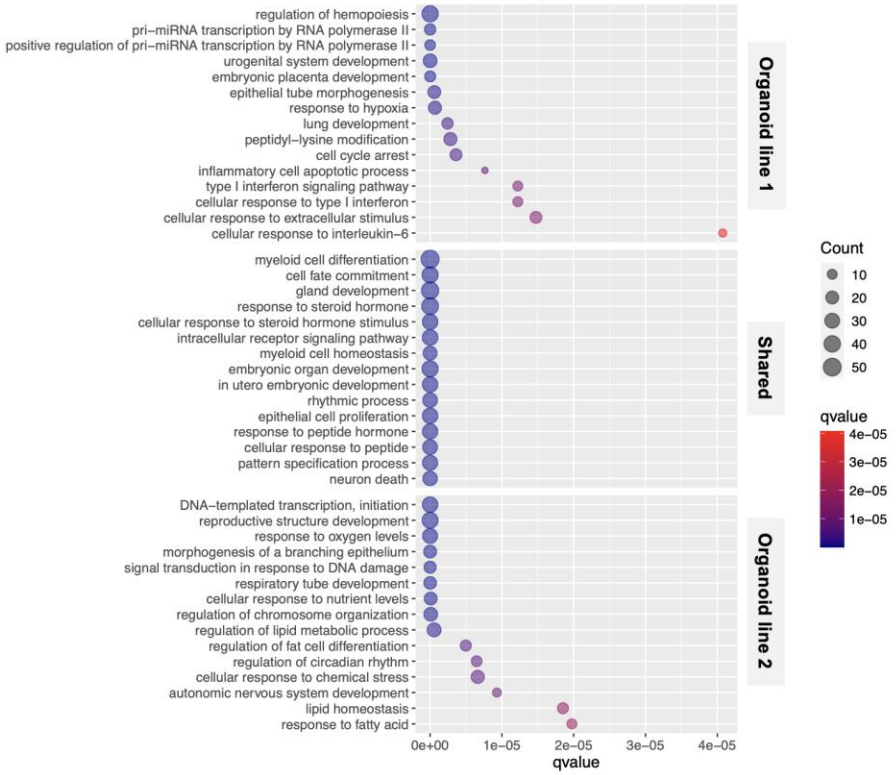

B

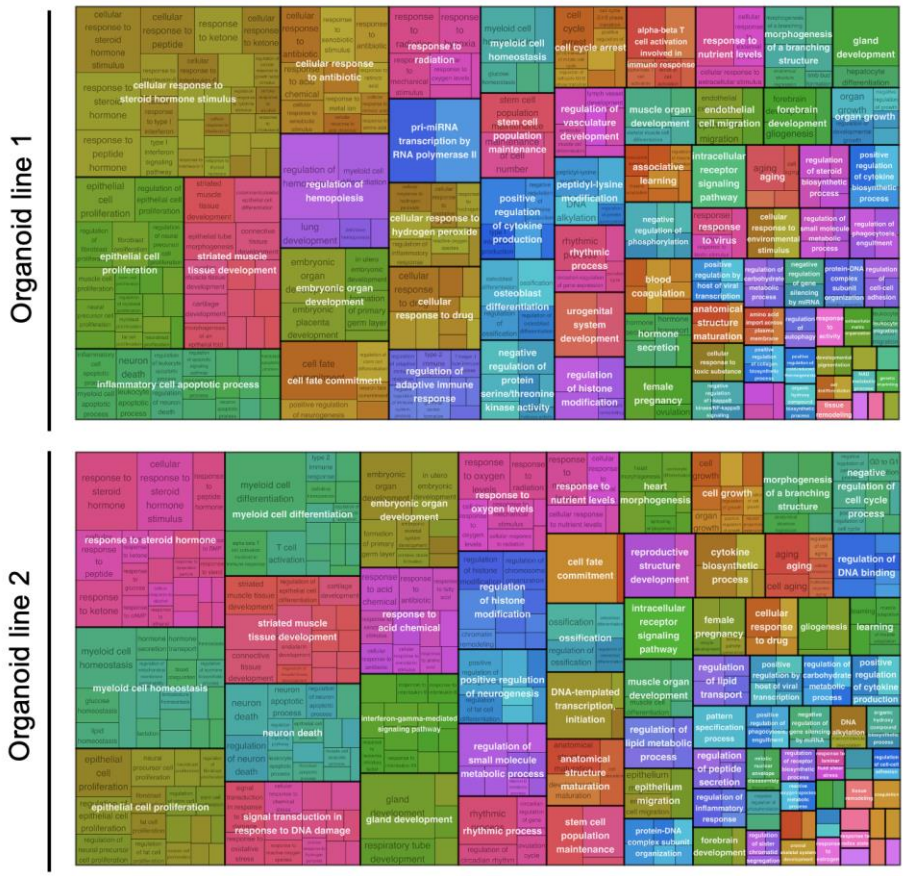

(Figure caption on the next page)

Supplementary Figure 4.18. Functional analysis of TF-TG networks upon *L. rhamnosus* exposure of organoids compared to undifferentiated controls. A) Revigo analysis of GO enriched functions of TF-DEG networks upon *L. rhamnosus* exposure of organoids compared to undifferentiated controls (t = 0 hours). Results are split in different boxes based on the organoid line. **B)** Bubble plot showing the 15 top enriched GO functions of TF-DEG networks upon *L. rhamnosus* exposure of organoids compared to undifferentiated controls (t = 0 hours). The colour of the bubble indicates the q-value of the enriched function (lowest, blue; highest, red), while the size indicates the number of elements contributing to the enriched function indicated. Functions are split in different boxes based on whether they are enriched in organoid line 1 only, line 2 only or both lines. Plots were created using the ClusterProfiler package in R.

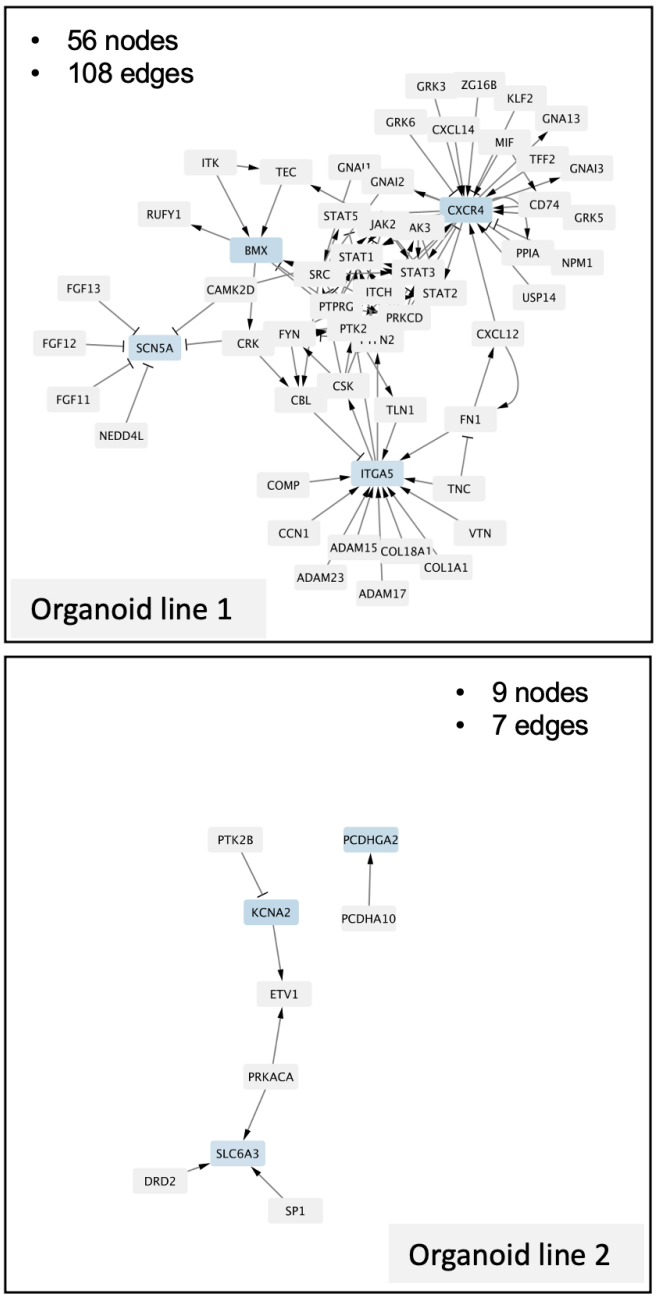

Enriched functions

- Peptydi-tyrosine modifications
- Regulation of (epithelial) morphogenesis
- JAK-STAT signalling
- Immune processes related to bacterial entry
- Positive regulation of cell adhesion
- ECM organization
- Hemostasis

Supplementary Figure 4.19. Interaction networks of DEGs and their direct interactors upon *L. rhamnosus* exposure. Networks: colour of the nodes indicates Log2FoldChange of DEGs (|Log2Foldchange| > 1, adjusted p-value < 0.05) in differentiated organoids exposed to *L. rhamnosus*-derived metabolites compared to differentiated organoid controls (t = 72 hours) in organoid line 1 (top) and 2 (bottom). Enriched functions: Top enriched functions in treated differentiated organoids compared to differentiated organoid controls in organoid line 1 or 2 identified by GO overrepresentation analysis of first neighbour networks of DEGs (|Log2Foldchange| > 1, adjusted p-value < 0.05). Networks were created in Cytoscape (version 3.8.2).

A

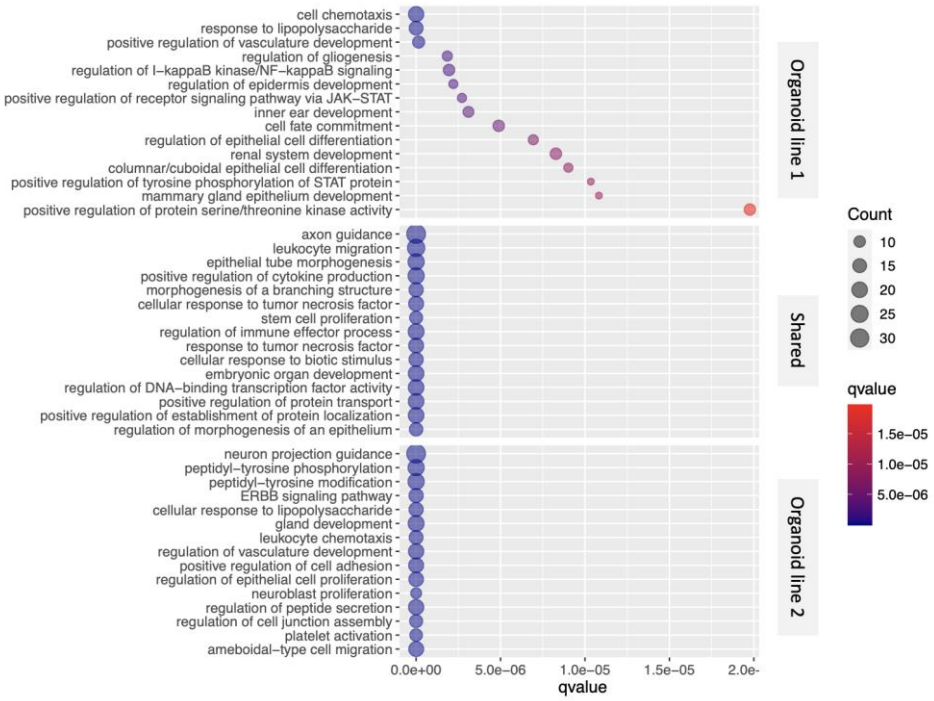

B

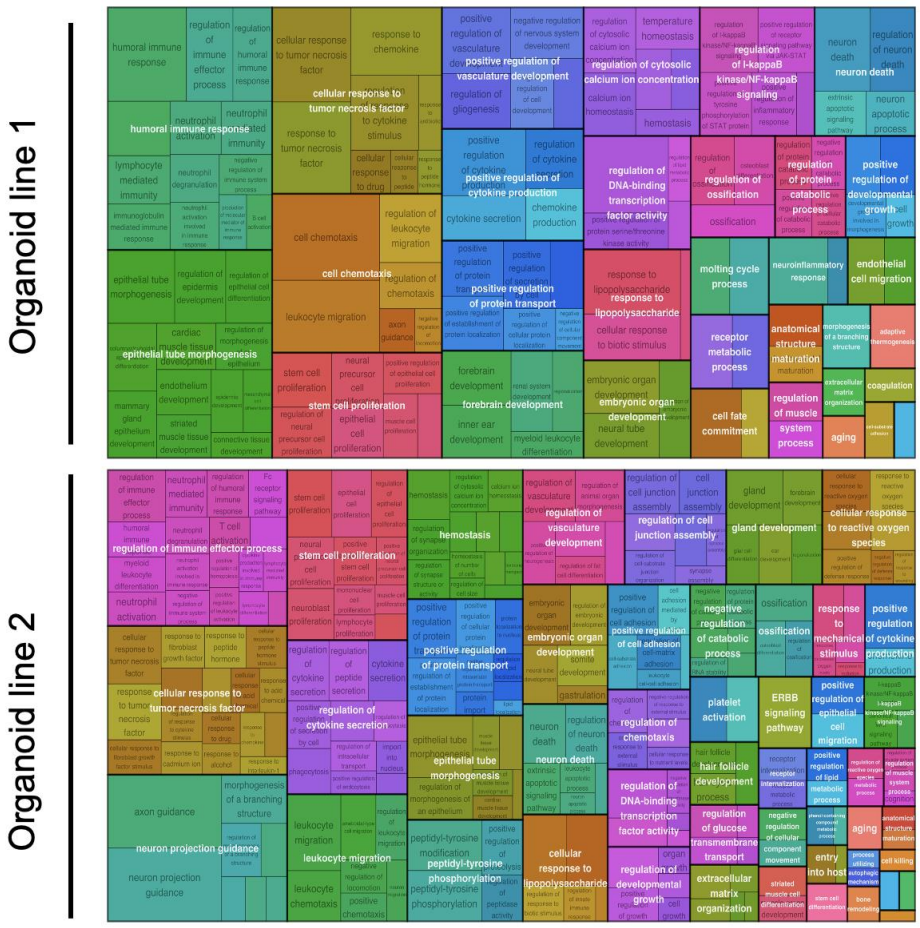

(Figure caption on the next page)

Supplementary Figure 4.20. Enriched GO functions in first neighbour networks of DEGs upon *B. breve UCC2003* exposure. A) Bubble plot showing the 15 top enriched GO functions of first neighbour networks of DEGs (adjusted p-value < 0.05, |Log2FoldChange| > 1) upon *B. breve UCC2003* sup. exposure of organoids compared to differentiated controls (t = 72 hours). The colour of the bubble indicates the q-value of the enriched function (lowest, blue; highest, red), while the size indicates the number of elements contributing to the enriched function indicated. Functions are split in different boxes based on whether they are enriched in line 1 only, line 2 only or both lines. Plots were created using the ClusterProfiler package in R. **B)** Revigo analysis of GO enriched functions of first neighbour networks of DEGs (adjusted p-value < 0.05, |Log2FoldChange| > 1) upon *B. breve UCC2003* exposure of organoids compared to differentiated controls (t = 72 hours). Results are split in different boxes based on the organoid line.

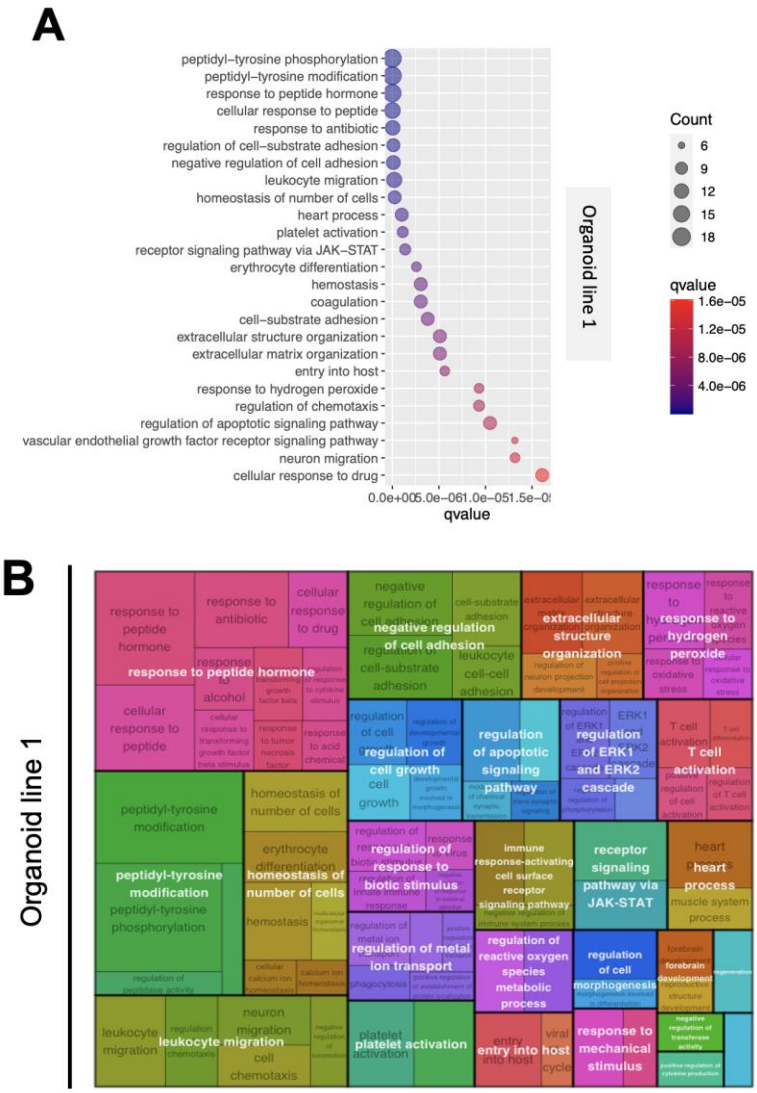

Supplementary Figure 4.21. Enriched GO functions in first neighbour networks of DEGs upon *L. rhamnosus* exposure. A) Bubble plot showing the 25 top enriched GO functions of first neighbour networks of DEGs (padj < 0.05, |Log2FoldChange| > 1) upon *L. rhamnosus* sup. exposure of organoids compared to differentiated controls (t = 72 hours). The colour of the bubble indicates the q-value of the enriched function (lowest, blue; highest, red), while the size indicates the number of elements contributing to the enriched function indicated. Functions are split in different boxes based on whether they are enriched in line 1 only, line 2 only or both lines. Results are shown for organoid line 2 only as no results were found for organoid line 1. Plots were created using the ClusterProfiler package in R. **B)** Revigo analysis of GO enriched functions of first neighbour networks of DEGs (padj < 0.05, |Log2FoldChange| > 1) upon *L. rhamnosus* sup. exposure of organoids compared to differentiated controls (t = 72 hours). Results are shown for organoid line 2 only as no results were found for organoid line 1.

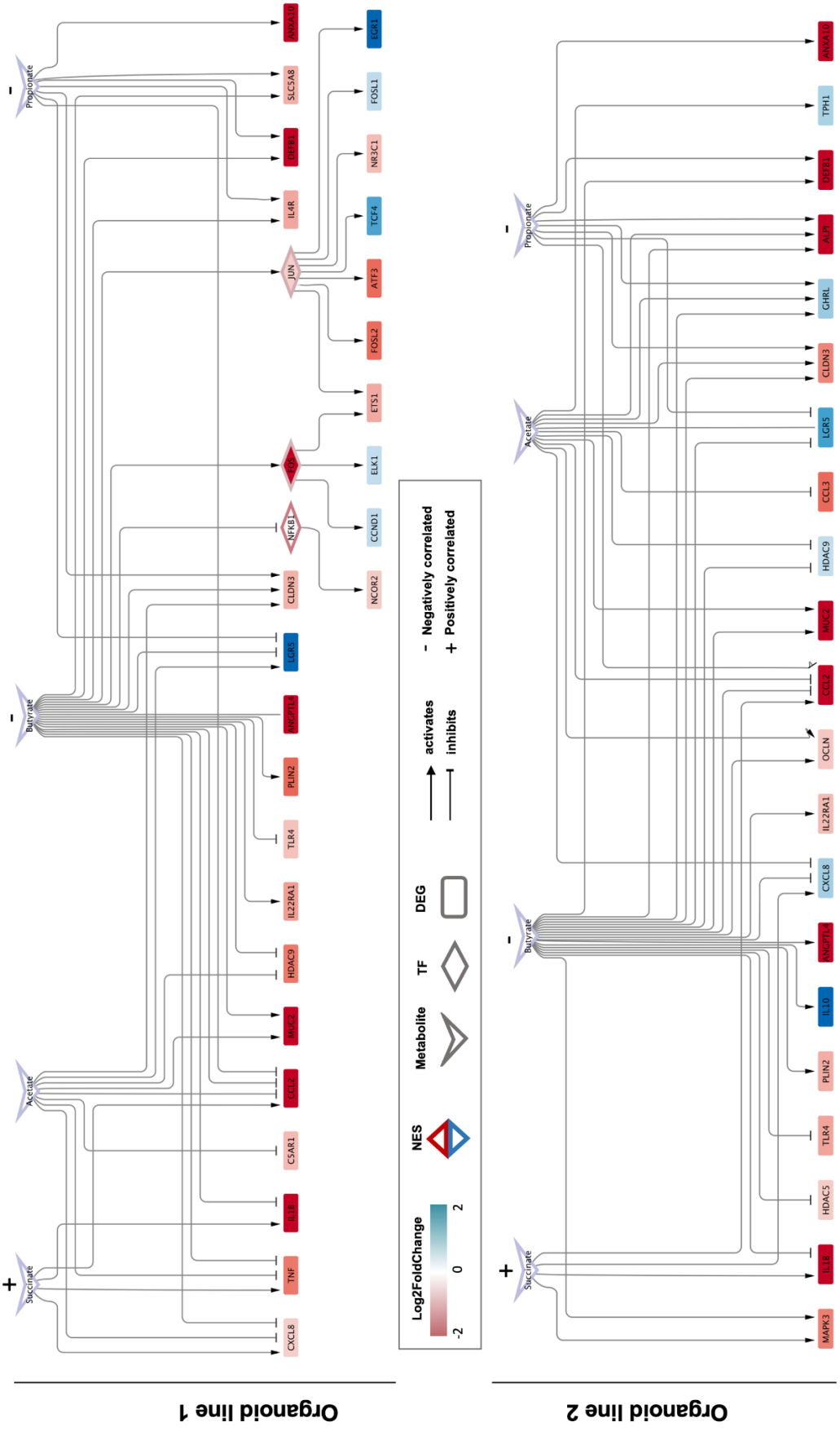

(Figure caption on the next page)

Supplementary Figure 4.22. Metabolite-host gene networks upon *B. breve* UCC2003 sup. exposure of organoids compared to undifferentiated controls. Metabolite-host gene networks showing *B. breve* UCC2003-produced metabolites and their affected target genes. Affected host genes are either predicted TFs or affected DEGs (|Log2FoldChange| > 0.5, adjusted p-value < 0.05) in organoids exposed to *B. breve* UCC2003 sup. compared to undifferentiated controls (t = 0 hours). The edge colour indicates the NES of the TF (red, activated (NES>0); blue, inhibited (NES < 0), while the colour gradient of the node indicates the Log2FoldChange of the DEG (red, upregulated; blue, downregulated). Arrows indicate the direction of the regulation, either activation (pointed arrow) or inhibition (T arrow). The shape indicates whether the node is a metabolite (arrow), TF (rhombus) or DEG (rectangle). Networks were created in Cytoscape (version 3.8.2).

Supplementary Table 4.1. TFs regulated upon *B. breve* UCC2003 and *L. rhamnosus* sup. exposure of organoids compared to differentiated controls.

Condition	Number	Gene name
Organoid line comparison		
L. rhamnosus		
Shared	5	*ZNF263, SP1, E2F1, ESR1, TP53*
Organoid line 1	7	*NFKB1, JUN, RELA, HIF1A, ATF4, EGR1, FOS*
Organoid line 2	1	*SP3*
B. breve UCC2003		
Shared	13	*EGR1, FOS, NFKB1, ZNF263, SP1, STAT3, MYC, FOXL2, JUN, RELA, TP53, STAT1, TEAD1*
Organoid line 1	1	*LYL1*
Organoid line 2	20	*CLOCK, RARA, ETS1, SMAD2, SP3, CEBPB, CEBPA, USF1, BACH1, HIF1A, E2F1, E2F6, MAFK, ZNF740, REL, ATF2, ETS2, SMAD3, ESR1, CREB1*
Bacterial treatment comparison		
Organoid line 1		
Shared	8	*ZNF263, NFB1, JUN, RELA, SP1, EGR1, FOS, TP53*
L. rhamnosus	4	*HIF1A, E2F1, ATF4, ESR1*
***B. breve* UCC2003**	6	*STAT1, TEAD1, LYL1, STAT3, MYC, FOXL2*
Organoid line 2		
Shared	6	*ZNF263, SP3, SP1, E2F1, TP53, ESR1*
L. rhamnosus	0	-
***B. breve* UCC2003**	27	*CLOCK, RARA, ETS1, EGR1, FOS, SMAD2, NFKB1, CEBPB, CEBPA, STAT3, MYC, FOXL2, USF1, JUN, BACH1, HIF1A, RELA, E2F6, MAFK, STAT1, ZNF740, REL, TEAD1, ATF2, ETS2, SMAD3, CREB1*

Supplementary Table 4.2. TFs regulated upon *B. breve* UCC2003 and *L. rhamnosus* sup. exposure of organoids compared to undifferentiated controls.

Condition	Number	Gene name
Organoid line comparison		
L. rhamnosus		
Shared	16	*ETS1, ZNF263, NFKB1, SP1, CEBPA, MYC, FOXP1, ESRRA, RELA, HIF1A, E2F1, TP53, STAT1, TEAD1, NR2F1, ESR1*
Organoid line 1	5	*SOX2, MEF2A, POU2F2, MEIS2, BHLHE40*
Organoid line 2	33	*ARNT, KLF4, IRF4, EGR1, CREM, MAF, MAFF, PBX2, IKZF1, STAT3, HMBOX1, TFAP2A, CTCF, TFAP4, KLF1, MXI1, JUN, MAX, FOXM1, ARID3A, GATA3, NFE2, MAFB, GATA6, RFX1, GFI1B, E2F4, LYL1, ASCL1, GABPA, FOXA1, TFAP2C, SPI1*
***B. breve* UCC2003**		
Shared	22	*IRF4, ZNF263, SP4, POU2F2, CTCF, HIF1A, RELA, TP53, STAT1, LYL1, BCL6, MEF2A, EGR1, NFKB1, BCL3, SP1, CEBPA, MYC, JUN, E2F1, E2F4, ZBTB7A*
Organoid line 1	34	*ETS1, ELK, FOS, PAX5, STAT3, FOXL2, FOXP1, MEIS2, LEF1, BACH1, FOXK2, MAFK, BHLHE40, MEF2B, JUND, ATF3, FOXP2, SPI1, KLF5, RARA, CEBPB, IRF1, IRF3, MAX, MEF2C, TCF7L2, MAFB, TEAD1, NRF1, AR, SNAI2, ETS2, TCF7, KLF9*
Organoid line 2	18	*ONECUT1, POU2F1, TBX21, HNF4A, NFYB, NFE2, TFAP2C, POU5F1, MEIS1, ZEB2, GRHL2, TFAP2A, SOX13, IRF2, HNF4G, FOXA1, ESR1, PDX1*
Bacterial treatment comparison		
Organoid line 1		
Shared	17	*MEF2, ETS1, ZNF263, NFKB1, POU2F2, SP1, CEBPA, MYC, FOXP1, MEIS2, HIF1A, RELA, E2F1, TP53, STAT1, TEAD1, BHLHE40*
L. rhamnosus	4	*SOX2, ESRRA, NR2F1, ESR1*
***B. breve* UCC2003**	39	*KLF5, IRF4, RARA, ELK1, EGR1, FOS, SP4, PAX5, CEBPB, BCL3, STAT3, IRF1, FOXL2, CTCF, LEF1, JUN, MAX, IRF3, BACH1, FOXK2, MEF2C, MAFK, TCF7L2, MAFB, NRF1, MEF2B, LYL1, E2F4, ZBTB7A, AR, SNAI2, ETS2, JUND, ATF3, TCF7, KLF9, FOXP2, BCL6, SPI1*
Organoid line 2		
Shared	21	*IRF4, ZNF63, CTCF, RELA, HIF1A, NFE2, TP53, STAT1, LYL1, TFAP2C, EGR1, NFKB1, SP1, CEBPA, TFAP2A, MYC, JUN, E2F1, E2F4, FOXA1, ESR1*
L. rhamnosus	28	*ARNT, ETS1, MAF, MAFF, PBX2, STAT3, HMBOX1, FOXP1, KLF1, ARID3A, GFI1B, ASCL1, GABPA, SPI1, KLF5, CREM, IKZF1, MXI1, ESRRA, TFAP4, MAX, FOXM1, GATA3, MAFB, GATA6, RFX1, TEAD1, NR2F1*
***B. breve* UCC2003**	19	*ONECUT1, SP4, SPIB, TBX21, POU2F2, HNF4A, NFYB, POU5F1, BCL6, MEF2A, MEIS1, ZEB2, BCL3, GRHL2, SOX13, IRF2, HNF4G, ZBTB7A, PDX1*

Supplementary Table 4.3. Raw metabolite concentration (in mM) for single metabolites in *B. breve* UCC2003 cultures over time as measured by 1H-NMR.

Metabolite Time (hrs)	Acetate	Butyrate	Ethanol	Formate	Lactate	Propionate	Succinate
0	2.5769	1.1927	1.8069	0.5686	0.0251	0.6003	0.1955
6	2.6700	1.2877	1.9096	0.6830	0.0366	0.5812	0.2235
12	2.9237	1.4930	1.9606	0.8051	0.0578	0.5348	0.2439
24	2.6247	1.3420	1.8484	0.8135	0.0908	0.3694	0.1730
36	2.6359	1.3279	1.8070	0.8485	0.1092	0.3744	0.1619
48	2.7652	1.3170	1.7491	0.8503	0.0800	0.3804	0.1561
72	2.9410	1.3199	1.6878	0.9489	0.0914	0.4842	0.1420
96	2.9026	1.2527	1.6893	0.8275	0.0473	0.5152	0.1451
120	2.9091	1.2770	1.6534	0.8236	0.0569	0.5155	0.1479
144	2.9164	1.1971	1.7465	0.8368	0.1047	0.5716	0.1365
168	3.2711	1.2555	1.8228	0.7232	0.0284	0.8475	0.1470
192	2.4451	1.5576	1.5159	0.3014	0.0174	0.8339	0.1417
216	2.5748	1.5836	1.5584	0.3223	0.0302	0.8813	0.0938
240	2.7049	1.4664	1.5913	0.2071	0.0209	0.8840	0.0807
264	2.8995	1.4630	1.6827	0.3713	0.0248	0.8878	0.1018
288	2.9876	1.4515	1.6491	0.4523	0.0215	0.8864	0.1254
312	3.0454	1.5245	1.5700	0.1907	0.0410	0.9612	0.1471
336	3.0909	1.3428	1.5747	0.2865	0.0458	0.9780	0.1169
360	3.2763	1.3590	1.6800	0.4020	0.0839	1.0284	0.1273
384	3.1694	1.3551	1.5865	0.3707	0.0651	1.0240	0.1146
408	3.1565	1.3657	1.6155	0.4373	0.0506	1.0242	0.1136

Supplementary Table 4.4. Spearman correlation between 16S reads of *B. breve* UCC2003 and identified metabolites. Statistical significance was calculated by performing a Spearman correlation test. Obtained p-values were adjusted for multiple comparisons using Benjamini & Hochberg correction. Statistical significance is indicated as follows: N.S. not significant; * adjusted p-value < 0.05; **adjusted p-value < 0.01; *** adjusted p-value < 0.001.

Metabolite	Correlation coefficient	Adjusted p-value	Statistical significance
Ethanol	0.84	0.000	***
Succinate	0.68	0.005	**
Formate	0.65	0.008	**
Lactate	0.56	0.023	*
Acetate	-0.14	0.673	N.S.
Propionate	-0.50	0.045	*
Butyrate	-0.51	0.046	*

Appendix 2: Supplementary data for Chapter 5

This appendix contains all the supplementary material for **Chapter 5**.

- **Supplementary Figure 5.1.** Intracellular signalling networks of ileal and colonic infected immature enterocytes upon SARS-CoV-2 infection.
- **Supplementary Figure 5.2.** Overview of intracellular signalling upon SARS-CoV-2 infection in colonic infected immature enterocytes, reconstructed using the CARNIVAL.
- **Supplementary Figure 5.3.** Overview of intracellular signalling upon SARS-CoV-2 infection in ileal infected immature enterocytes, reconstructed using CARNIVAL.
- **Supplementary Figure 5.4.** Ligands driving interactions between colonic and ileal infected immature enterocytes and resident immune cells upon infection in the colon and ileum.
- **Supplementary Figure 5.5.** Receptors participating in intercellular interactions between infected immature enterocytes and resident immune cells upon infection in the colon and ileum.
- **Supplementary Figure 5.6:** Ligand–receptor interactions between infected immature enterocytes and resident immune cells upon infection in the colon and ileum.
- **Supplementary Figure 5.7.** Intercellular interactions with upregulated and downregulated ligands of colonic and ileal infected immature enterocytes.

A

ViralLink

Colon

Network characteristics

Network parameter	Statistics
Number of nodes	1423
Number of edges	9971
Average number of neighbours	14
Network diameter	10
Path length	4

Node table

	Viral miRNAs or proteins	Human Binding proteins	Intermediary signalling proteins	TFs	Differentially expressed ligands	Total
Viral miRNA specific	19	107	120	4	2	**252**
Viral protein specific	28	236	223	4	2	**493**
Shared	0	66	565	29	18	**678**
Total	**47**	**409**	**908**	**37**	**22**	**1423**

Ileum

Network characteristics

Network parameter	Statistics
Number of nodes	1316
Number of edges	7935
Average number of neighbours	12
Network diameter	9
Path length	4

Node table

	Viral miRNAs or proteins	Human Binding proteins	Intermediary signalling proteins	TFs	Differentially expressed ligands	Total
Viral miRNA specific	28	125	242	6	1	**402**
Viral protein specific	19	214	169	2	1	**405**
Shared	0	54	399	29	26	**508**
Total	**47**	**393**	**810**	**37**	**28**	**1315**

B

CARNIVAL

Colon

Network characteristics

Network parameter	Statistics
Number of nodes	147
Number of edges	279
Average number of neighbours	3.782
Network diameter	15
Path length	6.375

Node table

	Viral miRNAs or proteins	Human Binding proteins	Intermediary signalling proteins	TFs	Differentially expressed ligands	Total
Viral miRNA specific	4	0	31	22	0	**57**
Viral protein specific	16	25	4	10	0	**55**
Shared	0	2	1	11	21	**35**
Total	**20**	**27**	**36**	**43**	**21**	**147**

Ileum

Network characteristics

Network parameter	Statistics
Number of nodes	274
Number of edges	479
Average number of neighbours	3.219
Network diameter	9
Path length	3.353

Node table

	Viral miRNAs or proteins	Human Binding proteins	Intermediary signalling proteins	TFs	Differentially expressed ligands	Total
Viral miRNA specific	4	0	154	1	3	**162**
Viral protein specific	17	30	15	0	1	**61**
Shared	0	1	0	25	21	**49**
Total	**21**	**31**	**169**	**26**	**25**	**272**

(Figure caption on the next page)

Supplementary Figure 5.1. Intracellular signalling networks of ileal and colonic infected immature enterocytes upon SARS-CoV-2 infection. A, B) Characteristics of causal networks of SARS-CoV-2-infected colonic and ileal immature enterocytes reconstructed using ViralLink (A) or CARNIVAL (B). For each network the number of interacting partners (nodes), number of interactions (edges), average number of neighbours, network diameter and characteristics path length are indicated under “Network characteristics”. Within the “Node table”, columns indicate the types of nodes in the different layers of the network, including SARS-CoV-2 proteins or miRNAs, human binding proteins, intermediary signalling proteins, TFs and differentially expressed ligands. Where an interacting partner (human protein/gene) was found to act in multiple layers of the network, it was assigned to a layer based on the following priority: differentially expressed ligands, human binding proteins, TFs, intermediary signalling proteins. Ligands have Log2FoldChange > |0.5| and adjusted p-value < 0.05. Within the “Node Table”, rows indicate whether the node or edge belong to intracellular signals stemming from viral miRNA only, viral protein only or both (“shared”).

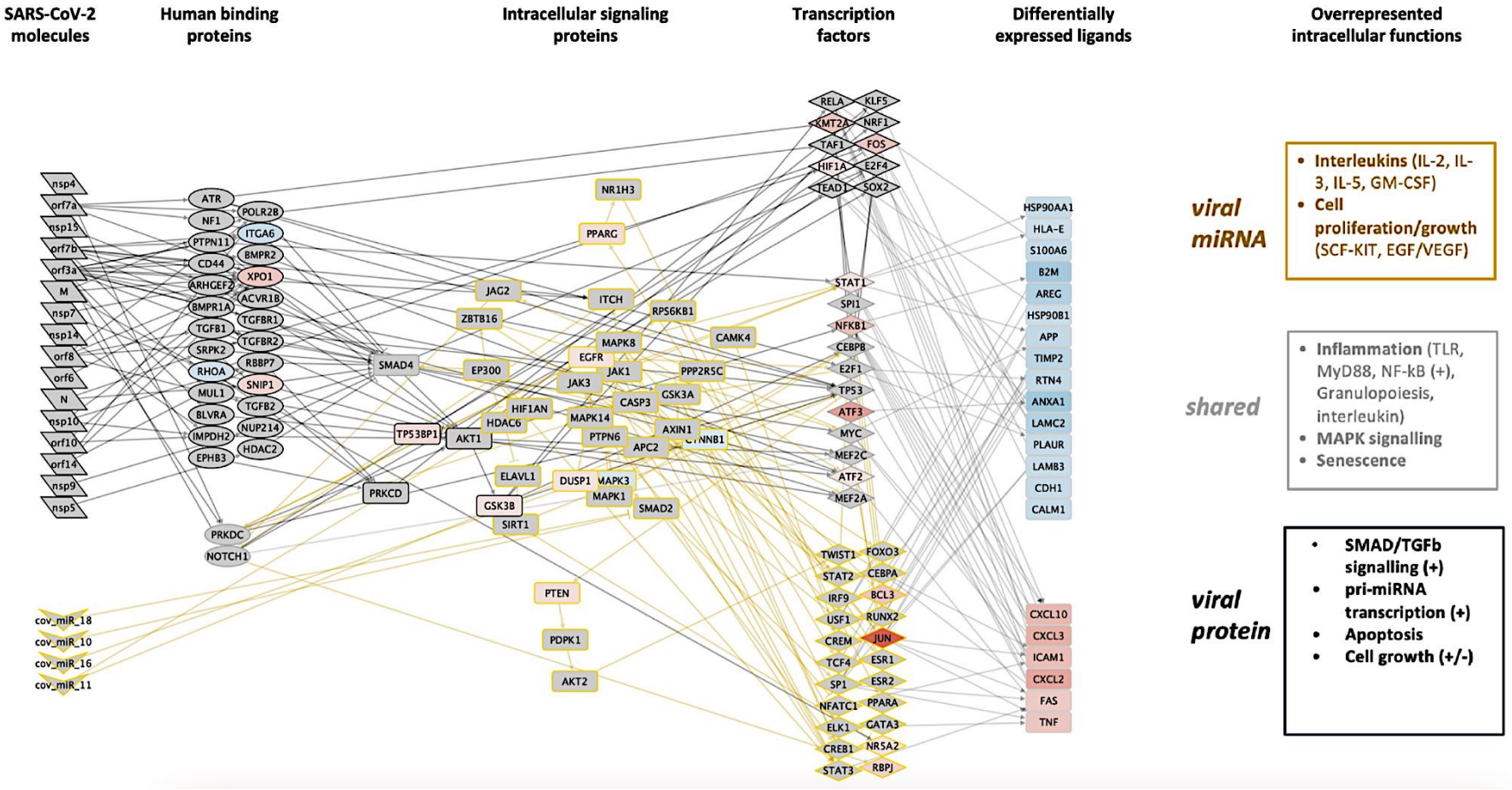

(Figure caption on the next page)

Supplementary Figure 5.2. Overview of intracellular signalling upon SARS-CoV-2 infection in colonic infected immature enterocytes, reconstructed using the CARNIVAL. From left to right: signalling cascade going from the upstream perturbation (SARS-CoV-2 proteins or miRNAs interacting with human binding proteins) to the downstream perturbation, transcription factors (TFs) regulating the differentially expressed ligands. Diamonds indicate the most active transcription factors after infection and the ovals are the perturbed human binding proteins. Rectangles are signalling intermediate proteins linking these two. Parallelograms and downward arrows indicate SARS-CoV-2 proteins and miRNAs, respectively. The colour of the node indicates activation (red) or inhibition (blue) upon SARS-CoV-2 infection vs uninfected condition. Connecting edges show the direction of the interaction, as activation (pointed arrow) or inhibition (T shape arrow). Differentially expressed ligands for which no upstream signalling was identified, but downstream intercellular connections were predicted are excluded from this figure. Differentially expressed ligands are grouped based on the direction of regulation, which is indicated with blue when downregulated (bottom) and red when upregulated (top) when comparing SARS-CoV-2 infected vs uninfected conditions. Colours of the nodes edge and of the functional analysis boxes indicate if the original network was a miRNA only (yellow), viral protein only (black) or both viral protein and miRNA (grey). Functional overrepresentation analysis was carried out for the “PPI layer” of the intracellular network which includes human binding proteins, intermediary signalling proteins and TFs (adjusted p-value < 0.05, n > 3).

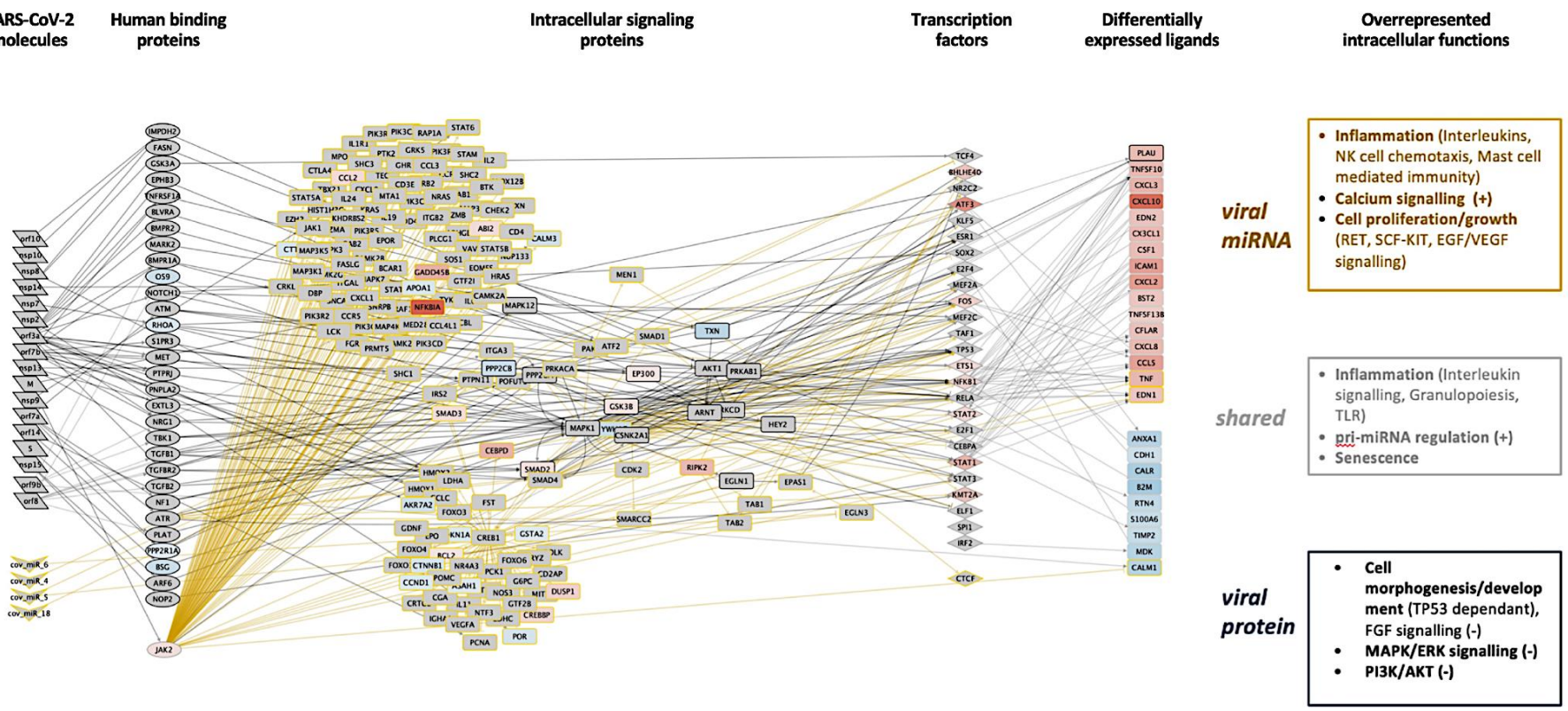

(Figure caption on the next page)

Supplementary Figure 5.3. Overview of intracellular signalling upon SARS-CoV-2 infection in ileal infected immature enterocytes, reconstructed using CARNIVAL. From left to right: signalling cascade going from the upstream perturbation (SARS-CoV-2 proteins or miRNAs interacting with human binding proteins) to the downstream perturbation, transcription factors (TFs) regulating the differentially expressed ligands. Diamonds indicate the most active transcription factors after infection and the ovals are the perturbed human binding proteins. Rectangles are signalling intermediate proteins linking these two. Parallelograms and downward arrows indicate SARS-CoV-2 proteins and miRNAs, respectively. The colour of the node indicates activation (red) or inhibition (blue) upon SARS-CoV-2 infection vs uninfected condition. Connecting edges show the direction of the interaction, as activation (pointed arrow) or inhibition (T shape arrow). Differentially expressed ligands for which no upstream signalling was identified, but downstream intercellular connections were predicted are excluded from this figure. Differentially expressed ligands are grouped based on the direction of regulation, which is indicated with blue when downregulated (bottom) and red when upregulated (top) when comparing SARS-CoV-2 infected vs uninfected conditions. Colours of the nodes edge and of the functional analysis boxes indicate if the original network was a miRNA only (yellow), viral protein only (black) or both viral protein and miRNA (grey). Functional overrepresentation analysis was carried out for the “PPI layer” of the intracellular network which includes human binding proteins, intermediary signalling proteins and TFs (adjusted p-value < 0.05, n > 3).

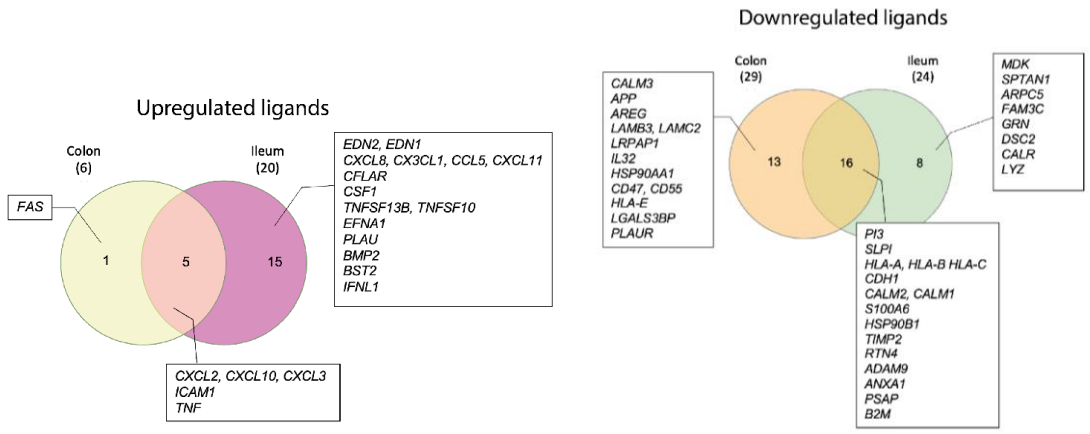

Supplementary Figure 5.4. Ligands driving interactions between colonic and ileal infected immature enterocytes and resident immune cells upon infection in the colon and ileum. Venn diagrams showing the number of ligands of the infected immature enterocytes–immune cells intercellular network that are unique or shared between the ileum and colon. Upregulated and downregulated ligands are shown separately.

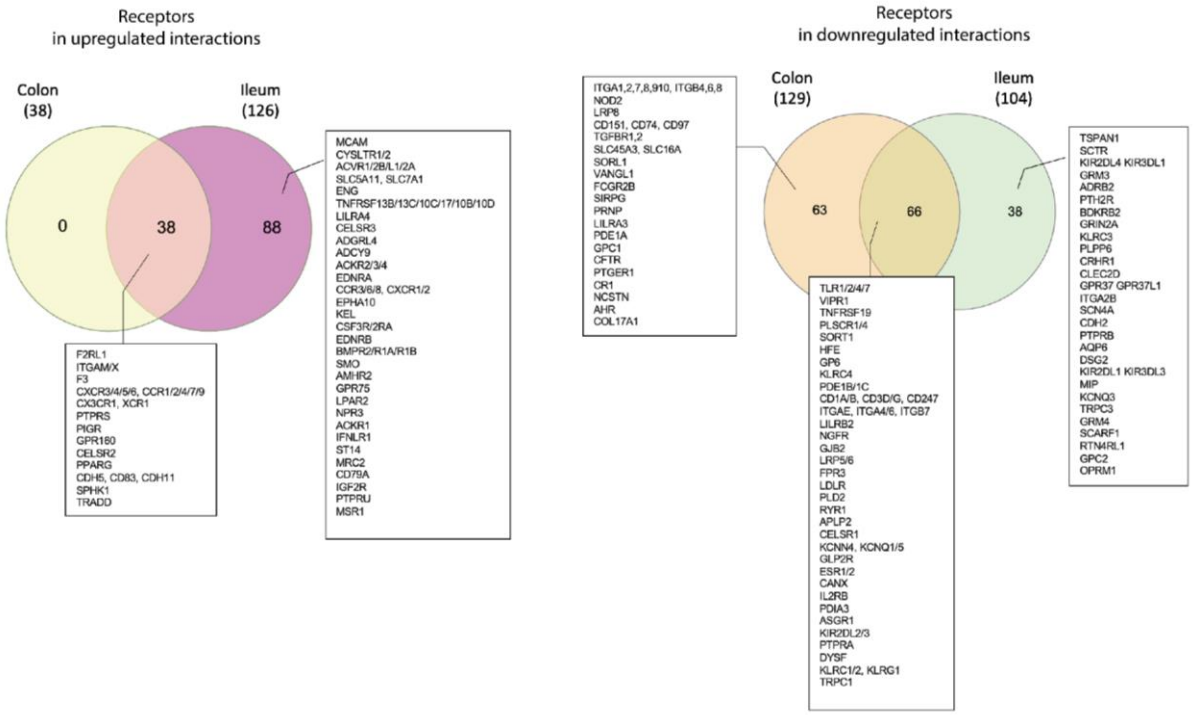

Supplementary Figure 5.5. Receptors participating in intercellular interactions between infected immature enterocytes and resident immune cells upon infection in the colon and ileum. Venn diagrams showing the number of receptors in the infected immature enterocytes–immune cells intercellular networks that are unique or shared between the ileal and colonic networks. Receptors targeted by upregulated ligands and downregulated ligands are shown separately.

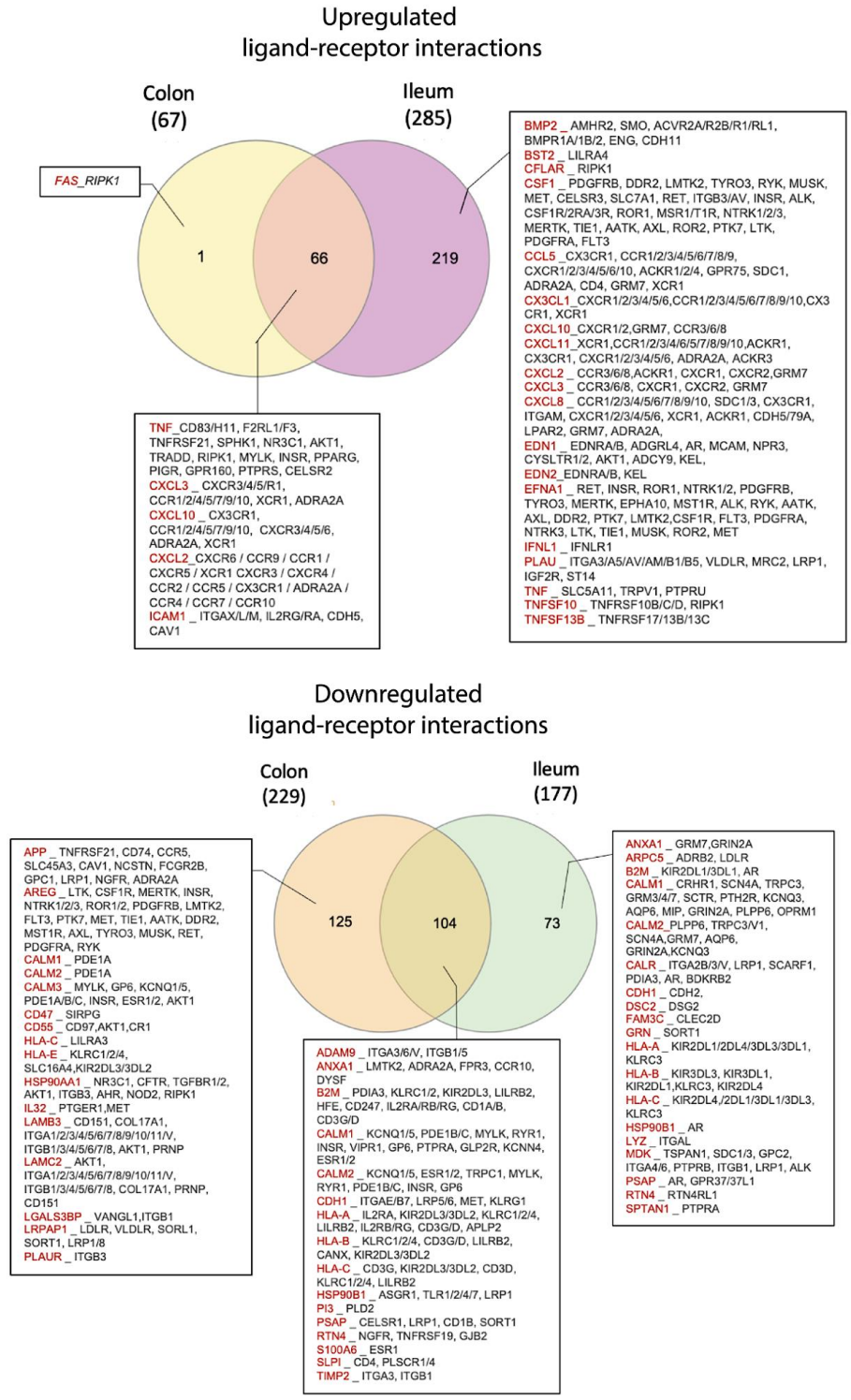

Supplementary Figure 5.6: Ligand–receptor interactions between infected immature enterocytes and resident immune cells upon infection in the colon and ileum. Venn diagrams showing the number of ligand–receptor interactions in the infected immature enterocytes–immune cells intercellular networks that are unique or shared between the ileum and colon. Intercellular interactions driven by upregulated and downregulated ligands are shown separately.

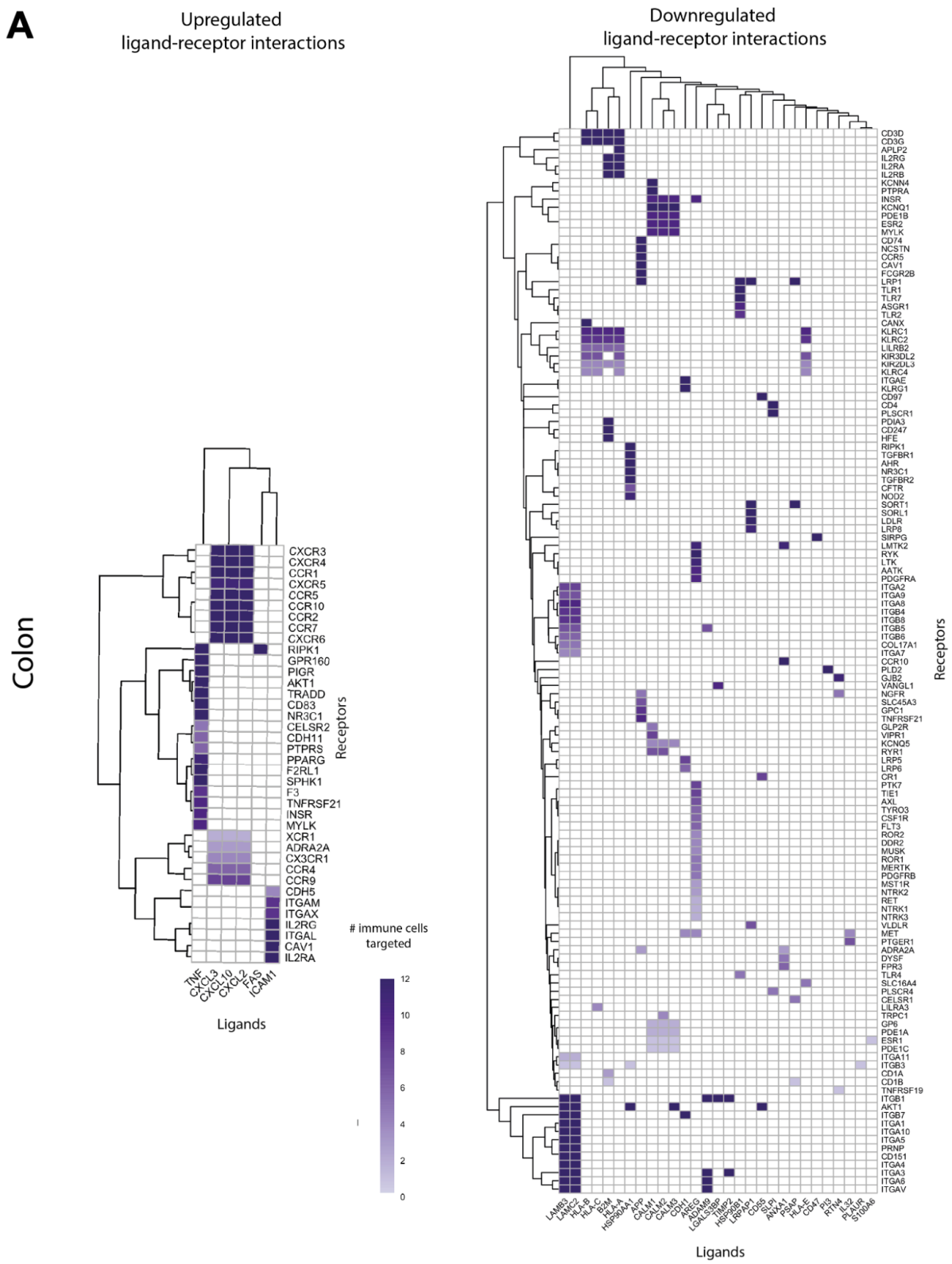

(Figure continues on the next page)

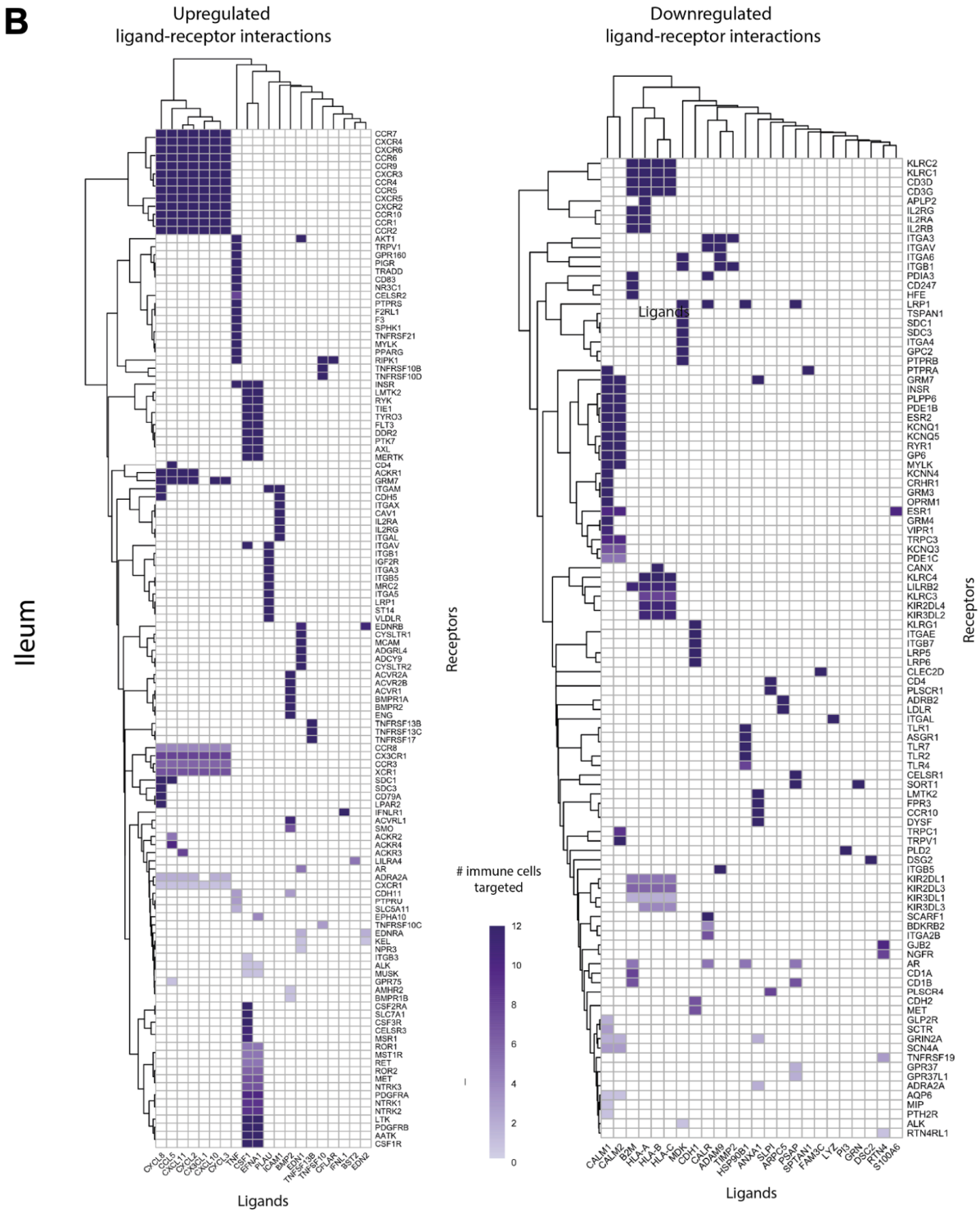

Supplementary Figure 5.7. Intercellular interactions with upregulated and downregulated ligands of colonic and ileal infected immature enterocytes. A, B) Interactions driven by upregulated and downregulated ligands in the colon (A) and ileum (B) are shown separately. The number of immune cells involved in ligand-receptor interaction pairs is indicated in purple.

Appendix 3: Peer-reviewed publications

A correction notice has been published, see:
https://doi.org/10.1093/ecco-jcc/jjac104

Journal of Crohn's and Colitis, 2021, 1222–1235
doi:10.1093/ecco-jcc/jjaa257
Advance Access publication December 20, 2020
Review Article

Review Article

Organoid-based Models to Study the Role of Host-microbiota Interactions in IBD

Martina Poletti,[a,b,†] Kaline Arnauts,[c,d,†] Marc Ferrante,[c,e] Tamas Korcsmaros[a,b]

[a]Earlham Institute, Norwich Research Park, Norwich, UK [b]Quadram Institute, Norwich Research Park, Norwich, UK [c]Department of Chronic Diseases, Metabolism and Ageing [CHROMETA], Translational Research Center for Gastrointestinal Disorders [TARGID], KU Leuven, Leuven, Belgium [d]Department of Development and Regeneration, Stem Cell Institute Leuven [SCIL], KU Leuven, Leuven, Belgium [e]Department of Gastroenterology and Hepatology, University Hospitals Leuven, KU Leuven, Leuven, Belgium

[†]These authors contributed equally.

Corresponding author: Marc Ferrante, MD, PhD, Department of Gastroenterology and Hepatology, University Hospitals Leuven, KU Leuven, Herestraat 49, 3000 Leuven, Belgium. Tel.: +32 16 344225; email: marc.ferrante@uzleuven.be

Abstract

The gut microbiota appears to play a central role in health, and alterations in the gut microbiota are observed in both forms of inflammatory bowel disease [IBD], namely Crohn's disease and ulcerative colitis. Yet, the mechanisms behind host-microbiota interactions in IBD, especially at the intestinal epithelial cell level, are not yet fully understood. Dissecting the role of host-microbiota interactions in disease onset and progression is pivotal, and requires representative models mimicking the gastrointestinal ecosystem, including the intestinal epithelium, the gut microbiota, and immune cells. New advancements in organoid microfluidics technology are facilitating the study of IBD-related microbial-epithelial cross-talk, and the discovery of novel microbial therapies. Here, we review different organoid-based *ex vivo* models that are currently available, and benchmark their suitability and limitations for specific research questions. Organoid applications, such as patient-derived organoid biobanks for microbial screening and 'omics technologies, are discussed, highlighting their potential to gain better mechanistic insights into disease mechanisms and eventually allow personalised medicine.

Key Words: Inflammatory bowel disease; microbiota; organoids; *in vitro* models

Introduction

Both forms of inflammatory bowel disease [IBD], Crohn's disease [CD] and ulcerative colitis [UC], are thought to be driven by environmental factors in genetically susceptible individuals, resulting in an exacerbated immune response towards components of the gut microbiota.[1] However, the underlying mechanisms are not yet completely understood. In particular, whether the loss of tolerance towards the microbiota is a cause or consequence of the disease, and what the exact effect is of the interactions between intestinal epithelial cells and the dysbiotic microbiota, remain unclear.

Growing evidence suggests that the cross-talk between the luminal microbiota and the intestinal epithelium plays a key role in the onset of IBD.[2] The intestinal microbiota interacts with the epithelium of the gut through metabolites or other released factors,[3–5] and contributes to the intestinal barrier functions and integrity,[3,4] modulates the host immune system,[6] and prevents colonisation of pathobionts.[6] Microbial metabolites such as short chain fatty acids [SCFAs], produced by microbial fermentation of dietary fibre in the gut, also serve as an energy source[7] and as immunomodulators.[8]

Alterations in microbiota composition and homeostasis ['dysbiosis'] have been observed in both forms of IBD,[9–11] overall

with a decrease in gut microbial diversity and a shift in the balance between commensal and pathobionts.[12] For example, a reduction in the Firmicutes phylum and an increase in Proteobacteria has repeatedly been observed.[13] This change in microbiota is also associated with a shift in fermentations products, such as SCFAs.[14] For instance, a decrease in butyrate-producing species has been observed in UC.[15]

In addition, the intestinal epithelium plays a key role in IBD.[16–18] This is illustrated by the presence of several IBD-associated genetic defects associated with bacterial sensing [*NOD2*], inflammation [*IL-23R*], autophagy [*ATG16L1*], endoplasmic reticulum stress, and epithelial barrier [*HNF4α*, *CDH1*, *MEP1A*, *CARD15*, *ATG16L1*] functions in epithelial cells.[19,20] In IBD, intestinal epithelial cell dysfunction promotes increased epithelial barrier dysfunction and permeability.[21–23] In a healthy condition, the presence of a single mucus layer in the small intestine and bi-layered mucus structure in the colon—with an impermeable inner layer and a permeable outer layer—prevents intestinal epithelial cells from being in direct contact with commensal bacteria and potential pathogens.[24] In IBD, changes in the integrity of the inner layer due to defects in mucus production result in intestinal barrier dysfunction.[25] As a consequence, increased bacterial and metabolite translocation are observed,[26,27] overall resulting in immune cell activation and inflammation.[28] Pro-inflammatory factors released in the intestinal mucosa during active disease progressively damage the epithelial layer.[26,27] Despite the importance of dysfunctional epithelial-microbial cross-talk in both types of IBD, the exact cause and mechanism of these interactions are yet not completely understood.

Strong evidence supports a causal role for the gut microbiota in IBD development.[29] Using mouse colonic inflammation models, it was observed that only conventionally raised mice developed inflammation, whereas germ-free mice [with no microbiota] did not.[30] Furthermore, transferring the gut microbiota from a colitis mouse model to a wild-type mouse resulted in the induction of inflammation.[31] In addition, recurrence of CD in patients who had undergone an [ileocolonic] resection could be prevented in the absence of faecal stream [and thus microbiota],[32] and triggered in the presence of intestinal fluids.[32,33]

Because of the strong relationship between dysbiosis and IBD, probiotics formulations,[34,35] SCFAs,[8,36] and faecal microbiota transplantation [FMT][37,38] have been explored for their ability to restore the microbiota composition and inflammatory status associated with IBD.[39] However, understanding of the effectiveness and mechanisms is still lacking.[40,41] It remains unclear which bacteria [single, or complex mixtures] are required to induce and maintain remission in IBD patients. Moreover, given the heterogeneous nature of IBD, it is likely that a microbial intervention will need to be tailored for each individual to reduce dysbiosis and promote immune tolerance and homeostasis in IBD.

Understanding the complex interactions between the microbiota and the intestinal epithelium, and how they impact on the individual's disease onset and progression, is essential. To achieve this, specific *in vitro* systems mimicking the intestinal epithelium in a representative model are needed. The development of intestinal organoids—three-dimensional [3D] *in vitro* models of the human intestinal epithelium—has represented a major advancement in the field [Figure 1A]. The use of organoids to study host-microbe interactions has been previously reviewed.[42] However, novel exciting organoid systems have brought many new possibilities especially relevant for IBD research.

In this review, we present the evolution of the organoid [derived] models available [Figure 2A], from basic 3D organoid models and their 2D counterparts, to more complex microfluidic-based systems [Figure 1B-C]. The suitability of these systems will be benchmarked for their ability to model the complex interactions happening in IBD, specifically host-microbiota interactions, for specific research questions [Table 1]. Finally, we present the main applications and future trends [Figure 2B].

2. Patient-derived Organoids to Investigate Host-microbiota Interactions

The study of the host-microbiota cross-talk *in vivo* is limited by the relative inaccessibility of the human digestive tract. Faecal samples can be easily obtained, but intestinal aspirates and biopsies are less accessible in adequate numbers.[43] Manipulation and precise control over experimental variables in human studies, including host and microbial genetics, also remains a difficult task. The effects of the microbiota are location [eg, sites of inflammation] and time dependent,[11] and *in situ* spatio-temporal measurements of microbiota and host responses at sufficient resolution are not currently possible in humans.

Microbiota studies have been generally carried out in mice,[44] thanks to their similar gastrointestinal architecture, and because they allow an easier sample collection and better control over both diet and genetics.[45] However, mouse models are unable to fully represent the physiological conditions of the human gut,[46] nor can they perfectly recapitulate human disease.[47] Alternatively, colonic cell lines such as Caco-2, T84, and HT-29 have also been employed.[48–50] Yet, cell lines do not reflect tissue heterogeneity or location-specific characteristics [duodenum, colon, etc].[51]

Patient-derived intestinal organoids represent a unique tool to study host-microbiota cross-talk, overcoming some of the disadvantages associated with human studies, mouse models, and cell lines. Furthermore, organoids allow repeated experiments and maintain organ, disease, and patient characteristics.[52,53]

2.1. Patient-derived intestinal organoids

Intestinal organoids are 3D *in vitro* epithelial structures derived from primary tissue, capable of self-renewal and self-organisation, recapitulating the architecture and function of the human gastrointestinal tract.[54] Intestinal organoids can be derived either from adult human intestinal stem cells [hASCs], hASCs containing crypts,[55] or human induced pluripotent stem cells [iPSCs].[56] Stem cells are embedded in a cell culture matrix, mimicking the extracellular matrix [ECM], which allows the self-assembly of a crypt-villi structure including the luminal surface of epithelium projected towards the centre of the organoid and the basolateral side in contact with the ECM and surrounding medium [Figure 1A].

Whereas ASC-derived organoids can be differentiated into the different intestinal epithelial cell types,[55] iPSC-derived organoids also contain the intestinal mesenchyme.[56] Furthermore, iPSC-derived organoids have a low grade of maturation and therefore resemble more fetal tissue compared with ASC-derived organoids—so they are less favourable to model adult tissue biology. Organoids derived from human biopsies maintain the crypt-villi structure of the intestine, and retain the genetic background and transcriptional and epigenetic characteristics of the intestinal segment [duodenum, jejunum, ileum] they were derived from.[57–60] Organoids from IBD patients maintain disease-specific characteristics,[61] including altered gene expression profiles associated with absorptive and secretory functions.[62] The acute transcriptional inflammatory phenotype is

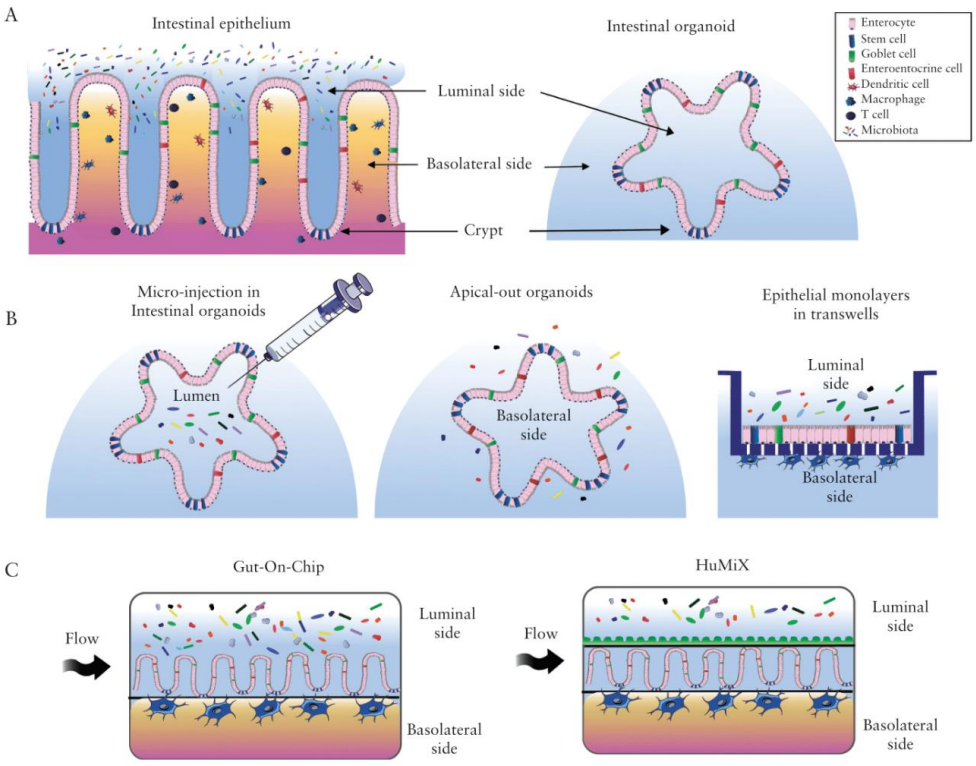

Figure 1. [A] The intestinal epithelium and the organoid model. [B] 3D organoids and organoid-derived models. [C] Microfluidics models.

lost during organoid culture but can be re-induced after inflammatory stimulation,[57] and an accumulation of somatic mutations in inflamed UC mucosa has been associated with disease duration.[63]

Contrary to intestinal cell lines, differentiated intestinal organoids contain all the epithelial cell lineages populating the intestinal crypt,[55] including rare cells [enteroendocrine, tuft, or M cells][64–66] or cells that could not be previously cultured *in vitro* [eg, Paneth cells].[67] By manipulating the culture conditions, organoids can also be maintained in a non-differentiated status, containing mainly intestinal stem cells and progenitor cells.[52] In this way, IBD organoids represent a unique tool to investigate the cell-type specificity of host-microbial interactions in a patient-specific manner.

Below, we will introduce the different organoid models that enable us to investigate the interactions between intestinal epithelial cells and the microbiota. The limitations and advantages of each model are summarised in Table 2. Some of these models have already demonstrated the ability to grow organoid-derived cells within the epithelial chamber, and others can accommodate them but with some optimisation required.

2.2. Microinjection of 3D organoids

3D organoids have closed structures, with the apical side of the epithelium, where most microbiota-epithelial interactions take place, projected inwards and therefore not very easily accessible. Different techniques can be employed to expose organoids to the microbiota, which include addition of metabolites, selected species of bacteria, or mixtures of complete patient-derived [filtered] faecal samples either by microinjection techniques or addition to the media.

Microinjection of microorganisms directly into the lumen of the differentiated 3D organoids has been employed in several laboratories, representing a useful technique to access the apical side of the epithelium.[68–70] The lumen of organoids is characterised by hypoxic conditions.[42] This facilitates the introduction of facultative or obligate anaerobic bacteria [Figure 1B], such as *Clostridium difficile*,[70] *Escherichia [E] coli*,[71] *E.coli* ECOR2,[72] and faecal matter containing complex microbiota.[73]

The microinjection technique presents some limitations: a stable co-culture with obligate anaerobic bacteria cannot be sustained for a long period of time, due to the presence of small amounts of oxygen in the organoid lumen; it requires a very specialised set-up and training[73]; and leakage of injected bacteria towards the basolateral side can influence the readout. However, microinjection represents a very useful approach when studying facultative anaerobes and for high-throughput applications, especially when an automated set-up and appropriate training are available.[73]

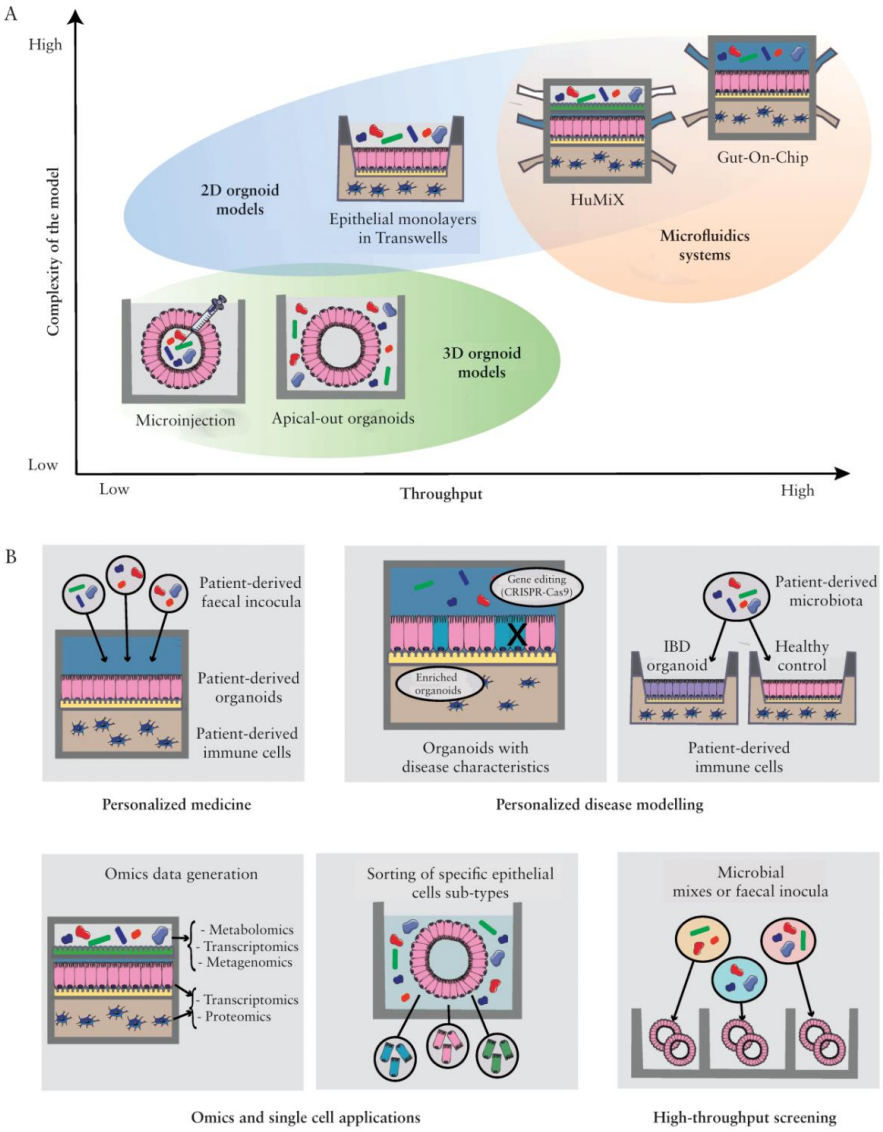

Figure 2. Organoid-based models, [A] evolution; [B] and applications.

2.3. 3D organoids with reversed polarity

Recently, the ability to grow reversed polarity ['apical-out'] organoids has made the apical side of the epithelium easily accessible, making it possible to evaluate epithelial-microbe interactions by adding the microbes directly in the culturing medium,[74] which is technically more convenient than microinjection [Figure 1B]. By understanding how matrix proteins control the epithelial [and thus organoid] polarity, researchers digested the matrix 'bubble', by using the chelator EDTA to disrupt divalent cation-dependent polymerisation of the ECM protein laminin. Upon continuation of the organoid culture in

Table 1. Benchmarking the different organoid models for host-microbiota studies in IBD.

Model complexity	In the Gut-Chip, peristalsis allows higher epithelial differentiation resulting in better mucus production. In HuMiX, this is achieved with an artificial mucus layer. The introduction of organoids [possible in all models], and other cell types [anaerobe Transwell, HuMiX, anaerobic Gut-Chip] can make the model more complete
Type of inoculum	The anaerobic Gut-Chip, HuMiX, and microinjection are preferred when co-culturing complex microbiota, whereas other models are more suitable for single bacteria or metabolites
Anaerobiosis	Strict anaerobes can be introduced within HuMiX, the anaerobic Gut-Chip [longer assays], or 3D organoids and the anaerobe Transwell [shorter assays]. Conversely, apical-out organoids and Transwells can only sustain the growth of facultative anaerobes for short-term assays
Nature of the interaction	Transwells and apical-out organoids provide a direct microbial-epithelial [villus] interface, which is relevant in IBD where the mucus barrier is often disrupted. Instead, because HuMIX presents a physical separation between microbes and epithelial cells, it is more suitable to study metabolites
Co-culture time	Static systems such as Transwells, microinjection, apical-out organoids, can sustain co-cultures for short times [<24 h], whereas the constant medium flow within the anaerobic Gut-Chip allows co-cultures for up to 5 days. HuMiX has been used for 24 h only, but could accommodate longer assays
Outcome measures	3D organoids and Transwells allow high-throughput experiments, and can be used to evaluate transcriptional gene expression. In contrast, microfluidics systems such as the anaerobic Gut-Chip and HuMiX allow selected conditions to be studied in depth, for long-term transcriptional and metabolic profiling
Availability/cost	Apical-out organoids, microinjection, and Transwells models allow low-cost and widely replicable assays. Conversely, the anaerobic Transwell model, HuMiX, and the anaerobic Gut-Chip are less accessible, and their associated cost is higher

IBD, inflammatory bowel disease.

Table 2. Criteria to evaluate for selection of the appropriate organoid models to study the host-microbiota cross-talk in IBD

Model	Micro-injection	Apical-out organoids	Anaerobe Transwell	Anaerobic Gut-on-Chip	HuMiX
Epithelial layer: organoids?	Yes	Yes	Yes	Yes	No, but feasible
Differentiation	Crypt-villi	Crypt-villi	Monolayer	Crypt-villi	N/A
Mucus layer	Goblet cells [low expression]	Goblet cells [low expression]	Goblet cells [low expression]	Goblet cells [high expression]	Artificially added
Peristalsis	No	No	No	Yes	No
Type of inoculum [Single bacteria, complex community, metabolites]	Single, metabolites, complex [short term]	Single, metabolites	Single, metabolites, complex [short term]	Single, metabolite, complex	Single, metabolites, complex
Strict anaerobiosis feasible?	No	No	Yes	Yes	Yes
Direct contact between microbiota and epithelial cells?	Yes	Yes	Yes	Yes	No [separated by nonporous membrane]
Duration of the co-culture	<4 days	1 h	24 h	5 days	24 h
Possibility to add other cell types [eg, immune cells]	No	No	Short term in lower compartment	PBMCs, endothelial cells	CD4 + T cells
Outcome measures					
Integrity of the barrier	FITC-dextrans	FITC-dextrans	Transepithelial electrical resistance, FITC-dextrans	Cascade blue tracing	FITC-dextrans
Microbiota profiling [16S rRNA sequencing, proteomics..]	No	Yes	Yes	Yes	Yes
Sampling microbiota during co-culture	No	No	No	Yes	Yes
Organoid profiling [qPCR, RNA sequencing, western blot, microscopy, cytokine production]	Yes	Yes	Yes	Yes	Yes
Microscopy of the epithelium during co-culture	Yes	Yes	Yes	Yes	No
High-throughput?	Yes, provided specialised equipment	Yes	Yes	No	No
Availability and cost of the equipment used?	Low cost, wide availability	Low cost, wide availability	Low cost, medium availability	High cost, low availability	High cost, low availability

IBD, inflammatory bowel disease; FITC, fluorescein isothiocyanate; PBMC, peripheral blood mononucleat cells; NA,not available.

suspension using low-attachment plates, an inversion of the organoid polarity with the apical side on the 'outside' could be observed after only 3 days. These early 'apical-out' organoids continued to mature, including the different polarised differentiated cell types.[74]

This model has been used to study infection by invasive enteropathogens [*Salmonella enterica* serovar Typhimurium and *Listeria monocytogenes*], but could possibly be applied to study interactions with commensal microbes.[74] The use of apical-out organoids represents an easily applicable option to investigate interactions with aerobic bacteria or bacterial metabolites, allowing multiple conditions to be easily tested in a high-throughput set-up. Yet, further validation is needed to assess the reliability of the readouts, as this technique does not guarantee a complete polarity reversion, making it difficult to distinguish between apical and basolateral interactions. Compared with basal-out organoids, the composition of apical-out organoids is skewed towards absorptive enterocytes. In the future, a thorough characterisation of how polarity reversion affects apical-out organoids phenotype, metabolism, and response to microbial challenge will be needed to understand critical similarities and differences between this model and self-organised and polarised organoids.[74]

2.4. Organoid-derived epithelial monolayers on Transwells

To make the apical side more accessible, another advance has been made by the linearisation of 3D organoids into 2D systems [Figure 1B]. Human small intestinal[75,76] or colonic[77] organoids created from patient biopsies can be cultured using the standard protocols,[52] fragmented into small clumps of cells/single cells, and subsequently plated onto a extracellular matrix-coated dish-well or Transwell insert, to create an organoid-derived monolayer.[76,78,79] Differentiation towards the different epithelial cell lineages occurs during the time period [± 7 days] of linearisation of the cells towards a strong, intact monolayer. Upon differentiation, the production of mucus by goblet cells is observed.[78]

In this model, the introduction of microorganisms is executed via addition to the culture media [Figure 2A].[78,80,81] This model enables co-culture of organoids with aerobic bacteria and microbial-derived metabolites for several hours [<24 h for bacteria, <48 h for metabolites][78,79,82,83] in an easily applicable set-up, and enables comparison of several conditions in one experiment. However, co-culture with strictly anaerobic bacteria is not feasible in this particular model as the system is kept in aerobic conditions to guarantee the organoid survival.

2.5. The anaerobic Transwell model

Recently, various strategies have been developed to overcome this limitation by maintaining the apical chamber of a Transwell insert in an anaerobic environment, while keeping the basolateral chamber in aerobic conditions.[84–86]

In one model, the enteroid anaerobe co-culture [EACC] system, human jejunal organoid-derived monolayers grown on Transwell inserts were placed onto modified gaskets sealed in place using double-sided adhesive tape on a gas-permeable plate. When keeping the entire system in an anaerobic chamber, co-culture with the obligate anaerobic bacteria *Bacteroides thetaiotaomicron* and *Blautia sp.* could be sustained for at least 24 h.[84] This cost-effective model has the advantages of enabling co-culture with anaerobic species for a limited time period [due to its static nature], and the possibility to employ in high-throughput experiments. However, it is not yet commercially available, and reproduction of the model could be time-consuming and would require optimisation.

In another model, the intestinal hemi-anaerobic co-culture system [iHACS], human colonic-derived epithelial monolayers are grown on Transwell inserts whose upper compartment is sealed off by a plug, enabling the co-culture with obligate anaerobe bacteria *Bifidobacterium adolescentis* and *Akkermansia muciniphila* for 24 h. Upon availability of the plug, the model can be implemented in every laboratory, although co-culture is also limited to 24 h.[85]

Finally, an alternative model has been developed where human colonic-derived epithelial monolayers are seeded within a microfabricated insert with tailored oxygen permeability properties, allowing the creation of an oxygen gradient between the luminal and basal compartments [0.8 ± 0.1% O_2; 11.1 ± 0.5% O_2]. Within this device, epithelial cells grown in the basolateral compartment polarise and remain viable during co-culture with facultative and obligate anaerobes *Lactobacillus rhamnosus*, *Bifidobacterium adolescentis*, and *Clostridium difficile* within the luminal compartment up to 24 h.[86] The disadvantage of this model is that the culture area is relatively large [equivalent to a 12-well Transwell insert], thus requiring a substantial amount of starting material for the epithelial compartment.

3. Towards More Physiologically Relevant Organoid Models

Organoids are composed of epithelial cell types only.[87] Depending on the proposed research question, this can be advantageous as it eliminates the confounding factor given by the presence of other cell types. This aspect is very important for IBD, in which defects in several epithelial cell type functions have been observed.[18] However, for other questions, more 'complex' *in vitro* research models must include other cell types known to be essential in intestinal physiology and pathophysiology,[54,88] including a functional immune system, enteric nerves, or nutrients providing the mesenchymal niche.[89] Co-culture with immune cells [macrophages,[83] neutrophils,[71] T lymphocytes,[90] and intraepithelial lymphocytes,[91]] as well as fibroblasts,[92] adipocytes,[93] and enteric nervous system cells,[94] have been key to gain knowledge on the role of these cell types in host-microbial interactions in IBD.[95]

Maintaining the gut microbiota and host cells in a co-culture system is currently challenging. Host cells require an aerobic environment, whereas most members of the microbiota are facultative or obligate anaerobes, requiring an environment which is [virtually] oxygen-free. In addition, both host and bacterial cells require a specific medium supporting their growth and metabolism, resulting in a significant challenge to properly model microbiota host-interactions in the gastrointestinal tract.[53]

Furthermore, the static nature of culture conditions of organoids results in microbial overgrowth and potential damage to epithelial host cells due to nutrients and oxygen depletion, and accumulation of organic waste [eg, acetate or lactate]. So far, this issue has been tackled by keeping the microbial and epithelial culture compartments separate,[96] or by using a short co-culture time [from half an hour to several hours], followed by bacterial elimination using bacteriostatic antibiotics.[97] However, to properly mimic host-microbiome interactions *in vitro*, viable and functional intestinal tissue and microbial cells must be kept within the same confined space for a longer period of time.[98,99] The introduction of fluid flows facilitating nutrient and oxygen uptake, and fluid shear stresses providing physiologically relevant mechanical signals to organoid cells, has represented a possible solution to tackle this problem.[100]

Organoids also lack peristalsis-like motion, which is important to stimulate *in vitro* intestinal differentiation, providing an improved *in vitro* model of the intestinal epithelium.[101,102] Finally, organoid-derived monolayers lack the crypt-villus structure to properly mimic the host-microbial interactions in the gut; however, recent studies show that this organisation is an attainable goal.[103] Another challenge is the replication of the mucus layer,[24] including the small intestinal single layer and the colonic double layer composed of inner and outer mucus layers associated with different densities and distinct microbial communities.[104]

3D human intestinal organoids are able to recapitulate mucus production as observed *in vivo*. However, this is enclosed in the central lumen, making it difficult to investigate its role in host-microbiota interactions during IBD.[105] Conversely, ileal and duodenal organoid-derived monolayers cultured on a Transwell only show the production of a thin mucus layer [<36 µm thick].[78,79] Hence, these models are currently unable to reproduce the physiologically important bilayer structure seen in human colonic mucus.[105]

4. Microfluidic-based and Organoid-on-chip Models

The development of microfluidic devices incorporating organoid-derived cells has overcome some of these limitations, providing a more representative and physiologically relevant model to investigate host-microbiota interactions. Within these models, cells are cultured with organ-relevant spatiotemporal chemical gradients and dynamic mechanical cues, to reconstitute the structural tissue arrangements and functional complexity of the living organism *in vitro*.[106] The use of these *in vitro* models to study host-microbe interactions has been previously reviewed.[107]

4.1. Gut-on-chip

Several 'gut-on-chip' devices have been developed.[99,108–110] A gut-on-chip device consists of two channels simulating the gut lumen and a blood vessel, separated by an ECM-coated membrane and Caco-2 cells[99] [Figure 1C]. In contrast to static cell monolayers or organoids, fluid flow and peristalsis-like deformations applied to the epithelial layer stimulate Caco-2 cells to differentiate into the four different types of intestinal epithelial cells, and to organise in villus-like structures.[111] Endothelial cells and blood peripheral mononuclear cells can also be introduced in the lower channel, to obtain a more advanced system.[101]

However, gut-on-chip devices have some limitations, including the use of Caco-2 cells [as these cells are easier to introduce to the system and give rise to a confluent monolayer faster than organoids], and the ability to sustain the growth of multiple bacteria within the system only in a few cases[101]

4.2. Organoid-on-chip

Recently, 2D human-derived intestinal organoids have been introduced into gut-on-chip systems,[109] combining the advantage of organoids [tissue differentiation] with those of gut-on-chip [controllable flow, mechanical cues, and tissue-tissue interaction]. In the microfluidic primary human intestine chip model ['organoid-on-chip'], fragments from human duodenal organoids are plated onto an ECM-coated porous membrane, and primary human intestinal microvascular endothelial cells are seeded on the opposite side of the same membrane within a parallel channel. Similarly to the gut-on-chip model, fluid flow and peristalsis-like deformations promote epithelial multilineage differentiation and crypt-villi formation,[109] with the final organoid monolayer mimicking epithelial functions [proliferation and response to infection] better than the original 3D organoid.

One drawback of gut-on-chip and organoid-on-chip devices is the presence of an aerobic environment within the epithelial chamber, which prevents the introduction of strictly anaerobic bacteria,[99,101] thus failing to represent bacterial species that play a major role in the gut.[107,112]

This limitation has been addressed thanks to the development of a novel microfluidic device with a transluminal hypoxia gradient, which allows study of the effect of a complex living human gut microbiome [including obligate anaerobes] on the epithelium.[113] This anaerobic human gut-chip was used to successfully co-culture a fresh gut microbiome isolated from human infant stool samples with a human ileal organoid monolayer. The presence of a hypoxia gradient within this system helped to sustain a physiologically relevant level of microbial diversity, with ratios of Firmicutes and Bacteroidetes similar to those observed in human faeces, and an extended co-culture time [up to 5 days]. Collectively, this allows better modelling of the physiological interactions between the intestinal epithelium and the anaerobic gut microbiota.[113]

Another adaptation of the human gut-on-a-chip model is represented by the anoxic-oxic interface-on-a-chip [AOI Chip]. This device contains a controlled gradient of oxygen thanks to the flow of both oxic and anoxic media in the chip, and allows the co-culture of Caco-2 epithelial cells and the anaerobic *Bifidobacterium adolescentis* and *Eubacterium hallii,* for up to 1 week.[114]

Overall, organoid-on-chip systems have the advantage of enabling long co-cultures of a complex microbiota culture in direct contact with organoid-derived cells. In addition, these models support spontaneous goblet cell differentiation and accumulation of a mucus bilayer structure with impenetrable and penetrable layers, and a thickness similar to that observed in the human colon, while maintaining a subpopulation of proliferative epithelial cells.[115] However, these models are expensive, require specific training to use, and do not allow for high-throughput experiments. In addition, the anaerobic human gut-on-chips are not commercially available yet in the set-up used.

4.3. The human-microbial cross-talk module

Within the human-microbial cross-talk module [HuMiX], anaerobic bacteria can be maintained in an [almost] anoxic compartment[116] [Figure 1C]. This device is composed of three parallel microfluidic chambers [microbial, epithelial, and perfusion chamber] separated by semipermeable membranes, including specific controllable inlets for each chamber.[107,116,117] Currently, experiments have been performed with Caco-2 cells, but the implementation of organoids in the model is feasible without any further adaptations. Caco-2 cells are cultured for 7 days under continuous basal perfusion, followed by bacterial inoculation into the microbial chamber for 24 h co-culture in anaerobic sheer-free conditions. Following co-culture, the modular design of HuMiX allows easy disassembly and cell collection for detailed downstream analyses.[116]

Using this system, Caco-2 cells have been successfully co-cultured with the anaerobic bacteria *B.caccae* and *L.rhamnosus*,[116] as well as immune cells [CD4 + T cells].[116] In the future, this system will be further developed to become the so-called 'immuno-HuMiX', which will allow the coexistence of patient-derived microbiota, epithelial cells, and immune cells (eg, peripheral blood mononuclear cells [PBMCs]).

In HuMiX, the mucus-coated membrane separating the microbial and epithelial compartments enables the study of host-metabolite interactions but prevents the direct host-microbe contact. In addition, gut peristalsis and differentiation of the epithelium into various cell types is not present.[109,118] As mentioned above, the introduction of organoids is feasible but would require a significant amount of starting material, given the large seeding surface [8 cm^2], which would limit high-throughput experiments. As an advantage, multiple readouts [RNA sequencing/qPCR, immunostaining, western blot] are feasible within one device. Finally, the current 'microbial microchamber' is not completely devoid of oxygen, making this model less physiologically relevant and hindering the co-culture of strict anaerobes.[116]

5. Limitations of Current Organoid Models for Host-microbiota Studies and Future Challenges

Organoid technology is constantly evolving, and many challenges associated with these models need to be addressed in the near future. The economic burden of high-throughput experiments and required [commercially available] equipment for the different devices are still limiting factors.

The polymeric material [PDMS] used in gut-on-chips can often limit the applicability to drug studies by absorbing small molecules, due to its hydrophobic nature.[119,120] Alternative materials or surface-coating techniques are being investigated to tackle these issues in the future.[121–124] The 3D nature and structural complexity of organoids and organoids-on-chip also present clear challenges to microscopy imaging and image analysis. Methods to enable precise positioning and confinement of organoids,[125] tissue-clearing methods during staining protocols,[126] or the use of advanced 3D imaging techniques,[127] are being developed to tackle these issues.

To reduce the overall variability of organoid experiments and related read-outs, standardisation of organoid culturing methods, including the used expansion and differentiation media, is paramount. Intestinal organoid culture medium is commercially available [IntestiCult™ Organoid Growth Medium, Stemcell Technologies], but due to its relatively high cost, the majority of the research laboratories are producing growth factors themselves [Wnt3A, Noggin, R-Spondin], which may cause batch-to-batch variation and differences in the cultivation and differentiation state of organoids. In addition, enrichment for a particular or rare cell type should be attainable in a standardised way.[128–130] The Transwell model enables differentiation into the different lineages but maintains a linearised structure of the epithelium while microfluidic flow drives the cells into more physiological crypt-villi structures.[78,109]

Recreating the optimal co-culture conditions to keep the bacterial community representative of the starting composition and stable over time, while maintaining epithelial or immune cells viability, still remains a challenge. Even without co-culture with epithelial cells, the long-term culture of microbiota supporting both the metabolism and the composition of this complex community is currently challenging. The targeted culturing of selected species is feasible but, when culturing complete microbiota, the selection of a specific medium and culture conditions will inevitably favour the growth of certain phyla.[131] In addition, bacterial media often contain components that damage mammalian cells,[132] leading to necessary compromises in terms of the best medium to be used during the co-culture.

Furthermore, although IBD organoids derived from inflamed regions maintain disease- and patient-specific characteristics, they lose their acute inflammatory phenotype during organoid culture.[133,134] Previous studies have shown a differential response of epithelial cells to butyrate in the presence/absence of inflammation,[82] showing the need to unravel host-microbiota interactions with and without an acute inflammatory state, reflecting active and quiescent disease, respectively. Interestingly, a recent study has shown that exposure of organoids to a defined inflammatory mix is able to re-induce the inflammatory phenotype while maintaining patient specificity.[134]

6. Future Directions

6.1. The next generation co-culture model

Currently available models to study host-microbiota interactions in IBD are still not optimal and require compromising between models supporting high-throughput experiments, or those better representing the *in vivo* situation but limited in throughput and convenient handlings [Table 1]. To be able to study interactions with the microbiota, there is great need to develop a model that enables an aerobe-anaerobe interface in a commercially available setting, and can support high-throughput applications at the same time.

This would first of all require the presence of aerobe and anaerobe compartments, in which the direct interactions between a complex microbiota community and epithelial cells can be evaluated during long-term co-culture experiments. This can either be done by creating two separate compartments and performing co-cultures in an anaerobe environment, or by providing each compartment with the desired aerobic/anaerobic source.

Simultaneously, the presence of a representative mucus layer, with small intestinal organoids composed of single layer and colonic organoids composed of inner and outer mucus layers with different densities, would be essential to correctly mimic the *in vivo* situation.[24,104] In addition to mucin-like formulations, hydrogel-based materials[135] with enhanced functionalities [ie, spatial-temporal control of characteristics] will be more frequently used in future versions of organoid-on-chip systems, as they can be tailored to match some of the relevant properties and functions of intestinal mucin for specific applications.[136]

Furthermore, the presence of an oxygen gradient will be important to allow the establishment of separate microbial communities of mucosal and luminal microbiota along the direction of the oxygen gradient, which would reflect conditions closer to the *in vivo* situation.

Beyond the correct oxygen gradient and mucus layer, studies have highlighted the crucial importance of the *in vivo*-like intestinal tissue microenvironment in shaping the composition of the microbial community, as demonstrated by the mucus degrading-genus *Akkermansia,* which is found in great abundance within anaerobic gut-on-chips, but not in liquid cultures under the same oxygen and mucus conditions.[113] Growing organoids on structured surfaces such as polymeric microscaffolds will be key to better mimicking the native *in vivo*-like microenvironment of the gastrointestinal tract, including the crypt-villi architecture.[137] In this regard, the development of finly tuneable biomaterials, such as [functionalised] hydrogels, will be paramount in providing a better simulation of the extracellular matrix and the mechanics of soft tissues while supporting cell adhesion and protein sequestration,[138,139] also addressing the issues related to poorly defined compositions and batch-to-batch variability of organoid matrices used so far.[140–142]

Real-time evaluation of cell organisation and structure to monitor monolayer integrity and cell viability during organoid

differentiation and exposure to the microbiota, in addition to *ad-hoc* fine tuning of flow speed and oxygen concentrations, will also be key. To reduce the costs of the model [culturing of organoid cells, required media, and other components] the seeding surface should be limited, but enough to enable continuous sampling of the medium and allow several read-outs [RNA sequencing, proteomics, metabolomics, immunohistochemistry,..] of both microbial and host cells in each device.

The inclusion of several microsensors that can precisely monitor alterations over the complete time course of the experiment [oxygen concentrations, barrier integrity measurements, temperature, oxygen, pH, integrity, flow] are of major interest, together with regular, easily accessible sampling of the different compartments [epithelial cells, microbiota].[143]

To complement the model, co-culture with other cell types including separate medium compartments should be optimised. In combination with patient-specific epithelial cells and microbiota, the addition of immune cells brings these co-culture models to the next level for evaluation of patient-specific responses or preclinical testing of new compounds.

The implementation of advanced [microfluidics] organoid-based models not only requires specialised knowledge and training, but also involves substantial implementation costs. To this end, the development of automated systems capable of performing several standardised read-outs will be key to achieving the successful introduction of these systems in daily laboratory practice. In addition, this will also help reduce the experimental variability and allow comparison of experimental results among different groups, especially when it comes to preclinical testing of compounds or microbiota mixtures.

6.2. Applications

Organoids and organoid-derived models are amenable to various applications [Figure 2B]. These can be combined to understand the role of host-microbiota interactions in IBD pathogenesis, and aid in finding microbial interventions tailored to the single individual, resulting in better prevention strategies and treatment success.

6.2.1. 'Omics and single-cell approaches

The different models reviewed are amenable to 'omics data generation, which can be helpful to interrogate the role of the epithelial genetic [patient-derived or engineered] or epigenetic background [acquired from the persistent exposure to pro-inflammatory signals].[58,144] 3D organoid models and organoid monolayers on Transwells are more suited for generating a single type of 'omics readout in many different samples, whereas microfluidics systems such as HuMIX allow multiple 'omics readouts to be produced from the same sample in a selected number of conditions.

Gut microbes and their metabolites affect each intestinal epithelial subtype differently. To evaluate cell-specific responses, organoid differentiation can be skewed towards a specific lineage [eg, Paneth cells or goblet cells] before exposure to the bacterial mixture.[128] Alternatively, techniques such as fluorescense activated cell sorting [FACS][145] or mass cytometry[146] may allow the isolation of cells from organoids after exposure to microbiota, similarly to what has been achieved for mouse intestinal tissue.[147]

Recently, single-cell 'omics approaches have been applied to characterise individual cells in mouse organoids,[148] or organoids derived from active CD lesions,[149] and to investigate the differential response of intestinal cell types to bacterial infection.[150] In the future, a similar approach could be applied to provide new insights into the mechanisms by which the microbiota or specific probiotics may influence the function of specific subpopulations of cells in the gut in relation to IBD.

6.2.2. Personalised disease models

CRISPR/Cas9 genome editing technology has been employed to develop genetically defined cultures from organoids.[151–154] The manipulation of specific genes linked to genetic susceptibility could help gain a better understanding of disease mechanisms, also in relation to microbial exposure [eg, *GATM*, *NOD2*, *HNF4A*, *ATG16L1*,...]].[155] Such models could be employed to dissect the role of epithelium in early-onset IBD, where a specific genetic mutation of the intestinal epithelium causes a defect in barrier function[156] and no inflammation has developed yet. Organoids enriched for a specific cell type[157] can further help elucidate the role of specific epithelial subpopulations in modulating the adhesion of IBD-associated bacterial strains, such as the recently discovered sentinel goblet cells.[158]

Co-culturing IBD-derived and matched healthy organoids in parallel, followed by addition of patient-derived microbiota and immune cells, could also throw some light onto whether the loss of tolerance towards the microbiota is a cause or consequence of the disease, a fundamental question in IBD research.

6.2.3. Drug/microbial screening

Organoid biobanks can be established from patient-derived organoids. One example is the recently established biobank containing IBD-derived organoids from various parts of the gastrointestinal tract.[159] By employing high-throughput approaches,[160,161] these can be used to screen microbial species or their metabolites.[78,162–164] Because the screening is performed in subpopulations of organoids, such approaches are key when studying heterogeneous diseases such as IBD,[165–167] as they reduce the variability and allow precision medicine approaches. By doing so, patient treatments could be optimised before application, reducing treatment failure. The introduction of patient-derived or engineered organoids within microfluidics devices also helps re-create a better *in vivo*–like disease phenotype,[168] thereby facilitating the development of robust disease models for improved personalised drug screening and matching.[169,170] Overall, organoids are useful for target identification and validation in the early stages of drug discovery, thanks to their similarity with actual organs. Instead, organs-on-a-chip are more suited for subsequent efficacy and safety screening, as they provide a more reproducible and controllable environment.[171]

6.2.4. Personalised medicine and microbial therapies

Microfluidics devices can be employed to couple patient-derived intestinal organoids with host-specific isolated immune cells, PBMCs, or microbiota [faecal inocula or individual-specific isolates], allowing the establishment of models amenable to personalised medicine approaches.[172] For instance, these models could be exploited to define how different commensal microorganisms within a patient-specific microbiota community contribute to IBD pathophysiology.[173] On the one hand, these systems could help gain a better understanding of the causal relationship between the abundance of each individual genus of bacteria and the distinct functions of the co-cultured human intestinal epithelium. On the other hand, these systems could be used to unravel how a dysfunctional IBD-derived epithelial layer could impact on the diversity and composition of the microbiota, favouring the growth of specific pathogenic bacteria [eg, pathogenic *E. coli*], while reducing beneficial ones [eg, *Faecalibacterium prausnitzii*]. Overall, the integration of these approaches could result in the development of personalised microbial therapies, including

microbiome-based therapeutics such as genetically engineered commensal bacteria,[174] or to assess the efficacy of FMT in a patient-specific manner.[113]

7. Concluding remarks

In recent years, the fundamental role played by host-microbiota interactions in IBD has begun to be unravelled. However, further research needs to be carried out to understand whether it will be possible to resolve dysbiosis, and which elements of the microbiota and species are essential to do this. Moreover, it is likely that each microbial therapy will need to be tailored for each individual.

Intestinal organoids, alone or within a microfluidics system, have shown the potential to become the gold standard in the study of host-microbiota interactions in IBD in a patient-specific manner. However, so far studies that analytically compare organoid-based systems and benchmark them for their suitability to look at host-microbiota interactions in IBD have been lacking. In this review, we have presented a variety of models, from 3D organoids and 2D organoid-derived monolayers to organoid-on-chip systems, and discussed their advantages, limitations, and suitability for different research questions and applications.

In the future, the use of organoid models, in combination with the patient's specific microbiota composition and immune cells, will help to provide a better understanding of disease onset mechanisms and to identify the key bacterial species required for resolving dysbiosis. This understanding could lead to more targeted microbial therapies, which either alone or in combination with traditional approaches have the potential to revolutionise IBD management and ultimately improve patient outcomes.

Funding

This work was supported by a PhD Fellowship strategic basic research [SB] grant [1S49419N] from Research Foundation Flanders [FW] for KA, by a CREA research grant of the KU Leuven [CREA/12/031], and a research grant by the European Crohn's and Colitis Organisation [ZKC4621/10143459]. KA received a research grant of the Belgian IBD Research and Development [BIRD] group, a doctoral scholarship of the KU Leuven, and a grant of the Crohns and Colitis Ulcerosa Vereniging—VZW. MF is a senior clinical investigator of the FWO, Belgium. TK was supported by a fellowship in computational biology at the Earlham Institute [Norwich, UK] in partnership with the Quadram Institute [Norwich, UK] and was strategically supported by the BBSRC [BB/J004529/1, BB/P016774/1, and BB/CSP17270/1]. TK and MP were also funded by a BBSRC ISP grant for Gut Microbes and Health BB/R012490/1 and its constituent project[s], BBS/E/F/000PR10353, and BBS/E/F/000PR10355. MP was supported by the BBSRC Norwich Research Park Biosciences Doctoral Training Partnership [grant BB/M011216/1].

Conflict of Interest

MF reports financial support for: research, Amgen, Biogen, Janssen, Pfizer, Takeda consultancy, Abbvie, Boehringer-Ingelheim, MSD, Pfizer, Sandoz, Takeda, and Thermo Fisher; speaking, Abbvie, Amgen, Biogen, Boehringer-Ingelheim, Falk, Ferring, Janssen, Lamepro, MSD, Mylan, Pfizer, Sandoz, and Takeda. TK is supported by BenevolentAI and Unilever. MP and KA declare no conflict of interest.

Author Contributions

MP, KA: study concept and design, literature search, manuscript writing, and illustrations; MF, TK: study concept and design, supervision, and critical revision of the manuscript. All authors approved the final version of the manuscript for publication.

References

1. Geremia A, Biancheri P, Allan P, Corazza GR, Di Sabatino A. Innate and adaptive immunity in inflammatory bowel disease. *Autoimmun Rev* 2014;**13**:3–10.
2. Neurath MF. Host-microbiota interactions in inflammatory bowel disease. *Nat Rev Gastroenterol Hepatol* 2020;**17**:76–7.
3. Geva-Zatorsky N, Alvarez D, Hudak JE, *et al*. In vivo imaging and tracking of host-microbiota interactions via metabolic labeling of gut anaerobic bacteria. *Nat Med* 2015;**21**:1091–100.
4. Earle KA, Billings G, Sigal M, *et al*. Quantitative imaging of gut microbiota spatial organization. *Cell Host Microbe* 2015;**18**:478–88.
5. Peterson LW, Artis D. Intestinal epithelial cells: regulators of barrier function and immune homeostasis. *Nat Rev Immunol* 2014;**14**:141–53.
6. Zelante T, Iannitti RG, Cunha C, *et al*. Tryptophan catabolites from microbiota engage aryl hydrocarbon receptor and balance mucosal reactivity via interleukin-22. *Immunity* 2013;**39**:372–85.
7. Sanderson IR. Short chain fatty acid regulation of signaling genes expressed by the intestinal epithelium. *J Nutr* 2004;**134**:2450–4S.
8. Russo E, Giudici F, Fiorindi C, Ficari F, Scaringi S, Amedei A. Immunomodulating activity and therapeutic effects of short chain fatty acids and tryptophan post-biotics in inflammatory bowel disease. *Front Immunol* 2019;**10**:2754.
9. Kostic AD, Xavier RJ, Gevers D. The microbiome in inflammatory bowel disease: current status and the future ahead. *Gastroenterology* 2014;**146**:1489–99.
10. Joossens M, Huys G, Cnockaert M, *et al*. Dysbiosis of the faecal microbiota in patients with Crohn's disease and their unaffected relatives. *Gut* 2011;**60**:631–7.
11. Halfvarson J, Brislawn CJ, Lamendella R, *et al*. Dynamics of the human gut microbiome in inflammatory bowel disease. *Nat Microbiol* 2017;**2**:17004.
12. Ni J, Wu GD, Albenberg L, Tomov VT. Gut microbiota and IBD: causation or correlation? *Nat Rev Gastroenterol Hepatol* 2017;**14**:573–84.
13. Mirsepasi-Lauridsen HC, Vrankx K, Engberg J, *et al*. Disease-specific enteric microbiome dysbiosis in inflammatory bowel disease. *Front Med [Lausanne]* 2018;**5**:304.
14. Zeng MY, Inohara N, Nuñez G. Mechanisms of inflammation-driven bacterial dysbiosis in the gut. *Mucosal Immunol* 2017;**10**:18–26.
15. Machiels K, Joossens M, Sabino J, *et al*. A decrease of the butyrate-producing species Roseburia hominis and Faecalibacterium prausnitzii defines dysbiosis in patients with ulcerative colitis. *Gut* 2014;**63**:1275–83.
16. Zeissig S, Bürgel N, Günzel D, *et al*. Changes in expression and distribution of claudin 2, 5 and 8 lead to discontinuous tight junctions and barrier dysfunction in active Crohn's disease. *Gut* 2007;**56**:61–72.
17. Strugala V, Dettmar PW, Pearson JP. Thickness and continuity of the adherent colonic mucus barrier in active and quiescent ulcerative colitis and Crohn's disease. *Int J Clin Pract* 2008;**62**:762–9.
18. Coskun M. Intestinal epithelium in inflammatory bowel disease. *Front Med [Lausanne]* 2014;**1**:24.
19. Koch S, Nusrat A. The life and death of epithelia during inflammation: lessons learned from the gut. *Annu Rev Pathol* 2012;**7**:35–60.
20. McCole DF. IBD candidate genes and intestinal barrier regulation. *Inflamm Bowel Dis* 2014;**20**:1829–49.
21. Mankertz J, Schulzke JD. Altered permeability in inflammatory bowel disease: pathophysiology and clinical implications. *Curr Opin Gastroenterol* 2007;**23**:379–83.
22. Rioux JD, Xavier RJ, Taylor KD, *et al*. Genome-wide association study identifies new susceptibility loci for Crohn disease and implicates autophagy in disease pathogenesis. *Nat Genet* 2007;**39**:596–604.
23. Kaser A, Lee AH, Franke A, *et al*. XBP1 links ER stress to intestinal inflammation and confers genetic risk for human inflammatory bowel disease. *Cell* 2008;**134**:743–56.
24. Johansson ME, Sjövall H, Hansson GC. The gastrointestinal mucus system in health and disease. *Nat Rev Gastroenterol Hepatol* 2013;**10**:352–61.

25. Swidsinski A, Loening-Baucke V, Theissig F, *et al*. Comparative study of the intestinal mucus barrier in normal and inflamed colon. *Gut* 2007;**56**:343–50.
26. Sun J, Shen X, Li Y, *et al*. Therapeutic potential to modify the mucus barrier in inflammatory bowel disease. *Nutrients* 2016;**8**. doi:10.3390/nu8010044.
27. Johansson ME, Gustafsson JK, Holmén-Larsson J, *et al*. Bacteria penetrate the normally impenetrable inner colon mucus layer in both murine colitis models and patients with ulcerative colitis. *Gut* 2014;**63**:281–91.
28. Neurath MF. Targeting immune cell circuits and trafficking in inflammatory bowel disease. *Nat Immunol* 2019;**20**:970–9.
29. Gkouskou KK, Deligianni C, Tsatsanis C, Eliopoulos AG. The gut microbiota in mouse models of inflammatory bowel disease. *Front Cell Infect Microbiol* 2014;**4**:28.
30. Pils MC, Bleich A, Prinz I, *et al*. Commensal gut flora reduces susceptibility to experimentally induced colitis via T-cell-derived interleukin-10. *Inflamm Bowel Dis* 2011;**17**:2038–46.
31. Zhou J, Zhou Z, Ji P, Ma M, Guo J, Jiang S. Effect of fecal microbiota transplantation on experimental colitis in mice. *Exp Ther Med* 2019;**17**:2581–6.
32. Rutgeerts P, Goboes K, Peeters M, *et al*. Effect of faecal stream diversion on recurrence of Crohn's disease in the neoterminal ileum. *Lancet* 1991;**338**:771–4.
33. D'Haens GR, Geboes K, Peeters M, Baert F, Penninckx F, Rutgeerts P. Early lesions of recurrent Crohn's disease caused by infusion of intestinal contents in excluded ileum. *Gastroenterology* 1998;**114**:262–7.
34. Venturi A, Gionchetti P, Rizzello F, *et al*. Impact on the composition of the faecal flora by a new probiotic preparation: preliminary data on maintenance treatment of patients with ulcerative colitis. *Aliment Pharmacol Ther* 1999;**13**:1103–8.
35. Sheil B, Shanahan F, O'Mahony L. Probiotic effects on inflammatory bowel disease. *J Nutr* 2007;**137**:819S–24S.
36. van der Beek CM, Dejong CHC, Troost FJ, Masclee AAM, Lenaerts K. Role of short-chain fatty acids in colonic inflammation, carcinogenesis, and mucosal protection and healing. *Nutr Rev* 2017;**75**:286–305.
37. Moayyedi P, Surette MG, Kim PT, *et al*. Fecal microbiota transplantation induces remission in patients with active ulcerative colitis in a randomized controlled trial. *Gastroenterology* 2015;**149**: 102–9.e6.
38. Imdad A, Nicholson MR, Tanner-Smith EE, *et al*. Fecal transplantation for treatment of inflammatory bowel disease. *Cochrane Database Syst Rev* 2018;**11**:CD012774.
39. Hart AL, Stagg AJ, Frame M, *et al*. The role of the gut flora in health and disease, and its modification as therapy. *Aliment Pharmacol Ther* 2002;**16**:1383–93.
40. Sanders ME, Merenstein DJ, Reid G, Gibson GR, Rastall RA. Probiotics and prebiotics in intestinal health and disease: from biology to the clinic. *Nat Rev Gastroenterol Hepatol* 2019;**16**:605–16.
41. Fang H, Fu L, Wang J. Protocol for fecal microbiota transplantation in inflammatory bowel disease: a systematic review and meta-analysis. *Biomed Res Int* 2018;**2018**:8941340.
42. Bartfeld S. Modeling infectious diseases and host-microbe interactions in gastrointestinal organoids. *Dev Biol* 2016;**420**:262–70.
43. Dave M, Higgins PD, Middha S, Rioux KP. The human gut microbiome: current knowledge, challenges, and future directions. *Transl Res* 2012;**160**:246–57.
44. Faith JJ, Ahern PP, Ridaura VK, Cheng J, Gordon JI. Identifying gut microbe-host phenotype relationships using combinatorial communities in gnotobiotic mice. *Sci Transl Med* 2014;**6**:220ra11.
45. Kostic AD, Howitt MR, Garrett WS. Exploring host-microbiota interactions in animal models and humans. *Genes Dev* 2013;**27**:701–18.
46. Nguyen TL, Vieira-Silva S, Liston A, Raes J. How informative is the mouse for human gut microbiota research? *Dis Model Mech* 2015;**8**:1–16.
47. Seok J, Warren HS, Cuenca AG, *et al*.; Inflammation and Host Response to Injury, Large Scale Collaborative Research Program. Genomic responses in mouse models poorly mimic human inflammatory diseases. *Proc Natl Acad Sci U S A* 2013;**110**:3507–12.
48. Krishnan M, Penrose HM, Shah NN, Marchelletta RR, McCole DF. VSL#3 probiotic stimulates T-cell protein tyrosine phosphatase-mediated recovery of IFN-γ-induced intestinal epithelial barrier defects. *Inflamm Bowel Dis* 2016;**22**:2811–23.
49. Martz SL, Guzman-Rodriguez M, He SM, *et al*. A human gut ecosystem protects against C. difficile disease by targeting TcdA. *J Gastroenterol* 2017;**52**:452–65.
50. Munoz S, Guzman-Rodriguez M, Sun J, *et al*. Rebooting the microbiome. *Gut Microbes* 2016;**7**:353–63.
51. May S, Evans S, Parry L. Organoids, organs-on-chips and other systems, and microbiota. *Emerg Top Life Sci* 2017;**1**:385–400.
52. Sato T, Stange DE, Ferrante M, *et al*. Long-term expansion of epithelial organoids from human colon, adenoma, adenocarcinoma, and Barrett's epithelium. *Gastroenterology* 2011;**141**:1762–72.
53. Dotti I, Salas A. Potential use of human stem cell-derived intestinal organoids to study inflammatory bowel diseases. *Inflamm Bowel Dis* 2018;**24**:2501–9.
54. Fatehullah A, Tan SH, Barker N. Organoids as an in vitro model of human development and disease. *Nat Cell Biol* 2016;**18**:246–54.
55. Sato T, Vries RG, Snippert HJ, *et al*. Single Lgr5 stem cells build crypt-villus structures in vitro without a mesenchymal niche. *Nature* 2009;**459**:262–5.
56. Spence JR, Mayhew CN, Rankin SA, *et al*. Directed differentiation of human pluripotent stem cells into intestinal tissue in vitro. *Nature* 2011;**470**:105–9.
57. Middendorp S, Schneeberger K, Wiegerinck CL, *et al*. Adult stem cells in the small intestine are intrinsically programmed with their location-specific function. *Stem Cells* 2014;**32**:1083–91.
58. Kraiczy J, Nayak KM, Howell KJ, *et al*. DNA methylation defines regional identity of human intestinal epithelial organoids and undergoes dynamic changes during development. *Gut* 2019;**68**:49–61.
59. Cramer JM, Thompson T, Geskin A, LaFramboise W, Lagasse E. Distinct human stem cell populations in small and large intestine. *PLoS One* 2015;**10**:e0118792.
60. Dekkers JF, Berkers G, Kruisselbrink E, *et al*. Characterizing responses to CFTR-modulating drugs using rectal organoids derived from subjects with cystic fibrosis. *Sci Transl Med* 2016;**8**:344ra84.
61. d'Aldebert E, Quaranta M, Sébert M, *et al*. Characterization of human colon organoids from inflammatory bowel disease patients. *Front Cell Dev Biol* 2020;**8**:363.
62. Dotti I, Mora-Buch R, Ferrer-Picón E, *et al*. Alterations in the epithelial stem cell compartment could contribute to permanent changes in the mucosa of patients with ulcerative colitis. *Gut* 2017;**66**:2069–79.
63. Nanki K, Fujii M, Shimokawa M, *et al*. Somatic inflammatory gene mutations in human ulcerative colitis epithelium. *Nature* 2020;**577**:254–9.
64. de Lau W, Kujala P, Schneeberger K, *et al*. Peyer's patch M cells derived from Lgr5[+] stem cells require SpiB and are induced by RankL in cultured "miniguts". *Mol Cell Biol* 2012;**32**:3639–47.
65. Rouch JD, Scott A, Lei NY, *et al*. Development of functional microfold [M] cells from intestinal stem cells in primary human enteroids. *PLoS One* 2016;**11**:e0148216.
66. Basak O, Beumer J, Wiebrands K, Seno H, van Oudenaarden A, Clevers H. Induced quiescence of Lgr5+ stem cells in intestinal organoids enables differentiation of hormone-producing enteroendocrine cells. *Cell Stem Cell* 2017;**20**:177–90.e4.
67. Sato T, van Es JH, Snippert HJ, *et al*. Paneth cells constitute the niche for Lgr5 stem cells in intestinal crypts. *Nature* 2011;**469**:415–8.
68. Bartfeld S, Bayram T, van de Wetering M, *et al*. In vitro expansion of human gastric epithelial stem cells and their responses to bacterial infection. *Gastroenterology* 2015;**148**:126–36.e6.
69. McCracken KW, Catá EM, Crawford CM, *et al*. Modelling human development and disease in pluripotent stem-cell-derived gastric organoids. *Nature* 2014;**516**:400–4.
70. Leslie JL, Huang S, Opp JS, *et al*. Persistence and toxin production by Clostridium difficile within human intestinal organoids result in disruption of epithelial paracellular barrier function. *Infect Immun* 2015;**83**:138–45.
71. Karve SS, Pradhan S, Ward DV, Weiss AA. Intestinal organoids model human responses to infection by commensal and Shiga toxin producing Escherichia coli. *PLoS One* 2017;**12**:e0178966.
72. Hill DR, Huang S, Nagy MS, *et al*. Bacterial colonization stimulates a complex physiological response in the immature human intestinal epithelium. *Elife* 2017;**6**. doi:10.7554/eLife.29132.

73. Williamson IA, Arnold JW, Samsa LA, *et al*. A high-throughput organoid microinjection platform to study gastrointestinal microbiota and luminal physiology. *Cell Mol Gastroenterol Hepatol* 2018;**6**:301–19.
74. Co JY, Margalef-Català M, Li X, *et al*. Controlling epithelial polarity: a human enteroid model for host-pathogen interactions. *Cell Rep* 2019;**26**:2509–20.e4.
75. Foulke-Abel J, In J, Kovbasnjuk O, *et al*. Human enteroids as an ex-vivo model of host-pathogen interactions in the gastrointestinal tract. *Exp Biol Med [Maywood]* 2014;**239**:1124–34.
76. Ettayebi K, Crawford SE, Murakami K, *et al*. Replication of human noroviruses in stem cell-derived human enteroids. *Science* 2016;**353**:1387–93.
77. Wang Y, DiSalvo M, Gunasekara DB, *et al*. Self-renewing monolayer of primary colonic or rectal epithelial cells. *Cell Mol Gastroenterol Hepatol* 2017;**4**:165–82.e7.
78. VanDussen KL, Marinshaw JM, Shaikh N, *et al*. Development of an enhanced human gastrointestinal epithelial culture system to facilitate patient-based assays. *Gut* 2015;**64**:911–20.
79. In J, Foulke-Abel J, Zachos NC, *et al*. Enterohemorrhagic Escherichia coli reduce mucus and intermicrovillar bridges in human stem cell-derived colonoids. *Cell Mol Gastroenterol Hepatol* 2016;**2**:48–62.e3.
80. Bartfeld S, Clevers H. Organoids as model for infectious diseases: culture of human and murine stomach organoids and microinjection of helicobacter pylori. *J Vis Exp* 2015; published online Nov 12. doi:10.3791/53359.
81. Schlaermann P, Toelle B, Berger H, *et al*. A novel human gastric primary cell culture system for modelling Helicobacter pylori infection in vitro. *Gut* 2016;**65**:202–13.
82. Vancamelbeke M, Laeremans T, Vanhove W, *et al*. Butyrate does not protect against inflammation-induced loss of epithelial barrier function and cytokine production in primary cell monolayers from patients with ulcerative colitis. *J Crohns Colitis* 2019;**13**:1351–61.
83. Noel G, Baetz NW, Staab JF, *et al*. A primary human macrophage-enteroid co-culture model to investigate mucosal gut physiology and host-pathogen interactions. *Sci Rep* 2017;**7**:45270.
84. Fofanova TY, Stewart C, Auchtung JM, *et al*. A novel human enteroid-anaerobe co-culture system to study microbial-host interaction under physiological hypoxia. *BioRxiv* 2019; published online Feb 20. doi:10.1101/555755.
85. Sasaki N, Miyamoto K, Maslowski KM, Ohno H, Kanai T, Sato T. Development of a scalable coculture system for gut anaerobes and human colon epithelium. *Gastroenterology* 2020;**159**:388–90.e5.
86. Kim R, Attayek PJ, Wang Y, *et al*. An in vitro intestinal platform with a self-sustaining oxygen gradient to study the human gut/microbiome interface. *Biofabrication* 2019;**12**:015006.
87. Stelzner M, Helmrath M, Dunn JC, *et al*.; NIH Intestinal Stem Cell Consortium. A nomenclature for intestinal in vitro cultures. *Am J Physiol Gastrointest Liver Physiol* 2012;**302**:G1359–63.
88. Hollins AJ, Parry L. Long-term culture of intestinal cell progenitors: an overview of their development, application, and associated technologies. *Curr Pathobiol Rep* 2016;**4**:209–19.
89. Noben M, Vanhove W, Arnauts K, *et al*. Human intestinal epithelium in a dish: Current models for research into gastrointestinal pathophysiology. *United European Gastroenterol J* 2017;**5**:1073–81.
90. Rogoz A, Reis BS, Karssemeijer RA, Mucida D. A 3-D enteroid-based model to study T-cell and epithelial cell interaction. *J Immunol Methods* 2015;**421**:89–95.
91. Nozaki K, Mochizuki W, Matsumoto Y, *et al*. Co-culture with intestinal epithelial organoids allows efficient expansion and motility analysis of intraepithelial lymphocytes. *J Gastroenterol* 2016;**51**:206–13.
92. Pastuła A, Middelhoff M, Brandtner A, *et al*. Three-dimensional gastrointestinal organoid culture in combination with nerves or fibroblasts: a method to characterize the gastrointestinal stem cell niche. *Stem Cells Int* 2016;**2016**:3710836.
93. Takahashi Y, Sato S, Kurashima Y, *et al*. Reciprocal inflammatory signaling between intestinal epithelial cells and adipocytes in the absence of immune cells. *EBioMedicine* 2017;**23**:34–45.
94. Workman MJ, Mahe MM, Trisno S, *et al*. Engineered human pluripotent-stem-cell-derived intestinal tissues with a functional enteric nervous system. *Nat Med* 2017;**23**:49–59.
95. Kuhn K. Altered colonic intraepithelial lymphocyte composition and function in Crohn's Disease. *J Immunol* 2016;**196**:54.10.
96. Zachos NC, Kovbasnjuk O, Foulke-Abel J, *et al*. Human enteroids/colonoids and intestinal organoids functionally recapitulate normal intestinal physiology and pathophysiology. *J Biol Chem* 2016;**291**:3759–66.
97. Payne AN, Zihler A, Chassard C, Lacroix C. Advances and perspectives in in vitro human gut fermentation modeling. *Trends Biotechnol* 2012;**30**:17–25.
98. Park GS, Park MH, Shin W, *et al*. Emulating host-microbiome ecosystem of human gastrointestinal tract in vitro. *Stem Cell Rev Rep* 2017;**13**:321–34.
99. Kim HJ, Huh D, Hamilton G, Ingber DE. Human gut-on-a-chip inhabited by microbial flora that experiences intestinal peristalsis-like motions and flow. *Lab Chip* 2012;**12**:2165–74.
100. Qian X, Nguyen HN, Song MM, *et al*. Brain-region-specific organoids using mini-bioreactors for modeling ZIKV exposure. *Cell* 2016;**165**:1238–54.
101. Kim HJ, Li H, Collins JJ, Ingber DE. Contributions of microbiome and mechanical deformation to intestinal bacterial overgrowth and inflammation in a human gut-on-a-chip. *Proc Natl Acad Sci U S A* 2016;**113**:E7–15.
102. Gjorevski N, Sachs N, Manfrin A, *et al*. Designer matrices for intestinal stem cell and organoid culture. *Nature* 2016;**539**:560–4.
103. Wang Y, Gunasekara DB, Reed MI, *et al*. A microengineered collagen scaffold for generating a polarized crypt-villus architecture of human small intestinal epithelium. *Biomaterials* 2017;**128**:44–55.
104. Li H, Limenitakis JP, Fuhrer T, *et al*. The outer mucus layer hosts a distinct intestinal microbial niche. *Nat Commun* 2015;**6**:8292.
105. Lock JY, Carlson TL, Carrier RL. Mucus models to evaluate the diffusion of drugs and particles. *Adv Drug Deliv Rev* 2018;**124**:34–49.
106. Huh D, Torisawa YS, Hamilton GA, Kim HJ, Ingber DE. Microengineered physiological biomimicry: organs-on-chips. *Lab Chip* 2012;**12**:2156–64.
107. von Martels JZH, Sadaghian Sadabad M, Bourgonje AR, *et al*. The role of gut microbiota in health and disease: in vitro modeling of host-microbe interactions at the aerobe-anaerobe interphase of the human gut. *Anaerobe* 2017;**44**:3–12.
108. Walsh DI 3rd, Dydek EV, Lock JY, *et al*. Emulation of colonic oxygen gradients in a microdevice. *SLAS Technol* 2018;**23**:164–71.
109. Kasendra M, Tovaglieri A, Sontheimer-Phelps A, *et al*. Development of a primary human Small Intestine-on-a-Chip using biopsy-derived organoids. *Sci Rep* 2018;**8**:2871.
110. Villenave R, Wales SQ, Hamkins-Indik T, *et al*. Human gut-on-a-chip supports polarized infection of coxsackie B1 virus in vitro. *PLoS One* 2017;**12**:e0169412.
111. Kim HJ, Ingber DE. Gut-on-a-Chip microenvironment induces human intestinal cells to undergo villus differentiation. *Integr Biol [Camb]* 2013;**5**:1130–40.
112. Maier E, Anderson RC, Roy NC. Understanding how commensal obligate anaerobic bacteria regulate immune functions in the large intestine. *Nutrients* 2014;**7**:45–73.
113. Jalili-Firoozinezhad S, Gazzaniga FS, Calamari EL, *et al*. A complex human gut microbiome cultured in an anaerobic intestine-on-a-chip. *Nat Biomed Eng* 2019;**3**:520–31.
114. Shin W, Wu A, Massidda MW, *et al*. A robust longitudinal co-culture of obligate anaerobic gut microbiome with human intestinal epithelium in an anoxic-oxic interface-on-a-chip. *Front Bioeng Biotechnol* 2019;**7**:13.
115. Sontheimer-Phelps A, Chou DB, Tovaglieri A, *et al*. Human colon-on-a-chip enables continuous in vitro analysis of colon mucus layer accumulation and physiology. *Cell Mol Gastroenterol Hepatol* 2020;**9**:507–26.
116. Shah P, Fritz JV, Glaab E, *et al*. A microfluidics-based in vitro model of the gastrointestinal human-microbe interface. *Nat Commun* 2016;**7**:11535.
117. Eain MMG, Baginska J, Greenhalgh K, Fritz JV, Zenhausern F, Wilmes P. Engineering solutions for representative models of the gastrointestinal human-microbe interface. *Engineering* 2017;**3**:60–5.
118. Marzorati M, Vanhoecke B, De Ryck T, *et al*. The HMI™ module: a new tool to study the host-microbiota interaction in the human gastrointestinal tract in vitro. *BMC Microbiol* 2014;**14**:133.

119. Berthier E, Young EW, Beebe D. Engineers are from PDMS-land, biologists are from polystyrenia. *Lab Chip* 2012;**12**:1224–37.
120. van der Meer AD, van den Berg A. Organs-on-chips: breaking the in vitro impasse. *Integr Biol [Camb]* 2012;**4**:461–70.
121. Ren K, Zhao Y, Su J, Ryan D, Wu H. Convenient method for modifying poly[dimethylsiloxane] to be airtight and resistive against absorption of small molecules. *Anal Chem* 2010;**82**:5965–71.
122. Wong I, Ho CM. Surface molecular property modifications for poly[dimethylsiloxane] [PDMS] based microfluidic devices. *Microfluid Nanofluidics* 2009;**7**:291–306.
123. Domansky K, Leslie DC, McKinney J, *et al*. Clear castable polyurethane elastomer for fabrication of microfluidic devices. *Lab Chip* 2013;**13**:3956–64.
124. van Midwoud PM, Janse A, Merema MT, Groothuis GM, Verpoorte E. Comparison of biocompatibility and adsorption properties of different plastics for advanced microfluidic cell and tissue culture models. *Anal Chem* 2012;**84**:3938–44.
125. Karzbrun E, Kshirsagar A, Cohen SR, Hanna JH, Reiner O. Human brain organoids on a chip reveal the physics of folding. *Nat Phys* 2018;**14**:515–22.
126. Chen YY, Silva PN, Syed AM, Sindhwani S, Rocheleau JV, Chan WC. Clarifying intact 3D tissues on a microfluidic chip for high-throughput structural analysis. *Proc Natl Acad Sci U S A* 2016;**113**:14915–20.
127. Galland R, Grenci G, Aravind A, Viasnoff V, Studer V, Sibarita JB. 3D high- and super-resolution imaging using single-objective SPIM. *Nat Methods* 2015;**12**:641–4.
128. Jones EJ, Matthews ZJ, Gul L, *et al*. Integrative analysis of Paneth cell proteomic and transcriptomic data from intestinal organoids reveals functional processes dependent on autophagy. *Dis Model Mech* 2019;**12**. doi:10.1242/dmm.037069.
129. Park JH, Lee JM, Lee EJ, Hwang WB, Kim DJ. Indole-3-carbinol promotes goblet-cell differentiation regulating Wnt and notch signaling pathways AhR-dependently. *Mol Cells* 2018;**41**:290–300.
130. Fujii M, Matano M, Toshimitsu K, *et al*. Human intestinal organoids maintain self-renewal capacity and cellular diversity in niche-inspired culture condition. *Cell Stem Cell* 2018;**23**:787–93.e6.
131. Yousi F, Kainan C, Junnan Z, *et al*. Evaluation of the effects of four media on human intestinal microbiota culture in vitro. *AMB Express* 2019;**9**:69.
132. Allen-Vercoe E. Bringing the gut microbiota into focus through microbial culture: recent progress and future perspective. *Curr Opin Microbiol* 2013;**16**:625–9.
133. Noben M, Verstockt B, de Bruyn M, *et al*. Epithelial organoid cultures from patients with ulcerative colitis and Crohn's disease: a truly long-term model to study the molecular basis for inflammatory bowel disease? *Gut* 2017;**66**:2193–5.
134. Arnauts K, Verstockt B, Santo Ramalho A, Vermeire S, Verfaillie C, Ferrante M. Ex vivo mimicking of inflammation in organoids derived from patients with ulcerative colitis. *Gastroenterology* 2020;**159**:1564-7.
135. Leijten J, Seo J, Yue K, *et al*. Spatially and temporally controlled hydrogels for tissue engineering. *Mater Sci Eng R Rep* 2017;**119**:1–35.
136. Cook MT, Smith SL, Khutoryanskiy VV. Novel glycopolymer hydrogels as mucosa-mimetic materials to reduce animal testing. *Chem Commun [Camb]* 2015;**51**:14447–50.
137. Almany L, Seliktar D. Biosynthetic hydrogel scaffolds made from fibrinogen and polyethylene glycol for 3D cell cultures. *Biomaterials* 2005;**26**:2467–77.
138. Caliari SR, Burdick JA. A practical guide to hydrogels for cell culture. *Nat Methods* 2016;**13**:405–14.
139. Lee JH, Kim HW. Emerging properties of hydrogels in tissue engineering. *J Tissue Eng* 2018;**9**:2041731418768285.
140. Rossi G, Manfrin A, Lutolf MP. Progress and potential in organoid research. *Nat Rev Genet* 2018;**19**:671–87.
141. Cruz-Acuña R, García AJ. Synthetic hydrogels mimicking basement membrane matrices to promote cell-matrix interactions. *Matrix Biol* 2017;**57-58**:324–33.
142. Lou YR, Leung AW. Next generation organoids for biomedical research and applications. *Biotechnol Adv* 2018;**36**:132–49.
143. Bhatia SN, Ingber DE. Microfluidic organs-on-chips. *Nat Biotechnol* 2014;**32**:760–72.
144. Kraiczy J, Zilbauer M. Intestinal epithelial organoids as tools to study epigenetics in gut health and disease. *Stem Cells Int* 2019;**2019**:7242415.
145. Fujimichi Y, Otsuka K, Tomita M, Iwasaki T. An efficient intestinal organoid system of direct sorting to evaluate stem cell competition in vitro. *Sci Rep* 2019;**9**:20297.
146. Qin X, Sufi J, Vlckova P, *et al*. Cell-type-specific signaling networks in heterocellular organoids. *Nat Methods* 2020;**17**:335–42.
147. Wang F, Scoville D, He XC, *et al*. Isolation and characterization of intestinal stem cells based on surface marker combinations and colony-formation assay. *Gastroenterology* 2013;**145**:383–95.e1–21.
148. Brazovskaja A, Treutlein B, Camp JG. High-throughput single-cell transcriptomics on organoids. *Curr Opin Biotechnol* 2019;**55**:167–71.
149. Suzuki K, Murano T, Shimizu H, *et al*. Single cell analysis of Crohn's disease patient-derived small intestinal organoids reveals disease activity-dependent modification of stem cell properties. *J Gastroenterol* 2018;**53**:1035–47.
150. Haber AL, Biton M, Rogel N, *et al*. A single-cell survey of the small intestinal epithelium. *Nature* 2017;**551**:333–9.
151. Schwank G, Koo BK, Sasselli V, *et al*. Functional repair of CFTR by CRISPR/Cas9 in intestinal stem cell organoids of cystic fibrosis patients. *Cell Stem Cell* 2013;**13**:653–8.
152. Matano M, Date S, Shimokawa M, *et al*. Modeling colorectal cancer using CRISPR-Cas9-mediated engineering of human intestinal organoids. *Nat Med* 2015;**21**:256–62.
153. Drost J, Artegiani B, Clevers H. The generation of organoids for studying Wnt signaling. *Methods Mol Biol* 2016;**1481**:141–59.
154. Drost J, van Jaarsveld RH, Ponsioen B, *et al*. Sequential cancer mutations in cultured human intestinal stem cells. *Nature* 2015;**521**:43–7.
155. Limanskiy V, Vyas A, Chaturvedi LS, Vyas D. Harnessing the potential of gene editing technology using CRISPR in inflammatory bowel disease. *World J Gastroenterol* 2019;**25**:2177–87.
156. Uhlig HH. Monogenic diseases associated with intestinal inflammation: implications for the understanding of inflammatory bowel disease. *Gut* 2013;**62**:1795–805.
157. Kozuka K, He Y, Koo-McCoy S, *et al*. Development and characterization of a human and mouse intestinal epithelial cell monolayer platform. *Stem Cell Rep* 2017;**9**:1976–90.
158. Birchenough GM, Nyström EE, Johansson ME, Hansson GC. A sentinel goblet cell guards the colonic crypt by triggering Nlrp6-dependent Muc2 secretion. *Science* 2016;**352**:1535–42.
159. Zilbauer M, Kraiczy J. Epigenetics in gastrointestinal health and disease: spotlight on DNA methylation in the intestinal epithelium. *Nestle Nutr Inst Workshop Ser* 2017;**88**:35–44.
160. Gracz AD, Williamson IA, Roche KC, *et al*. A high-throughput platform for stem cell niche co-cultures and downstream gene expression analysis. *Nat Cell Biol* 2015;**17**:340–9.
161. Brandenberg N, Hoehnel S, Kuttler F, *et al*. High-throughput automated organoid culture via stem-cell aggregation in microcavity arrays. *Nat Biomed Eng* 2020;**4**:863–74.
162. Fujii M, Shimokawa M, Date S, *et al*. A colorectal tumor organoid library demonstrates progressive loss of niche factor requirements during tumorigenesis. *Cell Stem Cell* 2016;**18**:827–38.
163. van de Wetering M, Francies HE, Francis JM, *et al*. Prospective derivation of a living organoid biobank of colorectal cancer patients. *Cell* 2015;**161**:933–45.
164. Francies HE, Barthorpe A, McLaren-Douglas A, Barendt WJ, Garnett MJ. Drug sensitivity assays of human cancer organoid cultures. *Methods Mol Biol* 2019;**1576**:339–51.
165. Weiser M, Simon JM, Kochar B, *et al*. Molecular classification of Crohn's disease reveals two clinically relevant subtypes. *Gut* 2018;**67**:36–42.
166. Satsangi J, Silverberg MS, Vermeire S, Colombel JF. The Montreal classification of inflammatory bowel disease: controversies, consensus, and implications. *Gut* 2006;**55**:749–53.

167. Jostins L, Ripke S, Weersma RK, *et al.*; International IBD Genetics Consortium [IIBDGC]. Host-microbe interactions have shaped the genetic architecture of inflammatory bowel disease. *Nature* 2012;**491**:119–24.
168. Dutta D, Heo I, Clevers H. Disease modeling in stem cell-derived 3D organoid systems. *Trends Mol Med* 2017;**23**:393–410.
169. Astolfi M, Péant B, Lateef MA, *et al.* Micro-dissected tumor tissues on chip: an ex vivo method for drug testing and personalized therapy. *Lab Chip* 2016;**16**:312–25.
170. Mack DL, Guan X, Wagoner A, Walker SJ, Childers MK. Disease-in-a-dish: the contribution of patient-specific induced pluripotent stem cell technology to regenerative rehabilitation. *Am J Phys Med Rehabil* 2014;**93**:S155–68.
171. Esch EW, Bahinski A, Huh D. Organs-on-chips at the frontiers of drug discovery. *Nat Rev Drug Discov* 2015;**14**:248–60.
172. Ashley EA. The precision medicine initiative: a new national effort. *JAMA* 2015;**313**:2119–20.
173. Cirstea M, Radisavljevic N, Finlay BB. Good bug, bad bug: breaking through microbial stereotypes. *Cell Host Microbe* 2018;**23**:10–3.
174. Steidler L, Hans W, Schotte L, *et al.* Treatment of murine colitis by Lactococcus lactis secreting interleukin-10. *Science* 2000;**289**:1352–5.

npj | systems biology and applications

www.nature.com/npjsba

ARTICLE OPEN

Check for updates

Mapping the epithelial–immune cell interactome upon infection in the gut and the upper airways

Martina Poletti[1,2,14], Agatha Treveil[1,2,14], Luca Csabai[1,3], Leila Gul[1], Dezso Modos[1,2], Matthew Madgwick[1,2], Marton Olbei[1,2], Balazs Bohar[1,3], Alberto Valdeolivas[4,5], Denes Turei[4,5], Bram Verstockt[6,7], Sergio Triana[8,9], Theodore Alexandrov[10,11], Julio Saez-Rodriguez[4,5,11], Megan L. Stanifer[12], Steeve Boulant[12] and Tamas Korcsmaros[1,2,13]✉

Increasing evidence points towards the key role of the epithelium in the systemic and over-activated immune response to viral infection, including SARS-CoV-2 infection. Yet, how viral infection alters epithelial–immune cell interactions regulating inflammatory responses, is not well known. Available experimental approaches are insufficient to properly analyse this complex system, and computational predictions and targeted data integration are needed as an alternative approach. In this work, we propose an integrated computational biology framework that models how infection alters intracellular signalling of epithelial cells and how this change impacts the systemic immune response through modified interactions between epithelial cells and local immune cell populations. As a proof-of-concept, we focused on the role of intestinal and upper-airway epithelial infection. To characterise the modified epithelial–immune interactome, we integrated intra- and intercellular networks with single-cell RNA-seq data from SARS-CoV-2 infected human ileal and colonic organoids as well as from infected airway ciliated epithelial cells. This integrated methodology has proven useful to point out specific epithelial–immune interactions driving inflammation during disease response, and propose relevant molecular targets to guide focused experimental analysis.

npj Systems Biology and Applications (2022)8:15 ; https://doi.org/10.1038/s41540-022-00224-x

INTRODUCTION

Specialised epithelial cells lining the surface of the mammalian gastrointestinal tract form the primary line of defense against external stimuli, working in cohort with resident immune cells to maintain homeostasis and defend the body from infections. Although the role of both the epithelium and the immune system during infection have been assessed in previous studies, these components have often been investigated separately. While this knowledge has been instrumental in advancing medical research, the recent COVID-19 pandemic has pointed out the need for large-scale, integrative models to address key questions that cannot yet be solved with available experimental models. One example is: what is the role of an infected cell in inducing systemic inflammatory responses by communicating to resident immune cells? To address this critical question, existing yet often disconnected datasets and computational approaches can be leveraged to develop a complex but easily interpretable map of how viral molecules are able affect different cell populations in the gut, and how infected cells can in turn modulate local and systemic immune and inflammatory responses.

The recent COVID-19 pandemic is caused by infection with the severe acute respiratory syndrome coronavirus 2 (SARS-CoV-2). While SARS-CoV-2 mainly targets the lung and upper airways[1–3], other organs can be infected too, including the heart, kidney, brain, and the intestine[4]. In addition to directly infecting key organs, the main hurdle of SARS-CoV-2 infection is the excessive inflammatory response mediated by both the innate and adaptive immune systems[1,5]. The overactivated inflammatory response, also known as cytokine release syndrome (CRS) or cytokine storm, is the result of high levels of circulating cytokines and chemokines, and it is thought to be responsible for the severe COVID-19 symptoms some patients experience[6]. Yet, there is no clear understanding of which particular inflammatory pathways and cell types are responsible for driving this process, and whether some organs are more important than others in the initiation and maintenance of this syndrome[7]. The causal role of SARS-CoV-2 on intestinal damage and the role of the small intestine in contributing to CRS was recently highlighted[8,9].

Human intestinal organoids have been used as a tool to study SARS-CoV-2 infection in the gut and the inflammatory responses of specific intestinal epithelial cell types[10–13]. These studies provided evidence that SARS-CoV-2 is able to infect and actively replicate in human intestinal cells, in particular in enterocytes[10,13]. These studies also revealed that, contrary to the limited type I and type III interferon (IFN) immune response observed in the lungs[14,15], the response to SARS-CoV-2 infection in the gut is characterised by a cell-type specific inflammatory response that is important in the development of systemic reactions[11]. Examination of human intestinal samples has also shown that infection of gut epithelial cells results in the activation of local immune populations[16]. Yet, the exact effects of viral infection in the gut and the role of epithelial cell–immune cell interaction in

[1]Earlham Institute, Norwich Research Park, Norwich, UK. [2]Quadram Institute Bioscience, Norwich Research Park, Norwich, UK. [3]Department of Genetics, Eotvos Lorand University, Budapest, Hungary. [4]Faculty of Medicine, Heidelberg University, Heidelberg, Germany. [5]Institute for Computational Biomedicine, Heidelberg University Hospital, Heidelberg, Germany. [6]Department of Gastroenterology and Hepatology, University Hospitals Leuven, KU Leuven, Leuven, Belgium. [7]Department of Chronic Diseases and Metabolism, Translational Research in GI disorders, KU Leuven, Leuven, Belgium. [8]Structural and Computational Biology Unit, European Molecular Biology Laboratory, Heidelberg, Germany. [9]Collaboration for joint PhD degree between EMBL and Heidelberg University, Faculty of Biosciences, Heidelberg, Germany. [10]Skaggs School of Pharmacy and Pharmaceutical Sciences, University of California San Diego, La Jolla, CA, USA. [11]Molecular Medicine Partnership Unit (MMPU), European Molecular Biology Laboratory, Heidelberg, Germany. [12]Department of Infectious Diseases, Heidelberg University Hospital Heidelberg, Heidelberg, Germany. [13]Department of Metabolism, Digestion and Reproduction, Imperial College London, London, UK. [14]These authors contributed equally: Martina Poletti, Agatha Treveil. ✉email: t.korcsmaros@imperial.ac.uk

Published in partnership with the Systems Biology Institute

npj

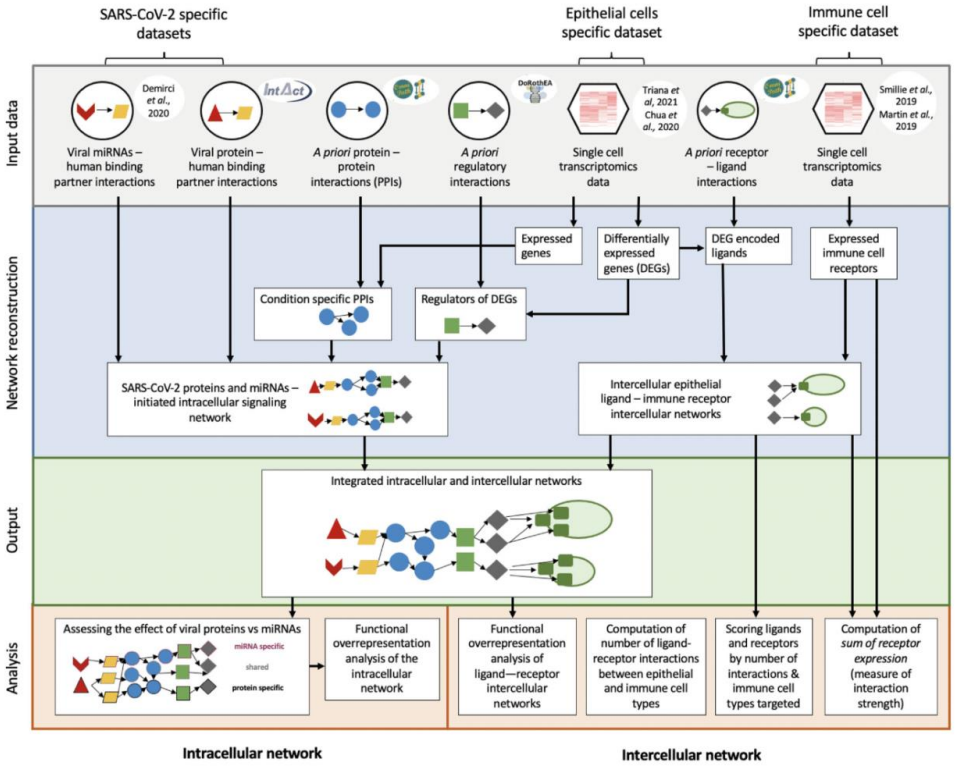

Fig. 1 Integrated workflow to analyse the intracellular and intercellular effect of SARS-CoV-2 in the gut. Schematic workflow illustrating the different analytical steps used to construct the intracellular and intercellular signalling networks between epithelial cells in SARS-CoV-2 infected intestinal organoids (ileal and colonic organoids, 24 h infection) or moderate COVID-19 upper airway ciliated epithelial and immune cell types.

mediating the inflammatory response of the body are not known. This information could ultimately aid the development of treatments and strategies to optimize the level and type of immune response as we would understand better the viral strategies that dysregulate our immune system. Due to the lack of adequate and complex experimental systems, to the best of our knowledge, no study has been carried out so far to analyse epithelial–immune crosstalk in the gastrointestinal tract upon SARS-CoV-2 infection.

Here, we introduce a computational framework to map epithelial–immune interactions, improve our understanding in the gut or in other organs by interpreting existing data better, and importantly, provide a short list of key molecules for targeted experimental validations. To achieve this, we integrated two previously developed intracellular modelling tools (ViralLink and CARNIVAL) with intercellular network approaches (from OmniPath)[17–19]. We present two proof of concept studies on intestinal organoids and upper airways ciliated cells. We used available SARS-CoV-2–human mRNA/protein–protein interaction predictions to model the effect of viral infection on intracellular signalling networks in host intestinal and ciliated cells, and applied published single-cell datasets to create cell-type, organ and context-specific epithelial–immune interaction maps. We demonstrated the importance and usefulness of this map with integrated analyses, which provided an improved understanding of the effect of viral infection on ileal, colonic and airway epithelial cells, and the role of epithelial–immune cell crosstalk during SARS-CoV-2 infection. Ultimately, this framework may help to find key intercellular inflammatory pathways involved in these crosstalks that could pave the way for potential successful strategies against the cytokine release syndrome associated-symptoms observed in severe cases of COVID-19. Importantly, the presented integrated framework will allow investigating other infections and conditions for which our analytical toolkits can be repurposed.

RESULTS

Reconstructing the intestinal epithelial–immune interactome

In our previous work, we identified a subpopulation of enterocytes as the prime target of SARS-CoV-2 (BavPat1/2020 strain), with directly infected cells showing a high pro-inflammatory response and little to no interferon-mediated response as the result of a SARS-CoV-2-mediated inhibition of interferon signalling[13]. These findings highlighted the key role of the gut as a pro-inflammatory reservoir, which primes for further investigation to be able to fully understand SARS-CoV-2 pathogenesis. Building on this study, we created an integrated bioinformatics framework that enables the investigation of the infected epithelial cell–immune cell crosstalk in a cell-type specific manner (Fig. 1). To do so, we exploited

a priori knowledge on ligand–receptor interactions [18] to construct intercellular networks connecting epithelial cells and resident immune cells using our previously generated single cell RNA-seq epithelial cell dataset of ileal and colonic organoids infected with SARS-CoV-2 (BavPat1/2020 variant)[13] and a separate lamina propria immune cell one[20,21].

First, we looked at the epithelial cell population with the highest number of ligands among the differentially expressed genes upon infection to assess which epithelial cell type could drive the response to SARS-CoV-2 infection. Our previous findings[13] had highlighted immature enterocytes (originally known as "immature enterocytes 2", an enterocyte subpopulation characterised by MMP7+, MUC1+, CXCL1+) as the epithelial population characterised by the highest number of differentially expressed genes upon infection (Supplementary Fig. 1). In accordance with this, we found that this population was also characterised by the highest number of differentially expressed ligands. Hence, differentially expressed ligands of colonic and ileal immature enterocytes were used to build epithelial–immune intercellular networks by connecting ligands to their binding receptors on immune cells (Fig. 1 and Methods).

To identify the main epithelial and immune cell types involved in intercellular crosstalk, the putative number of ligand–receptor interactions between each epithelial–immune cell type pair was computed. Specifically, all possible interactions between each set of up or downregulated epithelial ligands and each of the receptors expressed by the specific immune cell type (from[20] and[21]) were identified (Fig. 1 and Methods). While both bystander and infected cell populations were affected by viral infection, directly infected intestinal cell populations had a higher number of predicted interactions with immune cells compared to bystander cell populations in both colon and ileum, supporting a role for direct viral infection in altering intercellular signalling in the gut (Fig. 2a). In the colon, the higher number of epithelial–immune interactions was identified between downregulated ligands of infected immature enterocytes and plasma cells, as well as CD4+/CD8+ T cells, macrophages and dendritic cells (DCs) to a lesser extent (Fig. 2a). Conversely, in the ileum, the highest number of interactions was identified between upregulated ligands of infected immature enterocytes and IgA plasma cells, T resident memory (Trm) cells, dendritic cells and resident macrophages (Fig. 2a). Notably, the higher number of interactions in the ileum was not a result of a higher number of upregulated ligands (20), as this was similar to the number of downregulated ones (24) (Fig. 2a, b). Instead, the higher number of interactions was driven by upregulated ligands binding to multiple receptors on each immune cell targeted. A more detailed explanation can be found in the Supplementary Results.

With this integrated network reconstruction, we have shown the value of our framework in enabling the study of mechanistic details of the effect of SARS-CoV-2, or other viruses, on the human immune system.

The infected epithelial signalling network drives the epithelial–immune interactome

To further understand how SARS-CoV-2 infection drives altered ligand expression in infected intestinal epithelial cells, we used our integrated network model to reconstruct the altered intracellular signalling in directly infected immature enterocytes population driven by SARS-CoV-2. Within our framework, two separate bioinformatics tools, ViralLink and CARNIVAL, were used to construct an intracellular causal network linking perturbed human proteins interacting with SARS-CoV-2 viral proteins or miRNAs to activated transcription factors (TFs) regulating the differentially expressed ligands upon infection, through altered intracellular protein-protein signalling cascades (Fig. 1). By integrating tissue-specific epithelial data, we have constructed two separate causal networks for infected immature enterocytes of the ileum and colon, thus enabling us to distinguish tissue specific differences in infection response (Fig. 1). Detailed analysis of the colon and ileal intracellular network features can be found in the Supplementary Results. Furthermore, using multiple complementary methods of network analysis, we have highlighted the most likely signalling pathways affected upon infection. Finally, by integrating a priori information on SARS-CoV-2 miRNAs/proteins - human protein interactions, we have built separate sublayers of the networks representing altered signalling stemming from upstream perturbations caused by SARS-CoV-2 miRNAs, proteins or both. These networks allowed us to assess the contribution of each of these viral factors in altering the intracellular signalling cascade (Fig. 1 and Methods).

Functional analysis of the tissue-specific intracellular networks is useful to understand how SARS-CoV-2 infection in immature enterocytes affects their function through the modulation of intracellular signalling, and whether any differences in response exist between colon and ileum. Here, a functional overrepresentation analysis (Gene Ontology (GO) and Reactome) of the protein-protein interaction ("PPI") layer[22–25] of each intracellular causal sub-network (stemming from viral proteins, miRNAs, or both) was integrated in our framework to assess the contributions of SARS-CoV-2 miRNAs or proteins to the changes observed[22–25] (Fig. 1 and Methods). Functional analysis of the PPI layer of the intracellular networks built with ViralLink revealed an overrepresentation of pathways related to inflammation and chemotaxis (Nuclear Factor kappa-light-chain-enhancer of activated B cells (NF-kB) signalling, interleukin signalling, chemokine signalling) in both ileum and colon (Fig. 3). Additionally, we found the overrepresentation of functions related to interferon (IFN) signalling and Mitogen-Activated Protein Kinase (MAPK) signalling being overrepresented uniquely in the ileum in both viral protein and miRNA intracellular networks (Fig. 3b). An overrepresentation of laminin-driven interaction pathways, which we observed uniquely for viral miRNA intracellular network in both ileum and colon, could be indicative of an increased recruitment and adhesion of immune cells following infection (Fig. 3). Furthermore, an overrepresentation of pathways related to negative regulation of apoptosis, cell cycle, cell proliferation and growth was found in both ileal and colonic networks, suggesting an effect of SARS-CoV-2 on epithelial cell tissue renewal (Fig. 3). Interestingly, an overrepresentation of WNT signalling pathway, which is key for stem cell renewal, was found uniquely in the viral protein sub-network, in both tissues, while pathways related to the establishment of cell and tissue polarity were found uniquely in the colon, indicating an attempt for tissue healing following viral infection (Fig. 3).

Functional overrepresentation analysis of the PPI layer of the intracellular networks built with CARNIVAL confirmed similar affected functions upon infection as those found in the ViralLink networks, suggesting functional overlap between networks obtained using these two methods such as senescence or inflammation (Fig. 3 and Supplementary Figs. 3 and 4). Within the outlined framework, the choice of which tool (ViralLink or CARNIVAL) to be used to build the intracellular network for a particular study should be driven by the specific study aims and biological questions. Further information about similarities and differences between the two tools is available in the Methods and Supplementary Results.

Further analysis of these networks can help predict key transcription factors responsible for the upstream regulation of altered ligands upon infection. Here, we found that both colonic and ileal networks generated with CARNIVAL shared similar transcription factors, including ATF2/3, FOS, JUN, STAT1, and NFKB1, which were all upregulated in both tissues upon infection (Supplementary Figs. 3 and 4). These transcription factors play a role in interferon response (STAT1[26]), and inflammation (NFKB1[27]),

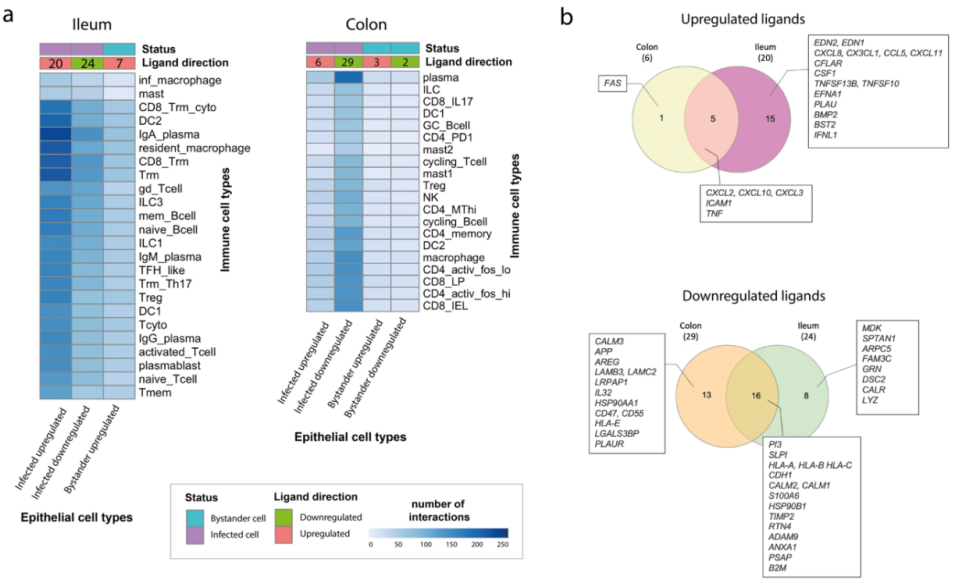

Fig. 2 Differentially expressed ligands driving upregulated and downregulated intercellular interactions between colonic and ileal infected immature enterocytes and resident immune cells upon infection in the colon and ileum. a Heatmap showing the number of interactions between immature enterocytes and resident immune cells. Interactions driven by upregulated and downregulated ligands (ligand direction) are shown separately for infected and bystander cells (status), and for ileum and colonic organoids. The intensity of the colour indicates the number of interactions with the immune cell types whose receptor is targeted by the epithelial cells ligands. The numbers on the ligand direction row refer to the number of upregulated or downregulated ligands driving the indicated interactions with immune cells for the different groups/conditions. Abbreviations: *Ileum:* inf_macrophage infected macrophage, mast mast cell, CD8_Trm_cyto Resident memory cytotoxic T cell, DC2 dendritic cell 2, Trm Tissue-resident memory T cell, gd_Tcell Gamma delta (γδ) T cells, ILC Innate lymphoid cell, mem_Bcell memory B cell, naive_Bcell naive B cell, TFH_like T follicular helper cells, Trm_Th17 Tissue-resident memory Th17 cells, Treg Regulatory T cell, Tcyto Cytotoxic T cell, Tmem Memory T cells. *Colon*: ILC Innate lymphoid cell, CD8_IL17 IL-17+ CD8+ T cells, DC dendritic cells, GC_Bcell Germinal center B cells, CD4_PD1 mast mast cell, Treg Regulatory T cell, NK Natural Killer cell, CD4_MThi high mitochondrial CD4+ T cell, CD4_memory CD4+ Memory T cell, CD4_activ_fos_high activated CD4+ T cells (high/low c-fos), CD8_LP CD8+ lymphocyte-predominant cells, CD8_IEL CD8+ intraepithelial lymphocytes. **b** Venn diagrams showing the number of ligands of the infected immature enterocytes–immune cells intercellular network that are unique or shared between the ileum and colon. Upregulated and downregulated ligands are shown separately. The full list of ligands is available as Table 1.

anti-apoptosis and cell growth (ATF2/3[28]), cell proliferation and differentiation (JUN, FOS[29]), suggesting an increase in these functions upon SARS-CoV-2 infection in both colon and ileum. Interestingly, viral miRNAs were predicted to target different intracellular signalling processes between colon and ileum (miR_10,11,16,18 in the colon and miR_4,5,6,18 in the ileum). Additionally, by analysing these networks, we observed that NOTCH1 and SMAD4, seem to be central to the intracellular signalling cascade in the colon, by receiving several signals driven by viral miRNAs and viral proteins, respectively (Supplementary Fig. 3). Interestingly, both the Notch and TGF-β SMAD-dependant signalling pathways are involved in intestinal epithelial cell homeostasis, including stem cell maintenance, progenitor cell proliferation[30] and maintenance of cell differentiation[31], suggesting a modulation of these pathways upon infection. In the ileal network, JAK2 and CREB1, as well as SMAD2, SMAD3 and ERK2 (MAPK1) seem to play a central role in the intracellular PPI signalling driven by viral miRNAs and viral proteins, respectively, and *JAK2* and both *SMAD2* and *SMAD3* were also upregulated upon infection (Supplementary Fig. 4). These transcription factors play a key role in the regulation of immunity (JAK2, CREB1;[32,33], cell proliferation and differentiation (MAPK1) and plasticity (SMAD2/3)[34,35], suggesting a positive regulation of these functions uniquely in the ileum upon infection.

Reconstruction and analysis of perturbed intracellular signalling in infected enterocytes using two complementary methods highlighted key pathways through which SARS-CoV-2 affects the infected cells, and pointed out transcription factors playing a major role during SARS-CoV-2 infection response.

Altered epithelial-derived ligands drive differential epithelial–immune crosstalk upon infection

To understand the functional impact of epithelial infection on the epithelial–immune interactome, we created intercellular networks by connecting upregulated and downregulated epithelial ligands of colonic and ileal infected immature enterocytes upon infection to their binding receptors on immune cells (Fig. 1 and Methods). Next, for each set of up and downregulated intercellular interactions, we looked at which ligands, receptors and immune cell types were involved in these intercellular interactions, assessing any potential similarities or differences between the colon and ileum (Fig. 1 and Methods). Here, we present the analysis relative to infected immature enterocytes–immune cell interaction, while the analysis relative to bystander immature enterocytes is available as Supplementary Results.

Upregulated ligands of infected immature enterocytes upon infection as well as binding receptors on immune cells were

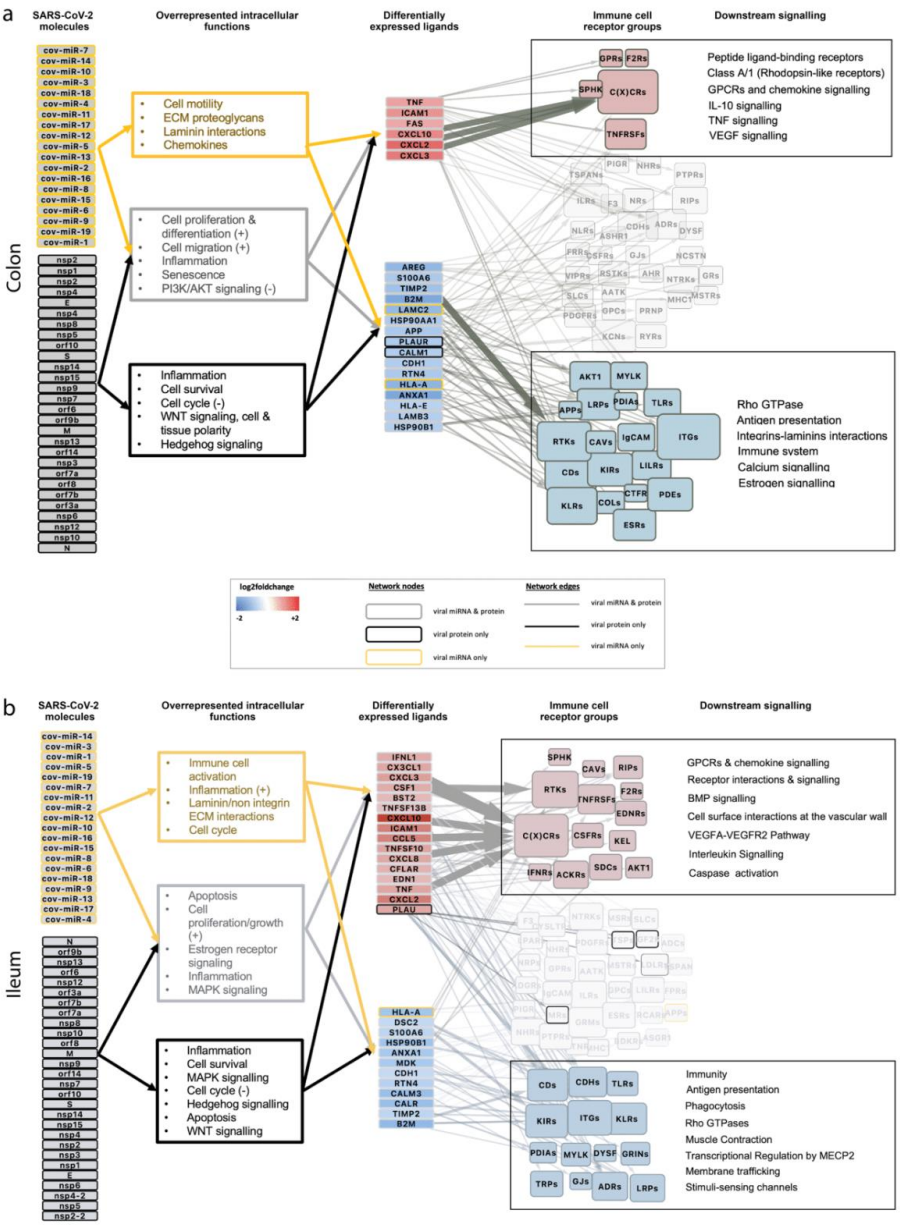

mainly shared among colon and ileum, resulting in most epithelial–immune interactions driven by upregulated ligands being similar in both tissues (one unique to colon, 219 unique to ileum, 66 shared) (Figs. 2b, 4a, b). A full list and detailed description of differences and similarities in ligands, receptors and upregulated intercellular interactions between colon and ileum can be found as Tables 1–3 and as Supplementary Results.

To understand which epithelial ligands and immune cell receptors were driving most epithelial–immune cell interactions, we scored ligands and receptors based on the number of

Fig. 3 Overview of intracellular and intercellular signalling of colonic and ileal infected immature enterocytes upon SARS-CoV-2 infection. a, b Overview of intracellular and intercellular signalling upon SARS-CoV-2 infection in colonic (**a**) and ileal (**b**) infected immature enterocytes and immune cell populations. From left to right: signalling cascade going from SARS-CoV-2 molecules (proteins or miRNAs) to differentially expressed ligands on immature enterocytes and binding receptor groups on immune cells. Intracellular network: SARS-COV-2 molecules are grouped separately if they are viral proteins (bottom) or miRNAs (top). Differentially expressed ligands for which no upstream signalling was identified, but downstream intercellular connections were predicted are excluded from this figure. Differentially expressed ligands are grouped based on the direction of regulation, which is indicated with blue when downregulated (bottom) and red when upregulated (top) when comparing SARS-CoV-2 infected vs uninfected conditions. Colours of the nodes and of the functional analysis indicate if the original network was a miRNA only (yellow), viral protein only (black) or both viral protein and miRNA (grey). Functional overrepresentation analysis was carried out for the "PPI layer" of the intracellular network which includes human binding proteins, intermediary signalling proteins and TFs (adj p value < 0.05, $n > 3$). Intercellular network: Size of the receptor node represents the sum of receptors within the group targeted by each incoming ligand. Functional analysis is indicated for ligand–receptor groups. Receptor groups layout is based on whether they contributed to the functional analysis of upregulated interactions (red) or downregulated interactions (blue). Receptor groups not contributing to any functions are indicated in light grey.

interactions they were involved in (Fig. 1 and Methods). In both tissues, chemokines (CXCLs) and tumour necrosis factor alpha (TNF-α) were among epithelial ligands (Fig. 5a, b), and chemokine receptors (CXCR 3,4,5,6 and CCR 1,2,5,7,9,10) among the receptors on immune cells driving the highest numbers of upregulated interactions (Fig. 6), overall pointing towards an increased immune cell recruitment upon infection[36]. The high number of upregulated interactions driven by chemokines could be attributable to the widespread presence of several different chemokine receptors on immune cells (Supplementary Fig. 8).

To decipher which specific epithelial ligands and immune receptors were driving the strongest epithelial–immune cell interactions, ligands and receptors participating in epithelial–immune interactions can be scored based on the "sum of receptor expression" value, which takes into account the number of interacting receptors and the level of receptor expression in each immune cell type (Fig. 1 and Methods). In the colon, the strongest upregulated interactions involved the epithelial TNF-α binding to B cells, T cells (CD4/CD8+), NK cells, macrophages and DCs, as well as epithelial chemokines (CXCL2,3, 10) binding to T cells (CD4/CD8+) and NK cells (Fig. 7a). Similarly, in the ileum the strongest upregulated interactions involved epithelial chemokines binding to T cells (Treg, Tcyto, Tmem, CD8 Trm cyto) as well as TNF-α and colony stimulating factor 1 (CSF1) binding to macrophages and DCs (Fig. 7b). Receptors driving the strongest upregulated interactions were mainly chemokine receptors (CXCRs, CCRs) in both colon and ileum, and Receptor Interacting Serine/Threonine Kinase 1 (RIPK1) in the colon only (Fig. 8).

Finally, functional overrepresentation analysis of the participating upregulated epithelial ligands and receiving receptors on immune cells can help to understand the role of each of these epithelial–immune interactions driven by infection (Fig. 1). In line with the extensive overlap in upregulated intercellular interactions (Fig. 4a and Supplementary Fig. 8), most functions were shared between colon and ileum, and included chemotaxis (GPCR signalling, chemokine signalling), immunity (interleukin signalling), apoptosis (caspase activation) and angiogenesis (VEGFA-VEGFR2 pathway) (Supplementary Fig. 9). One colonic-specific function was related to pro-inflammatory responses (TNF signalling) (Supplementary Fig. 9a) and one ileal-specific function was related to stem cell renewal (BMP signalling) (Supplementary Fig. 9b).

Downregulated ligands in infected immature enterocytes upon infection as well as targeted receptors on immune cells were tissue-specific to a large extent, resulting in a large proportion of downregulated interactions being tissue-specific (73 unique to ileum, 125 to colon) (Figs. 2b, 4a, b). A detailed description of differences and similarities in ligands, receptors and downregulated intercellular interactions between colon and ileum can be found as Supplementary Results.

In both tissues, a high number of downregulated interactions was driven by the epithelial ligands human leukocyte antigens (HLA-A/B/C), beta-2-microglobulin (B2M) and calmodulin (CALM1/2) (Fig. 5a, b), and integrins (ITGs), KLRCs and LDL Receptor Related Protein 1 (LRP1) in both colon and ileum (Figs. 4a and 6). Additionally, uniquely in the colon, the highest number of downregulated interactions was driven by two epithelial-derived laminins (LAMC2, LAMB3) (Fig. 2c), and by AKT1 (Protein kinase B, PKB) present on immune cell types (Figs. 4a and 6).

When investigating the strength of these intercellular interactions, we found that HLA-s (HLA-A, B, C) and B2M targeting T cells (colon: CD4/CD8+, Tregs; ileum: Trm, Tregs, cytotoxic T cells), NK cells (colon only), ILCs and macrophages (ileum only) represented the strongest downregulated interactions in both colon and ileum (Fig. 7). Additionally, uniquely in the colon, laminins (LAMB3, LAMC2) targeting T cells and macrophages represented the strongest downregulated interactions (Fig. 7). Receptors driving the strongest downregulated interactions were AKT1 uniquely in the colon (Fig. 8a) as well as integrins, KLRCs and LRP1 in both colon and ileum (Fig. 8a, b)

Functional overrepresentation analysis of the participating downregulated epithelial ligands and receiving receptors on immune cells (Fig. 1 and Methods) revealed shared functions related to antigen processing and cross-presentation (MHC class I–mediated), phagocytosis (endoplasmic reticulum (ER) phagosome pathway, signalling by RHO GTPases) and cell–cell communication (immunoregulatory interactions between a lymphoid and non-lymphoid cell) in both tissues, possibly suggesting decreased epithelial–immune cell crosstalk functions related to the activation of the innate and adaptive immune response[37] (Supplementary Fig. 9). Furthermore, several colon-specific functions were related to the extracellular matrix (ECM) organisation and integrin cell surface interactions, which play an important role in processes critical to inflammation, infection, and angiogenesis, thereby suggesting a negative regulation of these vital interactions uniquely in the colon[38] (Supplementary Fig. 9a). The only function uniquely overrepresented in the ileum was transcriptional regulation by MECP2 (Supplementary Fig. 9b), whose expression has been shown to play a role in intestinal morphology and function[39].

In conclusion, using our framework, we pinpointed tissue-specific and shared epithelial ligands and immune cell receptors participating in the intercellular signalling through which SARS-CoV-2 infected epithelial cells can affect the inflammatory responses of various immune cell types during infection (Fig. 9).

Implication of epithelial ligands in the inflammatory process

The analysis of our integrated framework of intracellular and intercellular signalling networks in intestinal epithelial cells upon infection has helped point out several differentially expressed ligands participating in epithelial–immune interactions potentially

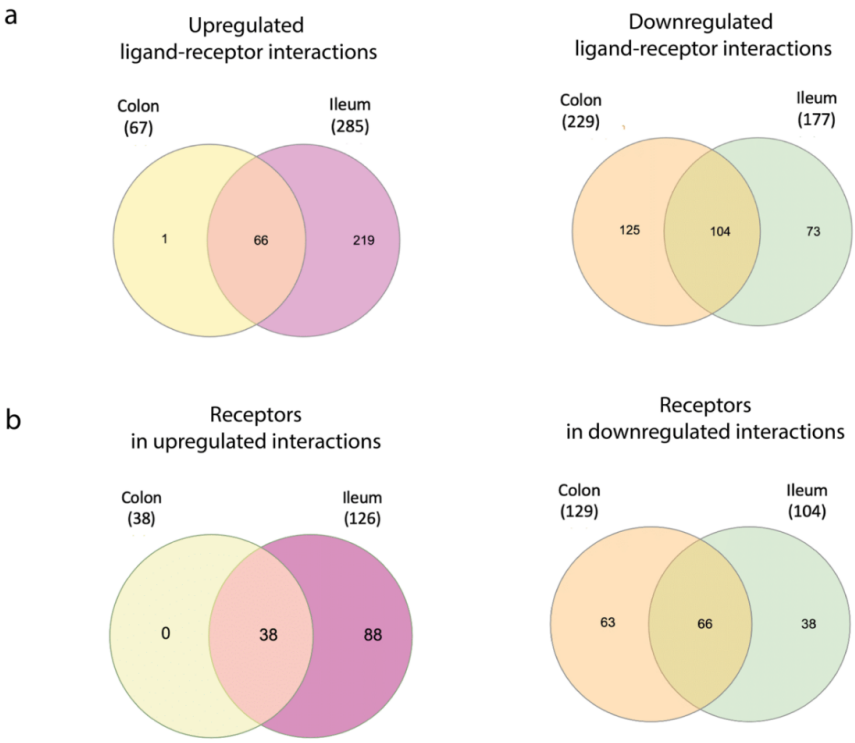

Fig. 4 Overview of upregulated and downregulated ligand–receptor interactions and participating receptors between infected immature enterocytes and resident immune cells upon infection in the colon and ileum. a Venn diagrams showing the number of ligand–receptor interactions in the infected immature enterocytes–immune cells intercellular networks that are unique or shared between the ileum and colon. Intercellular interactions driven by upregulated and downregulated ligands are shown separately. The full list of ligand–receptor interactions is available as Table 3. **b** Venn diagrams showing the number of receptors in the infected immature enterocytes–immune cells intercellular networks that are unique or shared between the ileal and colonic networks. Receptors targeted by upregulated ligands and downregulated ligands are shown separately. The full list of receptors is available as Table 2.

playing a role in driving the inflammatory process upon SARS-CoV-2 infection. To validate their importance during immune reactions, we integrated these predictions with independent data from three previously published studies (Fig. 1).

First, by comparing the differentially expressed ligands upon SARS-CoV-2 infection to DEGs in human colonic organoids exposed to inflammatory cytokines[40], we identified 24 ligands whose expression change is regulated by cytokines during intestinal inflammation (Table 4). These ligands are likely to contribute to the inflammatory responses upon infection. Next, by comparing ileal and colonic ligands to data from ImmunoGlobe, a manually curated intercellular immune interaction network[41] and ImmunoeXpresso, a collection of cell–cytokine interactions generated through text mining[42], we identified 12 ligands previously known to influence immune cell populations (Table 4). The full list of affected immune cell types for each epithelial ligand is available in Table 4. Finally, to understand which ileal and colonic ligands could explain blood cytokine level changes of COVID-19 patients via direct immune cell regulation, we used data from[5], and identified six ligands capable to create the detected blood cytokine levels during infection (Table 4).

Using this assessment, we were able to rank the differentially expressed ligands for their importance in the inflammatory process, and subsequently listed the 18 highest ranked ligands, for which there is strong evidence of their role in epithelial–immune cell interactions during the inflammatory SARS-CoV-2 disease response (Table 4). These ligands included CSF1, various chemokines (CXCL10, CXCL11, CXCL2, CXCL3, CCL5, CX3CL1, CXCL8), TNFa and TNFSF13b, and ICAM1 among the upregulated ones; and various laminins (LAMC2, LAMB3), AREG, B2M), human leukocyte antigens (HLAs) (HLA-A, HLA-B) and IL32 among the downregulated ones.

The intracellular and intercellular signalling are also altered in the upper airways in patients with moderate COVID-19

The presented integrated framework can also be applied to infected epithelial cell data from other organs to reveal the effects of viral infection on that specific organ's function. To show the ease of applicability of our framework to other infected tissues, we have employed it to analyse the effect of SARS-CoV-2 on the intracellular and intercellular signalling of upper airway ciliated epithelial cells during moderate COVID-19 cases (Methods and Fig. 1). Functional analysis of the PPI layer of the intracellular signalling network of infected ciliated cells upon moderate COVID-19 revealed an alteration of pathways related to cell motility and migration, cell adhesion mediated by the ECM (laminin, non-

Table 1. Ligands in ligand–receptor interactions in the colon and ileum.

Tissue	Direction	Number	Ligands
Colon only	Upregulated	1	FAS
Colon only	Downregulated	13	CALM3, APP, AREG, LAMB3, LRPAP1, IL32, CD47, HSP90AA1, CD55, LAMC2, HLA-E, LGALS3BP, PLAUR
Ileum only	Upregulated	15	EDN2, CXCL8, CX3CL1, CFLAR, CSF1, EDN1, TNFSF13B, TNFSF10, EFNA1, PLAU, CCL5, CXCL11, BMP2, BST2, IFNL1
Ileum only	Downregulated	8	MDK, SPTAN1, ARPC5, FAM3C, GRN, DSC2, CALR, LYZ
Colon and ileum	Upregulated	5	CXCL2, CXCL10, ICAM1, CXCL3, TNF
Colon and ileum	Downregulated	16	PI3, SLPI, HLA-A, CDH1, CALM2, S100A6, HSP90B1, TIMP2, RTN4, ADAM9, HLA-B, HLA-C, ANXA1, CALM1, PSAP, B2M

Table listing the number of ligands of infected immature enterocytes–immune cells intercellular network that are unique or shared between the ileum and colon.

Table 2. Receptors in ligand–receptor interactions in the colon and ileum.

Tissue	Direction	Number	Receptors
Colon only	Upregulated	0	–
Colon only	Downregulated	63	ITGA1,2,7,8,910, ITGB4,6,8, NOD2, LRP8, CD151, CD74, CD97, TGFBR1,2, SLC45A3, SLC16A, SORL1, VANGL1, FCGR2B, SIRPG, PRNP, LILRA3, PDE1A, GPC1, CFTR, PTGER1, CR1, NCSTN, AHR, COL17A1
Ileum only	Upregulated	88	MCAM, CYSLTR1/2, ACVR1/2B/L1/2 A, SLC5A11, SLC7A1, ENG, TNFRSF13B/13 C/10 C/17/10B/10D, LILRA4, CELSR3, ADGRL4, ADCY9, ACKR2/3/4, EDNRA, CCR3/6/8, CXCR1/2, EPHA10, KEL, CSF3R/2RA, EDNRB, BMPR2/R1A/R1B, SMO, AMHR2, GPR75, LPAR2, NPR3, ACKR1, IFNLR1, ST14, MRC2, CD79A, IGF2R, PTPRU, MSR1
Ileum only	Downregulated	38	TSPAN1, SCTR, KIR2DL4, KIR3DL1, GRM3, ADRB2, PTH2R, BDKRB2, GRIN2A, KLRC3, PLPP6, CRHR1, CLEC2D, GPR37, GPR37L1, ITGA2B, SCN4A, CDH2, PTPRB, AQP6, DSG2, KIR2DL1, KIR3DL3, MIP, KCNQ3, TRPC3, GRM4, SCARF1, RTN4RL1, GPC2, OPRM1
Colon and ileum	Upregulated	38	F2RL1, ITGAM/X, F3, CXCR3/4/5/6, CCR1/2/4/7/9, CX3CR1, XCR1, PTPRS, PIGR, GPR160, CELSR2, PPARG, CDH5, CD83, CDH11, SPHK1, TRADD
Colon and ileum	Downregulated	66	TLR1/2/4/7, VIPR1, TNFRSF19, PLD2, PLSCR1/4, SORT1, HFE, GP6, KLRC1/2/4, KLRG1, PDE1B/1 C, PDIA3, CD1A/B, CD3D/G, CD247, ITGAE, ITGA4/6, ITGB7, LILRB2, NGFR, GJB2, LRP5/6, FPR3, LDLR, RYR1, APLP2, CELSR1, KCNN4, KCNQ1/5, GLP2R, ESR1/2, CANX, IL2RB, ASGR1, KIR2DL2/3, PTPRA, DYSF, TRPC1

Table listing number of receptors involved ligand–receptor interactions in the infected immature enterocytes–immune cells intercellular network that are unique or shared between the ileum and colon. The direction column indicates the direction of the expression change of the epithelial ligand driving each intercellular interaction.

integrins interactions), pro-inflammatory signalling pathways (Interleukin, MAPK, PI3K, NF-kB signalling), cell cycle arrest and intestinal homeostasis (Supplementary Fig. 12).

Intercellular interactions between upper airways ciliated epithelial cells and resident immune cells were mainly driven by upregulated ligands, particularly chemokines (CXCL1/3/6) and HLAs (HLA-A/B/C) binding to chemokine receptors (CCRs, CX(3)CRs) and CD3D/G, KLRs and KIRs (expressed on T-cells and NK cells), respectively (Supplementary Fig. 12 and Supplementary Fig. 13a, b). Interestingly, the strongest upregulated interactions were driven by chemokines and HLAs targeting T-cells (cytotoxic and regulatory), macrophages (resident and non-resident) and B cells, with a second cluster of slightly weaker interactions including NK, dendritic and mast cells (Supplementary Fig. 13c). Together, these results point towards increased recruitment and antigen presentation to these immune cell types. Functional overrepresentation analysis showed that upregulated interactions were related to chemokines/cytokines signalling, antigen processing and presentation, activation of the innate and adaptive immune system and general defense response (Supplementary Fig. 12).

Conversely, downregulated interactions were driven by epidermal growth factor receptor (EGFR) binding to several different receptors, and the ECM protein Tenascin C (TNC) binding to integrins (ITGs) on immune cells (Supplementary Fig. 12 and Supplementary Fig. 13a, b). Downregulated interactions involved most immune cells, with the strongest interactions targeting non-resident macrophages and regulatory T cells (Supplementary Fig. 13c). Functional overrepresentation analysis showed that downregulated interactions were involved in haemostasis and cell adhesion processes mediated by the ECM components (integrin, laminin, syndecan) (Supplementary Fig. 12).

DISCUSSION

In this work, we have developed an integrated framework to model how altered intracellular signalling in epithelial cells drives a different epithelial–immune interactome upon infection. As a proof of concept study, we first applied this model to highlight the putative role of the gut during the immune response following SARS-CoV-2 infection, showing how several intracellular and intercellular mechanisms are affected, with key differences between colon and ileum. A visual schematic of our key findings can be found in Fig. 9. Additionally, we proved the applicability of this framework to other tissues of interest by analysing intra and intercellular interactions of the upper airway epithelium in moderate COVID-19 patients, confirming many of the findings highlighted in the literature, and pointing out key cell–cell interactions of interest.

SARS-CoV-2 has been shown to actively infect and reproduce in the human gut and in human gastrointestinal organoids[10,11,13]. However, the exact effect of intestinal inflammation and the role of epithelial–immune interactions in the hyperinflammatory

Table 3. Ligand–receptors in intercellular interactions in the colon and ileum.

Tissue	Direction	Number	Ligand–receptor interactions
Colon only	Upregulated	1	FAS _ RIPK1
Colon only	Downregulated	125	APP _ TNFRSF21, CD74, CCR5, SLC45A3, CAV1, NCSTN, FCGR2B, GPC1, LRP1, NGFR, ADRA2A
			AREG _ LTK, CSF1R, MERTK, INSR, NTRK1/2/3, ROR1/2, PDGFRB, LMTK2, FLT3, PTK7, MET, TIE1, AATK, DDR2, MST1R, AXL, TYRO3, MUSK, RET, PDGFRA, RYK
			CALM1 _ PDE1A
			CALM2 _ PDE1A
			CALM3 _ MYLK, GP6, KCNQ1/5, PDE1A/B/C, INSR, ESR1/2, AKT1
			CD47 _ SIRPG
			CD55 _ CD97, AKT1, CR1
			HLA-C _ LILRA3
			HLA-E _ KLRC1/2/4, SLC16A4, KIR2DL3/3DL2
			HSP90AA1 _ NR3C1, CFTR, TGFBR1/2, AKT1, ITGB3, AHR, NOD2, RIPK1
			IL32 _ PTGER1, MET
			LAMB3 _ CD151, COL17A1, ITGA1/2/3/4/5/6/7/8/9/10/11/V, ITGB1/3/4/5/6/7/8, AKT1, PRNP
			LAMC2 _ AKT1, ITGA1/2/3/4/5/6/7/8/9/10/11/V, ITGB1/3/4/5/6/7/8, COL17A1, PRNP, CD151
			LGALS3BP _ VANGL1, ITGB1
			LRPAP1 _ LDLR, VLDLR, SORL1, SORT1, LRP1/8
			PLAUR _ ITGB3
Ileum only	Upregulated	219	BMP2 _ AMHR2, SMO, ACVR2A/R2B/R1/RL1, BMPR1A/1B/2, ENG, CDH11
			BST2 _ LILRA4
			CFLAR _ RIPK1
			CSF1 _ PDGFRB, DDR2, LMTK2, TYRO3, RYK, MUSK, MET, CELSR3, SLC7A1, RET, ITGB3/AV, INSR, ALK, CSF1R/2RA/3R, ROR1, MSR1/T1R, NTRK1/2/3, MERTK, TIE1, AATK, AXL, ROR2, PTK7, LTK, PDGFRA, FLT3
			CCL5 _CX3CR1, CCR1/2/3/4/5/6/7/8/9, CXCR1/2/3/4/5/6/10, ACKR1/2/4, GPR75, SDC1, ADRA2A, CD4, GRM7, XCR1
			CX3CL1_CXCR1/2/3/4/5/6, CCR1/2/3/4/5/6/7/8/9/10, CX3CR1, XCR1
			CXCL10_CXCR1/2, GRM7, CCR3/6/8
			CXCL11_XCR1, CCR1/2/3/4/6/5/7/8/9/10, ACKR1, CX3CR1, CXCR1/2/3/4/5/6, ADRA2A, ACKR3
			CXCL2 _ CCR3/6/8, ACKR1, CXCR1, CXCR2, GRM7
			CXCL3 _ CCR3/6/8, CXCR1, CXCR2, GRM7
			CXCL8 _ CCR1/2/3/4/5/6/7/8/9/10, SDC1/3, CX3CR1, ITGAM, CXCR1/2/3/4/5/6, XCR1, ACKR1, CDH5/79A, LPAR2, GRM7, ADRA2A,
			EDN1 _ EDNRA/B, ADGRL4, AR, MCAM, NPR3, CYSLTR1/2, AKT1, ADCY9, KEL
			EDN2_EDNRA/B, KEL
			EFNA1 _ RET, INSR, ROR1, NTRK1/2, PDGFRB, TYRO3, MERTK, EPHA10, MST1R, ALK, RYK, AATK, AXL, DDR2, PTK7, LMTK2, CSF1R, FLT3, PDGFRA, NTRK3, LTK, TIE1, MUSK, ROR2, MET
			IFNL1 _ IFNLR1
			PLAU _ ITGA3/A5/AV/AM/B1/B5, VLDLR, MRC2, LRP1, IGF2R, ST14
			TNF _ SLC5A11, TRPV1, PTPRU
			TNFSF10 _ TNFRSF10B/C/D, RIPK1
			TNFSF13B _ TNFRSF17/13B/13C
Ileum only	Downregulated	73	ANXA1 _ GRM7, GRIN2A
			ARPC5 _ ADRB2, LDLR
			B2M _ KIR2DL1/3DL1, AR
			CALM1 _ CRHR1, SCN4A, TRPC3, GRM3/4/7, SCTR, PTH2R, KCNQ3, AQP6, MIP, GRIN2A, PLPP6, OPRM1; CALM2_PLPP6, TRPC3/V1, SCN4A, GRM7, AQP6, GRIN2A, KCNQ3
			CALR _ ITGA2B/3/V, LRP1, SCARF1, PDIA3, AR, BDKRB2
			CDH1 _ CDH2,
			DSC2 _ DSG2
			FAM3C _ CLEC2D
			GRN _ SORT1
			HLA-A _ KIR2DL1/2DL4/3DL3/3DL1, KLRC3
			HLA-B _ KIR3DL3, KIR3DL1, KIR2DL1, KLRC3, KIR2DL4
			HLA-C _ KIR2DL4/2DL1/3DL1/3DL3, KLRC3

Table 3 continued

Tissue	Direction	Number	Ligand–receptor interactions
			HSP90B1 _ AR LYZ _ ITGAL
			MDK _ TSPAN1, SDC1/3, GPC2, ITGA4/6, PTPRB, ITGB1, LRP1, ALK
			PSAP _ AR, GPR37/37L1
			RTN4 _ RTN4RL1
			SPTAN1 _ PTPRA
Colon and ileum	Upregulated	66	TNF_CD83/H11, F2RL1/F3, TNFRSF21, SPHK1, NR3C1, AKT1, TRADD, RIPK1, MYLK, INSR, PPARG, PIGR, GPR160, PTPRS, CELSR2
			CXCL3 _ CXCR3/4/5/R1, CCR1/2/4/5/7/9/10, XCR1, ADRA2A
			CXCL10 _ CX3CR1, CCR1/2/4/5/7/9/10, CXCR3/4/5/6, ADRA2A, XCR1
			CXCL2_CXCR6 / CCR9 / CCR1 / CXCR5 / XCR1 CXCR3 / CXCR4 / CCR2 / CCR5 / CX3CR1 / ADRA2A / CCR4 / CCR7 / CCR10
			ICAM1 _ ITGAX/L/M, IL2RG/RA, CDH5, CAV1
Colon and ileum	Downregulated	104	ADAM9 _ ITGA3/6/V, ITGB1/5
			ANXA1 _ LMTK2, ADRA2A, FPR3, CCR10, DYSF
			B2M _ PDIA3, KLRC1/2, KIR2DL3, LILRB2, HFE, CD247, IL2RA/RB/RG, CD1A/B, CD3G/D
			CALM1 _ KCNQ1/5, PDE1B/C, MYLK, RYR1, INSR, VIPR1, GP6, PTPRA, GLP2R, KCNN4, ESR1/2
			CALM2 _ KCNQ1/5, ESR1/2, TRPC1, MYLK, RYR1, PDE1B/C, INSR, GP6
			CDH1 _ ITGAE/B7, LRP5/6, MET, KLRG1
			HLA-A _ IL2RA, KIR2DL3/3DL2, KLRC1/2/4, LILRB2, IL2RB/RG, CD3G/D, APLP2
			HLA-B _ KLRC1/2/4, CD3G/D, LILRB2, CANX, KIR2DL3/3DL2
			HLA-C _ CD3G, KIR2DL3/3DL2, CD3D, KLRC1/2/4, LILRB2
			HSP90B1 _ ASGR1, TLR1/2/4/7, LRP1
			PI3 _ PLD2
			PSAP _ CELSR1, LRP1, CD1B, SORT1
			RTN4 _ NGFR, TNFRSF19, GJB2
			S100A6 _ ESR1
			SLPI _ CD4, PLSCR1/4
			TIMP2 _ ITGA3, ITGB1

Table listing the number of ligand–receptor interactions in infected immature enterocytes–immune cells intercellular network that are unique or shared between the ileal and colonic networks. The direction column indicates the direction of the expression change epithelial ligand driving each intercellular interaction. Interactions are indicated as follows: ligand_receptor1, receptor2, receptor3. Receptors belonging to the same class (e.g. calmodulins) are indicated as follows: CALM1/2/3.

immune response ("cytokine storm") characterising many COVID-19 patients are not known[5,6]. Accurately modelling these interactions could help identify potential targets that are key to selectively disrupt such cell–cell interactions underlying extreme inflammatory conditions during SARS-CoV-2 infection. This would be extremely important given the failure of most randomised control trials associated with pro-inflammatory drug candidates for COVID-19[43].

The altered epithelial–immune cell crosstalk during SARS-CoV-2 infection has been explored within the nasopharynx and lungs using scRNA seq data[44]. This study found stronger epithelial–immune cell interactions in critically ill patients based on ligand–receptor expression profiles, highlighting the importance of the crosstalk between infected cells and local immune cells in the disease course. However, to our knowledge, no prior study has been carried out so far to investigate the effect of viral infection in host intestinal cells, and the role and contribution of intestinal epithelial cell–immune cell crosstalk during SARS-CoV-2 infection.

In this work, we developed an integrated pipeline to model the effect of intracellular signalling perturbation in epithelial cells on the epithelial–immune interactome in the gut. As a proof-of-concept, we exploited our previously published data on SARS-CoV-2 (BavPat1/2020) infection in intestinal organoids[13] to investigate the effect of SARS-CoV-2 proteins and potential miRNAs on ileal and colonic epithelial cell intracellular signalling and function. We added in a distinguishable way the analysis of these potential miRNAs encoded by SARS-CoV-2, as previous studies highlighted the regulatory role of similar miRNAs produced by RNA viruses and their ability to downregulate host genes and affecting host functions[45–47]. Furthermore, we modelled how specific epithelial ligands, whose expression was altered upon infection, were driving specific epithelial–immune interactions *via* their altered binding to receptors expressed on resident immune cell populations[20,21].

While our previous data pointed towards immature enterocytes as the prime target of SARS-CoV-2 infection, the application of our integrated pipeline allowed us to model how this epithelial population, when directly infected, also drives the majority of interactions with gut resident immune cells stemming from their differentially regulated ligands by SARS-CoV-2 (Fig. 2a). Upon infection of immature enterocytes, intracellular signalling pathways were altered, with a direct effect on pathways of inflammation, apoptosis, cell survival and cell death (Fig. 3). Pathways related to cell cycle (negative regulation of G2/M transition) and cell proliferation were also altered upon infection (Fig. 3), in line with a previous phosphoproteomics study finding a correlation with cell cycle arrest upon SARS-CoV-2 infection[48].

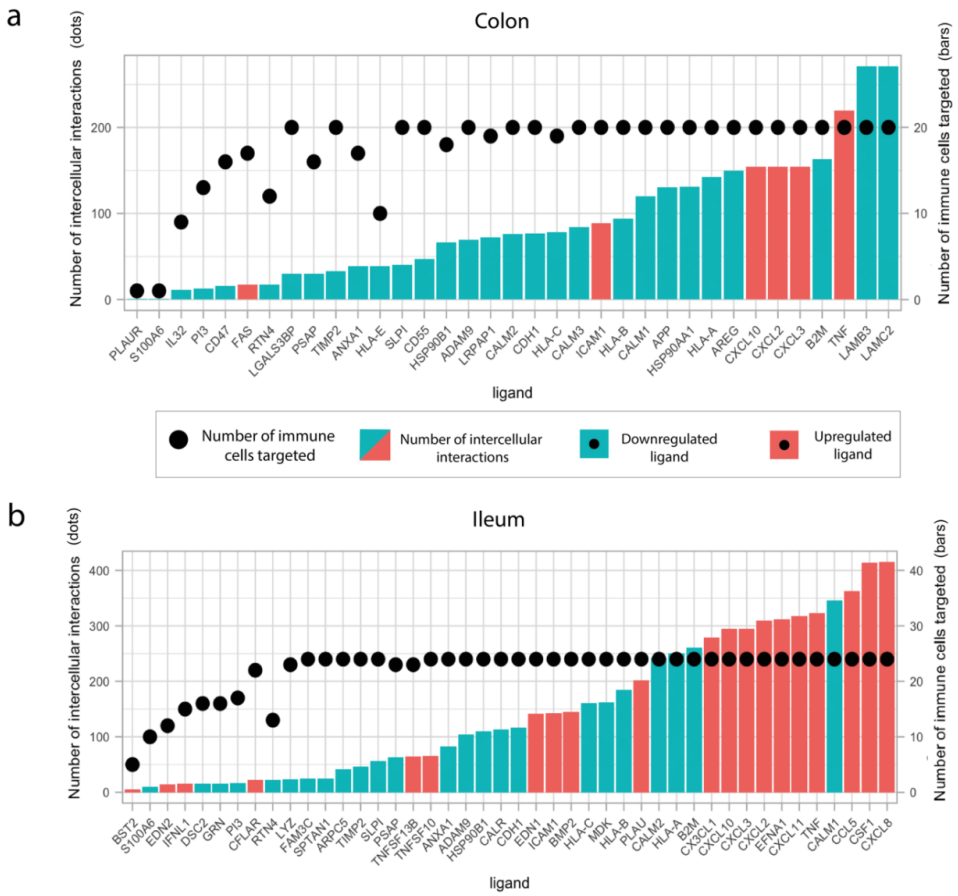

Fig. 5 Overview of upregulated and downregulated ligands and ligand–receptor interactions between infected immature enterocytes and resident immune cells upon infection in the colon and ileum. a, **b** Bar plot showing the upregulated and downregulated ligands in the colonic (**a**) and ileal (**b**) infected immature enterocytes–immune cell network scored by number of interactions (height of the bar plot) and number of immune cells targeted (black dots). Upregulated ligands are shown in red and downregulated ligands in blue.

Finally, pathways involved in cell differentiation, cell migration and epithelial polarisation were also modulated upon infection (Fig. 3), which to our knowledge no other study had highlighted before.

By using available ligand–receptor interaction data, we aimed to understand how infected gut epithelial cells recruit resident immune cell populations to find key interactions driving the immune response during infection. Our analysis revealed that IgA plasma cells were the immune cell population with the highest number of cell–cell interactions upon infection, with the highest number of epithelial–immune interactions driven by downregulated epithelial ligands (29) in the colon, and upregulated epithelial ligands (20) in the ileum (Fig. 2a). A possible explanation for these observed tissue-specific differences and on the role of IgA plasma cells can be found in the Supplementary Discussion section.

By further analysing the specific ligand–receptor interactions driving epithelial–immune crosstalk upon SARS-CoV-2 infection, we could observe that strong upregulated interactions upon infection were mostly shared by both colon and ileum, and were represented by chemokine and TNF-α driven interactions, possibly reflecting a general effect of the inflammation process (Figs. 6 and 7). Functional analysis highlighted a relation to proinflammatory signalling pathways, including TNF-α signalling, interleukin signalling and chemotaxis via GPCR signalling, overall suggesting an increasing recruitment and cell adhesion of these immune cell populations upon infection (Supplementary Fig. 9). Notably, four chemokine receptors identified by our study (CXCR6 in the ileum, CCR1/2 and CCR9 in both ileum and colon) are coded in a genomic region found to be a COVID-19 risk locus on chromosome 3, further validating our predictions[49].

Conversely, we could observe that strong downregulated interactions were driven by epithelial HLAs (HLA-A, B, C) and B2M, a subcomponent of the major histocompatibility complex I (MHC I) in both tissues (Fig. 6). According to our analysis, these ligands were mainly binding to KLR receptors, which are mainly presented on NK cells (Fig. 6, Supplementary Fig. 8).

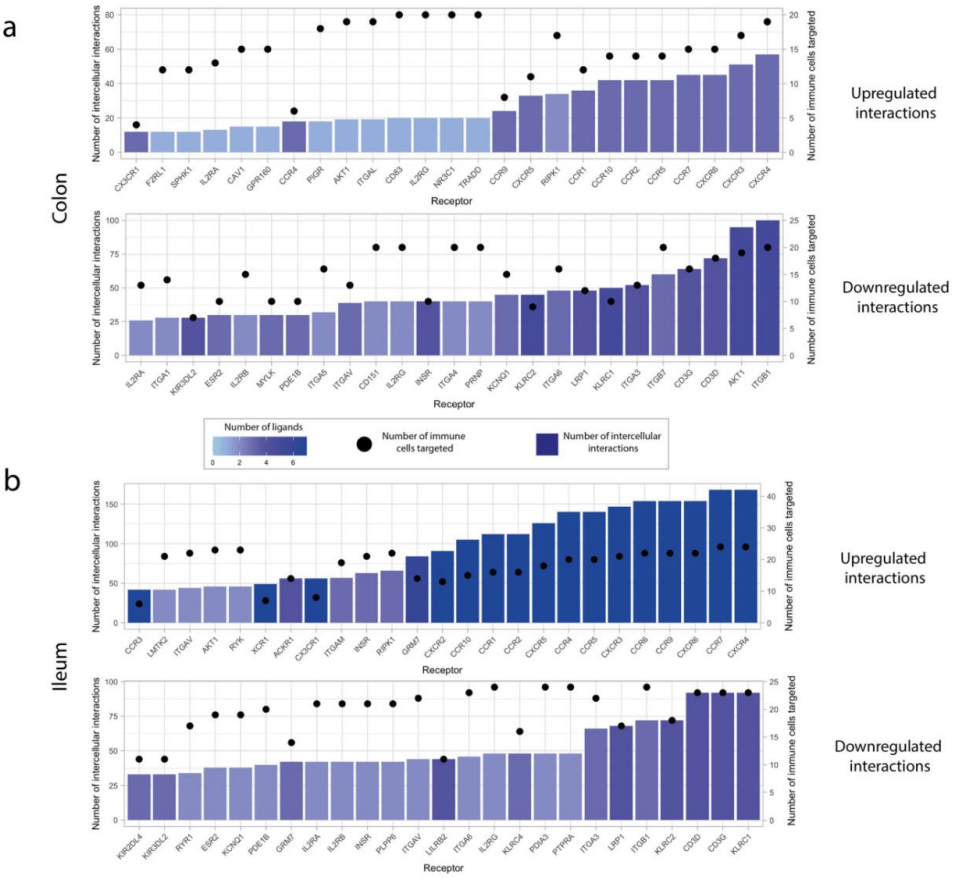

Fig. 6 Receptors involved in intercellular interactions between colonic and ileal infected immature enterocytes and resident immune cells. a, **b** Bar plot showing the immune receptors targeted by upregulated (top graph) and downregulated (bottom graph) ligands in colonic (**a**) and ileal (**b**) infected immature enterocytes, scored by number of interactions (height of the bar plot) and number of immune cells targeted (black dots). The colour of the bar plots indicates the number of ligands targeting each of the receptors indicated. This plot only shows the top 25 receptors by number of interactions, and the full plot is available as Supplementary Fig. 6.

Downregulation of HLA-KLR interactions may represent an immune evasion mechanism[50] that a recent study proposed as a way SARS-CoV-2 protein ORF8 uses to escape host immune surveillance[51].

Uniquely in the colon, strong downregulated interactions were driven by epithelial laminins (LAMB3 and LAMC2) and integrins, with T cells and macrophages as the main immune cell types targeted upon infection (Figs. 6 and 7). Laminin–integrin binding contributes to focal adhesion of immune cells to the inflamed tissue[52], and downregulation of laminins could represent an additional strategy for immune evasion following viral infection uniquely in the colon. Furthermore, laminins are known to play a role in shaping the architecture of intestinal mucosa, and an altered expression has been observed in Crohn's disease, a type of IBD, driven by pro-inflammatory cytokines TNF-α and IFN-γ[53–55]. Finally, an additional mechanism that SARS-CoV-2 may use to evade the immune response via the downregulation of calmodulin-phosphodiesterases interactions is further discussed in the Supplementary Discussion section.

With our integrated framework, we provided a key tool to study the effect of intracellular signalling perturbation in gut epithelial cells driving differential epithelial–immune interactions. By applying this workflow on SARS-CoV-2 infected organoids scRNA seq data, we confirmed many of the previous findings about SARS-CoV-2 infection, including the induced pro-inflammatory responses driven by chemokines and the role played by T cells (Fig. 9). Additionally, we uncovered mechanisms by which SARS-CoV-2 may evade the immune responses by interfering with epithelial–immune cell connections. Such mechanisms include downregulation of antigen presentation mediated by HLAs-KLR interactions and of focal adhesion pathways mediated by laminin–integrins interactions (Fig. 9).

In this work, we highlighted a set of intestinal epithelial ligands and immune cell populations implicated in altered epithelial–immune interactions during SARS-CoV-2 infection,

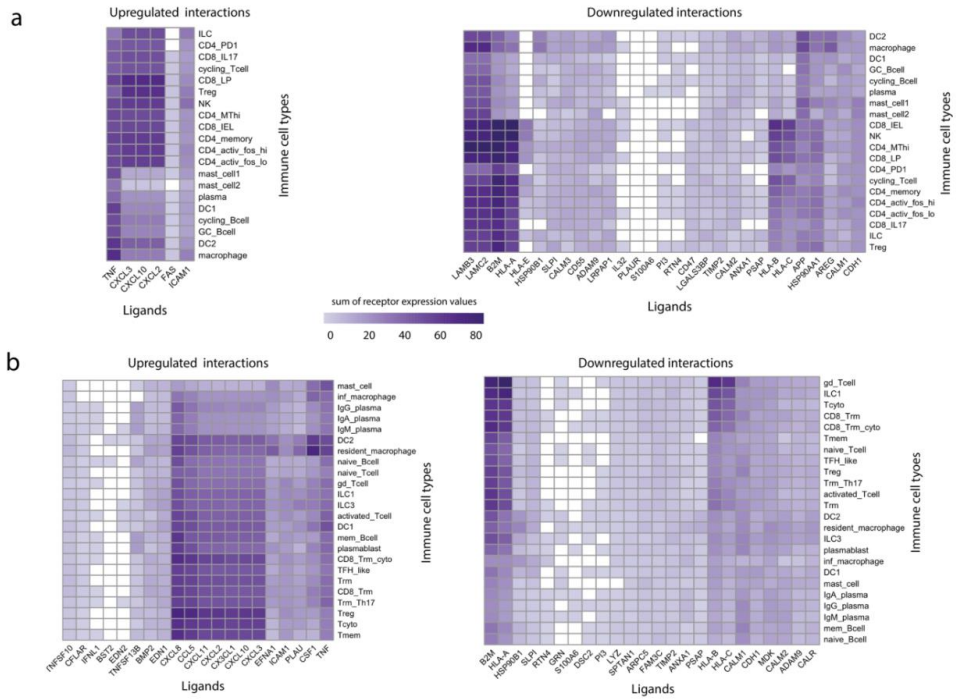

Fig. 7 Ligands of infected immature enterocytes involved in the strongest up and downregulated interactions upon SARS-CoV-2 infection in the colon and ileum. a, **b** Heatmap showing the upregulated and downregulated interactions in the colon (**a**) and ileum (**b**) between intestinal epithelial ligands and resident immune cells upon infection of immature enterocytes with SARS-CoV-2. The strength of the interaction is expressed by accounting for the number of interactions between epithelial ligands and immune receptors and the level of receptor expression of immune cells. The strength of the interaction, named "sum of expression values", is visualised using a colour gradient from white (weakeast interactions) to purple (strongest interactions). Abbreviations: *Ileum*: inf_macrophage infected macrophage, mast mast cell, CD8_Trm_cyto Resident memory cytotoxic T cell, DC2 dendritic cell 2, Trm Tissue-resident memory T cell, gd_Tcell Gamma delta (γδ) T cells, ILC Innate lymphoid cell, mem_Bcell memory B cell, naive_Bcell naive B cell, TFH_like T follicular helper cells, Trm_Th17 Tissue-resident memory Th17 cells, Treg Regulatory T cell, Tcyto Cytotoxic T cell, Tmem Memory T cells. *Colon*: ILC Innate lymphoid cell, CD8_IL17 IL-17+ CD8+ T cells, DC dendritic cells, GC_Bcell Germinal center B cells, CD4_PD1 mast mast cell, Treg Regulatory T cell, NK Natural Killer cell, CD4_MThi high mitochondrial CD4+ T cell, CD4_memory CD4+ Memory T cell, CD4_activ_fos_high activated CD4+ T cells (high/low c-fos), CD8_LP CD8+ lymphocyte-predominant cells, CD8_IEL CD8+ intraepithelial lymphocytes.

which could potentially drive the excessive inflammatory processes seen in severe COVID-19 patients (Table 4). Further experimental validation of bioinformatics predictions is key to validate these processes and the main molecules and cell types involved. To this end, intestinal organoids represent an excellent in vitro model to enable such validations[56]. Currently, introduction of immune cells to an organoid system is a challenging task. Yet, a recent study where human intestinal CD4+ T cells have been co-cultured with human intestinal organoids[57], may represent a promising set-up for future studies to investigate epithelial–immune cell interactions during SARS-CoV-2 induced inflammation in the gut. As reviewed recently by[58,59], such co-culture systems could be excellent to study intestinal host-microbe interactions, including the detailed experimental analysis of SARS-CoV-2 infection.

Nonetheless, our integrated workflow presents some limitations. When constructing the intracellular causal network, the effect of SARS-CoV-2 proteins towards human binding partners was always considered as inhibitory. However, this is not always the case. In the future, with increasingly available data, a more refined model could be generated. Furthermore, two different single cell transcriptomics datasets were used for colonic and ileal immune cell populations, due to the unavailability of both datasets from the same experiment. Similarly, IBD uninflamed data and healthy data were used for the ileum and colon respectively, as healthy control scRNAseq immune cell data for both tissues was not available at the time of the analysis. Finally, the a priori resources used to infer the intracellular and intercellular interaction networks may have some intrinsic limitations associated with them[60]. Specific tools such as LIANA (LIgand–receptor ANalysis frAmework; https://github.com/saezlab/liana) could be used in the future to compare across several resources available, helping to choose the one(s) providing the best overall prediction.

With our integrated workflow, we established a computational method to evaluate the effect of viral infection on host intestinal epithelial cell functions and how this consequently modulates the epithelial–immune crosstalk and immune activation. To demonstrate its applicability to other tissues, we analysed the intracellular and intercellular signalling of upper airway epithelial data of moderate COVID-19 cases. Although no specific information about the infecting SARS-CoV-2 strain was available, we were able to

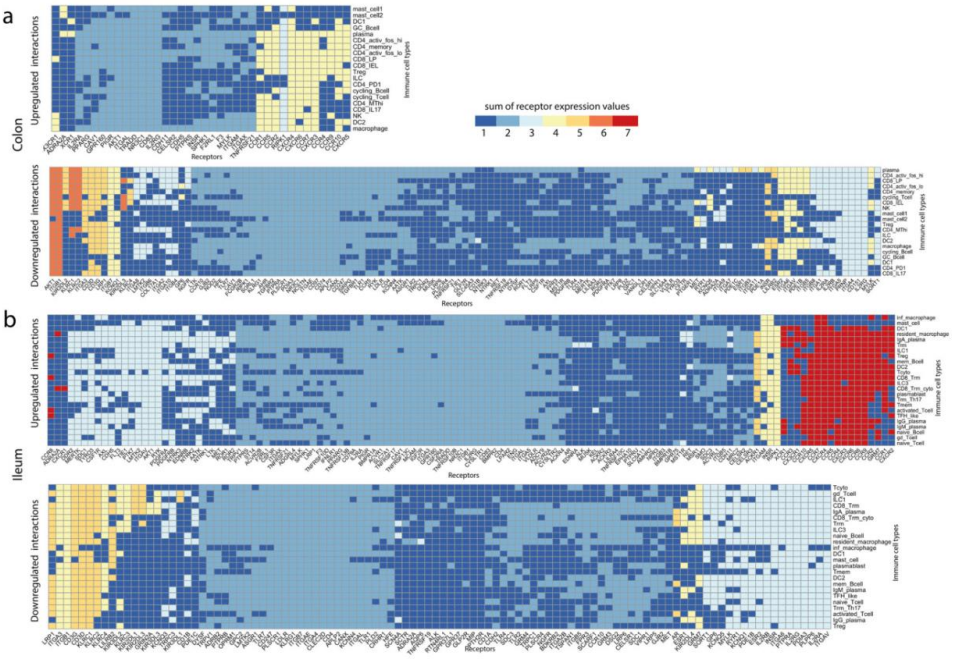

Fig. 8 Receptors on immune cell types involved in the strongest up and downregulated interactions upon SARS-CoV-2 infection in the colon and ileum. a, **b** Heatmap showing the upregulated and downregulated interactions in the colon (**a**) and ileum (**b**) between receptors and resident immune cell types upon infection of immature enterocytes with SARS-CoV-2. The number of interactions in which each receiving receptor on immune cell types is involved is visualised using a colour gradient from blue (weakest interactions) to red (strongest interactions). Abbreviations: *Ileum*: inf_macrophage infected macrophage, mast mast cell, CD8_Trm_cyto Resident memory cytotoxic T cell, DC2 dendritic cell 2, Trm Tissue-resident memory T cell, gd_Tcell Gamma delta (γδ) T cells, ILC Innate lymphoid cell, mem_Bcell memory B cell, naive_Bcell naive B cell, TFH_like T follicular helper cells, Trm_Th17 Tissue-resident memory Th17 cells, Treg Regulatory T cell, Tcyto Cytotoxic T cell, Tmem Memory T cells. *Colon*: ILC Innate lymphoid cell, CD8_IL17 IL-17+ CD8+ T cells, DC dendritic cells, GC_Bcell Germinal center B cells, CD4_PD1 mast mast cell, Treg Regulatory T cell, NK Natural Killer cell, CD4_MThi high mitochondrial CD4+ T cell, CD4_memory CD4+ Memory T cell, CD4_activ_fos_high activated CD4+ T cells (high/low c-fos), CD8_LP CD8+ lymphocyte-predominant cells, CD8_IEL CD8+ intraepithelial lymphocytes.

confirm several general findings related to COVID-19 infection previously highlighted in the literature. Following infection of ciliated cells, pro-inflammatory signalling pathways (interleukin, MAPK and NF-kB signalling) were altered, indicating an activated immune status, as previously reported[48,61–63]. Upregulated interactions were driven by chemokines binding to T cells (cytotoxic and regulatory) and macrophages, in line with the known role of chemokines in driving inflammation and immune cell recruitment[14,64] and the role played by T cells macrophages in the innate and adaptive immune response to SARS-CoV-2[65,66]. Additionally, upregulated interactions were also driven by HLAs, which are part of the MHC I complex, whose association with symptom severity has been previously highlighted[67]. Interestingly, the upregulation of intercellular interactions driven by HLAs is the opposite of the effect found in the intestine, which may represent a key difference in the response to SARS-CoV-2 between these two tissues. Finally, we found strong downregulated interactions between Tenascin C (TNC) and integrins, which were related to cell adhesion processes mediated by the ECM components. This is in line with a study finding that proteins associated with focal adhesion and the ECM receptors were decreased in COVID-19 lung tissue, which could indicate a dysregulation of the extracellular microenvironment in this tissue, revealing a possible mechanism of SARS-CoV-2-related lung damage[68].

To conclude, we demonstrated that this workflow is not limited to the gut, but it can be easily applied to other organs and cell types (e.g. lung, kidney, heart), provided the right input data is available. The workflow is translatable and both the epithelial and the immune component are replaceable. Furthermore, the presented workflow is transferable to understand any past or future infectious disease, when transcriptomic data of infected and control tissue and viral interactors are available. In this way, our workflow could potentially and efficiently be used in any other infection studies to shed light on the potential intervention points between immune cells and infected cells.

METHODS

Intercellular analysis

Input data

Intestinal epithelial cells: Single cell transcriptomics data of colonoids and enteroids infected with SARS-CoV-2 (BavPat1/2020 strain) was obtained from[69]. Single cell transcriptomics data of upper airway epithelial cells from moderate COVID-19 patients were obtained from[44]. Strain-level information about the infecting SARS-CoV-2 variant was not available in this study. The R packages 'Mast' and 'Seurat' were used to identify

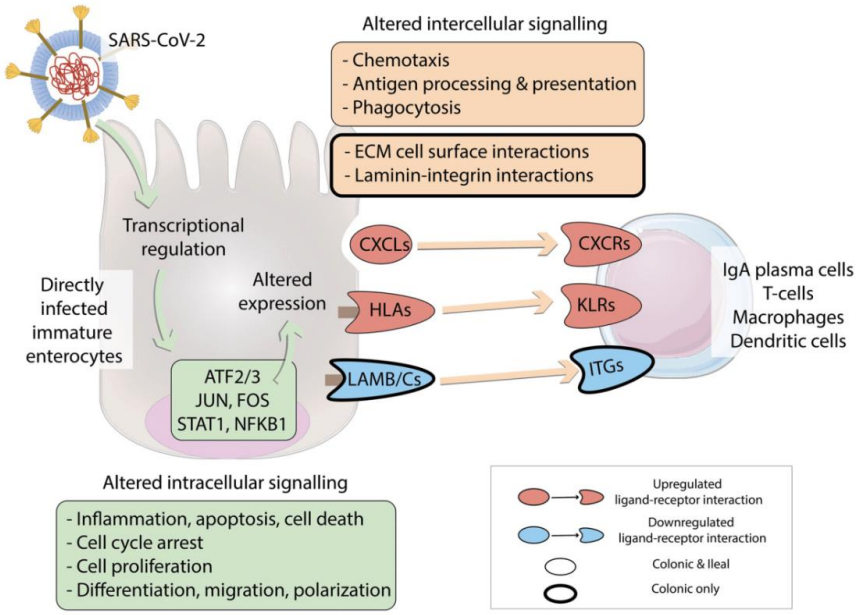

Fig. 9 Overview of intracellular and intercellular signalling upon SARS-CoV-2 infection of colonic and ileal immature enterocytes and resident immune cells. SARS-CoV-2 directly infects colonic and ileal immature enterocytes. Upon infection, transcription factors ATF2/3, JUN, FOS, STAT1 and NFKB1 are modulated, resulting in altered intracellular signalling pathways and altered ligands expression, including upregulation of chemokines (CXCLs) and human leukocyte antigens (HLAs), and downregulation of laminins (LAMB/Cs). Altered ligands expression drives differential intercellular interactions between epithelial ligands and immune cell receptors (chemokine receptors (CXCRs), killer cell lectin-like receptors (KLRs) and integrins (ITGs)) expressed on immune cells.

differentially expressed genes upon infection with SARS-CoV-2 for each epithelial cell type[70,71]. Specifically, directly infected or bystander cells from intestinal organoids treated with SARS-CoV-2 for 24 h were compared with the equivalent cell type from uninfected organoids. For the airway analysis, ciliated airway epithelial cells from moderate COVID-19 patients were compared with the equivalent cell type in control patients. This cell type was chosen as it is the most prevalent and most affected by SARS-CoV-2 infection together with secretory cell types[44]. Any genes with adjusted p value ≤0.05 and $|\log2 \text{ fold change (FC)}| \geq 0.5$ were considered significantly differentially expressed. Differential expression could only be calculated for cell types within a condition where data was available from ≥3 individual cells.

Intestinal resident immune cells: Single cell expression data from ileal and colonic resident immune cells was obtained from[20] and[21], respectively. For the analyses, data from healthy samples and uninflamed Crohn's disease samples was used for colonic and ileal immune cell populations, respectively. Single cell expression data of upper airway immune cells from moderate COVID-19 patients was obtained from[44].

Immune cell populations were identified through annotated clustering from[20,21,44]. Cell type labels were maintained as originally published. Following removal of all genes with count = 0, normalised log2 counts across all samples (separately for each cell type) were fitted to a gaussian kernel[72]. All genes with expression values above mean minus three standard deviations were considered as expressed genes for the given cell type in the given intestinal location. For the intercellular ligand–receptor predictions in the colon and ileum, a representative collection of immune cells relevant in gut inflammation and SARS-CoV-2 infection based on previous literature was selected, which included all macrophages, T cells, B cells, plasma cells, Innate Lymphoid Cells (ILCs), mast cells and a representative group of dendritic cells (DCs)[20,21,49,66,73]. For the ligand–receptor predictions of the upper respiratory tract, all immune cell types for which information was available were used in the analysis.

Defining ligand–receptor interactions between cell types. A list of ligand–receptor interactions was obtained from OmniPath on 23 September 2020 using the 'OmnipathR' R package[18]. Source databases used to retrieve the ligand–receptor interactions through OmnipathR included six independent resources (CellPhoneDB, HPMR, Ramilowski 2015, Guide2Pharma, Kirouac 2010, Gene Ontology)[25,74–78]. No weighing was performed on ligand–receptor interactions, and protein complexes were dealt with by including each of their individual proteins in the list.

Ligand–receptor interactions (intercellular interactions; full list available at https://github.com/korcsmarosgroup/gut-COVID) were predicted between epithelial cells types and resident immune cells according to the following conditions:

1. The ligand is differentially expressed in the epithelial cell (upon SARS-CoV-2 infection—in directly infected or bystander cells of the colon and ileum).
2. The receptor is expressed in the immune cell in the relevant dataset (ie, ileal or colonic immune cells).
3. The ligand–receptor interaction is present in OmniPath.

For the gut analysis, intercellular interactions were defined separately for directly infected epithelial cells and bystander epithelial cell populations in the ileum and in the colon. Enteroid epithelial data was paired with ileal immune cell data[20], while colonoid epithelial data was paired with colonic immune cell data[21]. For the upper airway analysis, ciliated cell data of moderate COVID-19 samples was paired with the same cell type of control samples[44]. Intercellular interactions were defined between every possible pair of epithelial cells and immune cells for each condition. Interactions derived from upregulated ligands ("upregulated interactions") were evaluated separately from interactions derived from downregulated ligands ("downregulated interactions").

Scoring of ligands, receptors and immune cell types involved in ligand–receptor interactions. To assess the importance of specific ligands,

Table 4. Key differentially expressed ligands produced by infected immature enterocytes drive the inflammatory process upon SARS-CoV-2 infection.

Ranking	Ligand	Ligand description	Organoid type	Expression change upon SARS-CoV-2 infection	Regulation by cytokines	Known to affect immune cells	Directly explain patients' blood cytokine levels
1	CXCL2	C-X-C Motif Chemokine Ligand 2	Colonic, Ileal	Up	IFNG, TNF, IL-17, IL-22 (up)	Neutrophils (1,2), fibroblasts, T cells, NK cell and CD8a + DCs (1), leukocytes (2)	✓
1	CXCL3	C-X-C Motif Chemokine Ligand 3	Colonic, Ileal	Up	TNF, IL-22 (up)	Neutrophils, fibroblasts (1), T cells (2)	✓
1	CXCL10	C-X-C Motif Chemokine Ligand 10	Colonic, Ileal	Up	IFNG, TNF (up)	DC, Th1, NK cells, B cells, monocytes (1), and 29 additional immune cell types (2)	✓
1	CSF1	Colony stimulating factor 1	Colonic	Up		35 immune cell types (2)	✓
1	CXCL11	C-X-C Motif Chemokine Ligand 11	Ileal	Up	n.d. (3)	DC (1,2), B cells, NK cells, Th1, monocytes, macrophages (1), lymphocytes, T cells, CD8+ alpha/beta T cell (2)	✓
2	TNFSF13B	TNF Superfamily Member 13b	Ileal	Up	n.d.	B cell, T cell, follicular B cell, naïve B cell, Th17, neutrophils, monocytes (2)	✓
2	LAMC2	Laminin Subunit Gamma 2	Colonic	Down	TNF, IL-22 (up)		
2	CCL5	C-C Motif Chemokine Ligand 5	Ileal	Up	n.d. (3)	T cells, basophils, eosinophils, macrophages, monocytes, NK cells, DC, Memory T cells, Th1 and Th2 (1), and 23 additional immune cell types (2)	
2	CX3CL1	C-X3-C Motif Chemokine Ligand 1	Ileal	Up	n.d. (3)	Monocytes, T cells, neutrophil, NK, DC, Mast cells and microglia (1), and 19 additional immune cell types (2)	
2	CXCL8	C-X-C Motif Chemokine Ligand 8	Ileal	Up	n.d. (3)	Neutrophils, macrophages, basophils, naïve T cells, CD8+ T cells, monocytes (1), and 44 additional immune cell types (2)	
3	ICAM1	Intercellular Adhesion Molecule 1	Colonic, Ileal	Up	IFNG, TNF, IL-22 (up)		
3	IL32	Interleukin 32	Colonic	Down	IFNG, TNF (up)		
3	AREG	Amphiregulin	Colonic	Down	IFNG (up), IL-13 (down)		
3	TNF	Tumour Necrosis Factor	Colonic, Ileal	Up	TNF, IL-22 (+)	Non-specific: 129 immune cell types (2)	
3	B2M	Beta-2-immunoglobulin	Colonic, Ileal	Down	IFNG (up)		
3	HLA-A	Major Histocompatibility Complex, Class I, A	Colonic, Ileal	Down	IFNG (up)		
3	HLA-B	Major histocompatibility complex, class I, B	Colonic, Ileal	Down	IFNG (up)		
3	LAMB3	Laminin Subunit Beta 3	Colonic	Down			

Table showing a list of top-ranked differentially expressed ligands in infected immature enterocytes which were identified to drive inflammation upon SARS-CoV-2 infection. The ranking of the ligands was performed using multiple criteria as explained in the Methods. 'Organoid type' indicates whether the expression change of the ligand was found in ileal or colonic infected immature enterocytes upon SARS-CoV-2 infection, respectively. 'Expression change upon SARS-CoV-2 infection' indicates the direction of expression change of the ligand in infected immature enterocytes upon SARS-CoV-2 infection. 'Regulation by cytokines' indicates whether ligand expression was found to be regulated by cytokines during inflammation based on results from[40]. Ileal data was not available (n.d.) in this study, so no conclusion could be drawn for ileal ligands. 'Known to affect immune cells' indicates whether the ligand was found to be regulated by immune cells using data from ImmunoGlobe[41] and ImmuneXpresso[42] databases. 'Directly explain patient blood cytokine levels' indicates whether the ligand was found to directly regulate blood cytokine levels in COVID-19 patients from[5].

receptors and immune cell types, additional parameters were computed using the ligand–receptor network. First, the number of interactions between each epithelial and immune cell type was computed by summing up all the possible interactions between each differentially expressed epithelial ligand and each of the receptors expressed by the specific immune cell type. Second, the number of immune cell types involved in each ligand–receptor pair was computed by counting the number of different immune cell types which were expressing the receiving receptor. Third, for each ligand, a "sum of receptor expression value" was computed for each interacting immune cell type, based on the number of interacting receptors and the mean expression level of the interacting receptors.

Data visualisation. Venn diagrams were generated using the 'gplots' R package. Heatmaps were generated using the 'ggplot2' and 'pheatmap' packages[79,80]. Barplots were generated with the 'ggplot2' package. Network visualisations were done using Cytoscape (version 3.8.2) (Shannon et al. 2003; Su et al. 2014). All scripts used to generate these plots are available on the Github repository of the project (https://github.com/korcsmarosgroup/gut-COVID).

Intracellular analysis

Two previously established tools were employed to predict the effect of SARS-CoV-2 infection on epithelial cells: ViralLink and CARNIVAL[17,19]. Both tools, using related but distinct methods, infer causal molecular interaction networks. These networks link perturbed human proteins predicted to interact with SARS-CoV-2 viral proteins or miRNAs, to transcription factors known to regulate the observed differentially expressed ligands in infected epithelial cells.

Input data. To reconstruct the intracellular causal networks, three different a priori interactions datasets were used. Information on viral proteins and their interacting human binding partners was obtained from the SARS-CoV-2 collection of the IntAct database on 1st October 2020[81,82]. Predicted SARS-CoV-2 miRNAs and their putative human binding partners were obtained from[45]. Intermediary signalling protein interactions known to occur in humans were obtained from the core protein-protein interaction (PPI) layer of the OmniPath collection using the 'OmnipathR' R package on 7th October 2020[83]. Only directed and signed interactions were included. Interactions between human transcription factors (TFs) and their target genes (TG) were obtained from the DoRothEA collection using the DoRothEA R package on 7th October 2020[84]. Only signed interactions of the top three confidence levels (A, B, C) were included.

Normalised transcript counts and differentially expressed ligands were obtained from single cell transcriptomics data of (i) colonoids and enteroids infected with SARS-CoV-2 obtained from[13], or (ii) upper airways samples of moderate COVID-19 patients from[44], as previously described.

ViralLink pipeline. Intracellular causal networks were inferred using the ViralLink pipeline, as described in[17]. Briefly, a list of expressed genes in infected immature enterocytes (originally known as "immature enterocytes 2" (MMP7+, MUC1+, CXCL1+)) from SARS-CoV-2-infected ileal and colonic organoids[13] or ciliated epithelial cells from moderate COVID-19 samples[44] was generated from a normalised count table by fitting a gaussian kernel[72]. The list of expressed genes in the infected immature enterocytes population or COVID-19 ciliated epithelial cells was subsequently used to filter the a priori molecular interactions from OmniPath and DoRothEA, to obtain PPI and TF-TG sub-networks where both interacting molecules are expressed (described as "contextualised" networks). Transcription factors regulating the differentially expressed ligands were predicted using the contextualised DoRothEA TF—TG interactions and scored as described in[17]. Human binding proteins of viral proteins and viral miRNAs obtained from the IntAct database[81,82] and[45], respectively, were connected to the listed TFs through the contextualised PPIs using a network diffusion approach called Tied Diffusion Through Interacting Events (TieDIE)[85]. In this model, all viral protein—human binding protein interactions were assumed to be inhibitory in action, based on likely biological function, and given a lack of clear literature evidence of proven action. All viral miRNA—human binding protein interactions were set as inhibitory based on biological action of miRNAs[86]. The final reconstructed network contains "nodes", which refers to the interacting partners, and "edges", which refers to the interaction between nodes. Nodes include viral proteins and miRNAs, human binding proteins, intermediary signalling proteins, TFs and differentially expressed ligands. Edges include activatory or inhibitory interactions.

For ileal, colonic and upper airways data, separate networks were generated using the viral miRNA and viral protein as perturbations, and subsequently joined using the "Merge" function within Cytoscape to generate the final intracellular network. Nodes and edges were annotated according to their involvement in networks downstream of viral miRNAs or proteins. Further analyses were performed separately on the different layers of the network: miRNA specific, protein specific or shared nodes.

CARNIVAL pipeline. Intracellular causal networks were inferred using CARNIVAL and associated tools for analyses of expression data as described in[19]. For simplicity, we refer to the pipeline as described in[19] as the CARNIVAL pipeline. Briefly, PROGENy is used to infer pathway activity from the log2 FC of the infected immature enterocytes 2 gene expression data[87]. Next, using the TF-TGs interactions (from DoRothEA) and the differential expression data from infected organoids, VIPER was used to score TF activity based on enriched regulon analysis[88]. Here, only the top 25 TFs regulating at least 15 target genes were taken forward, and a correction for pleiotropic regulation was included. Finally, CARNIVAL applied an integer linear programming approach to identify the most likely paths between human interaction partners of viral proteins or miRNAs and the selected TFs, through PPIs from OmniPath, considering the activity scores from PROGENy and VIPER. Viral protein—human binding protein interactions signs were specified to CARNIVAL as 'inhibitory', based on likely biological function, and given a lack of clear literature evidence of proven action. All viral miRNA—human binding protein interactions were also set as inhibitory based on biological action of miRNAs[86].

Network functional analysis

Functional overrepresentation analysis was performed on the networks constructed as above-mentioned using the R packages 'ClusterProfiler' and 'ReactomePA', for Gene Ontology (GO)[25]) and for Reactome[22–24] annotations, respectively. For the intercellular network, the analysis was carried out separately for ligand–receptor intercellular interactions driven by either upregulated or downregulated ligands. A complete list of ligand–receptor interactions is available in the GitHub repository of the project (https://github.com/korcsmarosgroup/gut-COVID). For the upregulated interactions, a list of upregulated ligands and their connecting immune receptors was used as the test. For the downregulated interactions, a list of downregulated ligands and their connecting immune receptors was used. Where a list of ligands plus receptors contained <5 genes, it was excluded from the analysis. All ligands and receptors from the original ligand–receptor network used as prior knowledge input for the intercellular analysis was used as the statistical background.

For the intracellular network, the analysis has been done separately for each of the sub-networks (viral protein specific, viral miRNA specific, or shared). For each sub-network, a set of genes that were human binding proteins, intermediary proteins and TFs in the network ("PPI layer") was used as a test list, and a set of all nodes from the original OmniPath PPI interaction network used as prior knowledge input for the intracellular analysis was used as the statistical background. For the Reactome pathway enrichment analysis the IDs were converted to Entrez Gene ID within the 'ReactomePA' package. Functional categories with adjusted p value ≤ 0.05 and with gene count >3 were considered significantly overrepresented.

Selection of ligands involved in the inflammatory process

To show how our approach could help point out specific epithelial-derived ligands driving the inflammatory process upon SARS-CoV-2 infection, the list of differentially expressed ligands in infected immature enterocytes in both colon and ileum was validated using independent data from three previously published studies. To identify ligands whose expression was induced by cytokines, ligands were compared to DEGs in human colonic organoids exposed to cytokines from[40]. To identify ligands already known to influence immune cell population, ligands were compared to two databases: ImmunoGlobe, a manually curated intercellular immune interaction network[41], and ImmunoeXpresso, a collection of cell–cytokine interactions generated through text mining[42]. Finally, to identify ligands that could directly explain blood cytokine level changes in COVID-19 patients via direct immune cell regulation, ligands were compared to the data from a large dataset we recently manually compiled using COVID-19 patient publications[5].

DATA AVAILABILITY

The necessary input data for the workflow and the full ligand–receptor interaction tables are available in the GitHub repository of the project (https://github.com/korcsmarosgroup/gut-COVID). All other relevant data is in the main text and in Supplementary files.

CODE AVAILABILITY

The code of the entire workflow is available in the GitHub repository of the project (https://github.com/korcsmarosgroup/gut-COVID).

Received: 5 November 2021; Accepted: 4 April 2022;
Published online: 02 May 2022

REFERENCES

1. Tay, M. Z., Poh, C. M., Rénia, L., MacAry, P. A. & Ng, L. F. P. The trinity of COVID-19: immunity, inflammation and intervention. *Nat. Rev. Immunol.* **20**, 363–374 (2020).
2. Mick, E. et al. Upper airway gene expression reveals suppressed immune responses to SARS-CoV-2 compared with other respiratory viruses. *Nat. Commun.* **11**, 5854 (2020).
3. Peacock, T. P. et al. The SARS-CoV-2 variant, Omicron, shows rapid replication in human primary nasal epithelial cultures and efficiently uses the endosomal route of entry. Preprint at https://www.biorxiv.org/content/10.1101/2021.12.31.474653v1 (2022).
4. Gupta, A. et al. Extrapulmonary manifestations of COVID-19. *Nat. Med.* **26**, 1017–1032 (2020).
5. Olbei, M. et al. SARS-CoV-2 causes a different cytokine response compared to other cytokine storm-causing respiratory viruses in severely ill patients. *Front. Immunol.* **12**, 629193 (2021).
6. Arunachalam, P. S. et al. Systems biological assessment of immunity to mild versus severe COVID-19 infection in humans. *Science* **369**, 1210–1220 (2020).
7. Stone, J. H. et al. Efficacy of tocilizumab in patients hospitalized with Covid-19. *N. Engl. J. Med.* **383**, 2333–2344 (2020).
8. Kale, S. D. et al. "Small" intestinal immunopathology plays a "Big" role in lethal cytokine release syndrome, and its modulation by interferon-γ, IL-17A, and a Janus kinase inhibitor. *Front. Immunol.* **11**, 1311 (2020).
9. Martin-Cardona, A. et al. SARS-CoV-2 identified by transmission electron microscopy in lymphoproliferative and ischaemic intestinal lesions of COVID-19 patients with acute abdominal pain: two case reports. *BMC Gastroenterol.* **21**, 334 (2021).
10. Lamers, M. M. et al. SARS-CoV-2 productively infects human gut enterocytes. *Science* **369**, 50–54 (2020).
11. Stanifer, M. L. et al. Critical role of type III interferon in controlling SARS-CoV-2 infection in human intestinal epithelial cells. *Cell Rep.* **32**, 107863 (2020).
12. Zang, R. et al. TMPRSS2 and TMPRSS4 promote SARS-CoV-2 infection of human small intestinal enterocytes. *Sci. Immunol.* **5**, 47 (2020).
13. Triana, S. et al. Single-cell analyses reveal SARS-CoV-2 interference with intrinsic immune response in the human gut. *Mol. Syst. Biol.* **17**, e10232 (2021).
14. Blanco-Melo, D. et al. Imbalanced host response to SARS-CoV-2 drives development of COVID-19. *Cell* **181**, 1036–1045.e9 (2020).
15. Hadjadj, J. et al. Impaired type I interferon activity and inflammatory responses in severe COVID-19 patients. *Science* **369**, 718–724 (2020).
16. Guo, M., Tao, W., Flavell, R. A. & Zhu, S. Potential intestinal infection and faecal–oral transmission of SARS-CoV-2. *Nat. Rev. Gastroenterol. & Hepatol.* **18**, 269–283 (2021).
17. Treveil, A. et al. ViralLink: an integrated workflow to investigate the effect of SARS-CoV-2 on intracellular signalling and regulatory pathways. *PLoS Comput. Biol.* **17**, e1008685 (2021).
18. Türei, D. et al. Integrated intra- and intercellular signaling knowledge for multicellular omics analysis. *Mol. Syst. Biol.* **17**, e9923 (2021).
19. Liu, A. et al. From expression footprints to causal pathways: contextualizing large signaling networks with CARNIVAL. *NPJ Syst. Biol. Appl.* **5**, 40 (2019).
20. Martin, J. C. et al. Single-cell analysis of Crohn's disease lesions identifies a pathogenic cellular module associated with resistance to anti-TNF therapy. *Cell* **178**, 1493–1508.e20 (2019).
21. Smillie, C. S. et al. Intra- and inter-cellular rewiring of the human colon during ulcerative colitis. *Cell* **178**, 714–730.e22 (2019).
22. Yu, G., Wang, L.-G., Han, Y. & He, Q.-Y. clusterProfiler: an R package for comparing biological themes among gene clusters. *OMICS* **16**, 284–287 (2012).
23. Yu, G. & He, Q.-Y. ReactomePA: an R/Bioconductor package for reactome pathway analysis and visualization. *Mol. Biosyst.* **12**, 477–479 (2016).
24. Fabregat, A. et al. The Reactome Pathway Knowledgebase. *Nucleic Acids Res.* **46**, D649–D655 (2018).
25. Ashburner, M. et al. Gene Ontology: tool for the unification of biology. *Nat. Genet.* **25**, 25–29 (2000).
26. Ivashkiv, L. B. & Donlin, L. T. Regulation of type I interferon responses. *Nat. Rev. Immunol.* **14**, 36–49 (2014).
27. Cartwright, T., Perkins, N. D. & Wilson, L. C. NFKB1: a suppressor of inflammation, ageing and cancer. *FEBS J.* **283**, 1812–1822 (2016).
28. Persengiev, S. P. & Green, M. R. The role of ATF/CREB family members in cell growth, survival and apoptosis. *Apoptosis* **8**, 225–228 (2003).
29. Mehic, D., Bakiri, L., Ghannadan, M., Wagner, E. F. & Tschachler, E. Fos and jun proteins are specifically expressed during differentiation of human keratinocytes. *J. Invest. Dermatol.* **124**, 212–220 (2005).
30. Carulli, A. J. et al. Notch receptor regulation of intestinal stem cell homeostasis and crypt regeneration. *Dev. Biol.* **402**, 98–108 (2015).
31. Yamada, Y. et al. Functional roles of TGF-β1 in intestinal epithelial cells through Smad-dependent and non-Smad pathways. *Dig. Dis. Sci.* **58**, 1207–1217 (2013).
32. Shuai, K. & Liu, B. Regulation of JAK-STAT signalling in the immune system. *Nat. Rev. Immunol.* **3**, 900–911 (2003).
33. Wen, A. Y., Sakamoto, K. M. & Miller, L. S. The role of the transcription factor CREB in immune function. *J. Immunol.* **185**, 6413–6419 (2010).
34. Valcourt, U., Kowanetz, M., Niimi, H., Heldin, C.-H. & Moustakas, A. TGF-beta and the Smad signaling pathway support transcriptomic reprogramming during epithelial-mesenchymal cell transition. *Mol. Biol. Cell* **16**, 1987–2002 (2005).
35. Osaki, L. H. & Gama, P. MAPKs and signal transduction in the control of gastrointestinal epithelial cell proliferation and differentiation. *Int. J. Mol. Sci.* **14**, 10143–10161 (2013).
36. Alejo, A. et al. Chemokines cooperate with TNF to provide protective anti-viral immunity and to enhance inflammation. *Nat. Commun.* **9**, 1790 (2018).
37. Mantegazza, A. R., Magalhaes, J. G., Amigorena, S. & Marks, M. S. Presentation of phagocytosed antigens by MHC class I and II. *Traffic* **14**, 135–152 (2013).
38. Mezu-Ndubuisi, O. J. & Maheshwari, A. The role of integrins in inflammation and angiogenesis. *Pediatr. Res.* **89**, 1619–1626 (2021).
39. Millar-Büchner, P. et al. Severe changes in colon epithelium in the Mecp2-null mouse model of Rett syndrome. *Mol. Cell. Pediatr.* **3**, 37 (2016).
40. Pavlidis, P. et al. Cytokine responsive networks in human colonic epithelial organoids unveil a novel molecular stratification of inflammatory bowel disease. *SSRN J.* https://doi.org/10.2139/ssrn.3823433 (2021).
41. Atallah, M. B. et al. ImmunoGlobe: enabling systems immunology with a manually curated intercellular immune interaction network. *BMC Bioinforma.* **21**, 346 (2020).
42. Kveler, K. et al. Immune-centric network of cytokines and cells in disease context identified by computational mining of PubMed. *Nat. Biotechnol.* **36**, 651–659 (2018).
43. Abubakar, A. R. et al. Systematic review on the therapeutic options for COVID-19: clinical evidence of drug efficacy and implications. *Infect. Drug Resist.* **13**, 4673–4695 (2020).
44. Chua, R. L. et al. COVID-19 severity correlates with airway epithelium-immune cell interactions identified by single-cell analysis. *Nat. Biotechnol.* **38**, 970–979 (2020).
45. Saçar Demirci, M. D. & Adan, A. Computational analysis of microRNA-mediated interactions in SARS-CoV-2 infection. *PeerJ* **8**, e9369 (2020).
46. Griffiths-Jones, S., Saini, H. K., van Dongen, S. & Enright, A. J. miRBase: tools for microRNA genomics. *Nucleic Acids Res.* **36**, D154–8 (2008).
47. Bruscella, P. et al. Viruses and miRNAs: more friends than foes. *Front. Microbiol.* **8**, 824 (2017).
48. Bouhaddou, M. et al. The global phosphorylation landscape of SARS-CoV-2 infection. *Cell* **182**, 685–712.e19 (2020).
49. Schultze, J. L. & Aschenbrenner, A. C. COVID-19 and the human innate immune system. *Cell* **184**, 1671–1692 (2021).
50. Koutsakos, M. et al. Downregulation of MHC class I expression by influenza A and B viruses. *Front. Immunol.* **10**, 1158 (2019).
51. Park, M. D. Immune evasion via SARS-CoV-2 ORF8 protein? *Nat. Rev. Immunol.* **20**, 408 (2020).
52. Simon, T. & Bromberg, J. S. Regulation of the immune system by laminins. *Trends Immunol.* **38**, 858–871 (2017).
53. Mahoney, Z. X., Stappenbeck, T. S. & Miner, J. H. Laminin alpha 5 influences the architecture of the mouse small intestine mucosa. *J. Cell Sci.* **121**, 2493–2502 (2008).
54. Bouatrouss, Y., Herring-Gillam, F. E., Gosselin, J., Poisson, J. & Beaulieu, J. F. Altered expression of laminins in Crohn's disease small intestinal mucosa. *Am. J. Pathol.* **156**, 45–50 (2000).
55. Francoeur, C., Escaffit, F., Vachon, P. H. & Beaulieu, J.-F. Proinflammatory cytokines TNF-alpha and IFN-gamma alter laminin expression under an apoptosis-independent mechanism in human intestinal epithelial cells. *Am. J. Physiol. Gastrointest. Liver Physiol.* **287**, G592–8 (2004).
56. Kim, J., Koo, B.-K. & Knoblich, J. A. Human organoids: model systems for human biology and medicine. *Nat. Rev. Mol. Cell Biol.* **21**, 571–584 (2020).
57. Schreurs, R. R. C. E., Baumdick, M. E., Drewniak, A. & Bunders, M. J. In vitro co-culture of human intestinal organoids and lamina propria-derived CD4 + T cells. *STAR Protoc.* **2**, 100519 (2021).

58. Poletti, M., Arnauts, K., Ferrante, M. & Korcsmaros, T. Organoid-based models to study the role of host-microbiota interactions in IBD. *J. Crohns Colitis* **15**, 1222–1235 (2021).
59. Min, S., Kim, S. & Cho, S.-W. Gastrointestinal tract modeling using organoids engineered with cellular and microbiota niches. *Exp. Mol. Med.* **52**, 227–237 (2020).
60. Dimitrov, D. et al. Comparison of Resources and Methods to infer Cell–Cell Communication from Single-cell RNA Data. Preprint at https://www.biorxiv.org/content/10.1101/2021.05.21.445160v1 (2021).
61. Su, C.-M., Wang, L. & Yoo, D. Activation of NF-κB and induction of proinflammatory cytokine expressions mediated by ORF7a protein of SARS-CoV-2. *Sci. Rep.* **11**, 13464 (2021).
62. Mardi, A., Meidaninikjeh, S., Nikfarjam, S., Majidi Zolbanin, N. & Jafari, R. Interleukin-1 in COVID-19 Infection: Immunopathogenesis and Possible Therapeutic Perspective. *Viral Immunol.* **34**, 679–688 (2021).
63. Vaz de Paula, C. B. et al. IL-4/IL-13 remodeling pathway of COVID-19 lung injury. *Sci. Rep.* **10**, 18689 (2020).
64. Koenig, L. M. et al. Blocking inflammation on the way: Rationale for CXCR2 antagonists for the treatment of COVID-19. *J. Exp. Med.* **217**, 9 (2020).
65. Yang, D. et al. Attenuated interferon and proinflammatory response in SARS-CoV-2-infected human dendritic cells is associated with viral antagonism of STAT1 phosphorylation. *J. Infect. Dis.* **222**, 734–745 (2020).
66. Sette, A. & Crotty, S. Adaptive immunity to SARS-CoV-2 and COVID-19. *Cell* **184**, 861–880 (2021).
67. Castelli, E. C. et al. MHC variants associated with symptomatic versus asymptomatic SARS-CoV-2 infection in highly exposed individuals. *Front. Immunol.* **12**, 742881 (2021).
68. Leng, L. et al. Pathological features of COVID-19-associated lung injury: a preliminary proteomics report based on clinical samples. *Signal Transduct. Target. Ther.* **5**, 240 (2020).
69. Triana, S., Stanifer, M. L., Boulant, S. & Alexandrov, T. COVID19_July.rda. *Figshare* https://doi.org/10.6084/m9.figshare.13703752.v1 (2021).
70. Hao, Y. et al. Integrated analysis of multimodal single-cell data. *Cell* **184**, 3573–3587.e29 (2021).
71. McDavid, A., Finak, G. & Yajima, M. MAST: Tools and methods for analysis of single cell assay data in R. *R package version 1.18.0* https://github.com/RGLab/MAST/ (2021).
72. Beal, J. Biochemical complexity drives log-normal variation in genetic expression. *Eng. biol.* **1**, 55–60 (2017).
73. Filbin, M. R. et al. Longitudinal proteomic analysis of severe COVID-19 reveals survival-associated signatures, tissue-specific cell death, and cell–cell interactions. *Cell Rep. Med.* **2**, 100287 (2021).
74. Ben-Shlomo, I., Yu Hsu, S., Rauch, R., Kowalski, H. W. & Hsueh, A. J. W. Signaling receptome: a genomic and evolutionary perspective of plasma membrane receptors involved in signal transduction. *Sci. STKE* **2003**, RE9 (2003).
75. Ramilowski, J. A. et al. A draft network of ligand-receptor-mediated multicellular signalling in human. *Nat. Commun.* **6**, 7866 (2015).
76. Pawson, A. J. et al. The IUPHAR/BPS Guide to PHARMACOLOGY: an expert-driven knowledgebase of drug targets and their ligands. *Nucleic Acids Res.* **42**, D1098–106 (2014).
77. Vento-Tormo, R. et al. Single-cell reconstruction of the early maternal-fetal interface in humans. *Nature* **563**, 347–353 (2018).
78. Kirouac, D. C. et al. Dynamic interaction networks in a hierarchically organized tissue. *Mol. Syst. Biol.* **6**, 417 (2010).
79. *ggplot2: Elegant Graphics for Data Analysis*. (Springer-Verlag New York, 2016).
80. Kolde, R. Pheatmap: pretty heatmaps. *R. package version 1. 2* **1**, 726 (2012).
81. Hermjakob, H. et al. IntAct: an open source molecular interaction database. *Nucleic Acids Res.* **32**, D452–5 (2004).
82. Orchard, S. et al. The MIntAct project - IntAct as a common curation platform for 11 molecular interaction databases. *Nucleic Acids Res.* **42**, D358–63 (2014).
83. Türei, D., Korcsmáros, T. & Saez-Rodriguez, J. OmniPath: guidelines and gateway for literature-curated signaling pathway resources. *Nat. Methods* **13**, 966–967 (2016).
84. Garcia-Alonso, L., Holland, C. H., Ibrahim, M. M., Turei, D. & Saez-Rodriguez, J. Benchmark and integration of resources for the estimation of human transcription factor activities. *Genome Res.* **29**, 1363–1375 (2019).
85. Paull, E. O. et al. Discovering causal pathways linking genomic events to transcriptional states using Tied Diffusion Through Interacting Events (TieDIE). *Bioinformatics* **29**, 2757–2764 (2013).
86. Huang, R. S. et al. Population differences in microRNA expression and biological implications. *RNA Biol.* **8**, 692–701 (2011).
87. Schubert, M. et al. Perturbation-response genes reveal signaling footprints in cancer gene expression. *Nat. Commun.* **9**, 20 (2018).
88. Alvarez, M. J. et al. Functional characterization of somatic mutations in cancer using network-based inference of protein activity. *Nat. Genet.* **48**, 838–847 (2016).

ACKNOWLEDGEMENTS

M.O., A.T., L.G., and M.P. are supported by the UKRI Biotechnological and Biosciences Research Council (BBSRC) funded Norwich Research Park Biosciences Doctoral Training Partnership (grant numbers BB/M011216/1 and BB/S50743X/1). The work of T.K. and D.M. was supported by the Earlham Institute (Norwich, UK) in partnership with the Quadram Institute (Norwich, UK) and strategically supported by the UKRI BBSRC UK grants (BB/J004529/1, BB/P016774/1, and BB/CSP17270/1). T.K. and D.M. were also funded by a BBSRC ISP grant for Gut Microbes and Health BB/R012490/1 and its constituent projects, BBS/E/F/000PR10353 and BBS/E/F/000PR10355. T.A. and S.T. acknowledge the funding from the Darwin Trust of Edinburgh and from the ERC Consolidator grant METACELL from European Union's Horizon 2020 programme. T.A. and S.T. acknowledge support from the EMBL Genomics Core Facility and particularly help from Vladimir Benes. B.V. is supported by the Clinical Research Fund (KOOR) University Hospitals Leuven. S.B. was supported by research grants from the Deutsche Forschungsgemeinschaft (DFG): project numbers 415089553 (Heisenberg program), 240245660 (SFB1129), 278001972 (TRR186), and 272983813 (TRR179), the state of Baden Wuerttemberg (AZ: 33.7533.-6-21/5/1) and the Bundesministerium Bildung und Forschung (BMBF) (01KI20198A). M.L.S. was supported by the DFG (416072091) and the BMBF (01KI20239B). D.T. was supported by the Federal Ministry of Education and Research (BMBF, Computational Life Sciences grant no. 031L0181B) to J.S.R.

AUTHOR CONTRIBUTIONS

M.P and A.T contributed equally to this manuscript. M.P., A.T., L.C., L.G. and D.M. contributed to the study design, data analysis and drafting the manuscript. M.M., M. O. and B.B. contributed to the initial input data processing and bioinformatics pipeline development. A.V., D.T., S.T. contributed with data generation and supervision during data analysis and bioinformatics pipeline development. B.V., T. A., J.S.R., M.L.S., S.B. and T.K. led the initial study design, supervised the work and contributed to writing the manuscript. All authors read and approved the manuscript.

COMPETING INTERESTS

The Authors declare no Competing Non-Financial Interests but the following Competing Financial Interests: B. Verstockt reports financial support for research from Pfizer; lecture fees from Abbvie, Biogen, Chiesi, Falk, Ferring, Galapagos, Janssen, MSD, Pfizer, R-Biopharm, Takeda and Truvion; consultancy fees from Janssen, Guidepont and Sandoz, all outside of the submitted work; JSR received funding from GSK and Sanofi and consultant fees from Travere Therapeutics.

ADDITIONAL INFORMATION

Supplementary information The online version contains supplementary material available at https://doi.org/10.1038/s41540-022-00224-x.

Correspondence and requests for materials should be addressed to Tamas Korcsmaros.

Reprints and permission information is available at http://www.nature.com/reprints

Publisher's note Springer Nature remains neutral with regard to jurisdictional claims in published maps and institutional affiliations.